An Axisymmetrical Model for A Single Vertical Pile in Sand

Gamal Abdelaziz

A Thesis
In
The Department
of
Building, Civil & Environmental Engineering

Presented in Partial Fulfillment of the Requirements
For the Degree of Doctor of Philosophy at
Concordia University
Montreal, Quebec, Canada

September 2000

0-612-59226-X

ABSTRACT

An Axisymmetrical Model For A Single Vertical Pile In Sand

Gamal Abdelaziz, Ph.D.

Concordia University, 2000

This study presents numerical and theoretical investigations on the bearing capacity of a single pile in sand under axisymmetrical loading conditions. An extensive literature review for the existing theories is presented. The published reports showed a wide range of discrepancies exists among previous theories developed to predict bearing capacity of a single pile in sand. A numerical pile load-testing program was carried out using finite element technique to cover a wide rang of pile geometry and sand states. Mohr-Coulomb criteria were used to model the sand behavior. Linear strain quadrilateral elements were employed to model soil and pile. A chain of slip elements was placed around the pile to model the slippage between sand and pile. The numerical model was validated against field load tests data. The numerical model was then used to analyze stresses influencing the pile behavior in sand and to establish the pile failure mechanism. The stresses and coefficient of earth pressure acting on the pile shaft were reported. A new failure mechanism was developed which varies with: pile geometry, coefficient of earth pressure, shaft roughness and angle of shearing resistance of sand.

A theoretical model was developed to predict the ultimate bearing capacity of a single pile in sand, utilizing the proposed failure mechanism. A data analysis procedure was employed to develop the new model parameters predictive formulas. An approximate method to predict the coefficient of earth pressure acting on the pile shaft was developed and used extensively in the theoretical model. A sensitivity analysis was conducted on the varying parameters of the theoretical model. The theoretical model incorporates salient features previously omitted in conventional bearing capacity theories: treating the bearing capacity of a single pile in sand under axisymmetrical conditions, adopting the punching shear failure as a principle failure mode, and accounting for the interdependence between skin friction and tip resistances. The theoretical model showed that the average unit skin and tip resistances increase, but at a lower rate below the critical depth. These findings concur with the recent research conclusions, which indicate that the average skin resistance tends to increase with depth. A computer program "G-Pile" was developed to facilitate the massive mathematical calculations of the theoretical model. The computer program "G-Pile" was used to produce data for charts of the factors needed to predict the bearing capacity of a single pile in sand. A design procedure is proposed and verified against field test results, good agreement was achieved. Recommendations are given for future research.

ACKNOWLEDGMENTS

In the name of Allah, the most Gracious, the most merciful

All praises and thanks are to Almighty, Allah, the Lord of the worlds, the sustainer of the universe, and the ruler of the day of resurrection. He provided me with all means of support, guidance, patience and abilities to complete this work.

I wish to express my gratitude to my supervisor, Dr. A. M. Hanna, for his continuous encouragement and valuable assistance over the years. His deep interest in this investigation and his guidance, made it possible to complete this research.

I would like to thank Dr. Hani Keira, adjunct professor, for his valuable discussions over the years.

I am thankful for the comments of many individuals whom I have contacted at various stages of this work, either in person or by correspondence, for their comments:

- Dr. G.G. Meyerhof (Nova Scotia Technical College, Canada)
- Dr. A. Britto and Dr. Gunn, M.J. Professors, (Cambridge University, U.K.) for technical support provided for using the finite element program CRISP.
- Dr. F. Tavenas (Rector, Laval University, Canada)

I am thankful to the Egyptian government, Missions Department, for financial support during the initial period of this research program. Also financial support from National Science and Engineering Research Council of Canada (NSERC) and Faculty of Engineering at Concordia University, are greatly appreciated. The Student's awards granted by Concordia University (1995-1999) are highly appreciated, without these supports this work could not come to life.

I would like to express my deep thanks to Ms. Patericia Verret, Manger, Graduate Awards Office, Concordia University, for her kind assistance and encouragement during my staying at Concordia.

My deep gratitude is due to my wife, Somaia for her, kindness and patience, without her continuous encouragements I could not have done this work.

I wish to express my sincere gratitude to my parents, for their love, support and favourite encouragements over the years.

To my family:

My parents and my brothers;

My wife and my children

TABLE OF CONTENTS

CHAPTER 3

NUMERICAL MODELING

CHAPTER 4

LIST OF FIGURES

PAGE

CHAPTER 2

LITERATURE REVIEW

CHAPTER 3

NUMERICAL MODELING

CHAPTER 4

THEORTICAL MODEL

APPENDIX I

APPLICATION OF METHOD OF SLICES

LIST OF TABLES

CHAPTER 2

CHAPTER 3

CHAPTER 4

CHAPTER 1

INTRODUCTION

1.1 General

The role of foundation is to transmit loads from the superstructure to the ground safely and without excessive settlement. Whenever soil of poor bearing capacity is encountered, a decision has to be made concerning the use of deep foundations. If the cost and difficulty of conventional foundations is considerable then piled foundations are normally used to transfer the load from the superstructure through weak compressible strata onto stiffer and less compressible soils or onto rock.

1.2 Problem Definiation And Motivation

The ultimate vertical pile load in sand is generally divided into two components, point load or tip load, and shaft or skin resistance. The static formula method (Sowers,G., 1970) is commonly used to determine the ultimate axial bearing capacity of a pile, Q_u; the equation and terminology used are:

$$Q_u = Q_p + Q_s = q_o A_p + f_s A_s \quad ...(1.1)$$

Where:

Q_p = ultimate point capacity;

Q_s = ultimate shaft capacity;

q_o = ultimate unit point resistance;

f_s = ultimate unit shaft resistance;

A_p = area of pile point; and

A_s = area of pile shaft.

1.2.1 Point Resistance

In all of the theoretical solutions, the ultimate unit point resistance, q_o, is given in simplified form utilizing cohesionless soil and a circular pile cross section as the commonly used form (Coyle and Sulaiman, 1970):

$$q_o = p_o N^*_q \qquad ...(1.2)$$

in which:

p_o = effective overburden pressure at the pile point level;

N^*_q = bearing capacity factors, usually depending upon the soil shearing resistance angle ϕ' and the assumed pattern or mechanism of failure.

In most of the theories the basic parameters, in addition to the pile geometry, are, the internal shearing resistance angle, ϕ', which is used to determine the bearing capacity factor, N_q, and the effective confining pressure of the soil. All of the bearing capacity theories require the evaluation of N^*_q for use in Equation 1.2. Among all conventional theories it is evident that there are major deviations from one theory to another, leading to the conclusion that the true failure mechanism is not, generally, well understood.

1.2.2 Shaft Resistance

The magnitude of the ultimate unit shaft resistance f_s is commonly determined using

$$f_s = K\, p' \tan \delta \qquad ...(1.3)$$

in which:

K = lateral earth pressure coefficient;

p' = average effective overburden along the segment of pile shaft being considered

$\tan\delta$ = coefficient of friction between the pile and the soil.

The determination of the ultimate unit shaft resistance, f_s is based on the laws of mechanics considering friction between solid surfaces. Factors K and tan δ need to be established in order to determine unit side resistance. Through the literature only one value is suggested by the different authors, regardless of pile geometry or soil conditions. Significant differences between the published values of ($K_s \tan\delta$) exist.

It has been shown that the variation of the values of N_q and K is so wide that the choice of one theory over another is a difficult exercise in engineering judgment. In view of these serious limitations, rational approaches are clearly needed to provide a unique theoretical basis for estimating the ultimate bearing capacity of an axially loaded single pile in sand.

1.3 Purpose and Scope of the Thesis

The objectives of the present research program are:

1- To review the existent design theories of pile foundations.

2- To develop a numerical model to examine the effect of various factors influencing the bearing capacity of a single pile driven in sand.

3- To establish a practical design procedure to estimate the coefficient of earth pressure acting on the pile shaft.

4- To develop a rational theory which is capable of incorporating some of the new factors usually omitted in the literature; these include the bearing capacity problem being treated as an axisymmetric case; the effect of pile geometry, adopting punching shear failure as a unique failure mode for pile foundation in sand, utilizing the variable failure mechanism and variable coefficient of earth pressure acting on the pile shaft, K_s. To produce design charts for the common bearing capacity factors: N^*_q and ($K_s \tan\delta$).

1.5 Organizanon of the Thesis

The historical development of the subject of this thesis is introduced in chapter 2. The numerical investigation of a single pile in sand using the finite element technique is carried out in chapter 3. The development of an axisymmetrical theoretical model for pile bearing capacity, presented in chapter 4. Following a sensitivity analysis for the new proposed model, the validity of the proposed model is verified by the analysis of field load tests. Chapter 4 introduces a rational design procedure for estimating bearing capacity of single piles driven in sand using design charts. Conclusions drawn from the present study and recommendations for future study are given in chapter 5.

CHAPTER 2

LITERATURE REVIEW

2.1 Introduction

Pile foundations are used extensively around the world to support both inland and offshore structures, including nuclear plants and oil drilling platforms. They are mainly used in sites where the presence of soft soil layers would cause excessive deformation or failure of more conventional types of foundations. The two major categories of piles in common use are: friction or floating piles, whose load carrying capacity depends mostly on the amount of frictional resistance that can develop at the interface between the pile shaft and the soil; and end bearing piles, which rely primarily on the concentrated soil resistance at the tip of the pile.

Many research reports dealing with the ultimate bearing capacity of pile foundations have been listed in the literature during the past four decades. Despite the progress made during this period, there remain a number of conflicting theories which form the basis for determining both ultimate load capacity and load displacement of a single pile in sand. In this chapter, a brief review of the methods developed for evaluating and predicting pile bearing capacity in sand are given. It should be noted that, in most of the given solutions, a unique factor "ϕ", angle of shearing resistance of sand, is considered. A few theories consider factors other than "ϕ" to affect the problem of bearing capacity of a single pile in sand.

2.2 Histrocal Devlopment

There are two approaches employed in the study of the behavior of pile foundations: theoretical and experimental, as shown in Figure 2.1. For many years, purely theoretical and empirical approaches were employed and the design of pile foundations was based on a combination of empiricism and experience. However, in the past three decades, a gradual change has taken place in pile design procedures, from the essentially empirical methods towards methods with a sounder theoretical basis. This change has resulted from the wider use of pile foundations and the need to support large loads on piles, especially in the case of the foundations of offshore structures. Accordingly, improvement of design procedures has rapidly developed, particularly due to the availability of powerful numerical techniques for analyzing this complex problem. Most of these methods involve the use of one (or more) of the following analytical techniques as reported by Poulos (1989):

(a) simplified analytical methods involving the consideration of independent horizontal "slices" of pile and soil (e.g. Randolph and Wroth 1978);

(b) boundary element methods, employing either load-transfer functions to represent the interface response (e.g. Coyle and Reese (1966), Kraft et. al. (1981)) or elastic continuum theory to represent the soil mass response (e.g. Butterfield and Banerjee (1971), Banerjee (1978), Banerjee and Davies (1978), Poulos and Davis (1980));

(c) finite element methods (e.g. Desai (1974), Valliappan et. al. (1974), Balaam et. al. (1975), Ottaviani (1975), Jardine et. al. (1986)), in which a variety of constitutive soil models can be utilized, and such factors as soil non-homogeneity and anisotropy can be taken into account.

This chapter summarizes the available literature relevant to the scope of the present research, i.e. the bearing capacity of a single pile driven in sand under axisymmetric static loading.

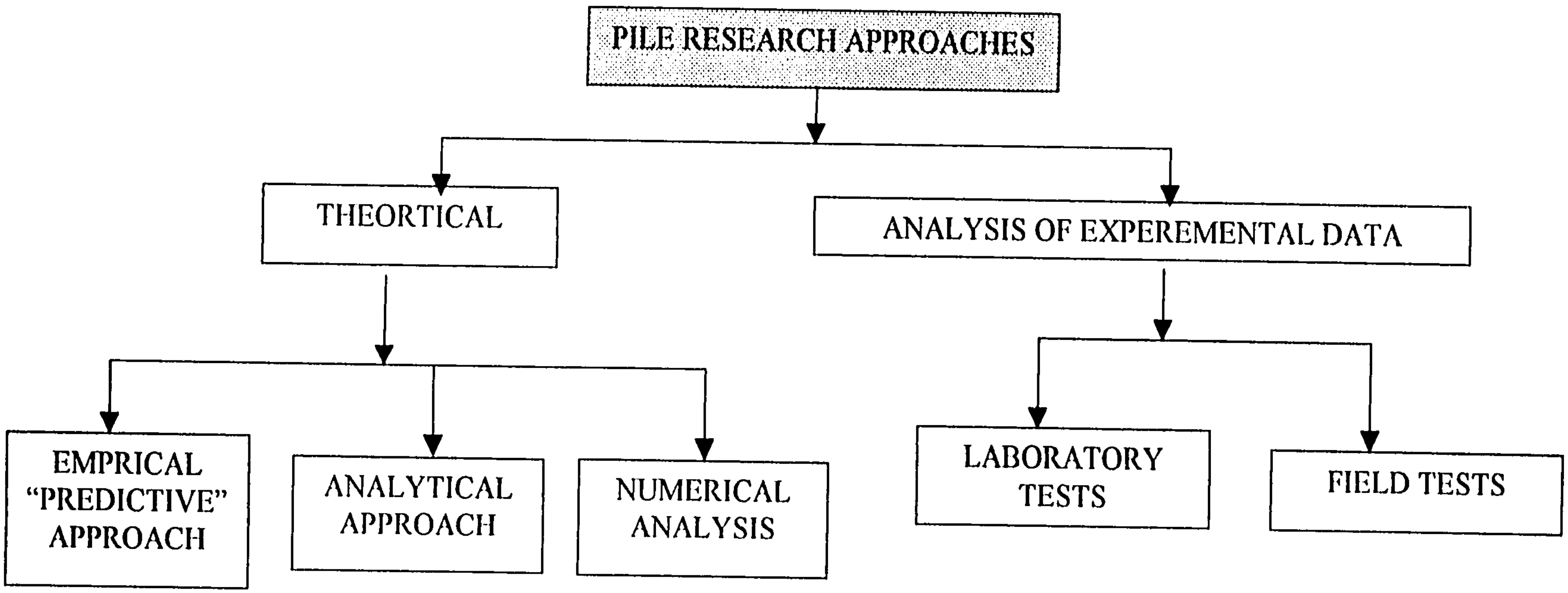

Figure 2.1 Pile Research Approaches

2.3 Static Analysis

In static analysis, the ultimate bearing capacity of a single pile driven in a homogenous sand deposit generally consists of two components: namely the load transmitted along the pile shaft and the load at the pile tip. These two components are usually referred to as the skin friction (shaft resistance) and point (tip) resistance, (Figure 2.2)

Hence,

$$Q_u = Q_s + Q_p = f_s \times A_s + q_p \times A_p \qquad \text{...(2.1)}$$

Where

Q_u = ultimate bearing capacity of the pile

Q_s = skin friction

Q_p = point resistance.

f_s = the average unit skin friction on shaft

A_s = area of the pile shaft

q_p = the unit bearing capacity of pile point

A_p = area of the pile cross section

The tip resistance "Q_p"is based on the estimated general shear strength failure mechanism of the soil and the effective stress method is used to evaluate the side friction of the sand.

2.3.1 Shaft Resistance

The theoretical determination of skin friction for piles in sand has received little attention in the literature and only a few methods have been reported. This can be explained by the fact that the interaction between the soil and the pile is very complex and poorly understood. Accordingly, the determination of the ultimate unit skin friction, q_s, is performed based on the

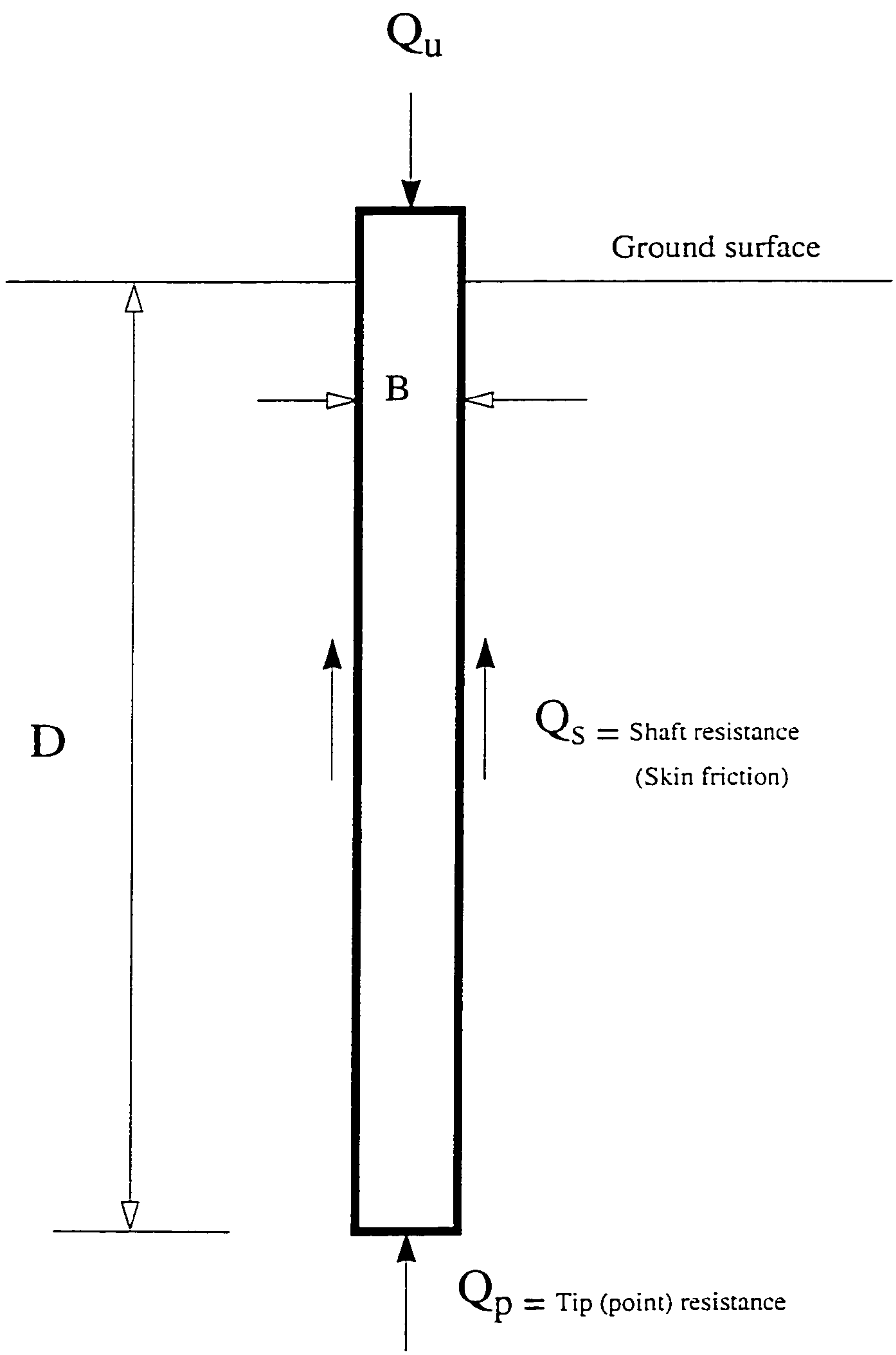

Figure 2.2 Ultimate Bearing Capacity - Static Method

laws of mechanics considering friction between solid surfaces. The shaft resistance of the pile is usually evaluated by integrating the pile-sand shear stress τ_f at depth z over the surface area of the shaft. The shear stress is usually assumed to be a function of the effective lateral stress σ'_n exerted on the pile by surrounding sand at the same depth. It is given by the following formula:

$$\tau_f = \left(\sigma'_n \tan\delta_z\right) \qquad \text{...(2.2)}$$

Where

δ_z = angle of friction between the pile and the sand at depth z.

$\tan\delta_z$ = coefficient of friction between the pile and the soil at the depth z.

The effective lateral stress σ'_n can be expressed in terms of the effective vertical stress σ'_z as:

$$\sigma'_n = K_z \sigma'_z \qquad \text{...(2.3)}$$

Where:

K_z = Coefficient of lateral earth pressure on pile shaft at the depth z.

From equation (2.3) and equation (2.4),

$$\tau_f = \sigma'_z K_z \tan\delta_z \qquad \text{...(2.4)}$$

By integrating over the depth D, Q_s can be found as:

$$Q_s = \int_0^D (\pi B)(\tau_f)(dz) \qquad \text{...(2.5)}$$

$$Q_s = \pi B\left(\int_0^D \sigma'_z\right) K_z \tan\delta_z dZ \qquad \text{...(2.6)}$$

Where:

B = pile diameter

D = pile embedment length

The effective vertical stress σ'_z is usually taken as equal to the effective overburden pressure at the same depth ($\gamma' z$), while K_z and δ_z are taken as average values K_s and δ, respectively, over the entire pile length.

$$Q_s = \pi B(K_s)\tan\delta\left(\int_0^D \gamma' z dz\right) = \frac{1}{2}\pi B(K_s \tan\delta)\gamma' D^2$$

$$Q_s = \left(\frac{1}{2}K_s \gamma' D \tan\delta\right)A_s = f_s A_s \qquad \text{...(2.7)}$$

Where:

γ' = effective unit weight of sand

$$f_s = 0.5\ K_s\ \gamma'\ D\ \tan\delta \qquad \text{...(2.8)}$$

Equation (2.7) appears simple but entails difficulties in its application, especially in estimating the average coefficient of earth pressure K_s. The magnitude of K_s has been found to depend on many factors (McCleland et al.,1967), such as:

(1) angle of shearing resistance ϕ,

(2) soil deformation characteristics,

(3) the initial state of stress of the sand layer,

(4) pile shape (straight-sided or tapered),

(5) pile installation method: bored, driven (pushed or hammered), and

(6)loading direction.

Figure 2.3 shows typical values of K_s suggested by Meyerhof (1976), while table 2.1 introduces a set of reported values of K_s found in the literature compiled by Coyle and Castello, (1981). Table 2.2 provides representative values of δ (the average angle of friction between sand and different pile materials), "δ" was determined by Potyondy (1961) and Brooms& Silberman (1964), using direct shear machines.

Based on measurements of skin friction on instrumented piles driven in homogeneous sand, it is found that the local unit skin friction f_z distribution along pile shafts is parabolic as shown in Figure 2.4 (D'Appolonia & Romualdi, 1963; Mohan et al., 1963; Vesic, 1967b; Coyle & Suliman, 1967).

Mohan,et al., 1963 suggested that the reduction of local unit friction in the lower region of the pile shaft driven in sand is related to the decrease of lateral earth pressure (which developed in the pile tip vicinity) caused by the radial movement of sand within the shear zone.

2.3.2 Point Resistance:

The theoretical determination of the point load has received extensive attention through the years. The theoretical approach to solve this problem was initiated by Caquot and Buisman in the mid-1930's. They have extended the classical work on punching failure proposed by Prandtl and Reissner approximately 15 years earlier to solve the problem of a single pile driven in sand. Following the same basic approach, several different solutions were presented with different assumptions concerning the failure pattern, and, accordingly, new empirical corrections rather than modifications were introduced Coyle, (1981). In all of the theoretical solutions, the ultimate unit point resistance, q_p, is given by:

$$q_p = S_q \sigma'_o N^*_q + S_c C N^*_c + S_\gamma \gamma' B \ N^*_\gamma \qquad ...(2.9)$$

Where

Table 2.1 Typical Values of Earth Pressure Coefficient for Pile Foundation Compiled by Coyle and Castello (1981).

AUTHOR	BASIS OF RELATIONSHIP	SOIL TYPE	VALUES OF K
Brinch Hansen	Theory	Sand	$\cos^2 \phi$
Lundgren (1960)	Pile test	Sand	0.8
Henry	Theory	Sand	K_p
Ireland (1957)	Pulling tests	Sand	1.75 to 3
Meyerhof (1951)	Analysis of field data	Loose sand Dense sand	0.5 1.0
Mansur-Kaufman (1958)	Analysis of field data	Silt	0.3 (compression) 0.6 (tension)
Lambe-Whitman (1969)	Guess	-	2
Kezdi (1958)	Theory	Granular	K_p

Table 2.2 Angle of Friction Between Sand and Pile Material.

PILE MATERIAL	POTYONDY (1961)		BROMS & SILBERMAN (1964)
Steel	Surface condition	δ/ϕ	δ
	Smooth	0.54	20°
	Rough	0.76	
Wood	Parallel to grain	0.76	0.75 ϕ
	At right angle to grain	0.88	
Concrete	Smooth	0.76	0.66 ϕ
	Grained	0.88	
	Rough	0.98	

ϕ = Angle of shearing resistance of sand (degrees).
δ = Angle of friction between sand and pile material (degrees).

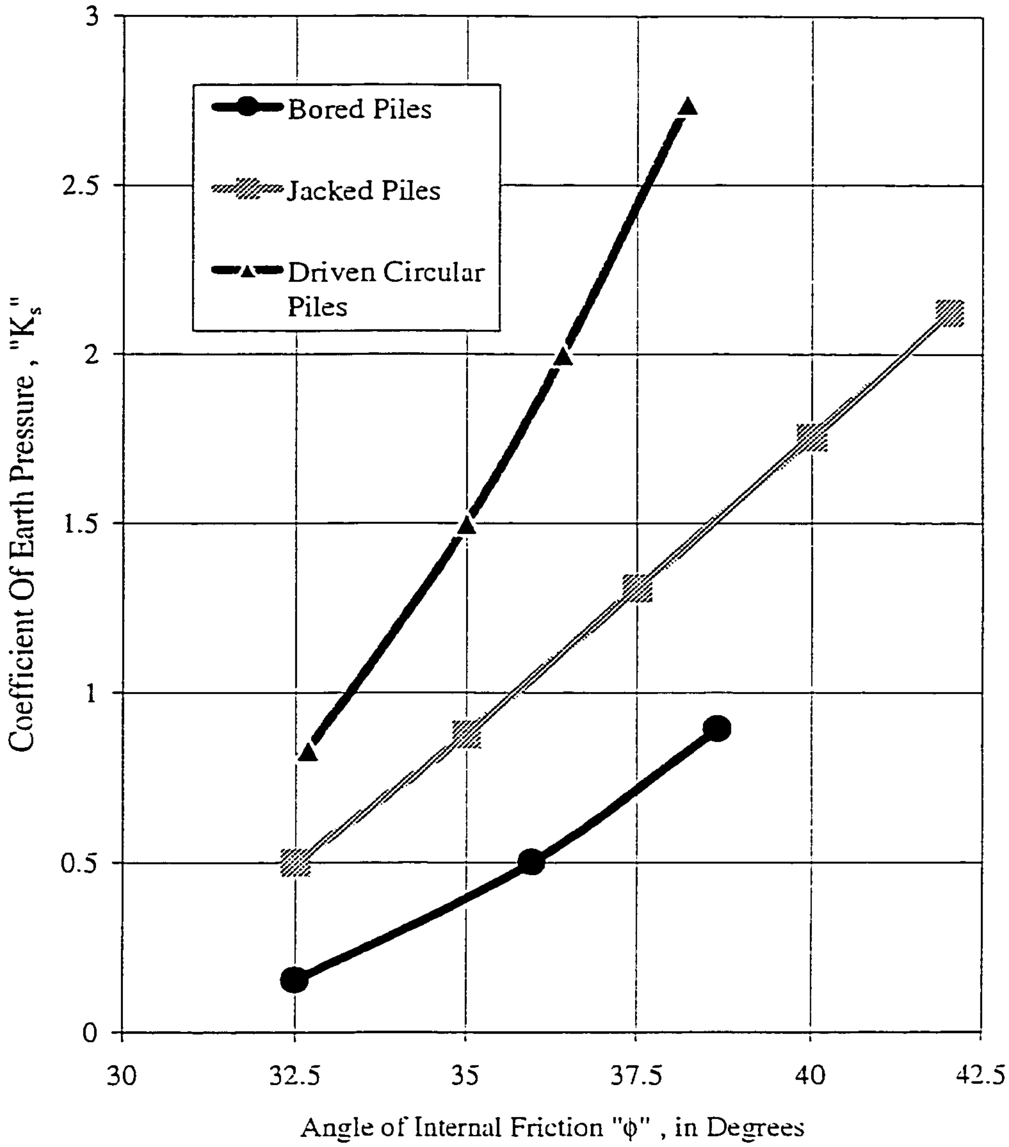

Figure 2.3 Coefficient of Earth Pressure "K_s" Acting on Piles shafts above Critical Depth in Sand (After Meyerhof, 1976)

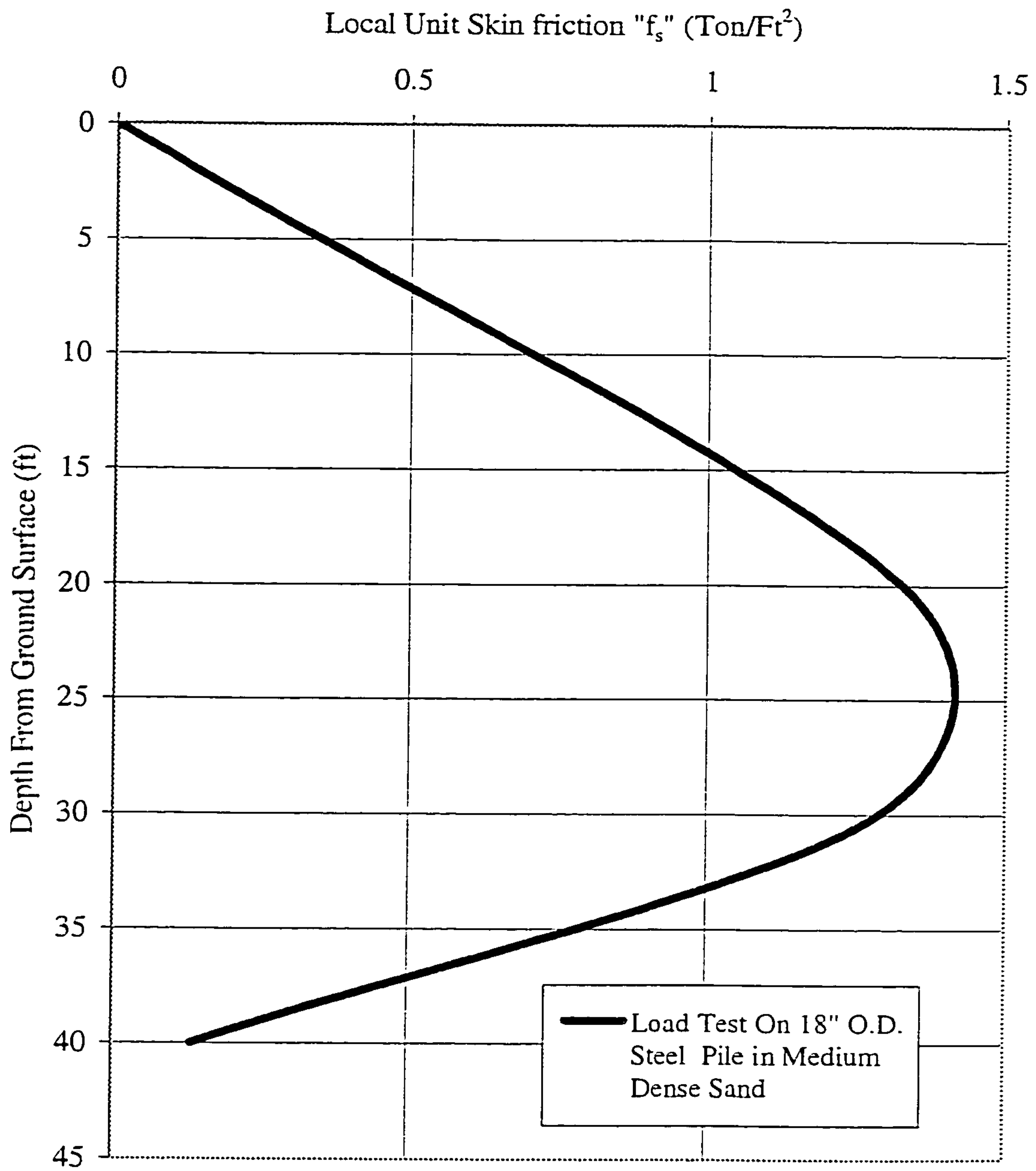

Figure 2.4 Distribution of Local Unit Skin Friction "f_s" over the Pile Shaft (After Vesic , 1967)

S_q, S_c, S_γ = shape factors.

N^*_q, N^*_c, N^*_γ = bearing capacity factors.

σ'_o = effective overburden pressure at the pile tip.

C = cohesion of the soil.

γ' = effective unit weight of the soil below the pile tip.

B = pile diameter.

Since the present study is limited to the case of cohesionless soils, the second term of the equation can be eliminated. Furthermore, comparison of two remaining terms show that the third term is relatively small and can be neglected. In addition, since most piles have circular or square cross sections where the shape factor is the same (Vesic, 1967a), it is reasonable to use a new bearing capacity factor, N^*_q, that incorporates this constant shape factor. Eliminating the second and third terms from equation(2.9) and multiplying by the pile tip area, A_p, to get the ultimate point resistance:

$$Q_p = (\sigma'_o N_q)A_p \qquad ...(2.10)$$

Where:

σ'_o = effective vertical stress at the pile tip level

N^*_q = a bearing capacity factor

A_p = cross section area of the pile tip

Historically, the evaluation of N_q evolved from an early solution for the problem of a rigid stamp penetrating into an incompressible rigid solid (Prandtl, 1921; Reissner, 1924). Later, approximate theoretical methods following the same general approach were used to solve bearing capacity problems of shallow foundations.

Numerous theories can be found in the literature to predict the tip component for the bearing capacity of a single pile based on different assumed shear failure patterns within classical plasticity theory. Also, various assumptions concerning the effect of the state of stress in the soil surrounding the pile have been sometimes considered. Table (2.3) lists some of these methods used in prediction of the tip resistance component of a single pile in sand.

As can be seen from table (2.3), there is a relatively wide range of values of interface friction angle (δ), and the theoretical stress coefficient (K). These parameters were usually selected to account for the testing procedures that caused lateral stresses against the pile after installation, and the uncertainty in the evaluation of the earth pressure coefficient at rest (K_o). The fact that many investigators used empirical correlations to estimate K_o indicates either a lack of confidence in these results or lack of experience with this type of data. Discrepancies exist in the evaluation of the earth pressure coefficient at rest (K_o) and the angle of interface friction (δ), and further, a large difference in the pile capacity calculation is found.

In the literature, the difference in pile capacity was found to be in the order of 170% for HP piles, 130% for pipe piles, 275% for slurry piers, and 110% for cased piers. These differences between pile capacities can also be attributed to the discrepancies among the published values of the bearing capacity factor N_q. Figure (2.6) shows variations of N_q values according to different investigators. These variations are a direct impact of ignoring the influence of many factors and presenting the N_q values as a function of a unique factor: angle of shearing resistance (ϕ) only.

TABLE 2.3 Summary of Most Common Used Static Formulas (After Finno, et..al., 1989)

REFERENCE	SHAFT RESISTANCE	TIP	PILE TYPE	K_S	δ	N_S
Poulos-Davis, (1980)	Fw(Ks tan σ'_{vo})	$N_q\sigma_{vb}$	HP Other	0.8 0.4	30 30	0.46 0.46
Bustamante, Van Impe, 1986	$\propto_s q_c R_t/N_o$	$\propto_s q_c$	-	-	-	-
Tomlinson, 1967	$(K/K_o)K_{oz}\tan(\delta/\phi)\phi_z\sigma'_{vo}$	$N_q\sigma_{vb}$	HP Pipe Slurry Cased	K_o pmt 0.5 K_o pmt 0.67K_o pmt 0.67K_o pmt	2/3 ϕ spt 2/3ϕ spt 0.8 ϕ spt 2/3 ϕ spt	- - - -
Meyerhof, 1956	$K' \tan \delta\sigma_{vo}'$	q_c	Driven Drilled	1.5 – 2.3 1	40-44.5 40-46	1.26-2.26 0.84-1.04
Mosher, 1984	f-z curve	f-z curve	-	-	-	-
Kulhawy, 1983	K tan $\delta\sigma'_{vo}$ cpt Correlations	$N_q\sigma_{vb}$	-	-	-	-
Meyerhof, 1976	N/50	$N_q\sigma_{vb}$	-	-	-	-
Meyerhof, 1976	1.3 K tan $\delta\sigma'_{vo}$	$N_q\sigma_{vb}$	HP Pipe Slurry Cased	0.5 0.57 0.45 0.5	35	0.35 0.4 0.32 0.35
De Beer, 1972	cpt Correlations	cpt Correl ations	-	-	-	-
API, RP2A, 1987	K tan $\delta\sigma'_{vo}$	$N_q\sigma_{vb}$	HP Pipe	0.8 0.9	15-35	0.21-0.56 0.24-0.63
Nottingham, 1975	Limiting f_s	$N_q\sigma_{vb}$	Driven Drilled	1 1	24.6 30	0.46 0.58
Nordlund, 1980	$K\left[\dfrac{\sin(w+\delta)}{\cos w}\right]\sigma'_{vo}$	$N_q\sigma_{vb}$	HP Pipe Drilled	K_o pmt K_o pmt 0.4	26 34 37	0.3
Reese-O'Neill, 1988	$\beta\sigma'_{vo}$	$N_q\sigma_{vb}$	-	-	-	-
Coyle-Castello, 1981	K tan $\delta\sigma'_{vo}$(pipe) f_s (HP)	$N_q\sigma_{vb}$ $N_q\sigma_{vb}$	Pipe	0.7	30.4-31.2	0.41-0.42
Cand. Found. Engrg. Manual	$\beta\sigma'_{vo}$	$N_q\sigma_{vb}$	Driven	-	-	-
Denis-Olson, 1983	cpt f_s	$N_q\sigma_{vb}$	-	-	-	

δ = Mobilized friction angle along the side off the pile
α = Empirical factor
k = Ratio of horizontal to vertical stress
q_c = Static cone resistance
N_s = Dimensionless bearing capacity factor that relates f_s to σ'_{vo}
σ'_{vo} = Initial vertical stress
N_q = Dimensionless bearing capacity factor
σ_{vb} = Effective stress at the tip of the pile
N = Average standard penetration resistance

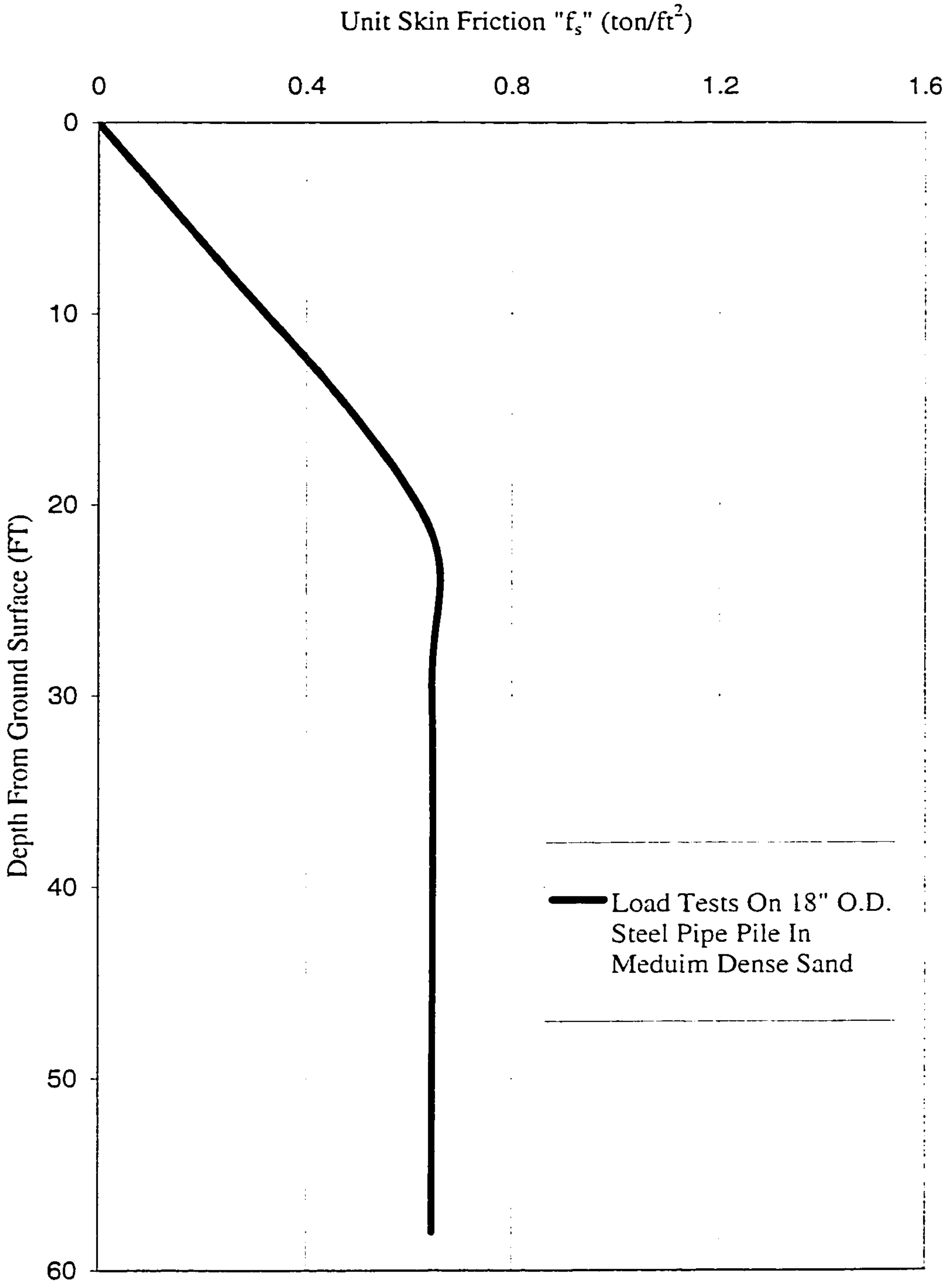

Figure 2.5 Variation of Unit Skin Friction "f_s" Versus Depth
(After Vesic, 1967-a)

2.3.2.1 Failure Mechanism

Many investigators proposed failure mechanisms to estimate the ultimate point resistance of single driven piles in sand.

Terzaghi (1943) extended his solution for the bearing capacity of a shallow foundation to the case of a single pile. Referring to Figure 2.7, the mechanism of pile failure involves the downward movement of the volume I (cone BCB'), which in turn displaces the soil outward and upward with the failure surfaces (volumes II, II', III& III') ending at the pile tip level (D'B'BD). These generated displacements are resisted by:

- The weight of an annulus of soil depicted in cross section by volumes IV and IV',
- The skin friction between the pile shaft and the soil (f_s) and
- The shear forces resisting upward movement of the annulus of soil along its outer surface area (τ).

The degree of shear mobilization of soil on this surface is unknown.

Terzaghi assumed that the tip resistance of a single pile may be determined by:

$$q_p = 1.3c\, N_c + \gamma_1\, D\, N_q + 0.6\, \gamma\, B\, N_\gamma \qquad \text{...(2.11)}$$

where:

N_c, N_q, N_γ = bearing capacity factors

c = soil cohesion

D = pile embedment length

γ = soil unit weight

Equation (2.11) is almost the same equation used for the ultimate bearing capacity of a shallow circular foundation except for the term ($\gamma_1 D$) which represents the pressure at the pile

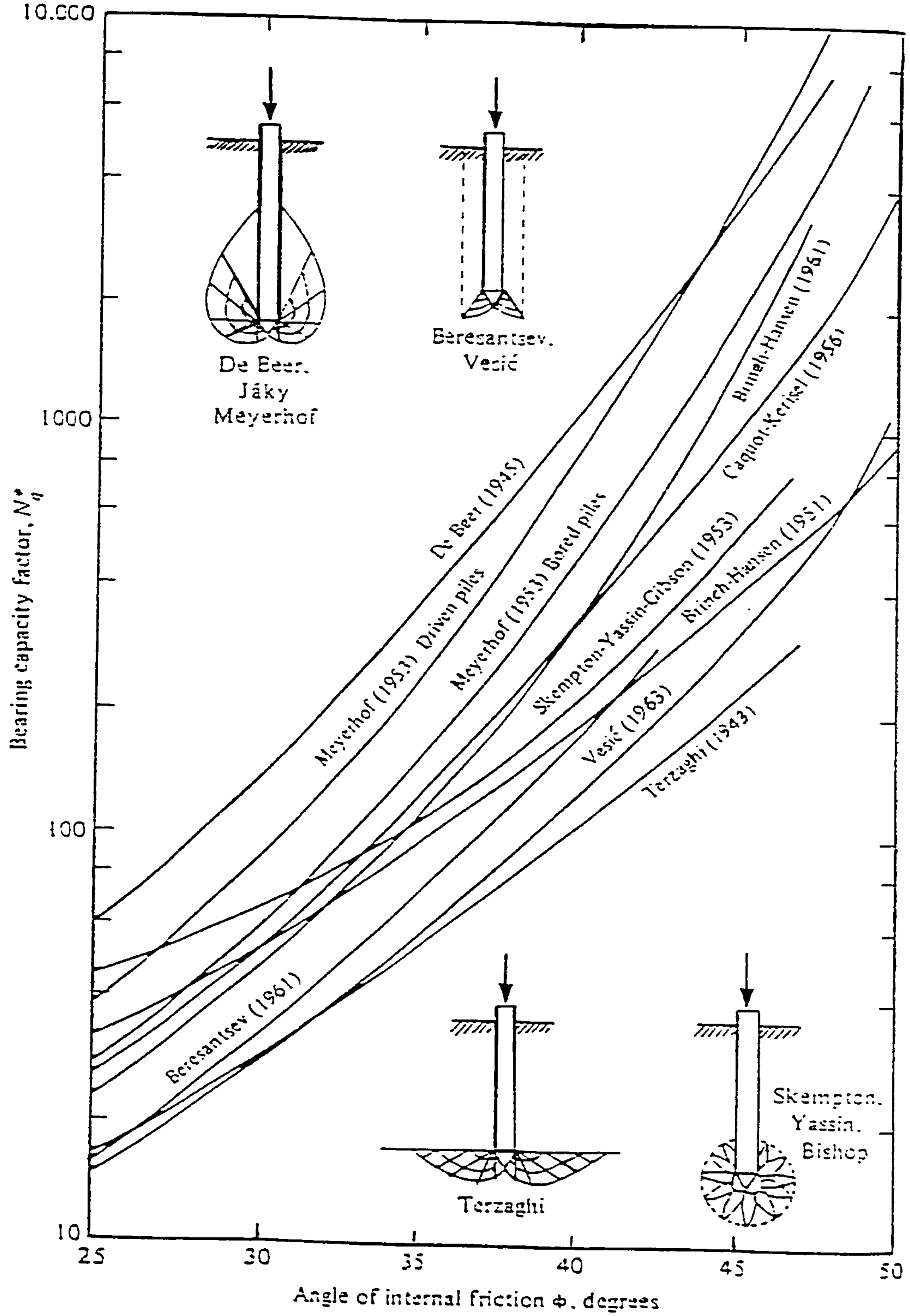

Figure 2.6 Bearing Capacity Factor N_q Versus Angle of Shearing Resistance ϕ According to Various Authors

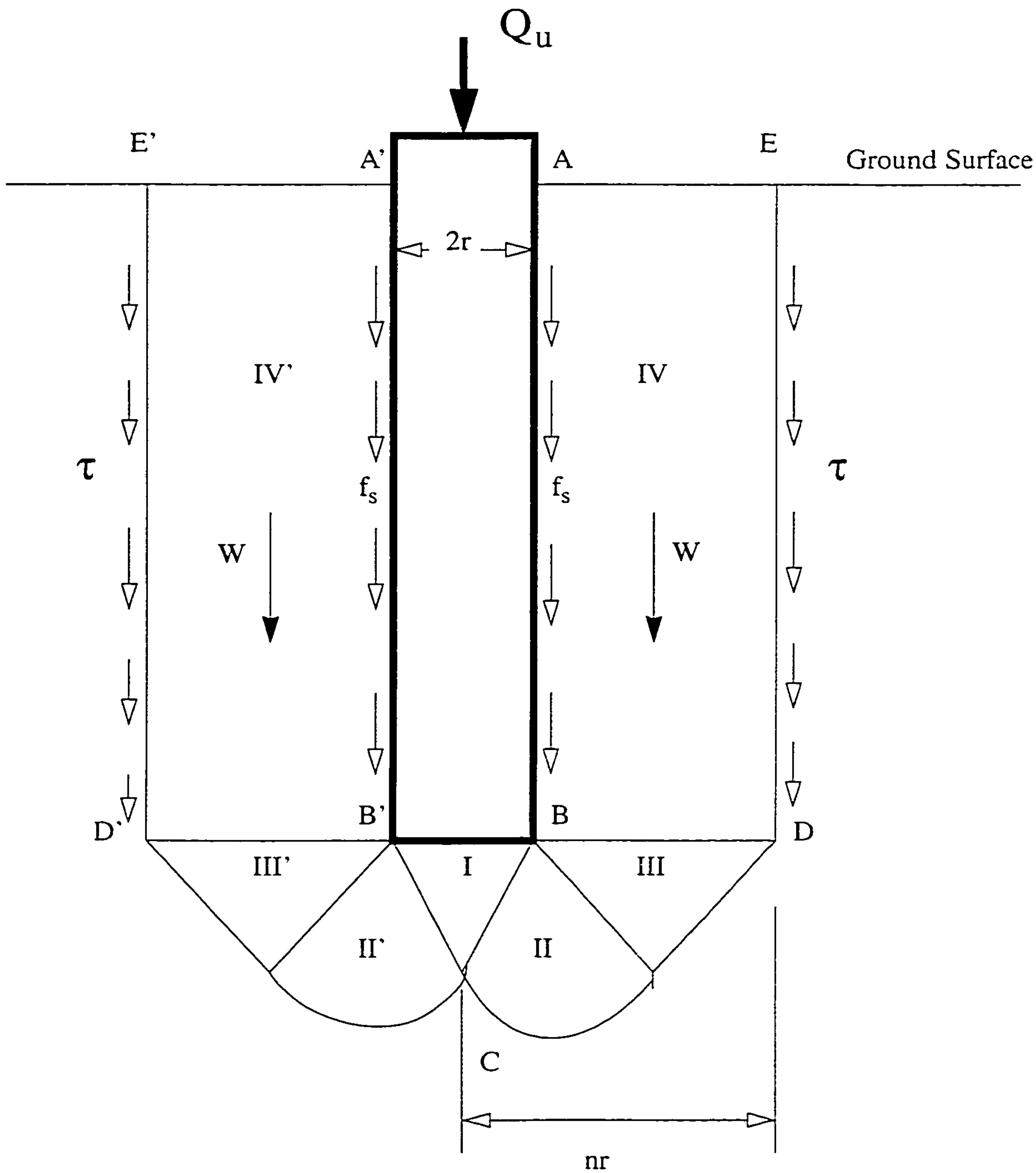

Figure 2.7 Assumed Failure Mechanism (Terzaghi, 1943)

tip level as a resultant resisting effects of the pile shaft skin friction (f_s), shear forces on the outer surface of the soil annulus (τ), and the weight of the soil annulus (w). Terzaghi suggested the value of γ_1 as:

$$\gamma_1 = \gamma + \frac{2(f_s + n\tau)}{(n^2 - 1)r} \qquad ...(2.12)$$

where

f_s = average unit skin friction along pile shaft

τ = average shear stress on the outer surface of the soil annulus

n = a factor indicating the magnitude of the outer radius of the soil annulus which is selected to minimize q_p for the given values of f_s, τ, γ and ϕ.

r = pile radius

γ = soil unit weight

According to Terzaghi, the full shear mobilization along the pile shaft and the unit skin friction f_s can be computed accordingly. However, estimating τ constitutes some difficulties due to the incomplete shear mobilization in the soil on the outer surface of the annulus. Terzaghi indicated that the volume compressibility of sand is the primary factor which influences the shear mobilization process.

Terzaghi's model is considered as one of the first original three dimensional treatments of a pile bearing capacity problem which dealt with the combined effect of shaft and tip resistances in the same failure mechanism. On the other hand, Terzaghi's model suffers some drawbacks. such as: no specific procedure to estimate the shear stress τ and the unit skin friction f_s were proposed. Thus, his model suffers serious limitations in practical applications.

Meyerhof (1951) introduced his general bearing capacity theory for shallow foundations assuming a failure mechanism as shown in Figure 2.8a. Three failure zones are proposed: elastic wedge (ABC), radial shear zone (BCD) which is a bounded by a log spiral (CD), and a mixed shear zone (BDEF). It should be noted that in his assumption for a shallow foundation failure mechanism, Meyerhof extended the failure surface to the ground level as shown in Figure 2.8a. Furthermore, he assumed the plane (BE), with inclination angle β, to be an equivalent free surface with normal and shear stresses, p_o and s_o, acting on it. The successful value of β is produced by having p_o and q_o values that simultaneously satisfy the equilibrium of the wedge (BEF). The state of stress on (BE) is determined from Mohr's circle on the basis of failure conditions on the planes (BD) and (DE). Upon implementation of the free surface (BE), a classical superposition method (Terzaghi, 1943) could be applied to determine the bearing capacity of the shallow strip footing taking into account the contribution of c, p_o, γ and ϕ. This gives the following equation:

$$q_u = cN_c + p_o N_q + \frac{1}{2}\gamma B N_\gamma \qquad ...(2.13)$$

Meyerhof (1951) extended his solution for shallow foundations to be applied to deep foundations (Figure 2.8b). He assumed that the failure surface does not reach the ground surface but reverts back onto the foundation shaft. Equation (2.13) is further simplified in the case of strip foundation in sand:

$$q_u = \frac{1}{2}\gamma B N_{\gamma q} \qquad ...(2.14)$$

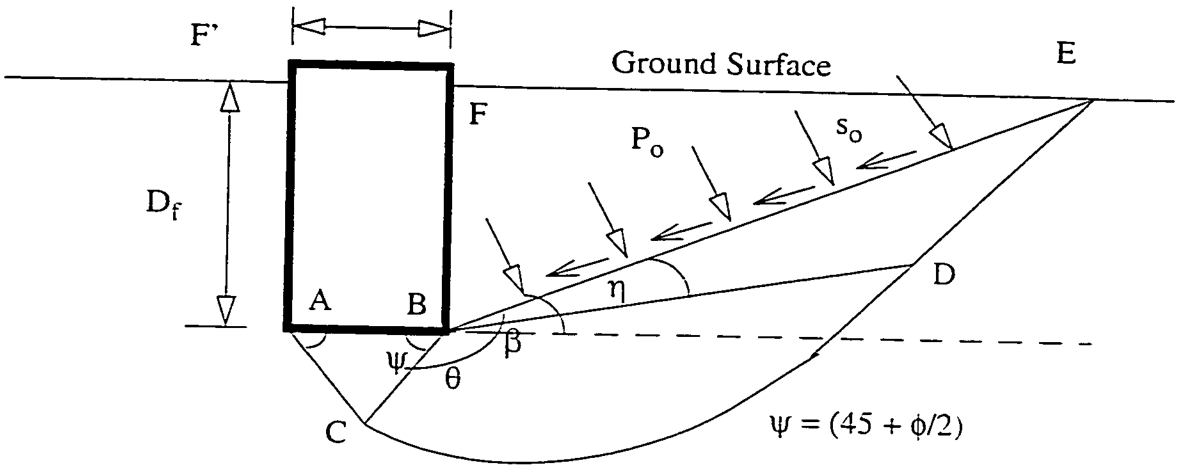

(a) Shallow Foundation

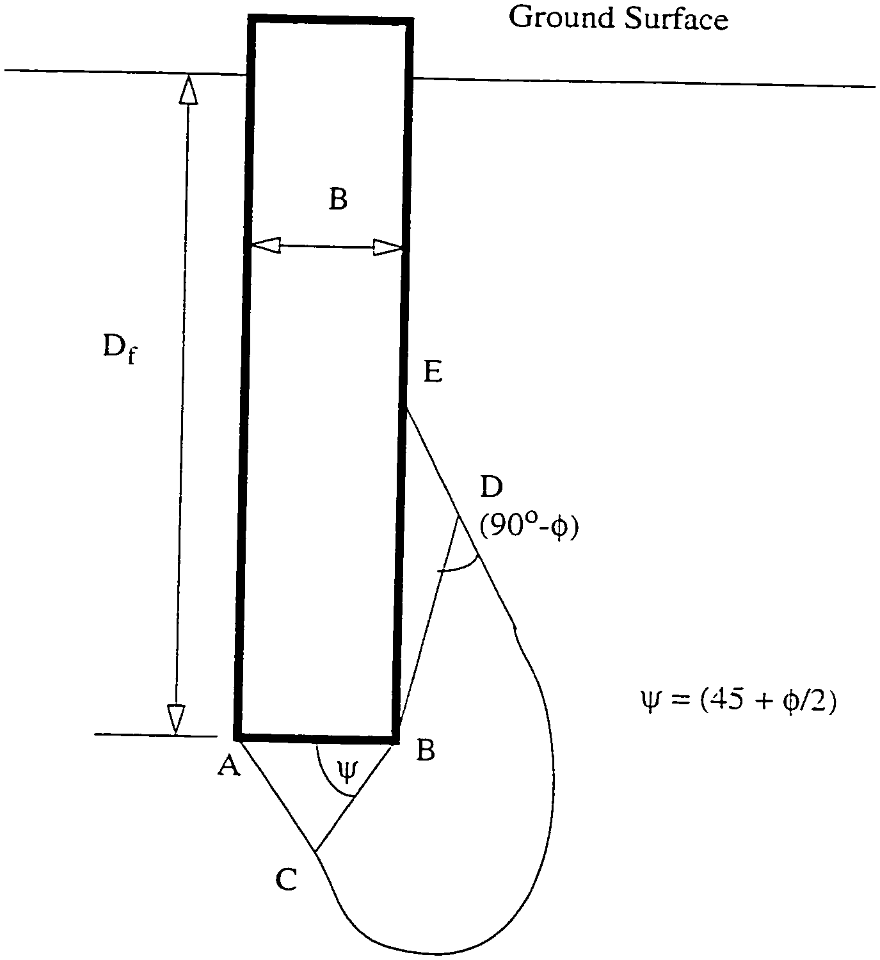

(b) Deep Foundation

Figure 2.8 Assumed Failure Pattern by Meyerhof (1951) where $N_{\gamma q}$ is a resultant bearing capacity factor combining N_γ and N_q.

Meyerhof's theory is capable of incorporating the effect of shaft roughness, (δ/ϕ), on the ultimate bearing capacity of a strip footing at any depth; and the effect of initial stress, implicitly indicated by the lateral coefficient K_o at-rest, on the shaft friction. He gave definite values for the coefficient of earth pressure on the shaft, K_s, (i.e., $K_s = 0.5$ for loose sand and 1.0 for dense sand). Further more, the failure mechanism introduced in Meyerhof's theory, which assumes that the general shear failure surface reverts back onto the shaft at great depth, has no experimental observations (Vesic, 1967-b; Durgunoglu and Mitchell, 1973).

A three dimensional analytical model was established by Skempton et al. (1953) to determine the bearing capacity of a single pile in sand (Figure 2.9). In this analysis, the assumed failure mechanism includes curved surfaces having circles as their vertical cross sections. These circles start at the apex of the cone, point (C), shown in Figure 2.9, and become tangent to vertical lines at the level of the pile tip at point (E), with its center at point (O) and radius "r". The center, O, thus, is always located at the pile tip level (i.e., line AE). The force system acting on a failure surface containing the central angle $\delta\theta$ includes:

- vertical skin friction component δs,
- vertical soil weight component δp,
- vertical shear force $\delta\tau$ on the cylindrical surface EF,
- inclined soil reaction component δR, and
- inclined resultant force component δQ_p on the central wedge ACA'.

The force δQ_p is assumed to act at one third the distance CE from the cone apex. Equilibrium conditions of zone ACE and the wedge ACA' lead to determination of δQ_p for a central angle

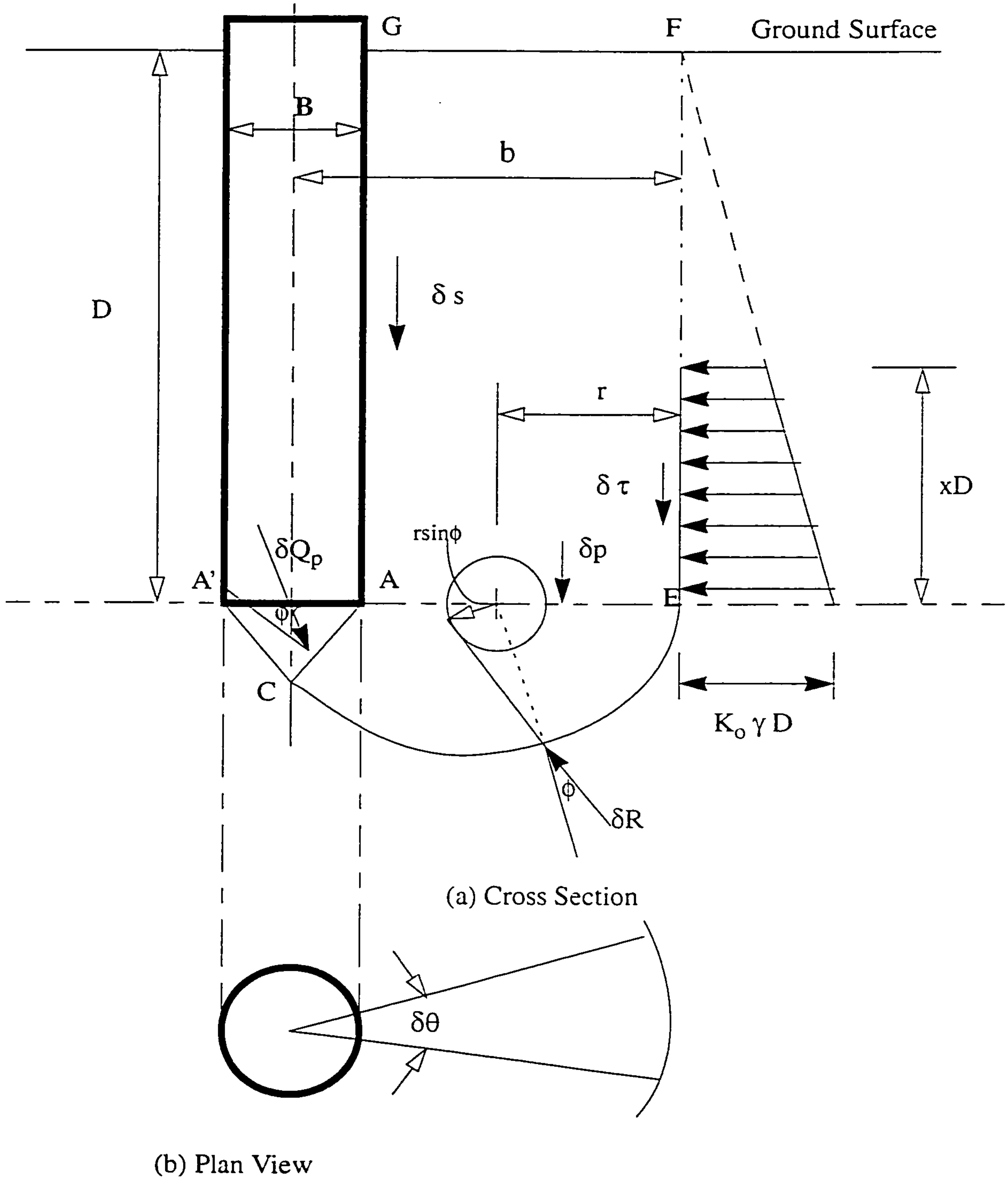

Figure 2.9 Assumed Slip Surfaces (Skempton's Model, 1953)

$\delta\theta$ and, subsequently, the bearing capacity factor N_q. Many trial calculations should carried out assuming different positions for the circle center along the pile tip level until a minimum value of N_q is obtained.

In this solution, if the effect of shear forces mobilized in the sand mass above the pile level are neglected (i.e., $\delta s = \delta\tau = 0$), then N_q is found to be a unique function of ϕ.

It was suggested that the shear stress τ at depth z may be determined by:

$$\tau = K_o \gamma z(\tan\phi) \qquad \text{...(2.15)}$$

where

K_o = coefficient of earth pressure at-rest

γ = unit weight of sand,

The shear stress was assumed to be applied over a length equal to xD where x is a factor that varies with the sand relative density D_R. The relationship between x and D_R is given in Figure 2.10. Based on these assumptions, N_q becomes a function of two factors: ϕ and the relative depth D/B. Thus, this model is considered to have gained some improvements for the common solution which adapted bearing capacity factor N_q as a function in a unique factor ϕ.

A failure mechanism quite similar to Terzaghi's was established in 1961, by Berezantzev et al. (Figure 2.11). It was assumed that the sand compaction under the pile tip causes the whole soil annulus to move downwards with respect to the remaining sand mass. This generates a resistance shear force T in an upward direction which is opposite to its counterparts in Terzaghi's and Skempton et al.'s failure mechanisms. The surcharge q_T at the pile tip level, assumed to be

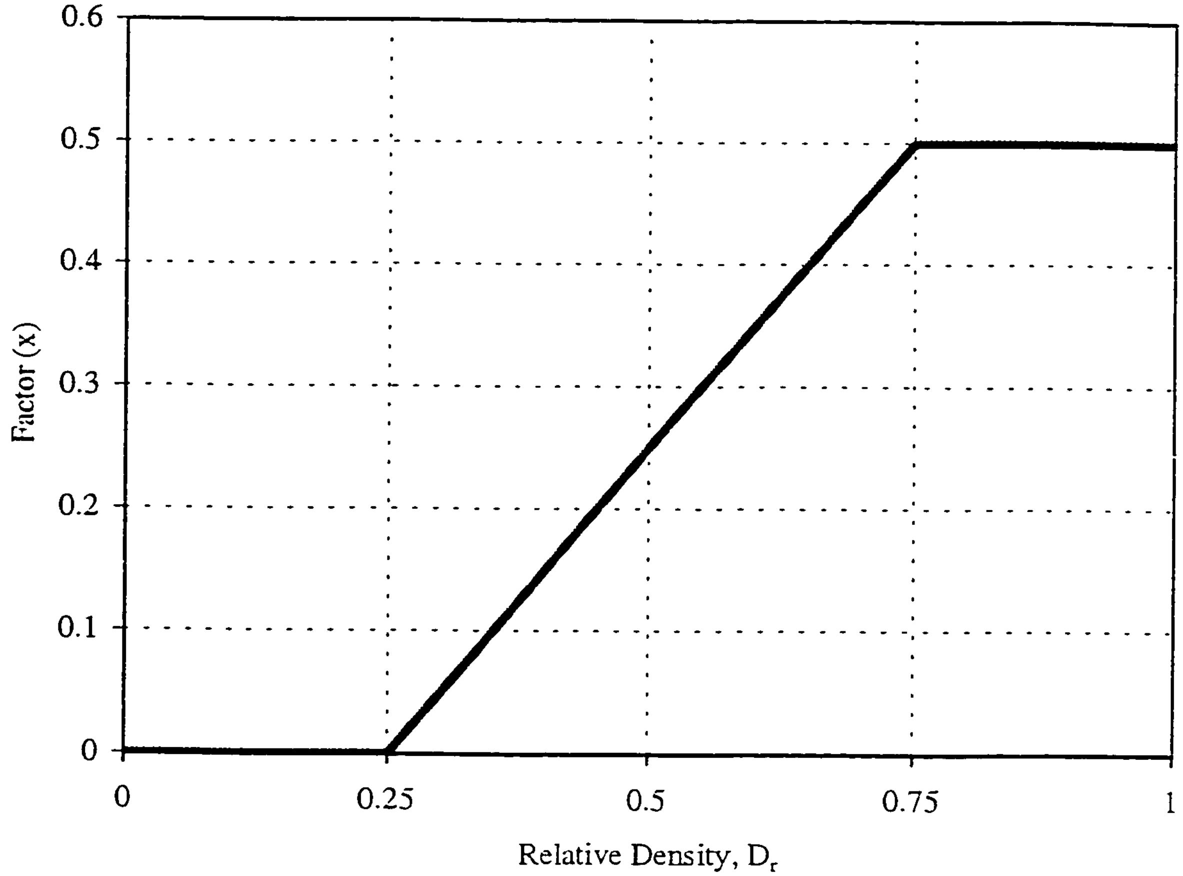

Figure 2.10 Variation of Factor x With Relative Density (Skempton et al., 1953)

calculated as the difference between the weight W of the annulus of soil and the shear force T on the outer surface of this volume, is determined as:

$$q_T = \alpha_T \gamma D \qquad ...(2.16)$$

where

α_T = a coefficient, function of D/B and ϕ

γ = unit weight of sand

D = pile embedment length

B = pile diameter

ϕ = angle of shearing resistance of sand

The unit point resistance of a single pile is given by:

$$q_u = A_k \gamma B + B_k q_T \qquad ...(2.17)$$

where A_k and B_k are bearing capacity factors.

The theory of limit equilibrium was applied to determine the radius of the annulus of soil, the lateral soil pressure on its outer surface, and the coefficients in equation (2.16) with respect to axisymmetric problems in a granular soil. It is of interest to note that Berezantzev's approach neglects the coupled effect of skin friction and point resistance in the same failure mechanism, in contrast to Terzaghi's assumption equation (2.12). Norlund (1963) and Vesic (1967-b) have made revision of different bearing capacity theories and recommended Berezantzev's approach as the theory that provided the best agreement with their experimental tests.

A two dimensional solution for estimation of ultimate bearing capacity for strip foundation at any depth was proposed by Hu (1965). Hu assumed a failure mechanism (Figure 2.12) that consists of the following zones:

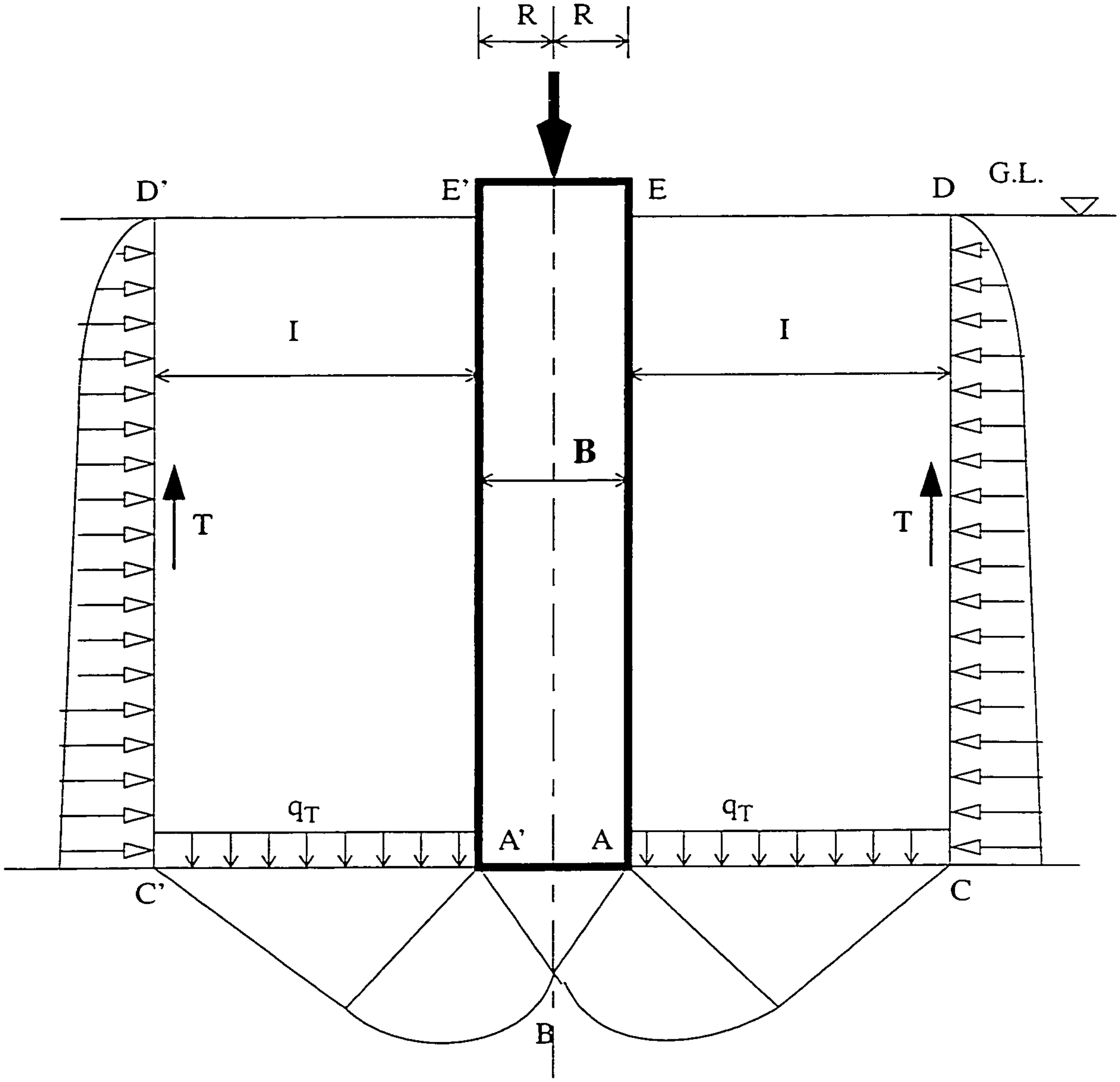

Figure 2.11 Assumed Failure Mechanism (After Berezantsev et al.,1961)

a- Triangle wedge (OCO'), below pile tip

b- Radial shear zone (OCE) bounded by a section of a log spiral having its pole at (O) and becoming tangent to a vertical plane (EF) at E.

c- Overburden zone (OEFG) comprising two weights, P_1 and P_2, acting through the centroids of the areas (OEH) and (EFGH).

The stress in the first and second zones are assumed to reach the plastic equilibrium state, while the stress in the third zone was assumed to be in a mixed shear state. The shear stresses along the interface (OE) are assumed to be fully mobilized. The model further neglects the effect of the shear resistance along the outer vertical failure surface (EF) and the skin friction along the foundation shaft (OG). The ultimate bearing capacity q_u is given by the following equation:

$$q_u = cN_c + p_o N_q + \frac{1}{2}\gamma B N_\gamma \qquad \text{...(2.18)}$$

where

p_o = overburden pressure at foundation level

To obtain the final base resistance, the shear resistance along (EF) and (OG) must be added to q_u. Equation (2.18) is further combined to give:

$$q_u = c\,N_c + \gamma B N_{\gamma q} \qquad \text{...(2.19)}$$

where $N_{\gamma q}$ is a resultant bearing capacity factor.

Hu's analysis has used a single failure surface to estimate N_c and $N_{\gamma q}$, while the conventional approach (Terzaghi, 1943; Meyerhof, 1951) uses two different failure surfaces in deriving N_c, N_q and $N\gamma$. This should be counted as a distinct feature of this theory.

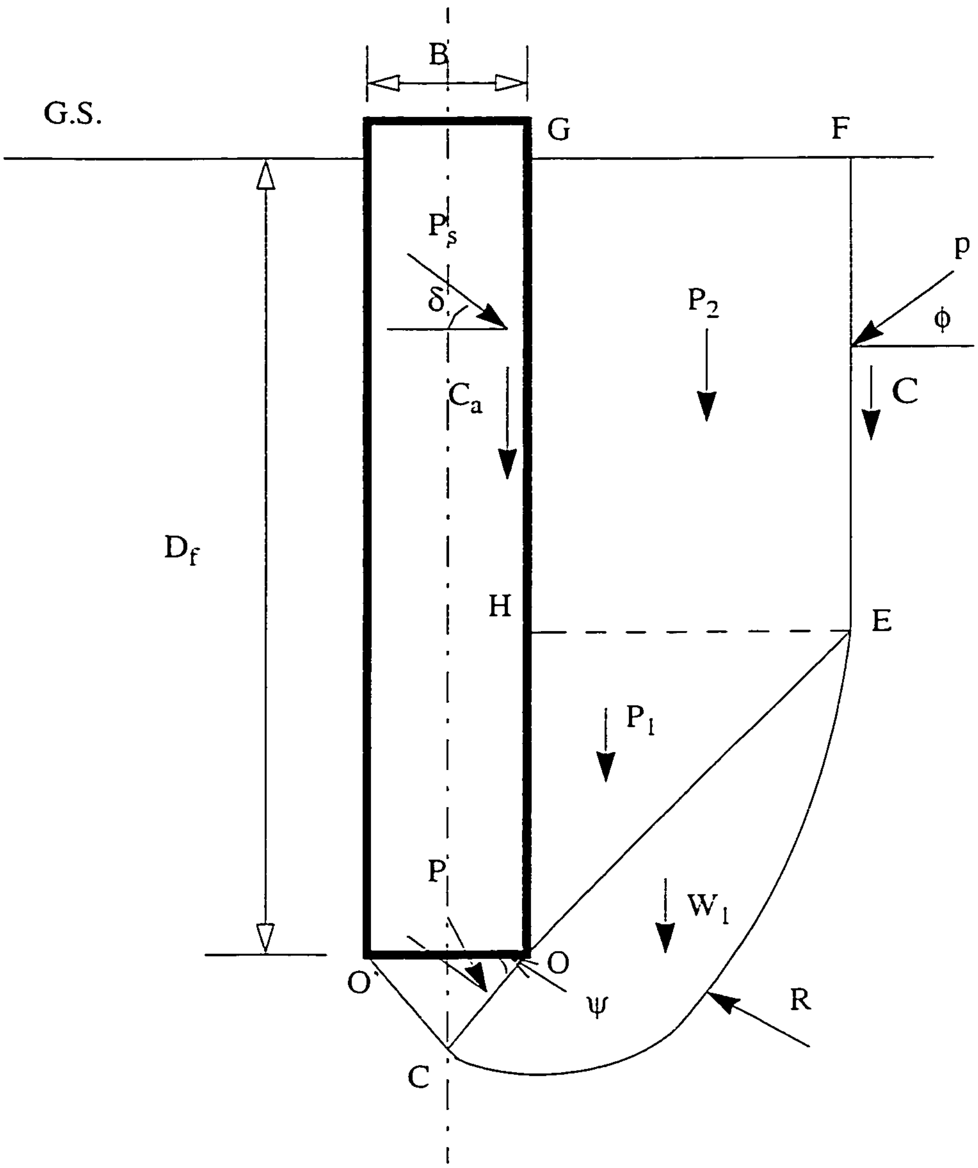

Figure 2.12 Failure Mechanism Assumed by Hu (Hu,1965)

Vesic (1967-b) developed a plane strain failure mechanism, Figure 2.13, to account for the local or punching shear failure of a strip foundation in sand at shallow depth (D/B < 4). He suggested a shear pattern that consisted of an elastic wedge, zone I, located between two plastic zones, II & II', bounded by sections of log spirals (CE) and (CD) having their poles located at point A and B, respectively. The failure surface develops only to a limited extent well below the pile tip level. He assumed the weight of the soil in the failure zones to be negligible compared to the overburden pressure, and by performing appropriate stress analyses along the limiting surface (BD) and (AE), Vesic's analysis gives the following equation for N_q:

$$N_q = e^{3.8\phi\tan\phi}\tan^2\left(45^\circ + \frac{\phi}{2}\right) \qquad ...(2.20)$$

Hu's failure mechanism was adopted by Durgunoglu and Mitchell (1973) to develop a theoretical basis for evaluating the static cone resistance. They introduced a resultant bearing capacity factor $N_{\gamma q}$ as a function of the following:

-apex angle of the cone,

-angle of shearing resistance ϕ,

-relative depth D/B,

-base roughness δ/ϕ,

-earth pressure coefficient on the shaft K_s, and

-coefficient of earth pressure at-rest K_o.

This analysis is considered an improvement on Hu's theory, because it took into account important parameters, such as K_o, K_s, and δ/ϕ, conventionally neglected in earlier theories. Drgunoglu and Mitchell's theory is not entirely congruent with experimental evidence, espe-

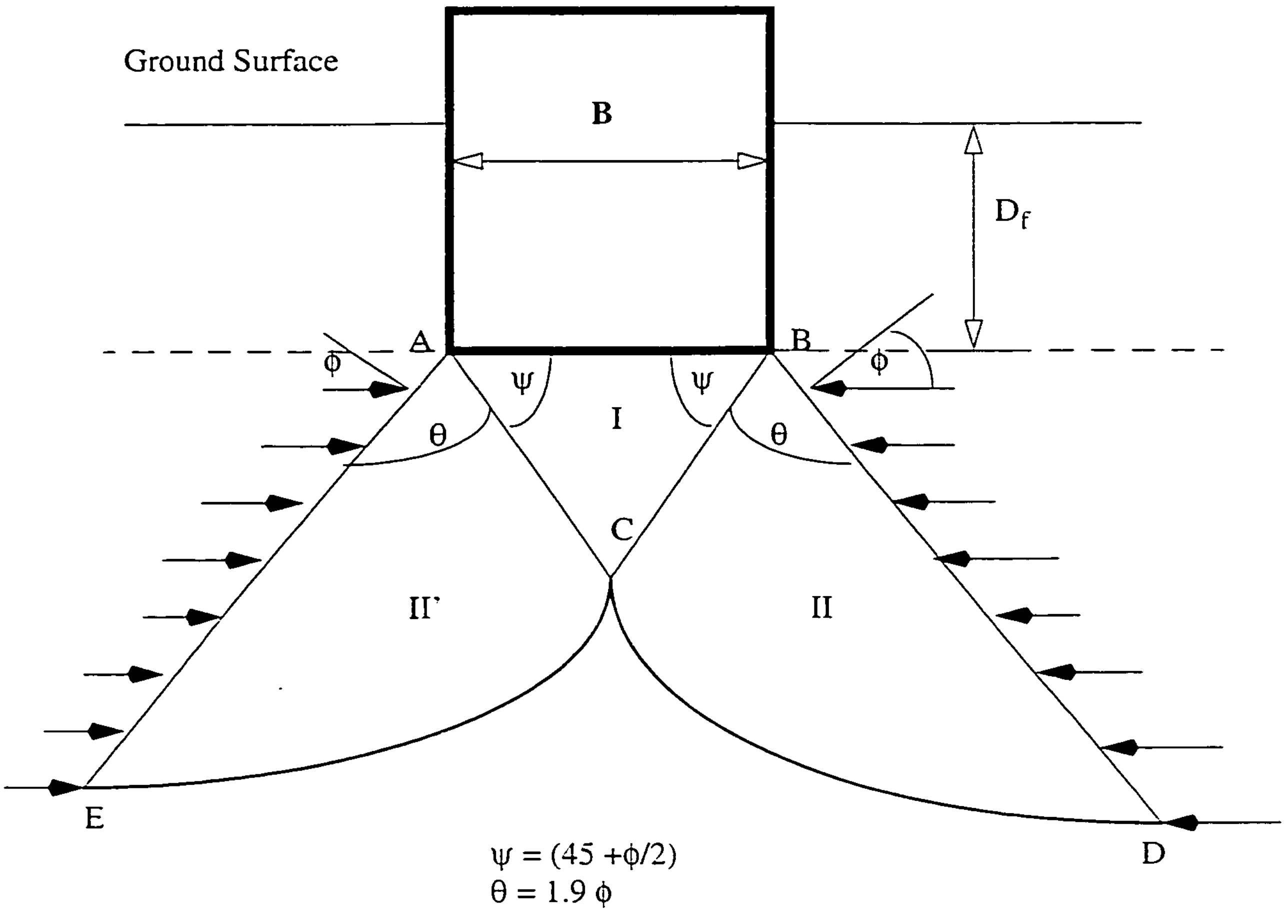

Figure 2.13 Failure Mechanism assumed by Vesic, 1967-b
Utilizing Punching and Local Shear Failure

cially at lower depths (Al-Wakati, 1975). If Drgunoglu and Mitchell Developed a relationship between K_o and K_s, including Q_s calculations in the same failure mechanism, these features would improve their theory which requires an empirical estimate of K_s in advance.

A two dimensional variable failure mechanism was introduced by Janbu and Senneset (1974). This analysis allows the critical shear zones beneath the pile tip to be adjusted to failure conditions. They derived bearing capacity factor N_q which is given by the following expression:

$$N_q = \tan^2\left(45^o + \frac{\phi}{2}\right)e^{(\pi - 2\beta)\tan\phi} \qquad ...(2.21)$$

where β is the angle of inclination of the terminal radial planes (AE) and (BD)- (Figure 2.14). Further improvements were added to the model by Janbu (1976), who produced a relationship to account for the partially mobilized shear strength along the assumed failure surface, and Equation (2.21) was developed into a generalized form:

$$N_q = \tan^2\left(45^o + \frac{\phi}{2}\right)e^{(\pi - 2\beta)(f\tan\phi)} \qquad ...(2.22)$$

in which f = degree of shear mobilization. To get good agreement with experimental data, β must be selected within the range $-15^o < \beta < +15^o$. With equation (2.21), Janbu apparently added a new outlook on the theory of bearing capacity of piles.

The following remarks should be noted about equation 2.22:

1- It was probably the first time that a theory of bearing capacity of piles depends on other factors than ϕ.

2- It suggests that N_q no longer depends uniquely on ϕ but is also a function of:

- the extent of the "plasticized" zone under the pile tip, and
- the degree of shear mobilization along the log spiral boundary of this zone.

3- In addition, it suggests that a variable failure mechanism may develop under the pile tip, although its mode of variation has not yet been adequately investigated. In this respect, how the angle β varies with ϕ, D/B or even K_o remains an interesting question for future research.

Vesic (1977) produced another model of incorporating soil compressibility into his assumptions. The shear failure pattern was established based on observations of experimental modeling and full-size pile tests (Figure 2.15). It consists of a highly compressed cone ABC (zone I), a radial shear zone BCD (zones II), and a plastic zone BD (zone III). Vesic assumed that the soil expands laterally into zone III and is compressed in zones I and II. This is will allow the pile to advance to lower depths. He further assumed that the average normal stress along BC is equal to the ultimate pressure needed to expand a spherical cavity in an infinite soil mass. The unit point resistance of a single pile is then given by:

$$q_p = cN_c + \sigma_m N_\sigma \qquad ...(2.23)$$

where

N_c, N_σ = bearing capacity factors

σ_m = mean normal ground stress

$\sigma_m = ((1+2Ko)/3) * \sigma_o'$

A three dimensional model developed by Nguyen, and Hanna, 1991, in an attempt to account for the punching shear failure, and the interdependence between point resistance and skin friction of a vertical pile driven in sand. As shown in Figure 2.17 the proposed critical shear surfaces in vertical section consists of 3 zones:

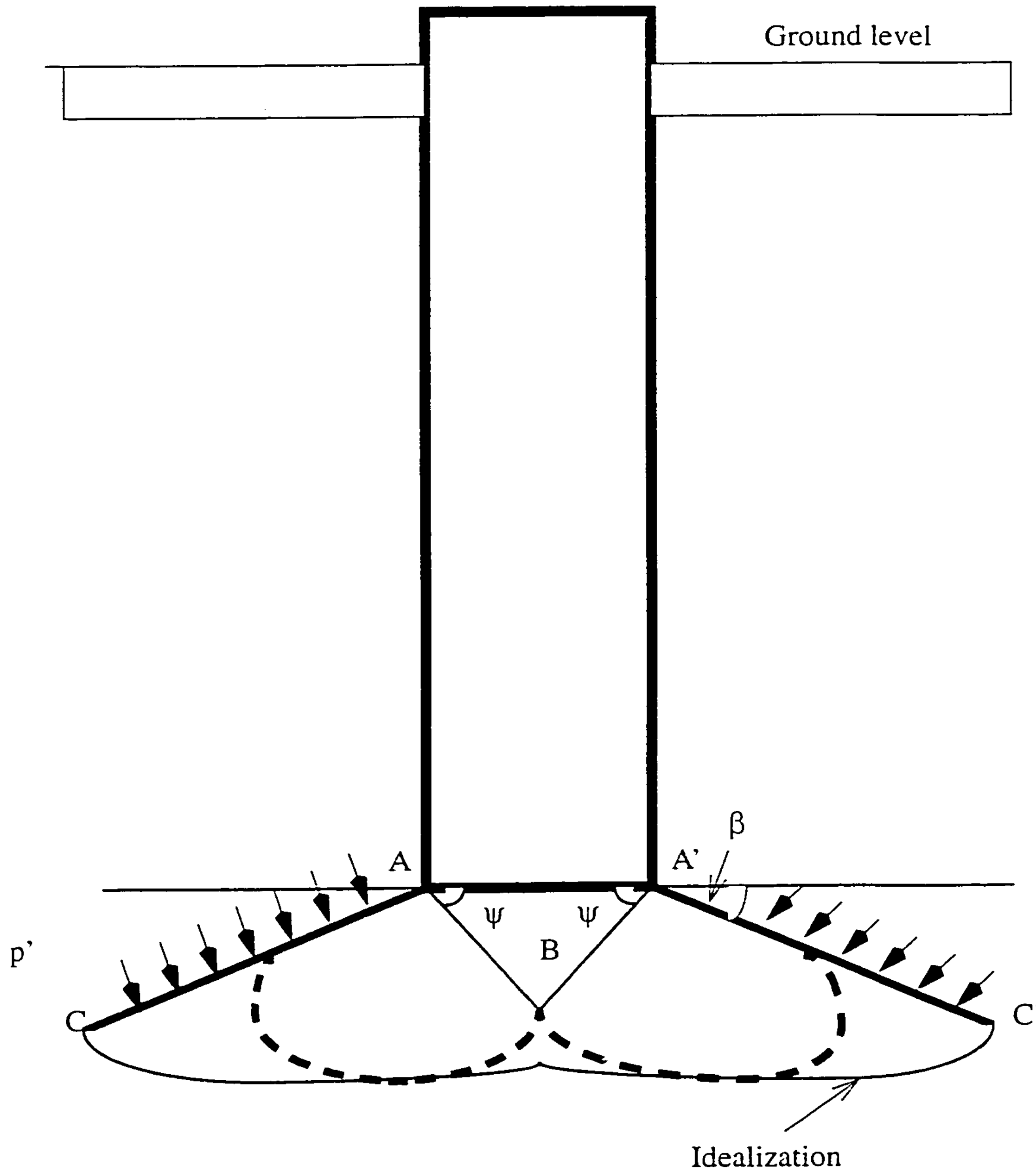

Figure 2.14 Janbu and Senneset Failure Mechanism (1974)

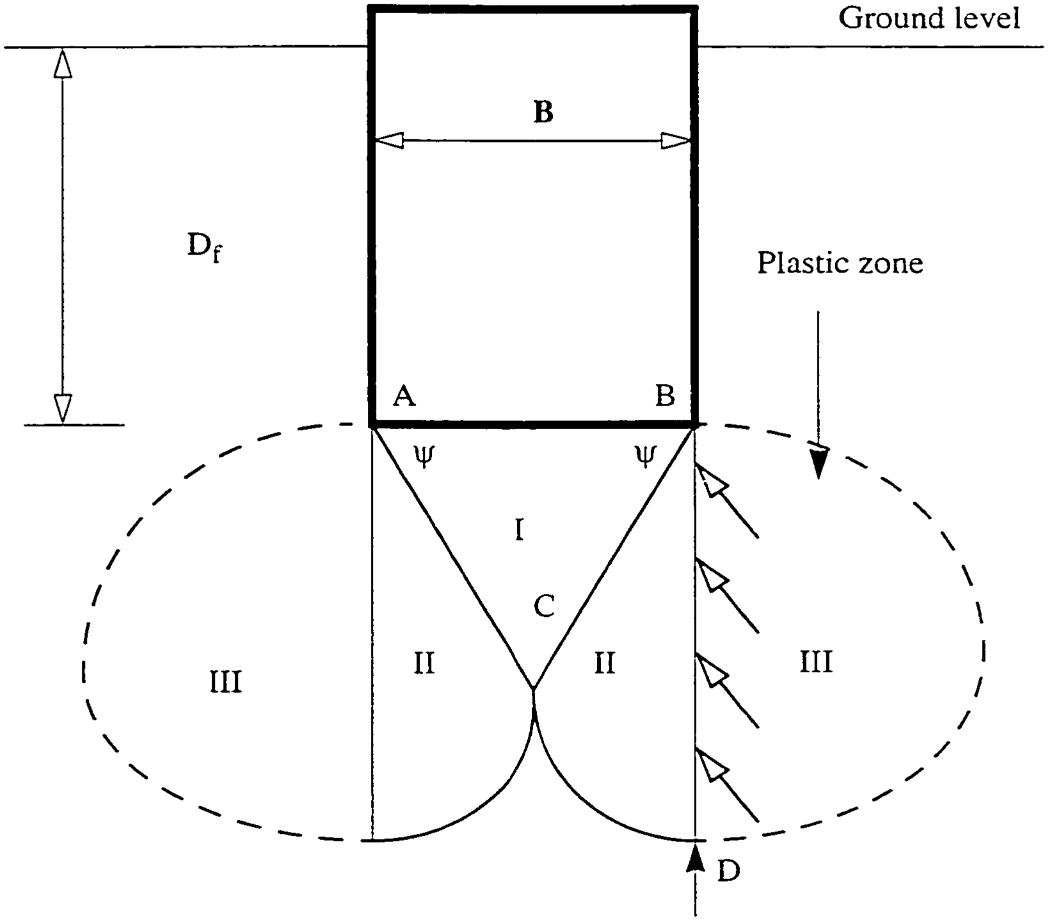

Figure 2.15 Vesic's Assumed Failure Surface Incorporating Soil Compressibility (After Vesic, 1977)

1) Zone I is a wedge shaped zone (aBa') located beneath the pile tip with its base angle Ψ :

$\Psi = (\pi/4 + \phi/2)$.

2)Zone II consists of two radial shear zones (Bac) and (Ba'c') bounded from below by the surfaces (Bc) and (Bc'), which are log spirals with their poles located at point a and a', respectively. These surfaces pass through the apex B of the wedge (aBa') and terminate at points c and c' located at a horizontal distance from the pile axis defined as radius of influence R.

3) Zone III includes two trapezoid shaped zones of mixed shear, (acde) and (a'c'd'e'), bounded laterally by the pile shaft and the outer boundaries (cd) and (c'd') of the zone of influence.

In this model the shear failure is assumed to be punching shear failure and the critical shear surfaces are not completely developed with the following assumptions:

i) The locally mobilized angle of shearing resistance ϕ_B along (Bc) and (Bc') varies along their lengths with its maximum value occurring at point B, equal to the angle of shearing resistance of sand, and its minimum value equal to zero at point c and c'.

ii)The shearing resistance is fully mobilized along both sides (aB) and (a'B) of the central wedge (aBa').

iii) Along the terminal radial surfaces (ac) and (a'c'), the locally mobilized angle of shearing resistance ϕ^*_β decreases linearly with the horizontal distance from the pile shaft, from a maximum value equal to ϕ at points a and a' to zero at point c and c'. In effect, the average mobilized angle of shearing resistance ϕ_β along ac and a'c' is equal to $\phi/2$.

iv) There is no shear mobilization assumed on the boundary surfaces (cd) and (c'd') of the zone of influence.

The problem was considered as axisymmetric loading, the longitudinal cross section (aOBcde) in Figure 2.17 was considered as one sector that revolves through an angle $\Delta\zeta$ around the axis of the pile to generate the volume which has been treated as a free body subjected to external forces using an equilibrium analysis.

Based on this analyses, the following relations were introduced to calculate skin friction and point resistance

$$Q_s = \frac{2\pi}{\Delta\zeta}(E_2 \tan\delta) \qquad ...(2.24)$$

Where

E_2 = Horizontal normal force acting on the surface AE.

δ = angle of friction between pile shaft and sand

$\Delta\zeta$ = central angle of rotation

$$Q_p = \frac{2\pi}{\Delta\zeta}(F_N \cos\psi + F_T \sin\psi) \qquad ...(2.25)$$

Furthermore:

Where:

F_N and F_T = normal and tangential forces acting on AB or A'B.

$\Psi = (\pi/4 + \phi/2)$.

To clarify the critical depth phenomena, Nguyen and Hanna, 1991 introduced a variable failure mechanism in their model by changing the model parameter angle β as the pile advances downwards in the sand medium (see Figure 2.17).

This model incorporated some features generally omitted in previous pile bearing capacity theories, such as:

i- Treating the pile bearing capacity problem as an axisymmetric case,

ii- Adopting punching shear associated with variable failure surfaces as the principle failure mode, and

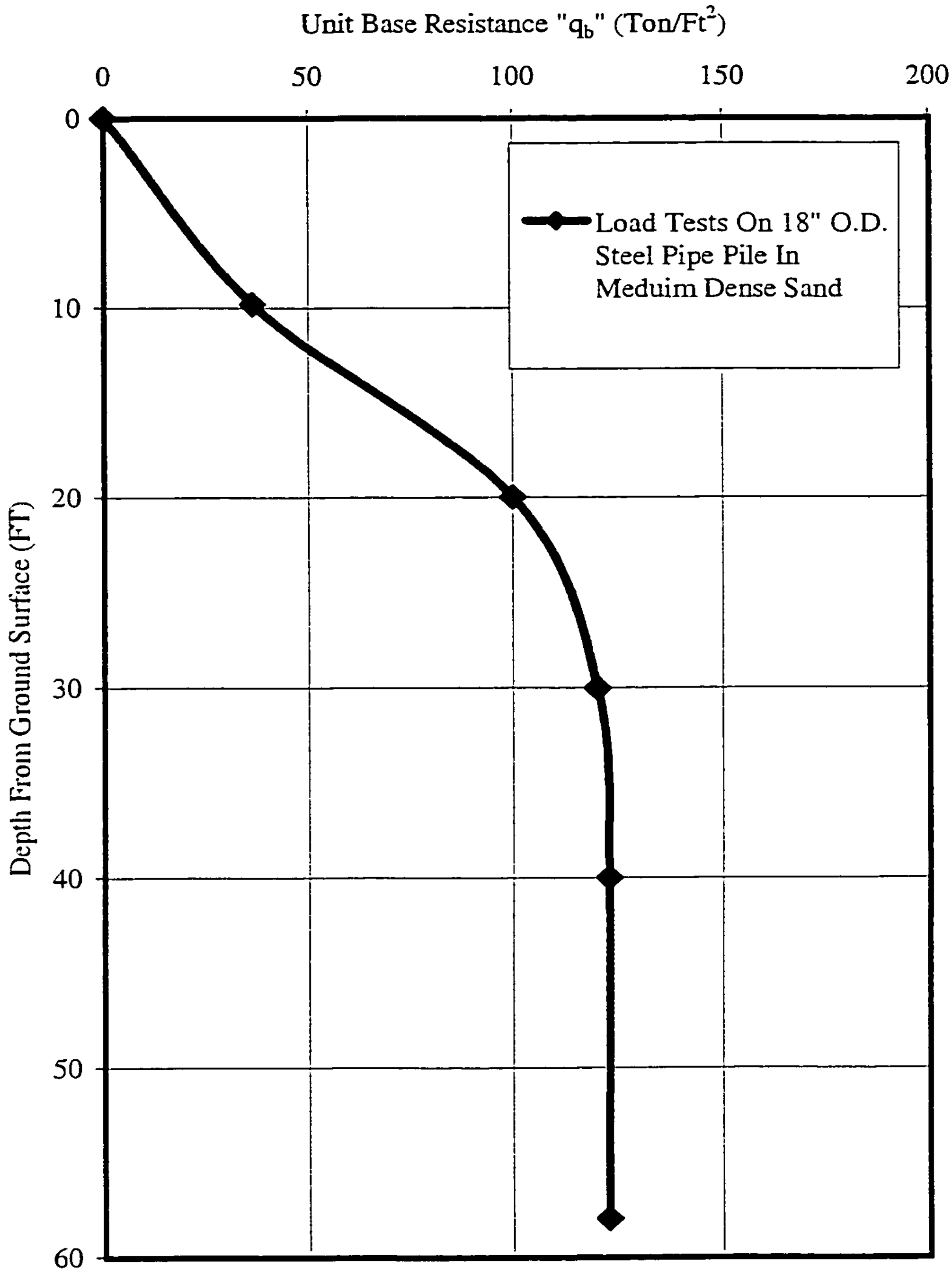

Figure 2.16 Variation of Unit Base Resistance "q_b" Versus Depth (After Vesic, 1967-b)

iii- Taking into account the interdependence between shaft and point resistances.

While the model introduced by Nugyen and Hanna, 1991 incorporated some important features which were omitted in the previous models, on the other hand it had the following drawbacks:

The model parameter angle β is an imaginary value which does not actually exist based on any evidence related to experimental or analytical analyses. Furthermore Nugyen and Hanna did not give any formulation to that parameter and in the suggested procedure one should run the program developed by the authors for a very wide range of angles β to match a value (based on another approach) and then use this value in analyzing the problem. This is not workable solution from a practical point of view.

2.4 Critical Depth

Extensive experimental investigation on full-scale piles under laboratory conditions (Kerisel, 1961; Vesic, 1967b) and pile load tests in the field (Vesic, 1967a; Tavenas, 1971; Hanna & Tan, 1973, Jardine and Lehane, 1993, Bond, et. al. 1997) showed that the average unit skin friction f_s increases linearly with depth, up to a depth beyond which f_s values remain constant or reduced. This depth was defined as “critical depth”. The critical depth was found to be a ratio of pile length to embedment depth, L/d, equal to 10 for loose sand and 20 for dense sand in the case of driven piles. Beyond this critical depth, f_s reaches asymptotically a constant value which depends only on the sand density and not on the effective overburden pressure (Figure 2.5). Recently, further accumulation of field evidence tends to challenge this conclusion. Coyle and Castello (1981) analyzed a large number of pile load tests and proposed design charts which clearly showed that the unit skin friction f_s continue to increase with

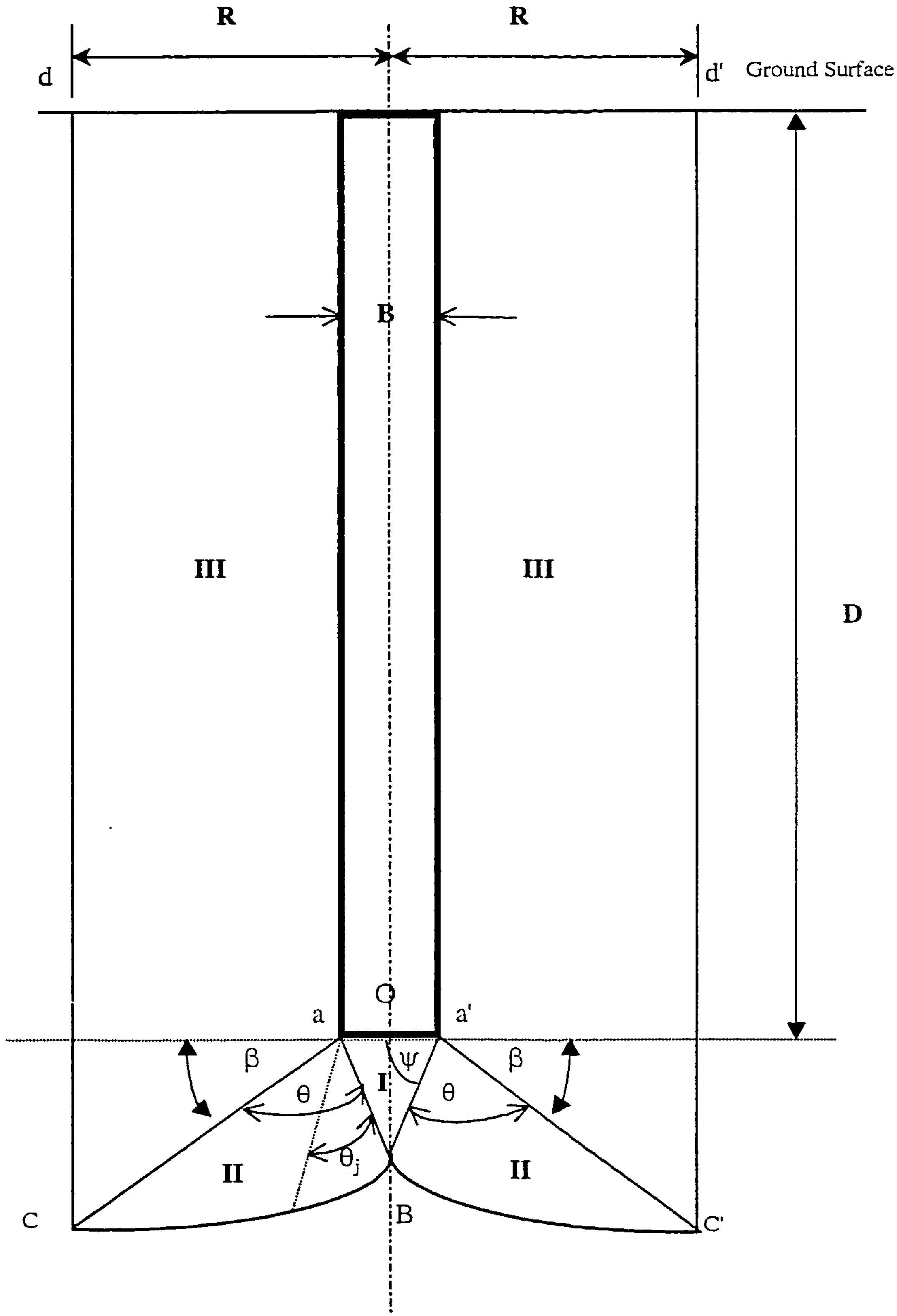

Figure 2.17 Assumed Failure Mechanism
(Nguyen, T.Q., and Hanna, A.M., 1991)

depth. Concurring with this view, Kulhawy (1984) argued that the apparent limiting value of f_s was purely coincidental, and even the whole critical depth concept was a fallacy. He claimed that the tip and side resistances of pile foundations do not reach a limit at a critical depth; instead, they increase with depth. For the tip, the rate of increase decreases with depth, primarily because of decreasing rigidity with depth. For side resistance, the rate is a function of increasing overburden and the decrease of K_0 with depth.

The critical depth ratio discussed above for the pile shaft resistance also applies to the pile end bearing resistance. Important studies by Kerisel (1961, 1964), Kerisel et al. (1965), Vesic (1963, 1964, 1967b) and Tavenas (1971) reported that the unit point resistance increases only to a certain depth and then reaches a constant value which depends only on the relative density of sand (Figure 2.15). Hanna and Tan (1973) reported a critical depth ratio of 40 for tip component in medium dense sand. This phenomenon of critical depth was attributed to arching which resulted in a relative constant vertical stress along the lower portion of the pile shaft and in the immediate vicinity of the pile tip (Vesic, 1967a). Experimental evidences of arching around the pile shaft were published by Robinshy and Mornson (1964) in their study of sand displacement around model piles using radiography techniques, and by Hanna and Tan (1973) who performed load tests on buried, instrumented model piles up to 1.5 in. in diameter. Meyerhof (1976) and Poulos and Davis (1980) subsequently incorporated Vesic's findings into practical design charts. Disagreements in the critical depth concept began to surface, especially after Vesic apparently abandoned further attempts to advocate his initial working hypothesis (Vesic, 1977). Hanna and Tan (1973) also pointed out the important effect of "locked-in stresses" existing in their model piles after installation, and questioned the validity of analyzing load distributions in piles without accounting for residual stresses. In 1981, Coyle and Castello proposed empirical design charts for piles in sand, which indicated that both the unit point resistance q_p and the average unit skin friction f_s continued to increase beyond the critical depth. In support of Coyle and Castello's charts, Zeitlen and Paikowsky (1982) suggested that the critical depth concept was not even necessary if proper allowances were made to account for the decrease of the angle of shearing resistance ϕ with increasing confining pressure. Accordingly, as ϕ decreased with depth, N_q and K_s also diminished with further pile penetration, resulting in relatively constant values of q_p and f_s. Altaee, et al, 1993, reported from an experimental field program that the critical depth appeared as a result of neglecting the influence of shallow depth variation of the earth pressure coefficient.

Fellenius, 1995, argued that the critical depth concept is a fallacy which resulted from misinterpretation of both field and laboratory tests. He further added that neglect of residual loads in full-scale test makes a measured load distribution looks like linear distribution below a certain depth. In the case of model scale pile, which are tested in shallow depths, neglect of stress-scale effects gives a similar error of interpretation. As the same results were obtained from field and laboratory, it is not surprising, therefore, that the fallacy so rapidly gained acceptance.

Finally, Kulhawy, 1995, based on his private communications in the early 1980's, with Vesic (to whom the concept generally has been attributed), claimed that Vesic stated the problem of critical depth as: "tentative working hypothesis and nothing more", and then Vesic's concept was disregarded by the mid 1970's.

2.5 Discussion

The previous literature review includes observations and conclusions on a number of investigators concerning phenomenons related to driven piles in cohesionless soil. As can be seen, the obtained values of N_q are a direct consequence of the assumed failure mechanism. which varied among the authors where in each theory different assumptions are made. It is also well known from the literature that all assumed failure patterns - except very few- consider a constant failure surface to fit all conditions depending on one unique factor (ϕ). It is not surprising to find serious discrepancies among published N_q values in the literature (Figure 2.6). On the other hand, the notion that N_q is a unique function of ϕ gradually loses its appeal because it presents an overly simplistic view of a highly complicated phenomenon.

The assumed failure mechanism was reported only to the tip resistance component and except for very few approaches, all methods assumed accumulation of the average unit of the skin resistance over the shaft. These accumulated calculations depend on different factors which differ from one theory to another (refer to table 2.3). Each investigator assumed a constant value for the average unit of skin resistance and/or constant value for angle of interface friction. The coefficient of earth pressure "K_s" acting on the pile shaft was always considered constant even with depth changes. Too many experimental data reported that K_s increases for shallow pile endowments and exceeds K_p. At full pile embedment and ultimate load. the coefficient of earth pressure K_s may greatly exceed K_p near the top of the pile and tend to be a lower limiting value of 0.5 near the pile base (Wersching 1987). Altaee, et al, 1993 reported from an experimental program for single pile driven in sand that the coefficient of earth pressure against the shaft is larger near the ground surface and that a constant coefficient does not develop until a depth of 3 m.

Meyerhof in 1959, and Norlund in 1963 dealt theoretically with the problem of the determination of the lateral earth pressure coefficients K. The assumption was made in both studies that the pile displaces the sand in a horizontal direction, without any vertical deformation. This displacement induces compaction in the surrounding soil which is maximum at the pile-soil interface. Since the wall pushes against the sand and the horizontal movement is large (equal to the pile radius), it is physically possible for the magnitude of the lateral earth Pressure coefficient, K, to be as high as the passive earth Pressure coefficient.

All methods reported in the literature are almost determine the skin resistance by accumulating the friction forces over the shaft as a linear distribution. Except very few, no rational theory developed to accommodate for the failure mechanism of the skin resistance component.

The classic theories of the bearing capacity of piles (for example; Terzaghi, 1943; Meyerhof, 1951; Skempton et al., 1953) are essentially based on the assumption that the soil is a rigid-plastic material, while the effect of compressibility of the soil is considered only empirical. It is also assumed that the strength parameters (c, ϕ) are constant regardless of the stress or strain level.

Most of the theories introduced in the literature dealt with the problem of bearing capacity of single pile in sand in the three dimensional case as an approximation extended from the plane strain solution.

It would be fair to say that the state of design methods for piles driven into sand is relatively unclear, and not yet well understood. There is still a pressing need for more theoretical and experimental investigations to generate a proper modeling of the problem which might lead to an enhanced solution in the future.

In summary, a rational bearing capacity theory for a single pile in sand should bring needed improvements in the shortcomings suffered by its predecessors. In this thesis, an attempt is made to develop a theoretical model depending on finite element analyses which are used widely in many successive cases in the geotechnical field to incorporate some salient features commonly omitted in the existing pile bearing capacity theories. These features include:

1. Treating the pile bearing capacity under an axisymmetric conditions.

2. Modeling of sand around the pile as an elasto-plastic material, considering the compressibility of the soil around the pile to observe the influence of different factors on the developed failure mechanism.

3. Develop a new predictive formulations for coefficient of earth pressure acting on the shaft as a varied parameter depending on several factors: δ, ϕ, and pile geometry.

4. Adopting varied failure mechanism which utilizing the punching shear failure as a unique failure mode for piles in sand.

5. Developing theoretical model to be used in predicting the ultimate bearing capacity of a single pile in sand as a function of many factors: pile geometry, relative shaft roughness δ/ϕ and angle of shearing resistance ϕ.

CHAPTER 3

NUMERICAL MODELLING

3.1 General

Numerical analyses using finite element techniques have been particularly popular in recent years in the field of foundation engineering. Based on the method described by Zienkiewicz (1977), a variety of finite element computer programs have been developed, with varieties of facilities to suit different needs. The behavior of soil can be approximated by the use of an appropriate stress-strain law applied to discrete elements. The finite element method provides a valuable analytical tool for the interpretation of foundations, where unusual geometry or three dimensional effects are significant. It is particularly relevant when we compare or back analyze the performance of a well instrumented prototype, or a full scale test in the field. Analyses for piles using the finite element method have been used by numerous researchers (Chen and Polous, 1993; Stewart, Jewell, and Randolph, 1993; Zaman, Najjar, and Muqtadir, 1993; Meibner and Shen, 1994; Nicola and Randolph, 1994; Law, 1982; Ottaviani, 1975). In particular, the analyses for axially loaded piles in sand have been reported by several researchers (Desai, 1974; Randolph and Wroth, 1978; Trochanis, Bielak and Christiano, 1988; Simonini, 1994).

3.2 Scope and Objectives

Due to the large number of parameters under consideration, which include geometries, loading conditions, and soil properties, some simplified assumptions have been considered in the literature. Assumptions were made to include perfect bonding between piles and soil, linear soil behavior, absence of degradation of soil properties, and elastic pile-soil interaction. These assumptions limit the range of applicability of these methods to particular soils or loading types, and they may predict a foundation response significantly different from the actual conditions. Three dimensional models employing nonlinear constitutive laws for soil present promise to model pile/soil interaction in a more realistic manner (Chow, 1986; Koumoto, 1985; Ottaviani,1975; Trochanis, et. al., 1988; Trochanis, et al, 1991& Zaman, et al, 1993). However, due to the computational limitations, only a few results have been obtained from these models. In addition, there is need to incorporate knowledge obtained from this type of sophisticated analysis into simpler models that can be used in practice by foundation designers.

In view of the above, the present chapter has the following objectives:

(1) To develop the numerical model for a single pile in sand

(2) To explore the mechanism of failure around a single pile in sand deposit due to the axisymmetrical loading conditions, which will provide the basis for rational theoretical model, to be presented in Chapter Four.

(3) To examine factors that should be incorporated in the analysis and the design of piles, which have been overlooked in the past.

The results of these analyses are expected to provide the basis for a rational theory for predicting the bearing capacity of a single pile in sand, which is presented in Chapter Four of this thesis.

3.3 Numerical Model

The numerical model developed in the present investigation was carried out using the finite element code CRISP94 (**CRI**tical **S**tate **P**rogram). It was initiated by Zytynsski (1976) and developed further by Britto & Gunn (1987), and modified at Cambridge University, U.K. It includes the following features:

(1) Undrained, drained and coupled consolidation analysis can be handled by the program either for two dimensional plane strain or axisymmetric loading conditions, or three dimensional plain strain solid bodies.

(2) The following soil models are available: Anisotropic linear elastic; inhomogenous linear elastic (properties vary linearly with depth); elastic-perfectly plastic with Von Mises, Tresca, Drucker-Prager, or Mohr-Coulomb yield criteria. For elastic-perfectly plastic models, the stress state is corrected back to the yield surface at each loading increment. Therefore, a limited increment size is required in order to achieve a reasonable convergence. It is worth mentioning that the program uses a tangent stiffness solution scheme in which the global stiffness matrix is updated at each increment.

3.3.1 Type and Size of Finite Element Mesh

The mesh used in the present study was determined according to the size of the pile and the amount of deformation expected during the analysis. Since the region of interest is limited to a few diameters around the pile, an axisymmetric analysis for a mesh whose axis coincides with the axis of the pile foundation is the most efficient solution. The choice of the number of elements and mesh design reflects a compromise between an acceptable degree of accuracy and computing time.

3.3.1.1 Boundary Conditions

The following boundary conditions are imposed on the mesh: the nodes belonging to the periphery of the cylindrical mesh are fixed against displacement in both horizontal directions, yet remain free to move vertically; and the nodes constituting the bottom of the mesh are fixed against displacement in both horizontal and vertical directions. Additional boundary conditions, which satisfy static loading, may have to be imposed in each case due to symmetry conditions, i.e., nodes lying on an axis of symmetry cannot be displaced perpendicularly to that axis. However, the boundary should be placed far enough from the region of interest in order not to affect the deformations within that region. The mesh is designed to be denser in the vicinity of the pile shaft, where the deformations and stresses are expected to have a major variation.

Randolph (1977) recommended boundry conditions for the finite element mesh to be 50 times the pile radius in the lateral direction, and to be 1.5 times the pile length below the tip in the vertical direction. Since the need is to study the failure pattern around the pile shaft, the boundary conditions used in this study will be as follows:

- The horizontal boundary was placed at least 50 times the pile radii measured from pile axis, see Figure 3.1.
- The vertical boundary was placed at 1.5 times the pile length below the pile tip.

These conditions will vary depending on pile geometry and the observed zone of failure around the shaft. Figures 3.1& 3.2 show schematic views of the adopted finite element meshes and the distribution of elements. These boundary conditions were imposed to minimize the boundary effect on the zone of interest (around the shaft), and to provide sufficient accuracy for the analyses.

3.3.1.2 Number of Elements

The number of elements required for the analysis to achieve sufficient accuracy is considered to be between 100 and 200 elements (Duncan, 1972 & Britto,1988). In this study several

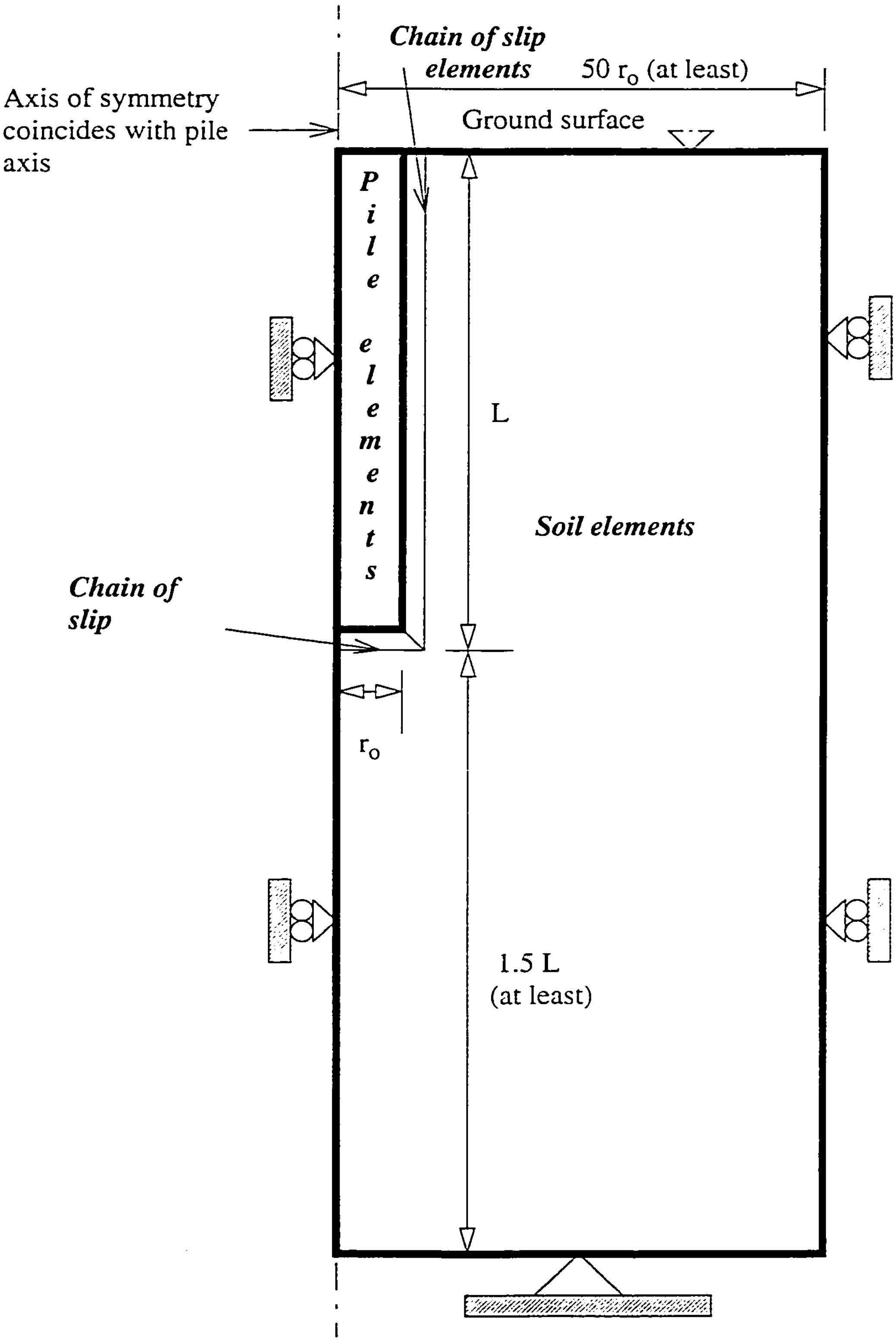

Figure 3.1 Pile-soil Interface System and Diagrammatic View of Boundary Conditions

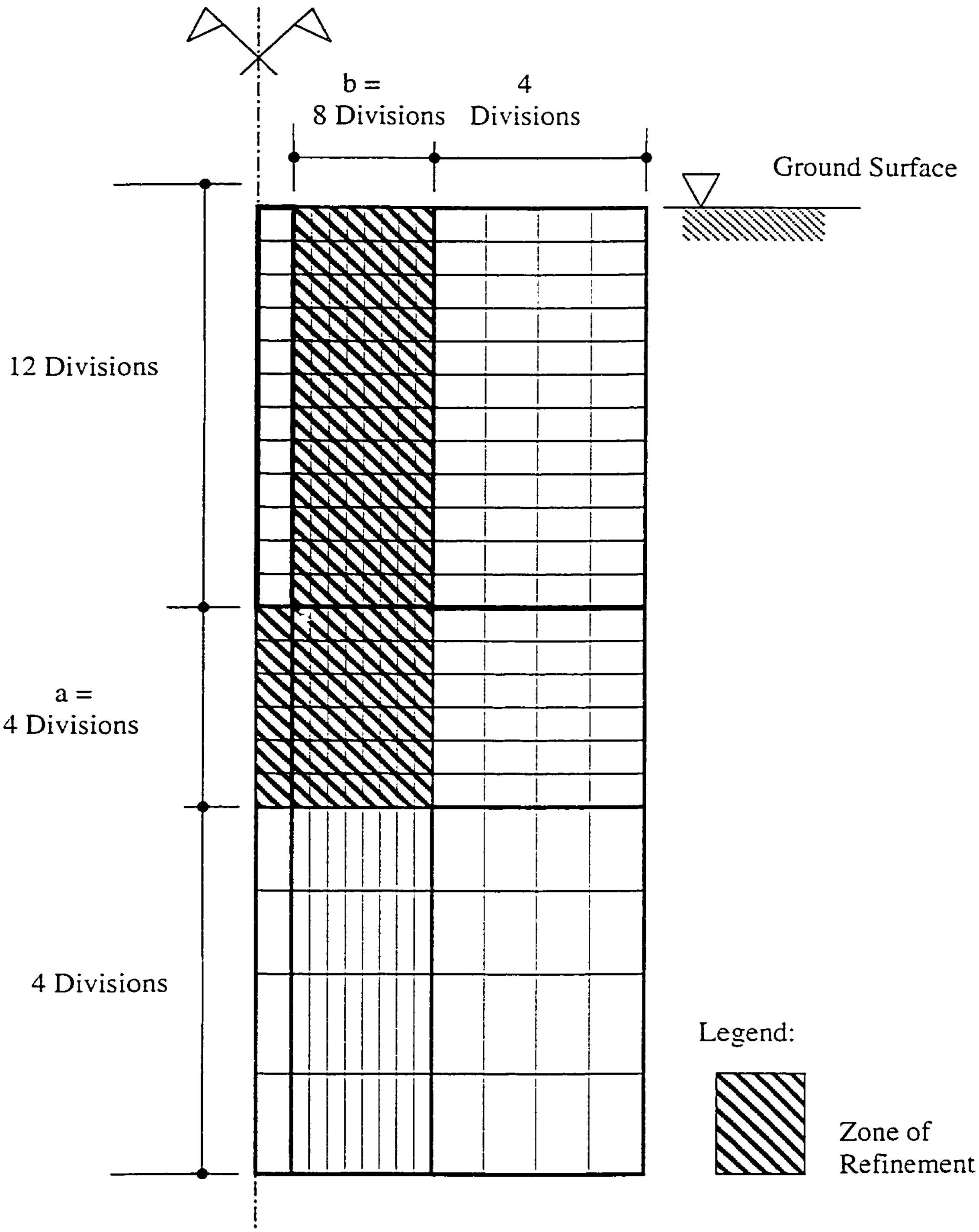

For a & b dimensions, refer to Table 3.5

Figure 3.2 Schematic View of the Finite Element Mesh
(Distribution of elements & Zone of Refinement)

meshes were examined to obtain the minimum number of elements necessary to produce accurate results. It was found that a minimum of 150 elements was required to achieve the desired accuracy. Increasing the number of elements beyond this number did not produce major changes in the results. In this study, 299 elements and 336 nodes were used and these numbers were sufficient for successful analysis. The distribution of elements is also displayed in Figure 3.2.

3.3.1.3 Types of Elements

The soil and the pile were modeled using eight-noded Linear Strain Quadrilateral elements "LSQ" with quadratic variation for the displacement along the sides of the element (Figure 3.3a). Smaller sized soil elements were selected in the vicinity of the pile where variations in stresses and strains were expected to be more significant. Furthermore, the aspect ratio for the used elements did not exceed 5. It was also recommended by Britto (1988) that the maximum aspect ratio required to provide a successful analysis should not exceed 10. In the present analysis, several meshes with different aspect ratios were examined. It was found that an aspect ratio of 10 provides the high level of accuracy for such analysis.

To model the interface behavior between the pile and the soil, a thin interface layer composed of 6-noded flat elements (Figure 3.3b), with a maximum aspect ratio between 10 and 100 was used (recommended by Britto,1988). This layer was placed between the pile and the soil to simulate the relative slippage between both soil and pile material. These elements can be used to simulate the interface between soil and structure in the case of smooth surfaces, or to simulate the case of slip after a limiting stress condition has been reached. These elements are placed all around the pile elements and along its entire length. In essence, these elements separate the pile perimeter nodes from the corresponding soil nodes; interface elements are

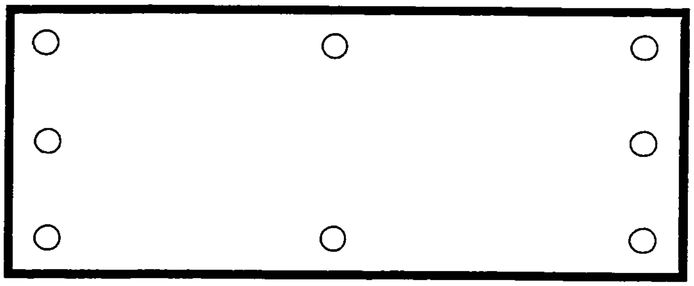

a - Eight-noded **L**inear **S**train **Q**uadrilateral elements
"**LSQ**" used to model soil and pile system.

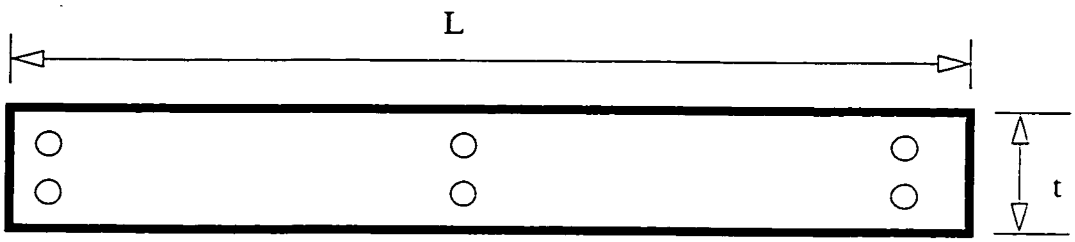

b- Interface slip elements L >> t

○ Unknown displacements (u, v, w)

Figure 3.3 Types of Elements Used in the analysis.

also placed around the soil column under the pile tip, so that slippage of the pile tip with respect to the surrounding soil can be modeled. It should be noted that the material properties for the slip element were determined based on the material properties for the adjacent soil.

3.4 Constitutive Laws

3.4.1 Model of Pile Material

The elements constituting the pile material were assumed to behave elastically at all times. The maximum stresses attained during this study did not exceed the yielding limit of the chosen material (reinforced concrete), thus validating the assumption of elastic pile behavior. Table 3.1 shows the typical elastic parameters required by the program to model the pile material.

Table 3.1 Typical Input Elastic Parameters Required by the Finite Element Code for Modeling Pile Material (Steel Pile)

Parameter	Definition	Adopted Values For Arkansas Pile Load Tests
Young's Modulus in X direction	Modulus of Elasticity (E) of pile material in horizontal direction	29×10^6 psi (after Armelah, 1986)
Young's Modulus in Y direction	Modulus of Elasticity (E) of pile material in vertical direction	29×10^6 psi (after Armelah, 1986)
Poisson's ratio ν_{hh}	Poisson's ratio (ν) for pile material in horizontal direction	0.3 (after Lambe, 1979)
Poisson's ratio ν_{vh}	Poisson's ratio for pile material in vertical direction	0.3 (after Lambe, 1979)
Shear modulus G_{hv}	$= E/(2(1+\nu))$	11.2×10^6 psi
K_w	Code = 0 for drained condition Code = 1 for undrained condition	$K_w = 0$ for the whole analyses
γ	bulk unit weight of pile material	7000 Ib./ft.^{3} (after Lambe, 1979)

3.4.2 Soil Model

The deformation of the soil was assumed to comprise a linear elastic stage, modeled by the classical theory of elasticity, and a nonlinear stage. The nonlinear constitutive model used for the soil was the Mohr-Coulomb plasticity model. This model was selected among the several soil models available in the library of CRISP because it can be implemented easily, its parameters can be related to the physical properties of the soil, and furthermore it is widely used in practice. In addition, a comparison between the results obtained by the Drucker-Prager, and Mohr-Coulomb models revealed close agreement between the two models, see Figure 3.4.

The criterion of Mohr-Coulomb is defined by the following relationship:

$$\tau = f(\sigma) \qquad ...(3.1)$$

where the limiting shear stress, τ, in a plane depends only on the normal stress, σ, acting in the same plane. Furthermore, the normal stress function, $f(\sigma)$, represents the failure envelope for the corresponding Mohr's circles, as shown in Figure (3.5).

Coulomb, much earlier, introduced his well known equation,

$$\tau = c + \sigma \tan(\phi) \qquad ...(3.2)$$

which is considered to be the simplest form of the Mohr failure envelope, where (c) represents the soil cohesion and (ϕ) represents the angle of shearing resistance of the soil. The Mohr failure criterion associated with the Coulomb equation is referred to as the Mohr - Coulomb criterion. The failure surface can be expressed in terms of principle stresses as follows:

$$\frac{(1-\sin\phi)}{2c \cdot \cos\phi} \times \sigma_1 - \frac{(1+\sin\phi)}{2c \cdot \cos\phi} \times \sigma_3 = 1 \qquad ...(3.3)$$

where: σ_1 and σ_3 are the major and minor principal stresses respectively.

Furthermore, this model was recommended by Gunn (1996) as the best available model in

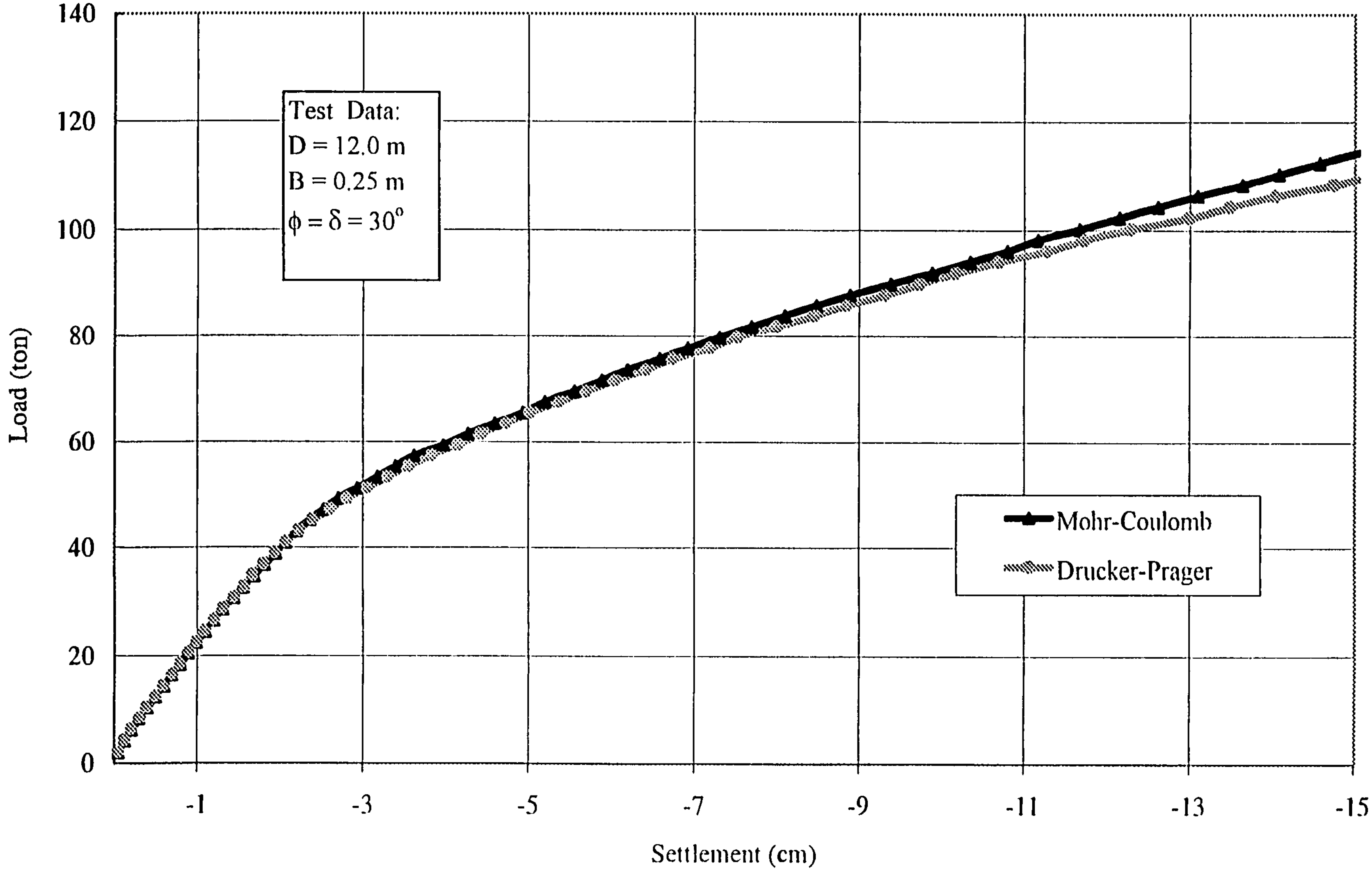

Figure 3.4 Comparison Between Different Soil Models

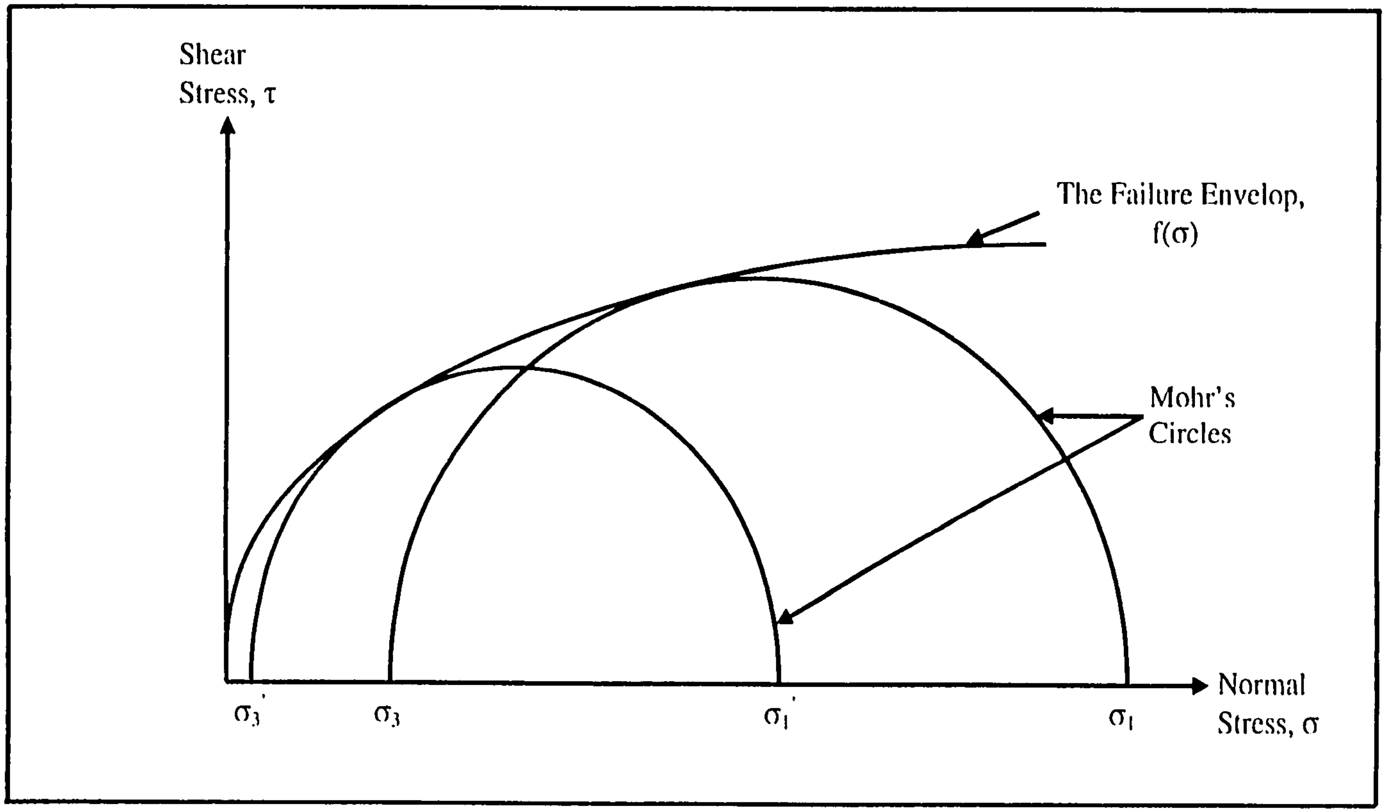

Figure 3.5 Mohr-Coulomb Failure Envelope

CRISP for such analysis. Table 3.2 introduces typical parameters required by CRISP for using the Mohr-Coulomb model.

Table 3.2 Typical Input Parameters Required for Modeling Sand Material (Adapted values for Arkansas pile load tests)

Parameter	Definition	Adapted values for Arkansas pile load tests	
		Soil Type (SP)	Soil Type (SM)
E_o	Young's Modulus at $Y=Y_o$	$2.16x\ 10^6$ Ib./ft.^{2} After Lambe (1977)	$1.65x\ 10^6$ Ib./ft.^{2} After Lambe (1977)
ν_s	Poisson's ratio	0.3 (After Desai, 1979)	0.3 (After Desai, 1979)
C_o	Cohesion at $Y=Y_o$	0.00	0.00
ϕ	Internal friction angle for soil	31° (After Desai, 1979)	32° (After Desai, 1979)
Y_o	Y - Coordinate where $E=E_o$ & $C= C_o$	0.00	0.00
K_w	Code = 1.0 for undrained condition = 0.0 for drained condi-	0.00	0.00
γ_s	Bulk unit weight for soil	62.5 Ib./ft.^{3} (After Desai, 1979)	62.4 Ib./ft.^{3} (After Desai, 1979)
m_e	Rate of increase of E with depth	0.00	0.00
m_c	Rate of increase of C with depth	0.00	0.00

The Origin of the Mesh is Located at the Bottom of the Mesh and Increases Upward i.e., Y-coordinates = 0.0 Found at the Bottom of the Mesh.

3.4.3 The Pile-Soil Interface Element Model

For a realistic model, a rough (or adhesive) interface is required between the pile shaft and the soil. A relative slippage should be permitted when the shear stress mobilized on the shaft exceeds the limiting value. Trochanis,et. al., (1988) in their finite element analyses results showed that inelastic soil behavior can significantly affect the response of piles, and pile/soil slippage is the most significant inelastic effect under purely axial loading. Furthermore, their findings concluded that the load-settlement behavior is the same for the elastic and the inelastic soil model. This implies that all significant nonlinearity, in this case, is caused by the slippage and not by the yielding of the soil.

A slip element was employed to simulate the interaction at soil/pile interface. The slip element used in the analysis was similar to the one proposed by Desai et. al. (1984). It was treated as a one dimensional element with six distinct nodes; three of each are on one side of the longitudinal direction of the element. This element is also formulated to behave as a linear elastic - perfectly plastic (Mohr - Coulomb material) which is governed by the following parameters:

- Soil cohesion, c
- Interface angle, δ
- Stiffness in the normal direction, $K_n = E(1-\nu)/(1+\nu)(1-2\nu)$,

  Where, E, ν are the modulus of elasticity and the Poisson's ratio respectively
- Shear modulus, $K_s = G = E/(2(1+\nu))$
- Residual shear modulus, K_{res} (usually equal to 0.01 to $0.001K_s$),
- Thickness of the element, t (usually: $0.1L > t > 0.01L$),

  where L = the element length.

According to the foregoing constitutive relationship, the slip element behaves elastically till the shear stress reaches the limiting shear stress as defined by the Mohr-Coulomb equation,

$$\tau = c + \sigma \tan(\delta) \qquad \ldots(3.4)$$

If the shear stress exceeds the limiting shear stress, the shear modulus, K_s, is replaced by the residual shear modulus, K_{res}, which permits the relative slippage between the soil and the pile. A comparative study was conducted on the results of two pile load tests, one using slip elements around the shaft and another using no slip elements. Two different meshes were designed for this analysis; both were similar except the placement of slip elements around the pile shaft. The obtained results are shown in Figure 3.6 in terms of pile load settlement curves. As can be seen, the assumption of perfect pile-soil bonding leads to an ultimate load several times higher than the one computed when slippage is taken into consideration. The same trend was found for pile settlement: the settlement needed for fully mobilized ultimate load is much higher than in the case of permitted slippage. These observations coincide with the results obtained by Trochanis,et al., (1988).

3.5 Finite Element Output

The results of the present numerical investigation are introduced in graphical forms. The following information is provided for each load test:

1. Deformed/undeformed mesh
2. Displacement vectors
3. Horizontal strain (ε_{xx})
4. Vertical strain (ε_{yy})
5. Horizontal stress (σ_{xx})
6. Vertical stress (σ_{yy})
7. Horizontal displacement (δ_x)
8. Vertical displacement (δ_y)

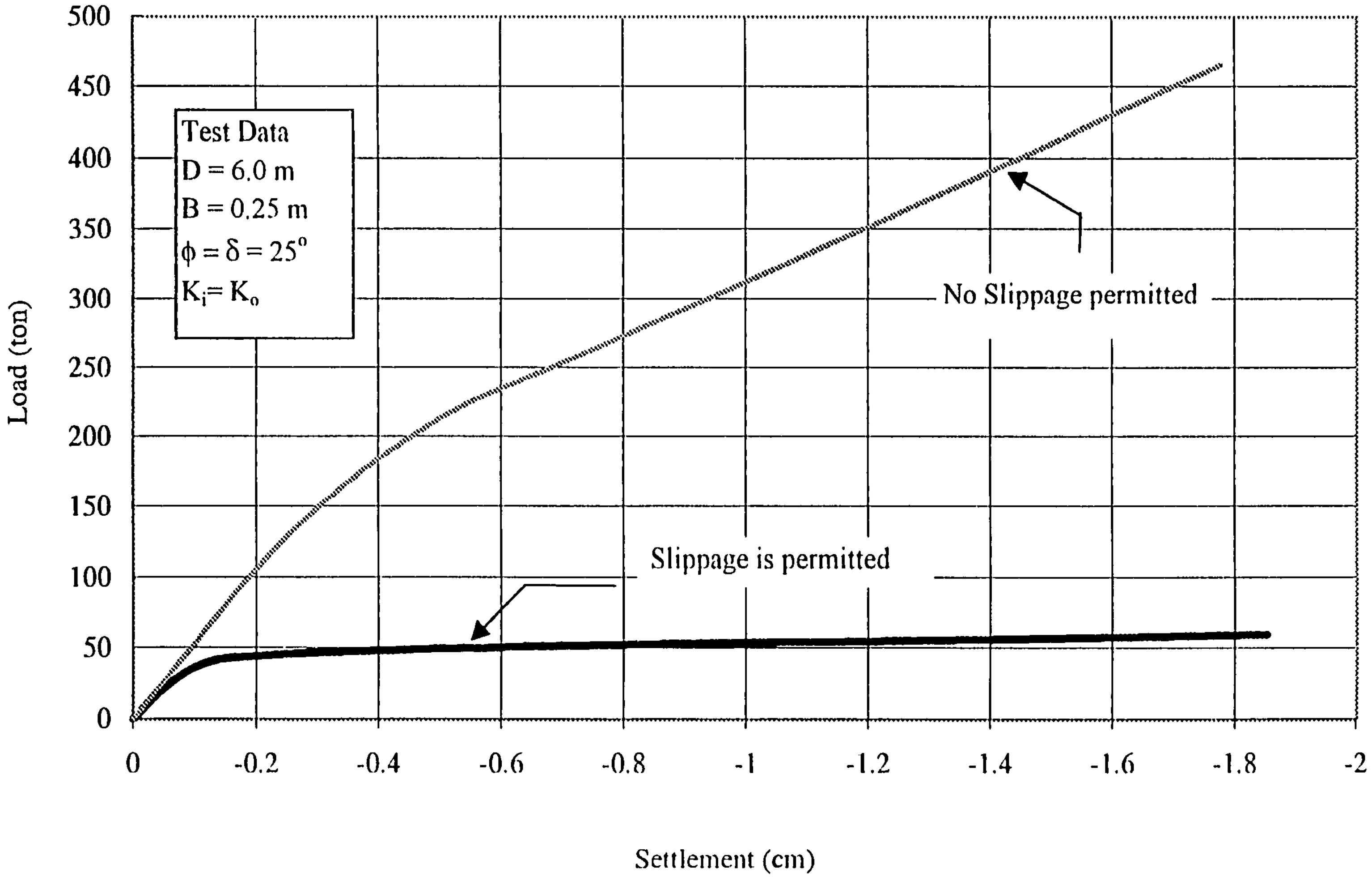

Figure 3.6 Load Settlement Relationships for Piles with and without Slippage

3.6 Model Validation

In order to establish confidence in the numerical procedure developed in this investigation, the numerical solutions were verified against field observations. In this chapter, several field pile load tests conducted by the United States Army Corps of Engineers (CE, 1964, as reported by Desai, 1974) were analyzed. Comparing the results of the present numerical analysis and the field data in terms of the tip settlement versus the total applied load and ultimate bearing capacities are presented in Table 3.3. A good agreement was achieved.

Table 3.3 Comparison of Load Carrying Capacity for Arkansas Pile Tests

Criterion	Ultimate Load Carrying Capacity		
	Pile # 2	Pile # 3	Pile # 10
Field measured (tons)	215	250	165
Finite element prediction present study (tons)	285	240	185
Error%	-32.5%	4.0%	-12.0%

3.6.1 Pile Load Tests

The U.S. Army Corps of Engineers has conducted a large number of field pile load tests. Tests from two sites will be considered: Arkansas Lock and Dam no. 4 (LD4) on the Arkansas River in Arkansas, and Jonesville Lock (JL) on the Black River in Louisiana, USA. Details regarding the pile test program have been fully described in a report by Fruco and Assoc., (1964) and in the paper by Mansur and Hunter (1970) and, further, were analyzed by Desai (1974a). Details of boring logs and other soil properties are adopted from Mansur and Hunter, (1970), Fruco and Assoc. (1964), and Desai, (1974a). All soil foundations and related pile material properties are presented in Tables 3.1 and 3.2 and Figure 3.7.

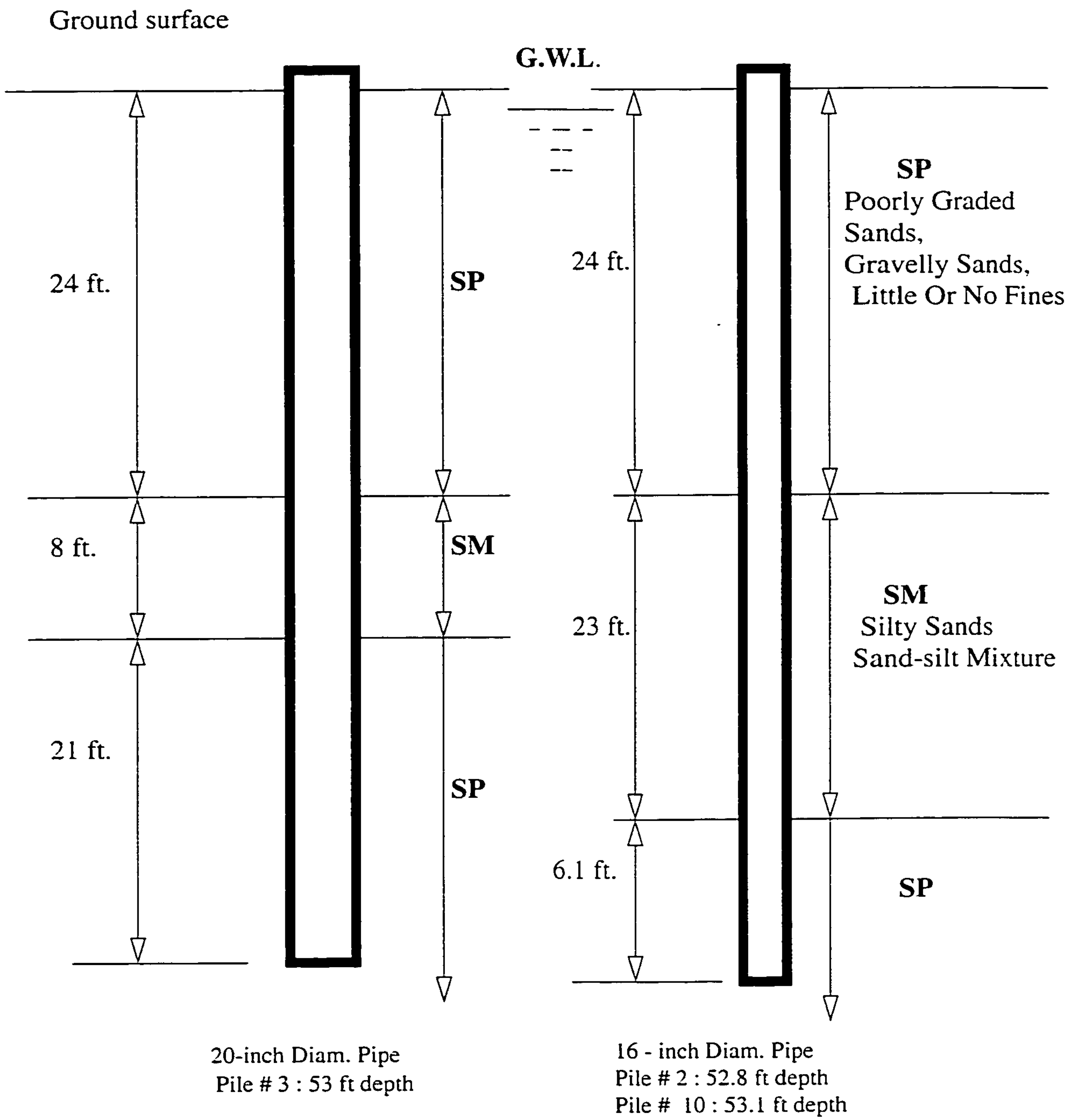

Figure 3.7 Field Data for Pile Load Tests
(Arkansas River 1964)

3.6.2.1 Finite Element Meshes

The pile-soil interface system was modeled as described in section 3.3. A mesh with 394 nodes and 351 elements was used to model pile load tests number 2 & 10, while a mesh with 316 nodes and 279 elements was used to represent pile load test number 3.

3.6.3 Interface Parameters

According To The U.S. Army Corps of Engineers, a number of direct shear tests were available to evaluate the angle of friction between the pile material and the sand (Desai, 1974a). Results of these tests indicate that the angle of friction between pile material and soil is 25° for **SP** soil and 27° for **SM** soil. These values were used in this analysis.

3.6.4 Test Procedure

1) The pile was assumed to be driven in a homogeneous, isotropic sand layer, i.e. no driving stresses were considered. The initial stresses in the soil mass were assumed to have a zero value at the ground surface and to increase linearly downward. The maximum vertical stress (σ_v) at the bottom of the mesh is equal to:

$$\sigma_v = \gamma . h \qquad ...(3.5)$$

and the maximum horizontal initial stress (σ_h) at the bottom of the mesh is equal to:

$$\sigma_h = K . \gamma . h \qquad ...(3.6)$$

Where:

K = coefficient of earth pressure

h = the total height of the mesh starting from the ground surface.

γ = unit weight of sand

2) With respect to the assumed soil and pile properties, the loads were applied in equal increments in a form of uniform compression stress acting on the cross section of the pile head. The load was then applied in equal increments of 17.5 tons (160 kN) for pile load test number 3 and 20 tons (178 kN) for pile load tests numbers 2 and 10. The stresses acting on the pile material did not exceed the maximum allowable stresses. A total of 60 increments was found enough to meet the requirements of the used soil model, and the desired accuracy.

3- The ultimate load was determined from plotting the total load/settlement relationship, i.e. the plunging failure load was estimated. The failure pattern which developed gradually was monitored.

These test procedures and assumptions were applied in all analyses included in the present study.

3.6.7 Analyses and Results

Three finite element analyses were performed for the three pile load tests at Lock and Dam No. 4, Arkansas River. Load/settlement relationships were established and the ultimate load for each test was determined by using the tangent method. The comparison between finite element analyses and field observations is presented in Table 3.3. It can be seen that the finite element predictions showed good correlation with the measured value. For any individual comparison, the two ultimate loads are not the same; this is expected because of the following two reasons: neglect of driving stresses; inaccuracy of adapted theoretical parameters such as modulus of elasticity, angle of interface friction between pile and soil, etc. These parameters were adapted from other similar soil data and not for the same site; moreover, the team that executes the loading test in any site does not determine such parameters. In general, one can conclude that a fair agreement between field and theoretical analysis is achieved.

3.7 Axisymmetrical Parametric Study

An axisymmetrical finite element analysis was performed in a form of limited parametric study with the following objectives:

1- To investigate the failure mechanism of a single pile in sand subjected to an axial load and to establish the parameters governing the mechanism.

2- To study the sensitivity of the governing parameters affecting the ultimate bearing capacity of the single pile in sand.

Table 3.4 Range of Pile Geometries Used in the Parametric Study

Group No.	Series No. 1 Pile diameter (B) 0.25 (m)		Series No. 2 Pile diameter (B) 0.40 (m)		Series No. 3 Pile diameter (B) 0.50 (m)		Series No. 4 Pile diameter (B) 0.75 (m)	
	D/B	Pile Length (D) m	D/B	Pile Length (D) m	D/B	Pile Length (D) m	D/B	Pile Length (D) m
1	12	3.00	12	4.80	12	6.00	12	9.00
2	24	6.00	24	9.60	24	12.00	24	18.00
3	36	9.00	36	14.40	36	18.00	36	27.00
4	48	12.00	48	19.20	48	24.00	48	36.00
5	72	18.00	72	28.80	72	36.00	72	54.00
6	96	24.00	96	38.40	96	48.00	96	72.00

3.7.1 Pile Geometry

A relatively wide geometric range was examined in order to gain better understanding of the failure mechanism of the soil surrounding the pile. Piles with diameter (B) starting from 0.25 m. up to 0.75 m, length (D) from 3.0 m up to 72 m and slenderness ratios (D/B) of 12 to 96 were used. The testing program consisted of 6 groups. Each group included 4 series, each series with one constant diameter and six different slenderness ratios (see table 3.4). Twenty four meshes were used, with 299 elements and 336 nodes for each mesh. Table 3.5 summarizes the dimensions and boundary conditions of these meshes, and Figure 3.2 shows the distribution of the element system used in the design of these meshes.

3.7.2 Soil Type

Three types of sand deposits were tested, loose, dense and medium-dense sand. Tables 3.6 & 3.7 give the soil and the slip element parameters used in the present study with relevant references. The slip element parameters were determined based on the adjacent soil properties (as recommended by the CRISP manual). The initial coefficient of earth pressure was considered as a parameter in this study. In all cases a value of the Coefficient of earth pressure at rest K_o for normally consolidated sand was the initial insitu value used for all pile load tests, based on the following relationship:

$$K_o = 1\text{-}\sin \phi$$

Table 3.6 Soil Parameters Employed in Parametric Study

Soil Type	Dry Unit Weight (After Das, 1995) γ_s (t/m^3)	Angel of Shearing Resistance (After Das, 1995) ϕ (Degrees)	Average Modulus of Elasticity (After Poulus, 1971) E_s (t/m^2)	Poisson's Ratio (After Das, 1995) ν_s
Loose Sand	1.65	25^o - 30^o	175	0.25
Medium Dense Sand	1.75	31^o- 37^o	350	0.33
Dense Sand	1.9	38^o - 45^o	700	0.42

3.7.3 Sensitivity Analysis of Finite Element Parameters

In order to investigate the influence of the different parameters, used in the present numerical

Table 3.5 Testing Program And Finite Element Meshes Used in Parametric Study (See Figure 3.2)

Mesh No.	Pile Diameter B (m)	Pile Depth D (m)	Selenderness Ratio D/B	Total Mesh Height L(m)	Vertical Height L_1(m)	Total Horizontal Width H(m)	Refinement zone dimensions	
							a (m)	b (m)
1	0.25	3.00	12	7.55	4.50	10.00	1.50	2.00
2	0.25	6.00	24	15.0	9.0	10.00	3.00	3.00
3	0.25	9.00	36	22.50	13.50	10.00	4.50	4.50
4	0.25	12.00	48	30.00	18.00	10.00	6.00	6.00
5	0.25	18.00	72	45.00	27.00	12.00	9.00	6.00
6	0.25	24.00	96	60.00	36.00	12.00	12.00	6.00
7	0.40	4.80	12	12.00	7.20	16.00	3.5	4.0
8	0.40	9.60	24	24.60	15.00	16.00	5.0	6.0
9	0.40	14.40	36	36.40	22.00	18.00	8.0	8.0
10	0.40	19.20	48	49.20	30.00	20.00	10.0	12.0
11	0.40	28.80	72	72.80	44.00	20.00	15.0	12.0
12	0.40	38.40	96	96.40	58.00	25.00	20.0	15.0
13	0.50	6.00	12	15.00	9.00	20.00	3.0	5.0
14	0.50	12.00	24	30.00	18.00	20.00	6.0	7.0
15	0.50	18.00	36	46.00	28.00	20.00	10.0	9.0
16	0.50	24.00	48	60.00	36.00	25.00	12.0	12.0
17	0.50	36.00	72	90.00	54.00	30.00	18.0	18.0
18	0.50	48.00	96	120.00	72.00	35.00	24.0	18.0
19	0.75	9.00	12	23.00	14.00	30.00	5.0	10.0
20	0.75	18.00	24	46.00	28.00	30.00	10.0	10.0
21	0.75	27.00	36	67.00	40.00	35.00	13.0	15.0
22	0.75	36.00	48	90.00	54.00	35.00	18.0	18.0
23	0.75	54.00	72	135.00	81.00	40.00	27.0	20.0
24	0.75	72.00	96	180.00	108.00	40.00	36.0	25.0

model, on the determined ultimate bearing capacity of a single pile in sand, the following parameters were examined:

a-Modulus of Elasticity "E" and Poisson's ratio "ν" of sand.

b- Angle of shearing resistance of the sand ϕ.

c- Slip element parameters: K_n, $K_s(G)$, K_{sres} & δ (theses parameters are defined in Table 3.7).

d- Coefficient of earth pressure at rest, K_o.

To carry out the sensitivity analysis, only one pile with diameter B = 0.40 m, depth D = 14.4 m and slenderness ratio D/B = 36 was used. Each parameter was subjected to change while other parameters remained constant at an intermediate values.

Table 3.7 Slip Element Parameters Employed in the Parametric Study

Soil Type	$K_n=E(1-\nu)/(1+\nu)*(1-2\nu)$ (t/m^2)	$K_s = G = E/2(1+\nu)$ (t/m^2)	K_{sres} = (0.01 to 0.001) (K_s) (t/m^2)	$\delta = \phi$ (Degrees)	Slip element thickness "t" (cm)
Loose Sand	210	70	1.00	25-30	2.0
Medium Dense Sand	519	132	1.32	31°- 37°	2.0
Dense Sand	1787	247	2.47	38° - 45°	2.0

3.7.3.1 Effect of Modulus of Elasticity "E" and Poisson's Ratio "ν"of Sand

Three values of modulus of Elasticity of sand "E" were employed to examine the sensitivity of this parameter on the determined bearing capacity; these values are 175, 350 & 700 ton/m^2. As expected, the bearing capacity of a pile increases due to the increase of the modulus value, while the associated settlement decreases (the results are shown in Figure 3.8). An average value of "E" for each sand density will be assigned; these values are given in Table 3.6. With

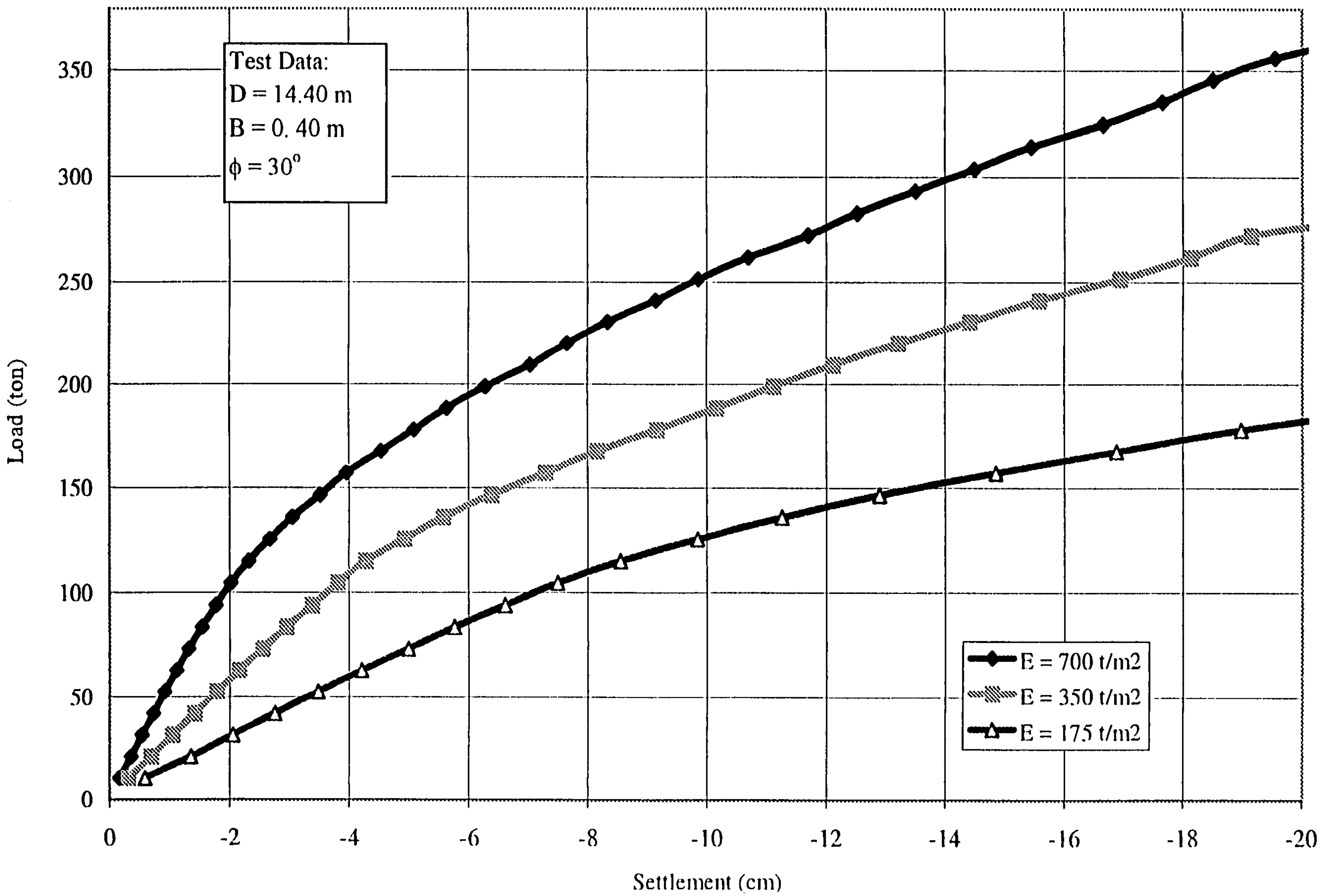

Figure 3.8 Effect of Modulus of Elasticity "E"

respect to effect of Poisson's ratio of sand "v", a three values of "v" were used. These values are: 0.25, 0.3 & 0.4, it can be noted that there is no significant change in the settlement and the bearing capacity due to change of "v". The results are shown in Figure 3.9.

3.7.3.2 Effect of Angle of Shearing Resistance "ϕ"

In order to examine the sensitivity of the angle of shearing resistance "ϕ" on the predicted bearing capacity, three values were used in this analysis: 30°, 35°, 38°. It was found that, as reported in the literature, the bearing capacity of a single pile in sand increases due to an increase of the angle of shearing resistance "ϕ". Figure 3.10 displays the results.

3.7.3.3 Effect of Slip Element Parameters K_n, K_s(G), K_{sres} & δ.

The theoretical relationships of each slip element parameter were given in table 3.7. For the parameter K_n, three values were employed to verify its sensitivity to the determined bearing capacity: 200, 520 & 750 t/m^2. Figure 3.11 shows these results. It can be noted that the effect of K_n on the bearing capacity of the pile is minor and can reasonably be neglected.

The parameter K_s was examined using the following values: 130, 300 & 500 t/m^2. The results are shown in Figure 3.12. It can be noted that K_s has no effect before the ultimate point (the point at maximum curvature), beyond which there was little or no change in load capacity behavior. The same trend was found in examining K_{sres}; the results are shown in Figure 3.13. Based on the above, the values for slip element parameters, K_s, K_{sres} & K_n should be assigned average values which are recommended in the program manual. These values depend on the adjacent soil properties, and are given in Table 3.7.

To examine the effect of angle of friction between the pile and sand"δ", three values were

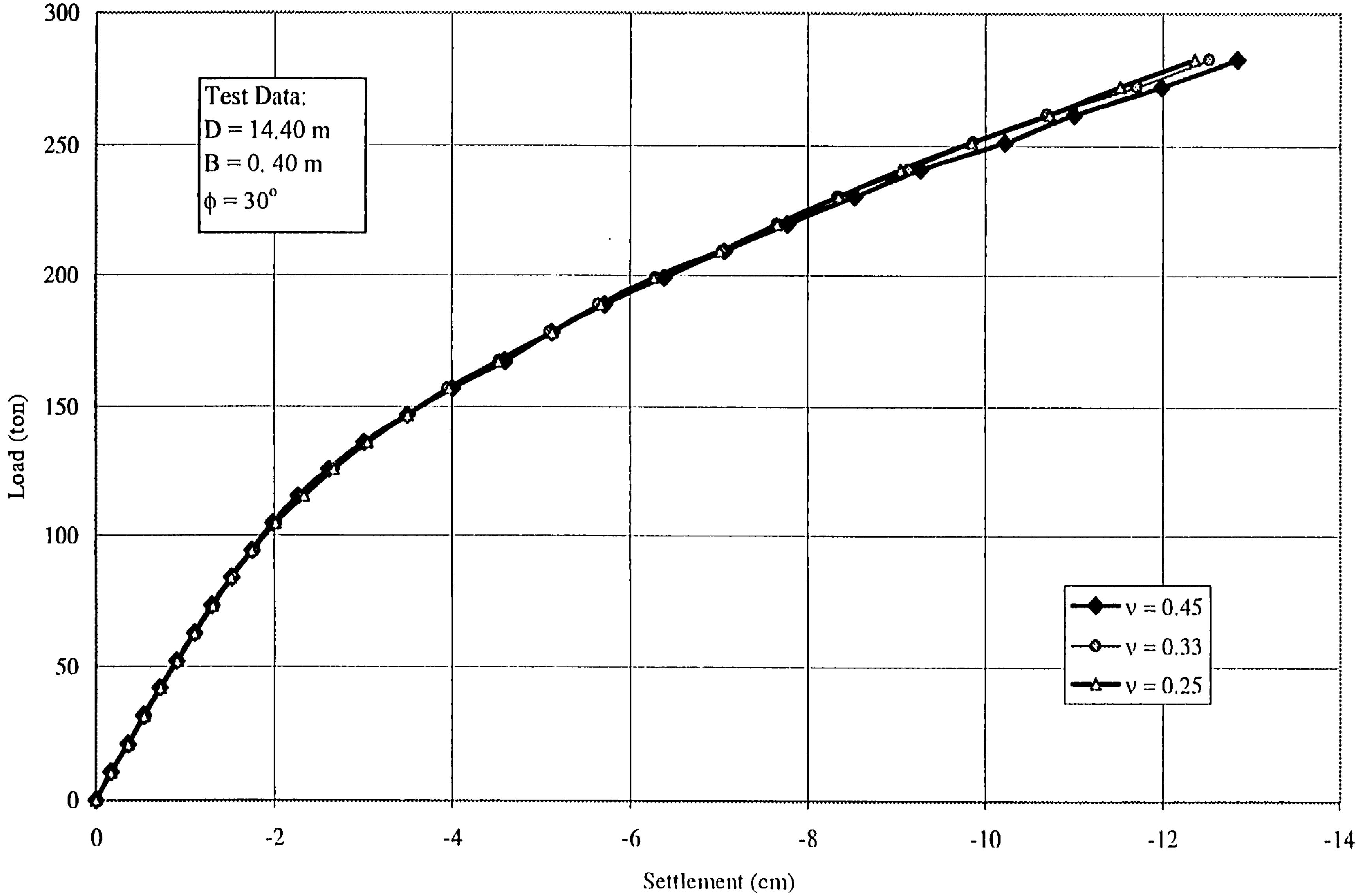

Figure 3. 9 Effect of Poisson's Ratio "ν"

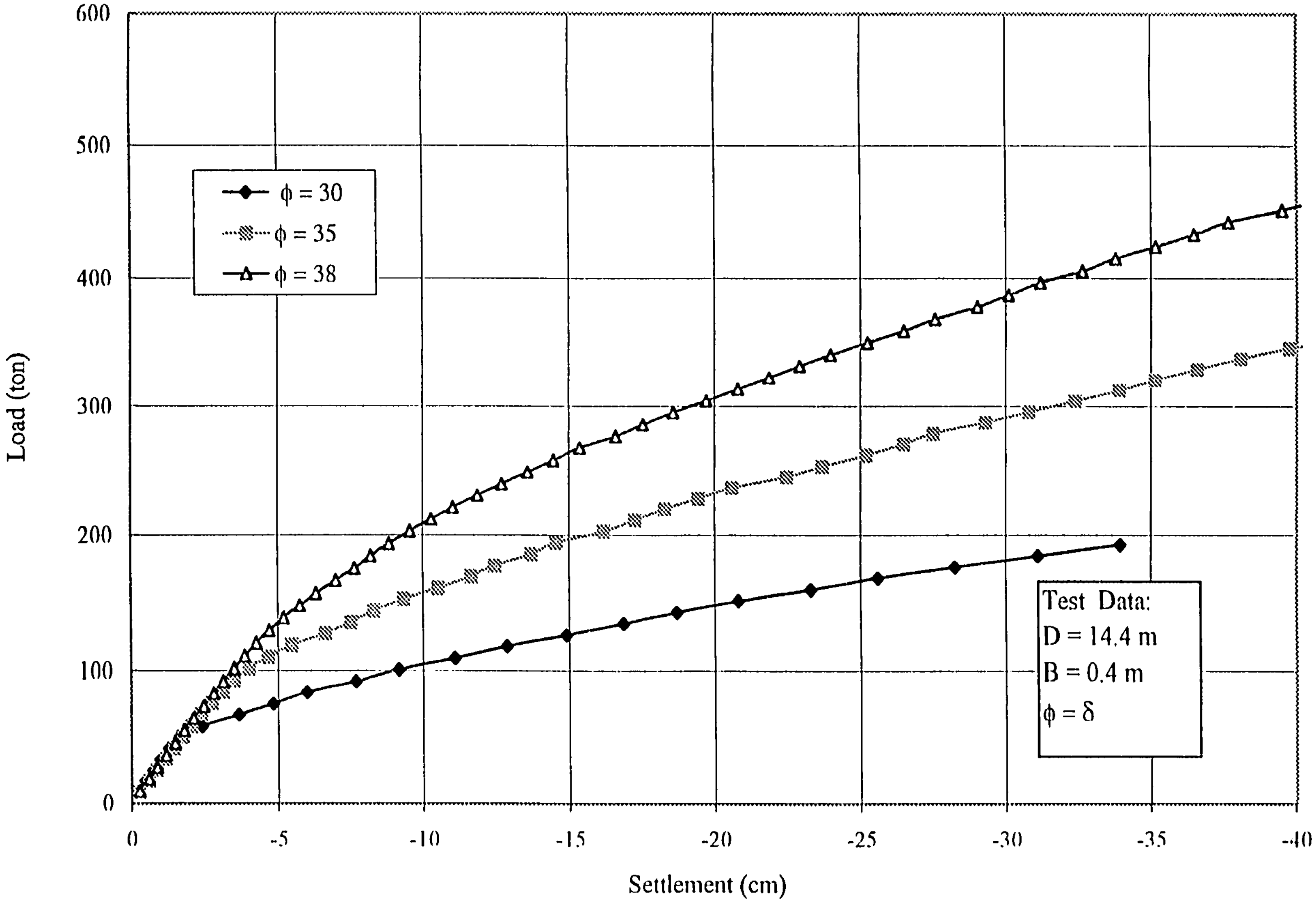

Figure 3.10 Effect of Angle of Shearing Resistance of Sand "ϕ"

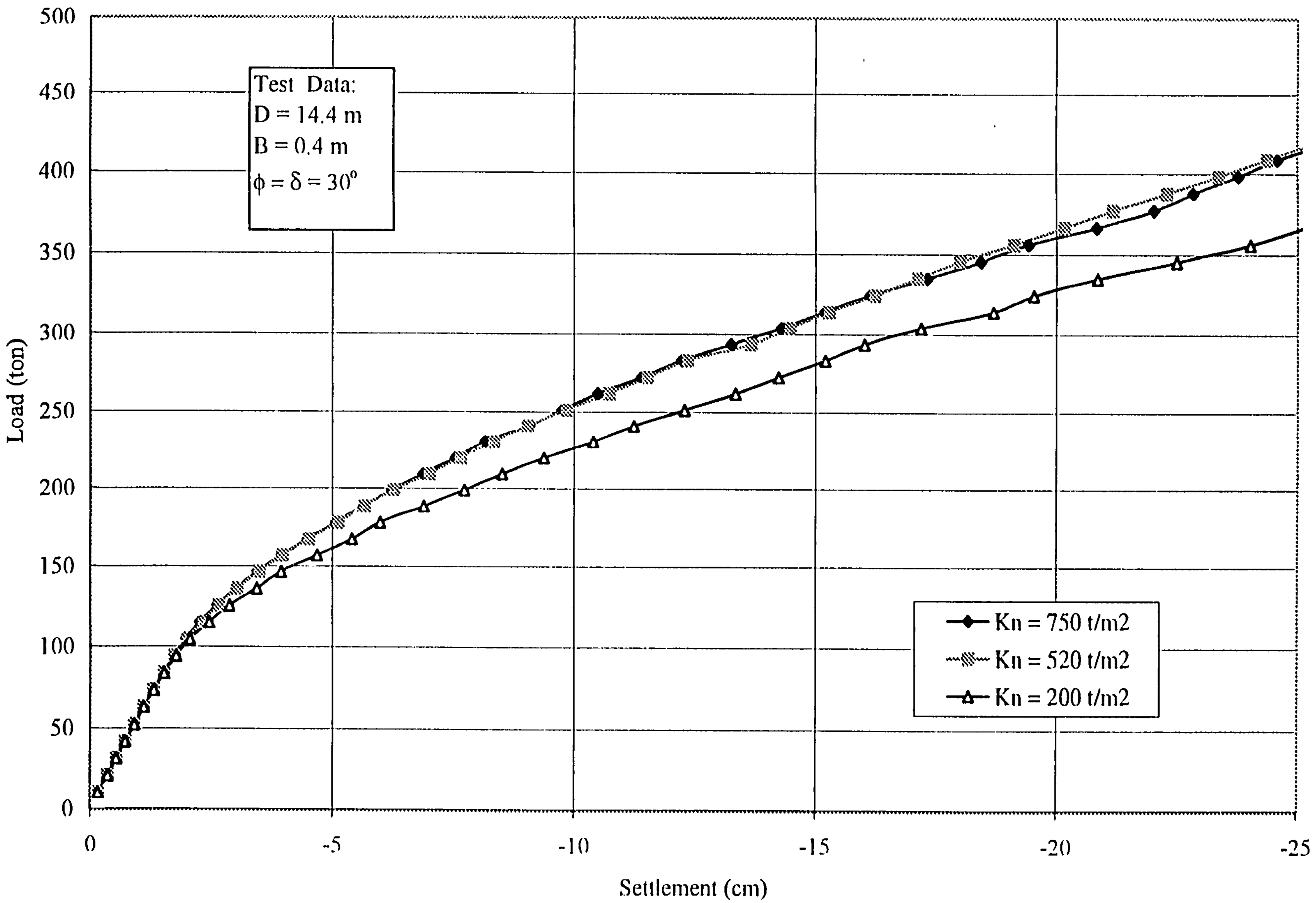

Figure 3.11 Sensitivity Analysis for Slip Element Parameter K_n

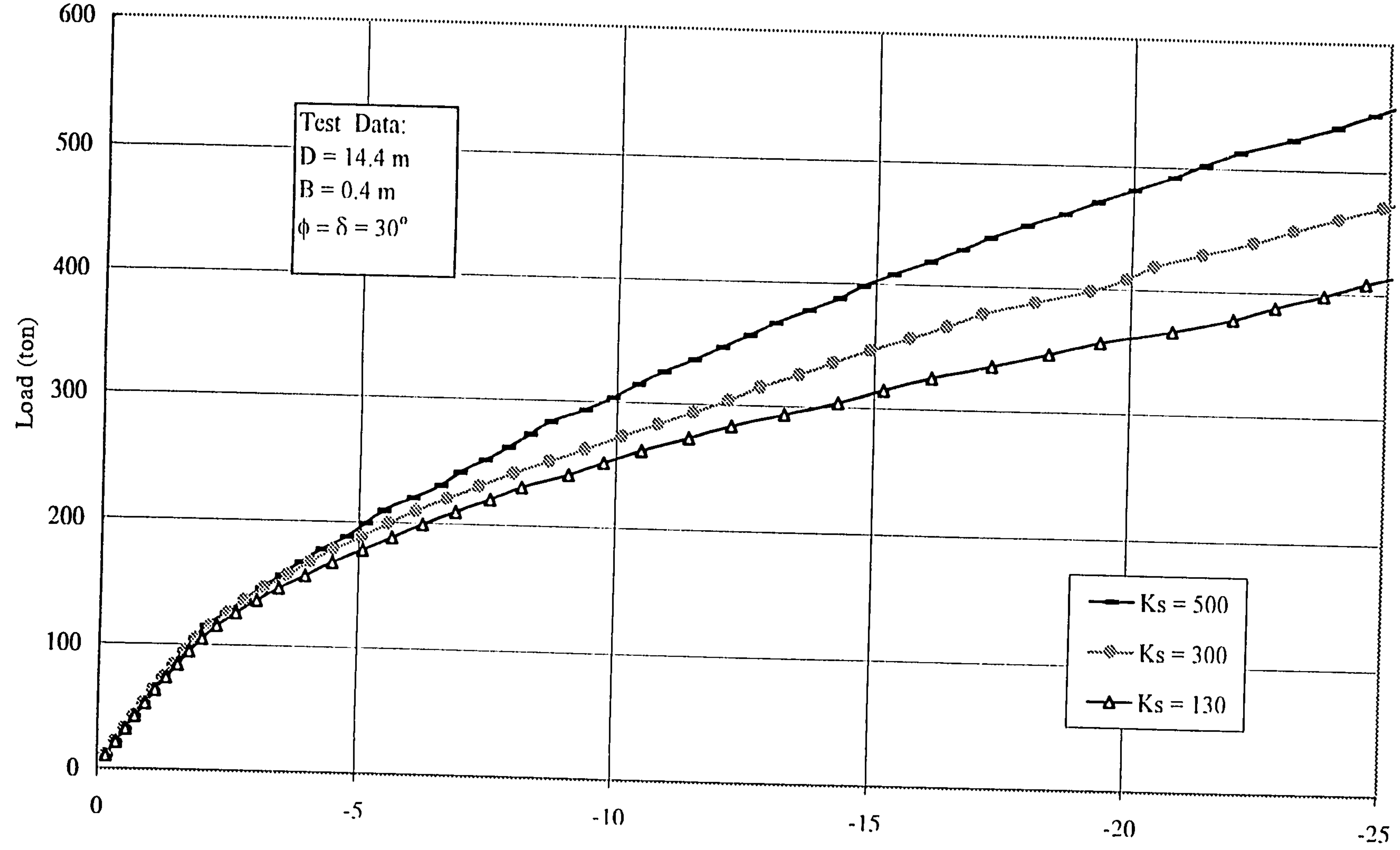

Figure 3.12 Sensitivity Analysis for Slip Element Parameter K_s

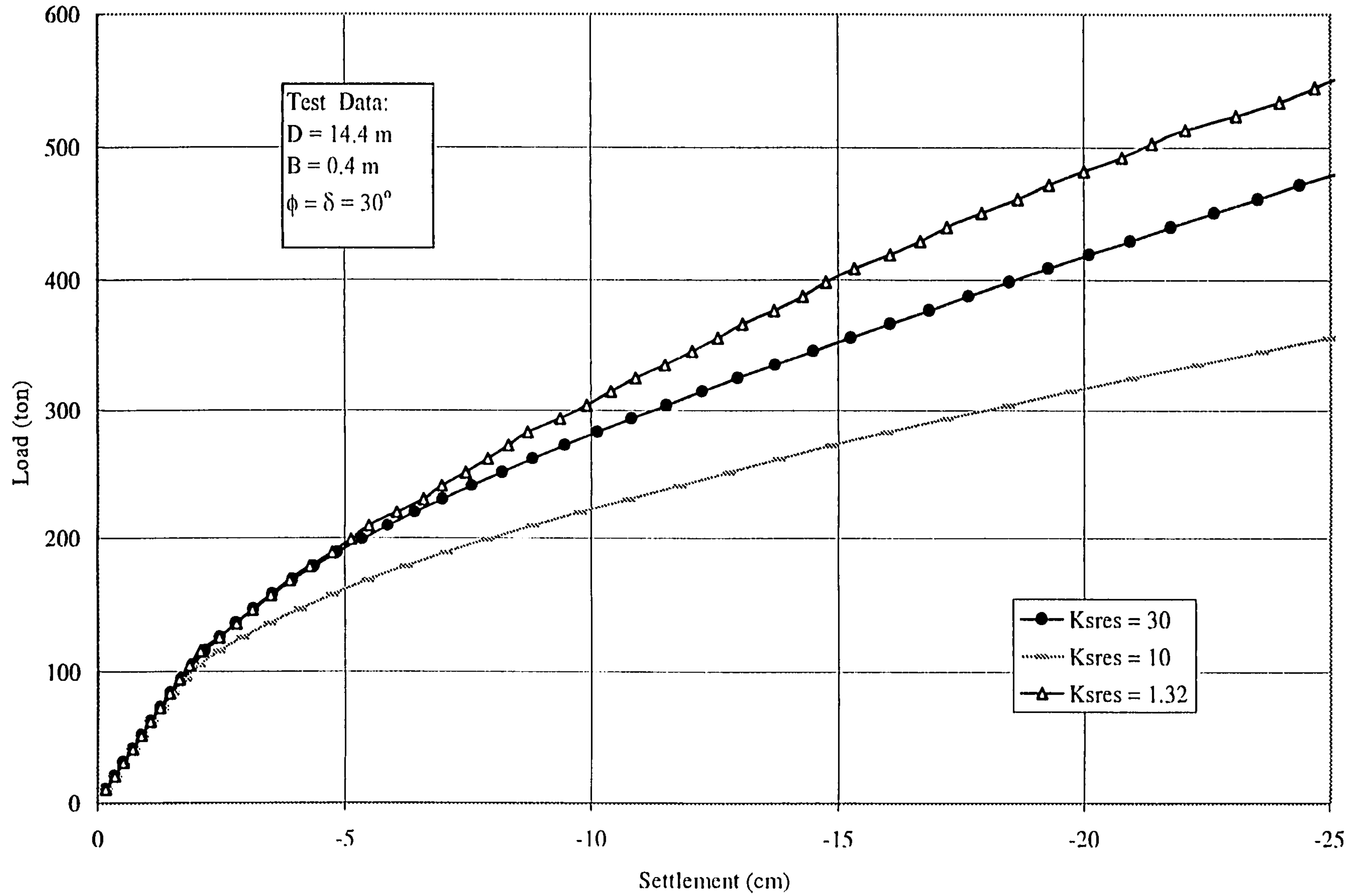

Figure 3.13 Sensitivity Analysis for Slip Element Parameter K_{sres}

used: δ/ϕ = 0.5, 0.7 & 1.0. Results are displayed in Figure 3.14. It can be noted that the bearing capacity and settlement increase with an increase of the angle "δ". Therefore the angle of friction between pile and sand "δ" will be considered as a parameter in the present investigation because it depends on the pile material and varies depending on the sand properties.

3.7.3.4 Effect of Initial Coefficient of Earth Pressure "K_i"

In order to investigate the importance of the coefficient of earth pressure in the present study, the coefficient of earth pressure "K_i" is assigned theses values: K_o, 4 K_o & 8K_o. It was found that the ultimate bearing capacity increases with an increase of the initial value of "K_i" (see Figure 3.15). Accordingly the intial value of K_i must be incorporated in determining the bearing capacity of a single pile.

3.7.3.5 Summary

Based on the sensitivity analysis conducted above, it can be concluded that the parameters affect the determination of the bearing capacity of a single pile in sand and, accordingly, will be considered in the present study:

a- Initial coefficient of earth pressure "K_i".

b- Angle of shearing resistance of the sand "ϕ".

c- Angle of friction between the pile material and the sand "δ".

3.8 Test Results

The following are the desired results of the numerical model developed in this investigation:

1- Load settlement curves for the skin, the tip and the total loads on the pile.

2- Incremental plot for the contour lines for factor of safety against shear failure.

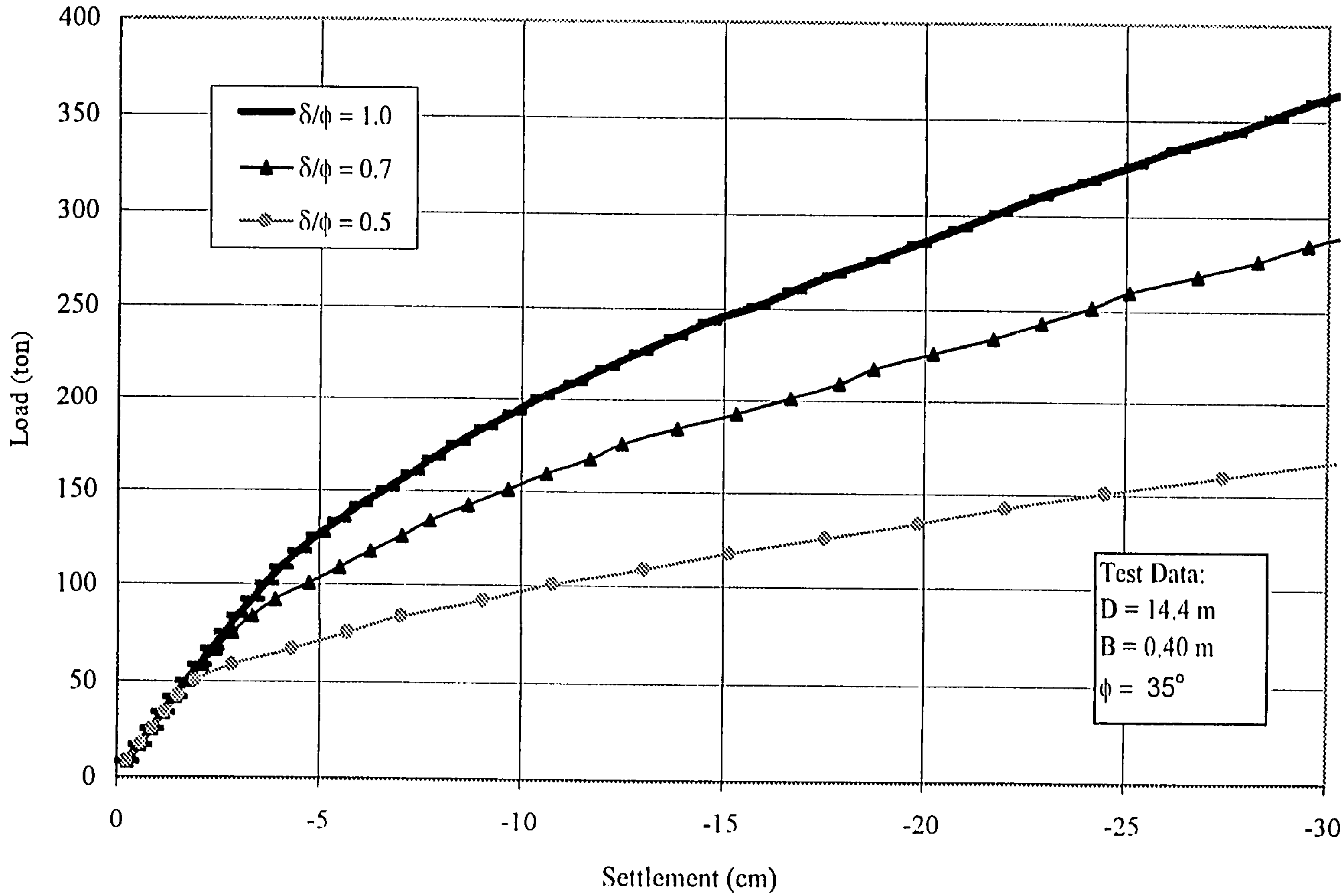

Figure 3.14 Effect of Angle of Friction Between Pile and Sand "δ"

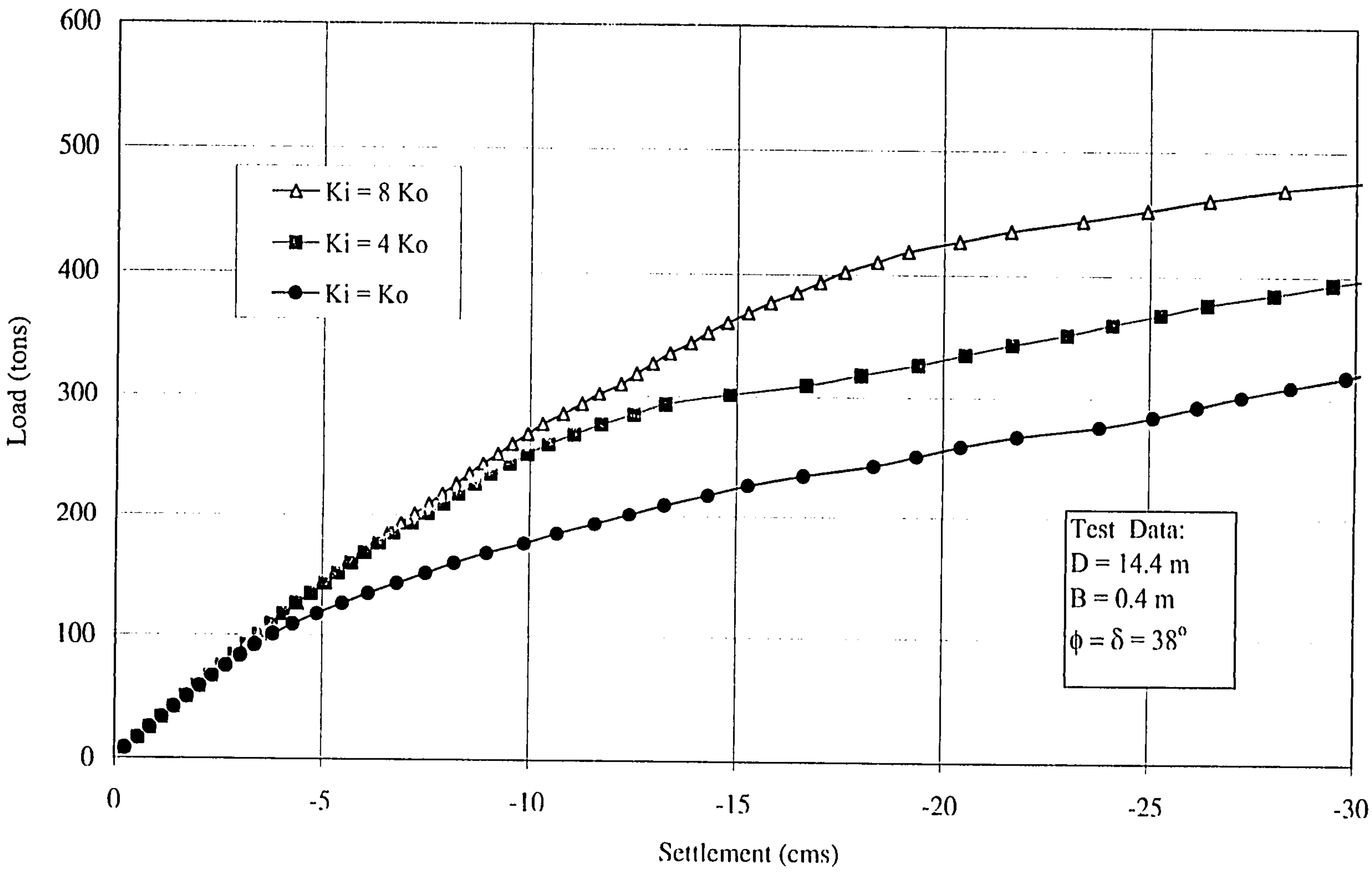

Figure 3.15 Effect of the Initial Coefficient of Earth Pressure "K_i"

3- Incremental plots for the progress of failed elements around the pile shaft.

4- incremental development of the shear stresses τ_{xy}., vertical stresses σ_y and horizontal stresses σ_x acting on the pile shaft:

5 - Incremental development of the coefficient of earth pressure acting on the pile shaft K_s.

These results will assist in determining the failure mechanism around the pile. The plots of τ_{xy}, σ_x ,σ_y & K_s are determined for the vertical and horizontal sections shown in Figure 3.16.

3.8.1 Typical Results for Pile Test

Due to the massive graphical results deduced from the finite element analysis and the relatively large number of tests performed in this investigation, typical results for load test will be introduced in this section for demonstration purposes. The load test was carried out for the pile diameter of (B = 0.25 m) and length (D = 12 m), i/e (D/B = 48); $\phi = \delta = 30^{o}$. A total stress of 2500 t/m^2 was applied into the pile cross section over a 60 increments; i.e. 41.67 t/m^2 per increment. The test was performed up to the failure point (the point of maximum curvature). where the stress at failure was 1042.02 t/m^2 which is equal to an ultimate load of 51.15 tons. Figure 3.17 shows the load-deformation relationship for this test. From this Figure 3.17, it can be noted that:

The ultimate load = 51.15 (tons), Skin ultimate resistance = 11.84(tons), Tip ultimate resistance = 39.31(tons) and the settlement at failure = 2.932 cm which took place at increment number 24. It should be mentioned here that total load was determined from the accumulation of the external applied load. The skin resistance is determined by integration of the local shear stresses (τ_{xy}) acting along the pile shaft at the point of failure, and tip resistance is equal to total load minus skin load. The settlement at failure is close enough to the limit of 10% of pile

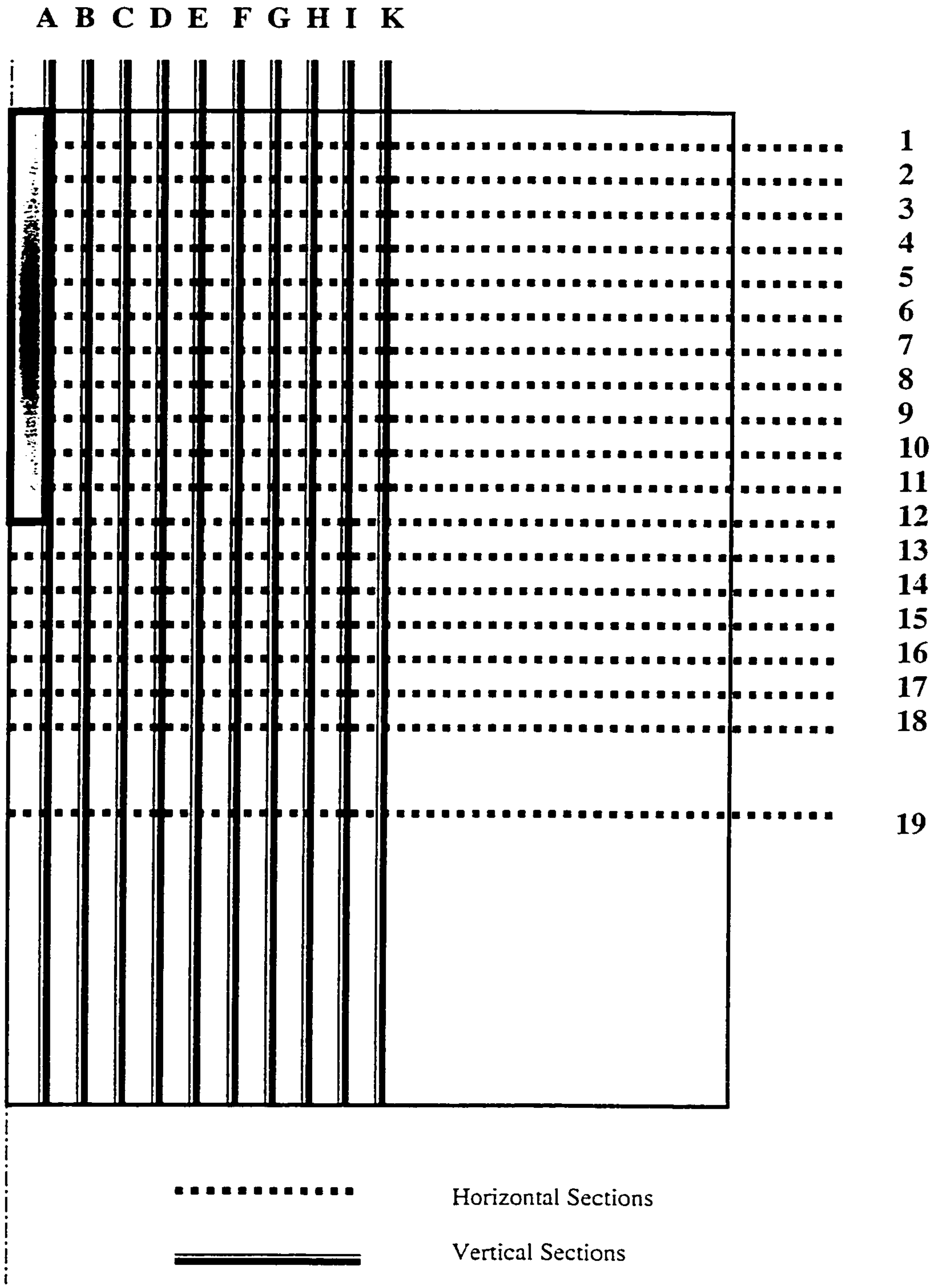

Figure 3. 16 Schematic View of the Locations of the Vertical and Horizontal Sections

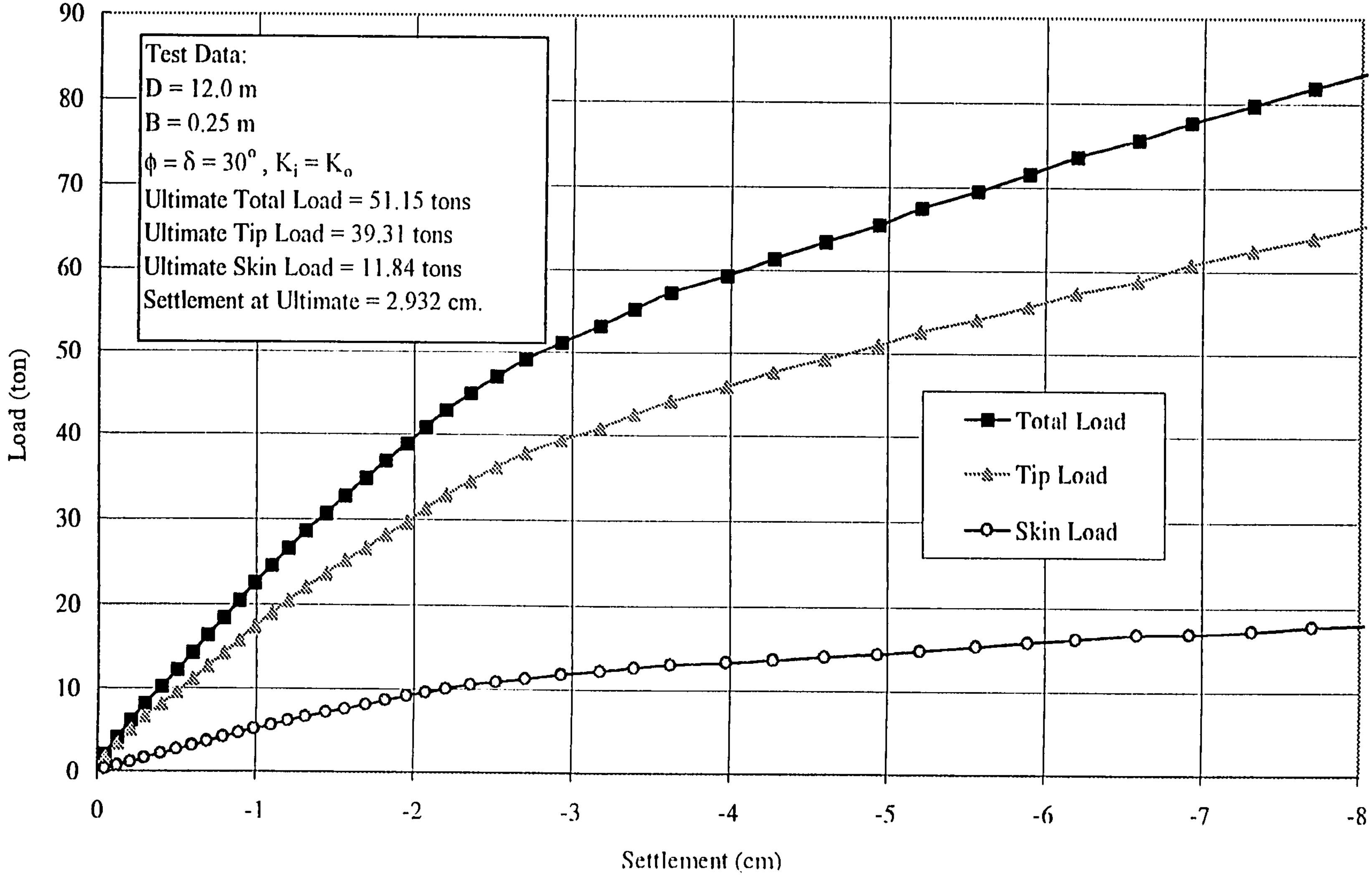

Figure 3.17 Load Settlement Relationship

diameter (2.5 cm) and does not exceed the value recommended by the "Canadian Foundation Engineering Manual, 1992".

3.8.2 Development of Horizontal Stresses (σ_x)

Confinement pressure is one of the major factors affecting the bearing capacity of a single pile in sand. It is responsible for a major part of the mobilized skin resistance on the pile shaft. In order to investigate the development of the horizontal stresses on the pile shaft, an incremental mobilization is introduced. The horizontal stresses at each increment were determined individually and the results are shown in Figure 3.18 for the vertical section located immediately adjacent to the pile shaft. It can be seen from this Figure (3.18), that the horizontal stress σ_x developed on the shaft, comparing with its determined value from overburden ($K_o*\sigma_y$), exhibits higher values at the zone below ground surface. This increase was found to be linear with a value of zero at the ground surface. While lower values of σ_x was found at the zone around tip. Furthermore, at the failure load, between these two zones the distribution of σ_x is almost equal to overburden value and linearly distributed. This trend can be identified by the following three zones:

a- Zone I: immediately beneath ground surface;

σ_x exhibited a noticeable increase beneath the ground level, which decreases with depth, up to the normal linear distribution at an approximate depth of 0.25 D. This can be attributed pile installation and ground subsidence which takes place around the pile. At a greater depth, the level of confinement increases which in return minimizing the possibility of horizontal movements around the shaft. This should explain the high level of shear mobilization within the upper zone.

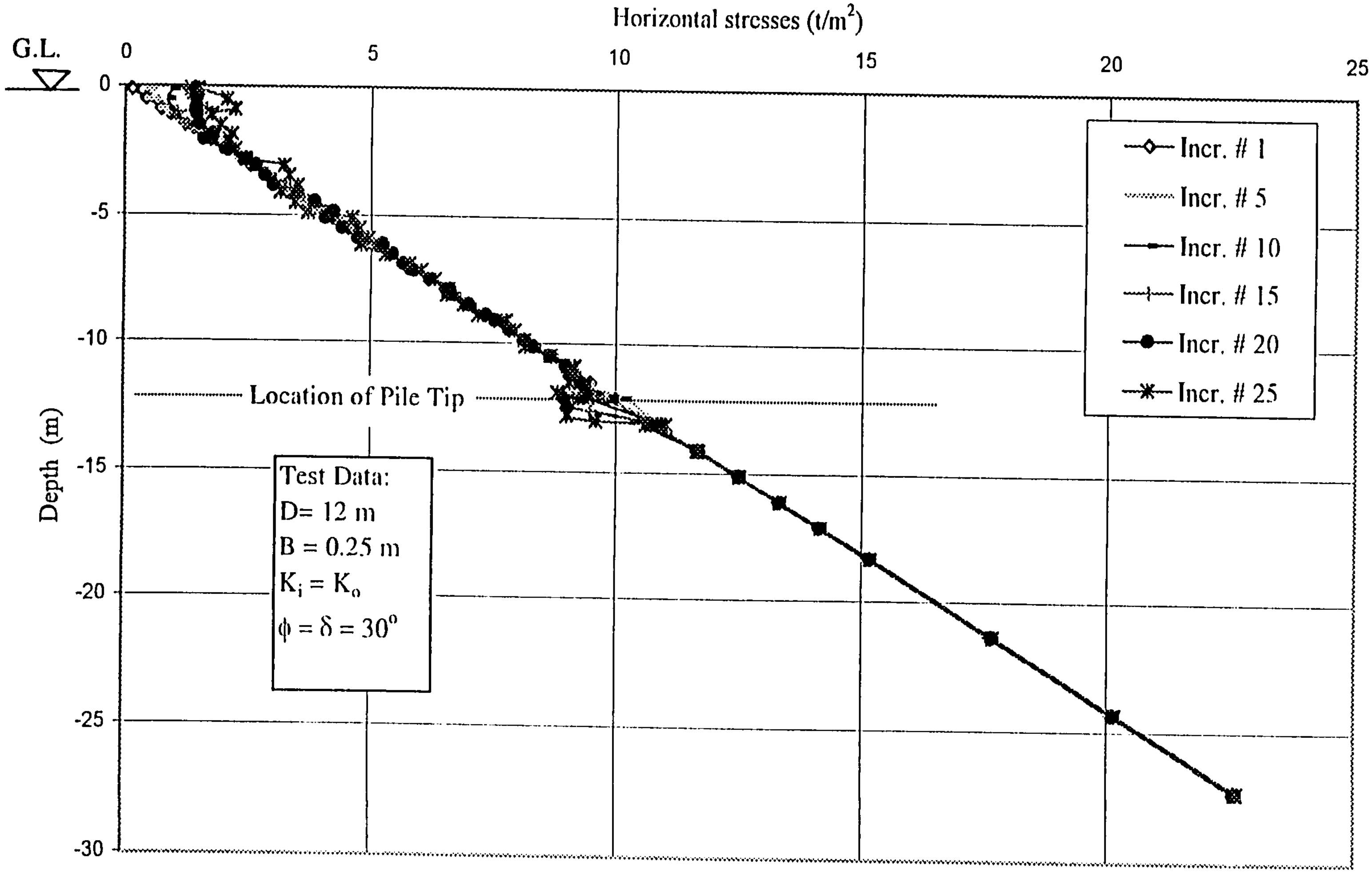

Figure 3.18 Development of Horizontal Stresses along Vertical sec. # 1
(located on pile shaft)

b- Zone II: located adjacent to pile tip;

σ_x decreased than the calculated linear magnitude ($K^*\sigma_y$) in this zone by about 20%; this is can be attributed to the advanced pile tip that crushs the soil particles, changing soil strength and coefficient of earth pressure in this area. Pushing soil particles aside to open for the shaft to penetrate the soil mass, causes an active earth pressure condition and a noticeable decrease in the σ_x value.

Figure 3.19 shows the developed horizontal stresses, at failure, over different vertical sections located horizontally at distances measured from the pile axis of symmetry. Figure 3.20 shows the distribution of the developed horizontal stresses, at the failure load, over horizontal sections covering the entire depth of the pile. The general locations of both vertical and horizontal sections are given in Figure 3.16.

Analysis of the developed σ_x over the vertical and the horizontal sections showed the following:

1- In general, the value of σ_x in vicinity of the pile shaft is relatively higher as compared to the values at the same level but far from the pile shaft. This trend is noticeable horizontally up to a distance equal to "R", which is named in this investigation as the radius of influence zone. Also it is noticeable in the vertical direction up to about 0.25 H_l from ground surface (see Figure 3.59 for location of H_l).

2- The decrease of σ_x occurred around the tip, is limited in the horizontal direction of about 5B from the tip, and vertically by distance above the tip level of about 7B, and below the tip level equal to about 6B. This trend provide the base for employing a varied radius of influence over the shaft.

3- At any point inside the soil mass, σ_x has the value of ($K_o^* \sigma_y$), which depends on the over-

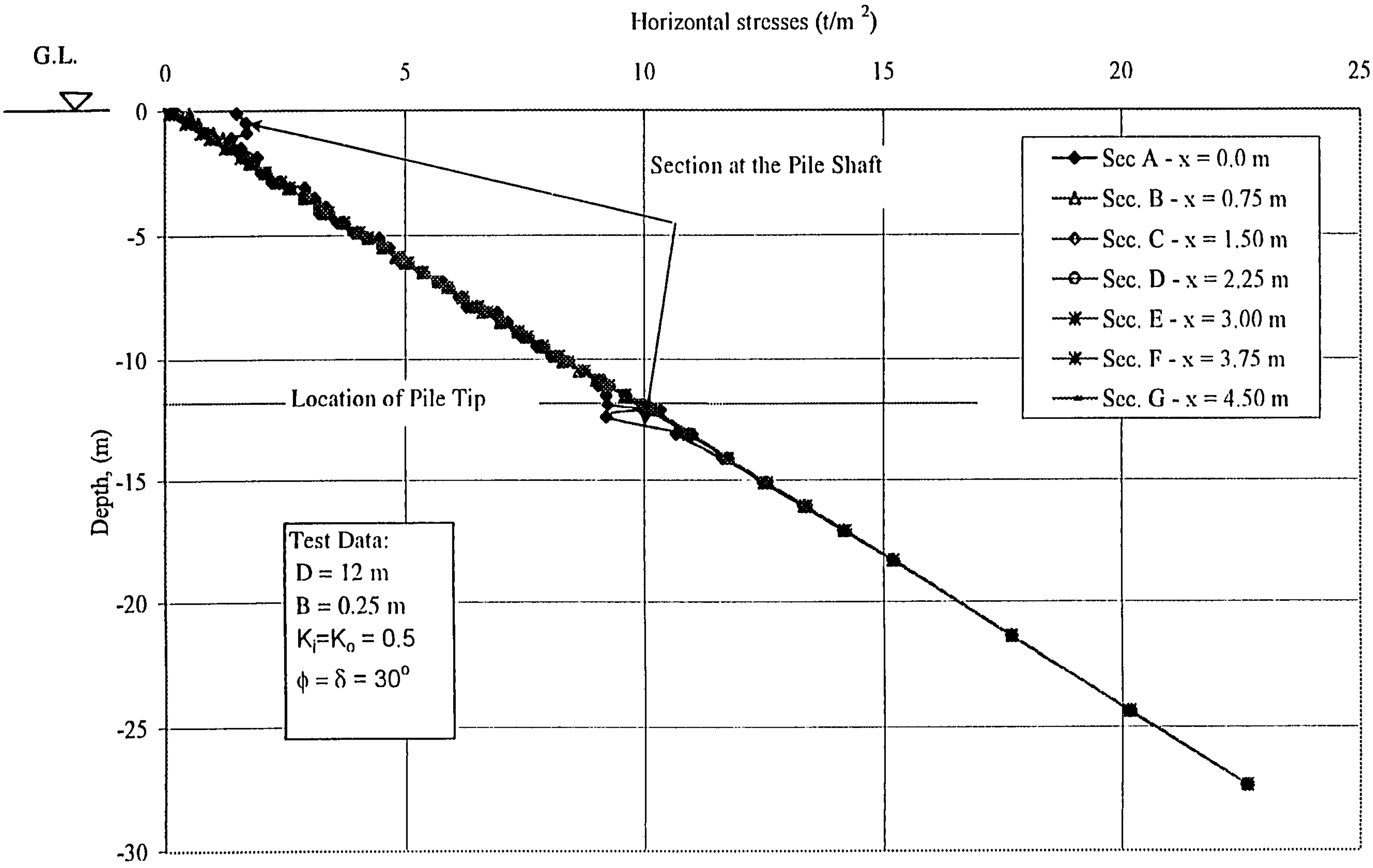

Figure 3.19 Horizontal Stresses Developed at Failure Along Different Vertical Sections Measured Horizontally From Pile Axis

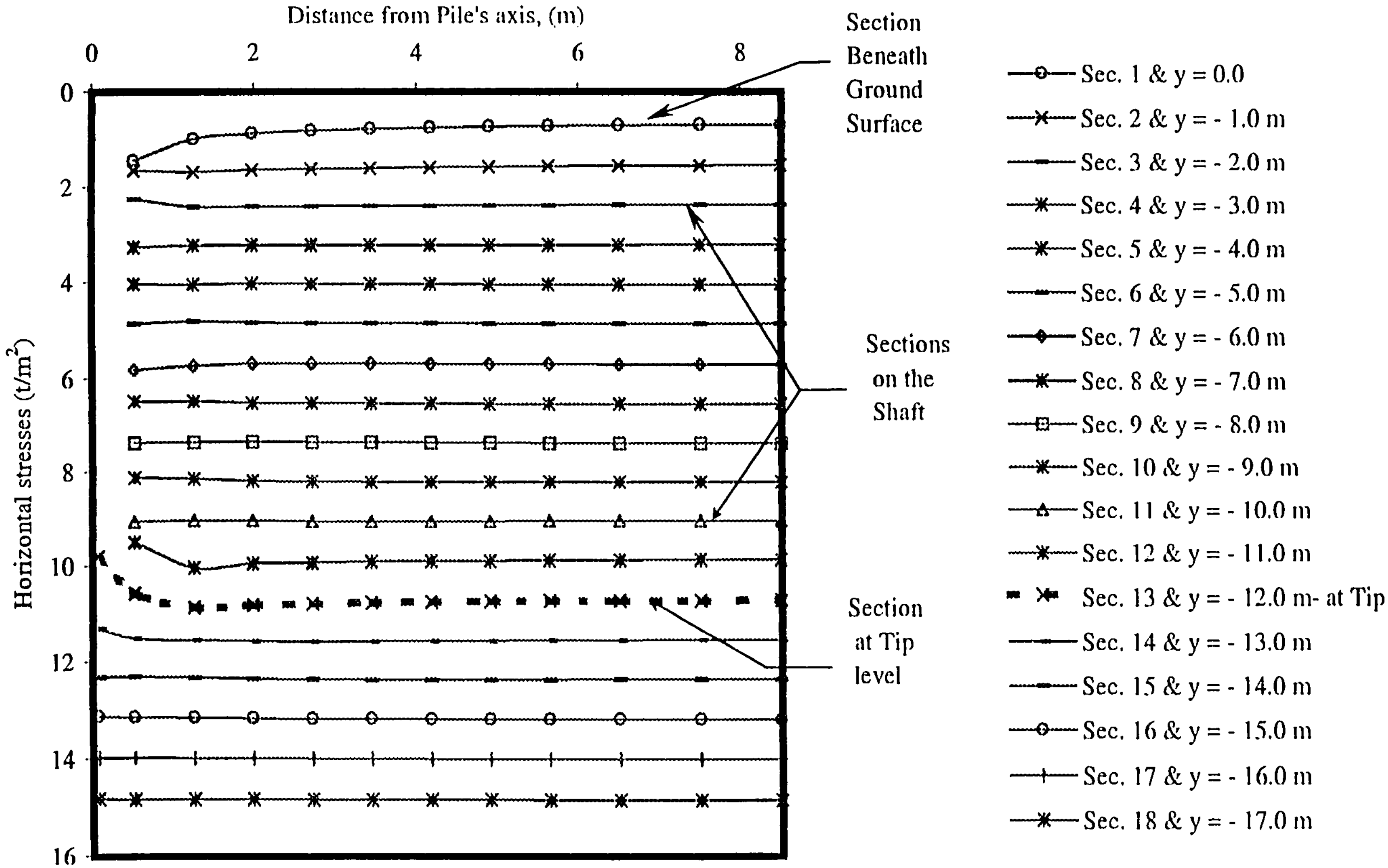

Figure 3.20 Comparison of Horizontal Stresses Developed at Failure Along Horizontal Sections Located at Various Depths. (Test Data: D=12.0 m, B= 0.25 m, $K_i = K_o$, $\phi = \delta = 30^o$)

burden pressure. An exception to this rule was found in the vicinity of the shaft, especially in the forgoing zones. This trend can explains the changes in sand angle of shearing resistance "ϕ" occurred around the shaft.

In order to determine the increase and/or decrease of σ_x acting on the shaft, a relative comparison is presented in Figure 3.21 which introduces the percentage of developed horizontal stresses acting at the shaft related to the insitu horizontal stresses. It should be noted that the meaning of positive sign is that the developed σ_x is higher than the insitu overburden one and vise versa. From Figure 3.21, the behavior of σ_x can be divided into three main trends:

a-Zone I: with a total height of about 0.25 H_l located beneath ground level. In this zone the soil experiences increase of horizontal stresses immediately beneath the ground level and this increase is terminated at a distance equal to the depth of about (0.25 H_l), where σ_x becomes equal to the insitu value.

b- **Zone II**: located near the tip, and having values lesser than the insitu overburden values; this trend can be related to the active pressure condition developed due to the pushing of soil by the shaft tip.

c- **Zone III**: located between zone I and II having σ_x value close to the value of the insitu horizontal component of overburden pressure where σ_x flocculates slightly around the insitu values. This zone can be called the neutralized zone.

Also from Figure 3.21 it can be noted that the developed σ_x just beneath the ground level is higher than any other level along the pile shaft; the percentage of increase is about 120%. This trend should explain the degree of mobilized skin friction beneath ground level, where the highest magnitude of σ_x took place, decreasing with depth. This explains the higher level of

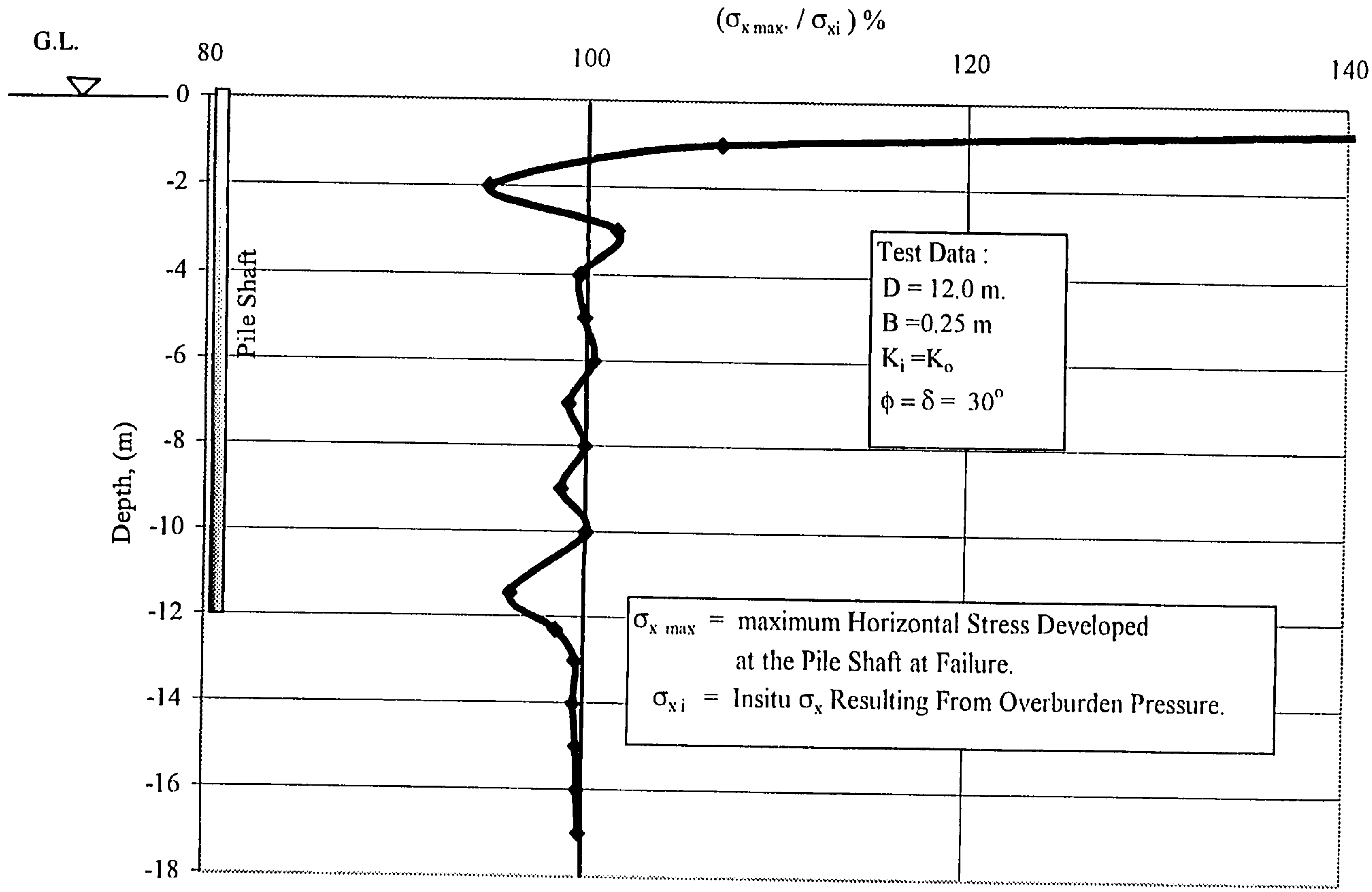

Figure 3.21 Percentage of Developed Horizontal Stresses to Insitu Versus Depth Along Vertical Section of Pile Shaft (at Failure).

skin resistance mobilization in this zone than in any other zone.

In view of the above, the following remarks can be given:

1- The horizontal pressures against the pile shaft are playing a major role in estimating the value of skin resistance.

2- The magnitude of σ_x acting on the shaft differs from one level to another and is not varied linearly as suggested in most of the literature.

3- The maximum value of σ_x acting on the shaft occurred beneath the ground surface and decreased with depth; this explains the higher degree of skin resistance mobilization which took place beneath ground surface and decreased with depth.

4- At the vicinity of the pile tip, the developed horizontal pressure is smaller than the overburden values (the -ve sign in Figure 3.21). This is due to the effect of the tip advancement in the soil, creating an approximately active earth pressure condition at this zone.

It is reasonable to state that the horizontal forces acting on the shaft must be considered in any equilibrium analysis, an additional horizontal force should be taken into account. This force is shown in Figure 3.22 as E_{R1} which resulted from the superposition of the additional horizontal pressure (in a form of triangle) acting on the shaft. It should be noted that this triangle was originally curved with zero value at ground level and it was approximated by a triangle to simplify calculations. This triangle has its base at the ground surface with a horizontal coordinate equal to the following empirical value:

$$C_x = K_s * \gamma * 0.25 * H_l \qquad ...(3.7)$$

Where:

K_s = Coefficient of earth pressure acting on the shaft

γ = Soil unit weight

L_x = Height of the additional pressure triangle = 0.25 * H_1

H_1 = Height of mobilized skin resistance zone measured from ground surface

This triangle will produce the horizontal force E_{R1}

Where:

$$E_{R1} = 1/2\ C_x * (0.25\ H_1) \qquad ...(3.8)$$

and acting horizontally at a distance equal to 2/3 (0.25 H_1) measured from ground surface.

3.8.3 Development of Vertical Stresses (σ_y)

A group of plots for developed vertical stresses over vertical and horizontal sections are introduced in this section. The plots over the vertical section introduces the changes of vertical stresses versus depth, and the plots over the horizontal sections will compare the developed vertical stresses at shaft with the instu values.

Figure 3.23 shows the development of vertical stresses acting on the vertical section located at the pile shaft. It can be seen from this Figure (3.23) that the distribution of vertical stresses over this section is almost linear, except at two zones. The first zone is located immediately beneath the ground surface, which believed to influence the mobilization of the skin resistance up to a depth of about 3B beneath the ground surface. The second zone is located beside the pile tip, where sudden increase in σ_y just beside the tip can be observed, and is believed to result from the mobilization of the tip resistance.

Figure 3.24 introduces a set of plots for the vertical stresses developed on vertical sections at various horizontal distances. This Figure 3.24 shows the following:

1- Distribution of σ_y is almost linear over the shaft, except at two zones:

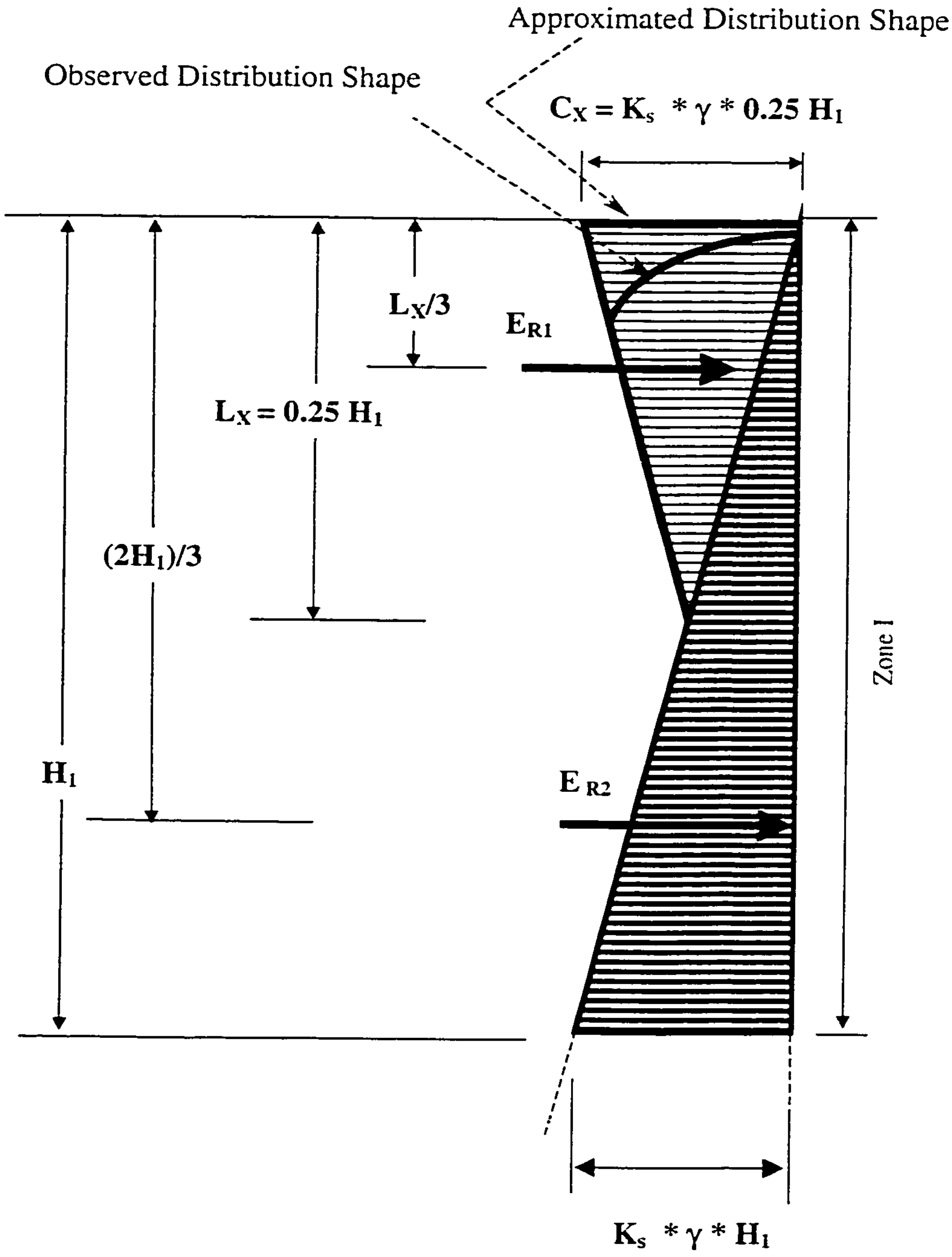

Figure 3.22 Horizontal Forces Acting on the Upper Part of The Shaft (Zone I)

a- immediately (few centimeters) beneath the ground surface where there is an increase of about 41% compared to the insitu value, similar to the trend observed for σ_x values.

b- in the vicinity of the tip, there is another increase, found to be about 26% greater than the insitu values. These observations are shown in Figure 3.25, where the percentage of the developed stress to insitu value of σ_y is plotted for the vertical section located on the shaft.

Figure 3.26 shows the development of σ_y at failure load along horizontal sections measured vertically from the ground surface. The following can be noticed:

1- At any horizontal plane, a higher magnitude of σ_y occurs near the pile shaft and decreases away from the shaft. This could reveal the effect of the influence zone which was evaluated by 5B in the middle of the shaft and 8B in the zone adjacent to the pile tip and beneath the ground surface.

2- Sharp increase in σ_y occurred just at tip level; this is expected due to the pile loading and its advances through the soil mass compressing the soil particles in this zone.

3- At vertical distance about 8B below the tip, the vertical stresses became equal to the insitu stresses. In other words, the influence of pile loading process on the soil mass is terminated at this distance. This may reveal the vertical influence below the pile tip.

In general, at any level within the soil mass $\sigma_y = \gamma * h$, where γ = unit weight of the soil and h is the vertical height above that level. Considering that the vertical level remains unchanged, accordingly, the only change to take place is the soil unit weight. This may explains densification process of sand which took place around the tip.

3.8.4 Development of Earth Pressure Acting on the Pile Shaft

In the literature, the distribution of earth pressure acting on the pile shaft is assumed to act

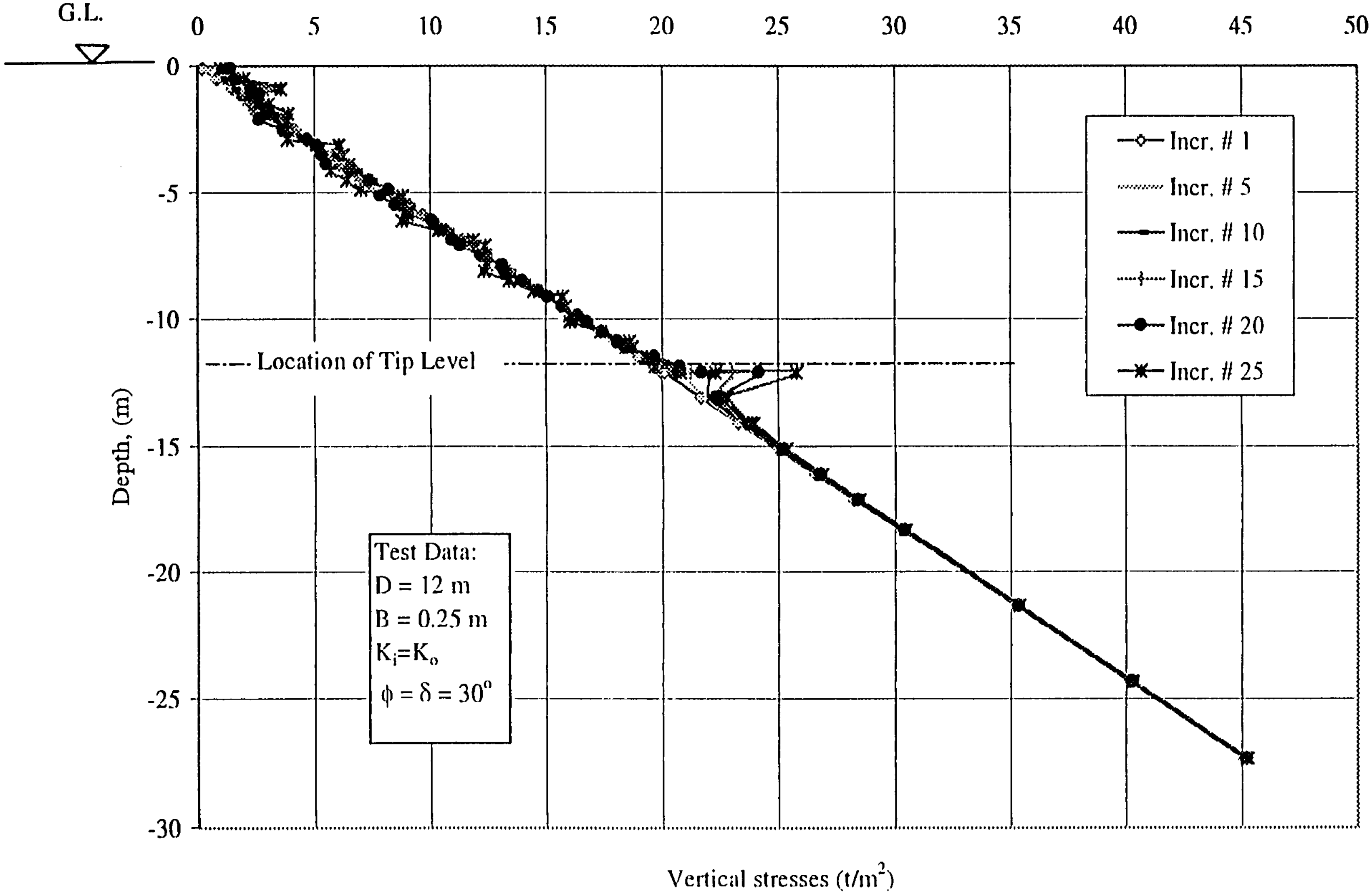

Figure 3.23 Development of Vertical Stresses at Vertical Section
(Located at Pile Shaft)

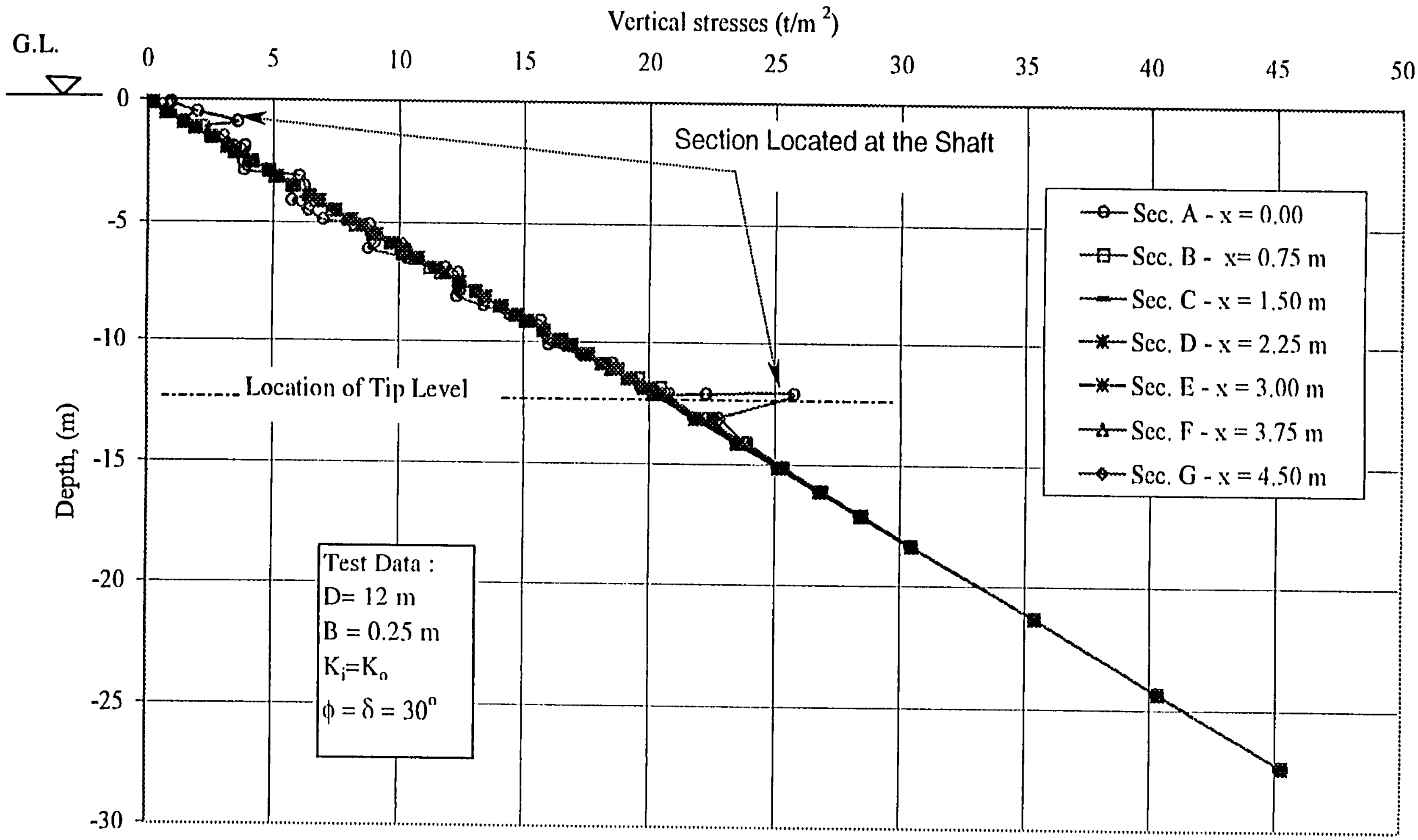

Figure 3.24 Comparison of Vertical Stresses Developed at Failure Along Different Vertical Sections Measured Horizontally From the Pile Axis

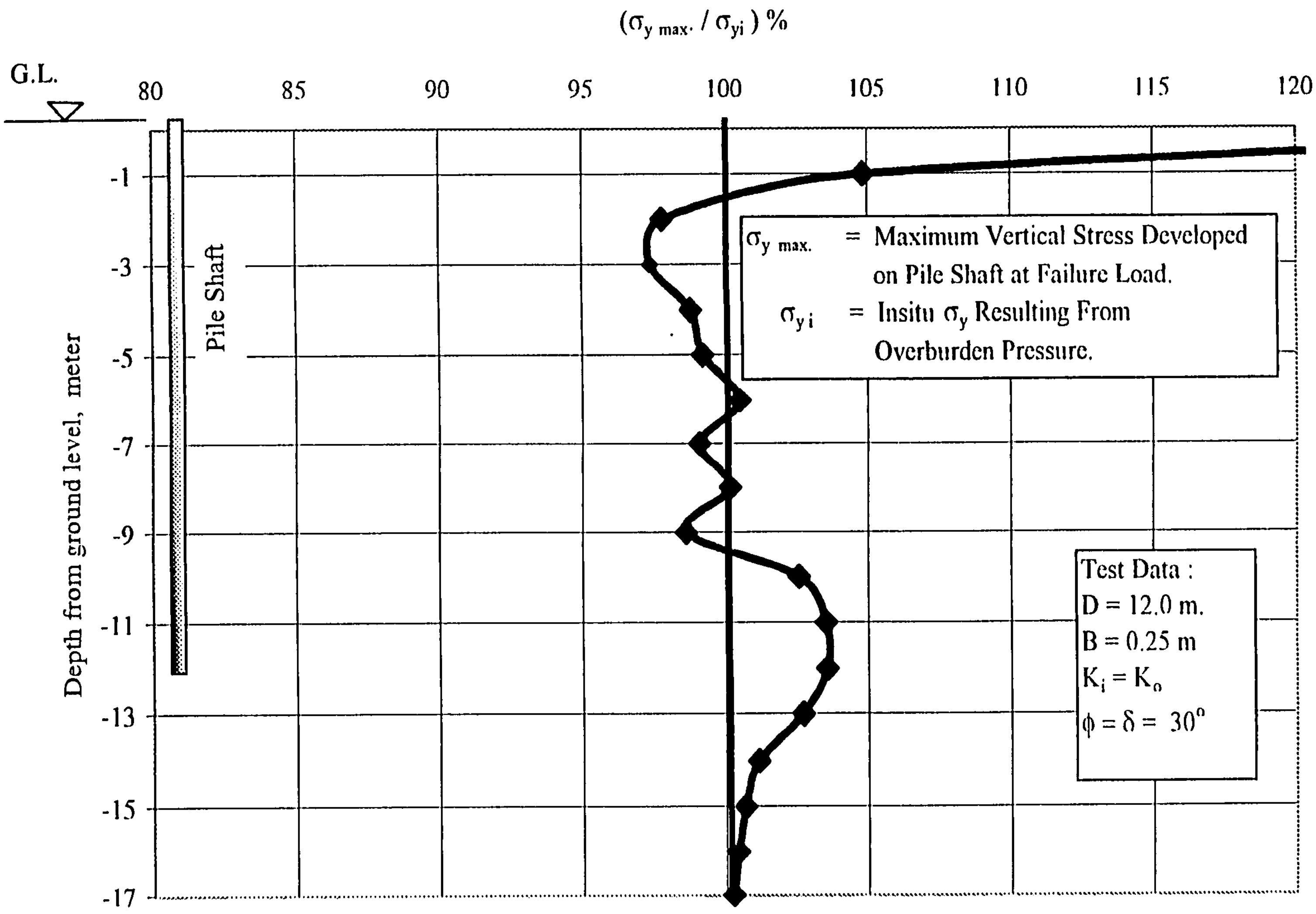

Figure 3.25 Percentage of developed (at Failure) to Insitu Vertical Stresses Versus Depth Along Vertical Section Located at the Pile Shaft

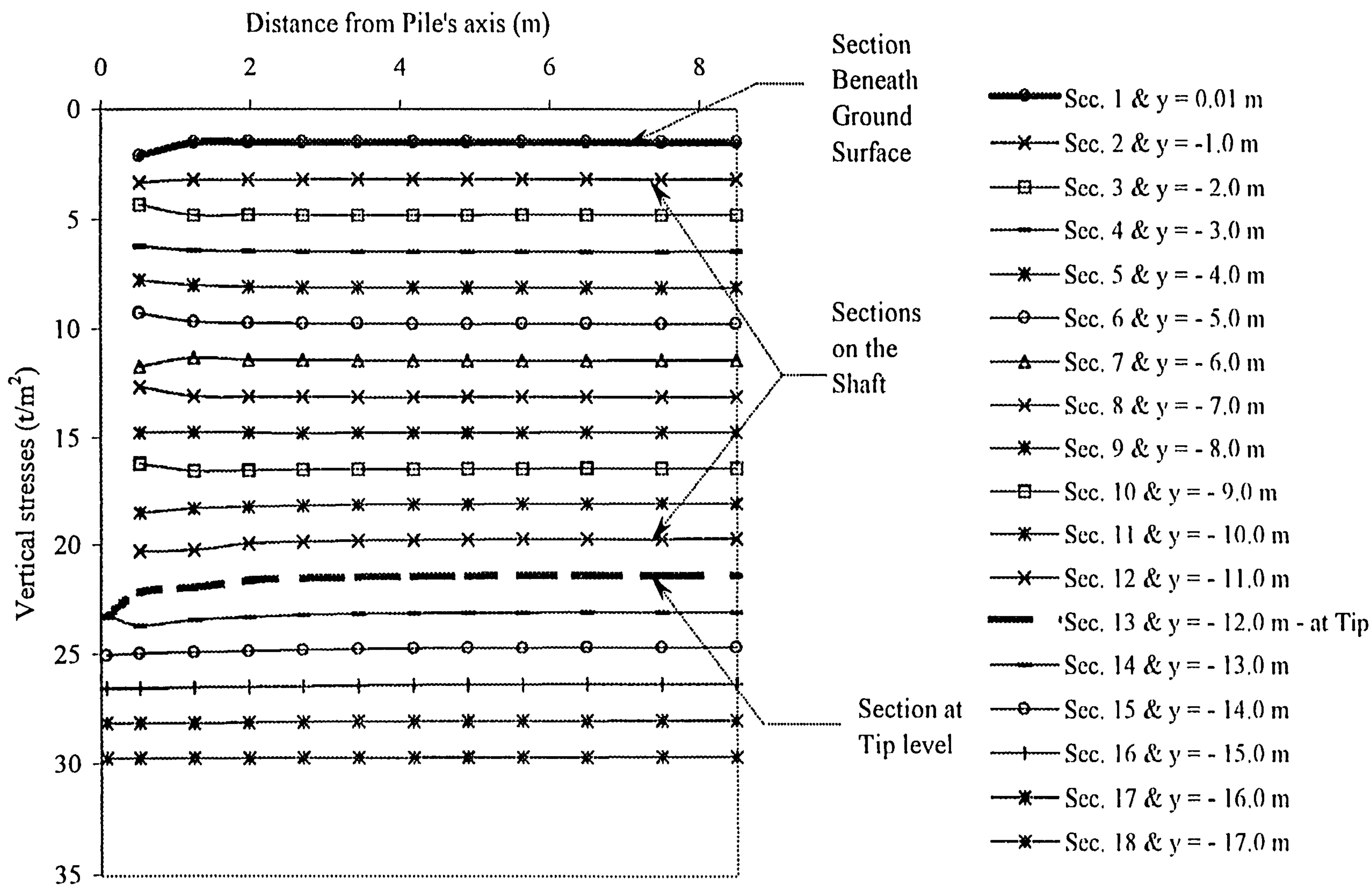

Figure 3.26 Vertical Stresses (at Failure) Developed Over Horizontal Sections Measured From Ground Level

(Test Data: D= 12m., B = 0.25m., $K_i = K_o$, $\phi = \delta = 30^o$)

linearly. Many theories considered the coefficient of earth pressure acting on the pile shaft K_s as a constant value based on the assumption of linear distribution. Many experimental data reported that K_s increases for short piles and may exceeds K_p. At a full pile embedment and at the failure load, the coefficient of earth pressure K_s may be closer to K_p near the top of the pile and tends to be a lower limiting value near the pile base.

Coefficient of earth pressure K_s is considered as a major factor affecting the value of skin resistance. The actual distribution of K_s over the shaft has not yet been well documented.

In this investigation the following terminology is used:

K_o = Coefficient of earth pressure at rest (for normally consolidated sand) = 1-sin ϕ

K_i = Insitu (initial) coefficient of earth pressure in the soil mass (before pile loading) = K_o

K_s = Coefficient of earth pressure acting on the pile shaft

K_{sg} = Coefficient of earth pressure acting on the pile shaft developed at ground surface

Figure 3.27 shows typical results of the determined coefficient of earth pressure, K_s on the shaft along the pile-soil interface.

From this Figure (3.27) it can be noted that: the highest value of K_s was developed immediately beneath the ground level, and decreases with depth up to a depth of about 8B from ground surface. Below this distance, the distribution remains constant, with a sudden reduction occurring in the vicinity of the pile tip. The distribution of the developed K_s on the shaft can be divided to the three following zones:

a- An upper zone (I) just beneath the ground surface and extended to a depth equal to about 8 B. The sand in this zone is subjected to densification due to the sudden subsidence in the ground surface around the shaft. Furthermore, during loading the pile, the soil moves towards the shaft. Therefore, a state of higher earth pressure (this could be a passive state) has been generated in this zone, i.e. $K_{sg} >> K_i$.

b- In zone II around the tip, the sand is also subjected to densification, where the movement of the pile is against the soil, and accordingly an active condition was developed ($K_s < K_i$).

c- In zone III, between zone I & II, the distribution of K_s at this zone, implies that there are no major movements which could change the at rest condition, accordingly, there was not enough influences to the skin resistance along pile length in this zone, ($K_s \equiv K_i$).

Figure 3.28 displays the coefficient of earth pressure developed over different vertical sections measured horizontally from the pile axis covering a total horizontal distance equal to 30 B From this Figure (3.28) it can be noted that:

1- Horizontally, the coefficient of earth pressure developed at ground surface is always higher than the insitu ($K_{sg} >> K_i$), where at the shaft ($K_{sg} = 1.55$) > ($K_i = 0.5$). Horizontally away from the shaft, K_{sg} became higher (at a distance equal to 3 B, $K_{sg} = 2.53$). And beyond the distance 3B, K_{sg} decreases. At a distance equal to 14.4 B, K_{sg} became equal to K_i. Beyond this distance the trend, differs and becomes ($K_{sg} < K_i$), where at a distance equal to 15 B, K_{sg} became equal to 0.46 < ($K_i = 0.5$). The trend will continues with increase of distance from the shaft, where at a distance equal to 30 B, K_{sg}, was found to be = 0.33 < ($K_i = 0.5$).

2- Vertically the increase of K_{sg} which occurred at the ground surface, is limited to a distance equal to about 8 B measured from the ground surface. Beyond this distance, K_{sg} became almost equal to the insitu value or higher, with a sudden decrease just at the tip. This decrease was found to be ($0.45 < Ki = 0.5$).

Figure 3.29 shows the coefficient of earth pressure developed over different horizontal sec-

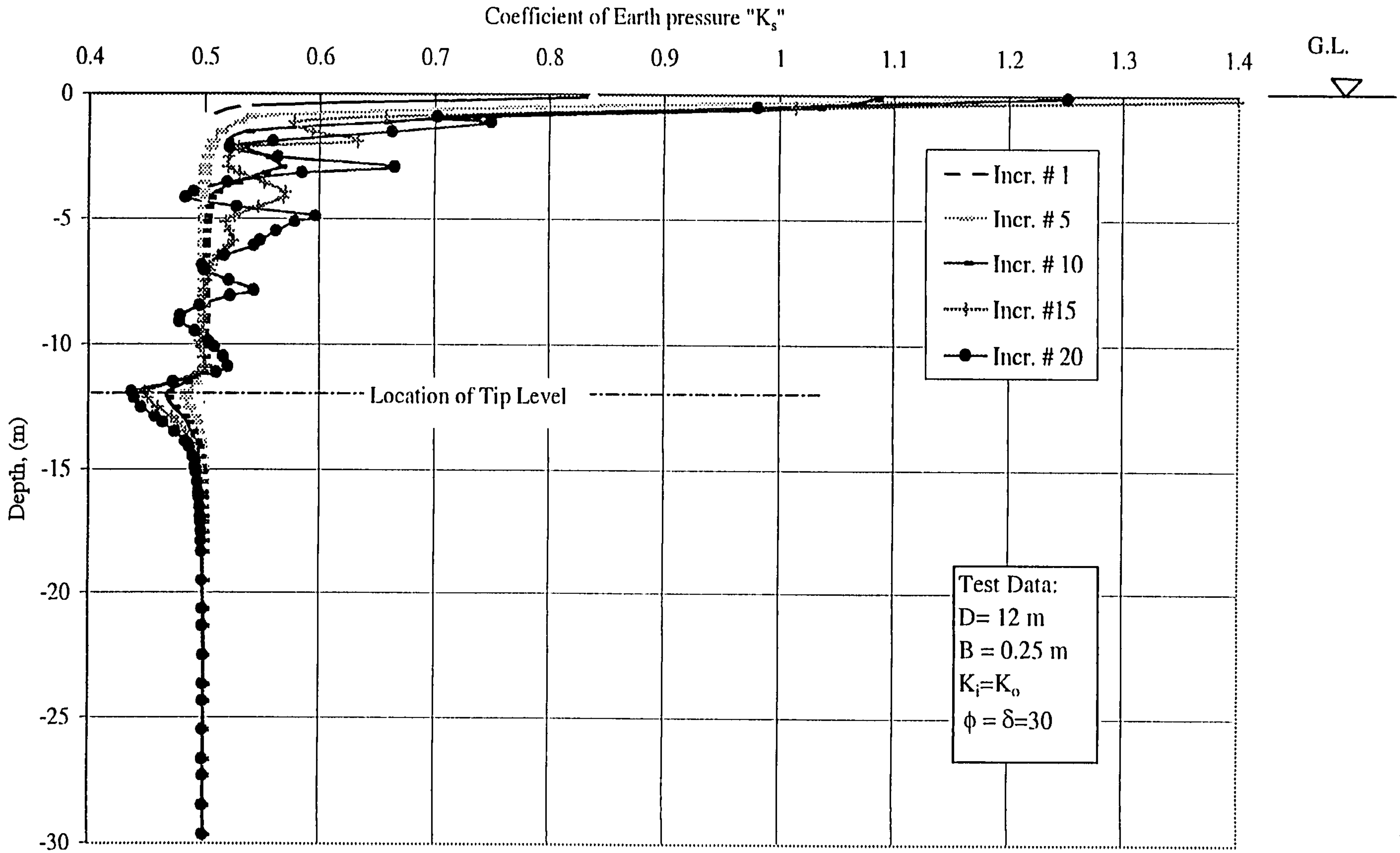

Figure 3.27 Development of Coefficient of Earth Pressure " K_s " along the Pile-soil Interface

tions located at vertical distances measured from ground surface. Figure 3.30 introduces the percentage of developed to insitu coefficient of earth pressure acting on the shaft K_s. The following observations can made from theses Figures (3.29, 3.30):

1- The influence zone in the considered test is found to be horizontally as follows (Figure 3.29):

a- Beneath ground surface (zone I): 14.4 B

b- Beside pile tip (zone II): 8B

c - Over the shaft between zone I and II (zone III): 5 B

2- The maximum percentage of K_s/K_i is found to be 140% and occurred beneath the ground surface, zone I, (Figure 3.30). Along the shaft, in zone III, this percentage is about 104%. At zone II, beside the tip, it was found to be 94%.

The above observations can be documented as follows:

1- The pile loading mechanism creates different states of stress zones around the shaft. The earth pressure coefficient in these zones varies between $K_s>K_i$ and $K_s<K_i$. The differences between each state are also extended to various vertical distance over the shaft. These observations make invalid the former assumptions for K_s - as a constant value for all the shaft length, resulting in linearly distributed horizontal pressures acting on the shaft. This trend was reported by several authors, Kulhawy (1984), Meyerhof (1976), Werching, (1987) and Altaee, et al (1992-a &b &1993).

2- It is found that K_s exhibits a higher value at the ground surface, which is called K_{sg}; this value is also variable depends on some other factors, i.e. δ,ϕ.

3- The values of developed coefficient of earth pressure at the shaft K_s are higher than the initial coefficient of earth pressure K_o; this increase is also varied depending on other factors, i.e.

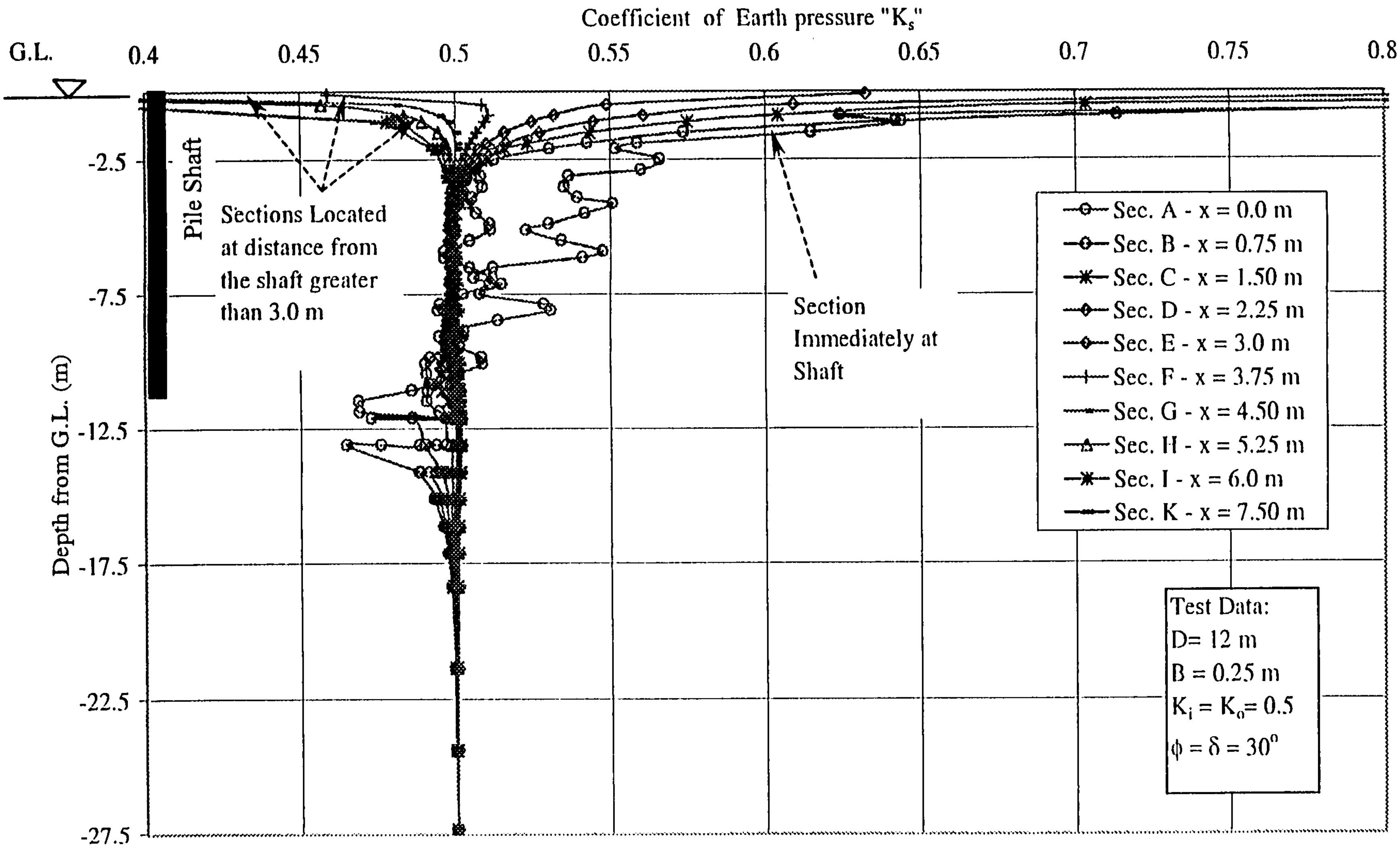

Figure 3.28 Development of Coefficient of Earth Pressure (at Failure) Along Different Vertical Sections at Various Horizontal Distances

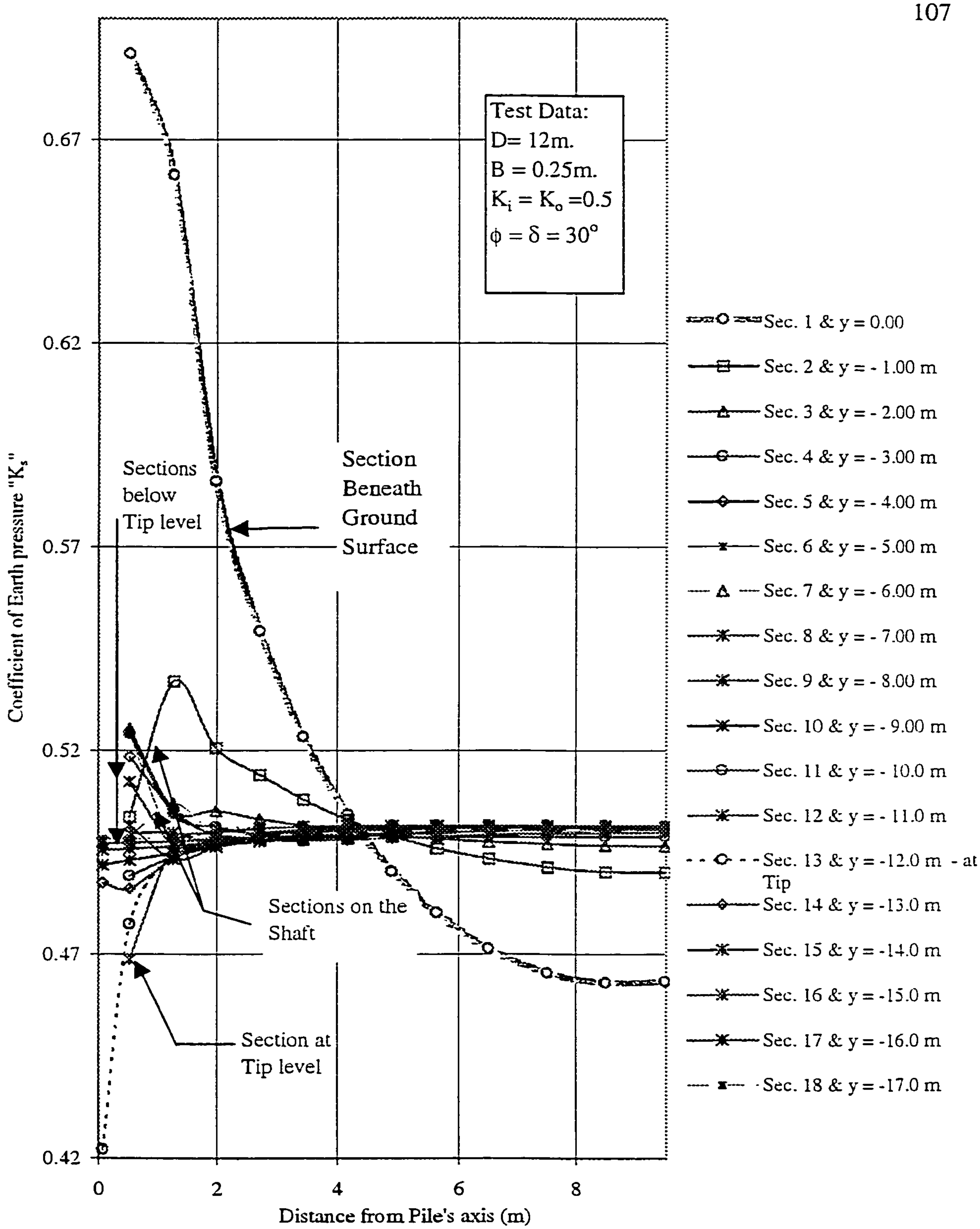

Figure 3.29 Coefficient of Earth Pressure Developed (at Failure) along Horizontal Sections at Various Depths

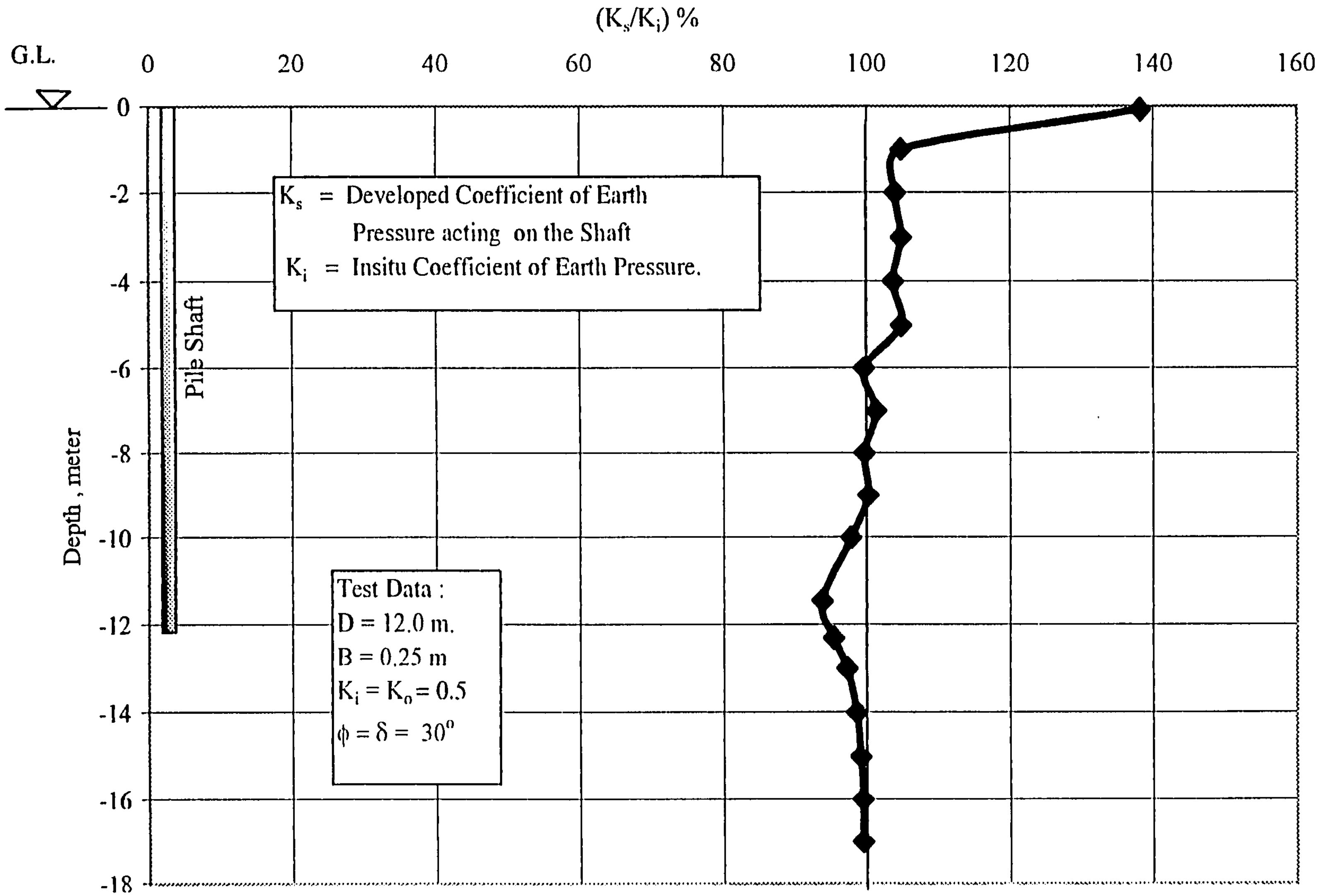

Figure 3.30 Percentage of (K_s/K_i) at Failure Versus Depth Along Vertical Section Located at Pile-soil Interface

δ, ϕ.

The forgoing conclusions stress the importance of obtaining new values for K_s for design purposes.

3.8.4.1 Coefficient of Earth Pressure Acting on the Pile Shaft K_s

It was found that the coefficient of earth pressure acting on the shaft K_s exhibits greater increase than the insitu values K_i, ($K_i = K_o = 1\text{-sin } \phi$). This increase is a direct reflect of stress state in soil mass and variable sand densities occurred due to pile loading. In order to show how much increase was found due to the different soil conditions, a ratio of K_s/K_i will be introduced in the following section. Table 3.8 shows the typical results of the coefficient of earth pressure acting on the shaft K_s. It should be noted here that the entire parametric study was performed taking into account $\delta/\phi = 1.0$. These results also are presented graphically in Figure 3.31. This Figure shows the relationship between the ratio of coefficient of earth pressure K_s/K_i and the angle of shearing resistance ϕ with respect to pile depth "D" and diameter "B". It can seen from this Figure (3.31) that:

1- At shallow depths, the ratio of K_s/K_i exhibits a higher increase than at greater depths.

2- K_s/K_i increases with the increase of pile width "B".

3- K_s/K_i increases with the increase of angle of shearing resistance "ϕ".

In order to establish a predictive function for K_s, using the entire output of the parametric study -shown in Figure 3.31- the following procedures were followed:

1- Average relationship of the ratio K_s/K_i at an angle of shearing resistance $\phi = 25^o$ with respect to pile width = 0.25 m, were produced. This relationship represents the lower envelop for all curves introduced in Figure 3.31 taking into consideration the range of pile depths between 3.0 m and 72.0 m. This relationship is introduced in Figure 3.32. The best fitting function to produce predictable equation is found to be as follows:

$$(K_s/K_i)_{(at\ \phi=25^o)} = 1.194 + D^* (-10.98+D^* (258.04 + D * (-1966.46 + D * (6405.12 + D * (-514.79))))) \qquad ...(3.9)$$

This process was carried out using a computer program that offers the best fit relationships for many engineering functions and develops corresponding equations. A comparison between all produced curves was carried out and the most reliable representation of the input data was chosen. Many trials have been done to determine the most efficient equation in terms of simplicity and reliability. The chosen equation was coded in subroutine to test the coverage range for its function, which was found accurate enough to cover the desired range.

2- The trend of K_s/K_i versus "ϕ" was found to be almost parallel for all values of "ϕ" with semi constant difference; this implies the concept of using one curve at the lowest value and additional increase due to extra values of "ϕ" can be added. The predictive function could be established for the lower value of "ϕ" (using Equation 3.9) and then an additional increase can be added to predict the higher values of "ϕ". The same trend can be approximated for the increase due to the increase of pile width "B". With respect to "ϕ", the maximum difference in K_s/K_i (between the value at "ϕ" = 25° and the value at "ϕ" = 45°) was found to be about 0.322. This amount was distributed among the range of ϕ = 25° to ϕ = 45° and additional increase to the predicted value of $(K_s/K_i)_{at\ \phi=25^o}$ will be added using the following equation:

$$K_{sI} = 0.0161*(\phi) - 0.4025 \qquad ...(3.10)$$

Equation 3.10 is presented graphically in Figure 3.33.

$$(K_s/K_i)_I = (K_s/K_i)_{at\ \phi=25^o} + K_{sI} \qquad ...(3.11)$$

Table 3.8 Parametric Study Results for Model Parameter:
Coefficient of Earth Pressure acting on Shaft "K_s"

Pile Geometry, m		Coefficient of Earth Pressure acting on Shaft "K_s"				
B	D	$\phi = 25°$	$\phi = 30°$	$\phi = 35°$	$\phi = 40°$	$\phi = 45°$
0.25	3	0.88	0.83	0.77	0.70	0.63
0.25	6	0.81	0.78	0.72	0.65	0.58
0.25	9	0.76	0.71	0.66	0.60	0.54
0.25	12	0.70	0.67	0.62	0.55	0.49
0.25	18	0.63	0.57	0.52	0.47	0.42
0.25	24	0.60	0.55	0.49	0.44	0.38
0.4	4.8	0.89	0.82	0.77	0.70	0.62
0.4	9.6	0.79	0.74	0.68	0.62	0.54
0.4	14.4	0.70	0.65	0.60	0.54	0.48
0.4	19.2	0.63	0.58	0.53	0.48	0.43
0.4	28.8	0.61	0.55	0.49	0.43	0.36
0.4	38.4	0.59	0.53	0.47	0.40	0.34
0.5	6	1.20	1.06	0.97	0.87	0.75
0.5	12	1.03	0.94	0.86	0.77	0.68
0.5	18	0.90	0.84	0.76	0.68	0.60
0.5	24	0.80	0.75	0.69	0.61	0.54
0.5	36	0.69	0.64	0.58	0.52	0.45
0.5	48	0.65	0.60	0.55	0.49	0.43
0.75	9	1.13	1.03	0.95	0.85	0.76
0.75	18	0.94	0.86	0.79	0.69	0.63
0.75	27	0.79	0.74	0.68	0.60	0.54
0.75	36	0.72	0.66	0.60	0.53	0.46
0.75	54	0.67	0.62	0.56	0.49	0.43
0.75	72	0.67	0.62	0.56	0.49	0.43

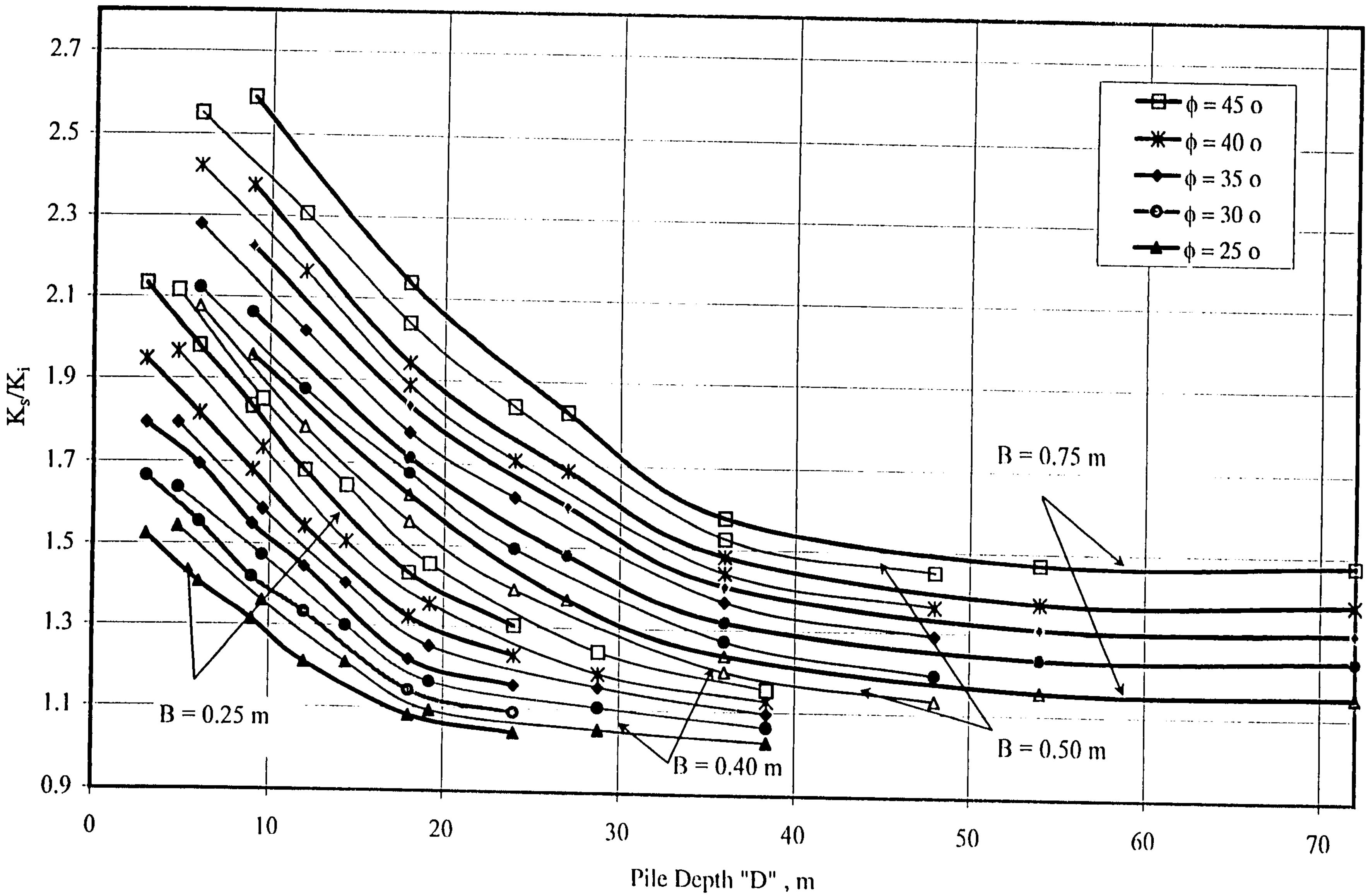

Figure 3.31 K_s/K_i Versus Pile Depth "D" with respect to angle of Shearing Resistance "ϕ" and Pile Width "B".

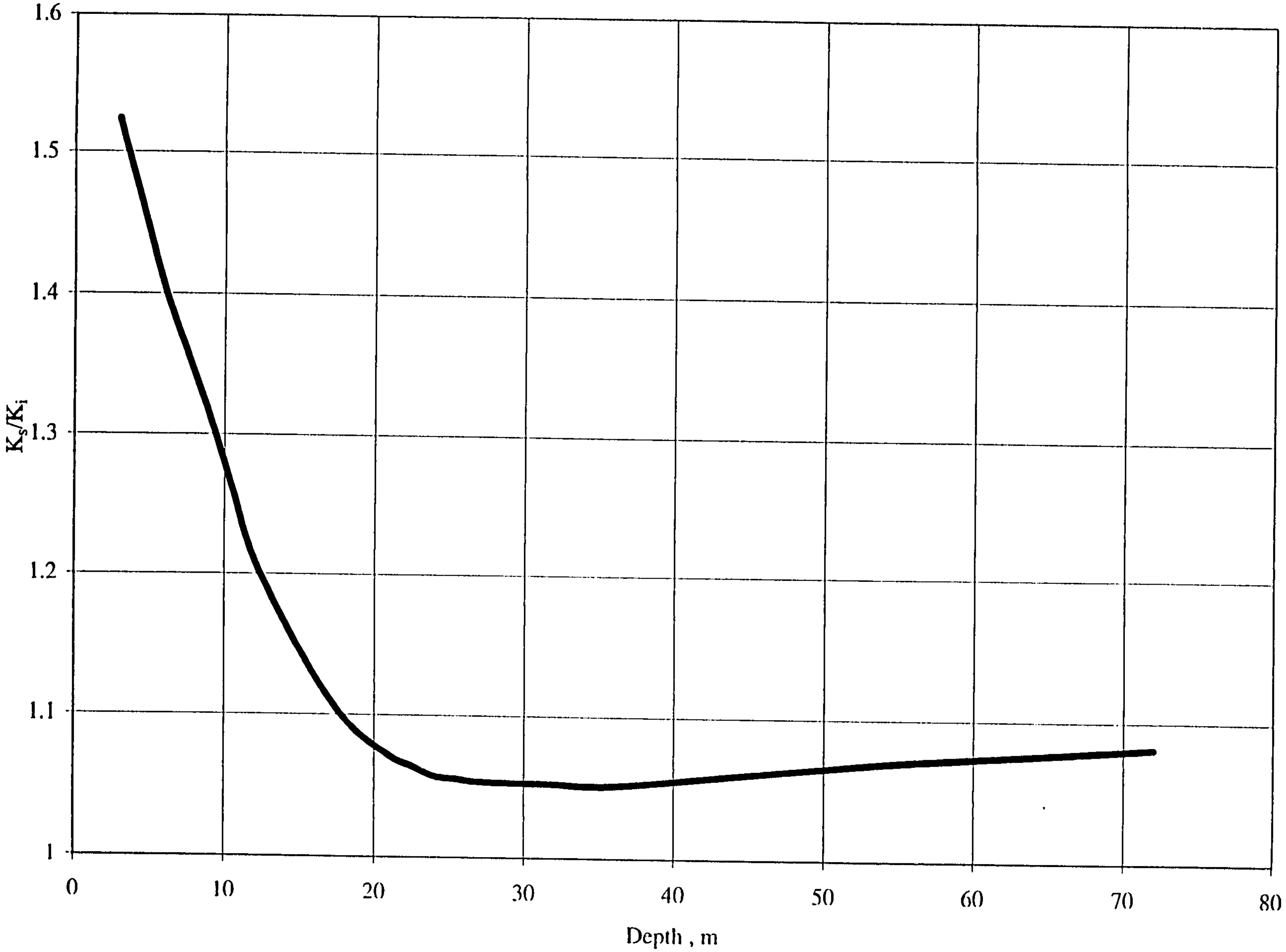

Figure 3.32 Average Value for K_s/K_i at ϕ=25° Versus Pile Depth

3- With respect to "B" the maximum difference in K_s/K_i (between the value at B= 0.25 m and B = 0.75 m) varied with depth and a function is needed to predict its value. This function is presented graphically in Figure 3.34, where the maximum difference between the value of K_s/K_i at B = 0.75m and B = 0.25 m was determined as an average of all series. The Equation for best fitting function of this data is given as follows:

$$K_{sB}=0.31+0.5015*(\mathrm{atan}((D-23.57)/(-5.178)+1.571))/\pi) \qquad ...(3.12)$$

$$Y_B=((B-0.25)/0.5)*K_{sB}$$

Equation 3.12 is presented graphically in Figure 3.34 and used to determine the increase of K_s/K_i due to the increase of "B"; this increase is dependent of the pile depth. Thus the pile depth is used to determine the corresponding increase of K_s/K_i due to the increase of "B".

$$(K_s/K_i)_{II} = (K_s/K_i)_I + Y_B \qquad ...(3.13)$$

3.8.4.2 Effect of Angle of Friction "δ" on the Value of K_s

Figures 3.35 to 3.39 show the results of selected pile load tests to present the variation of δ against K_s/K_i. From theses Figures 3.35 to 3.39, it can be noted that K_s increases with the increase of δ within the range of δ/ϕ = 2/3 to 1.0. While in the range of δ/ϕ = 1/2 to 2/3 it can be considered as a constant value with no major changes. The average rate of increase within this range is 36%. This amount of increase will be deducted, since the original studies were conducted using δ/ϕ=1.0, in the range of δ/ϕ = 2/3 to 1.0. And in the range of δ/ϕ = 1/2 to 2/3, K_s/K_i will take the same value based on its value at δ/ϕ = 2/3.

The best fitting function for this condition gave the following equation:

$$Y_2=0.37*(0.009*(\ln(e^{((\delta/\phi+0.17)/0.0045)}+e^{(186.6667)})$$

$$-\ln(e^{(224.4444)}+e^{((\delta/\phi)/0.0045)}))+0.34)/(0.64) \qquad ...(3.14)$$

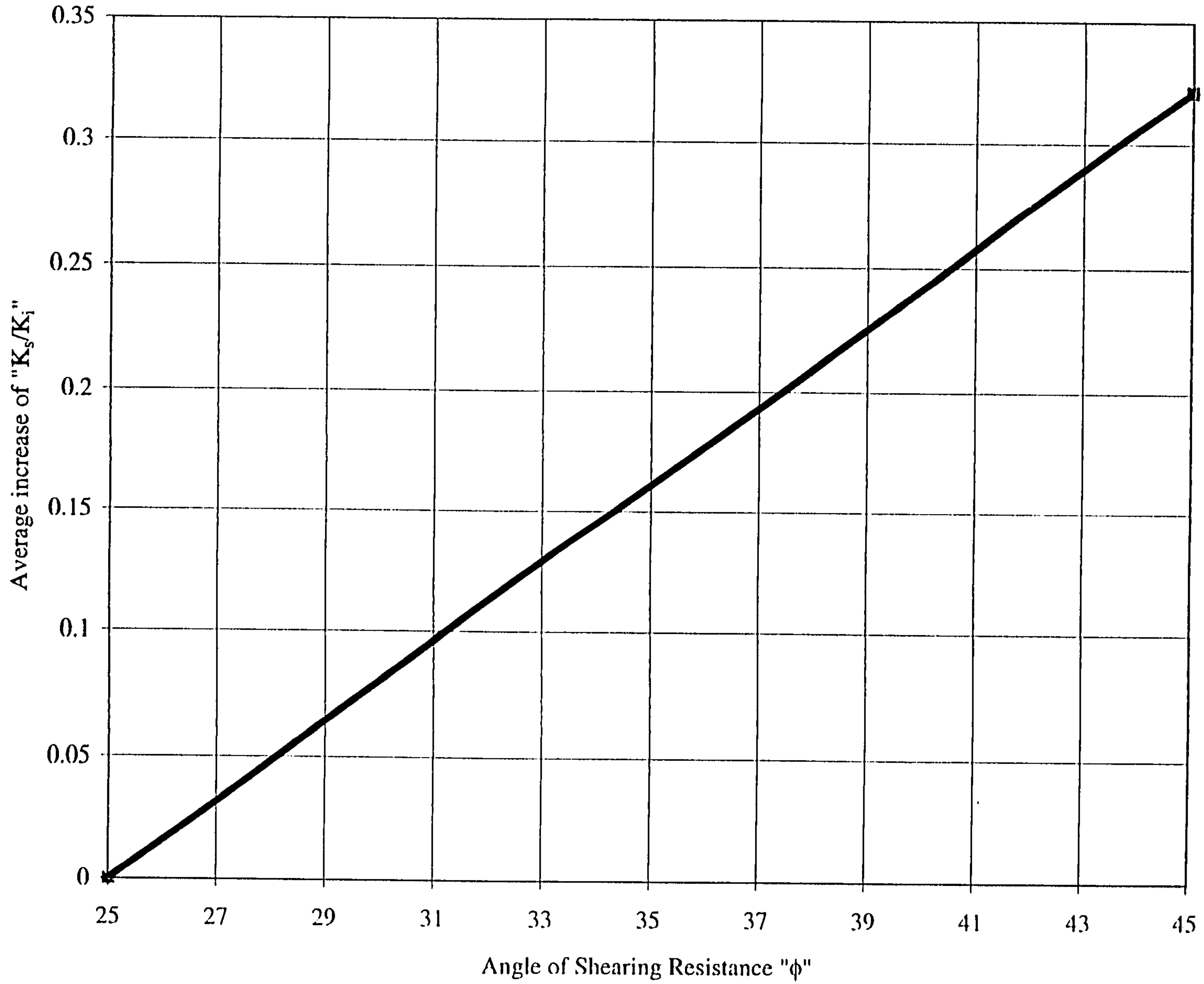

Figure 3.33 Average increase in "K_s/ K_i" due to the increase of "ϕ"

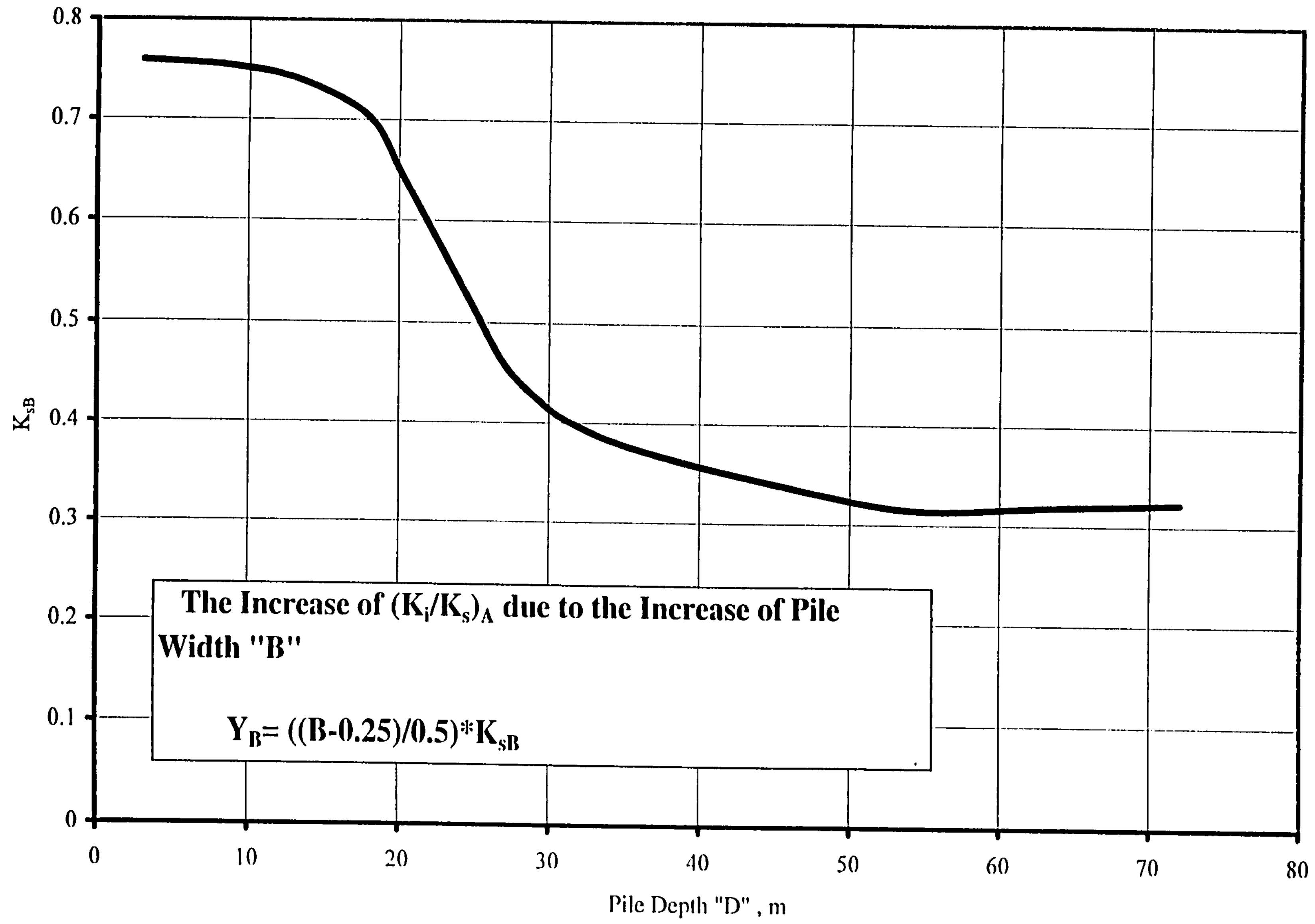

Figure 3.34 Rate of Increase in K_s/K_i (K_{sB}) Due to Increase of Pile Width "B"

$Y_K = 0.36 - Y_2$

Equation 3.14 was produced using the best fitting equation and is presented graphically in Figure 3.40.

$$(K_s/K_i) = (K_s/K_i)_{II} * (1 - Y_K) \qquad ...(3.15)$$

Finally

$$K_s = (K_s/K_i) * K_i$$

3.9 Suggested Method to Predict Coefficient of Earth Pressure Acting on the Shaft, K_s

Figure 3.41 introduces a graphic relationship for K_s/K_i and pile depth for different values of angle of shearing resistance ϕ, which resulted from the present investigation. The following steps are suggested to predict K_s based on the proposed method:

1- Use pile depth and angle of shearing resistance "ϕ" together to determine $(K_s/K_i)_A$ from Figure 3.41.

2- Determine the amount of increase due to increase of pile width B from Figure 3.34 by knowing pile depth D, "K_{sB}", getting $\{(K_s/K_i)_A + Y_B\}$

3- Determine the decrease due to decrease of δ/ϕ, Y_2, from Figure 3.40

$$(K_s/K_i) = \{(K_s/K_i)_A + Y_B\} - (0.36 - Y_2)$$

4- Finally: $K_s = (K_s/K_i) * K_i$

3.10 Development of Failure Pattern Around the Pile Shaft

The development of shaft and tip resistances is dictated by the amount of movement a pile experiences. It was reported in the literature that the amount of displacement needed for full mobilization of shaft resistance is much smaller than the amount needed for full mobilization

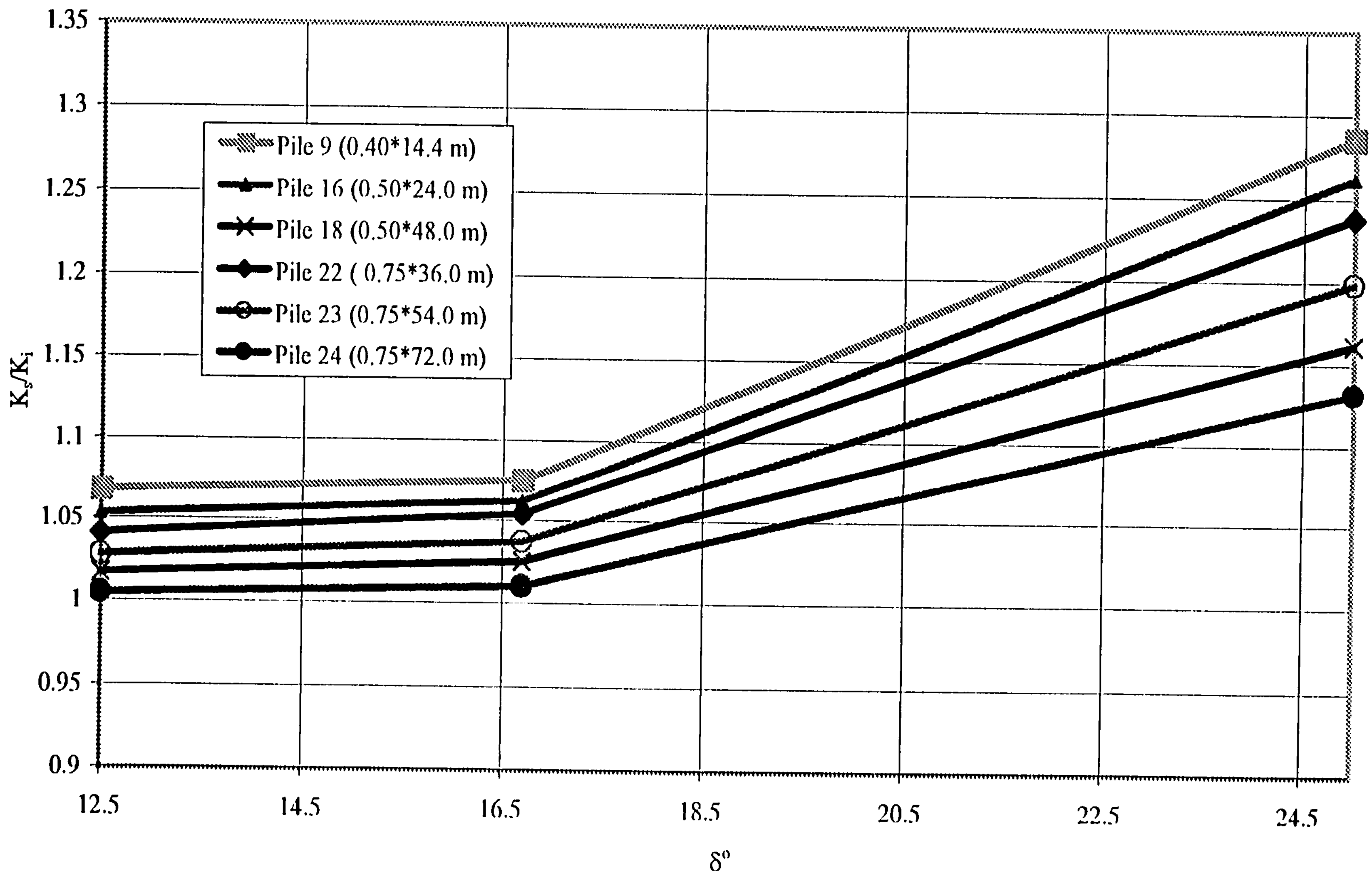

Figure 3.35 Selected Test Results to Determine the Effect of δ on K_s with Respect to Different Pile Slenderness Ratios (Case of ϕ=25^o)

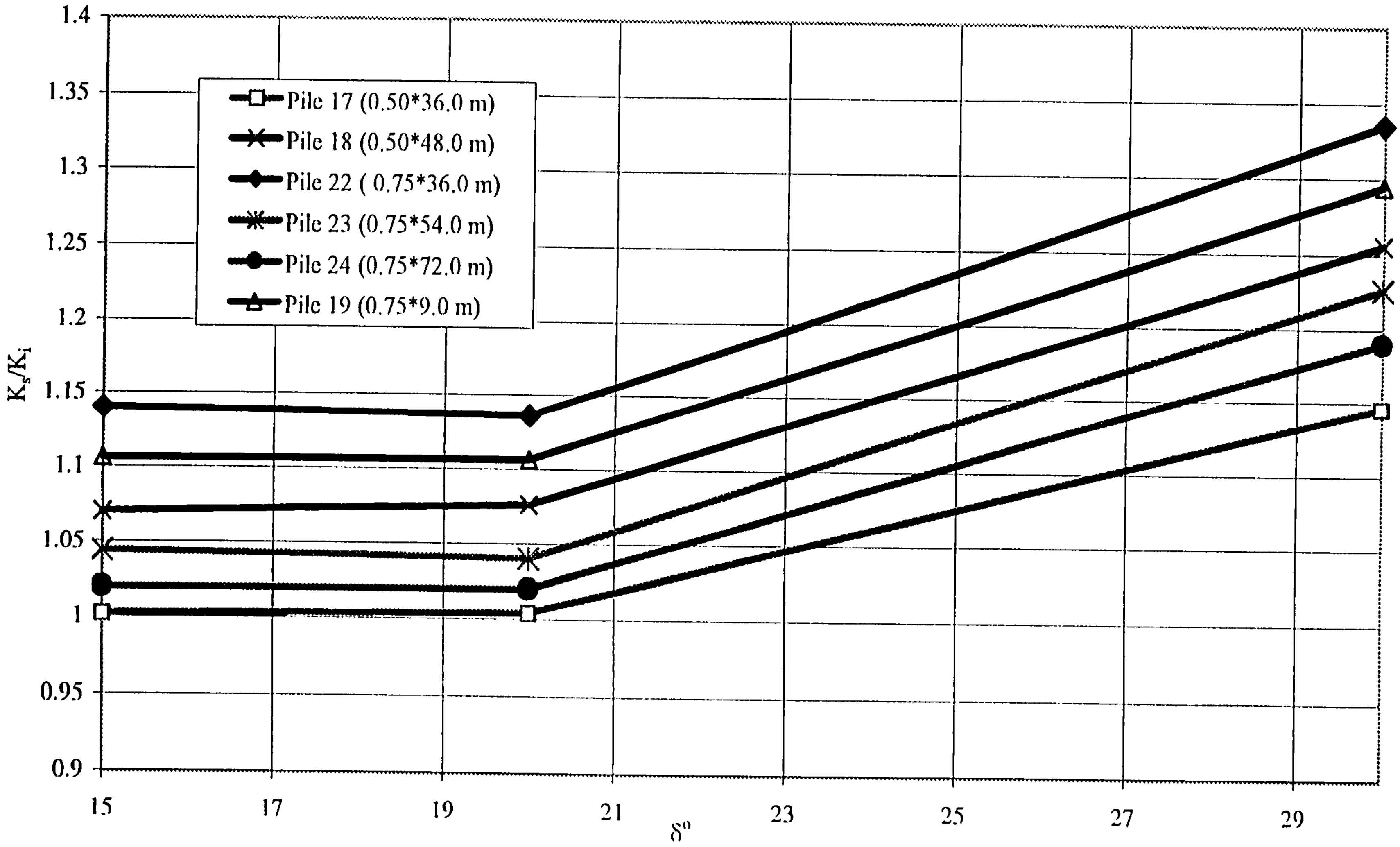

Figure 3.36 Selected Test Results to Determine the Effect of δ on K_s With Respect to Different Pile Slenderness Ratios (Case of $\phi=30^{\circ}$)

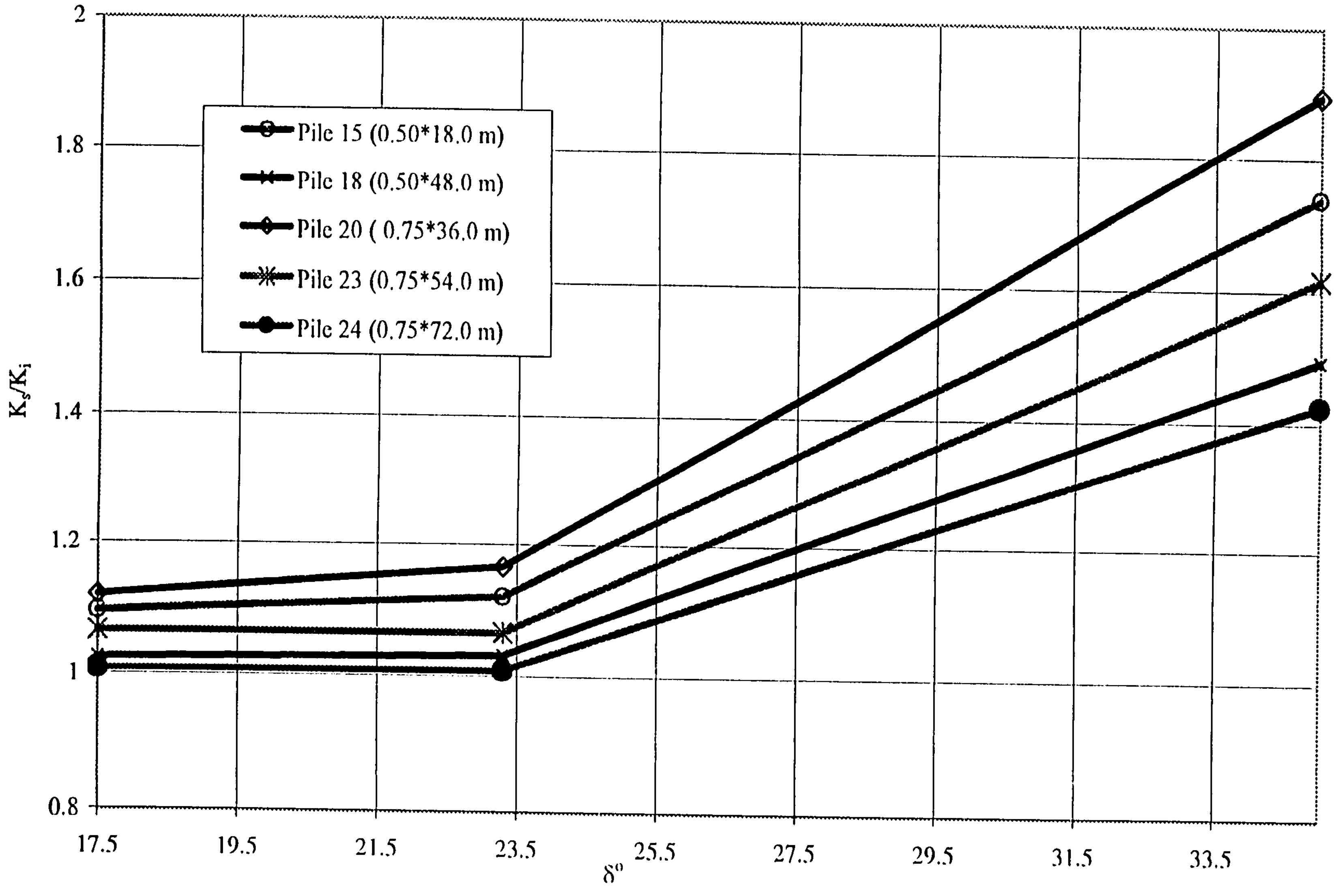

Figure 3.37 Effect of "δ" on K_s for different pile slenderness ratios (Case of $\phi=35^o$)

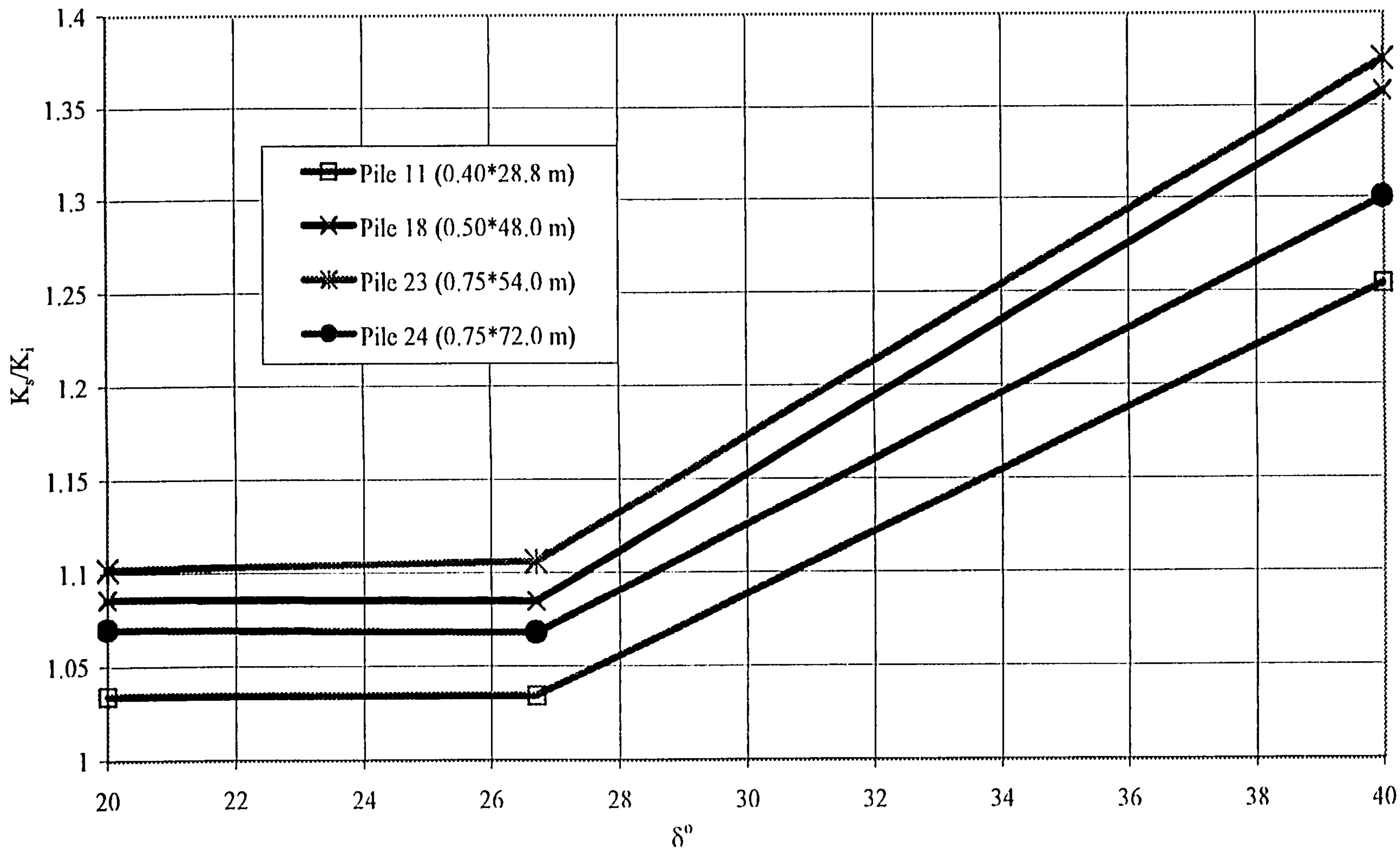

Figure 3.38 Effect of δ on K_s for different pile slenderness ratios

(Case of $\phi=40^{\circ}$)

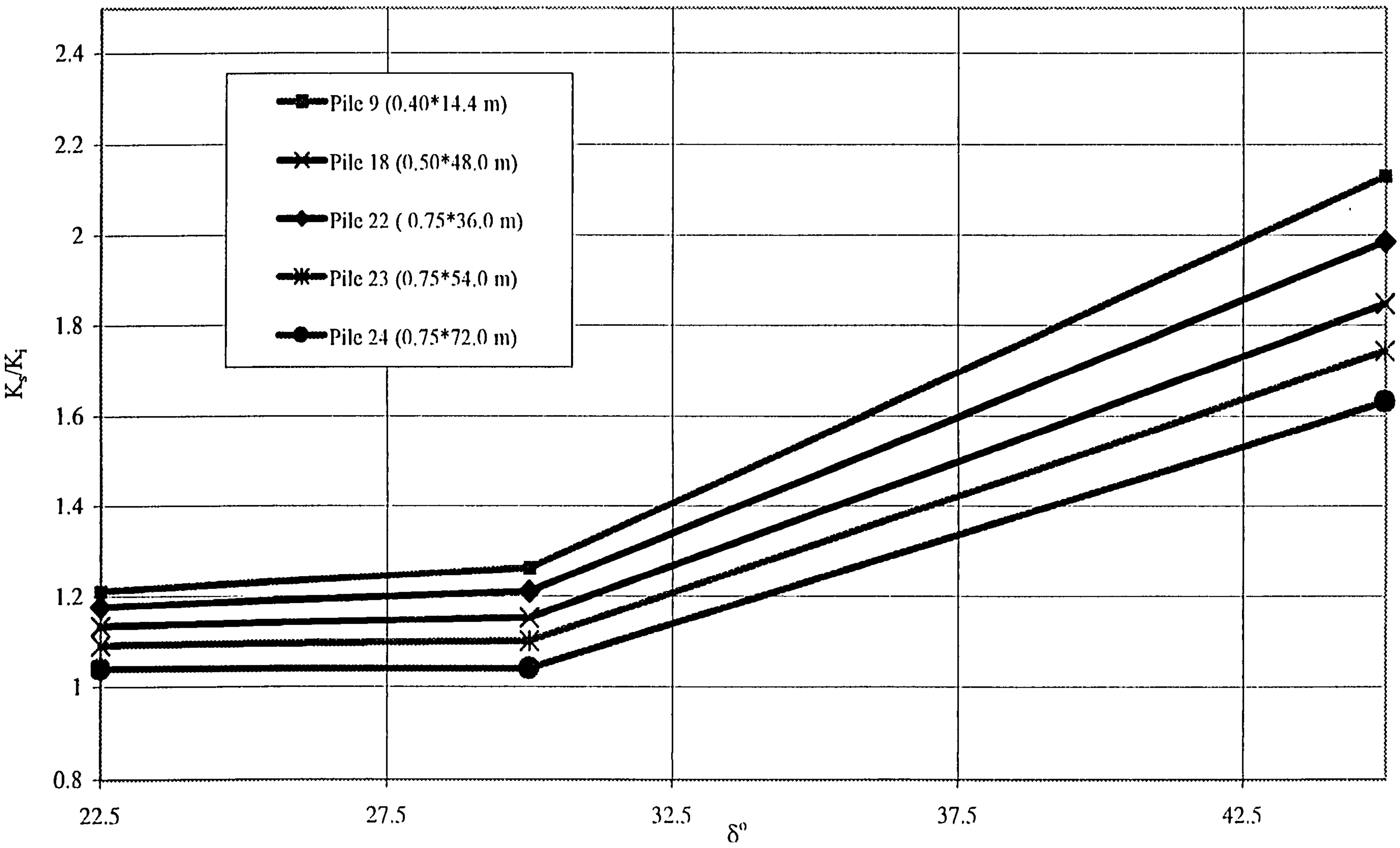

Figure 3.39 Effect of δ on K_s for different pile slenderness ratios

(Case of $\phi=45^o$)

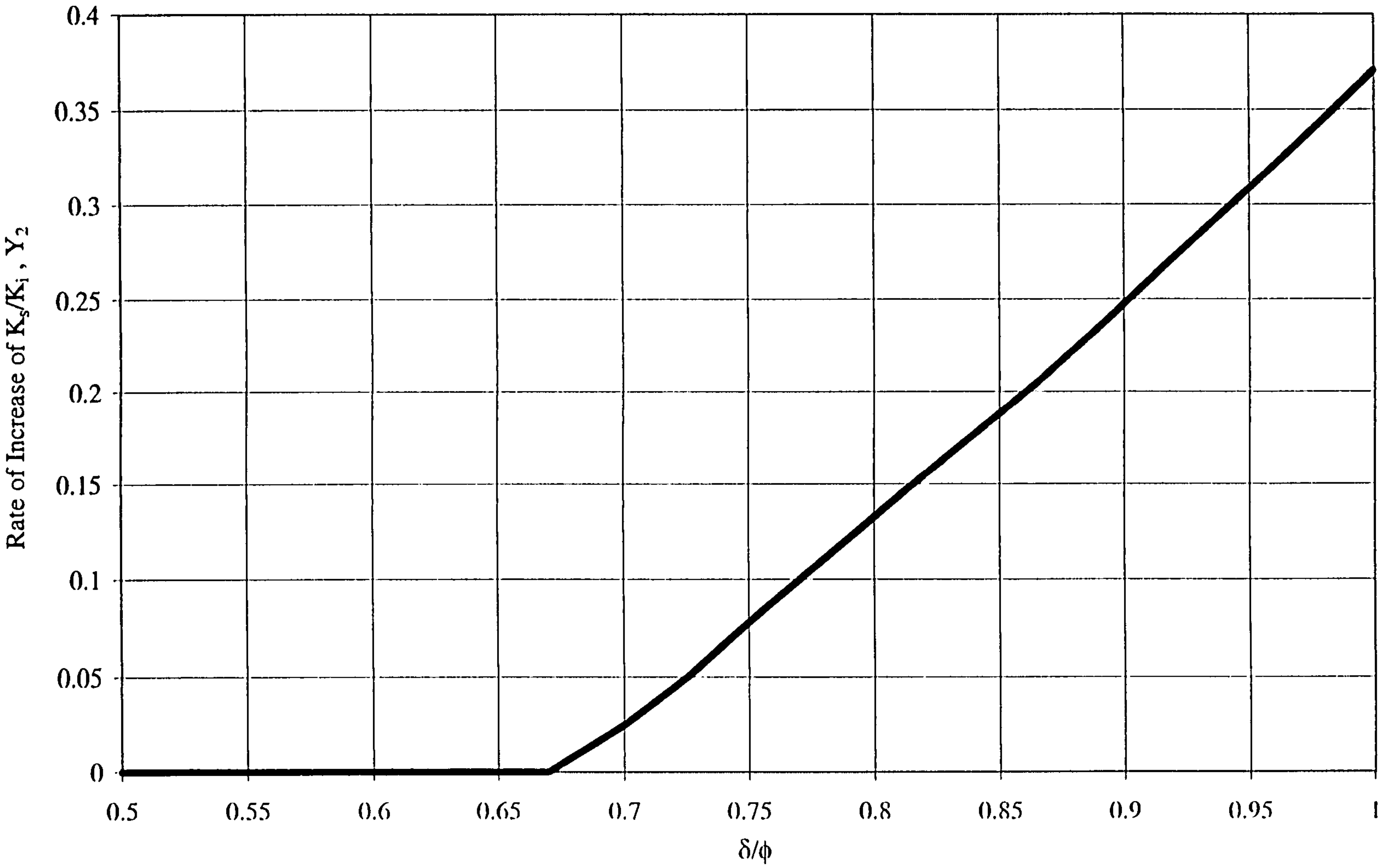

Figure 3.40 Rate of Increase of K_s/K_i Due to the Decrease of δ/ϕ

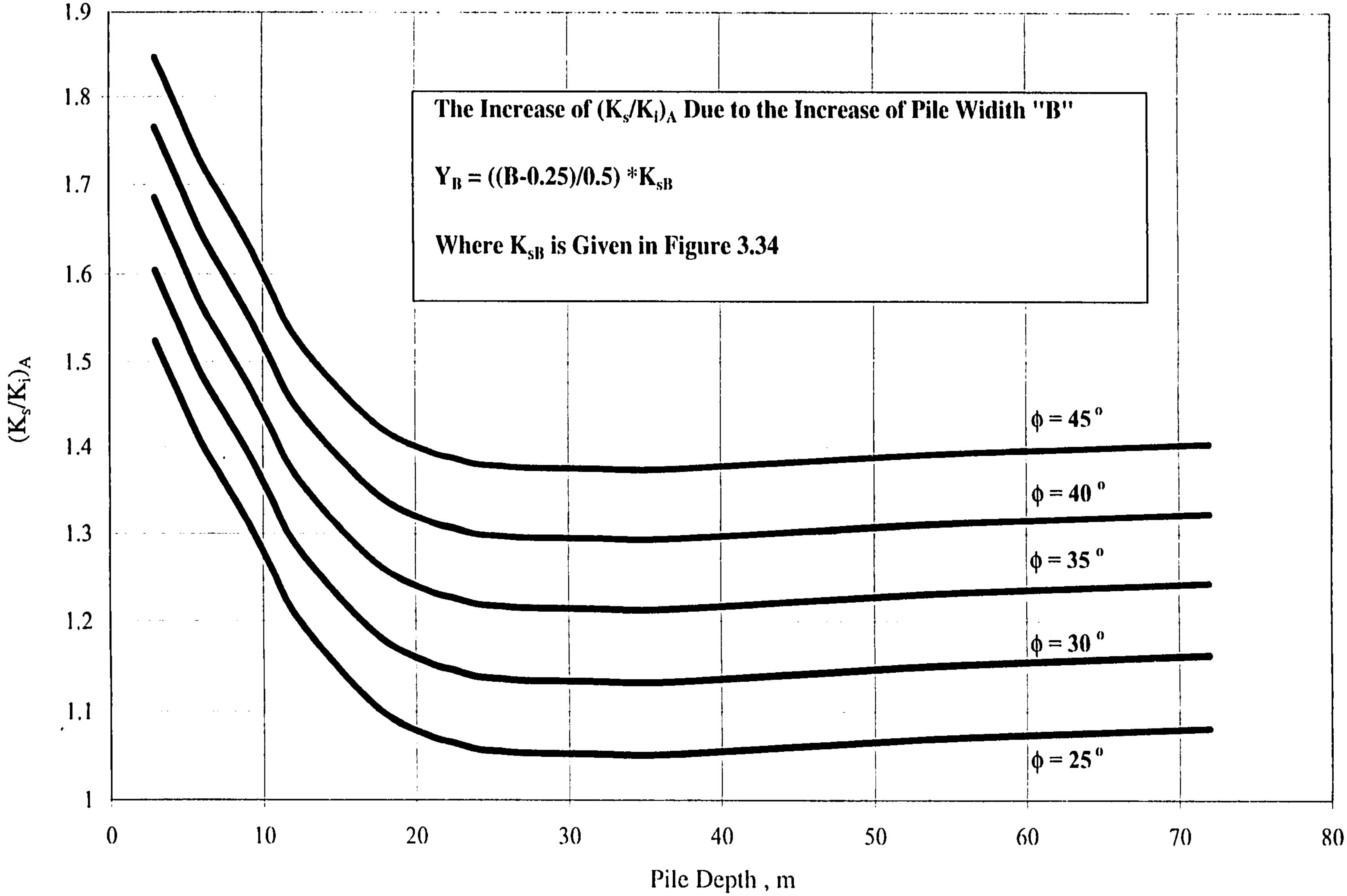

Figure 3.41 Design Chart of K_s/K_i Based on Pile Depth "D" and Width "B" (Based on Pile Width=0.25 m).

of the tip resistance.

3.10.1 Failure Pattern

In the following analysis, two methods were used to determine the failure pattern around the pile shaft as deduced from the finite element results. The first method is by producing the contour lines for the factor of safety (F.O.S) against shear failure for each increment of loading process and then determining the ultimate load corresponding to a factor of safety of unity. This indicates the boundaries of the failure pattern. The second method is by dedicating the failed soil elements around the shaft. The resulted failure area in this case must be the same as the observed using method one.

1- **Method I**:

From the results of the finite element analyses, the contour lines of stress ratio (t/s) which is equal to sine ϕ_m are plotted

Where:

t = the radius of Mohr's circle (effective stress) = $(\sigma_1-\sigma_3)/2$

and s = the coordinate of the center of Mohr's circle along the direct stress axis

= $(\sigma_1+\sigma_3)/2$

ϕ_m = mobilized angle of shearing resistance.

Thus,

$$t/s = \{(\sigma_1-\sigma_3)/2\}/\{(\sigma_1+\sigma_3)/2\} = (\sigma_1-\sigma_3)/(\sigma_1+\sigma_3) = \text{sine}\ \phi\ ,$$

$$\text{or} = \text{sine}\ \phi_m \qquad \text{...(3.16)}$$

The failure or slippage occurs at a point where (sine ϕ_m/sine ϕ) = 1.0, i.e. when $\phi_m = \phi$ where factor of safety against shear failure is equal to unity.

2- **Method II**:

The stress state for each element was determined immediately after each increment. The deduced stress was then compared with the allowable stress computed from the soil strength parameters. If the ratio is less than unity, this means that this element did not reach the failure state yet; i.e. for a ratio equal to or higher than one, the element is in a state of failure.

In this investigation, both methods were utilized to determine the failure pattern around the pile and the following procedure was used to determine the failure pattern around a single pile in sand:

1- For each test, several trials were carried out to estimate the magnitude of the ultimate load. Then double the estimated ultimate load was applied, divided over 60 increments in order to allow for close monitoring of the development of the failure pattern around the pile. In this investigation, the ultimate load was defined as follows:

a- In case of load-settlement, the curve exhibits plunging failure and the peak is easily defined. The ultimate load was taken as the load at which the plastic settlement curve breaks sharply, in other words, at the point of maximum curvature. This was recommended by Chellis (1961), with the condition that the corresponding settlement does not exceed the limit of B/30 plus the elastic settlement (Canadian Foundation Engineering Manual 1992).

b- In the case of plunging load, failure exhibited beyond the settlement limit and/or the load-settlement relationship is linear and has no defined maximum curvature. In this case the ultimate load was determined at a settlement equal to 10% of the pile diameter (Danish Standard, referred by Schultaze, 1964, Vesic, 1977, A. J., CIRIA, referred by Weltman, 1980& and Bishop, et al., 1948).

2- Plotting the total load-settlement relationship for each test can lead to determination of the increment number at which the ultimate load is reached.

3- Through close monitoring of the foregoing steps, the factor of safety against shear failure and the yielded elements, around the pile can be observed and accordingly, the critical slip surface at failure.

In the following section, typical results for the process of failure pattern development around the pile shaft is introduced.

3.10.2 Typical Results of the Failure Pattern Around the Pile Shaft

Using the same test data presented in all forgoing analyses, (pile depth = 12.0m, pile width = 0.25m, $\delta = \phi = 30^o$, $K_i = K_o$, refer to section 3.9) the following results are presented.

Figure 3.42 presents the development of failure pattern around the pile shaft, which started at loading increment number 11, in terms of failed elements around the shaft. Figure 3.43 shows an enlarged view of the pile head area for the contour lines of factor of safety against shear failure at the same increment.

Analysis of Figures 3.42 and 3.43 leads to the following observations:

1- It was observed that, the mobilization of skin resistance started first before the mobilization of tip resistance and this occurred at settlement of - 0.989 cm (at increment number 11) which is equal to about 33% of the total settlement at ultimate load. This reveals how small a movement is needed for the skin resistance to be mobilized before the tip resistance (in the test under consideration).

2- The failure mechanism begins around the pile head (at ground level), which represents the beginning of mobilized skin resistance. In the same Figure 3.42 (at increment number 11), the failed mechanism around the tip has not observed yet.

3 - The failed volume due to mobilized skin resistance can be approximated as an inverted cone with the base located at ground surface.

4 - The failed zone due to mobilization of skin resistance- at this increment- is extended horizontally to a distance of R = 2 B from pile axis, where B = pile diameter, and extended vertically from G.S. to a vertical distance H_1= 5 B.

Figure 3.44 presents graphical direction of internal movements around the pile in terms of displacement vectors. From this Figure 3.44, the following remarks can be made:

1- Higher movements are located around the pile shaft and decrees faraway from the shaft in both horizontal and vertical directions.

2- In the area deemed as mobilized skin resistance zone (upper part of the mesh), the direction of movement is against the pile shaft. In the area considered as tip resistance zone (around the tip), the movements are away from the pile.

3- In the zone between the above two mentioned zones, the movements are almost vertical (parallel to pile shaft).

In more detail Figure 3.45 introduces the contour lines for horizontal displacement at increment number 11. As can seen from this Figure 3.45, the horizontal movements in the mesh are generally categorized in two directions:

a- In the vicinity of the shaft head near G.S. the horizontal movements are negative, i.e. its direction is against the shaft, i.e. soil is compressing the shaft.

b- Near the tip, the horizontal movements are positive, i.e. its direction is away from the shaft, and pile is compressing the soil.

The principal strains around the shaft are introduced in Figure 3.46, where the concentration of strains are increased around the shaft and no major increase of strains is found outside this

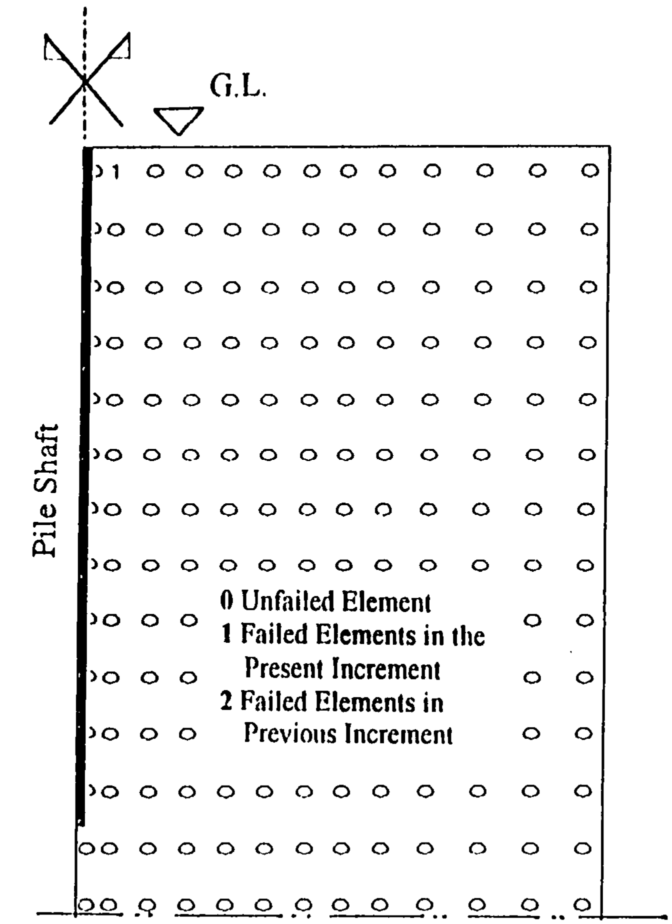

Figure 3.42 Failed Elements Around the Shaft, Increment Number 11. Test Data: D = 12 m, B = 0.25 m, $K_i = K_o$, $\phi = \delta = 30^o$.

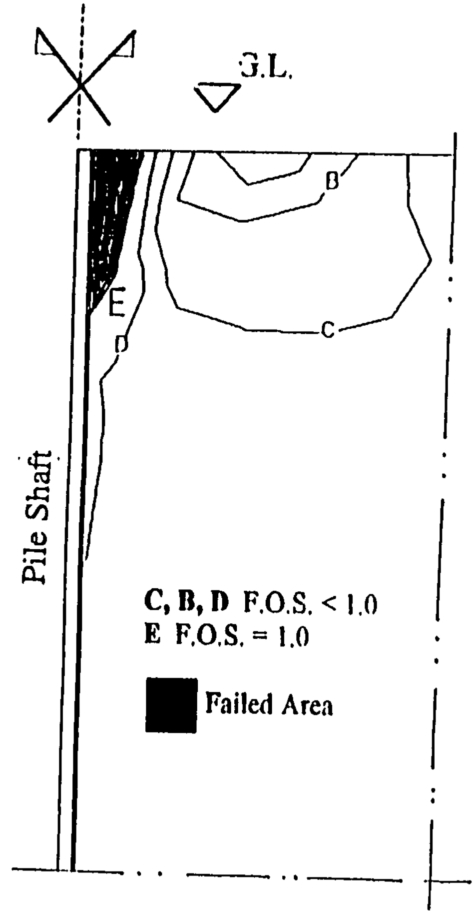

Figure 3.43 Contour Lines of Factor of Safety Against Shear Failure Around the Shaft, Increment Number 11. (Blow up View). Test Data: D = 12 m, B = 0.25 m, $K_i = K_o$, $\phi = \delta = 30^o$.

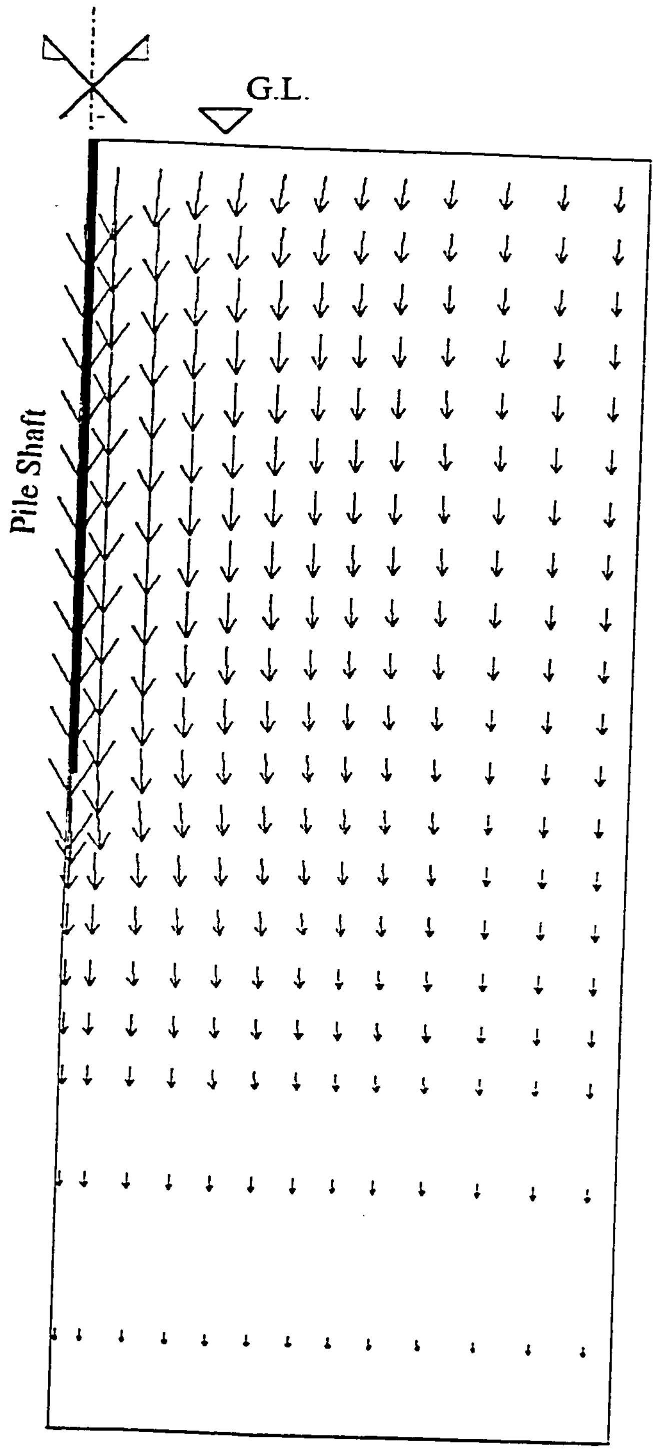

Figure 3.44 Displacement Vectors Around the Shaft, Increment Number 11.
Test Data: D = 12 m, B = 0.25 m, $K_i = K_o$, $\phi = \delta = 30°$.

area.

In order to follow up the progress of failure, the failed elements at increment number 28 are shown in Figure 3.47 and the corresponding contour lines for factor of safety against shear failure is presented in Figure 3.48. It was found that the mobilization of skin resistance extends in the vertical direction for a total distance of 6 B and one more failed element was added vertically in this increment. Also the mobilization of tip resistance started in this increment, where the first failed element is found to be just beneath the tip. Also the mobilized tip resistance was stared at this increment with a small bulb beneath the tip. This bulb has the following dimensions: horizontally 1.25 B, and vertically 3 B. It was found that the tip resistance started to mobilize at settlement equal to -3.62 cm.; it was developed immediately in the element beneath the tip. In general, the mobilized tip resistance took a shape very similar to a bulb. This bulb shape will be approximated by a log-spiral curve later on.

The displacement vectors at increment number 28 are shown in Figure 3.49. In this Figure 3.49, it is clear that the movements around the pile are composing a so-called arching effect. Beneath the ground surface the movements are towards the shaft and beside the tip, the movements are away from the shaft, and in between these two zones, the movements are vertical.

The skin resistance is fully mobilized at increment number 31, and no further propagation for this component was observed after this increment. This is shown in Figures 3.50 and 3.51, where the skin resistance was extend vertically to a distance of 13.25 B, and horizontally 3.75 B. This was the final incremental failure pattern that occurred due to skin resistance, this can be seen in Figure 3.50.

Further development of tip resistance was found in increment number 44. This is shown in Figures 3.52 and 3.53, where the failed elements and F.O.S. against shear failure around the

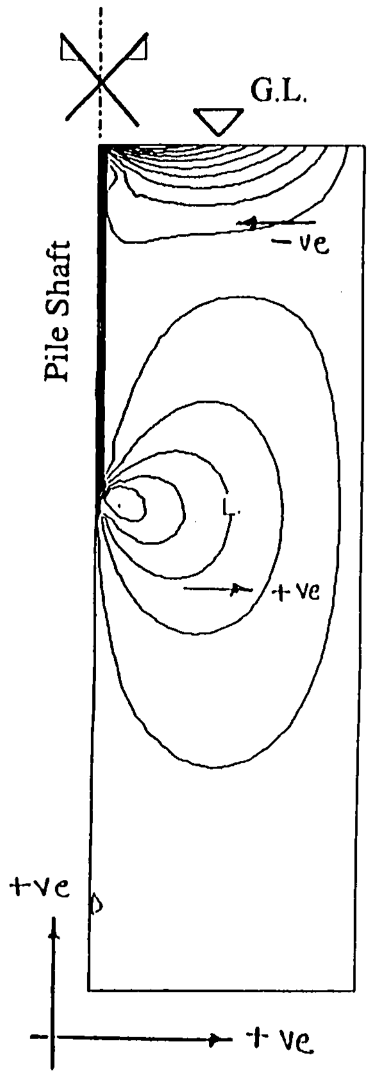

Figure 3.45 Contour Lines of Horizontal Displacement Around the Shaft, Increment Number 11. Test Data: D = 12 m, B = 0.25 m, $K_i = K_o$, $\phi = \delta = 30^o$.

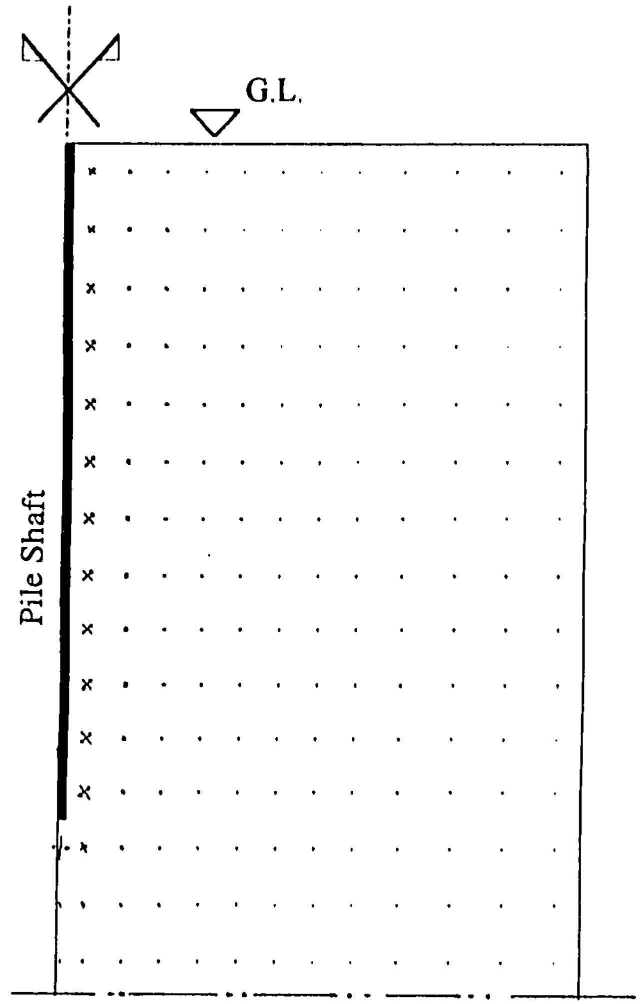

Figure 3.46 Principal Strains, Increment Number 11. Test Data: D = 12 m, B = 0.25 m, $K_i = K_o$, $\phi = \delta = 30^o$.

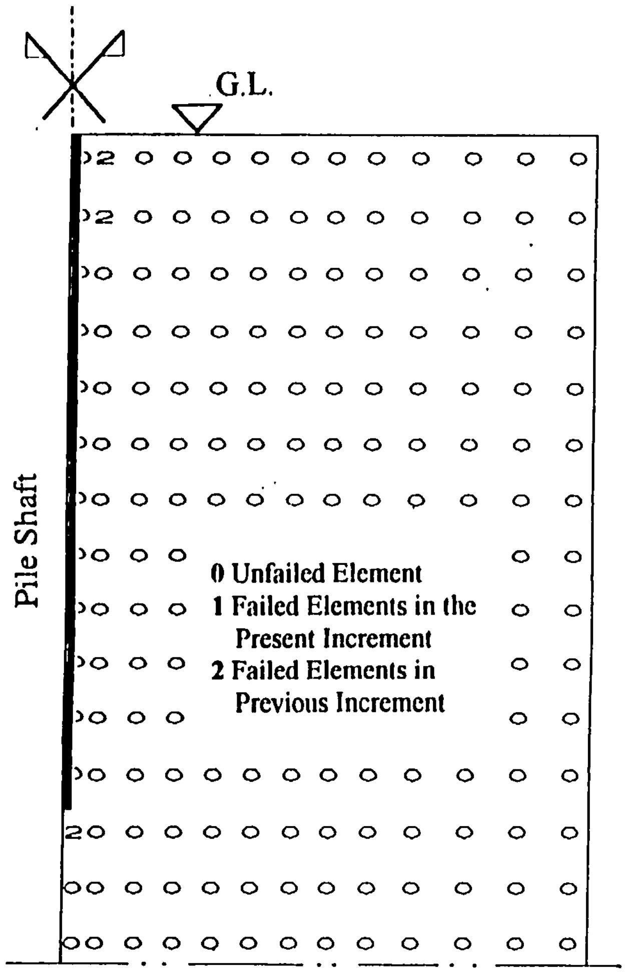

Figure 3.47 Failed Elements Around the Shaft, Increment Number 28. Test Data: $D = 12$ m, $B = 0.25$ m, $K_i = K_o$, $\phi = \delta = 30^o$.

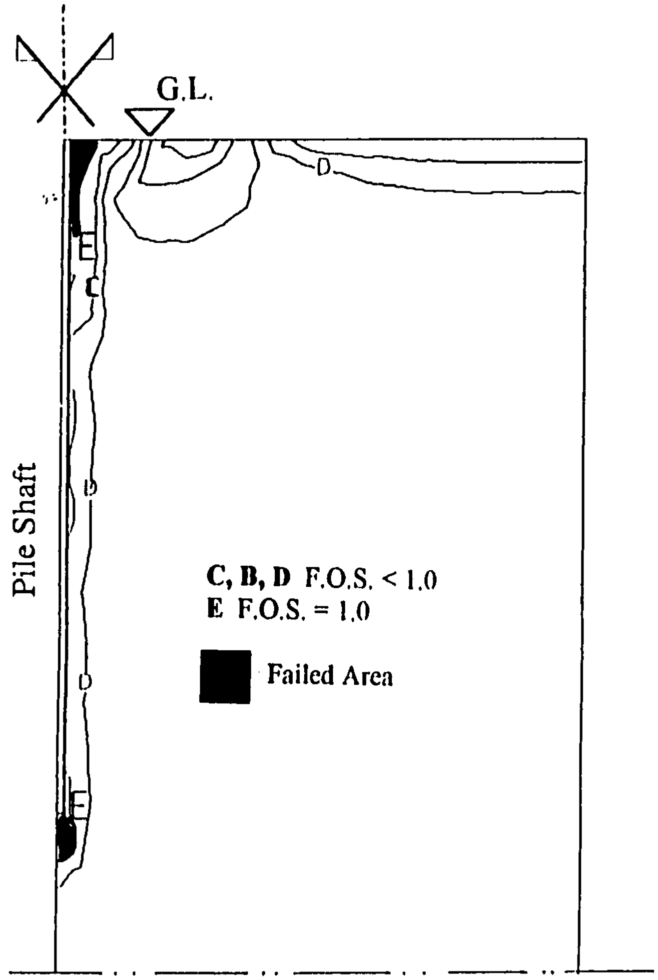

Figure 3.48 Contour Lines of Factor of Safety Against Shear Failure Around the Shaft, Increment Number 28. Test Data: $D = 12$ m, $B = 0.25$ m, $K_i = K_o$, $\phi = \delta = 30^o$.

tip are plotted. The failure around the tip is extended horizontally and one more failed element was added (Figure 3.52). The dimensions of failure pattern at this increment are: horizontally 2.15 B, and vertically 3.6 B above the tip level and 5.15 B beneath the tip level (Figure 3.53). The full mobilization of tip resistance was reached at increment number 48 and no further development was observed beyond this increment. This is shown in Figures 3.54 and 3.55. The total dimensions of failure pattern around the tip were found to be as follows: vertically 5.5 B below the tip level, and 3.35 B above the tip level. and horizontally 2.25 B.

Figure 3.56 shows the displacement vectors around the shaft at increment number 48. The same trend found before is reported here, where increased movements against the pile head and away from the tip are observed, while in between is vertical movement. This behavior can be related to the reported phenomenon in literature: arching effect. This phenomenon is believed to be responsible for the partially mobilized skin resistance and also the so-called critical depth phenomenon.

The development of horizontal displacements at both pile tip and head which occurred at different increments, is given in Table 3.9.

Table 3.9 Comparison Between Horizontal Displacements at Different Increments

Displacement	incr. # 12	incr. # 24	incr. # 28	incr. # 44
max. Horz. displacement at tip	$+0.96 \times 10^{-3}$	$+0.149 \times 10^{-2}$	$+0.843 \times 10^{-2}$	$+0.112 \times 10^{-1}$
max. Horz. displacement at head	-0.124×10^{-2}	-0.129×10^{-2}	-0.12×10^{-2}	-0.102×10^{-2}

Figure 3.57 shows graphically the development of horizontal displacements at the tip for

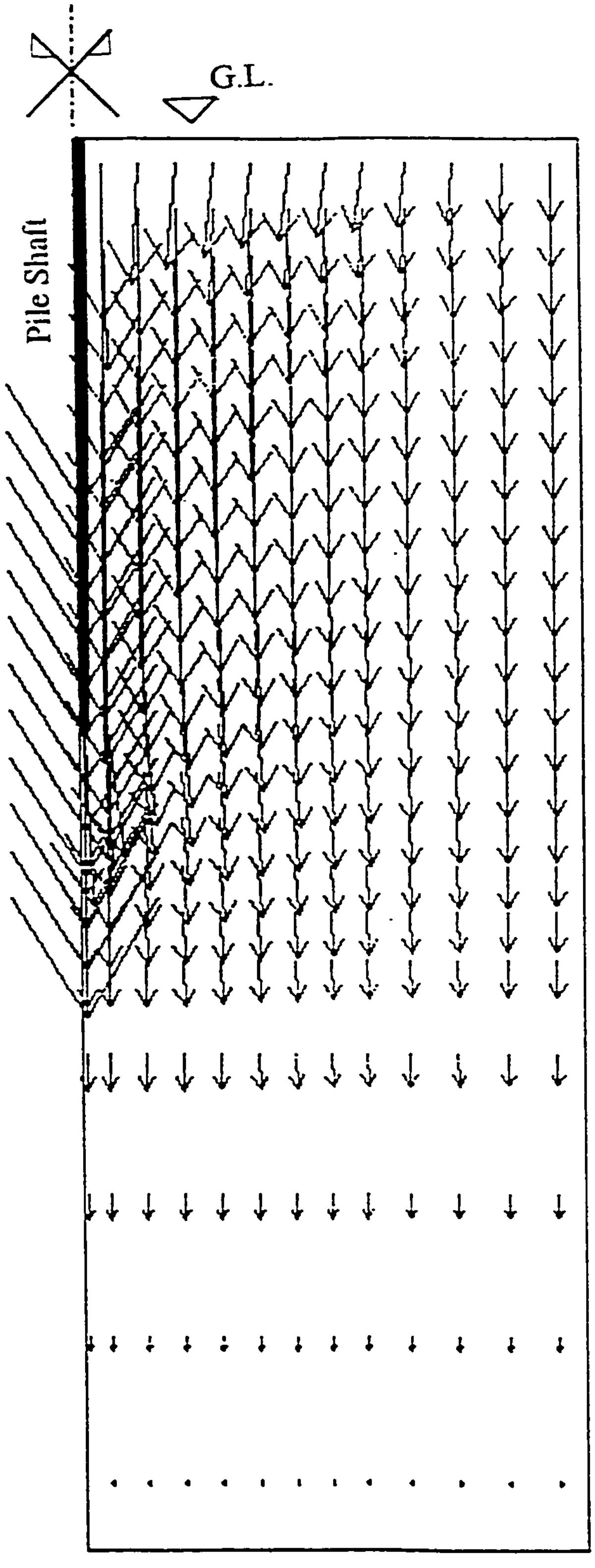

Figure 3.49 Displacement Vectors Around the Shaft, Increment Number 28.
Test Data: D = 12 m, B = 0.25 m, $K_i = K_o$, $\phi = \delta = 30°$.

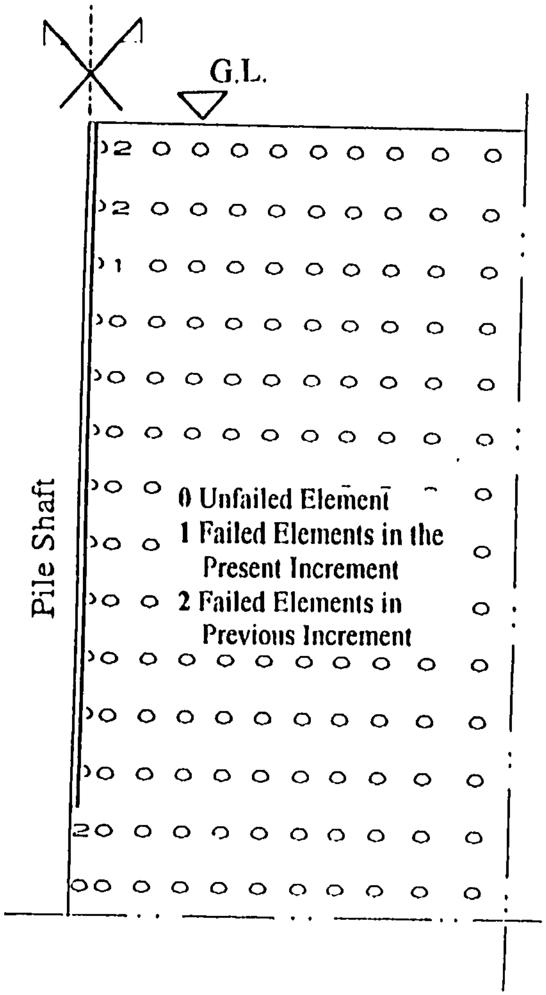

Figure 3.50 Failed Elements Around the Head, Increment Number 31. Test Data: D = 12 m, B = 0.25 m, $K_i = K_o$, $\phi = \delta = 30°$.

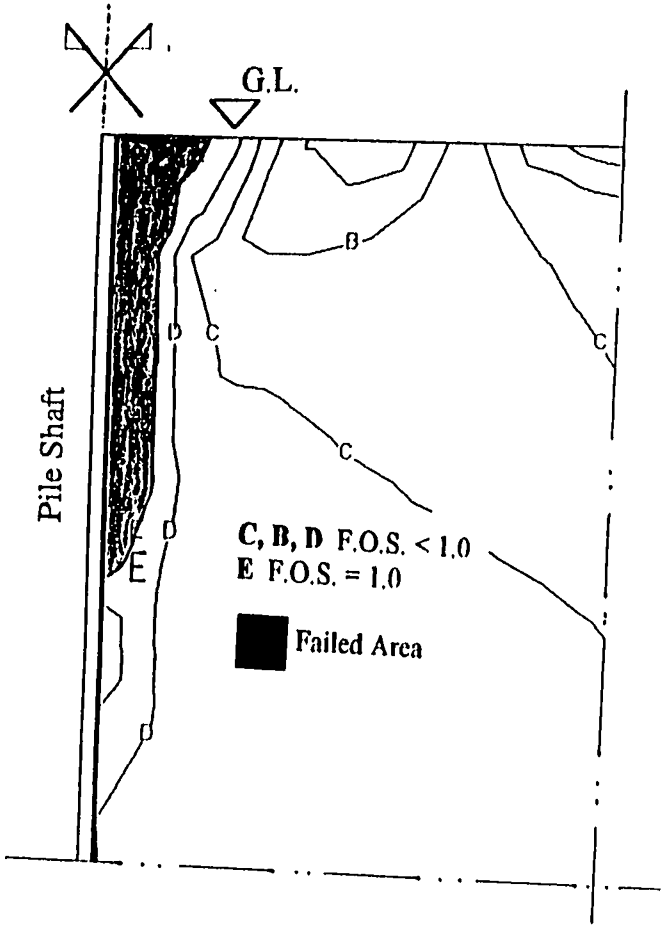

Figure 3.51 Contour Lines of Factor of Safety Against Shear Failure Around the Head, Increment Number 31. Test Data: D = 12 m, B = 0.25 m, $K_i = K_o$, $\phi = \delta = 30°$.

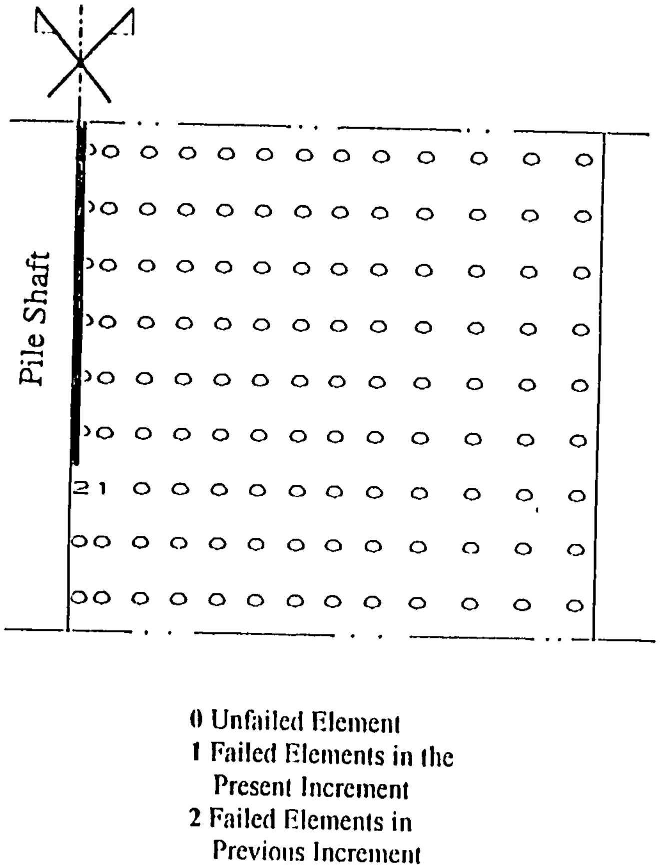

Figure 3.52 Failed Elements Around the Tip, Increment Number 44. Test Data: D = 12 m, B = 0.25 m, $K_i = K_o$, $\phi = \delta = 30^o$.

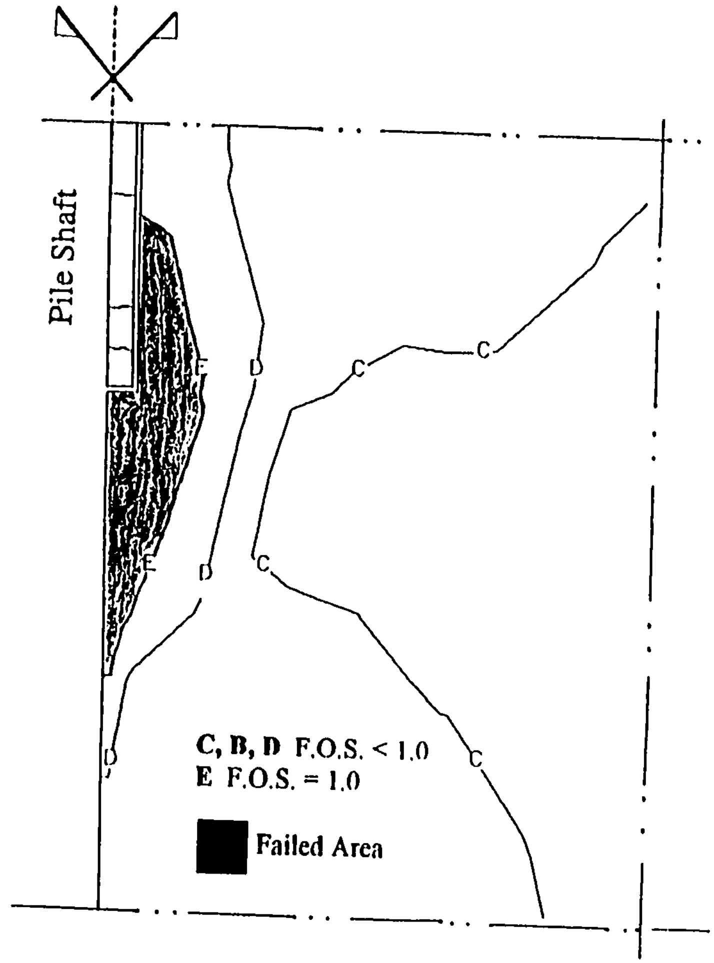

Figure 3.53 Contour Lines of Factor of Safety Against Shear Failure Around the Tip, Increment Number 44. Test Data: D = 12 m, B = 0.25 m, $K_i = K_o$, $\phi = \delta = 30^o$.

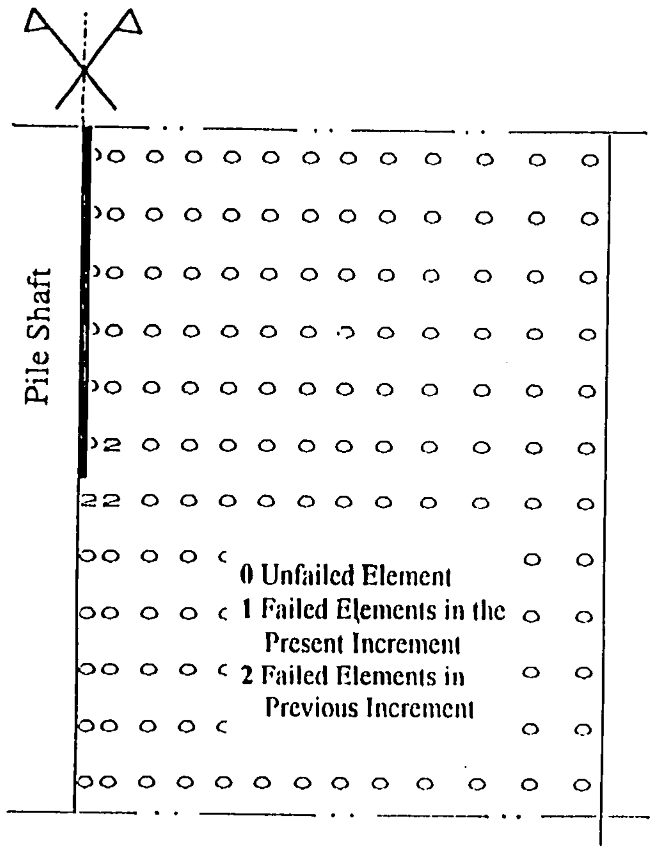

Figure 3.54 Failed Elements Around the Tip, Increment Number 48. Test Data: D = 12 m, B = 0.25 m, $K_i = K_o$, $\phi = \delta = 30^o$.

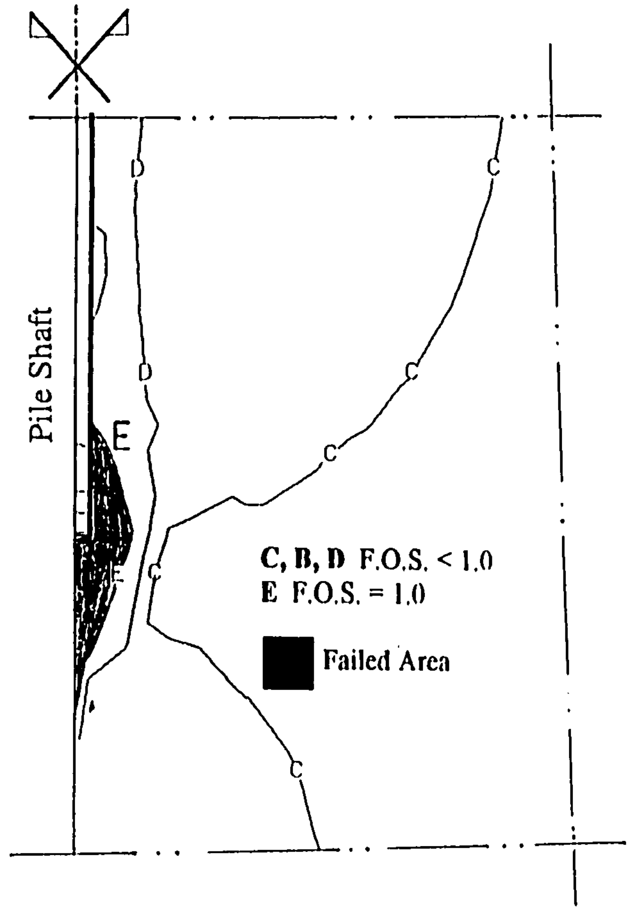

Figure 3.55 Contour Lines of Factor of Safety Against Shear Failure Around the Tip, Increment Number 48. Test Data: D = 12 m, B = 0.25 m, $K_i = K_o$, $\phi = \delta = 30^o$.

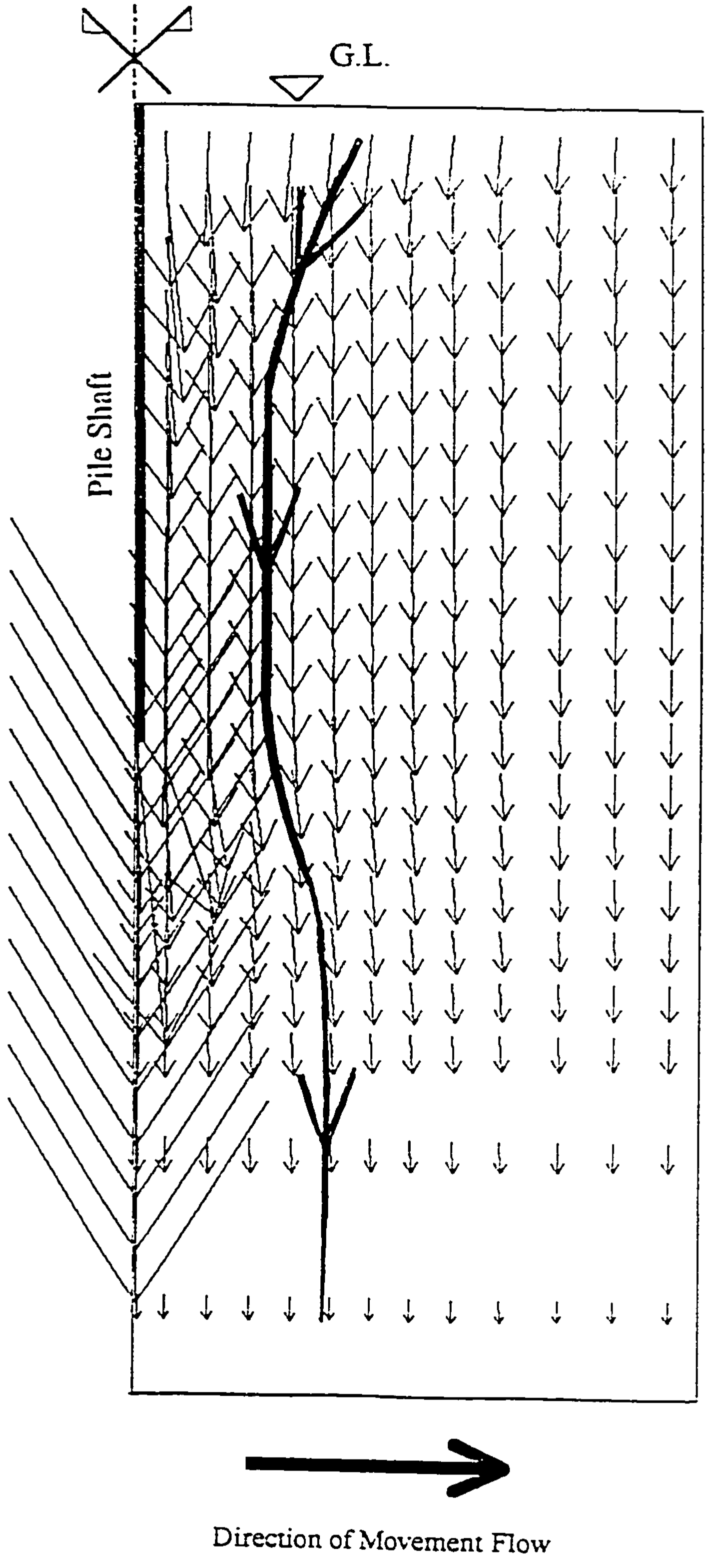

Figure 3.56 Displacement Vectors Around the Shaft, Increment Number 48
Test Data: D = 12 m, B = 0.25 m, $K_i = K_o$, $\phi = \delta = 30°$.

increments 11, 24, 28 and 44. This comparison reflects the mechanism of movements around the tip, where positive movements in the direction away from the tip are increased with loading increase. Figure 3.58 shows the development of horizontal displacements at the head for increments 11, 24, 28 and 44. Also the negative movements, against the pile head, increase up to increment number 31, where the skin resistance was fully mobilized and then decrease again with loading increase. These two Figures 3.57, 3.58 can help in understanding of the mechanism which control the failure pattern around the shaft where the mobilization of skin resistance needs a smaller amount of displacement to start mobilization. After full mobilization, the rate of displacement increase becomes much less than before full mobilization. On the other hand, the mobilization of tip resistance needs the amount of displacements to be much higher than those required by skin resistance and continue increasing with loading. The behavior is different in the two cases and contributes to better understanding of the failure mechanism around the shaft.

3.10.3 Failure Mechanism Around a Single Pile in Sand

With respect to the forgoing analyses of stresses and deformations around the pile shaft, the following remarks are due:

Three zones generally are expected to influence the stresses and deformations around the pile shaft:

a- Zone I located immediately beneath the ground surface and extending downward to a distance equal to $0.25H_1$ and horizontally to a distance of R or radius of influence, refer to Figure 3.59. This zone is subjected to a densification process due to pile loading and this reflects directly on the degree of mobilization of skin resistance which is highly mobilized beneath the ground surface.

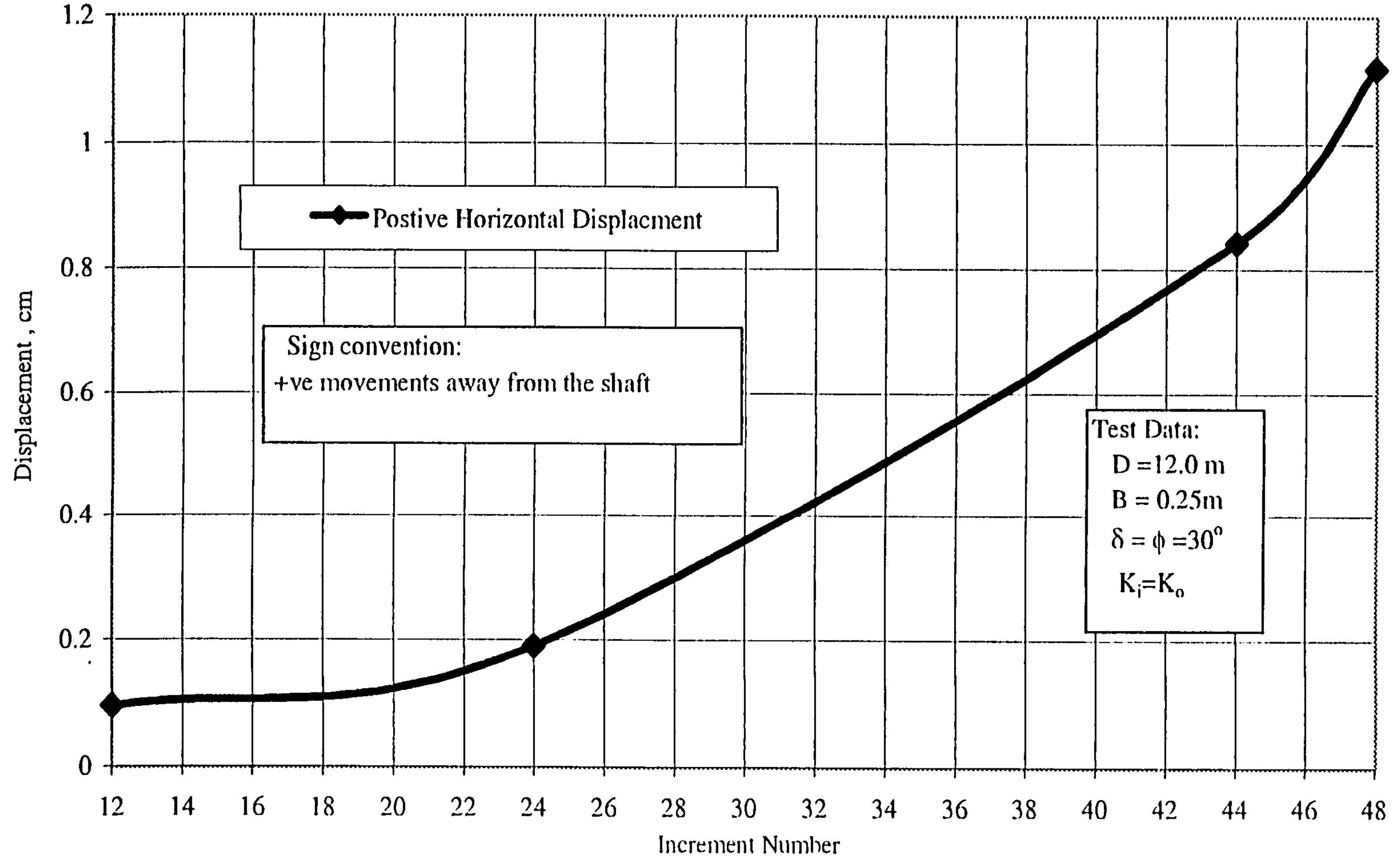

Figure 3. 57 Progress of Horizontal Displacement at Pile Tip Versus Loading Increments

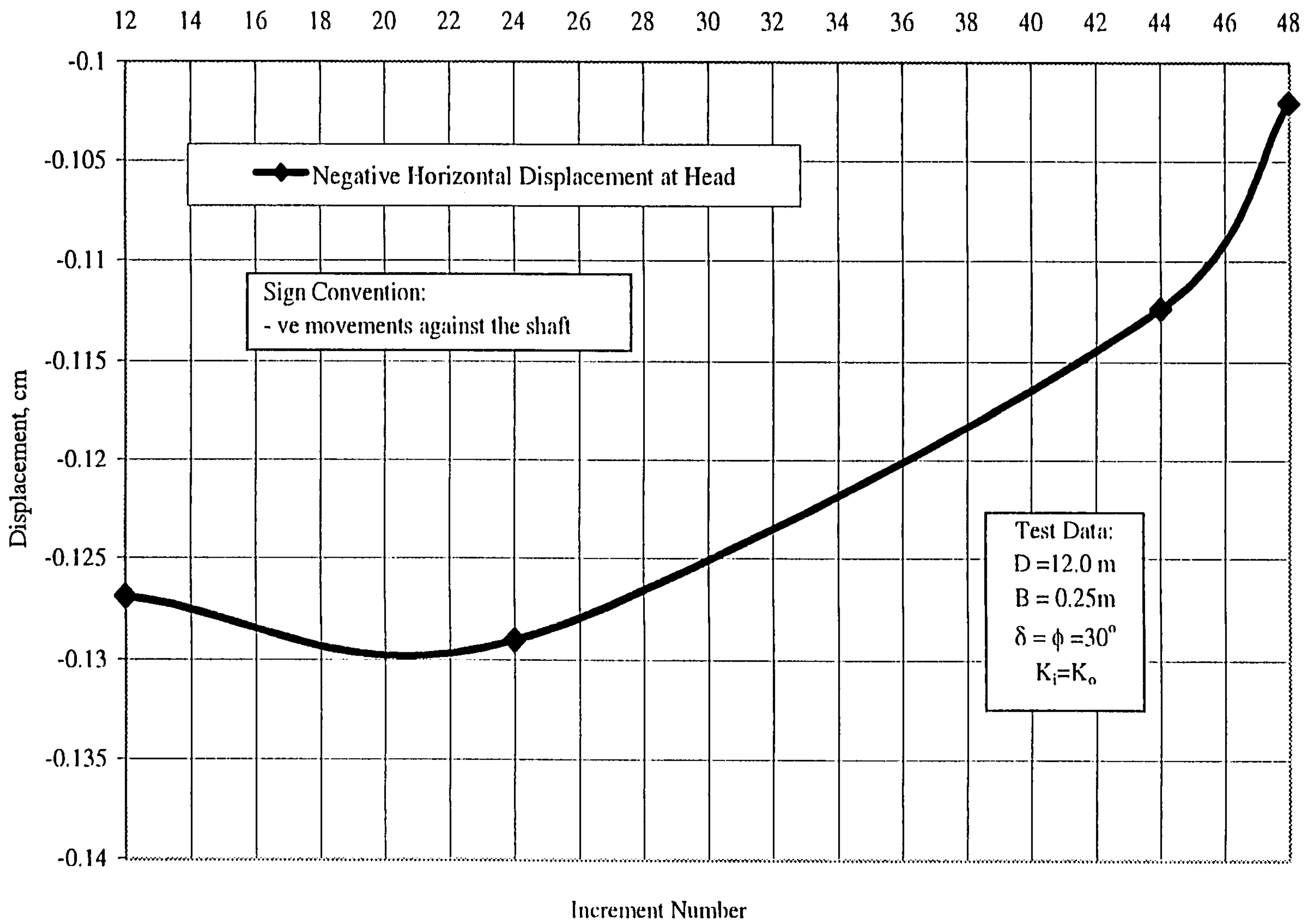

Figure 3.58 Progress of Horizontal Displacement at Pile Head Versus Loading Increments

b- Zone II which exists around the pile tip a few diameters above and a few diameters below with a total height of (L_1 +L_2 +L_3), refer to Figure 3.59. It is also subjected to a densification process due to the opening process for the advanced pile tip. The pile tip crushing and/or compacting the soil particles beneath and around creats an active earth pressure condition. And this process is actually deemed to influence the mobilization of tip resistance.

c- Zone III is located between the above two zones and is subjected to a loosening process and extends horizontally to a few diameters. In this zone the loosening process was found not sufficient to generate pressures against the shaft that could lead to increase in the degree of mobilization of skin resistance.

In summary, for the forgoing section about the development of failure pattern around a single pile in sand, the following conclusions are suggested (refer to Figure 3.59):

1- Failure pattern around the shaft is developed in two separate areas; around the pile head (skin resistance) and around the tip (tip resistance).

2- The volume of failure pattern due to mobilized skin resistance can be approximated to a converted cone, with its base at ground surface and an assumed base width equal to R (radius of influence measured from pile axis) and vertical height equal to assumed vertical distance H_1 measured from ground surface.

3- Failure pattern due to mobilized tip resistance can be approximated to a compacted cone beneath the tip, connected with a log-spiral curve extending to a horizontal distance r and then reverted back to the shaft with a vertical distance (L_1+L_2).

4- The developed failure mechanism can be assumed as shown in Figure 3.59. The model parameters: H_1, R, L_1,L_2,L_3 and r are variables and depend on several factors.

The factors involved in the assumed failure pattern were observed and the predictive equa-

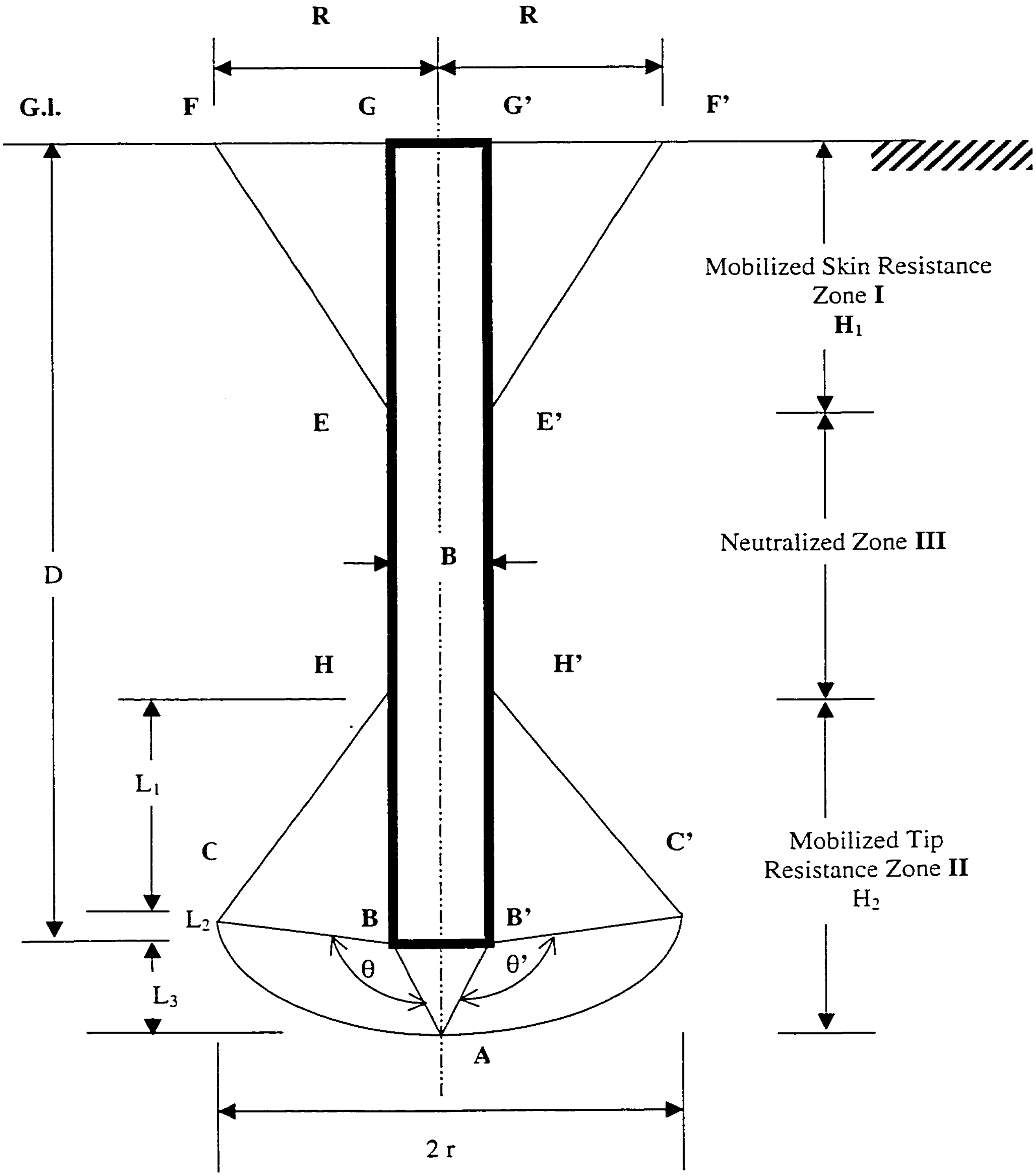

Figure 3.59 The Developed Failure Pattern Around Single Pile in Sand and The Influence Zones

tions for the model parameters were developed and introduced in the following sections.

3.11 Theoretical Model

3.11.1 General

It is concluded from the forgoing sections that the volume of soil involved in the failure mechanism around a single pile in sand can be approximated by two parts:

a- A conical volume with its base at ground level; base width is R or radius of influence at ground level and height H_1. This part is assumed to represent the failure mechanism due to mobilized skin resistance.

b- Second volume is a semi bulb shaped around the tip with a total height of (L_1+L_2+L_3) and width equal to r; where r is the radius of influence at the pile tip and with dimensions L_1,L_2 & L_3 as shown on Figure 3.59.

The parameters R, H_1, L_1,L_2, L_3 and r will be considered as the main parameters needed to establish the theoretical model to predict ultimate load for a single pile in sand. The proposed theoretical model will be introduced in Chapter Four of this thesis. The main objective of the following section is to develop a mathematical predictive equations to determine the variable model parameters.

3.11.2 Radius of Influence "R"

Radius of influence at ground surface R is the horizontal distance located at the ground surface measured from the pile axis of symmetry. This distance represents the base of the conical shaped failure zone due to mobilized skin resistance. Table 3.10 gives the output results for the parametric study.

Figure 3.60 introduces a graphical relationship between the radius of influence "R/D" versus pile depth "D" for angle of shearing resistance ϕ range from 25^{o} to 45^{o}, with respect to pile width "B", for a total of 120 tests. Analysis of this Figure 3.60 shows that R/D increases with the increase of ϕ in all series and decreases with respect to pile depth D.

In order to develop a representative equation for this trend; the following procedure was followed:

1- An estimated lowest envelop of R/D at $\phi = 25^{o}$ and B = 0.25m was produced graphically in Figure 3.61. The best fit Equation is as follows:

$$R/D_{(at\ \phi=25^{o})} = -0.23+0.0096*[\ln(D)]^2+0.93*[1.0/(\mathrm{sqrt}(D)]$$
$$-0.88*e^{-D} \qquad ...(3.17)$$

Where:

D = Pile Depth

and e = Euler's number = 2.71828

2- An additional increase of R/D due to the increase of ϕ is presented in Figure 3.62, where the average maximum difference between the value of "R/D" at $\phi = 25^{o}$ and at $\phi = 45^{o}$ is found to be about 0.0574. This amount was distributed over the range of 20^{o} which represents the corresponding maximum difference of ϕ. The best fitting equation for this function is as follows:

$$RF = -7.93016446E-21 + xR*0.0027 \qquad ...(3.18)$$

Where: $xR = (\phi-25)^{o}$

The value of R/D at any value of ϕ will be:

$$R/D_{(at\ any\ value\ of\ \phi)} = (R/D)_I = R_{(at\ \phi=25^{o})} + RF \qquad ...(3.19)$$

3- An average increase in R/D versus the increase in pile width "B" is presented in Figure 3.63. It should be noted that this increase was found to depend on pile depth "D" and deter-

Table 3.10 Parametric Study Results for Model Parameter: Radius of Influence "R"

Pile Geometry, m		Radius of Influence "R", meter				
B	D	$\phi = 25°$	$\phi = 30°$	$\phi = 35°$	$\phi = 40°$	$\phi = 45°$
0.25	3	0.823	0.879	0.978	1.11	1.27
0.25	6	1.04165	1.152	1.248	1.35	1.47
0.25	9	1.125	1.23	1.35	1.47	1.6
0.25	12	1.2	1.3	1.4	1.54	1.67
0.25	18	1.332	1.43	1.55	1.66	1.79
0.25	24	1.272	1.37	1.5	1.67	1.8
0.4	4.8	1.56	1.67	1.8	2.06	1.92
0.4	9.6	1.76	1.89	2	2.24	2.1
0.4	14.4	1.84	1.97	2.1	2.35	2.2
0.4	19.2	1.92	2.02	2.13	2.39	2.27
0.4	28.8	1.9	2	2.1	2.35	2.23
0.4	38.4	1.89	1.98	2.12	2.4	2.23
0.5	6	2.24	2.32	2.46	2.6	2.7
0.5	12	2.44	2.52	2.63	2.75	2.87
0.5	18	2.49	2.58	2.69	2.8	2.92
0.5	24	2.47	2.56	2.69	2.81	2.95
0.5	36	2.5	2.58	2.72	2.84	2.93
0.5	48	2.53	2.63	2.76	2.87	2.98
0.75	9	2.96	3.1	3.27	3.44	3.64
0.75	18	3.2	3.32	3.47	3.62	3.76
0.75	27	3.2	3.36	3.49	3.64	3.8
0.75	36	3.2	3.35	3.49	3.62	3.78
0.75	54	2.78	2.98	3.18	3.32	3.48
0.75	72	2.54	2.74	2.95	3.1	3.29

Table 3.11 Parametric Study Results for Model Parameter: Radius of Influence at Tip "r"

Pile Geometry, m		Radius of Influence at Tip "r", meter				
B	D	$\phi = 25°$	$\phi = 30°$	$\phi = 35°$	$\phi = 40°$	$\phi = 45°$
0.25	3	0.29	0.35	0.4125	0.447	0.547
0.25	6	0.35	0.42	0.48	0.52	0.5625
0.25	9	0.333	0.3717	0.4203	0.4617	0.56
0.25	12	0.381	0.4428	0.498	0.528	0.62
0.25	18	0.507	0.556	0.615	0.68	0.76
0.25	24	0.624	0.704	0.785	0.871	0.924
0.4	4.8	0.78	0.88	0.95	1.05	1.1376
0.4	9.6	0.7	0.81	0.94	1.09	1.22
0.4	14.4	0.76	0.91	1.03	1.14	1.31
0.4	19.2	0.86	1	1.14	1.28	1.4
0.4	28.8	1.13	1.36	1.524	1.64	1.81
0.4	38.4	1.33	1.54	1.82	2.01	2.22
0.5	6	1.26	1.37	1.51	1.64	1.78
0.5	12	1.1	1.27	1.44	1.59	1.76
0.5	18	1.09	1.26	1.4	1.58	1.77
0.5	24	1.15	1.28	1.44	1.63	1.87
0.5	36	1.37	1.56	1.78	1.97	2.23
0.5	48	1.47	1.67	1.86	2.09	2.38
0.75	9	2.01	2.28	2.49	2.65	2.9
0.75	18	1.94	2.17	2.4	2.63	2.9
0.75	27	1.94	2.18	2.4	2.65	2.94
0.75	36	2.13	2.31	2.52	2.772	3.096
0.75	54	2.21	2.48	2.68	2.93	3.24
0.75	72	2.36	2.64	2.93	3.2	3.5

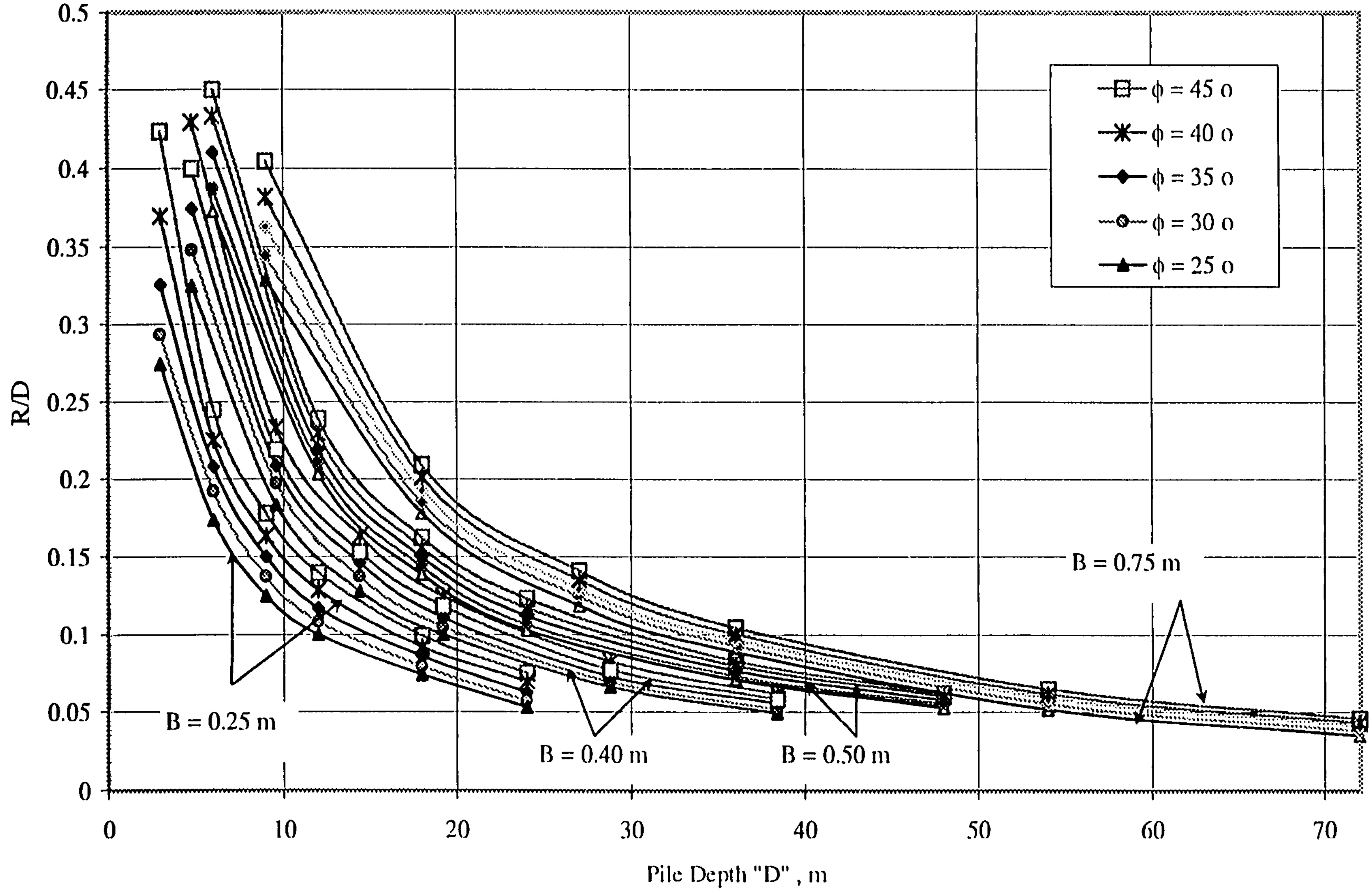

Figure 3.60 Relationship of Radius of Influence "R/D" Versus ϕ, D and B

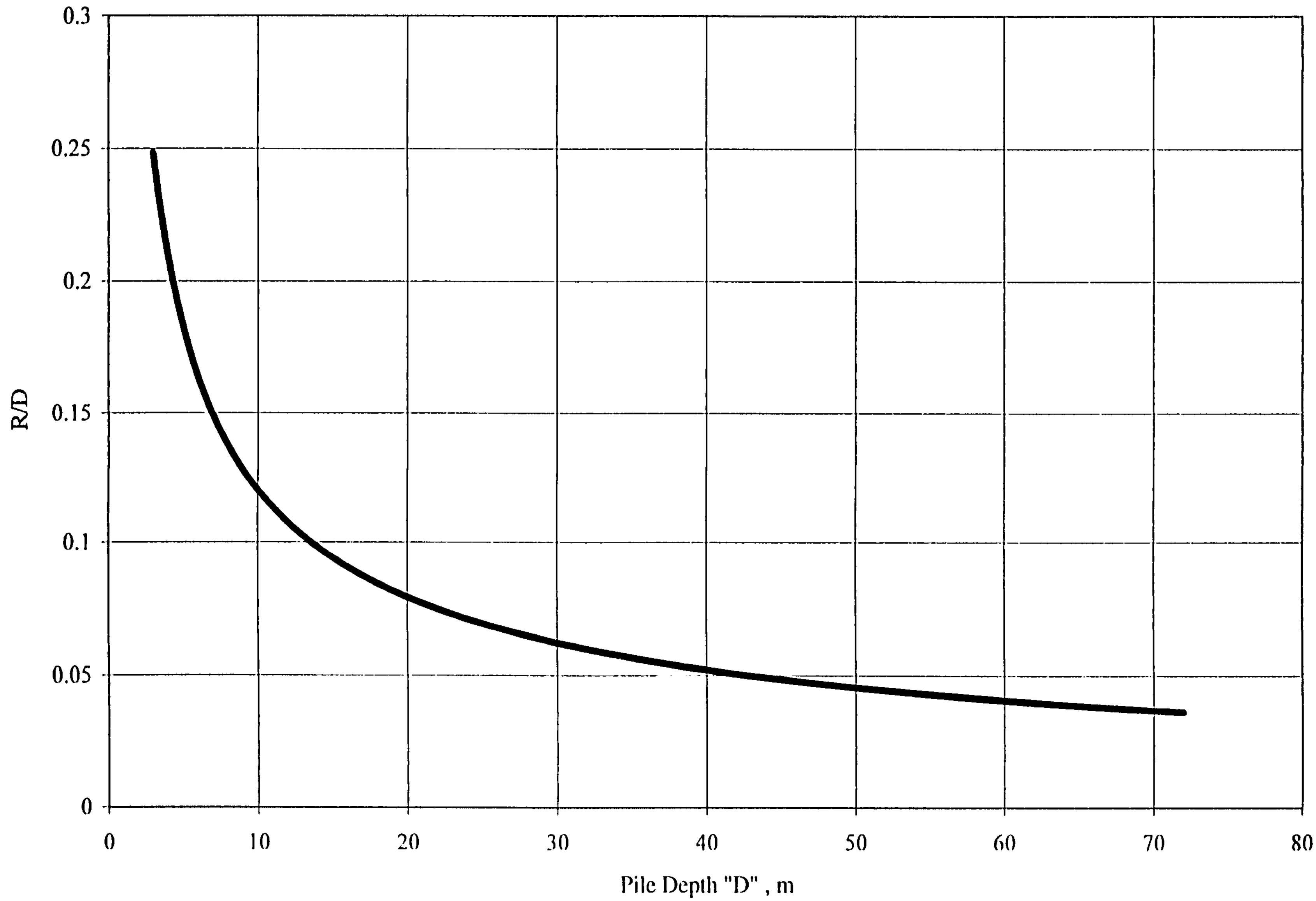

Figure 3.61 R/D Versus Pile Depth, "D" For Lower Envelope at $\phi = 25^{0}$ and B = 0.25 m

mined based on the average difference between values of R/D at B = 0.75 m and the lower values at B = 0.25 m for all series (refer to Figure 3.60). The predictive equation for this rate of increase which is presented graphically in Figure 3.63, is as follows:

$$RB=0.055 - 0.00069*D + (2.52E\text{-}06)*D^2 + 10.53*(\ln D/D^2) - 8.701*(1/D^2) \quad ...(3.20)$$

Then:

$$(R/D)_{II} = (R/D)_I + RB \quad ...(3.21)$$

R in meters, $R_I = (R/D)_{II} * D$

3.11.2.1 Effect of Angle of Friction δ on the Value of "R"

In order to determine the effect of changing the angle of friction between the pile and sand δ, a few selected tests were carried out in a form of parametric study. In performing these tests, all parameters were frozen at intermediate value while only δ was changed. Three values for δ were chosen: δ/ϕ = 1, 2/3 and 1/2. It is important to mention here that the whole parametric study was carried out considering the value of $\delta/\phi = 1.0$ for all tests and the effect of changing δ was investigated in a separate study.

Figures 3.64 to 3.68 show the relationship between δ in degrees and "R" in meters for a variety of pile load tests with different slenderness ratios. Each Figure shows this relationship for one value of φ. In the analysis of these Figures, it was found that "R" decreases with the decrease of δ, and the average of decrease due to the decrease of δ, was found to be about 30% in the range of $25^o < \phi < 45^o$. This rate of decrease is given in Equation 3.22:

$$RD = 0.3 - (0.6*(\delta/\phi - 0.5)) \quad ...(3.22)$$

Finally:

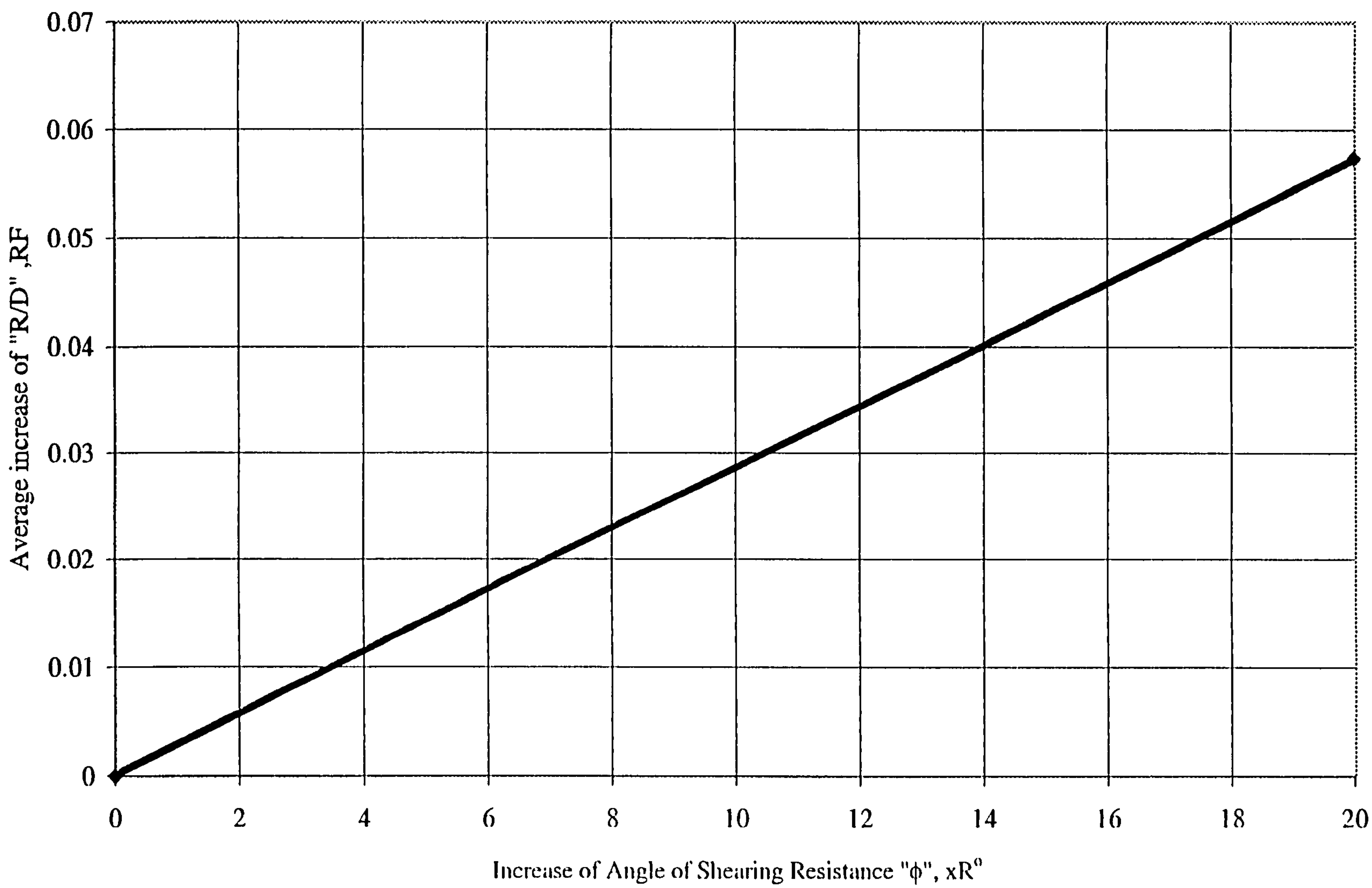

Figure 3.62 Average increase in "R/D" due to the increase of "ϕ"

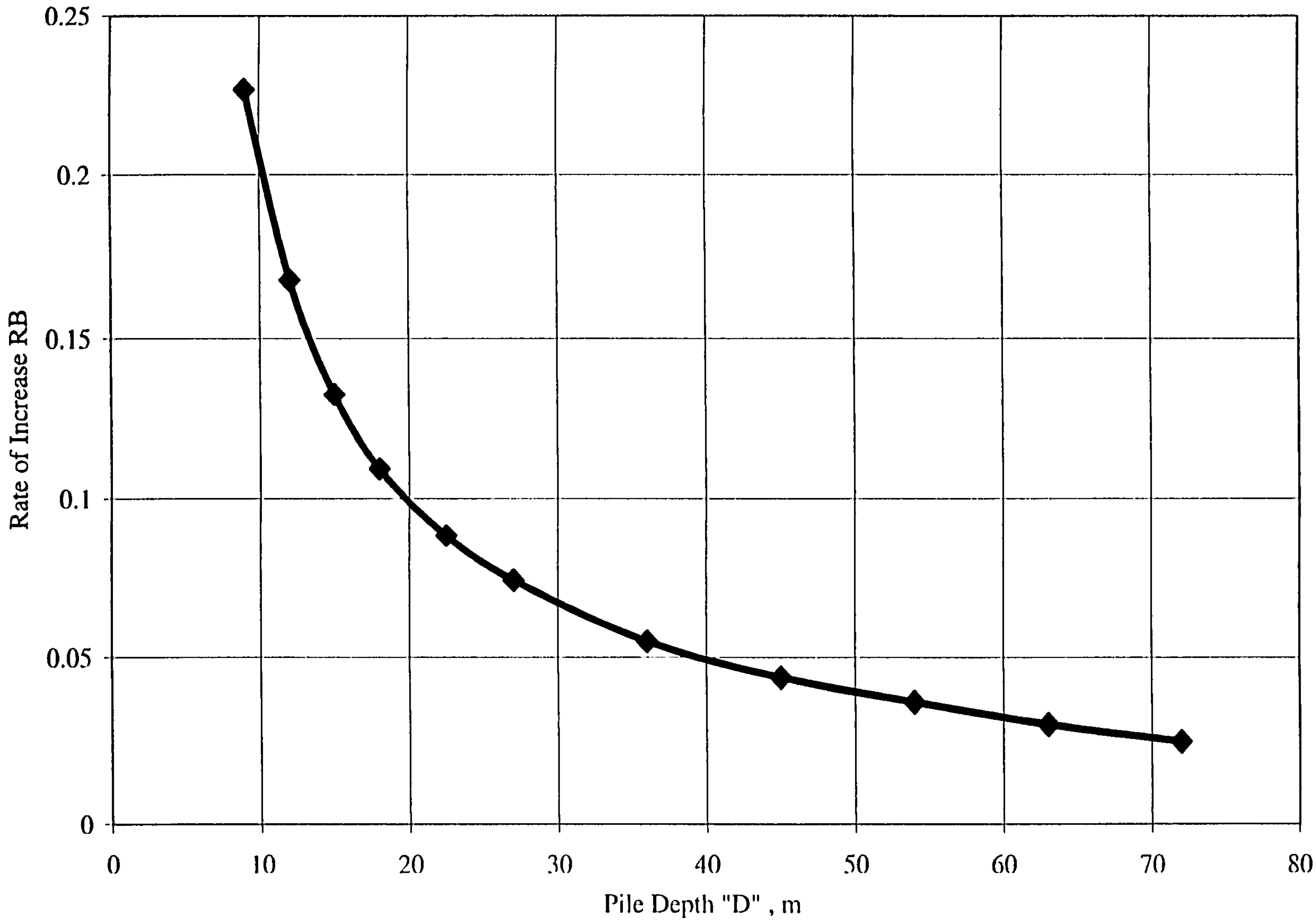

Figure 3.63 Rate of Increase in R/D due to Increase of Pile's Width "B"

$$R = R_I * (1 - RD) \qquad ...(3.23)$$

3.11.3 Radius of Influence at Tip "r"

Table 3.11 introduces the out-put results of the parametric study with respect to radius of influence at tip "r". Figure 3.69 introduces the relationship between "r" and Pile depth "D" in a form of four groups; each group represents one pile diameter and five values for angle of shearing resistance, "ϕ"; each point in this graph represents one test result with a total of 120 tests for radius of influence at tip "r". As can seen from this Figure 3.69 the value of "r" increases with respect to the increase of the following: angle of shearing resistance, ϕ, pile depth "D" and diameter "B".

In order to establish a general function to predict radius of influence at tip "r" with respect to the following parameters: angle of shearing resistance, ϕ, pile depth "D" and diameter "B", the following procedure was followed:

1- An average for the lowest values of "r" at ($\phi = 25^o$) and pile diameter = 0.25 meter were plotted against pile depth "D" in Figure 3.70. The following equation was established based on the best fitting equation for the forgoing data:

$$r_{(at\ \phi = 25^o)} = 0.43 + 4.89 * (11.96 * (\ln(e^{((D+33.91)/5.98)} + e^{(9.182)})$$

$$- \ln(e^{((14.852)+e(D/5.98)))} + 67.811) / (135.622) \qquad ...(3.24)$$

Where:

D = Pile depth in meters

2- As Equation 3.24 was determined based on a value of r at 25^o and B = 0.25m, the following two additions to the value of: $r_{(at\ \phi = 25^o)}$ were established:

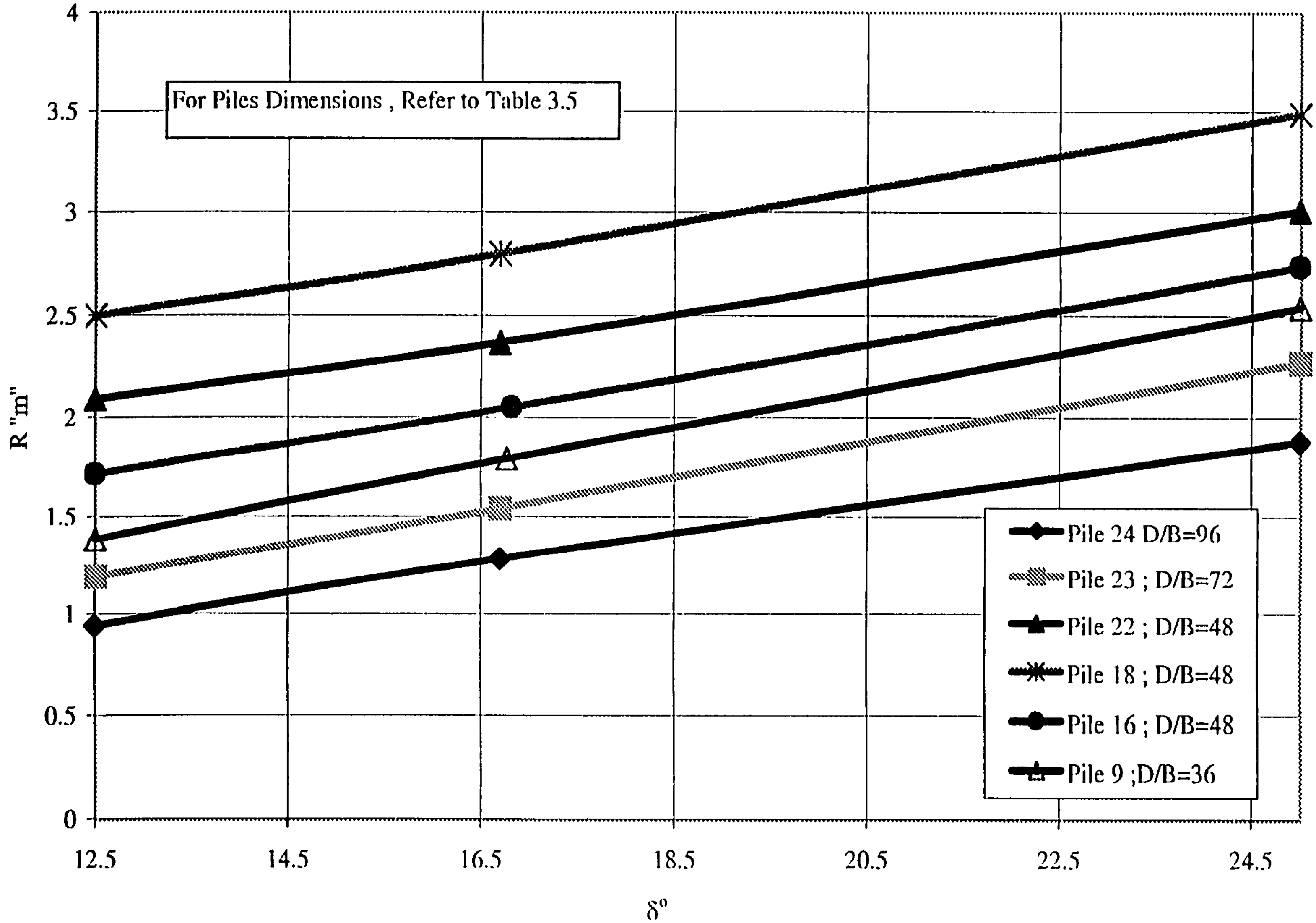

Figure 3.64 Effect of Change of Angle of Friction Between Pile and Sand "δ" on Radius of Influence "R" (Case of "ϕ" =25°)

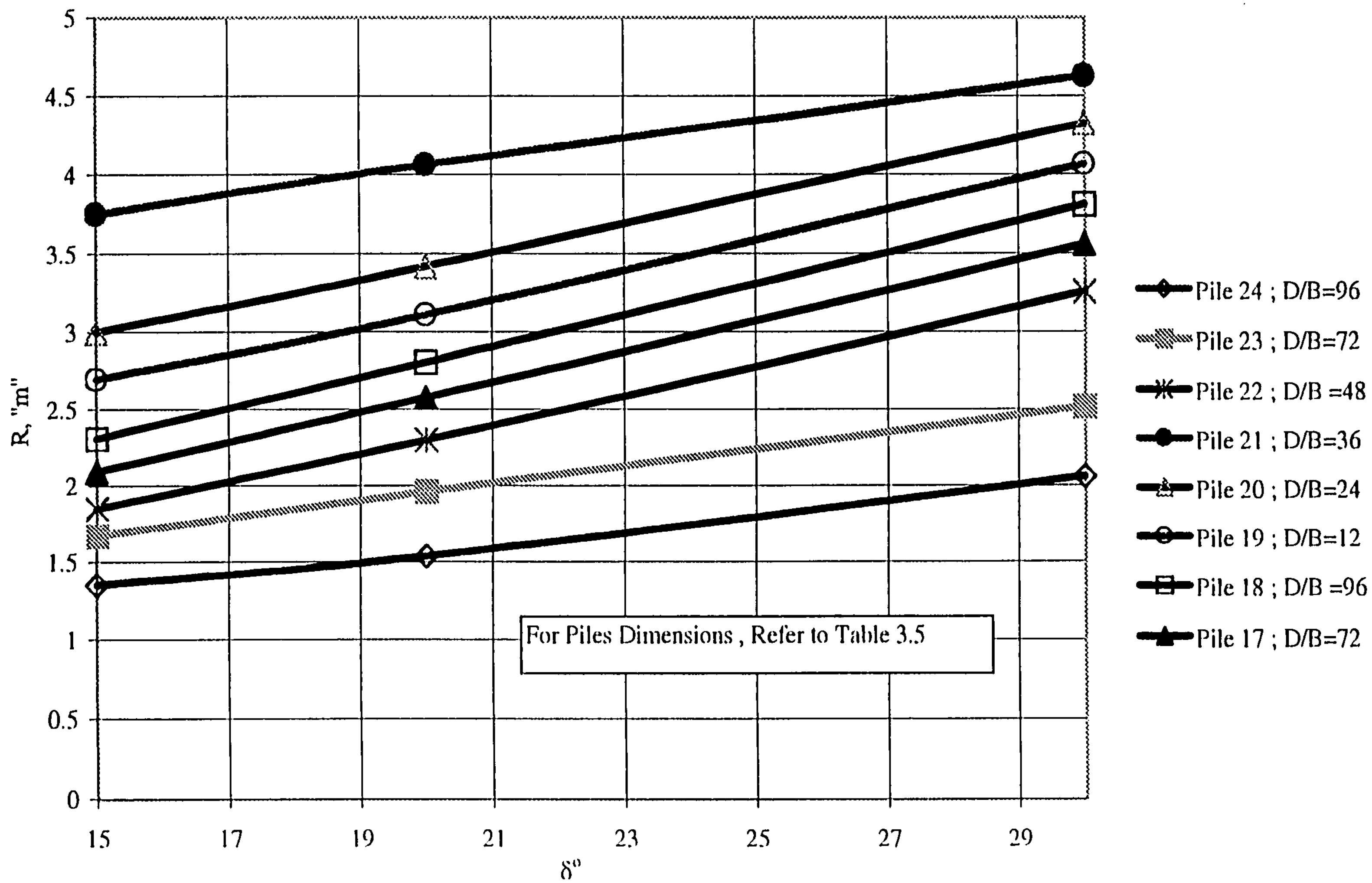

Figure 3.65 Effect of Change of Angle of Friction Between Pile and Sand "δ" on Raduis of Influnce "R"
(Case of $\phi = 30^{o}$)

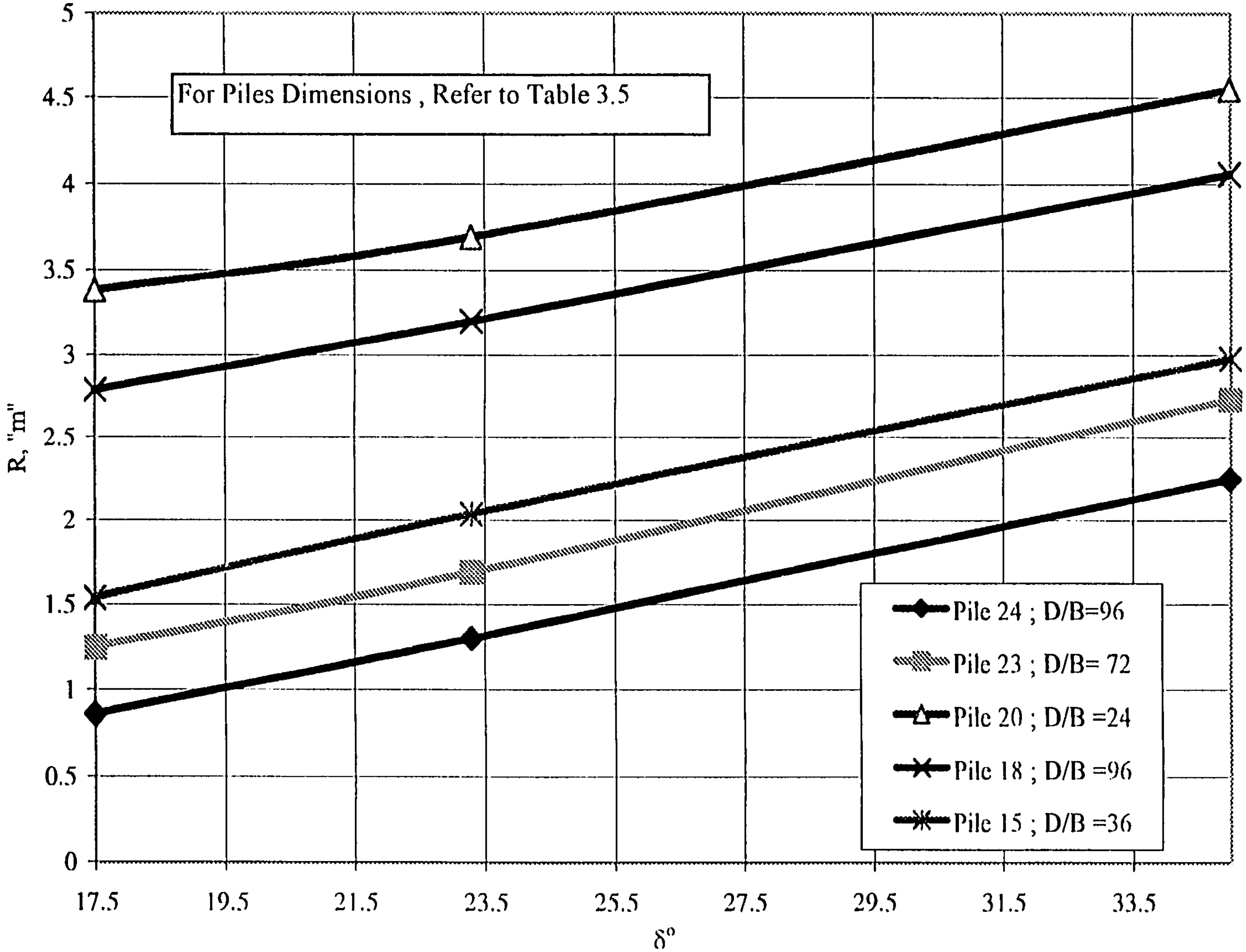

Figure 3.66 Effect of Change of Angle of Friction Between Pile and Sand "δ" on Raduis of Influnce "R"
(Case of $\phi = 35^o$)

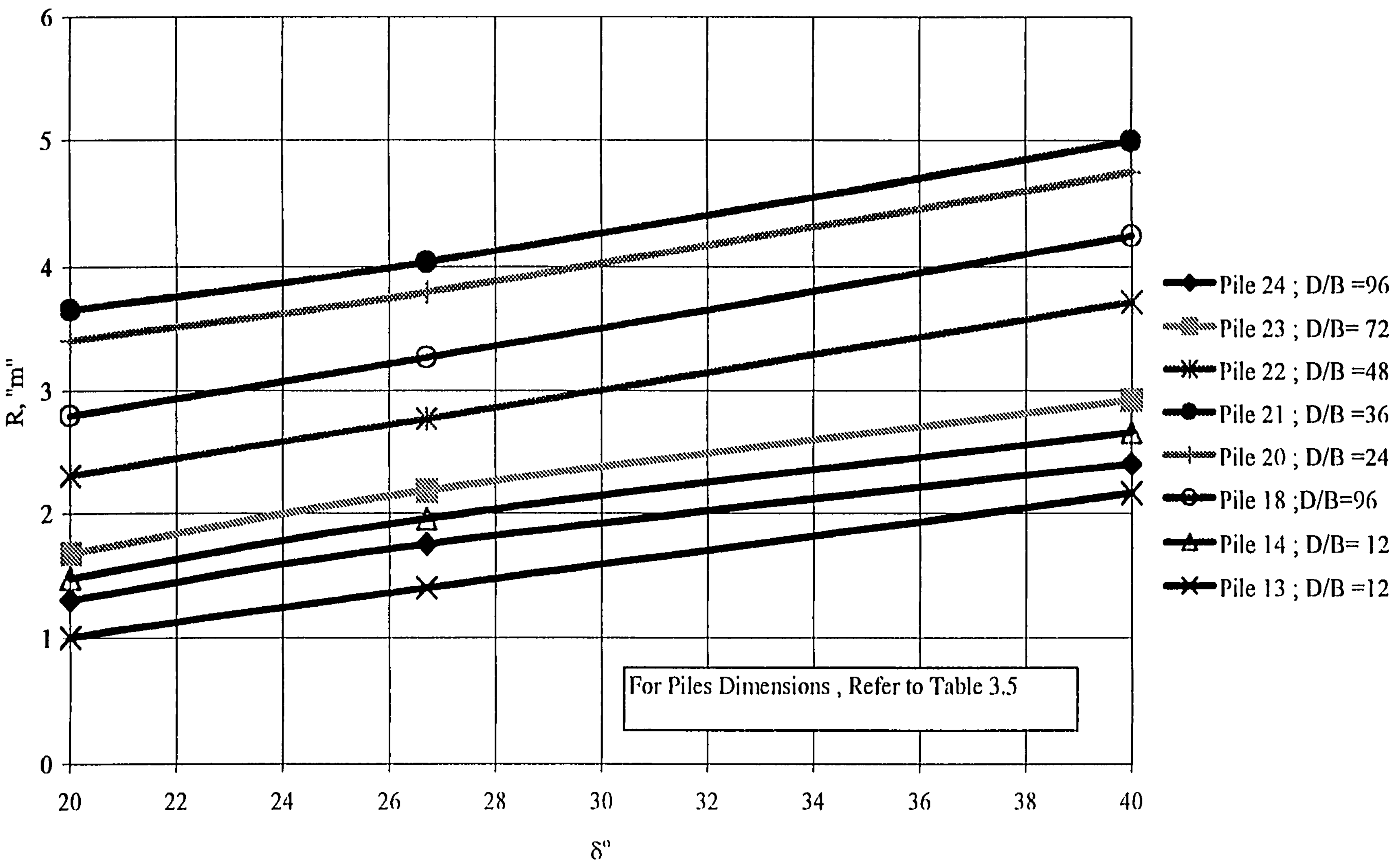

Figure 3.67 Effect of Change of Angle of Friction Between Pile and Sand "δ" on Raduis of Influnce "R"
(Case of $\phi = 40^{o}$)

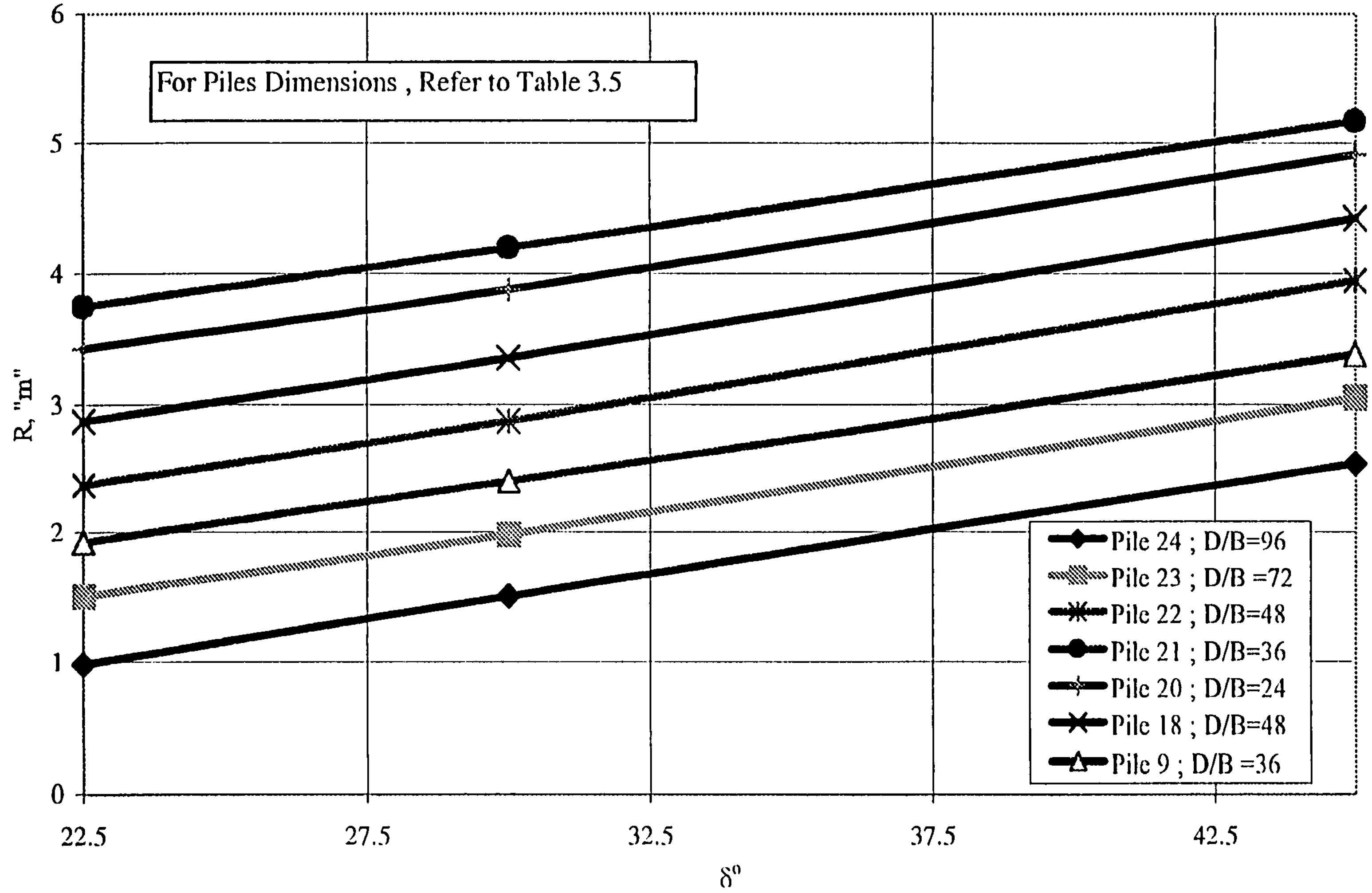

Figure 3.68 Effect of Change of Angle of Friction Between Pile and Sand "δ" on Raduis of Influnce "R"
(Case of $\phi = 45^o$)

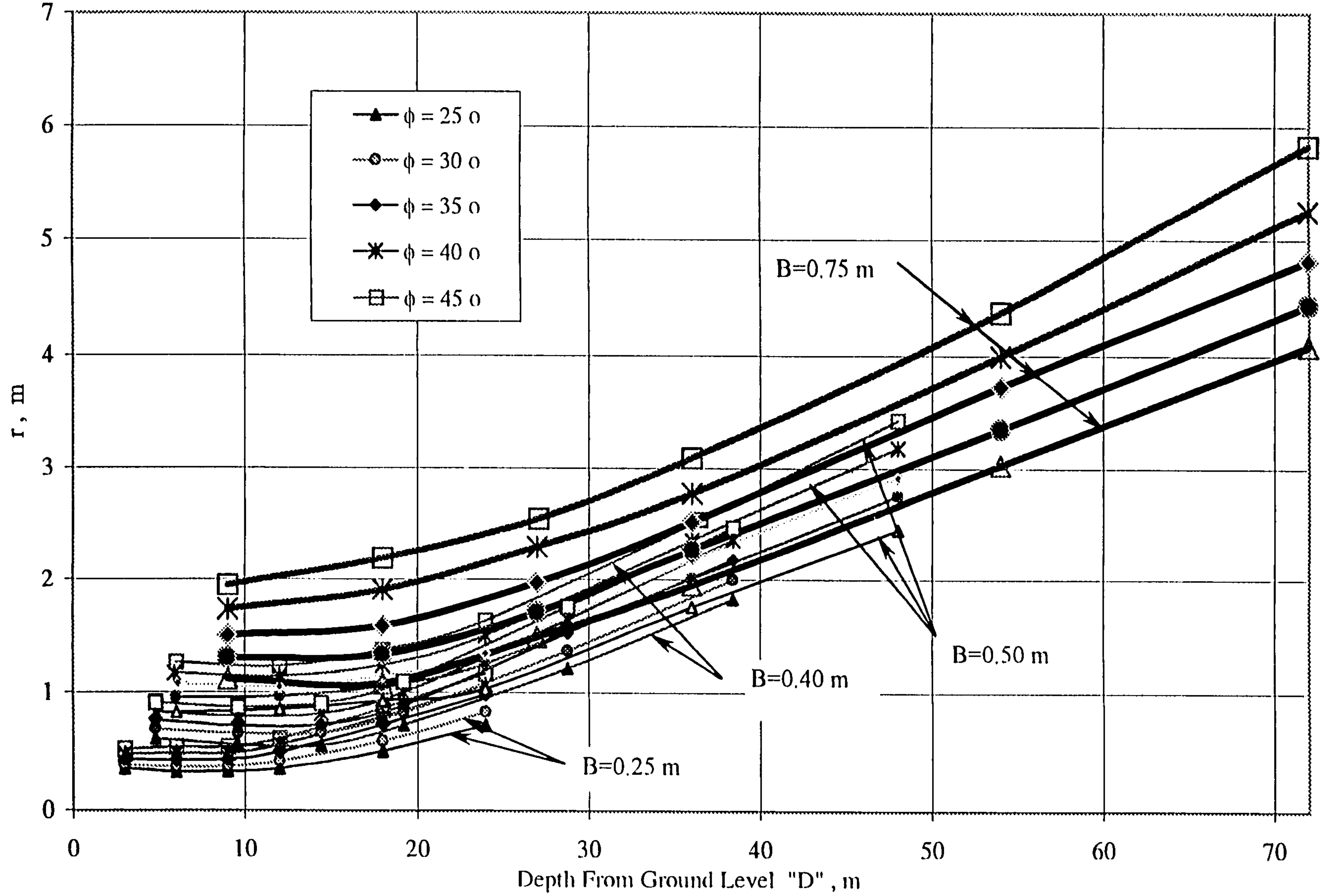

Figure 3.69 Relationship between Radius of Influence at Tip "r" ,
Angle of Shearing Resistance "ϕ" and Pile Depth with Respect to Pile Diameter "B"

a- Increase due to the increase of pile width B:

$$rB=0.004+0.293/(1.0+\exp(-(D-13.672)/-2.621)) \quad ...(3.25)$$

Equation 3.25 is given graphically in Figure 3.71.

Then:

$$(r)_I = r25 + ((0.75-B)/0.5)*rB \quad ...(3.26)$$

b - Increase due to the increase of ϕ:

The maximum average difference between r at 25^o and at r at 45^o was found to be 0.63 meter.

This difference was distributed over 20^o,and the following equation was produced:

$$r_\phi = 0.0315*(\phi - 25) \quad ...(3.27)$$

$$(r)_{II} = (r)_I + r_\phi \quad ...(3.28)$$

3.11.3.1 Effect of Shaft Relative Roughness δ/ϕ on Radius of Influence at Tip "r"

The same procedure followed to determinate the effect of changing "δ" on "R" was applied in the present section. Figures 3.72 to 3.76 introduce the effect of the changing of "δ" on "r" for selected pile load tests. Analysis of theses Figures 3.72 to 3.76 implies that no major effect should be considered. To determine the value of "r", equation 3.28 will be implemented and used for the whole analysis without modifications for such effect.

3.11.4 Vertical Distance H_1

The vertical distance H_1 is the vertical dimension of the conical-shape for the mobilized skin

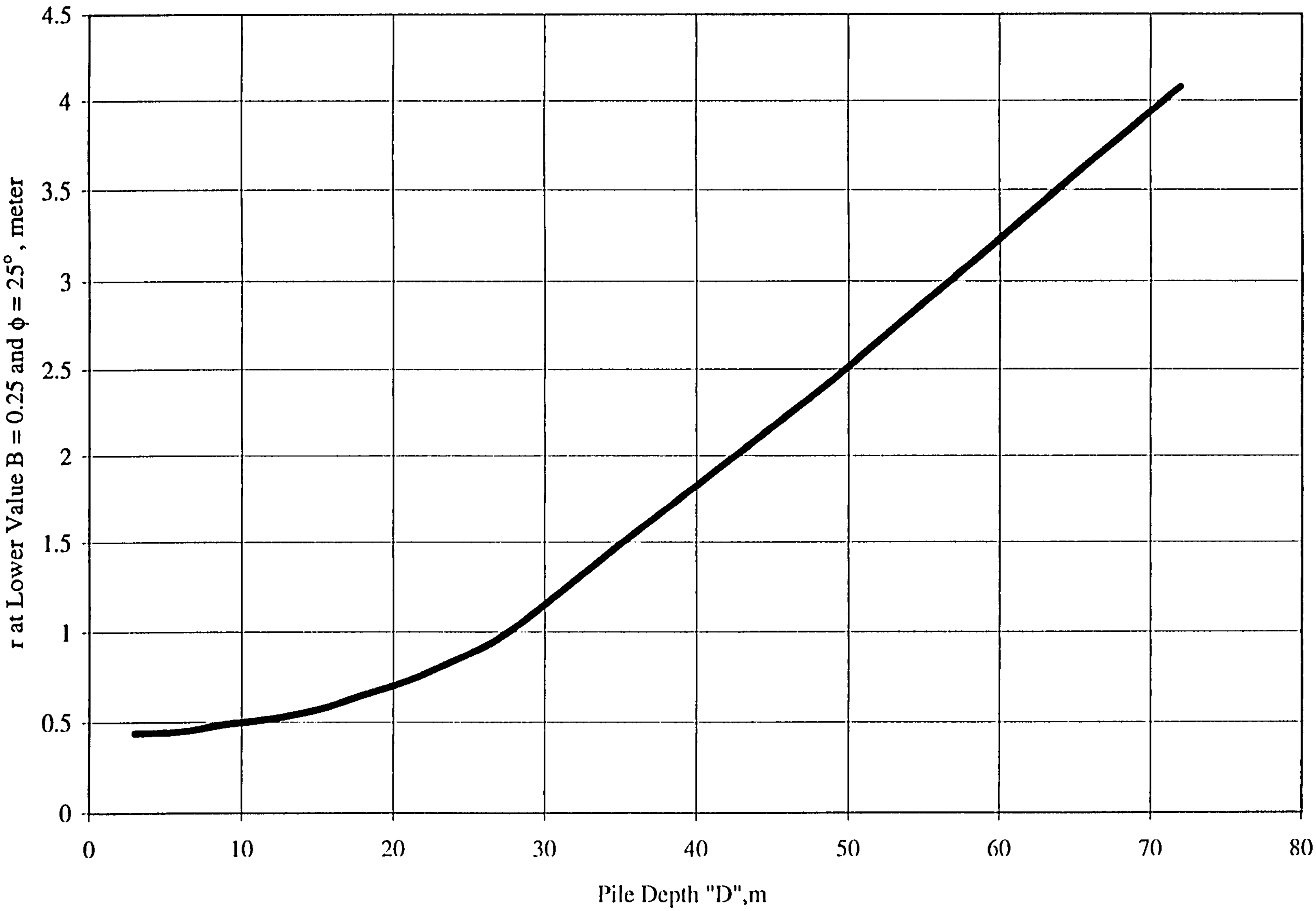

Figure 3.70 Relationship between Radius of Influence at Tip "r" and Pile Depth at Angle of Shearing Resistance "ϕ" =25^{0} and Pile Diameter "B = 0.25 m"

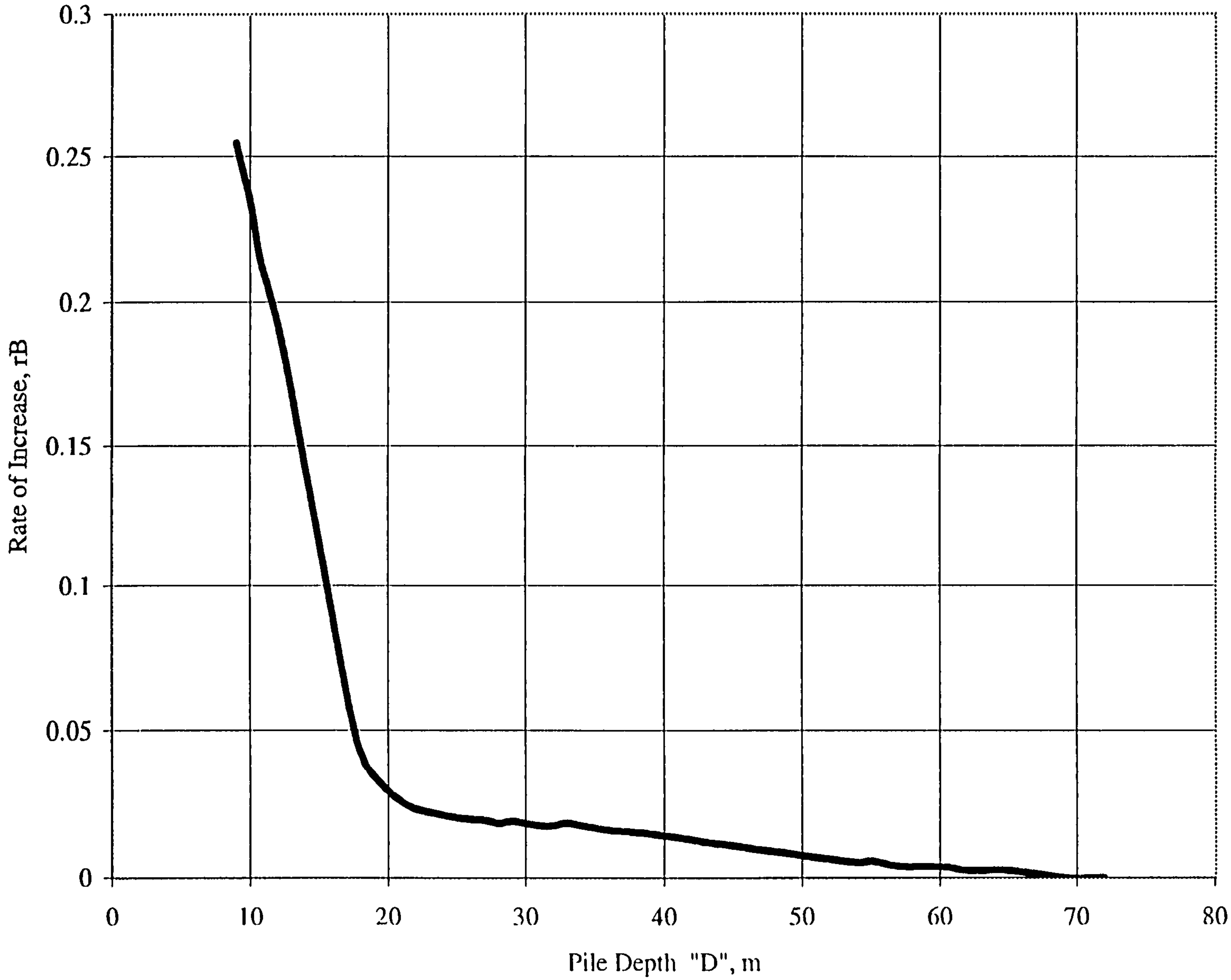

Figure 3.71 Rate of Increase of "r" Due to the Increase of B

resistance zone of the proposed theoretical model. It is measured from ground level with a total vertical distance H_l (Table 3.12 introduce the detailed parametric study results for H_l). Figure 3.77 produced the relationship between H_l in meters and ϕ, with respect to pile depth D and diameter B. From this figure 3.77 the following can be seen:

1- H_l increases with the increase of ϕ, and this increase is dependent on pile depth. The trend for all groups could be considered the same. An upper envelope for all groups is produced in Figure 3.78 based on average values at $\phi = 45^o$ and B = 0.75m. Equation 3.28 introduces the best fitting function for this envelope, it is also shown graphically in Figure 3.78.

$$H_{l(45)} = (0.16+D*(0.571+D*(-0.024+D*0.000678)))/$$

$$(1.0+D*(-0.048+D*(0.0011+D*7.514E-06))) \qquad ...(3.29)$$

2- For the relationship introduced in equation 3.29, two reductions should be applied:

a- Reduction due to the decrease of pile diameter B, "HB": equation 3.30 gives this reduction based on average decrease found in Figure 3.77. It is found that this reduction depends on pile depth "D".

$$HB=-3.66+(\log(D))*(5.75+(\log(D))*(1.89+(\log(D))*(-7.56+(\log(D))*$$

$$(4.64+(\log(D))*(-1.065+(\log(D))*0.086))))) \qquad ...(3.30)$$

Where: HB is in meters. Equation 3.30 is introduced graphically in Figure 3.79.

Then:

$$(H_l)_I = H_{l(45)} - HB \qquad ...(3.31)$$

b- Reduction due to the decrease of angle of shearing resistance ϕ, equation 3.32 introduce this decrease based on average observations of Figure 3.77.

$$Hf = -2.01+ 0.48*D - 0.033*D*SD + 20.29*\ln D/D^2 -21.97*e^{-D} \qquad ...(3.32)$$

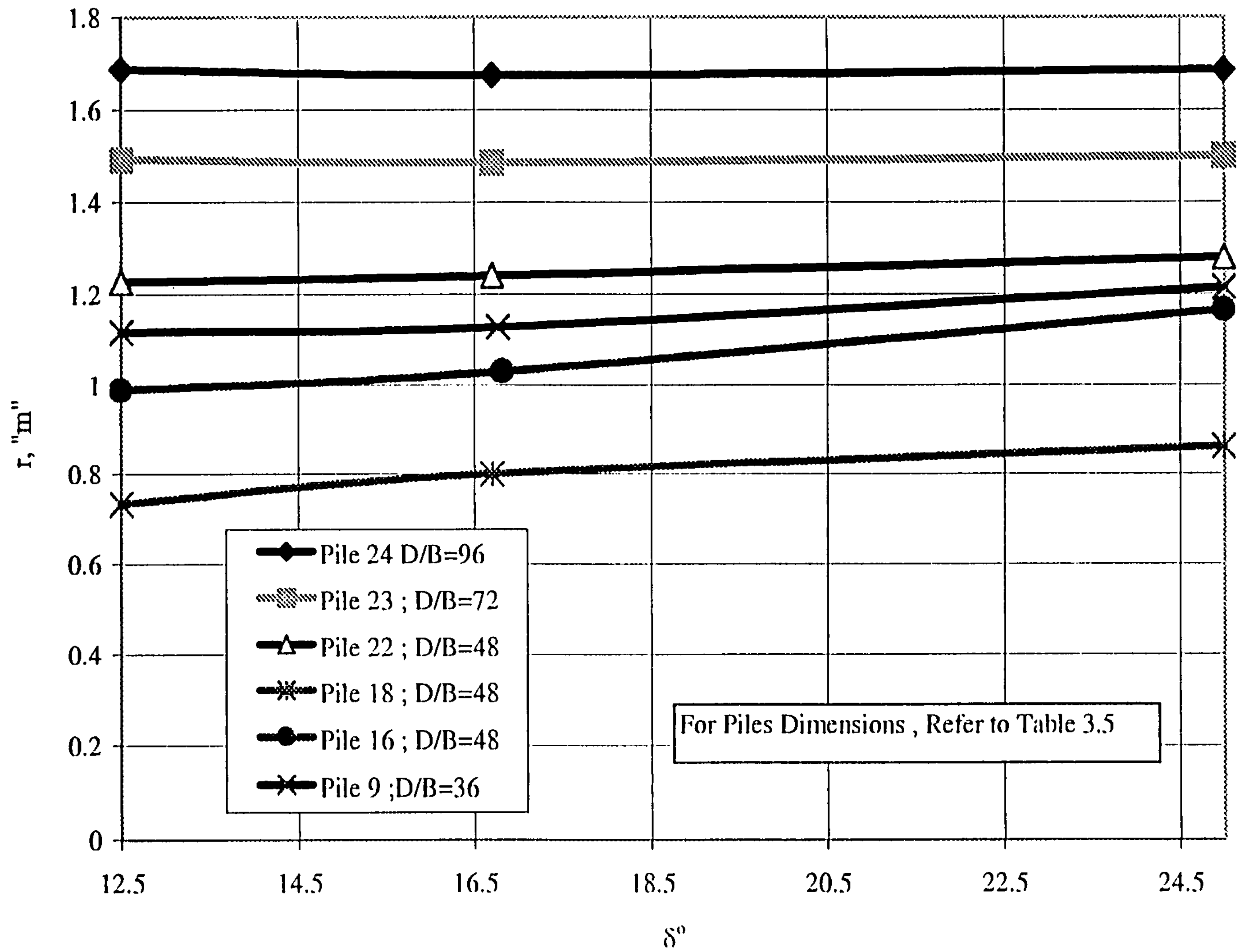

Figure 3.72 Effect of Change of Angle of Friction Between Pile and Sand "δ" on Radius of Influence at Tip " r" (Case of ϕ =25°)

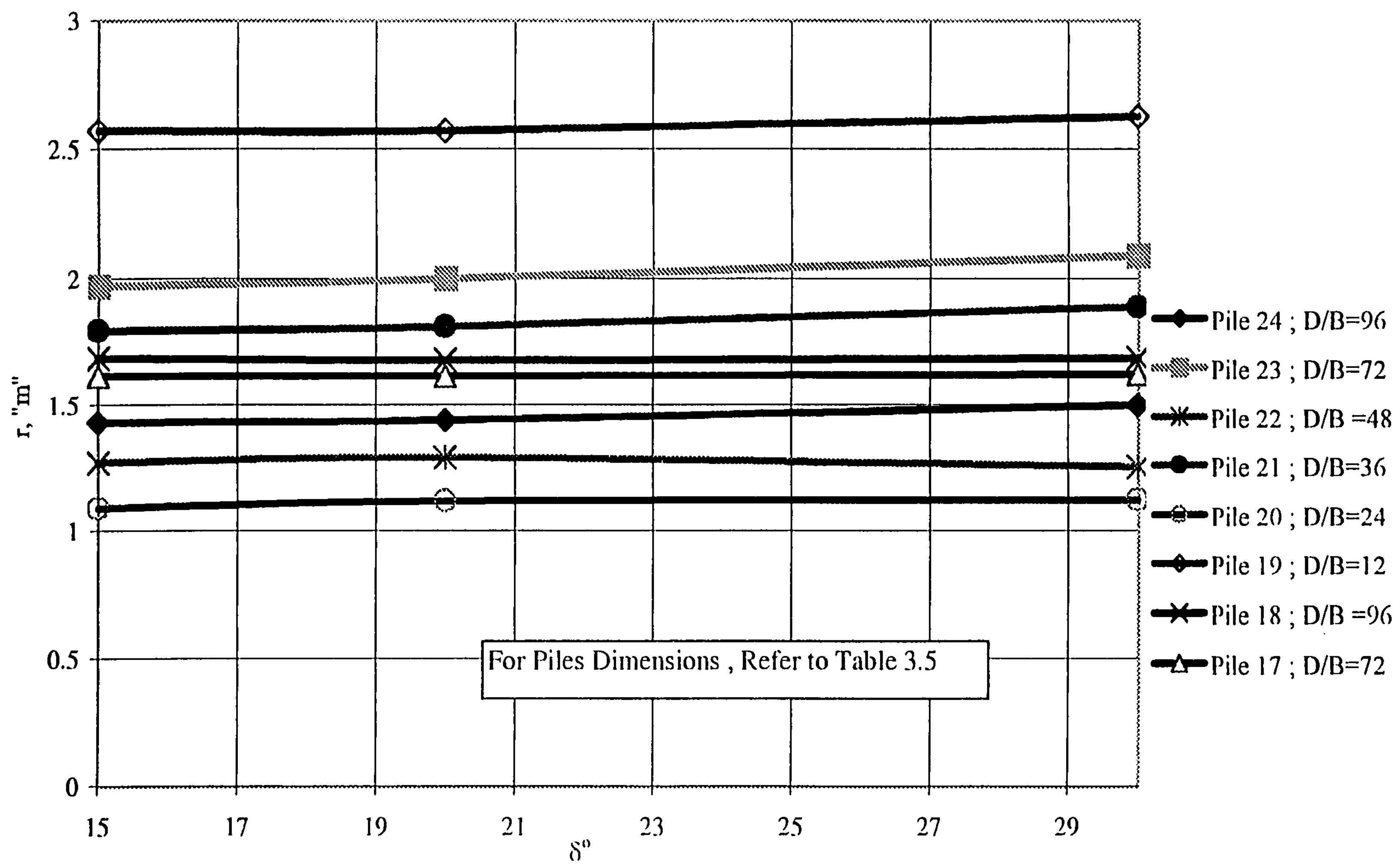

Figure 3.73 Effect of Change of Angle of Friction Between Pile and Sand "δ" on Radius of Influence at Tip " r" (Case of $\phi = 30^{\circ}$)

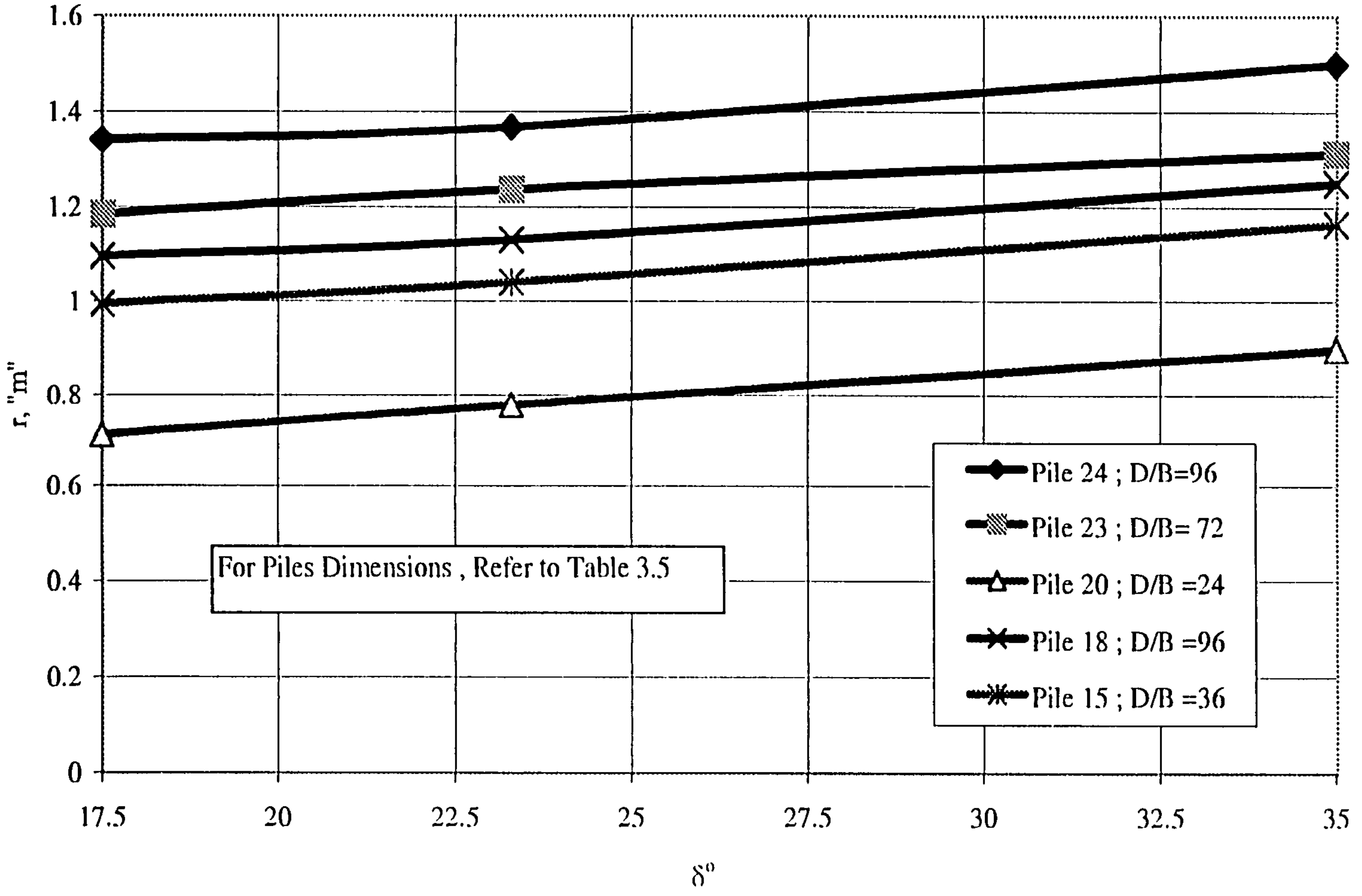

Figure 3.74 Effect of Change of Angle of Friction Between Pile and Sand "δ" on Radius of Influence at Tip " r" (Case of $\phi=35^0$)

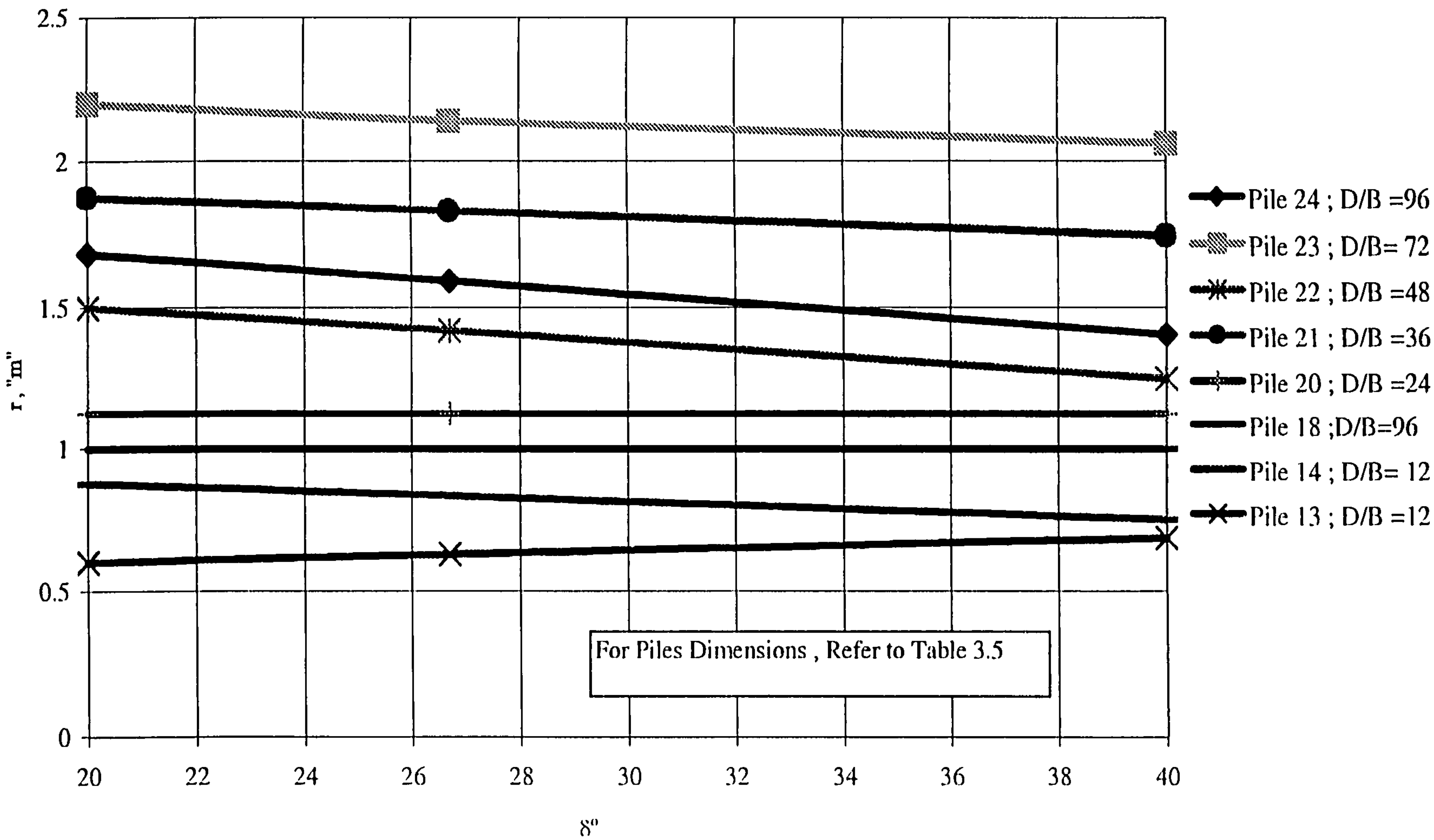

Figure 3.75 Effect of Change of Angle of Friction Between Pile and Sand "δ" on Radius of Influence at Tip " r" (Case of ϕ= 40°)

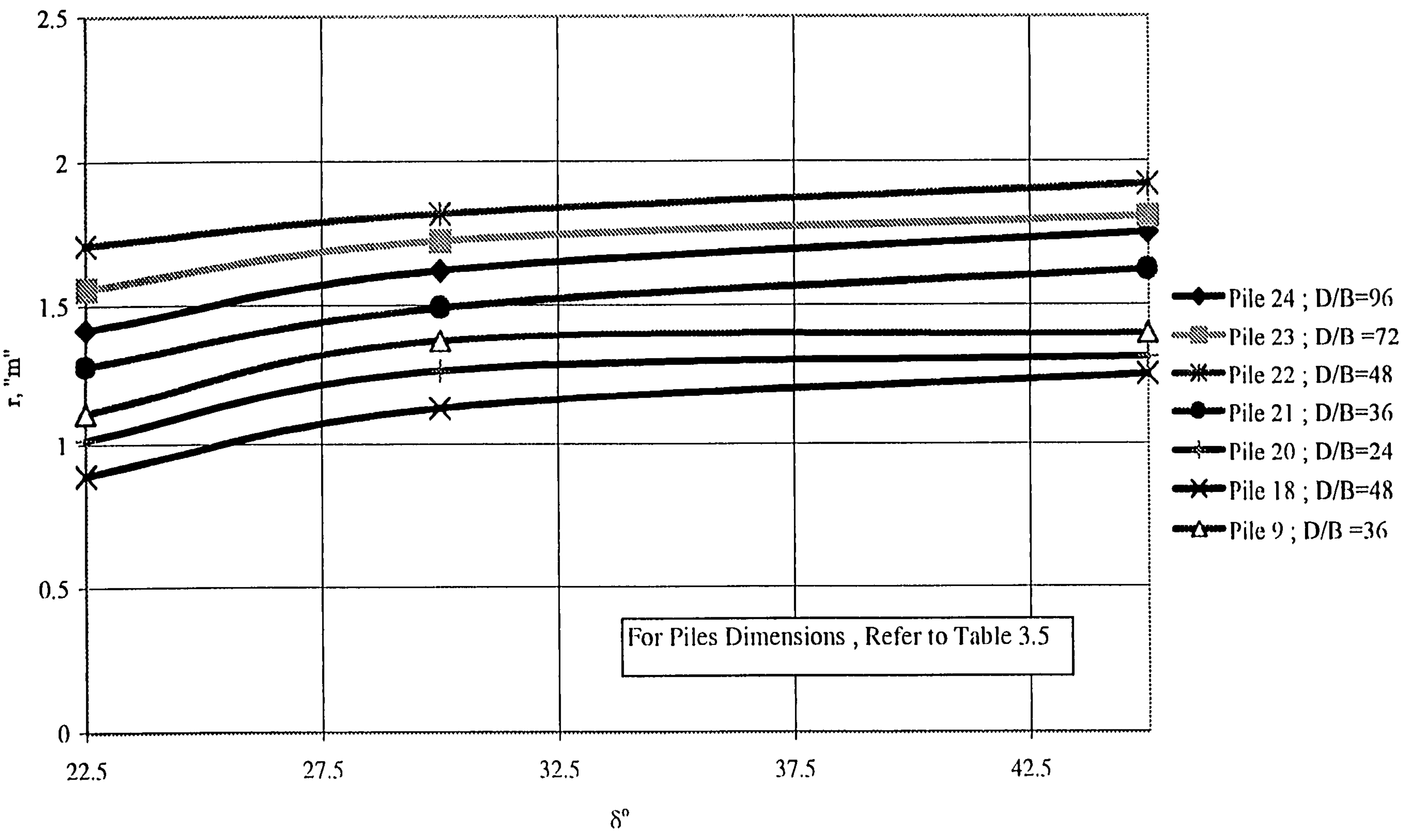

Figure 3.76 Effect of Change of Angle of Friction Between Pile and Sand "δ" on Radius of Influence at Tip " r" (Case of ϕ=45°)

Table 3.12 Parametric Study Results for Model Parameter: Vertical Distance "H_l"

Pile Geometry, m		Vertical Distance "H_l", meter				
B	D	$\phi = 25°$	$\phi = 30°$	$\phi = 35°$	$\phi = 40°$	$\phi = 45°$
0.25	3	1.224	1.386	1.539	1.68	1.86
0.25	6	2.418	2.706	3	3.324	3.738
0.25	9	3.24	3.798	4.365	4.95	5.517
0.25	12	3.6	4.428	5.04	5.904	6.672
0.25	18	3.924	4.752	5.634	6.732	7.758
0.25	24	3.984	5.112	6.192	7.44	8.664
0.4	4.8	2.141	2.376	2.621	2.904	3.149
0.4	9.6	4.224	4.752	5.27	5.789	6.25
0.4	14.4	5.573	6.422	7.157	8.093	8.827
0.4	19.2	6.451	7.334	8.314	9.312	10.23
0.4	28.8	6.71	7.978	9.302	10.71	12.15
0.4	38.4	7.565	9.062	10.68	12.4	14.13
0.5	6	3.24	3.576	3.882	4.248	4.578
0.5	12	6.504	7.044	7.656	8.304	9.036
0.5	18	8.928	10.19	11.25	12.29	13.32
0.5	24	10.56	12	13.61	15.07	16.54
0.5	36	11.63	14.11	16.56	18.94	21.38
0.5	48	13.01	15.79	19.1	21.74	24.77
0.75	9	4.464	4.833	5.247	5.787	6.327
0.75	18	9.09	9.972	10.96	11.74	12.78
0.75	27	11.83	13.55	15.42	16.9	18.6
0.75	36	13.39	15.2	17.46	19.62	21.49
0.75	54	14.2	16.96	19.6	22.41	25.38
0.75	72	16.27	19.01	22.68	25.49	29.16

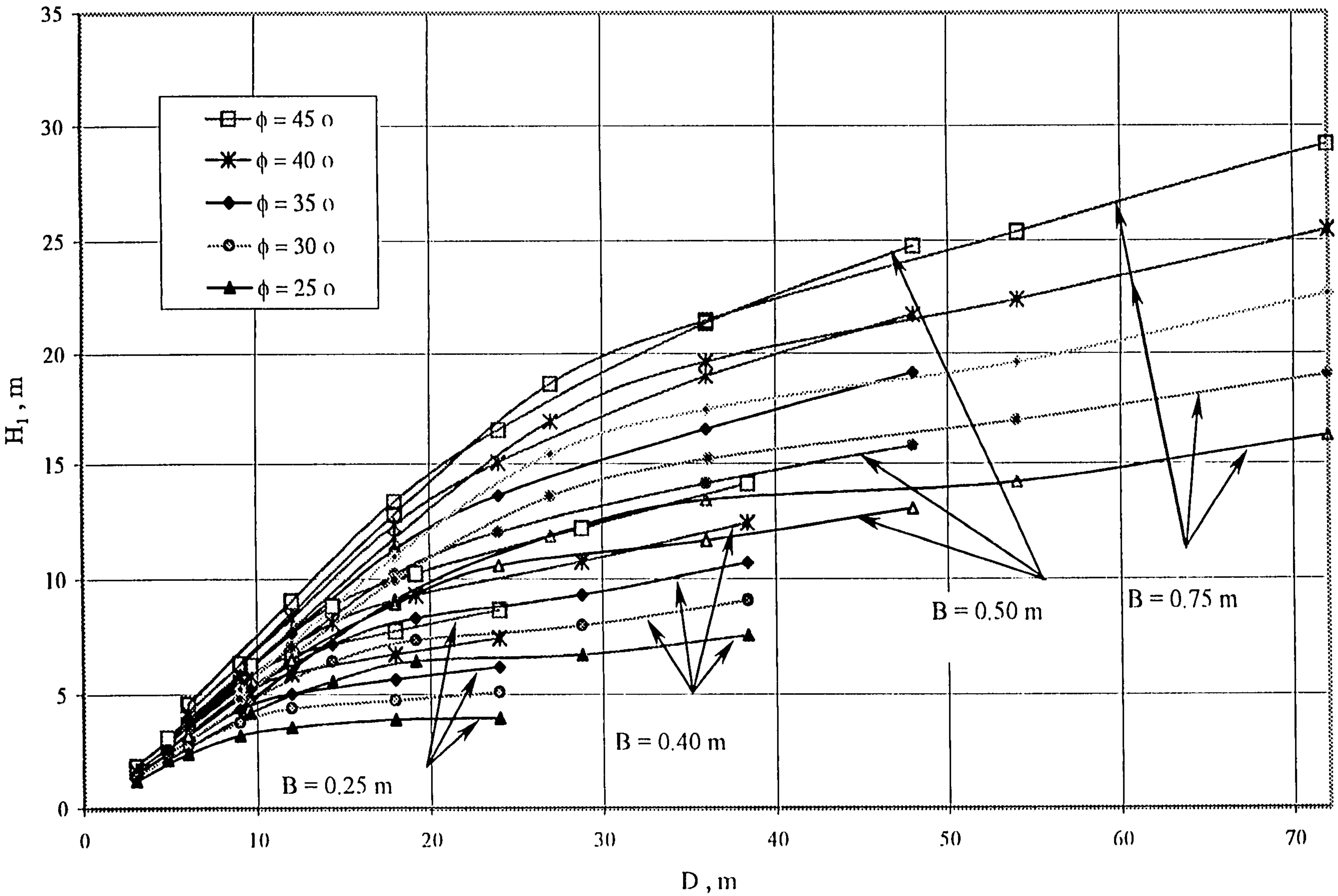

Figure 3.77 Relationship between H_1 and Pile Depth "D" With respect to φ , and Diameter "B"

Where: Hf is in meters. Equation 3.32 is introduced graphically in Figure 3.80.

The portion should be distributed is:

$$YHf = Hf * ((45-\phi)/20) \quad ...(3.33)$$

Thus:

$$(H_l)_{II} = (H_l)_I - YHf \quad ...(3.34)$$

3.11.4.1 Effect of Change of δ on the Value of H_l

Selected pile load tests were performed to determine the effect of changing of δ on the value of H_l. In this analysis all parameters were frozen except δ which was permitted to change. The results of these tests are introduced in Figures 3.81 to 3.85. It is obvious that H_l increases with the increase of δ/ϕ. This trend is clear between δ/ϕ =2/3 - 1.0, but it is very weak in the range of δ/ϕ=1/2 - 2/3. This behavior could be related to the degree of mobilization that requires higher friction for skin resistance to be fully mobilized. It was found that the rate of decrease of H_l due to the decrease of δ/ϕ varies from any value of φ to another value. An average decrease of δ in a form of meters per 1^o of δ is introduced in Figure 3.86. Equation 3.35 introduces this rate (H_{lrd}) as a trend line for the plotted data.

$$H_{lrd} = 0.0727*\phi - 1.2331 \quad ...(3.35)$$

For any value of φ, the corresponding value of rate of decrease in H_l per 1^o is determined from Equation 3.35. The value of H_l due to the decrease of δ is as follows:

$$H_l = (H_l)_{II} * D - (\phi-\delta)*H_{lrd} \quad ...(3.36)$$

3.11.5 Vertical Distances L_1,L_2& L_3 at the Mobilized Tip Resistance Zone

For these three distances composing the vertical dimensions for the failure zone around the

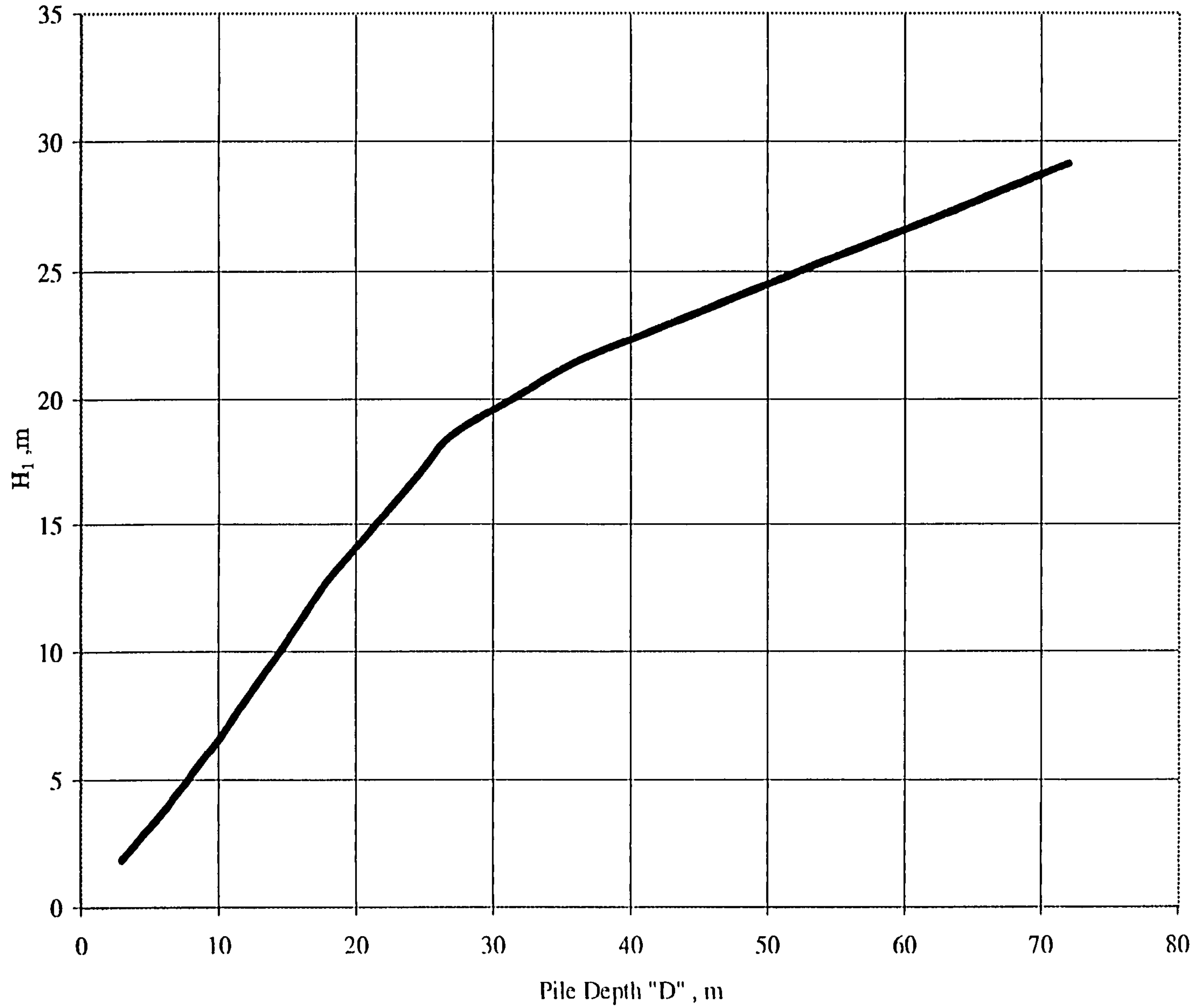

Figure 3.78 Relationship of H_1 Versus Pile Depth "D" at $\phi = 45^\circ$

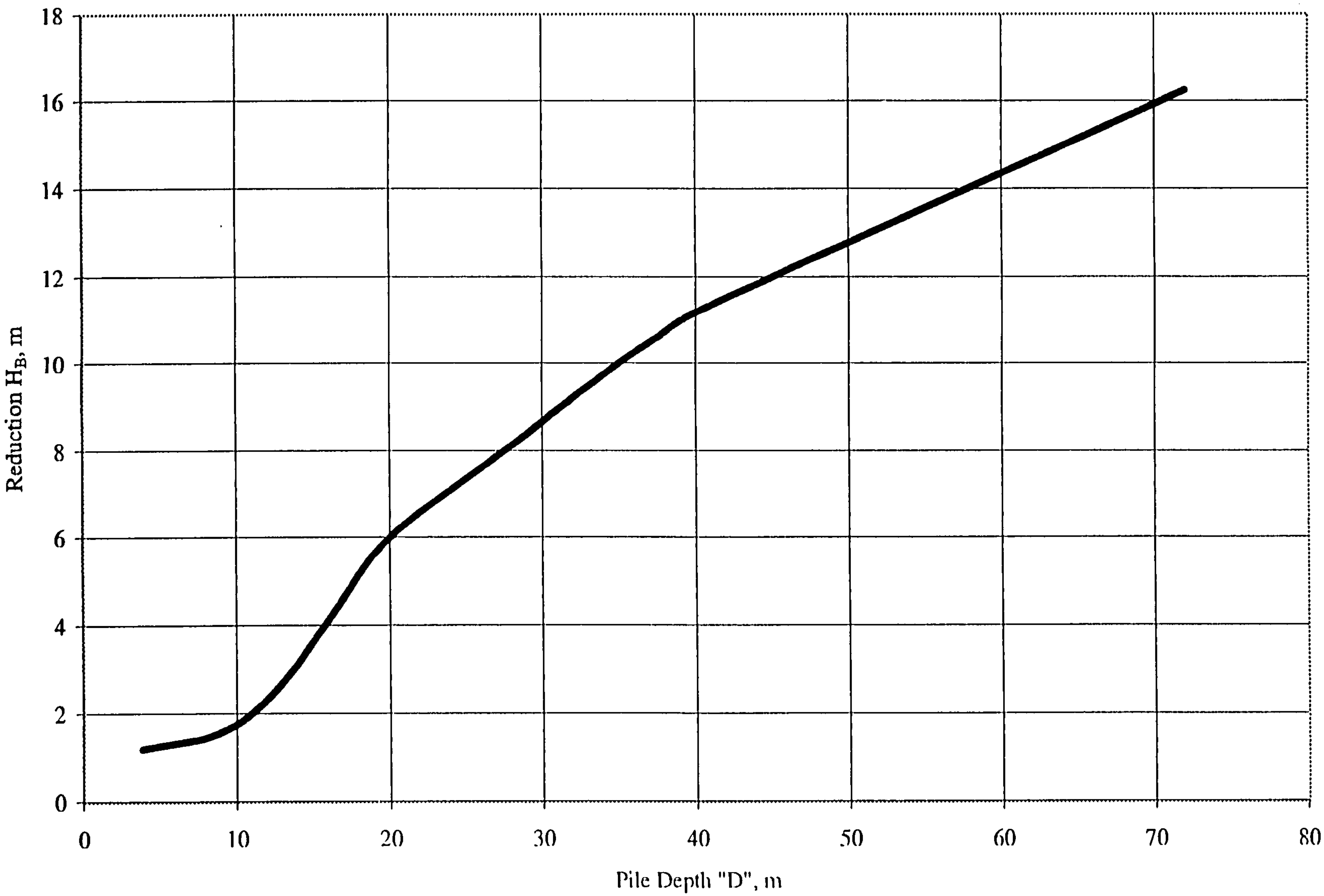

Figure 3.79 Reduction in H_1 Due to Decrease of Pile Diameter "B"

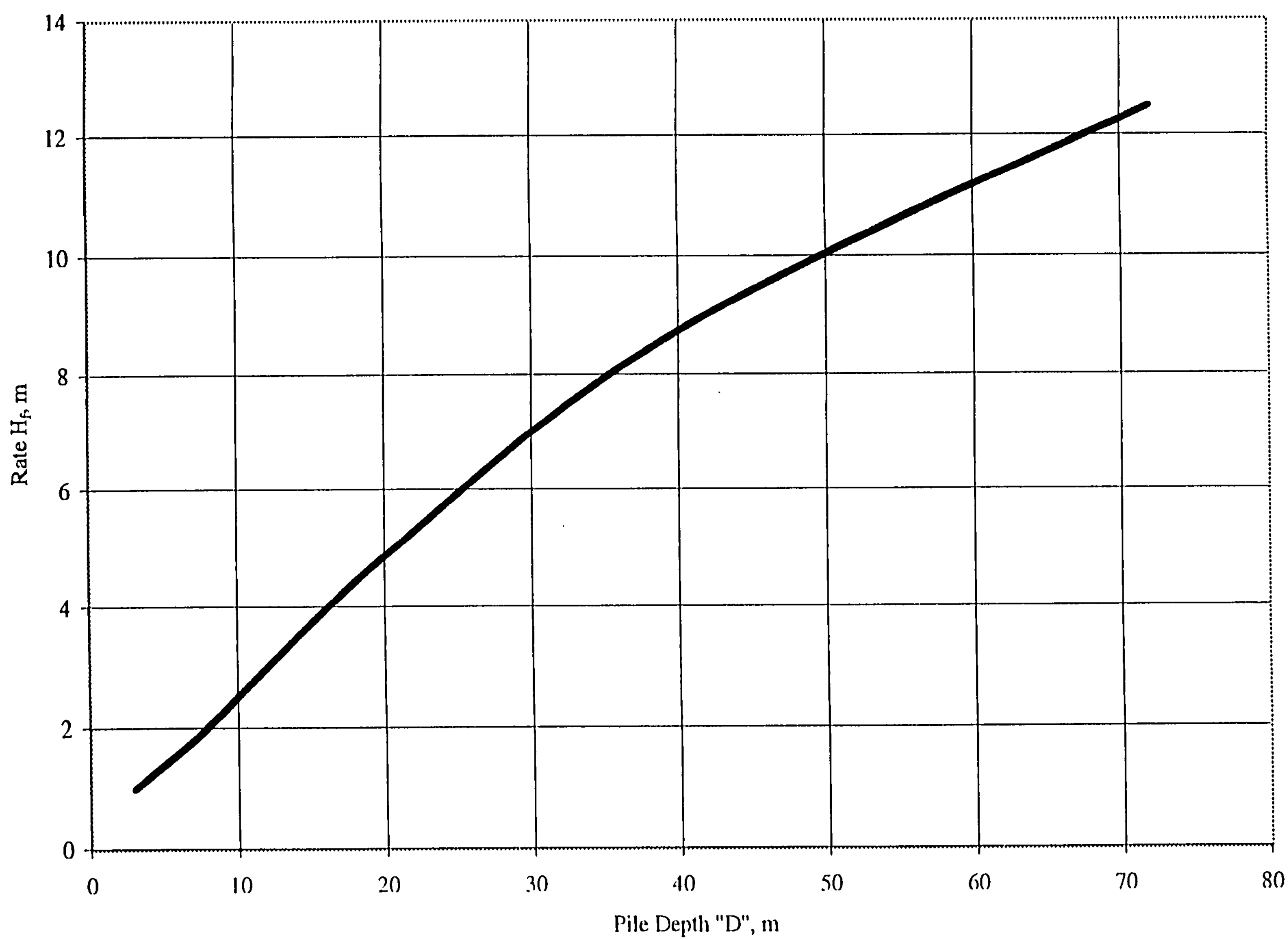

Figure 3.80 Rare of Decrease in H_1 Due to Decrease of Angle of Shearing resistance "ϕ"

tip, refer to Figure 3.59 for details. The first distance, L_3, is located beneath the tip and it represents the vertical limit of the propagation of the failure pattern beneath the tip, (Table 3.13 introduce the parametric study out-put for L_3). The out put results are presented graphically in Figure 3.87 where the relationship between L_3 and ϕ is introduced with respect to pile diameter "B" and depth "D". Analysis of this Figure 3.87 implies the following:

1- In general, L_3 increases with the increase of ϕ, but with respect to B, the increase is not noticeable. For this relationship, the best fitting equation is introduced in Figure 3.88 and Equation 3.37:

$$L_{3(45)} = 2.21 - 0.192 * D + 1.09 * D / \ln(D) - 5.152 * 1.0 / \ln(D) + 22.23 * \ln(D) / (D^2) \quad ...(3.37)$$

Equation 3.37 was interpolated based on the upper envelop for all series where $\phi=45^{o}$ and B = 0.75 m.

2- A reduction due to lower values of ϕ is needed to be deducted from Equation 3.37, since it represents the upper value of L_3 at $\phi=45^{o}$:

$$L_{3red} = - 0.0223*(\phi) + 1.0025 \quad ...(3.38)$$

Equation 3.38 was produced based on the average maximum difference between the value of L_3 at 45^{o} and at 25^{o} and is introduced graphically in Figure 3.89. The deduction should be applied as follows:

$$L_{3\ (dif)} = ((45-\phi)/20)*L_{3red} \quad ...(3.39)$$

Thus:

$$L_3 = L_{3(45)} - L_{3\ (dif)} \quad ...(3.40)$$

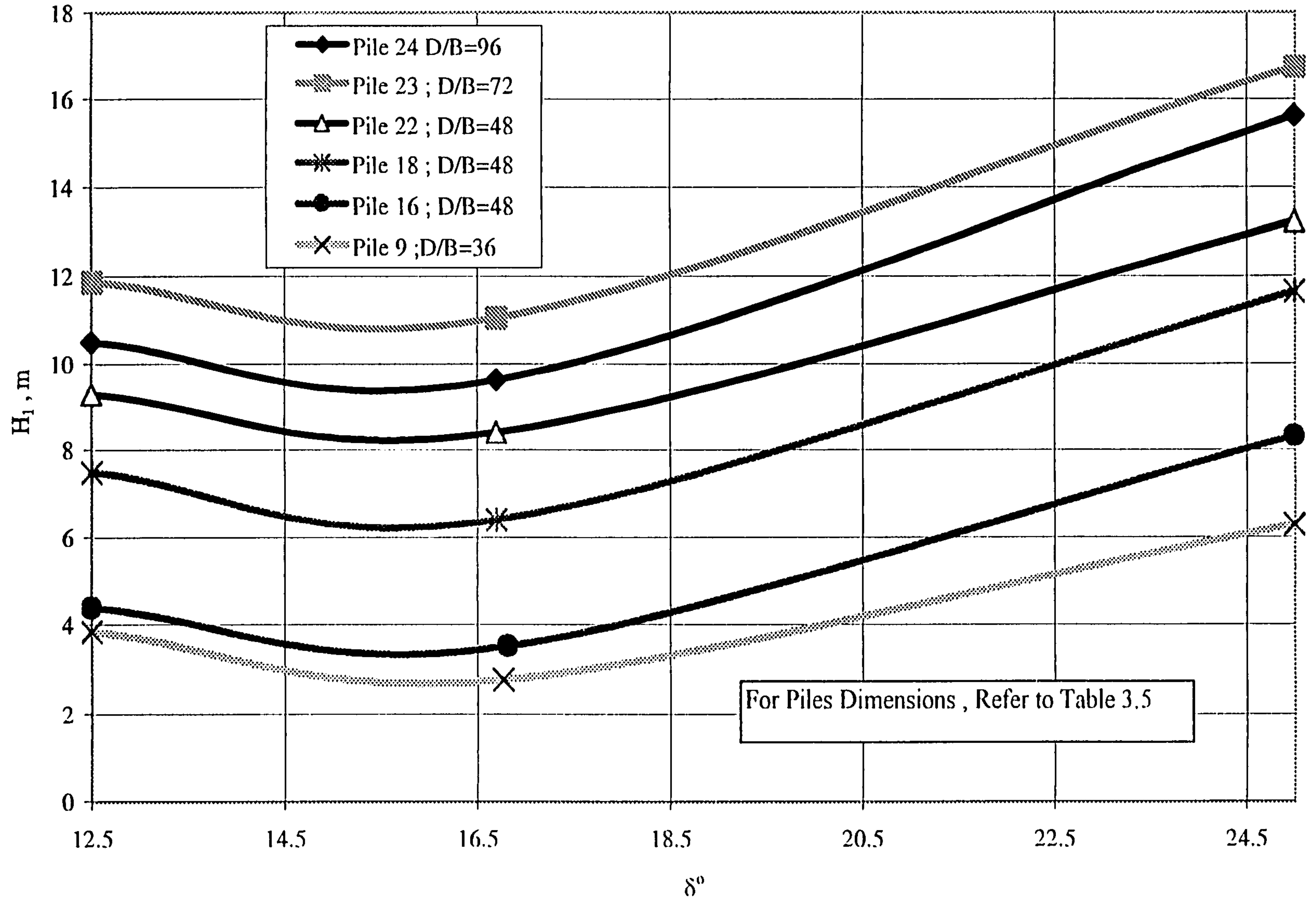

Figure 3.81 Effect of Changing of Angle of Friction "δ" between Pile and Sand on the Value of H_1 (Case of $\phi = 25^o$)

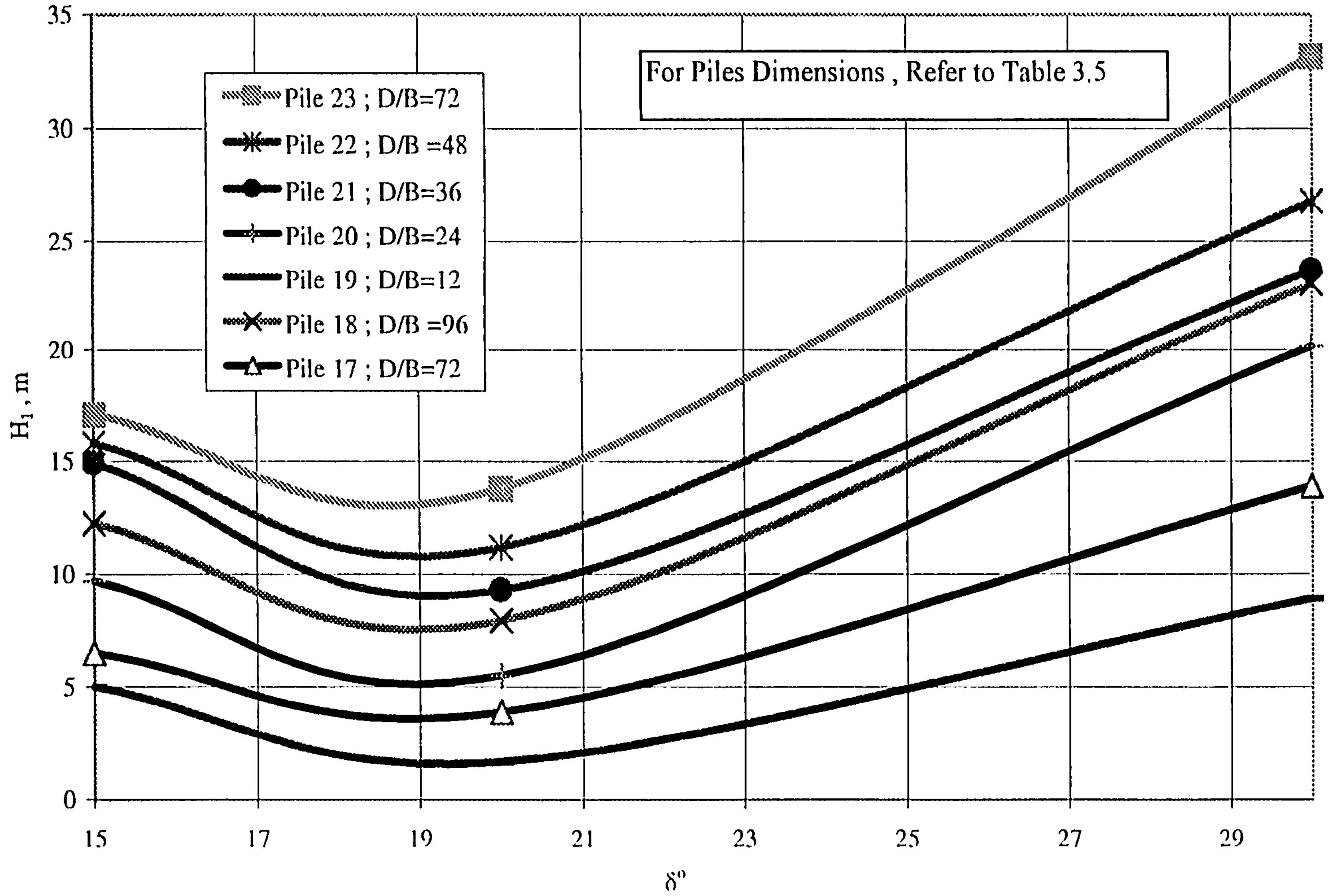

3.82 Effect of Changing Angle of Friction "δ" between Pile and Sand on the Value of H_1 (Case of ϕ =30°)

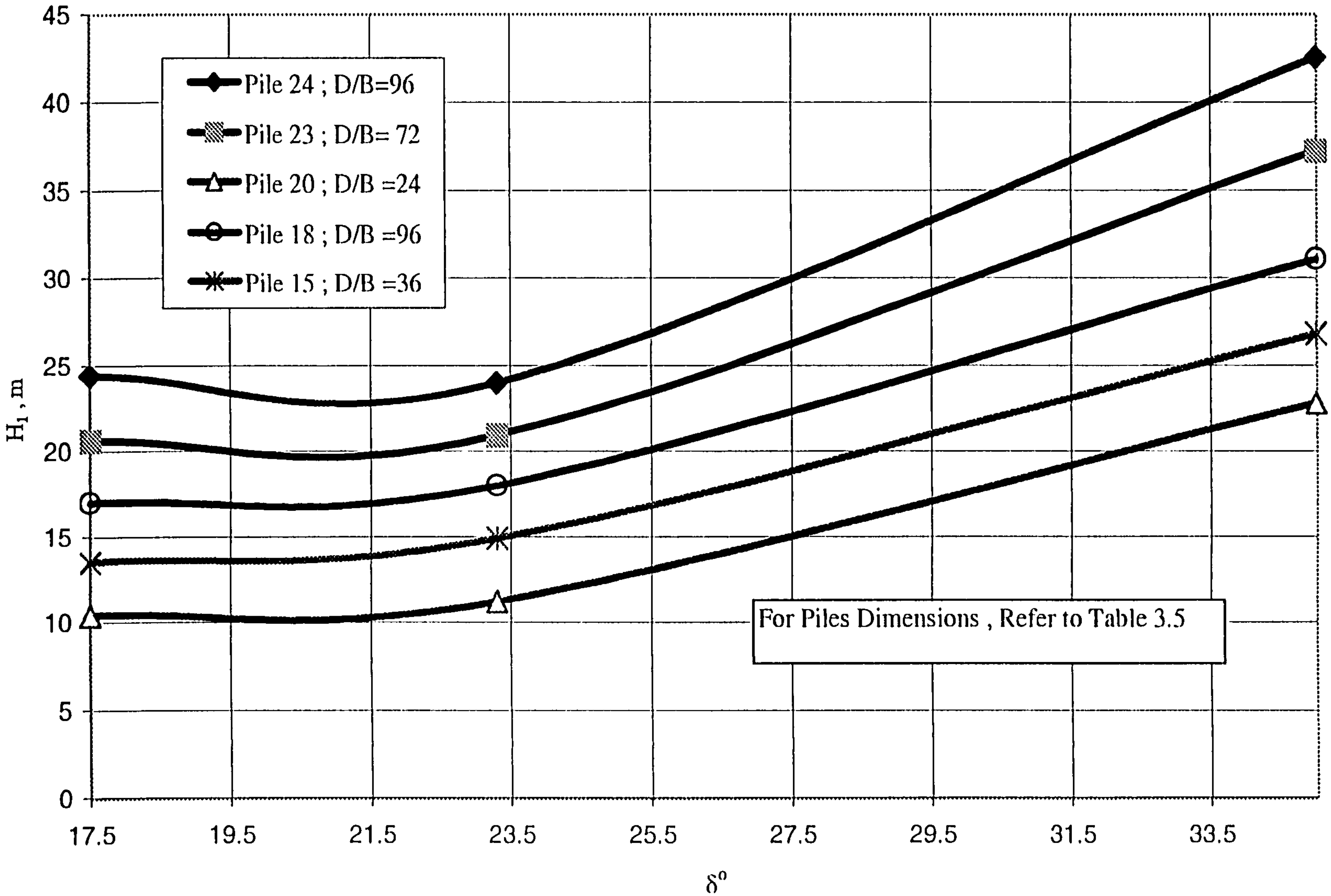

3.83 Effect of Changing Angle of Friction "δ" between Pile and Sand on the Value of H_1 (Case of ϕ =35^o)

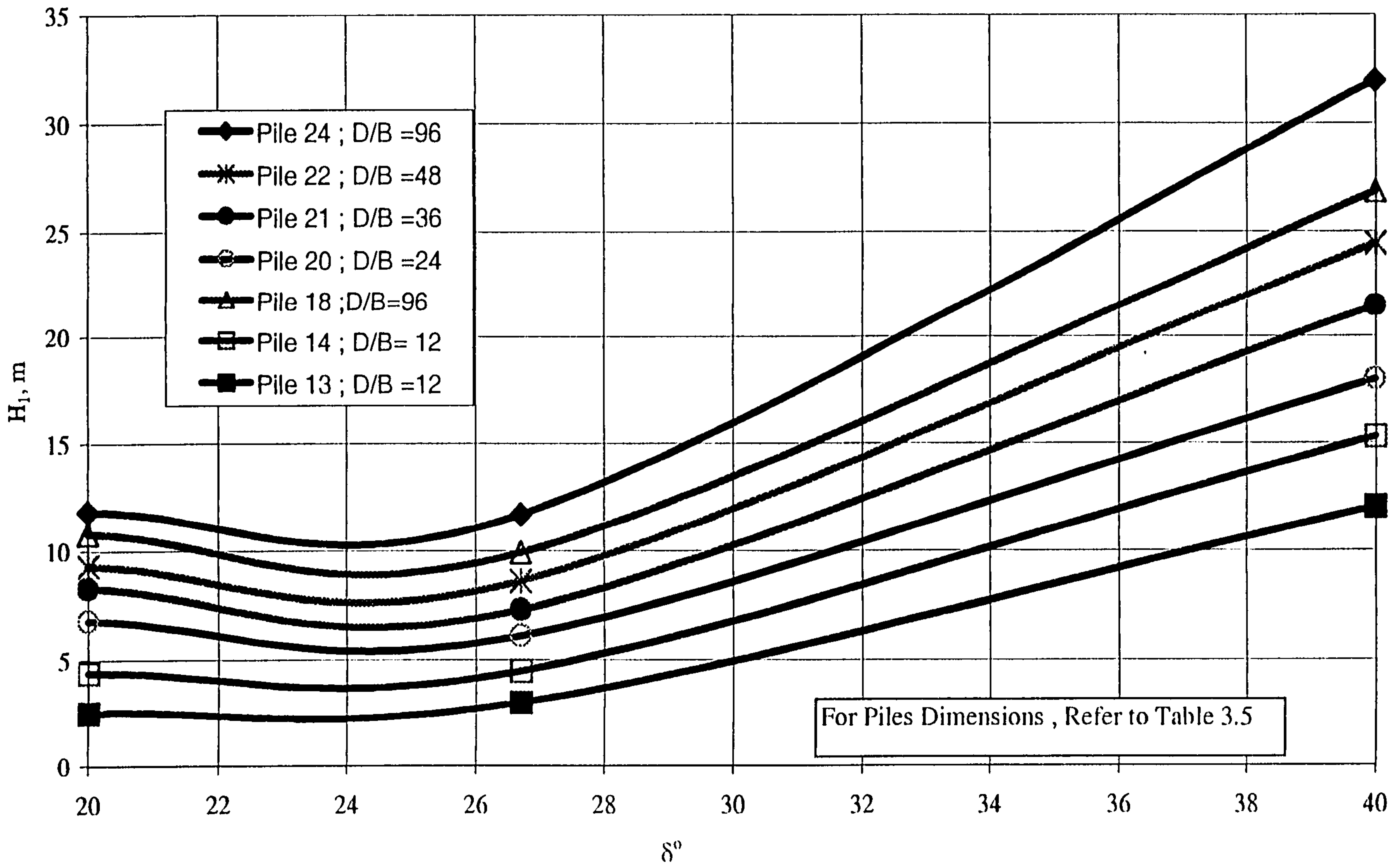

3.84 Effect of Changing Angle of Friction "δ" between Pile and Sand on the Value of H_1 (Case of ϕ =40°)

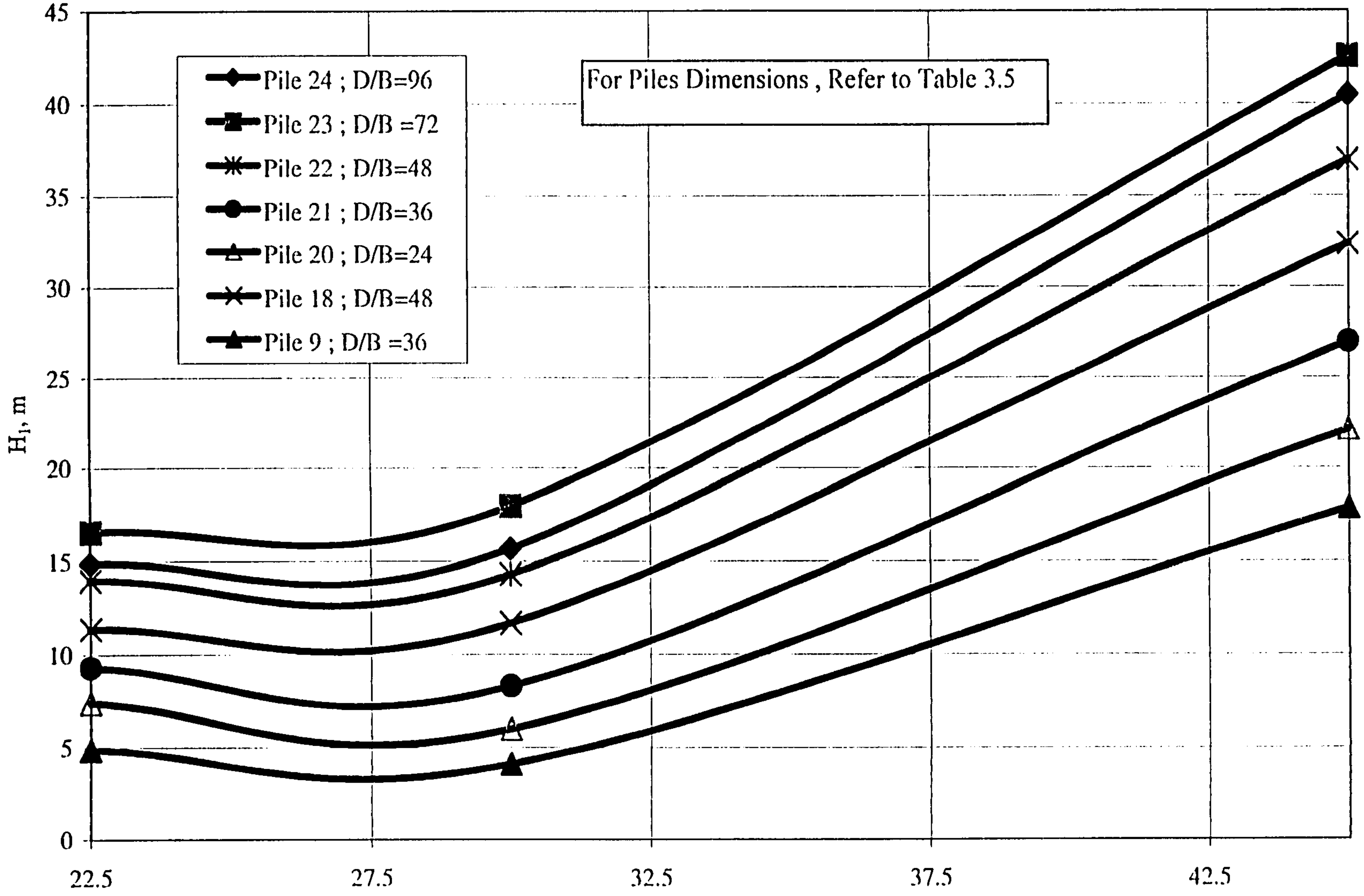

3.85 Effect of Changing Angle of Friction "δ" between Pile and Sand on the Value of H_1 (Case of ϕ =40°)

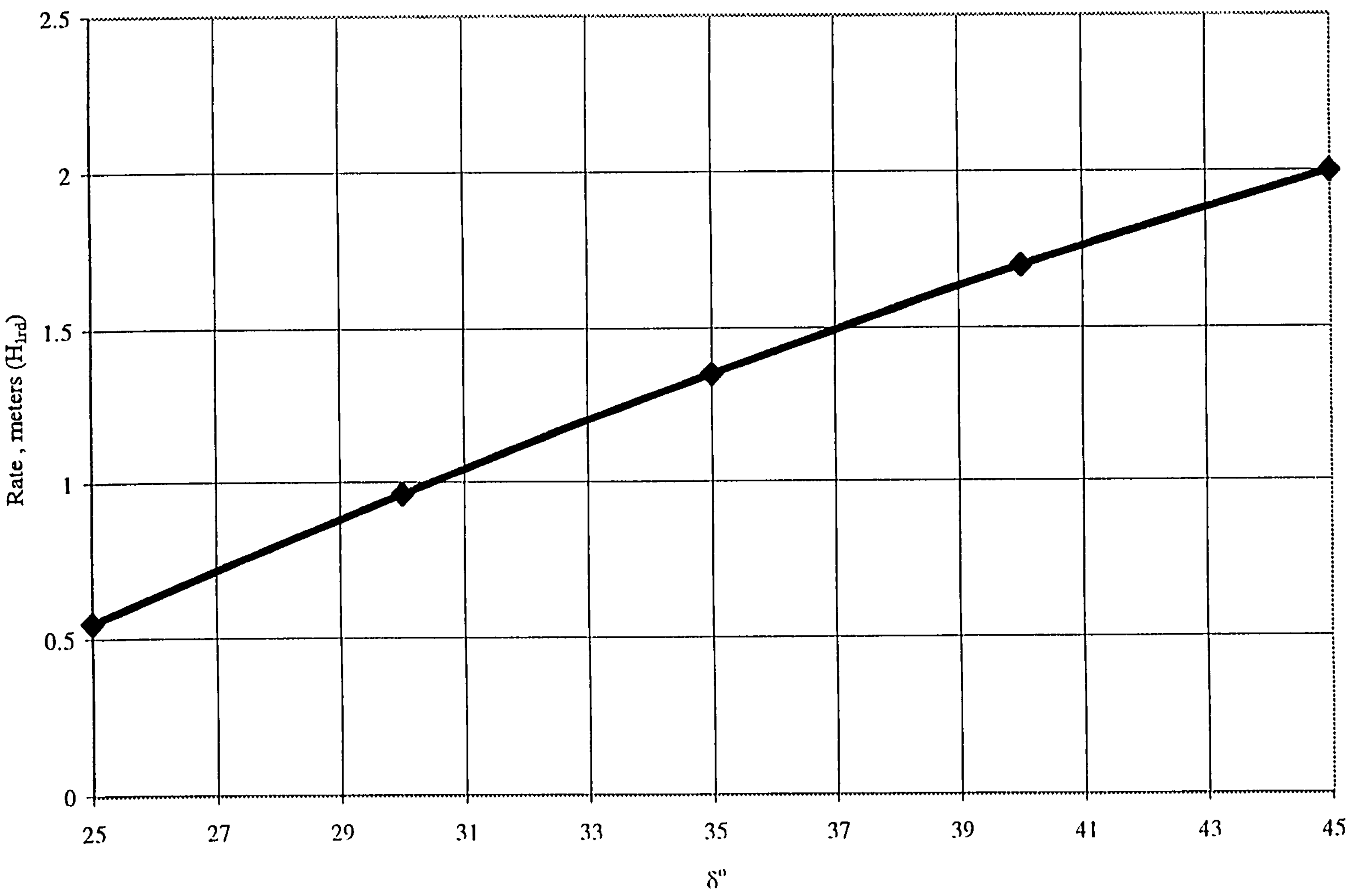

Figure 3.86 Rate of Decrease of H_1 (in meters) Versus each 1° of δ With Respect to Angel of Shearing Resistance "ϕ"

Table 3.13 Parametric Study Results for Model Parameter: Vertical Distance "L_3"

Pile Geometry, m		Vertical Distance "L_3", meter				
B	D	$\phi = 25°$	$\phi = 30°$	$\phi = 35°$	$\phi = 40°$	$\phi = 45°$
0.25	3	2.24	2.346	2.395	2.501	2.616
0.25	6	2.493	2.616	2.689	2.747	2.837
0.25	9	2.714	2.861	2.926	3.016	3.049
0.25	12	3.057	3.172	3.262	3.294	3.335
0.25	18	3.44	3.507	3.572	3.646	3.736
0.25	24	3.85	3.989	4.063	4.128	4.251
0.4	4.8	2.362	2.493	2.55	2.624	2.738
0.4	9.6	2.935	3.074	3.155	3.204	3.245
0.4	14.4	3.294	3.392	3.45	3.507	3.605
0.4	19.2	3.736	3.866	3.932	4.022	4.144
0.4	28.8	4.218	4.332	4.431	4.496	4.594
0.4	38.4	4.676	4.79	4.88	4.929	4.995
0.5	6	2.6	2.747	2.812	2.877	2.918
0.5	12	3.155	3.27	3.351	3.4	3.458
0.5	18	3.507	3.621	3.687	3.785	3.866
0.5	24	3.948	4.079	4.136	4.218	4.349
0.5	36	4.373	4.48	4.586	4.643	4.725
0.5	48	4.782	4.888	5	5.06	5.15
0.75	9	2.845	2.959	3.057	3.131	3.155
0.75	18	3.629	3.752	3.826	3.907	4.01
0.75	27	4.079	4.185	4.267	4.349	4.48
0.75	36	4.537	4.635	4.741	4.79	4.856
0.75	54	4.913	5.035	5.142	5.215	5.322
0.75	72	5.142	5.223	5.322	5.4	5.493

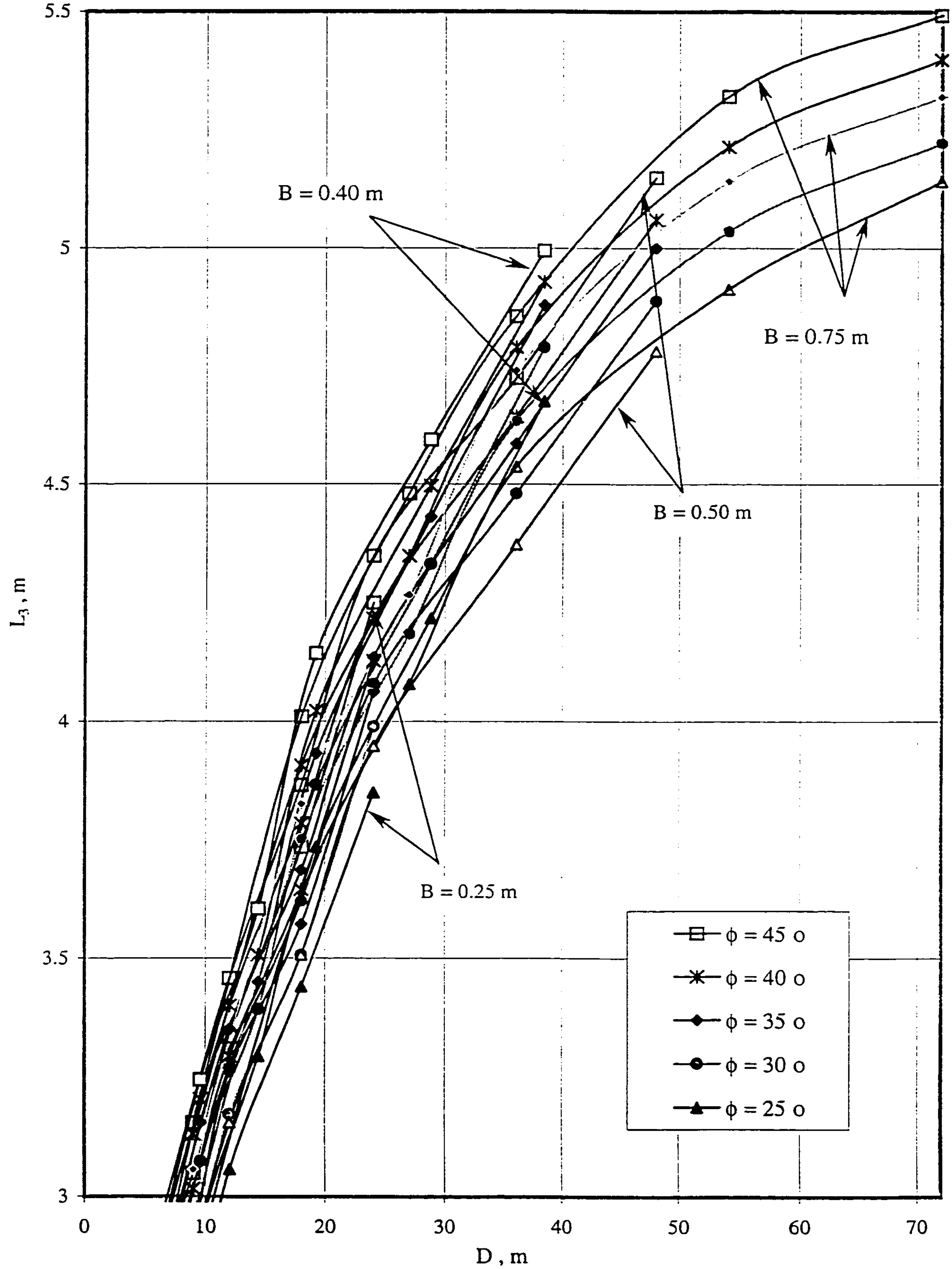

Figure 3.87 Relationship of (L_3, m) and ϕ , With respect to Pile Depth "D" and Diameter "B"

3.11.5.1 Effect of δ on L_3

A few selected pile load tests were performed to clarify the effect of change of δ on L_3, (refer to Figures 3.90 to 3.94). It was found that changing δ does not affect the value of L_3 and therefor the influence of δ against L_3 can be safely neglected. This behavior may be related to the location of L_3, which lies beneath the tip, where the relative movements between pile and soil should not have much effect in that location. The final value of L_3 will be predicted using Equation 3.40.

3.11.5.2 Analysis of L_2 and L_1

L_1 and L_2 are the vertical distances of the failed area around the tip which are located just above the tip level. For simplification and to keep the angle $\theta > 90.0^o$ (refer to Figure 3.59), L_2 will be empirically assumed as a constant ratio of pile depth and it will assumed to be equal 0.0001 D.

The results of analysis of parameter L_1 is introduced in Figure 3.95 and Table 3.14. The lower envelop of L_1 versus pile depth at ϕ=25^o is plotted in Figure 3.96 and given in Equation 3.41:

$$L_{1(25)} = (-0.029+\ln(D)*(0.091+\ln(D)*(0.124+\ln(D)* (-0.096+\ln(D)*0.016))))/(1.0+\ln(D)*(-0.355+\ln(D)* (-0.251+\ln(D)*(0.173+\ln(D)*(-0.037+\ln(D)*0.003))))) \quad ...(3.41)$$

This relationship is an average function to predict L_1 at its lower value for all series and generated from Figure 3.95. Additional increase due to increase of ϕ was produced in Figure 3.97 and Equation 3.42.

$$L_{1(\phi)} = (0.77+\ln(D)*(-0.32+\ln(D)*(-0.25+\ln(D)*(0.223+\ln(D)*$$

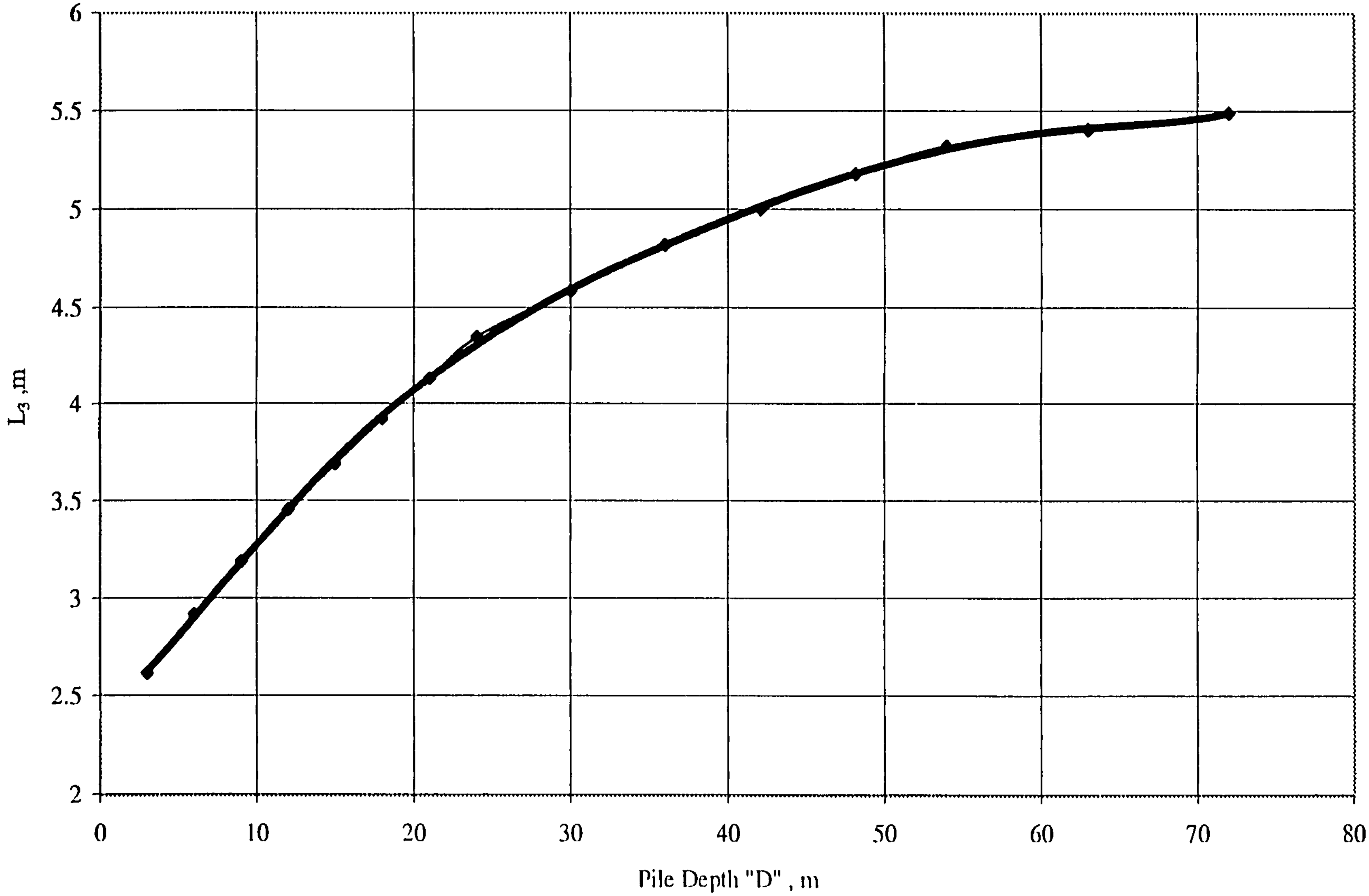

Figure 3.88 L_3 Versus Pile Depth at "$\phi=45^{o}$" in meters

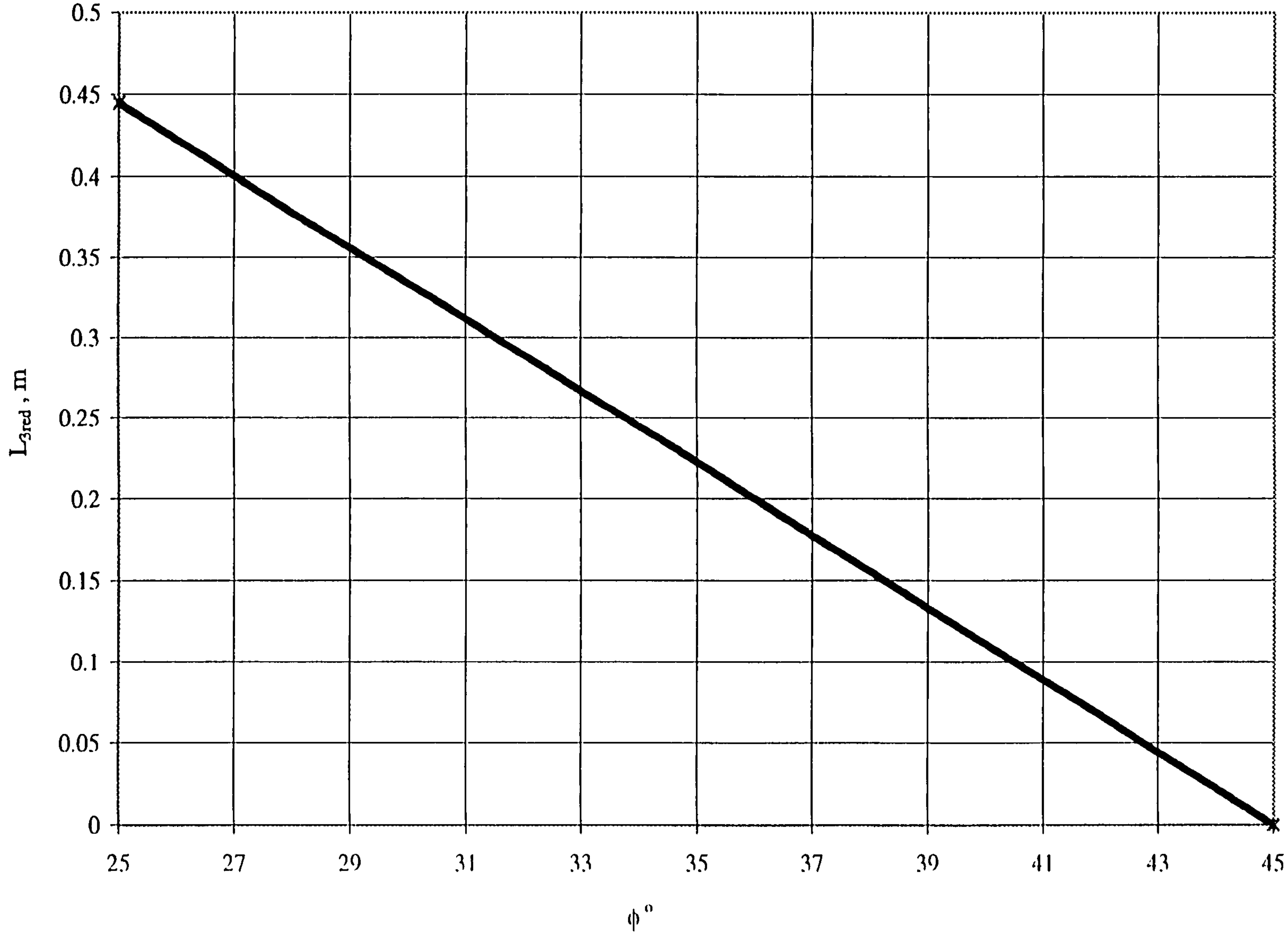

Figure 3.89 Rate of Decrease of L_3 Due to Decrease of "ϕ"

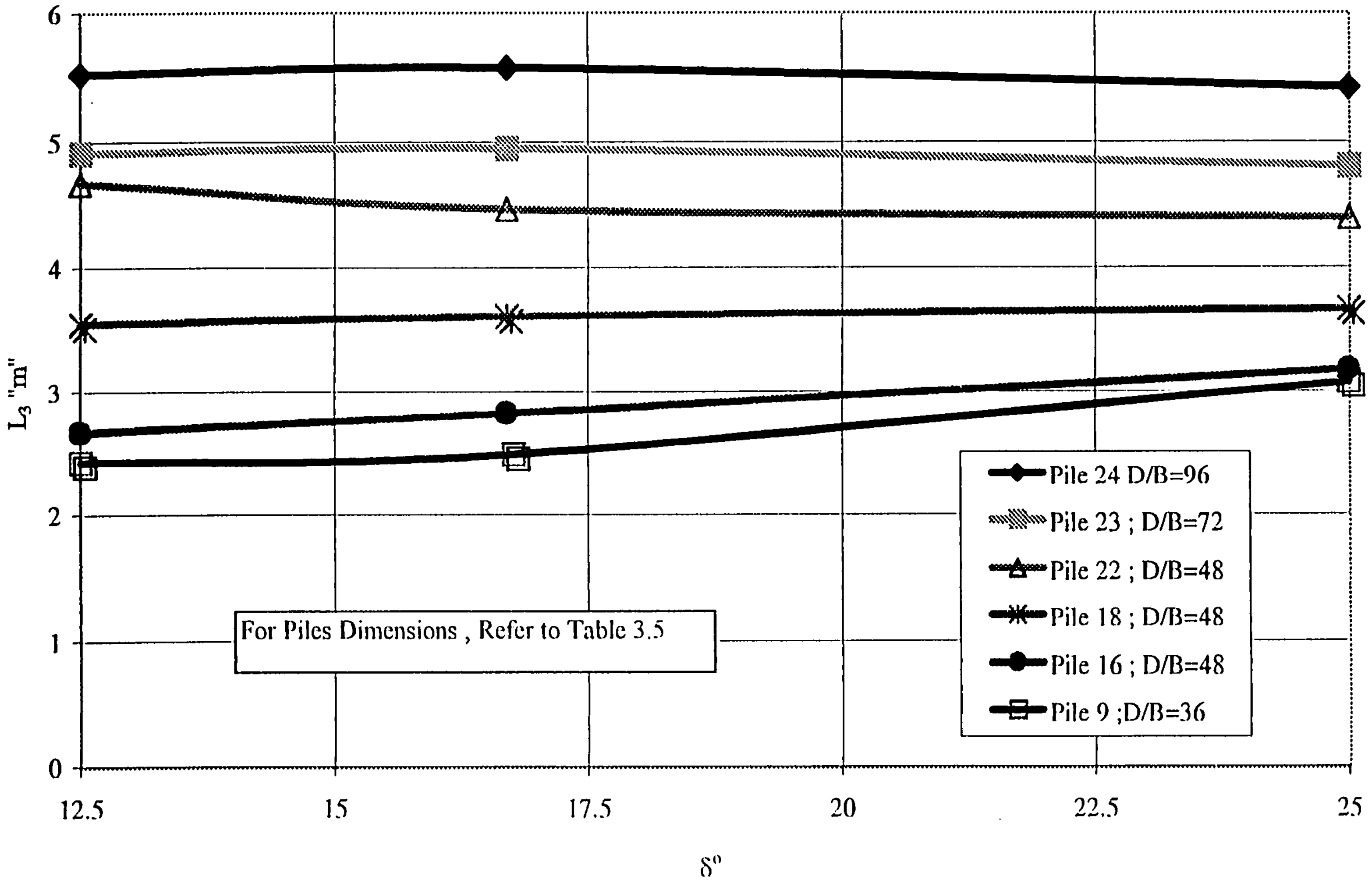

Figure 3.90 Effect of Changing Angle of Friction "δ"
Versus Model Parameter L_3 (Case of ϕ =25^{o})

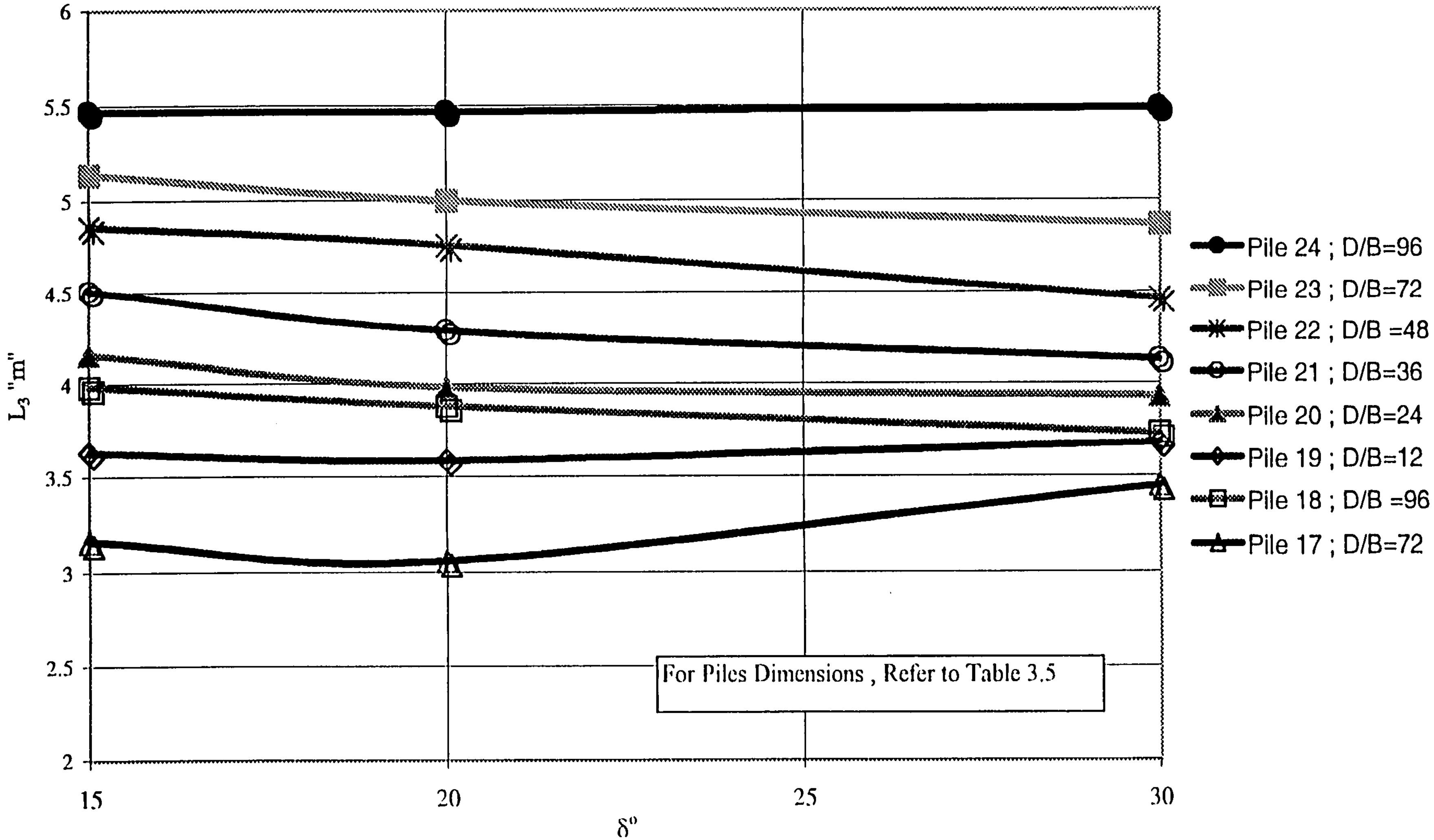

Figure 3.91 Effect of Changing Angle of Friction "δ"
Versus Model Parameter L_3 (Case of $\phi = 30^{o}$)

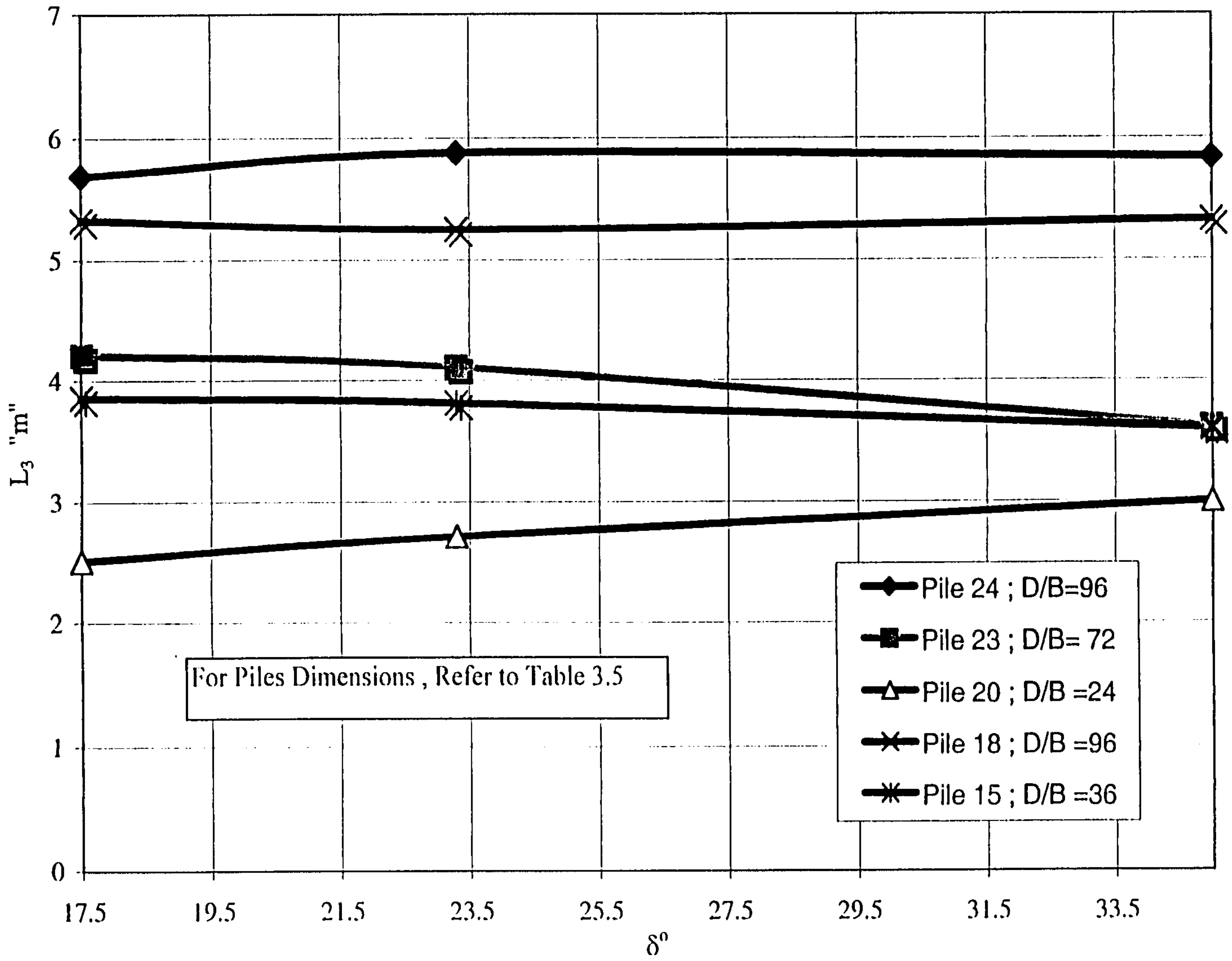

Figure 3.92 Effect of Changing Angle of Friction "δ" Versus Model Parameter L_3 (Case of $\phi=35^0$)

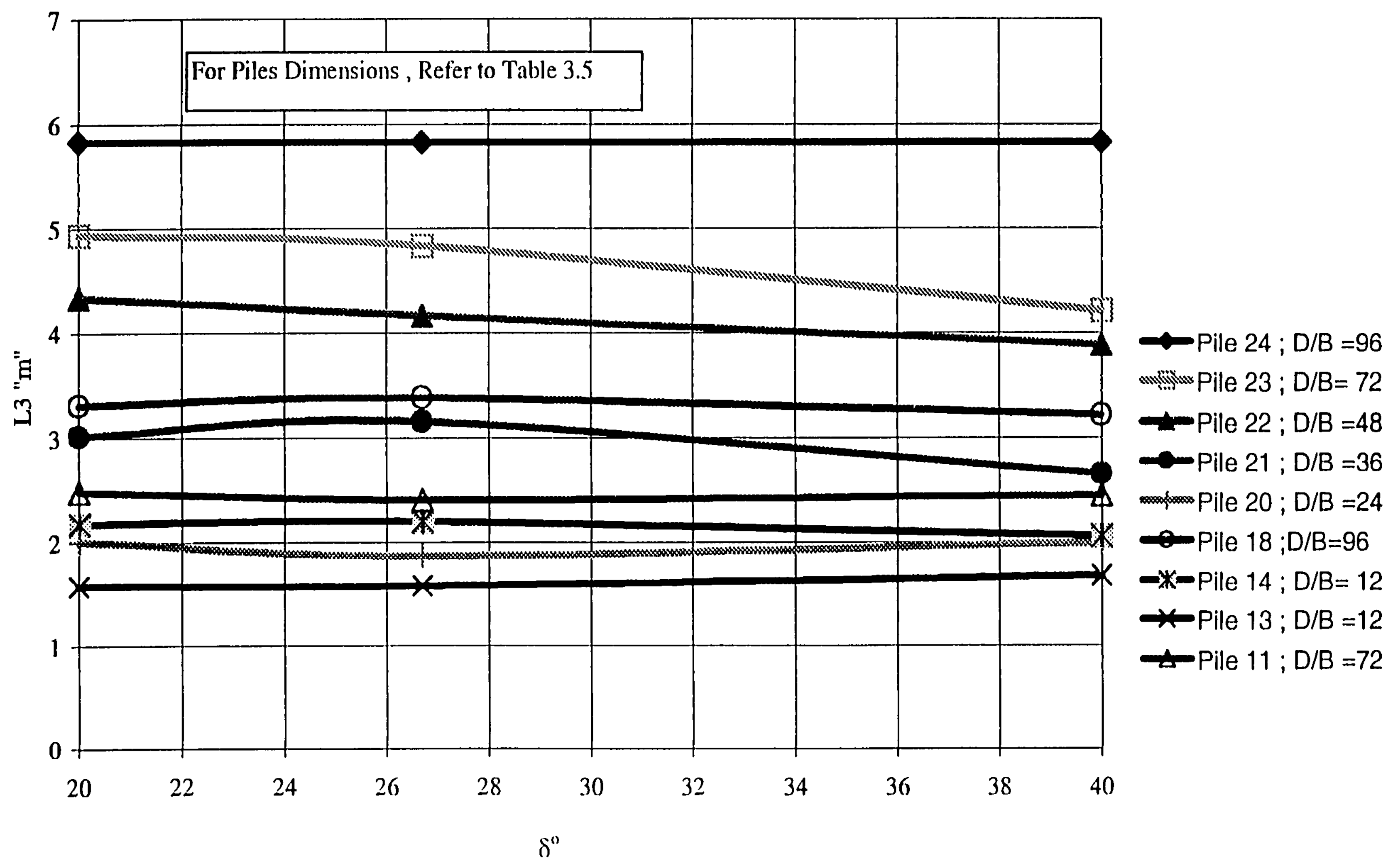

Figure 3.93 Effect of Changing Angle of Friction "δ"
Versus Model Parameter L_3 (Case of ϕ= 40°)

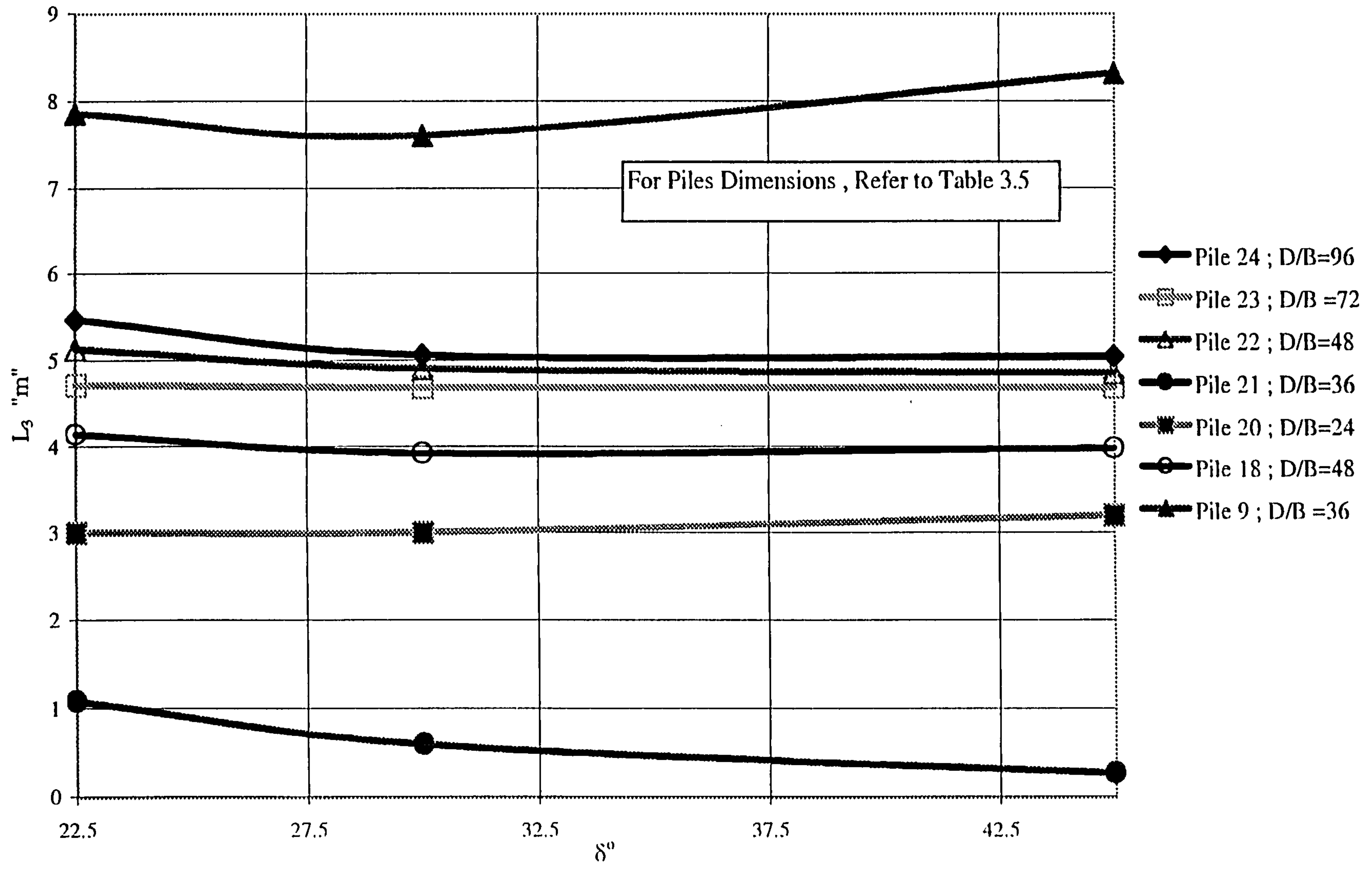

Figure 3.94 Effect of Changing Angle of Friction "δ" Versus Model Parameterr L_3 (Case of ϕ=45)

$$(-0.066+\ln(D)*0.0072)))))/(1.0+\log(D)*(-0.51+\ln(D)*$$

$$(-0.25+\ln(D)*(0.25+\ln(D)*(-0.07+\ln(D)*0.0072)))))\qquad ...(3.42)$$

Thus:

$$L_l = L_{l(25)} + (((\phi-25)/20)*L_{l(\phi)})\qquad ...(3.43)$$

It should be noted that the effect of higher values of "B" was omitted since it was found. from Figure 3.95, that the influence of B is almost negligible.

3.11.5.3 Effect of Change of δ on the Value of L_l

A few selected pile load tests were carried out to determine the effect of δ over L_l (refer to Figures 3.98 to 3.102). It was found that changing δ affects the value of L_l at a very slight rate that could be safely ignored, where no obvious effect could be taken into account.

3.12 Development of Shear Stresses (τ_{xy})

The exact distribution of shear stresses over the shaft is not yet well understood. Most of the solutions available in the literature assumed that the skin friction for a single shaft is a function of horizontal stress σ_x and a factor δ, which is the angle of friction between soil and pile material. Due to this relationship, the distribution of shear stress is assumed to be a straight line linearly increase with depth. The exact pattern of distribution of shear stresses is not yet well established. In the following section, analyses of shear stresses acting on the shaft τ_{xy} have been carried out. Figure 3.103 shows the progress of developed shear stresses at the pile-shaft interface. The following observations can be made from Figure 3.103:

1-The distribution of τ_{xy} over the shaft is not linear, it has a zero value at ground level and increases with depth. The shear stresses τ_{xy} exhibits a peak at certain depth from ground level.

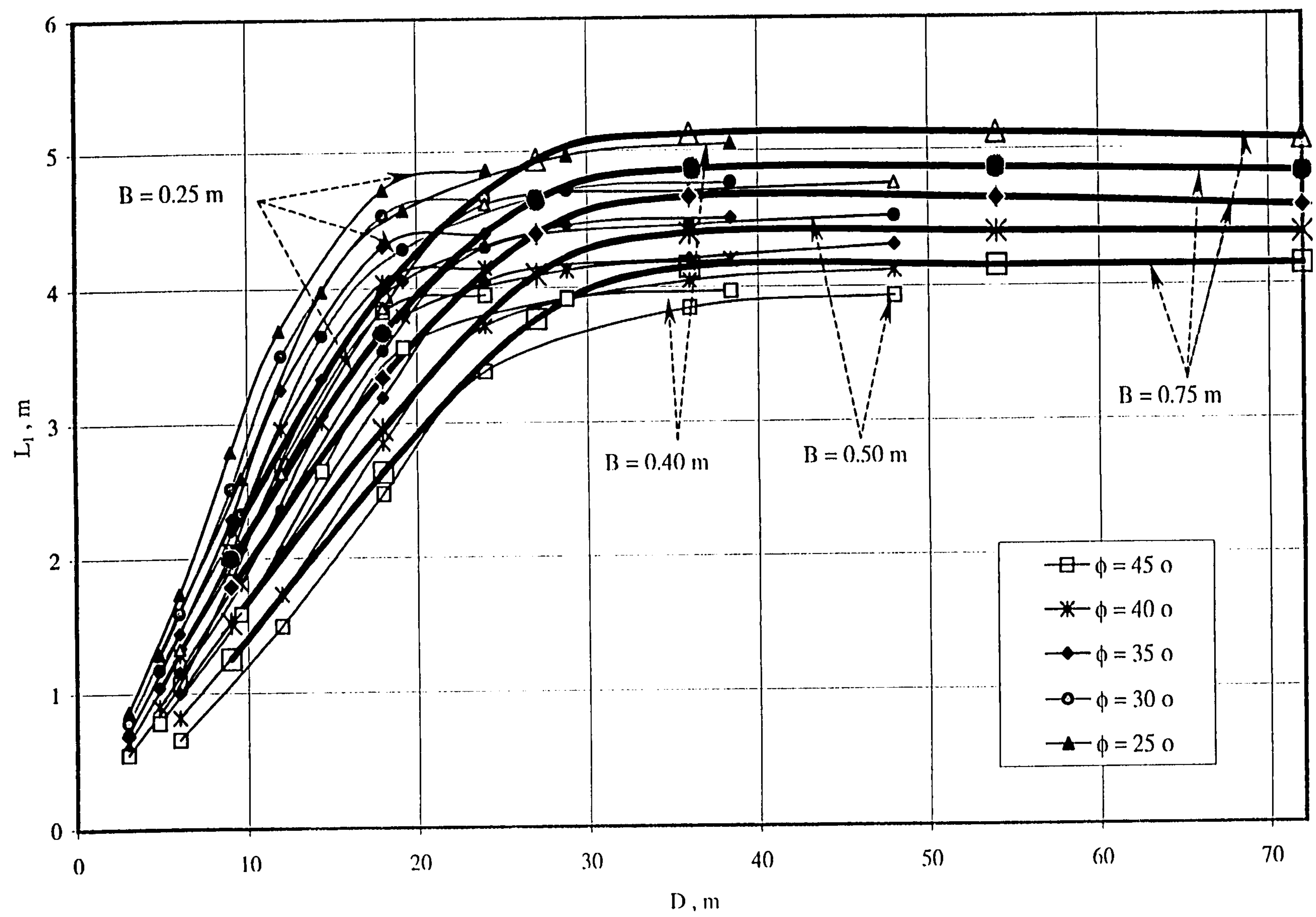

Figure 3.95 Vertical Distance L_1 Versus Pile Depth "D" With respect to Angle of Shearing Resistance "ϕ", and Pile Diameter "B"

Table 3.14 Parametric Study Results for Model Parameter: Vertical Distance "L_l"

Pile Geometry, m		Vertical Distance "L_l", meter				
B	D	$\phi = 25°$	$\phi = 30°$	$\phi = 35°$	$\phi = 40°$	$\phi = 45°$
0.25	3	0.858	0.777	0.7005	0.63	0.54
0.25	6	1.731	1.587	1.44	1.278	1.071
0.25	9	2.79	2.511	2.29	2.04	1.83
0.25	12	3.69	3.5	3.25	2.96	2.69
0.25	18	4.73	4.54	4.31	4.05	3.83
0.25	24	4.87	4.67	4.4	4.15	3.95
0.4	4.8	1.2816	1.164	1.0416	0.9	0.7776
0.4	9.6	2.592	2.328	2.0688	1.8096	1.5792
0.4	14.4	3.98	3.65	3.33	3.0096	2.6424
0.4	19.2	4.58	4.29	4.06	3.8	3.56
0.4	28.8	4.97	4.72	4.46	4.13	3.92
0.4	38.4	5.05	4.77	4.51	4.2	3.97
0.5	6	1.32	1.152	0.999	0.816	0.651
0.5	12	2.628	2.358	2.052	1.728	1.49
0.5	18	3.86	3.54	3.19	2.85	2.47
0.5	24	4.62	4.3	4.05	3.72	3.38
0.5	36	4.71	4.46	4.21	4.05	3.85
0.5	48	4.76	4.52	4.31	4.12	3.93
0.75	9	2.178	1.9935	1.7865	1.5165	1.2465
0.75	18	3.98	3.67	3.339	2.952	2.63
0.75	27	4.94	4.65	4.4	4.1	3.77
0.75	36	5.12	4.87	4.67	4.4	4.15
0.75	54	5.12	4.87	4.65	4.4	4.15
0.75	72	5.06	4.83	4.58	4.38	4.15

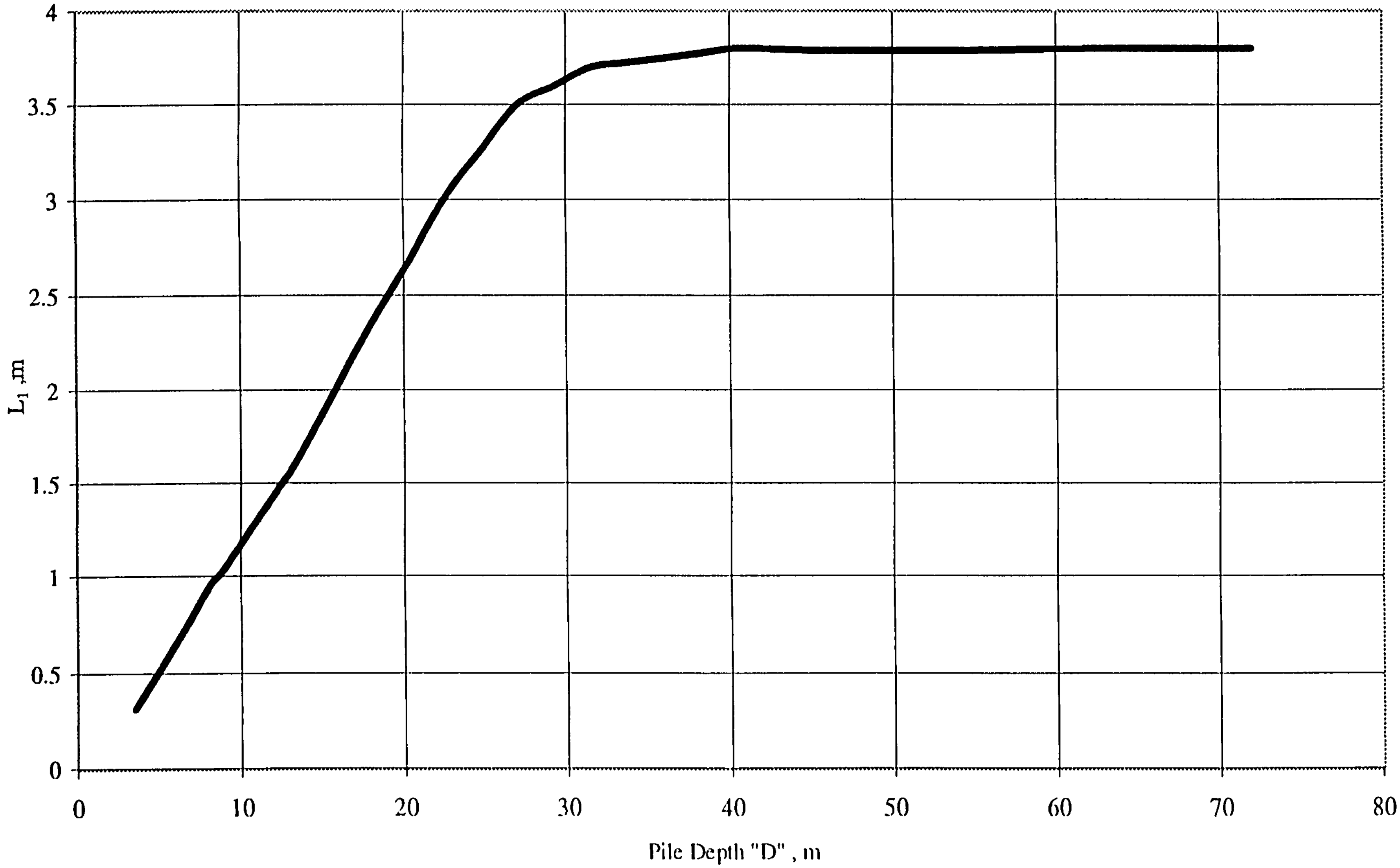

Figure 3.96 L_1 Versus Pile Depth, Case of $\phi=25^{\circ}$ (Lower Envelope)

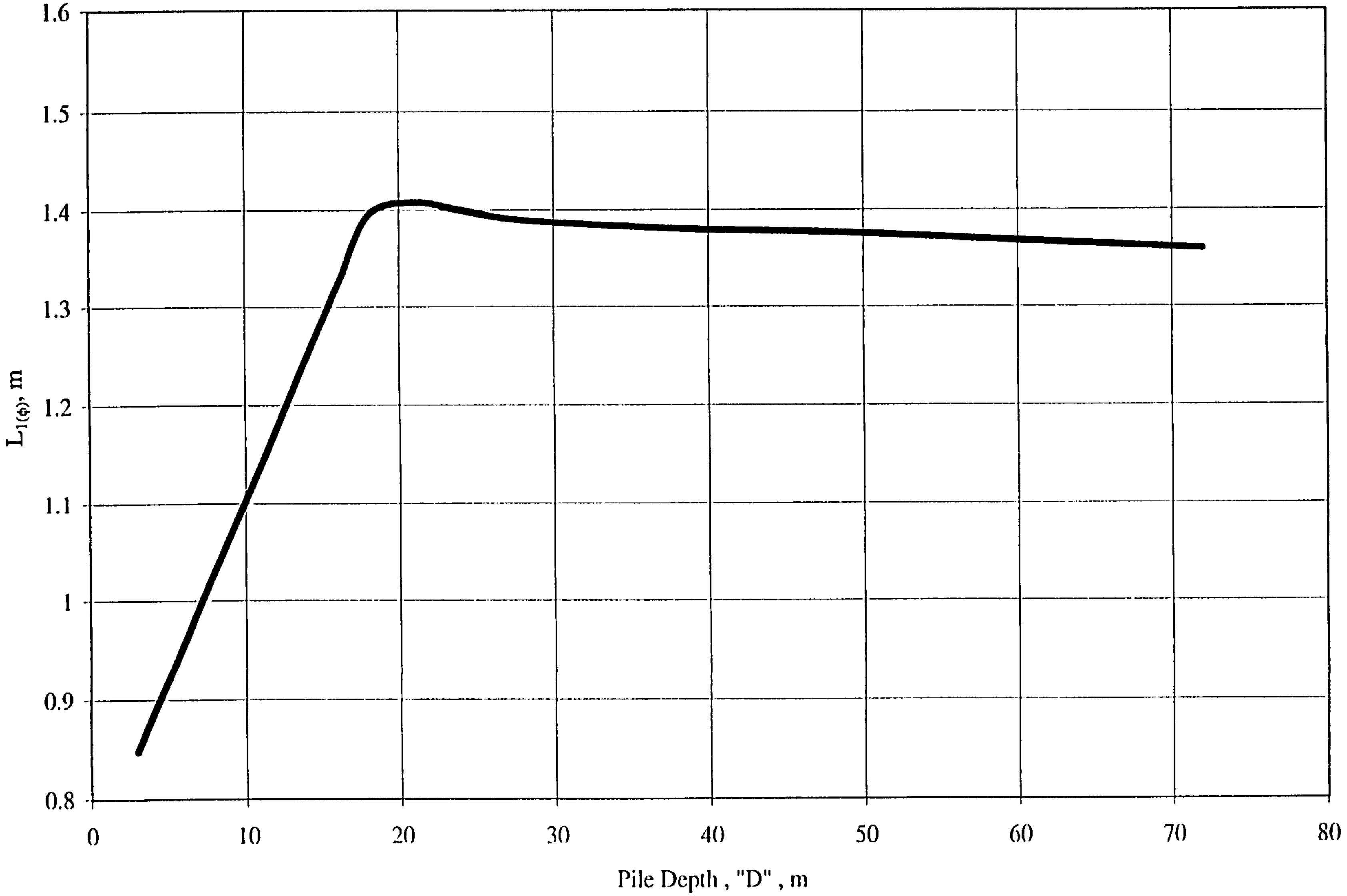

Figure 3.97 Average Rate of Increase in L_1 Due to Increase of ϕ

In this case it occurred at a depth equal to about 30 B. This behavior occurred in the zone of mobilized skin resistance, influence zone number I.

2- Zone II, located beside the tip, where the highest value of shear stresses (about 3.5 t/m^2) occurred, and diminished beneath the pile tip (at 6B beneath the tip). The shear stresses are negligible below that depth.

3- In general, the distribution of shear stresses can be described as follows:

- From ground level to a depth of about 30 B (zone I), τ_{xy} exhibits a sharp increase with depth.
- From depth equal to 30 B up to depth 44 B at tip level, the increase of τ_{xy} occurs with depth at a relatively lower rate.
- Between depths 44 B and 48 B (at the maximum pile embedment ratio), there is a noticeable increase in stresses occurred (this is the Zone II around tip).
- At a depth equal to about 4.5 B beneath tip, the stresses became almost negligible.

Figure 3.104 shows the distribution of shear stresses at failure at different vertical sections measured horizontally from the pile axis. Analyses of Figure 3.104 can give the following remarks:

1- The highest shear stresses are always around the shaft area.

2- The influence zone around the shaft, in this case, could be considered equal to about 6B.

3- At a horizontal distance equal to about 20 times the pile diameter, the shear stresses became negligible.

Figure 3.105 shows the distribution of developed shear stresses at failure, at different horizontal sections measured vertically from ground surface.

Analysis of this Figure 3.105 draws the following remarks:

1-τ_{xy} at ground surface is equal to zero and a high rate of increase occurs beneath the ground

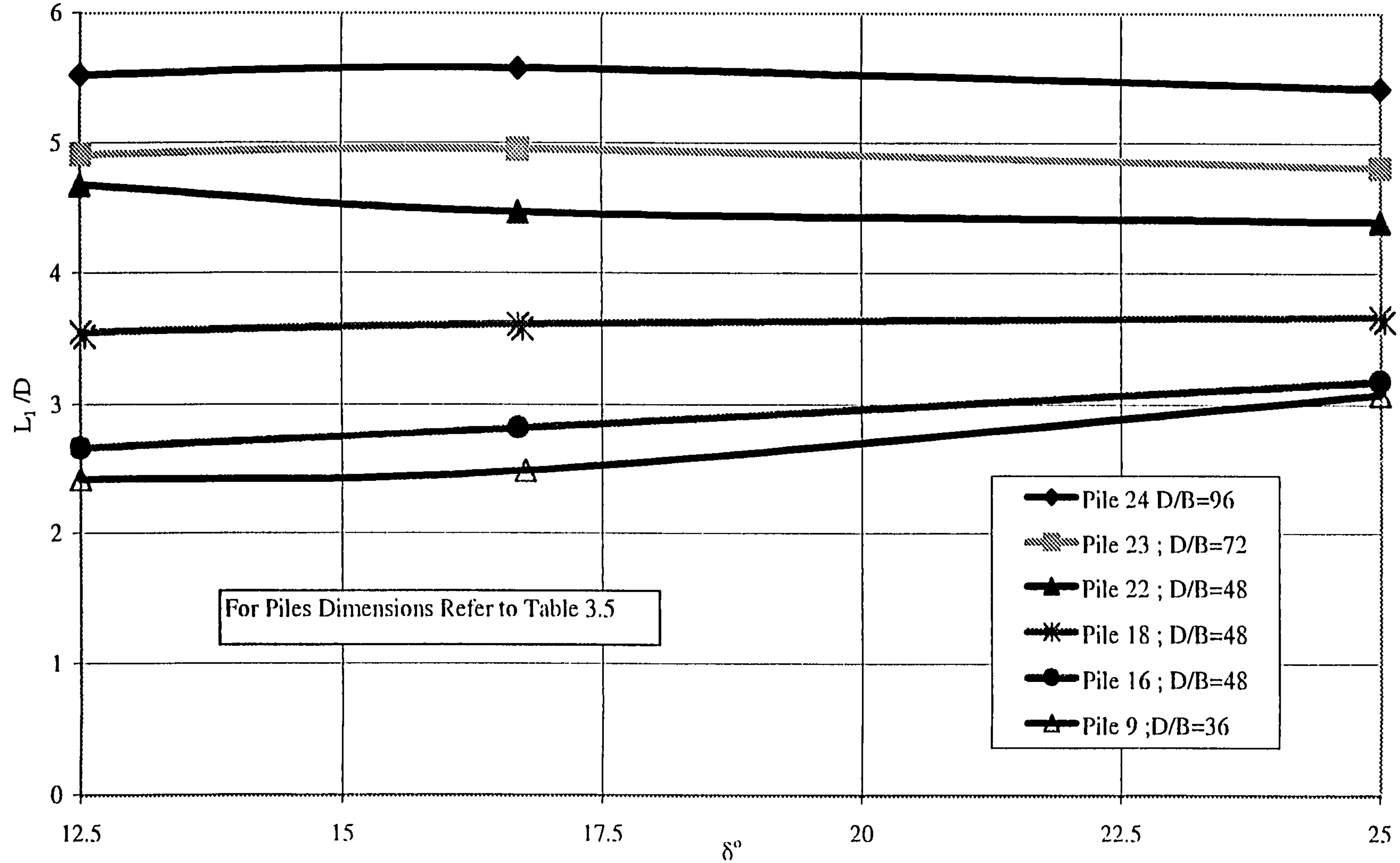

Figure 3.98 Effect of Changing Angle of Friction "δ" on Vertical Distance "L_1"
(Case of "φ" = 25°)

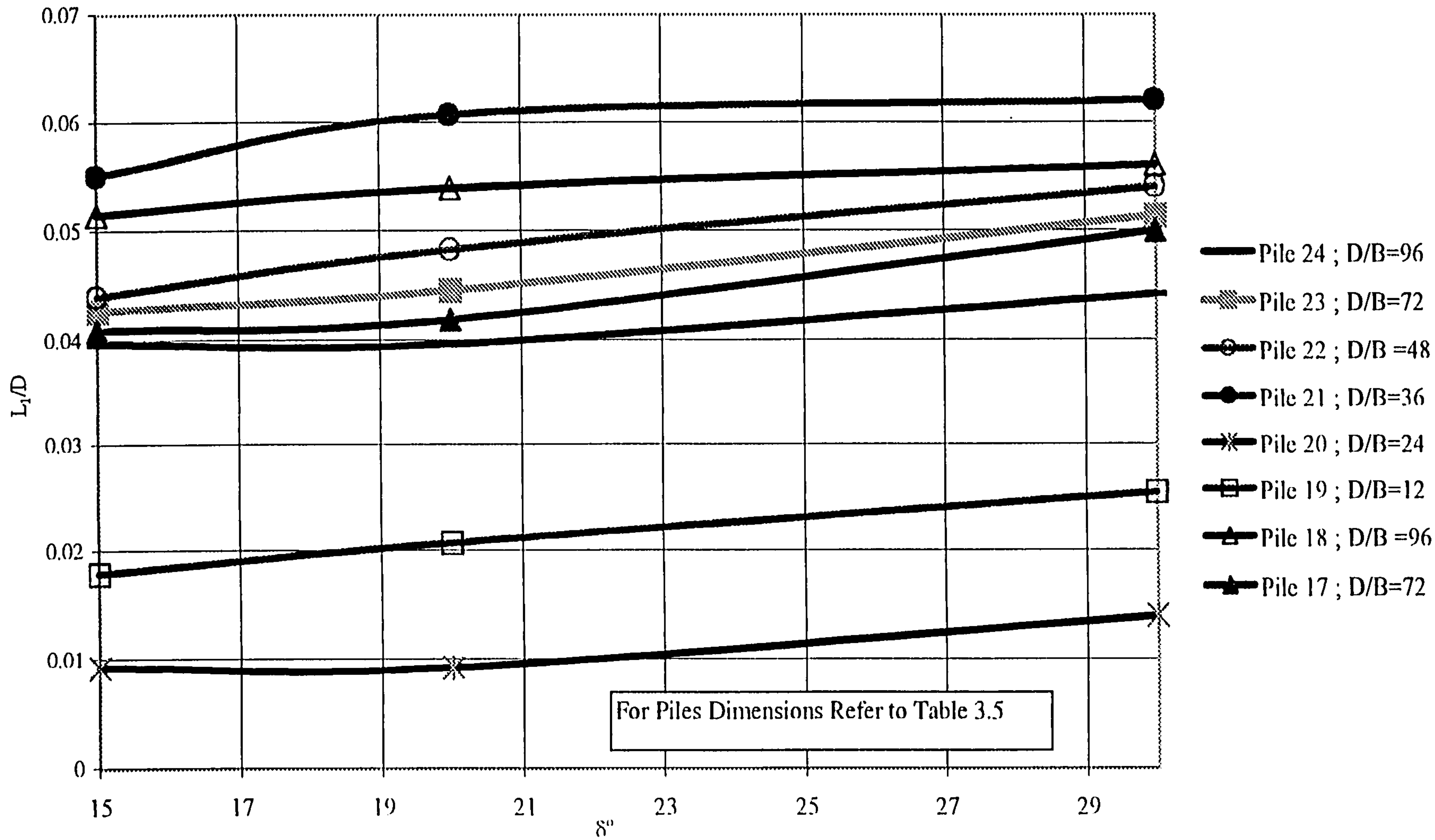

Figure 3.99 Effect of Changing Angle of Friction "δ" on Vertical Distance "L_1"
(Case of $\phi = 30^o$)

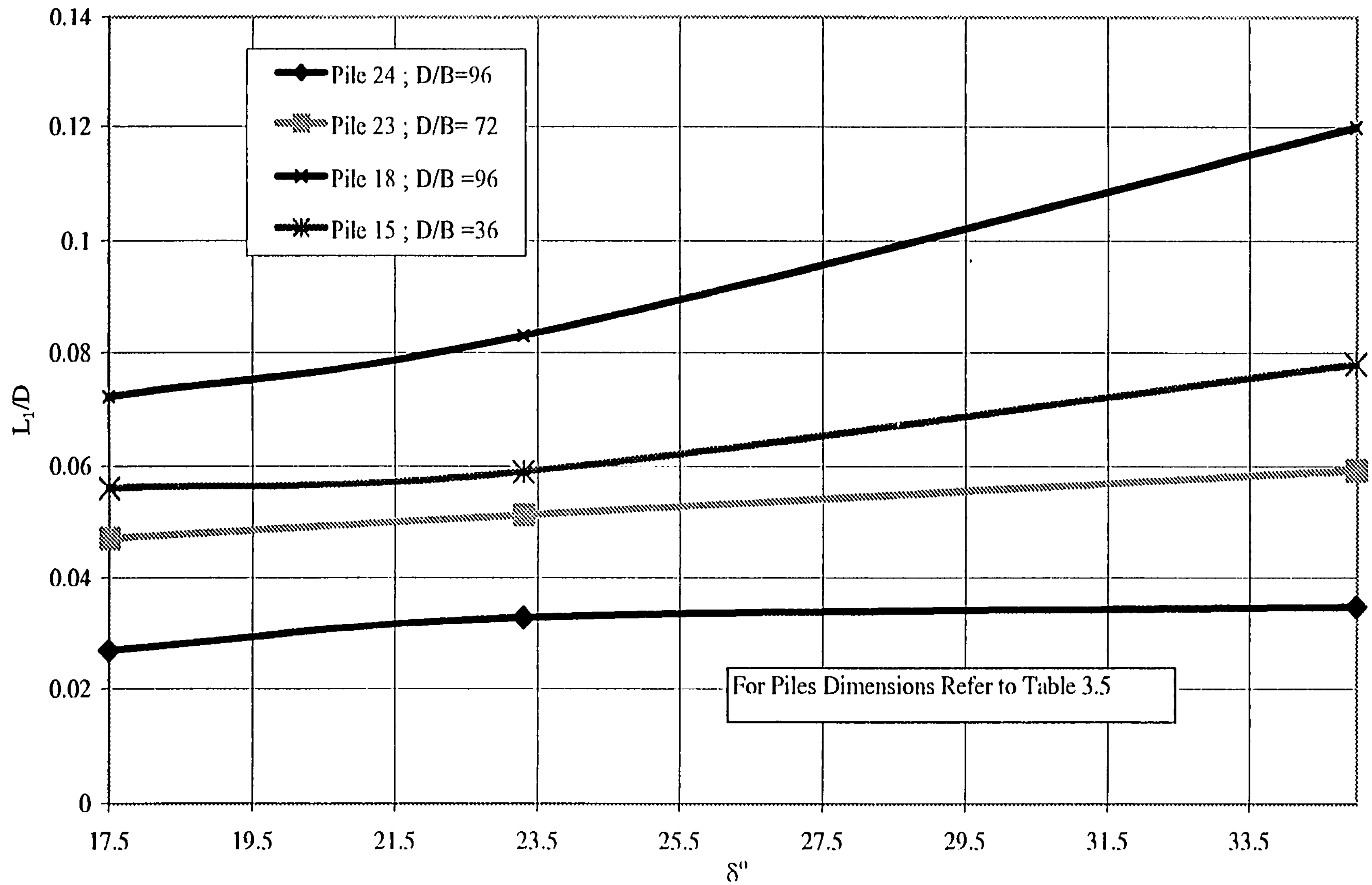

Figure 3.100 Effect of Changing Angle of Friction "δ" on Vertical Distance "L_1"
(Case of $\phi = 35^0$)

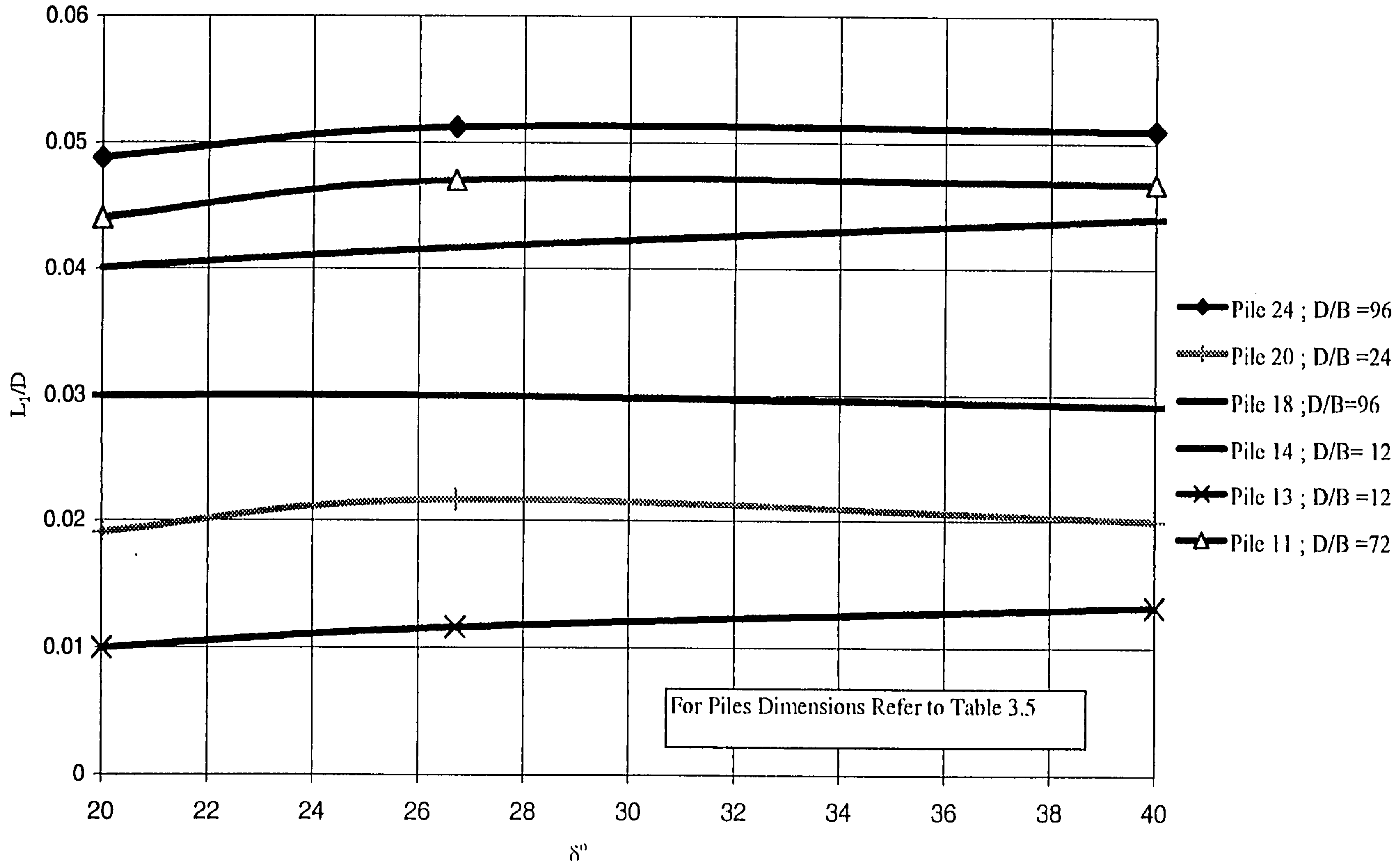

Figure 3.101 Effect of Changing Angle of Friction "δ" on Vertical Distance "L_1"
(Case of $\phi = 40^o$)

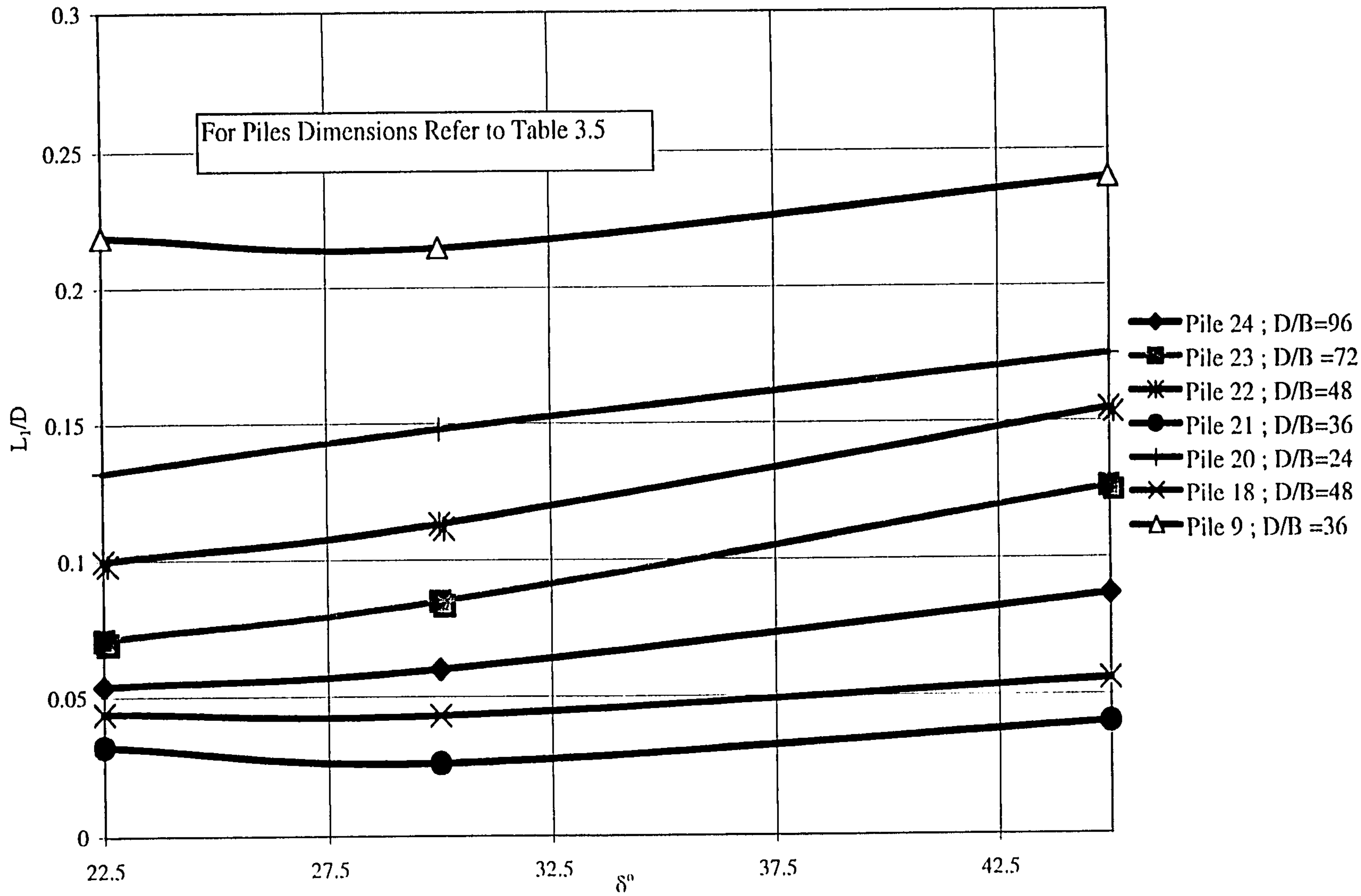

Figure 3.102 Effect of Changing Angle of Friction "δ" on Vertical Distance "L_1"
(Case of $\phi = 45^0$)

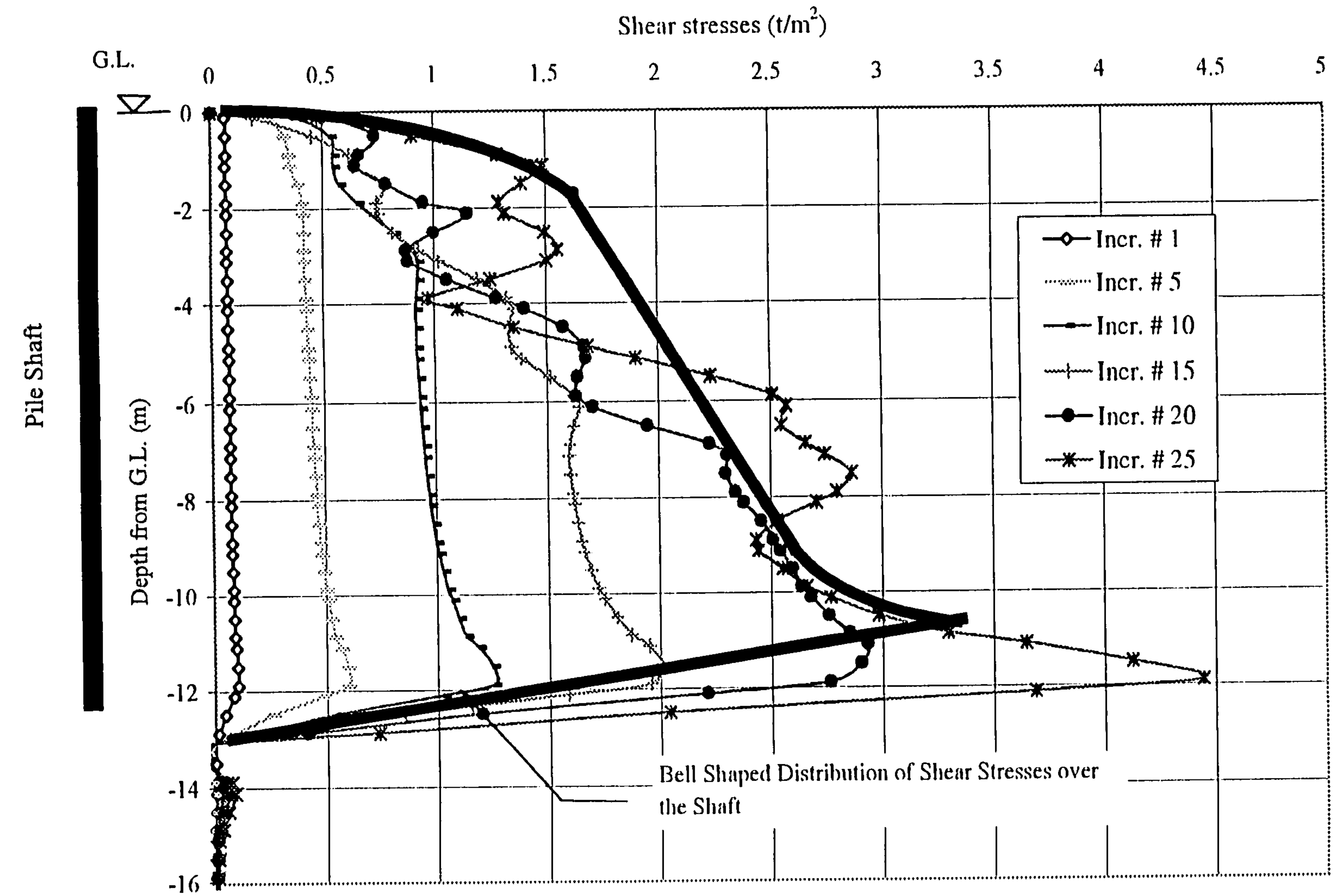

Figure 3.103 Incremental Development of Shear Stresses up to Failure Along Pile-Shaft Interface
(Test Data: D =12.0 m, B =0.25 m, $K_i = K_o$, $\phi = \delta = 30^o$)

level.

2- The shear stresses concentration occurred around the shaft up to a horizontal distance equal to about 5B. At distance equal to about 16 B, the stresses became almost negligible.

3- In the vertical direction, the influence beneath the tip level, was found to be in the order of 5B.

The conclusions from this section are:

1- The distribution of shear stresses τ_{xy} over the shaft can be approximated to bell shaped distribution, see Figure 3.104.

2- The developed τ_{xy} magnitude is dependent on the angle of friction between the pile material and the soil, and it varies with depth.

3- The horizontal and vertical influence zones around the shaft varies from level to level.

4- Shear stresses developed on the shaft are not constant ratio of horizontal stresses and are varied with depth.

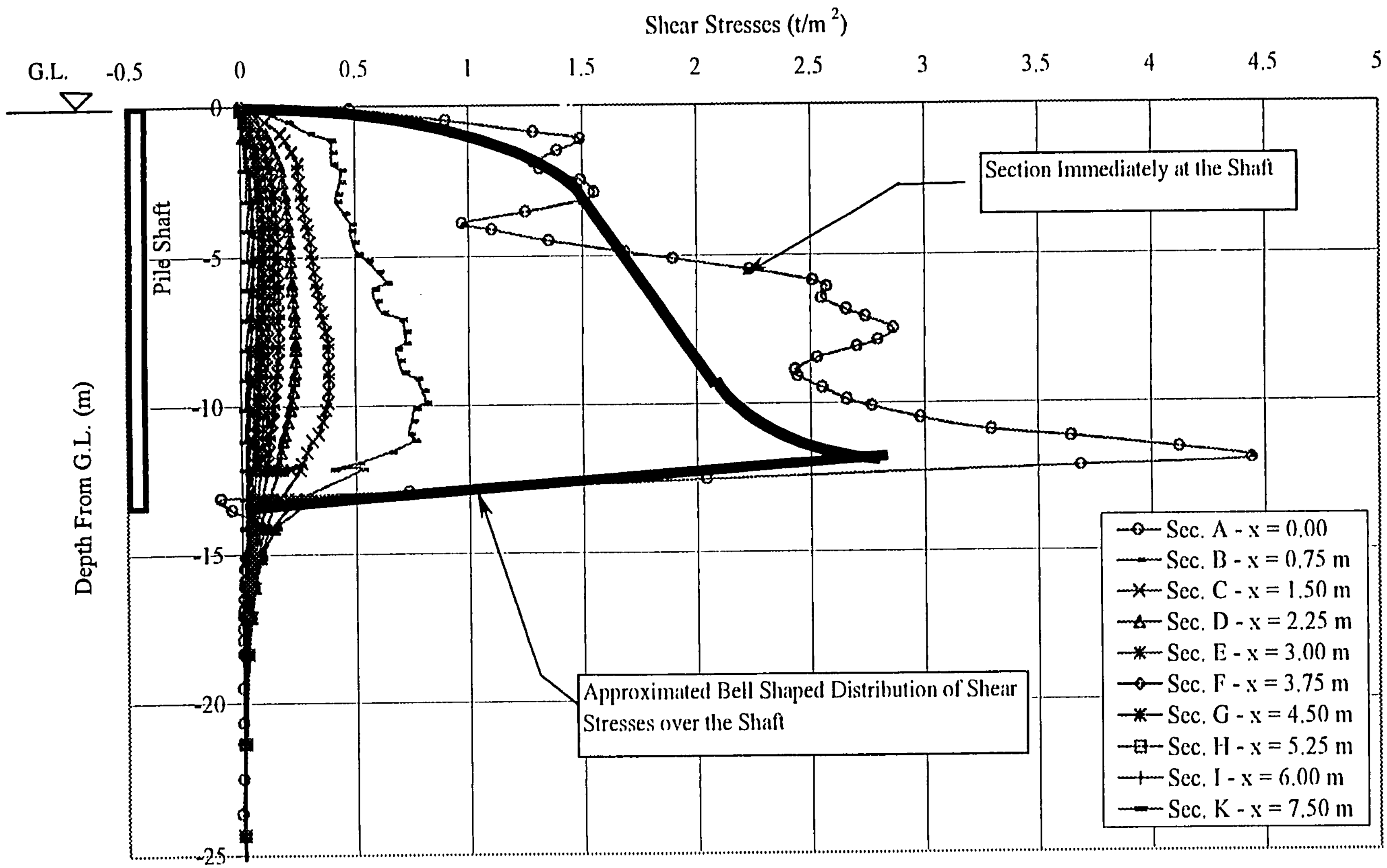

Figure 3.104 Comparison of Shear Stresses Developed at Failure Along Different Vertical Sections Measured Horizontally From Pile Axis (Test Data: D =12.0 m, B =0.25 m, $K_i = K_o$, $\phi = \delta = 30^o$)

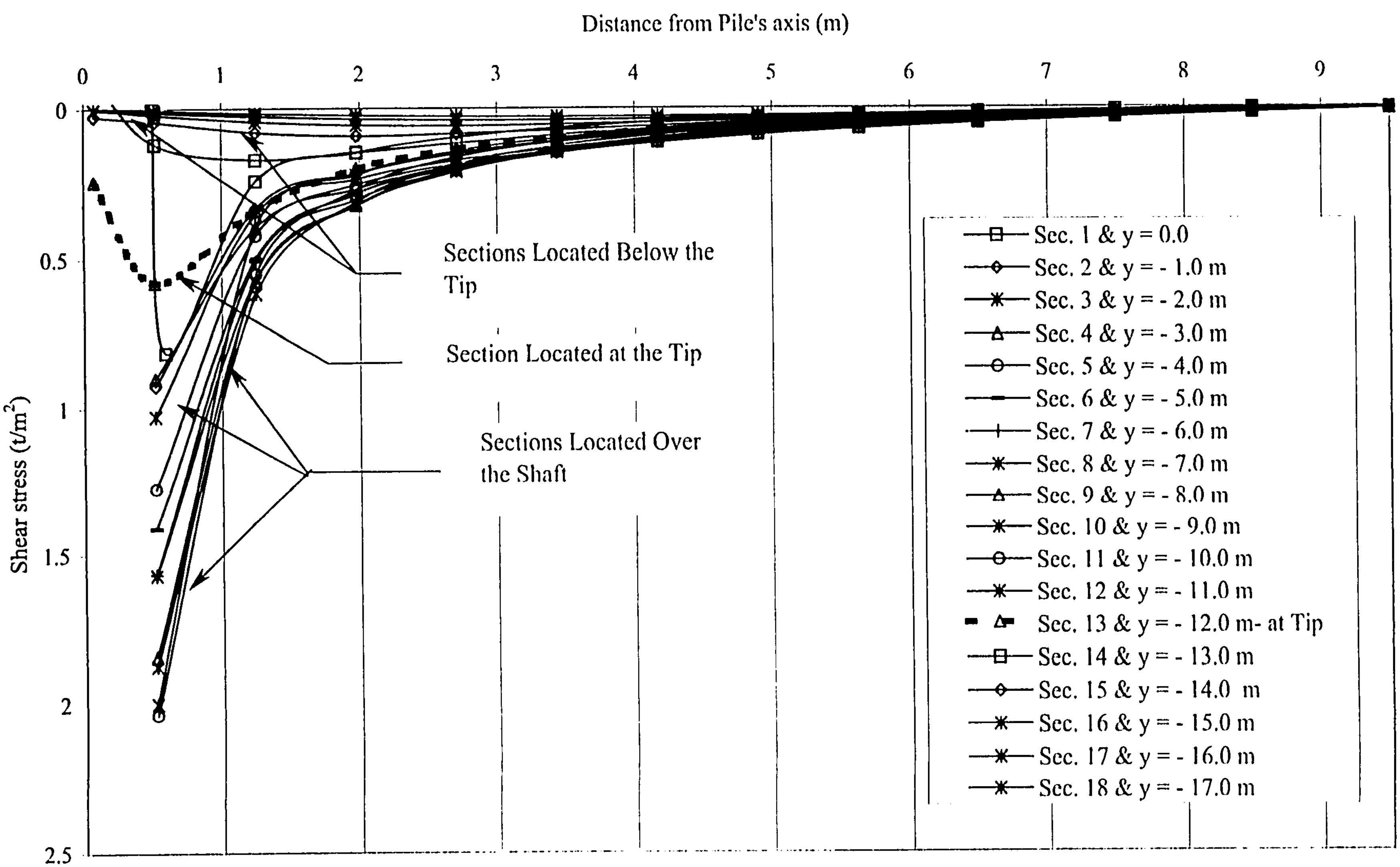

Figure 3.105 Comparison of Shear Stresses Developed at Failure Over Horizontal Sections Measured Vertically From Ground Level (Test Data: D =12.0 m, B =0.25 m, $K_i = K_o$, $\phi = \delta = 30^0$)

CHAPTER 4

THEORTICAL MODEL

4.1 GENERAL

In the literature bearing capacity theories were cited based on the assumptions that a failure mechanism develops around the pile tip and the shaft resistance is determined using simple mechanic laws. Except very few, no attempts were made to evaluate the failure mechanism due to skin resistance and its interaction with tip resistance. The state of stresses on the shear failure surfaces around the tip is either postulated as principle stresses (Berezantzev, 1961; Janbu, 1974) or derived from an earth pressure distribution prescribed on the pile shaft (Meyerhof, 1951; Hu, 1965; Durgonoglu and Mitchell, 1973). The influence of skin resistance on the tip resistance was ignored in most theories.

In the present chapter, an axisymmetrical Model for a single pile in sand is developed based on the results of the numerical model which was introduced in Chapter 3. The interdependence between shaft and tip resistances, and the effect of skin on tip resistance were accounted for. A new distribution of earth pressure acting on the shaft was introduced and used extensively in the proposed model.

4.2 Failure Mechanism

The proposed failure pattern varies with the following parameters: angle of shearing resistance of sand (ϕ), pile depth (D) and diameter (B), insitu coefficient of earth pressure (K_i) and relative roughness of the pile shaft (δ/ϕ). The proposed failure mechanism is presented in Figure 4.1. This failure mechanism is composed of two main parts: first is the shear failure sur-

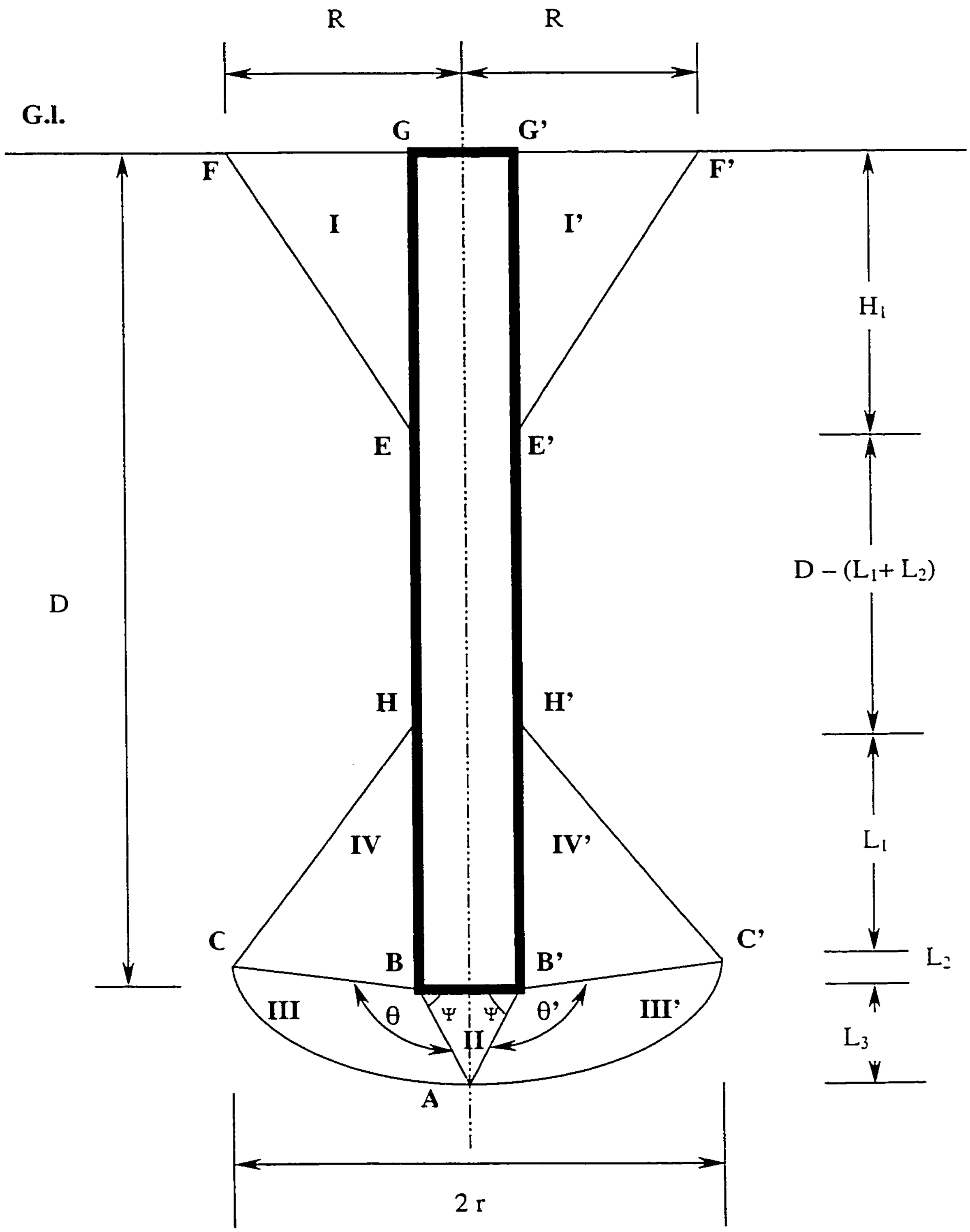

Figure 4.1 Assumed Failure Mechanism

face (Zone **I**) which developed around the pile shaft due to mobilization of skin resistance and second is the critical shear failure developed around the pile tip (Zones **II**, **III**, **IV**) due to mobilization of tip resistance. Specifically, theses Zones are as follows:

1) Zone **I** is the failure Zone which is developed as a result of mobilization of the skin resistance. This Zone composed of a conical shaped Volume, FGE, with total vertical height H_1 measured from ground surface and diameter R measured from the pile axis of symmetry. It should be noted here that, the surface FG was originally curved but it was considered as a plane in order to simplify calculations.

2) Zone **II** is a triangle wedge Zone ABB' located beneath the pile tip with a height of L_3 and base angle Ψ which varies depending on the Model parameter L_3 and pile diameter B, where:

$$\psi = \tan^{-1}(2L_3/ B)$$

and ψ is always less than 90^0 (refer to Figure 4.1).

3) Zone **III** consists of a radial shear Zone ABC bounded laterally by the surface AC which is a log spiral curve with its pole located at point B. This curve passes through the apex A of wedge ABB' and terminates at point C located at a horizontal distance of "**r**". The height of radial shear Zone III (the log-spiral) is composed of two distances, L_2 and L_3, where L_2 is the vertical distance above the pile tip level, and L_3 is the height of the cone-shaped Zone II below the tip level. The width of this Zone, "**r**", is measured from the pile axis of symmetry and is called the radius of influence at tip level.

4) Zone IV is composed of wedge Zone BCH, which is located above the radial shear Zone III and bounded externally by plane CH.

The model parameters: H_1, R, L_1, L_2, L_3 & **r** are vary depending on the following data: ϕ , δ;

D; B; and K_i.

4.2.1 Equilibrium Analysis

To carry out the equilibrium analyses utilizing the axisymmetrical cases of loading, it is sufficient to consider one sector of the Volume involved to revolve through the angle $\Delta\zeta$ around the pile axis (refer to Figure 4.2). The left half of the cross section of the proposed mechanism is assumed to revolve around the pile axis to generate the following Volumes:

1- Cross section FGE produces Volume $efge_1f_1g_1$ and is referred to as **Volume I** (refer to Figure 4.3). Figure 4.4 introduces the force system acting on this Volume as a free body subjected to the following forces:

a- Weight $\mathbf{W_1}$ of the soil wedge $efge_1f_1g_1$.

b- Earth pressure $\Delta\mathbf{E_1}$ and the shear force $\Delta\mathbf{Q_{s1}}$ acting on surface ee_1g_1g.

c- Normal horizontal forces $\mathbf{R_A}$ (resultant in central plan of the earth pressures forces $\mathbf{R_1}$& $\mathbf{R'_1}$, Figures 4.3 and 4.4), acting on tangelos planes efg and $e_1f_1g_1$ respectively.

d- Ground reaction acting on surface ee_1f_1f; $\mathbf{R_{GA}}$.Which is analyzes to horizontal component $\mathbf{E_2} = \mathbf{R_{GA}}$ *cos β and vertical component $\mathbf{T_2} = \mathbf{R_{GA}}$* sinβ.

2- Cross section ABO produces Volume $AObb_1$ and referred to Volumes **Volume II**. (Figure 4.5) shows a blow up view of this Volume and external acting forces:

a- Weight $\mathbf{W_2}$ of the soil wedge $AObb_1$.

b- Tangential Shear forces $\mathbf{F_T}$ and normal force $\mathbf{N_T}$ acting on surface Abb_1.

c- Normal resultant forces $\mathbf{R_{II}}$& $\mathbf{R'_{II}}$ of earth pressure acting on tangential planes AOb and AOb_1 respectively.

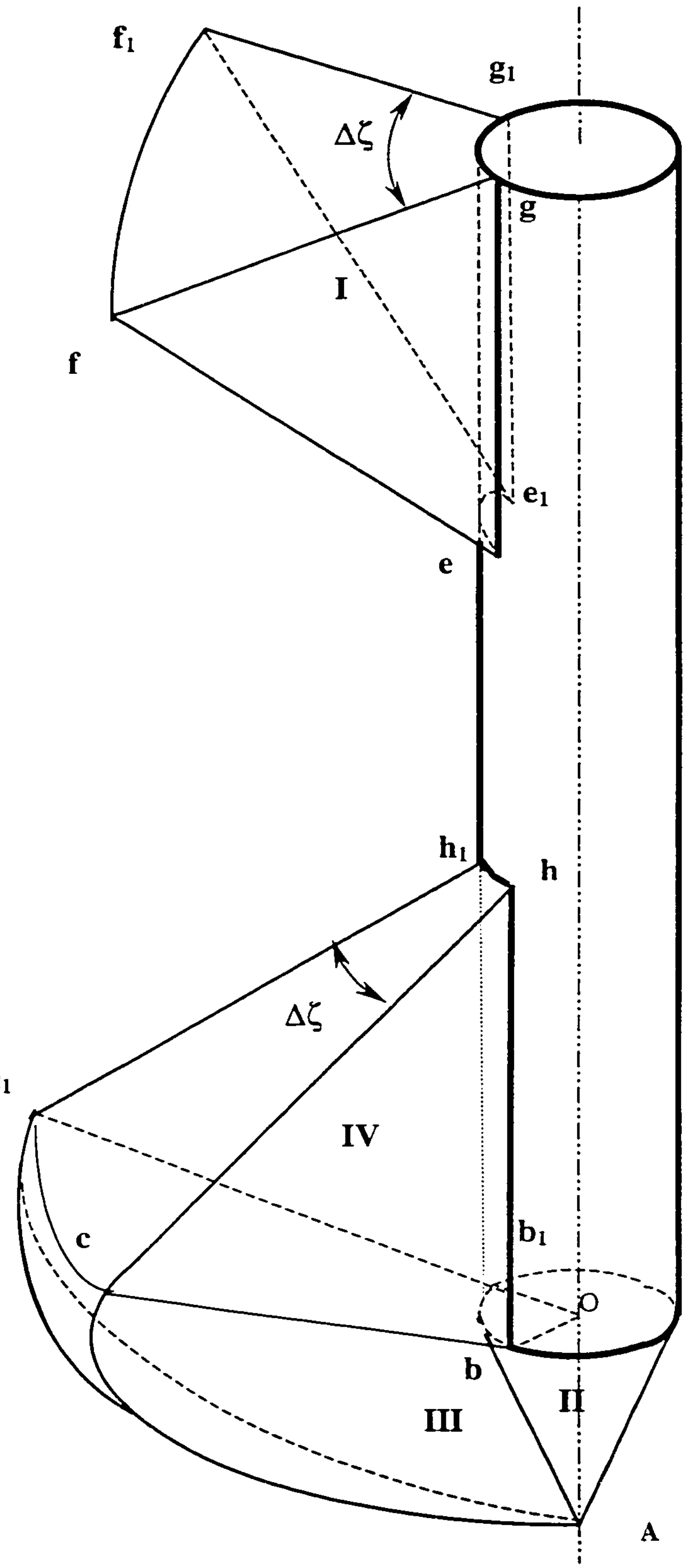

Figure 4.2 Volumes Generated by a Plane Cross Section Revolving Through a Central Angle Δζ Around Pile Axis

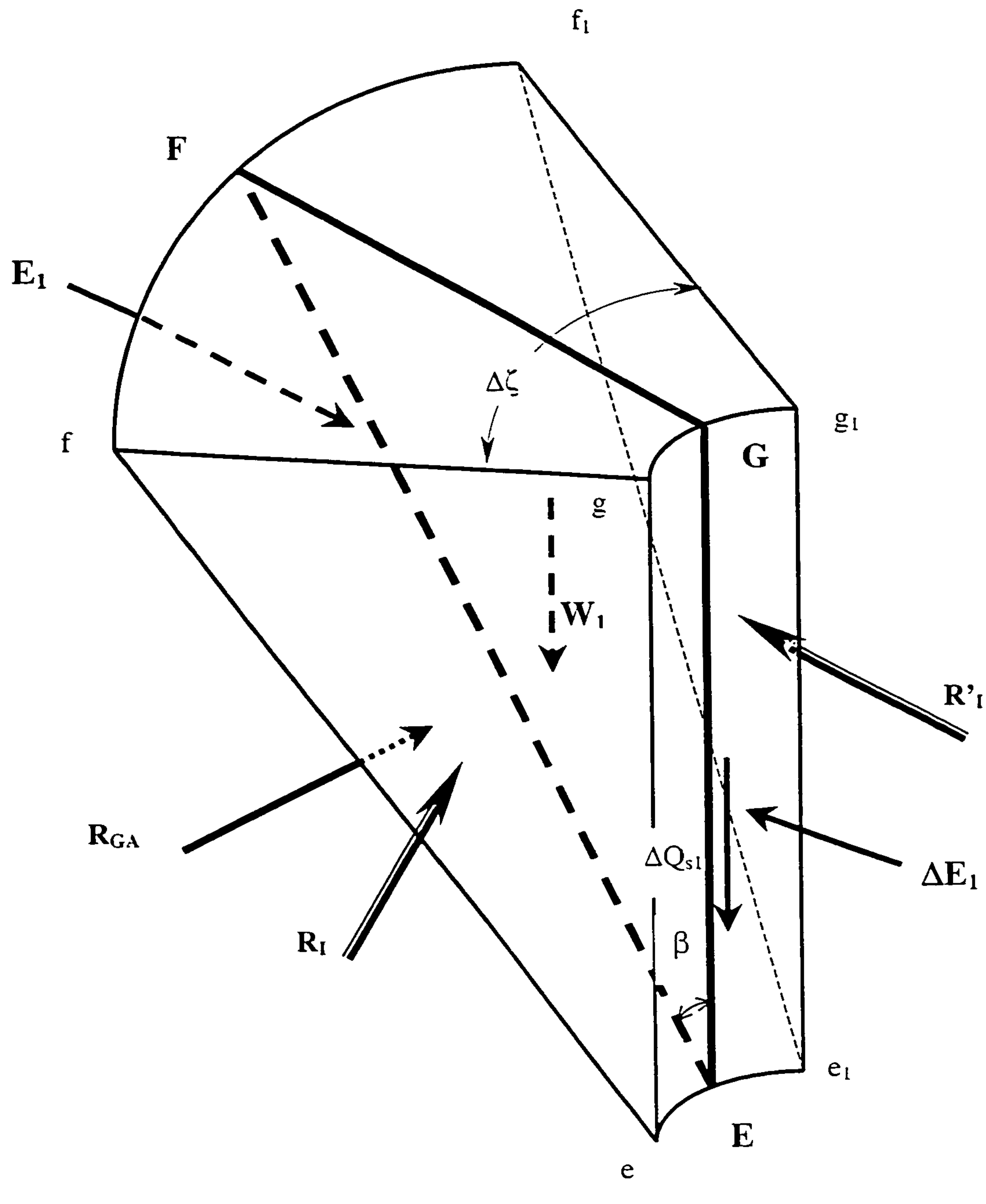

Figure 4.3 Enlarged View of Volume I (External Acting Forces)

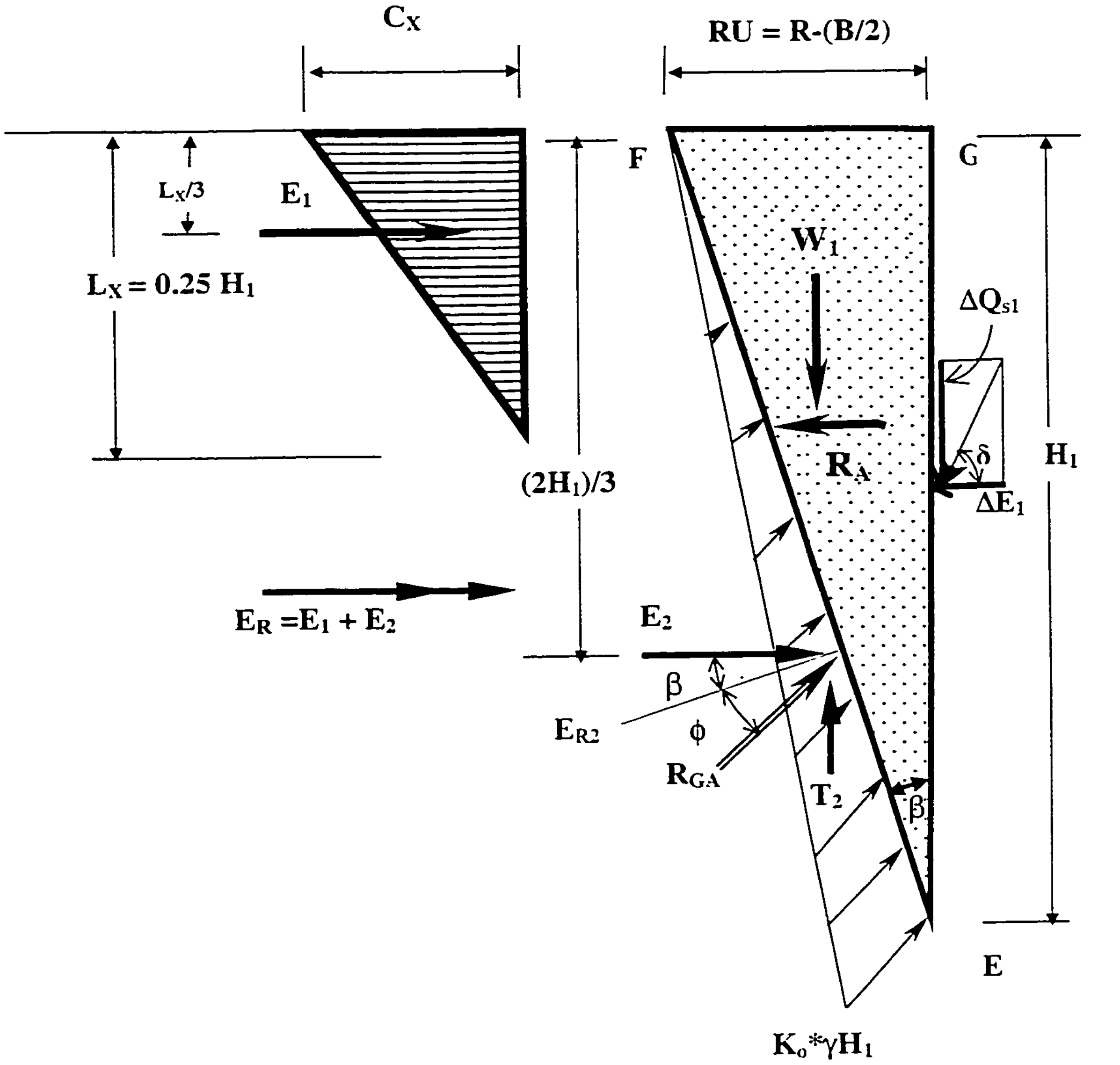

Distribution of the Additional Horizontal Earth Pressures (Due to Pile Loading)

Failure Pattern due to Skin Resistance (Plane of symmetry as one slice)

Figure 4.4 Acting forces as a Free Body Diagram of Zone I On the Central Plan

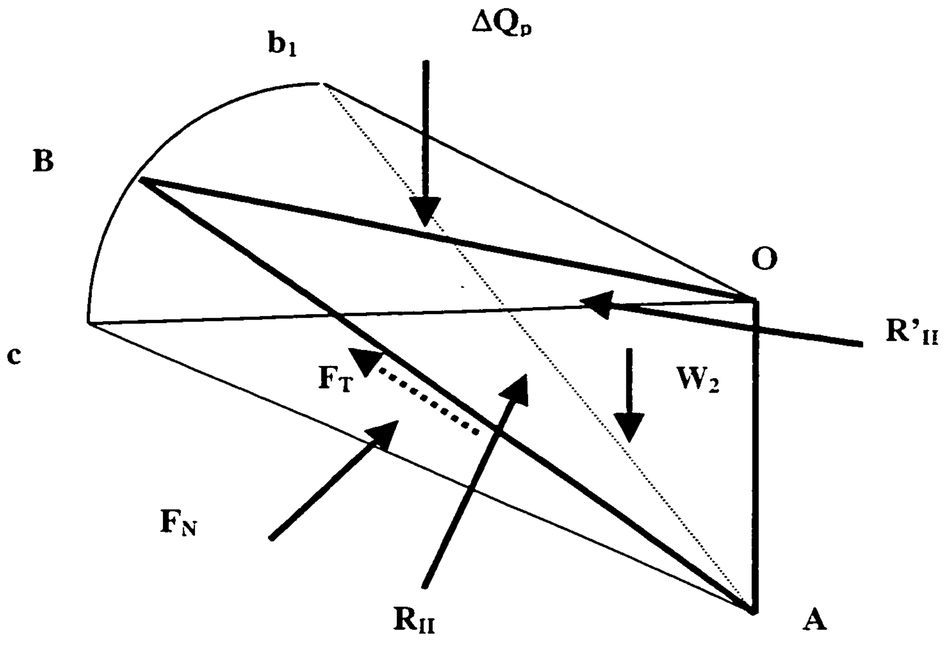

Figure 4.5 External Forces acting on Volumes II

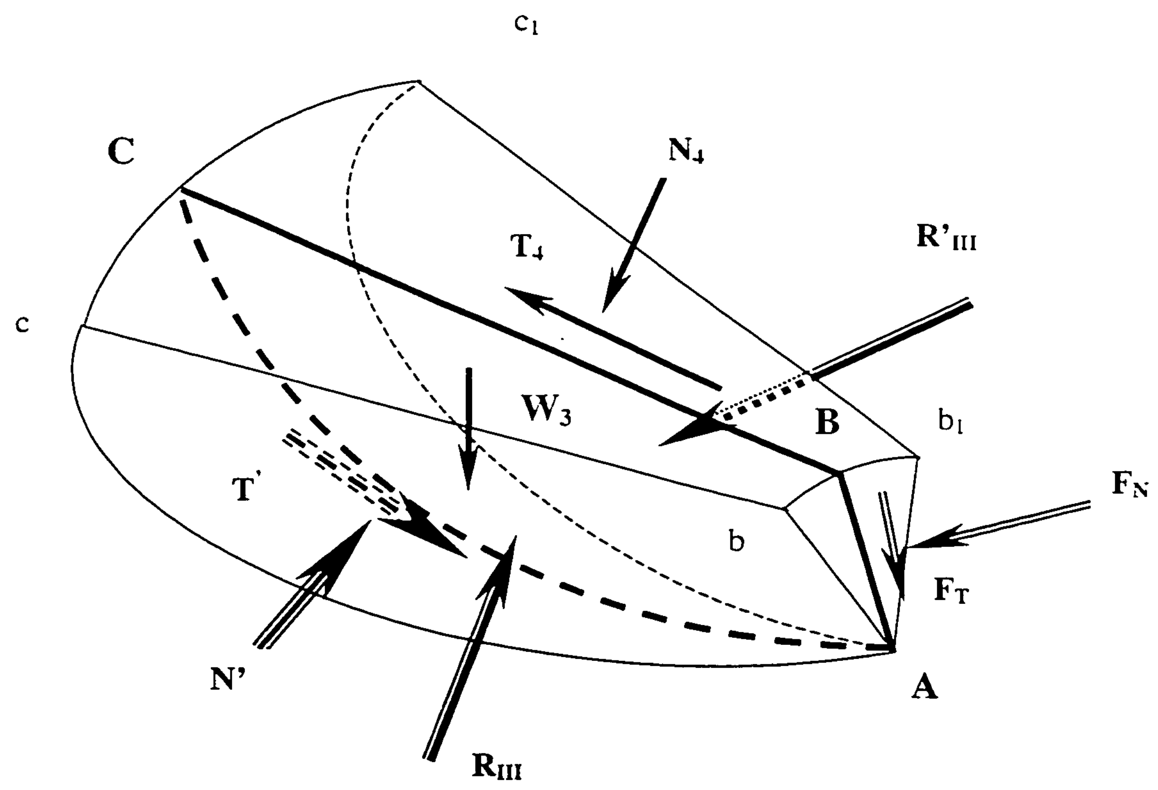

Figure 4.6 External Forces acting on Volumes III

d- Force $\Delta \mathbf{Q_p}$, the reaction force from the pile tip on the area Obb_1.

3- Cross section ABC produces Volume $Abcc_1b_1$ and referred to as **Volume III**. (Figure 4.6) shows a blow up view of this Volume as a free body subjected to the following force system:

a- Weight $\mathbf{W_3}$ of the soil wedge $Abcc_1b_1$.

b- Normal forces $\mathbf{N'}$, $\mathbf{F_N}$ & $\mathbf{N_4}$ acting on surfaces Acc_1, Abb_1 & bcc_1b_1 respectively.

c- Normal resultant forces R_{III}& $R^{'}_{III}$ of earth pressure acting on tangential planes Abc and Ab_1c_1 respectively.

d- Tangential Shear forces $\mathbf{T'}$, $\mathbf{T_4}$ and $\mathbf{F_T}$ acting on surfaces Acc_1, bcc_1b_1 & Abb_1 respectively.

The Mode of failure underneath the pile tip is assumed as punching shear failure (L'Herminier, 1953; Vesic, 1967b) and to facilitate this assumption, the locally mobilized angle of shearing resistance ϕ_β on the radial shear Zones **III &III'** (Refer to Figure 4.7) along line AC and AC' is taken equal to the angle of shearing resistance ϕ at point A and decrease to zero at point C& C', where at any arbitrary point j ϕ_β is given by:

$$\phi_\beta = \left(1 - \frac{\theta_j}{\theta}\right)\phi \qquad ...(4.1)$$

4- Cross section BCH produces Volume $bchh_1b_1c_1$ referred to as **Volume IV**, and is subjected to the following force system (refer to Figure 4.8):

a- Weight $\mathbf{W_4}$ of wedge $bchh_1b_1c_1$

b- Normal forces $\mathbf{N_{2A}}$ and $\Delta\mathbf{E_2}$ acting on surfaces bcc_1b_1 and bhh_1b_1 respectively.

c- Vertical force $\mathbf{W_G}$ acting on surface chh_1c_1 due to overburden pressure.

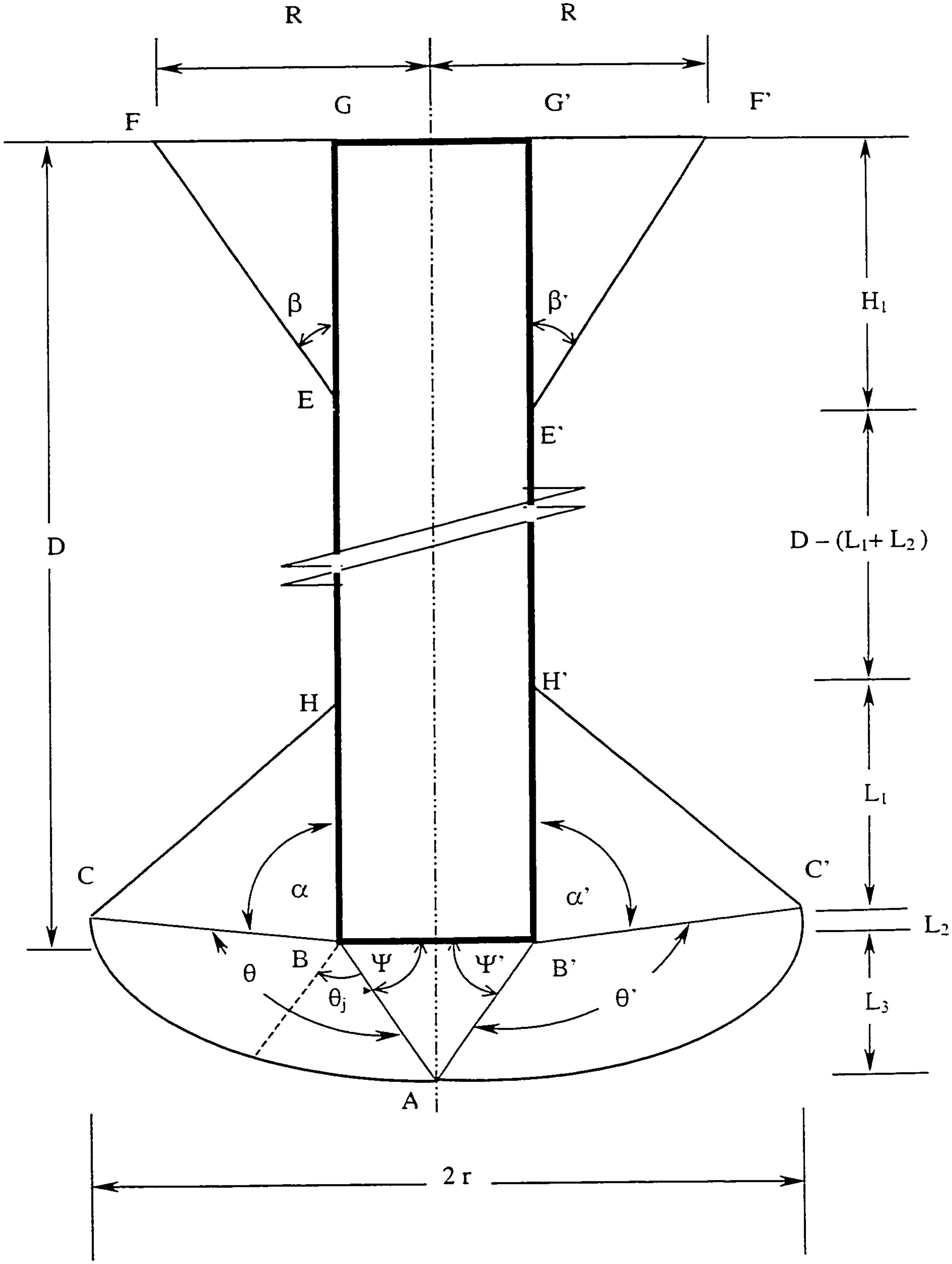

Figure 4.7 Geometry of the Log Spiral Curve at the Tip

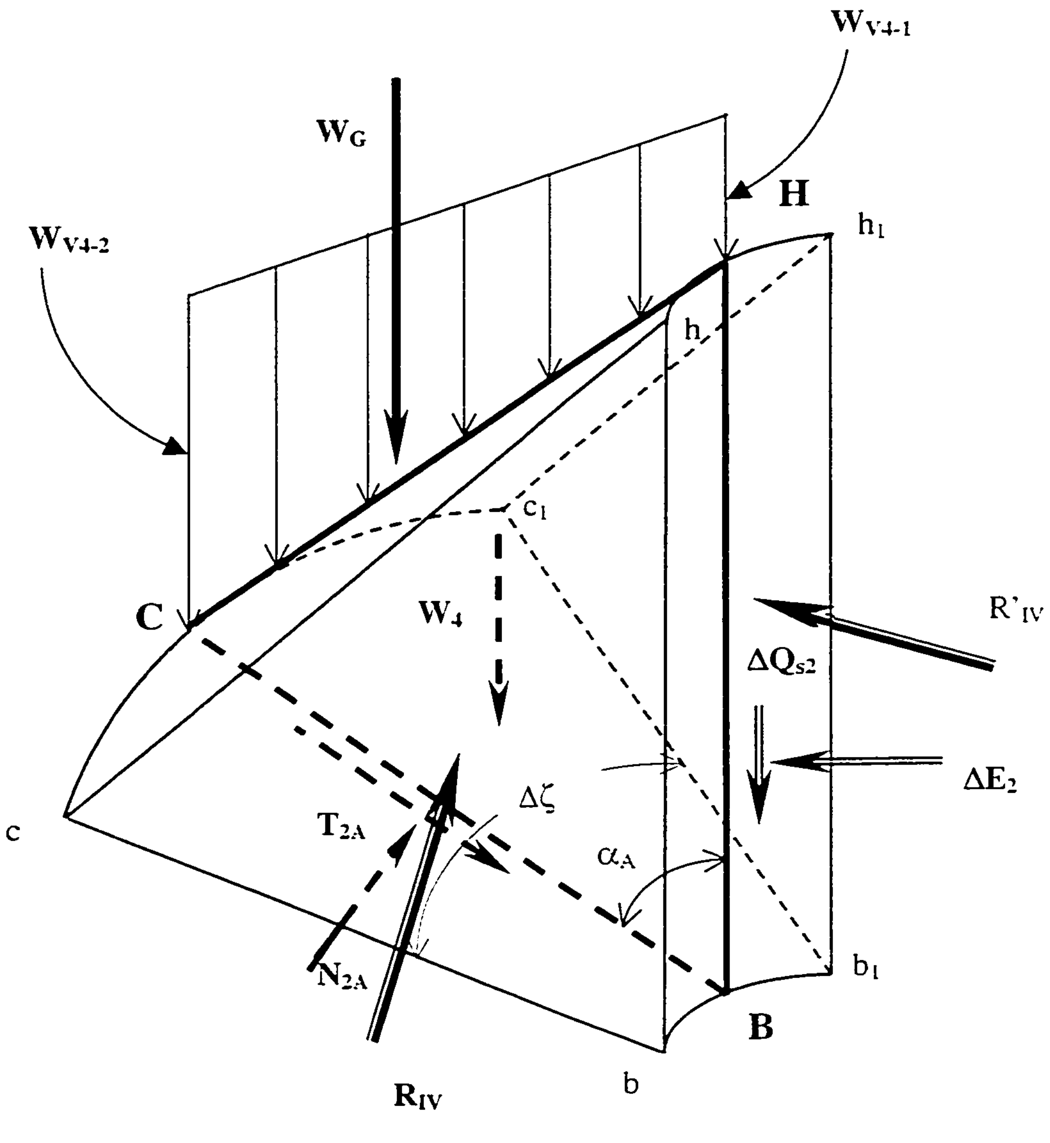

Figure 4.8 Enlarged View of Volume IV (External Forces)

d- Shear forces $\mathbf{T_{2A}}$ and $\Delta \mathbf{Q_{s2}}$ acting on surfaces bcc_1b_1 and bhh_1b_1 respectively.

e- Earth pressure forces $\mathbf{R_{IV}}$ and $\mathbf{R'_{IV}}$ acting on surfaces bhc and $b_1h_1c_1$ respectively.

Due to the axisymmetrical condition of the problem under consideration, it is possible to transform the three dimensional force system into a two dimensional one. Furthermore, the assumed force system is applied within the central plane of symmetry. The only exception to this assumption is the resultant forces R_I, R'_I; R_{II}, R'_{II}, R_{III}, R'_{III} and R_{IV} , R'_{IV} of earth pressure acting on tangential planes of Volumes I, II, III & IV respectively. These forces can be analyzed into components normal to plane of symmetry (canceling each other) and tangential components that lie in the plane of symmetry and which will play a role in the overall equilibrium of each Volume (refer to Figure 4.9).

4.3 Calculation of Skin Friction

The applied force system for Volume **I** is displayed in Figure 4.4. It is evident that all coplanar forces are applied in the plane of symmetry, as follows:

1- The weight $\mathbf{W_{1A}}$ of the soil Volume **I**. This Volume could be calculated using PappusGuldinus' theorem, i.e., area of triangle FGE multiplied by angle of rotation $\Delta\zeta$ in radians.

$$\mathbf{W_{1A}} = 1/2\ (R - B/2) * H_1 * \rho_{G1} * \gamma * \Delta\zeta\ \nu \qquad ...(4.2)$$

Where:

ρ_{G1} = Distance between centroid of Zone **I** and the pile axis $=\{(R-(B/2))/3\} + B/2$

2- The resultant $\mathbf{R_{1A}}$ of lateral forces $R_I \& R'_I$ can be calculated as follows (refer to Figure 4.10):

$$R_{1A} = R_{Ix} + R'_{Ix}$$

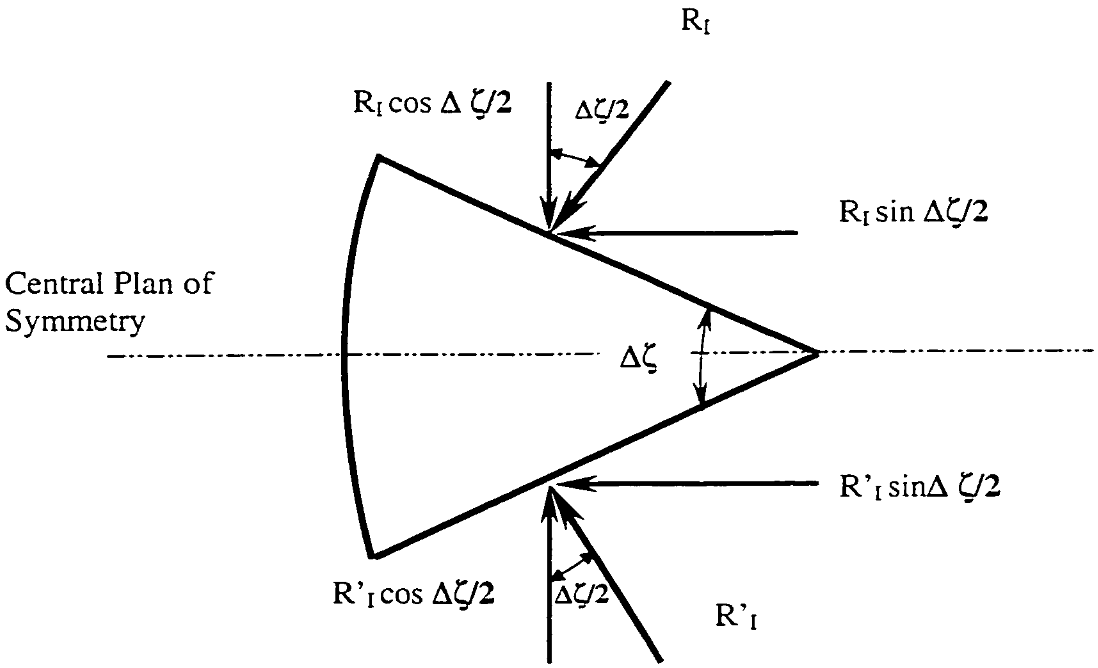

Figure 4.9 Plan View For Earth pressure Resultant Forces Acting on Assumed Vertical Failure Surfaces Volume **I**

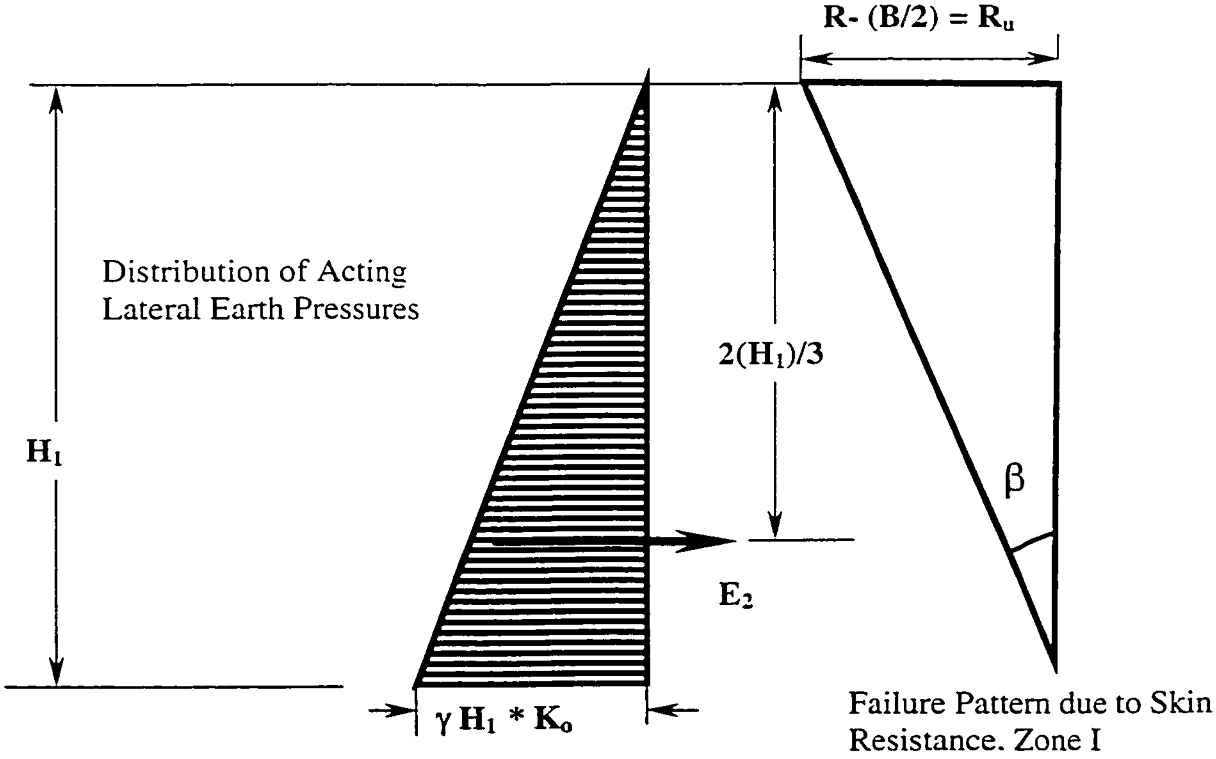

Figure 4.10 Illustrated Diagram for Calculation of Lateral forces Acting on Failure Zone I, R_I and R_I'.

$$R_{Ix} = R'_{Ix} = R_I \sin(\Delta\zeta/2) \quad = R'_I \sin(\Delta\zeta/2)$$

$$\mathbf{R_{1A}} = R_I \sin(\Delta\zeta/2) + R'_I \sin(\Delta\zeta/2)$$

$$\mathbf{R_{1A}} = 2\, R_I \sin(\Delta\zeta/2) = 2\, R'_I \sin(\Delta\zeta/2) \qquad \text{...(4.3)}$$

in which R_{Ix} & R'_{Ix} are components of forces R_I &R'_I (in x -direction) and parallel to the plane of symmetry FGE (refer to Figure 4.9).

Where R_I can be calculated as a hydrostatic pressure acting on the failure surface (refer to Figure 4.10):

$$R_I = \text{(average acting pressure on area for Zone I)} * \text{(area for Zone I)}$$

$$R_I = 1/2\ K_o *\gamma\,(H_l) * \text{(area FGE)}$$

$$R_I = 1/2\ K_o *\gamma\,(H_l) * (R\text{-}B/2)\ H_l$$

$$R_I = 1/4 * \gamma * K_o * H_l^2 (R\text{-}B/2) \qquad \text{...(4.4)}$$

Where:

H_l = Vertical height of Failure zone due to mobilization of Skin resistance

K_o = Coefficient of earth pressure at rest before the pile installation

R = Radius of influence at ground surface

B = Pile diameter

3- The additional earth pressure force E_l acting on the vertical height $0.25H_l$ is given by (refer to Figure 4.4):

$$E_l = {}^1/_2\,\gamma\, K_s\,(0.25\, H_l^2) * (R/2) * \Delta\zeta$$

$$E_l = 0.0625\ \gamma\, K_s\ H_l^2 * R * \Delta\zeta \qquad \text{...(4.5)}$$

where:

K_s = Developed coefficient of earth pressure acting on the pile shaft

γ = unit weight of sand

H_l = Model parameter, vertical height of mobilized skin resistance zone, and indicated as segment GE (Figures 4.3 and 4.4).

R = horizontal distance, radius of influence in meters, and indicated as segment GF (Figures 4.3 and 4.4).

$\Delta\zeta$ = central angle of rotation (in radians)

Once the free body forces are known for Zone I, the equilibrium can be calculated for the plane area EGF to determined ΔQ_s acting on the line GE. For this case, a generalized method of slices developed first by Sarma (1979), will be introduced in the following section.

Sarma assumed a general method which divided the soil mass enclosed in a plane slip surface into a number of slices. The slices are not necessary to be vertical nor the two sides of any slice to be parallel.

In his method, Sarma (1979) derived a recurrence relation between the normal forces E_i and E_{i+1} acting on the left and right sides, respectively, of an arbitrary slice i as follows (refer to Figure 4.11 and Appendix 1):

$$E_{i+1} = \frac{\cos(\phi_{Bi} - \alpha_i + \phi_{Si} - \omega_i)\cos\phi_{si+1}}{\cos(\phi_{Bi} - \alpha_i + \phi_{Si+1} - \omega_{i+1})\cos\phi_{Si}} E_i$$

$$+ \frac{(W_i + FV_i)(\cos\phi_{Si+1})\sin(\phi_{Bi} - \alpha_i)}{\cos(\phi_{Bi} - \alpha_i + \phi_{Si+1} - \omega_{i+1})}$$

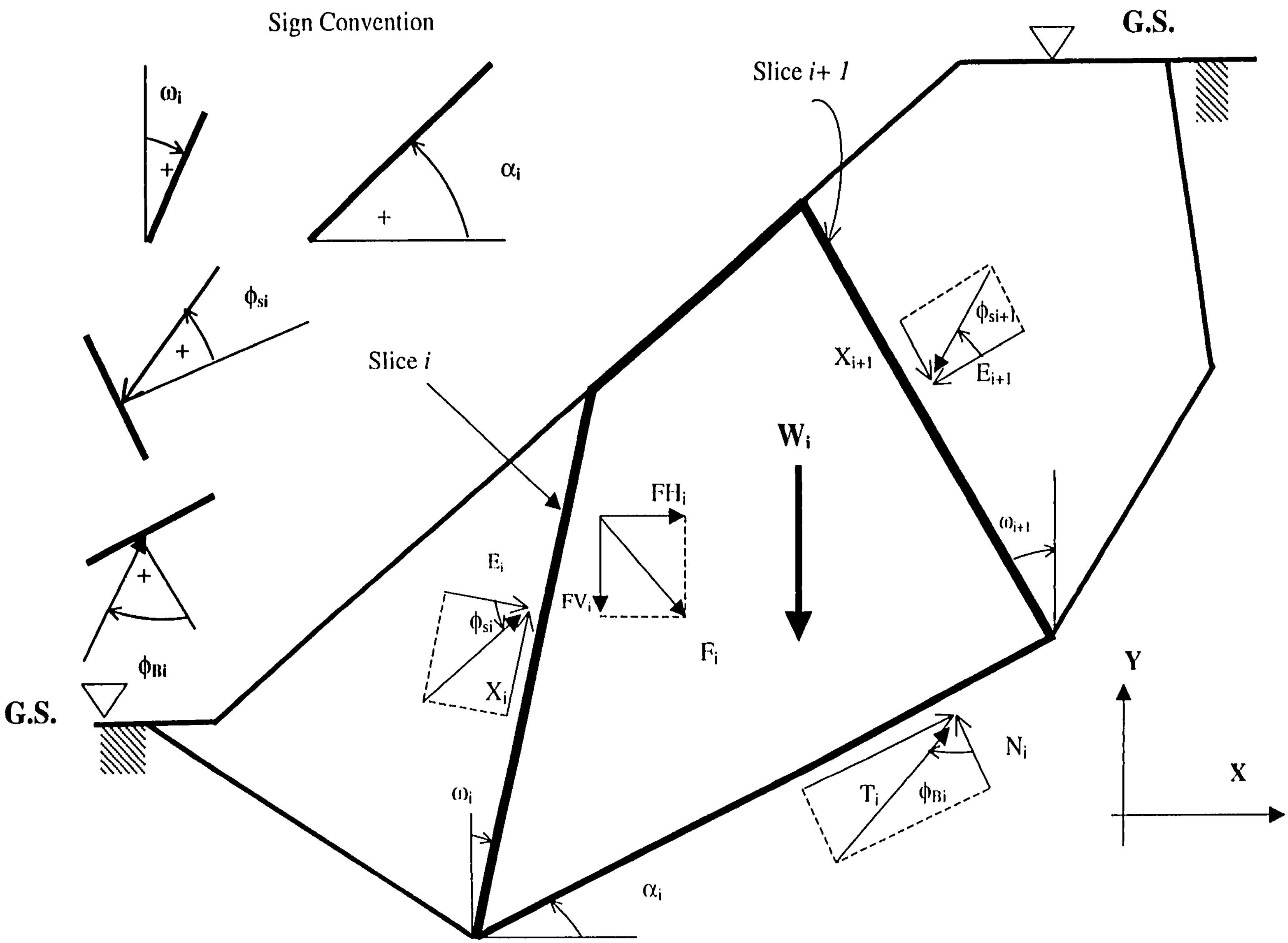

Figure 4.11 Notation and Sign Convention Used in Equation 4.7

$$+\frac{FH_i(\cos\phi_{Si+1})\cos(\phi_{Bi}-\alpha_i)}{\cos(\phi_{Bi}-\alpha_i+\phi_{Si+1}-\omega_{i+1})} \qquad ...(4.6)$$

where:

E_i, E_{i+1} = normal forces acting on the sides of slice i

α_i = basal slope of slice i

ω_i, ω_{i+1} = inclinations of sides of slice i

ϕ_{Bi} = mobilized angle of shearing resistance at mid point of the base of slice i

ϕ_{Si}, ϕ_{Si+1} = average mobilized angles of shearing resistance along sides of slice i

W_i = weight of slice i

F_i = resultant of external forces acting on slice i (other than E_i, E_{i+1}, W_i, N_i and T_i)

FH_i and FV_i = horizontal and vertical components of F_i.

Derivation of Equation 4.6 is given in Appendix 1. Figure 4.11 illustrates the general notations and sign conventions used.

For the slice EGF, to calculate the shear force ΔQ_{s1} along EG, it needs for ΔE_1 to be known first, refer to Appendix 1 for derivation of the following equations:

ΔE_1 is given by:

$$\Delta E_1 = E_1 + R_{GA} * \sin(90-\phi-\beta) - R_{1A} \qquad ...(4.7)$$

and

$$\Delta Q_{s1} = R_{GA} * \cos(90-\phi-\beta) - W_{1A} \qquad ...(4.8)$$

Where:

E_1 is given by equation 4.5.

β = Inclination angle of outer side of mobilized skin resistance zone

R_{1A} is given by equation 4.3.

R_{GA} = Ground reaction on surface FE and is equal to:

$$R_{GA} = 1/2\, \gamma\, H_1^2\, K_o * R/2 * \Delta\zeta \qquad ...(4.9)$$

The total skin resistance, Q_s is the sum of the two components, one is resulted from the analysis of forces of zone I; Q_{s1} and the other is resulted from the analysis of forces of zone IV, Q_{s2}.

For the analysis of zone 4, ΔQ_{s2} is given by the following Equation (refer to Appendix 1):

$$\Delta Q_{S2} = \Delta E_2 \tan\delta \qquad ...(4.10)$$

Where:

$$\Delta E_2 = \frac{W_{4G} + W_4 - A(R_4)}{A - \tan\delta} \qquad ...(4.11)$$

and:

$$A = \left(\frac{\sin\alpha_A + \tan\phi_\beta \cdot \sin(90 - \alpha_A)}{\cos\alpha_A - \tan\phi_\beta \cdot \cos(90 - \alpha_A)} \right)$$

Where α_A is the inclination angle of terminal radial surface BC, refer to Figure 4.12 and it is equal to:

$$\alpha_A = \tan^{-1} (\mathbf{r}\text{-}B/2) / L_2 \qquad ...(4.12)$$

W_4 = Self weight of slice 4 and it is equal to:

$$W_4 = 1/2\, (\mathbf{r}\text{-}B/2) * (L_1 + L_2) * \gamma * \rho_4 * \Delta\zeta \qquad ...(4.13)$$

ρ_4 = Distance between centroid of Zone **IV** and the pile axis $= \{(\mathbf{r}-(B/2))/3\} + B/2$

W_{4G} = Vertical reaction acting above slice CBH

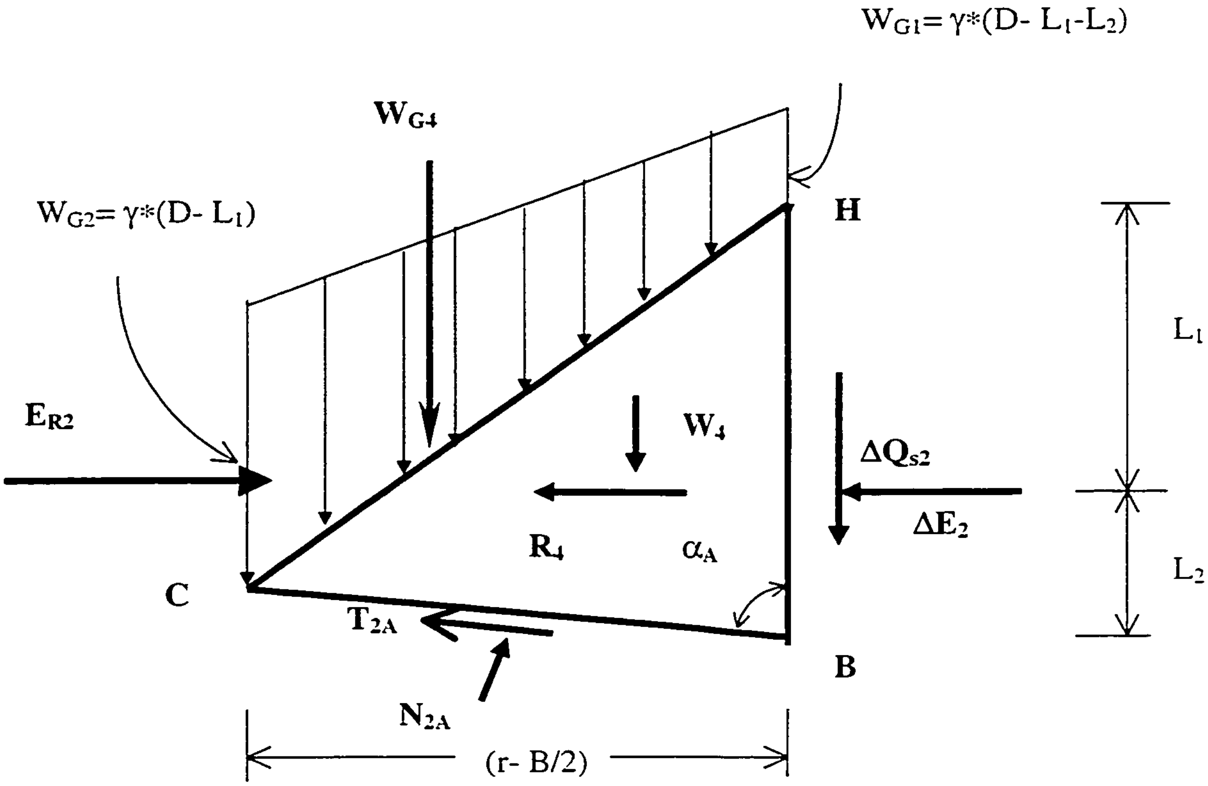

$$\alpha_A = \tan^{-1} (r- B/2)/ L_2$$

Figure 4.12 Free body For Zone IV

$$W_{4G} = 1/2\,(2D - L_1 - 2L_2)\,(\mathbf{r}/2)^*\Delta\zeta \qquad ...(4.14)$$

Then the normal force N_{2A} (refer to derivation in Appendix 1), acting on the surface between volume IV and III is given by:

$$N_{2A} = \frac{\Delta E_2 + R_4}{\cos\alpha_A - \tan\phi_\beta \cos(90 - \alpha_A)} \qquad ...(4.15)$$

And tangential force acting on the same surface T_{2A} is given by:

$$T_{2A} = N_{2A} \tan\phi_\beta \qquad ...(4.16)$$

Where:

ϕ_β = Average mobilized angle of shearing resistance on base BC.

and it assumed to be equal to $\phi/2$.

Once ΔQ_s is determined, calculating for a central angle of rotation equal to $\Delta\zeta$, the total skin friction Q_s is computed as:

$$Q_s = (\Delta Q_{s1} + \Delta Q_{s2})\left(\frac{2\pi}{\Delta\zeta}\right) \qquad ...(4.17)$$

4.4 Calculation of Point Resistance Q_P

4.4.1 General

The force $\mathbf{\Delta Q_p}$ is calculated, as the reaction force acting on the area bOb_1 (Figure 4.5). And the end bearing capacity $\mathbf{Q_p}$ is computed by integrating $\mathbf{\Delta Q_p}$ over a central angle of rotation of 2π around the pile axis.

To calculate $\mathbf{Q_P}$ it is essential to know the force components acting from the neighboring Volumes, Volume **III** and Volume **IV**. For the forces N_{2A} and T_{2A} acting from Volume **IV**, it is given in Equations 4.16 and 4.17 respectively as a result of equilibrium of Volume **IV**.

4.4.2 Equilibrium of Volume IV

To determine the forces T_4 and N_4, the equilibrium of Volume **IV** will be introduced here: Similar to the procedure which was followed for the equilibrium of Volume I. Refer to Figures 4.8 and 4.12.

1- The weight $\mathbf{W_4}$ of the soil induced in Volume **IV** is calculated using Pappus Guldinus' theorem, i.e., area of triangle BHC multiplied by angle of rotation $\Delta\zeta$ in radians.

$$\mathbf{W_4} = 1/2\,(\mathbf{r} - B/2) * (L_1 + L_1) * \rho_{G4} * \gamma * \Delta\zeta \qquad \text{...(4.18)}$$

Where:

ρ_{G4} = Distance between centroid of Zone **IV** and the pile axis $= \{(\mathbf{r}-(B/2))/3\} + B/2$

2- The resultant R_4 of lateral forces R_{IV} & R'_{IV} can be calculated as follows (refer to Figure 4.11):

$$R_4 = R_{IVx} + R'_{IVx}$$

$$R_{IVx} = R'_{IVx} = R_{IV} \sin(\Delta\zeta/2) = R'_{IV} \sin(\Delta\zeta/2)$$

$$R_4 = R_{IV} \sin(\Delta\zeta/2) + R'_{IV} \sin(\Delta\zeta/2)$$

$$R_4 = 2\,R_{IV} \sin(\Delta\zeta/2) = 2\,R'_{IV} \sin(\Delta\zeta/2) \qquad \text{...(4.19)}$$

Where R_{IVx} & R'_{IVx} are components of forces R_{IV} &R'_{IV} (in x -direction) and parallel to the plane of symmetry FGE; and where R_{IV} can be calculated as a hydrostatic pressure acting laterally on the failure surface:

R_{IV} = (average acting earth pressure on area for Zone IV) * (area for Zone IV)

$$R_{IV} = 1/2\ \gamma\ K_s\ (2D-L_1) * 1/2\ (\mathbf{r}-B/2) * (L_1 + L_2)$$

$$R_{IV} = 1/4\ \gamma\ K_s\ (2D-L_1) * (\mathbf{r}-B/2) * (L_1 + L_2) \qquad ...(4.20)$$

Where:

3- The resultant earth pressure forces E_{R4} acting on the vertical height (L_1+L_2) is given by:

$$E_{R4} = {}^1/_2\ K_s\ \gamma\ \{(2D-L_1-L_2)\}\ \Delta\zeta \qquad ...(4.21)$$

where:

K_s = Coefficient of earth pressure acting on the Pile Shaft

γ = unit weight of sand

4- Weight of soil mass:

$$W_{4G} = 1/2\ (W_{V1}+W_{V2}) = 1/2\ \gamma\ \{2D-L_1-2L_2\} \qquad ...(4.22)$$

5- Horizontal force ΔE_4, acting on the right side of slice **IV**, by using the same slice method used before in analyzing Zone I, is given by:

$$\Delta E_4 = E_4 \cdot \frac{\cos\left(\phi/2 - (270+\alpha) - \tan^{-1}((r')/L_1)\right)}{\cos(\phi/2 - (270+\alpha) + \delta)} + W_4 \frac{\cos\delta \sin(\phi/2 - (270+\alpha))}{\cos(\phi/2 + \delta - (270+\alpha))}$$

$$+ R_4\ \frac{\cos\delta\cos(\frac{\phi}{2} - (270+\alpha))}{\cos(\phi/2 + \delta - (270+\alpha))} \qquad ...(4.23)$$

Where the angles associated with the slice and using the same procedure followed in equation 4.6 are:

$\alpha = \tan^{-1} (\mathbf{r}-(B/2))/L_2$

$\omega_{i+1}=0$

$\omega_i= \tan^{-1} (\mathbf{r}')/L_1$

$\phi_{si}=$zero

$\phi_{si+1}=\delta$

$\alpha_i= 270+\alpha$

$\phi_{Bi}= \phi/2$

$\phi_{si+1}= \delta$

Where $\mathbf{r}'= \mathbf{r}-(B/2)$

Then ΔQ_s is given by:

$$\Delta Q_s= \Delta E_4 \tan \delta \qquad ...(4.24)$$

and equilibrium of Zone **IV** gives N_4 and T_4 as follows:

$$N_4 = (R_4+ \Delta E_4 - E_{R4})/ (\tan (\phi/2)*\cos\alpha - \sin \alpha) \qquad ...(4.25)$$

$$T_4= N_4 \tan (\phi/2) \qquad ...(4.26)$$

4.4.2.1 Calculation of $\mathbf{F_N}$ and $\mathbf{F_T}$

The normal and tangential forces $\mathbf{F_N}$ and $\mathbf{F_T}$ of Volume **III**, lie in the plane of symmetry ABO and act on the surface abb_1 of Volume **II** (Figure 4.5). Then from equilibrium consideration of forces acting on the Volume bb_1OA (i.e., Volume **II**), the calculation of $\mathbf{F_N}$ and $\mathbf{F_T}$ starts with analysis of external forces acting on the Volume $Abcc_1b_1$ (i.e., Volume **III**). The resultants of all these forces lie on the plane of symmetry ABC (Figure 4.6).

4.4.2.2 Equation of the log spiral BC

The log spiral AC has its pole located at point B, passes through point A, and terminates at point

C at a horizontal distance **r** from the pile axis, where **r** is the radius of influence of tip resistance. The general equation of a log spiral is given by:

$$r_s = r_o\, e^{b\theta} \qquad \text{...(4.27)}$$

in which r_s is the distance from the pole to an arbitrary point on the spiral, r_o is the distance from the pole to a selected reference point also located on the spiral, θ is the angle between these two lines, and b is a constant. Once r_o and b are known, the log spiral can be constructed. For the log spiral AC, its equation may be written as

$$r_s = (AB)\, e^{b\theta}$$

where AB is chosen as the reference radius r_o (refer to Figure 4.7). Since point C lies on the log spiral AC, BC is given by:

$$BC = (BA)\, e^{b\theta} \qquad \text{...(4.28)}$$

with θ = Angle ABC, Figure 4.7.

Then, From the geometry shown in Figure (4.7):

$$b = \frac{1}{\theta}\ln\left(\frac{CB}{AB}\right)$$

$$\theta = A\hat{B}C = (270 - \psi - \alpha)$$

$$BA = \frac{B}{2\cos\psi}$$

$$BC = \frac{r - \frac{B}{2}}{\cos\alpha} = \frac{2r - B}{2\cos\alpha}$$

where α is the slope of BC. The angle α is always < 90°, and $\psi = \tan^{-1}(2L_3/\ B)$ as assumed previously.

Substitute values of θ, AB and AC into Equation (4.28),

$$b = \frac{1}{(270-\psi-\alpha)}\ln\left(\frac{2r-B}{B}\left(\frac{\cos\psi}{\cos\alpha}\right)\right) \quad ...(4.29)$$

Hence, the equation of the log spiral AC may be expressed by:

$$r_s = \left(\frac{D}{2\cos\psi}\right)e^{b\theta} \quad ...(4.30)$$

in which ψ and b have been given.

It can be noted, that for a given pile diameter B and tip radius of influence **r**, b is a function of ϕ and α. As of the angle α varies depends on different factors, it can be said that the shape of the log spiral AC will also change. This is another distinct assumption made in connection with the postulated failure mechanism. In conventional analysis of pile bearing capacity, the failure surface is usually assumed to be a log spiral having the equation $r_S = \mathbf{r}_o{}^{\alpha\theta}$ with b = tan ϕ, resulting in the shape of the log spiral remaining unchanged with depth (i.e., Meyerhof. 1951; Hu, 1965; Vesic, 1967b).

4.4.2.3 Application of Method of Slices for Radial Shear Zone ABC

Once the radial shear Zone ABC is clearly defined, the analysis proceed with the division of this Zone into "n" slices, all sharing the same apex B. Each slice has inclined sides, an apex angle equal to (θ/n) and is subjected to a system of external forces such as shown in Figure 4.13. These forces consist of:

i) The weight w_i of the slice. Its Volume v_i may be calculated as the Volume generated by the plane area a_i of the slice revolving around the pile axis. By using the theorem of PappusGuldinus, v_i is given by:

$$v_i = a_i.\ \rho.\ \Delta\zeta$$

where

ρ_i = distance from the pile axis to the centroid of the generating area a_i

$\Delta\zeta$ = central of angle of rotation around the pile axis.

With the Volume v_i known, the weight w_i can be easily calculated by: $w_i = \gamma\, v_i$.

ii) The normal and tangential components of the side forces include N_i, T_i, N_{I+1} and T_{I+1} which are related by the expressions:

$$T_i = N_i \tan \phi_{si}$$

$$T_{i+1} = N_{i+1} \tan \phi_{si+1}$$

In which ϕ_{si} and ϕ_{si+1} are respectively the average mobilized angles of shearing resistance along the left and right sides of the slice i.

It is also assumed that the average mobilized angle of shearing resistance along the side of an arbitrary slice varies linearly with the polar angle measured from BA, between two limiting values: ϕ_β along BC and $\dot{}$ along BA (Figure 4.13). Mathematically, ϕ_{si} and ϕ_{si+1} with i > 1, may be expressed by:

$$\phi_{si} = \phi_\beta + (\phi - \phi_\beta)\left(\frac{\sum_{k=1}^{i-1} \Delta\theta_k}{\theta}\right) \qquad ...(4.31)$$

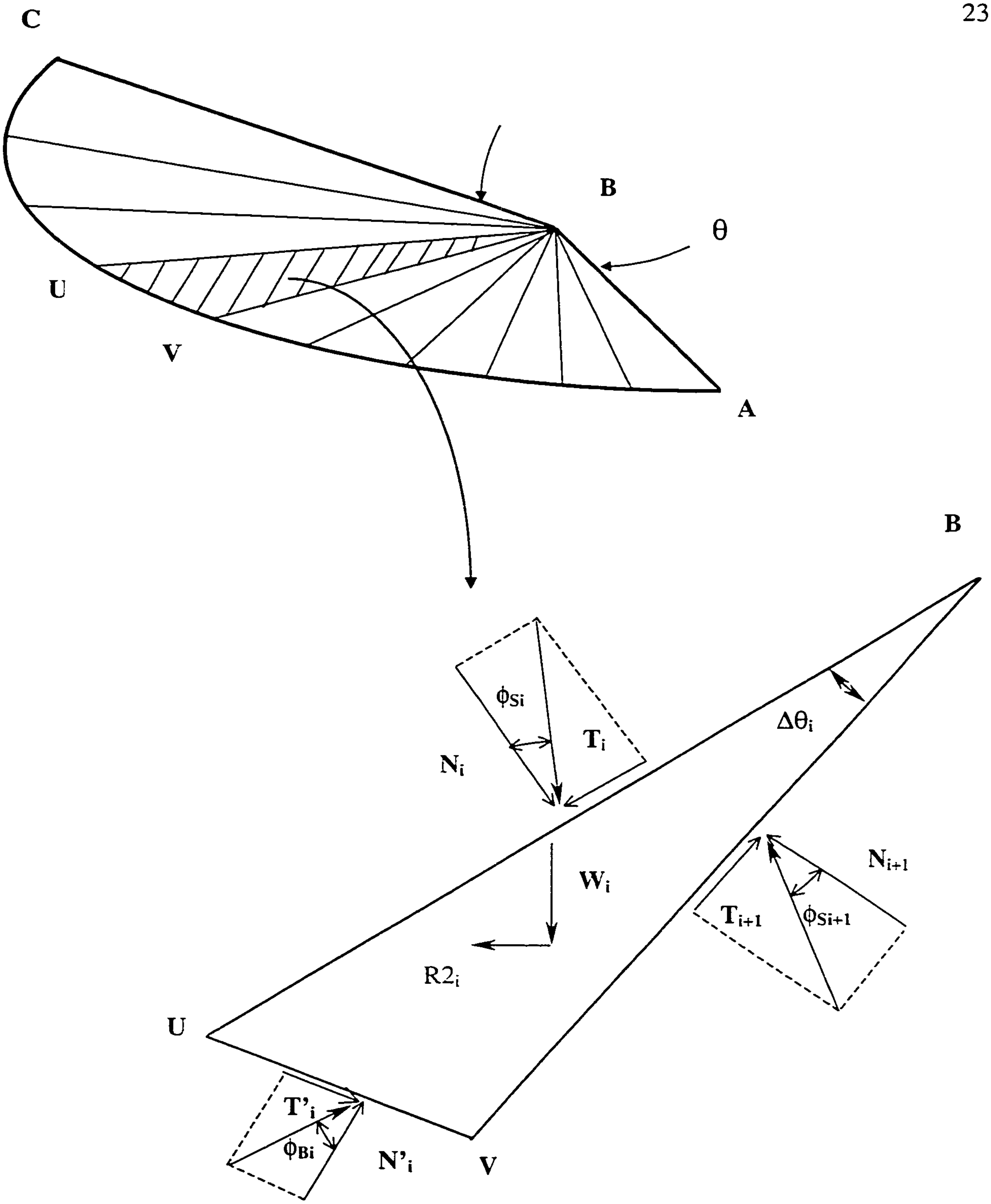

Figure 4.13 A Free Body Diagram of an Inclined Slice in the Radial Shear Zone III (Log-Spiral)

$$\phi_{si+1} = \phi_\beta + (\phi - \phi_\beta)\left(\frac{\sum_{k=1}^{i} \Delta\theta_k}{\theta}\right) \qquad \text{...(4.32)}$$

where

ϕ_β = average mobilized angle of shearing resistance along AC

$\Delta\theta_k$ = apex angle of a slice

θ = Apex angle of radial shear Zone ABC

iii) The normal and tangential components N'_i and T'_i of the soil reaction on the slice base are related by:

$$T'_i = N'_i \tan \phi_{\beta i}$$

In which $\phi_{\beta i}$, denoting the mobilized angle of shear resistance at the midpoint of the slice base, may be computed by Equation 4.1.

iv) R_{IIi} and R'_{IIi} represent the resultant forces of the earth pressure exerting on the area auv and $a_1u_1v_1$ (Figure 4.14a). The force RIIi, for instance, is then equal to the Volume of the truncated pressure prism acting on the area auv (Figure 4.14b).

$$R_{IIi} = 1/3\ (\text{Area auv})\ (p_a + p_u + p_v) \qquad \text{...(4.33)}$$

The lateral earth pressure p_a, p_u and p_v at points a, u and v on the tangential plane aBc are given by $K_o\,\gamma\,z_a$, $K_o\,\gamma\,z_u$, and $K_o\,\gamma\,z_v$, respectively; in which z_a, z_u, and z_v are depths of point a, u, and v. The resultant $R2_i$ of the forces R_{IIi} and R'_{IIi} is calculated by:

$$R2_i = R_{IIx} + R'_{IIx}$$

$$R2_i = R_{II}\sin\left(\frac{\Delta\zeta}{2}\right) + R'_{II}\sin\left(\frac{\Delta\zeta}{2}\right)$$

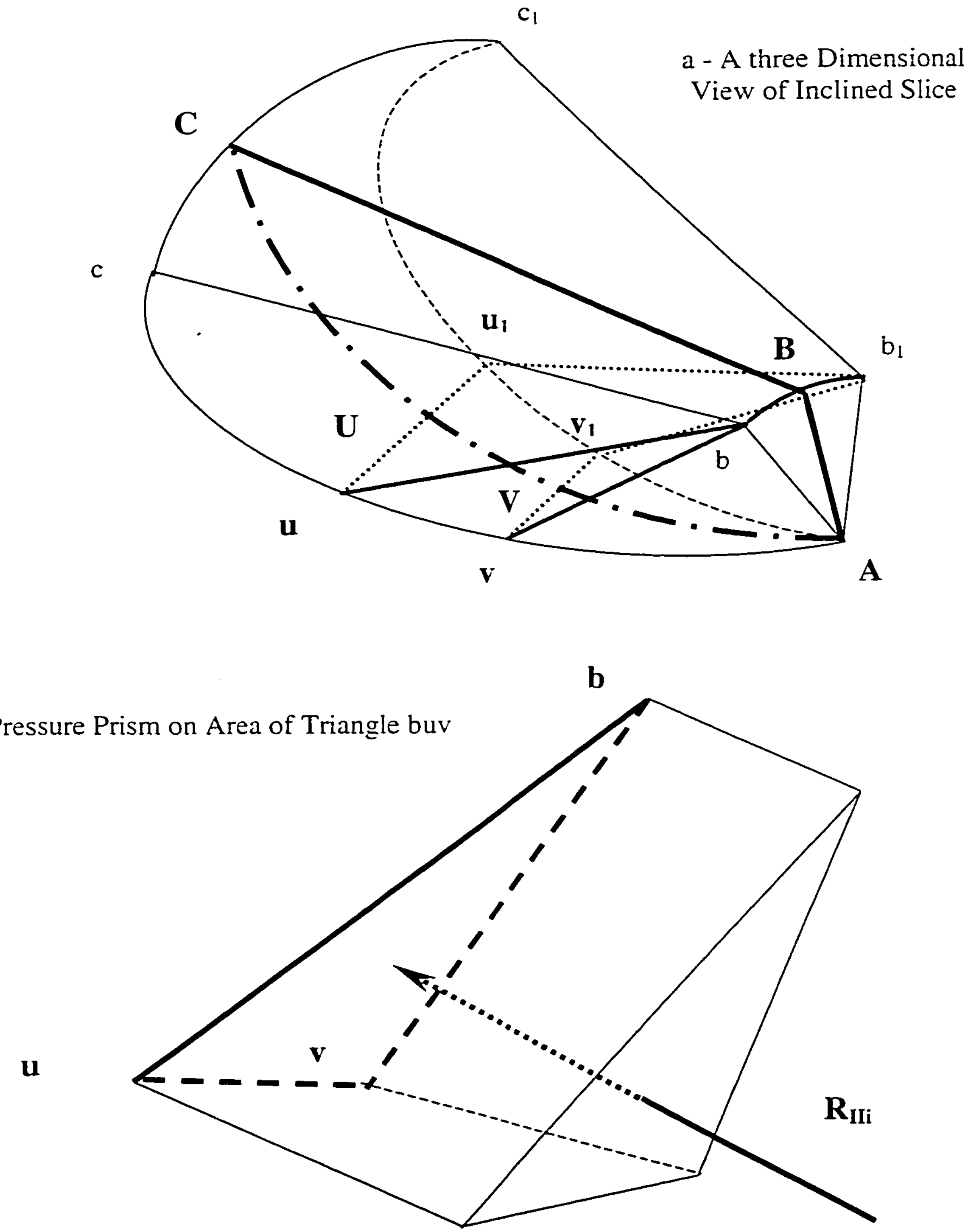

a - A three Dimensional View of Inclined Slice

b - Pressure Prism on Area of Triangle buv

Figure 4.14 Earth Pressure Acting on the Tangential Planes of an Inclined Slice

$$R2_i = 2R_{II}\sin\left(\frac{\Delta\zeta}{2}\right) = 2R'_{II}\sin\left(\frac{\Delta\zeta}{2}\right) \qquad ...(4.34)$$

in which $R_{IIx} = R'_{IIx}$ = components of the forces R_{II} and R'_{II} parallel to the plane of symmetry ABC.

For any slice, ϕ_{si}, ϕ_{si+1}, and ϕ_{Bi}, $R2_i$ and w_i may be calculated following the procedure just described. If the normal force N_i is known on the left side of the slice, then its counterpart N_{i+1} on the right side may be calculated, using Sarma's recurrence relation (Equation 4.6). As a result, with N_4, T_4 known from the analysis of Volume IV (see Figure 4.8), it is possible to start with the first slice, calculate N_2 then repeat the same procedure to calculate N_3 for the second slice and so on, until the forces $F_N = N_{n+1}$ and $F_T = T_{n+1}$ are computed for the right side of the n^{th} slice,

4.4.3 Equation of Point Resistance Q_P

In deriving an expression for Q_p, Volume II and its mirror image counterpart with respect to the pile axis (Figure 4.15a) were considered. The triangular area ABB' is subjected to a system of forces shown in Figure 4.15b. They include a pair of normal and tangential forces F_N and F_T acting along AB, another pair of forces, being the mirror images of F_N and F_T acting along AB', the weight $2W_1$ of the wedge of sand and the reaction $2\Delta Q_p$ from the pile tip. Due to symmetry, there is no resultant force of the earth pressure acting on the tangential planes bOA, b'OA, b_1OA and b'_1OA. With reference to Figure 4.15b, the equilibrium of forces in the vertical direction is given by:

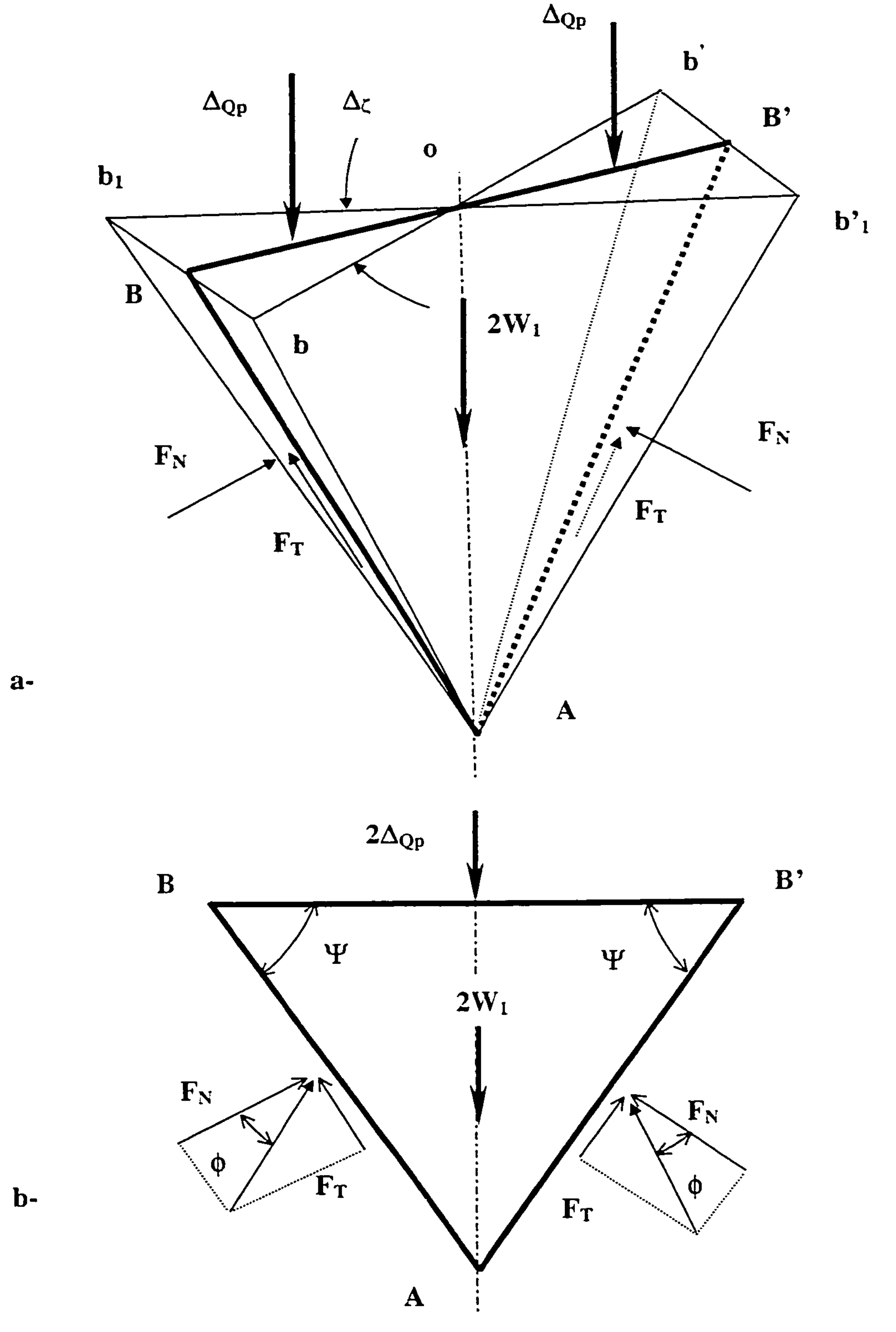

Figure 4.15 A Diagram of Forces Used to Compute Point Resistance Q_p

$$2(F_N \cos\psi + F_T \sin\psi) - 2W_1 - 2\Delta Q_p = 0$$

$$\Delta Q_p = F_N \cos\psi + F_T \sin\psi - W_1$$

Where ΔQ_p = pile load acting on the area bob_1 of the Volume aOa_1B

W_1 = weight of the Volume of sand bOb_1A (see Figure 4.15a)

The point resistance Q_p is then given by:

$$Q_p = (2\pi/\Delta\zeta)\Delta Q_p \qquad ...(4.35)$$

$$Q_p = (2\pi/\Delta\zeta)(F_N \cos\psi + F_T \sin\psi) - W_c \qquad ...(4.36)$$

in which W_C = weight of the cone of sand beneath the pile tip.

4.5 Computer Program Implementation

In order to facilitate the extensive numerical calculations of the new model, a computer program called G-Pile was written. The complete list of the code is given in Appendix II. The implemented program was used in the verification of the sensitivity of two groups of parameters:

1- Computations parameters such as:

a - Central angle of rotation around the axis of symmetry $\Delta\zeta$.

b- Number of slices "N_θ" used in the equilibrium of the radial shear zone, log-spiral curve.

2- Model parameters: H_1, R, L_1, L_3& **r** against the input parameters: D,B, ϕ, δ.

Also this program was used to develop the design charts.

To test the sensitivity of "N_θ" against the percentage of error in determining Q_u, the following test data were used:

Pile depth, D=24.0 m, Pile diameter, B = 0.405 m; Angle of shearing resistance of sand, ϕ = 31.2 °, angle of friction between sand and pile $\delta = 21.8^{o}$. The following depths 12, 24 & 36 meters were used to verify the effect of number of slices against the point bearing capacity "Q_p".

The comparisons between the three series of tests are shown in Figure 4.16. The effect of N_θ was found more significant against Q_p than against Q_s or Q_u, so that its effect was verified against Q_p, only. All parameters were frozen and therefore changing of N_θ were permitted for the range from 4 to 35. As can seen from this Figure 4.16, the trend of changing of N_θ against Q_p resulted in semi constant values up to certain number of slices, 13, and beyond this number it was found that some disturbance took place. For this reason, a number of slices equal to 13,which was found to be the maximum value to maintain the trend without disturbance, was considered enough to satisfy the required accuracy.

In order to verify the effect of the central angle of rotation $\Delta\zeta$, on the ultimate bearing capacity, Q_u, the same tests were repeated with respect to a change of $\Delta\zeta$, only, and all other parameters were frozen. The range of $\Delta\zeta$ was used from 0.5^o to 20^o; the results are shown in Figure 4.17, where a comparison between the three series of tests are displayed. From Figure 4.17, it is clear that the value of $\Delta\zeta$ has almost no effect on the magnitude of Q_u. Therefore a value of $\Delta\zeta=1^o$ was considered satisfactory to achieve reasonable accuracy.

4.6 Sensitivity Analysis for the Theoretical Model Parameters

A Sensitivity Analysis for the proposed model parameters is given in the following section.

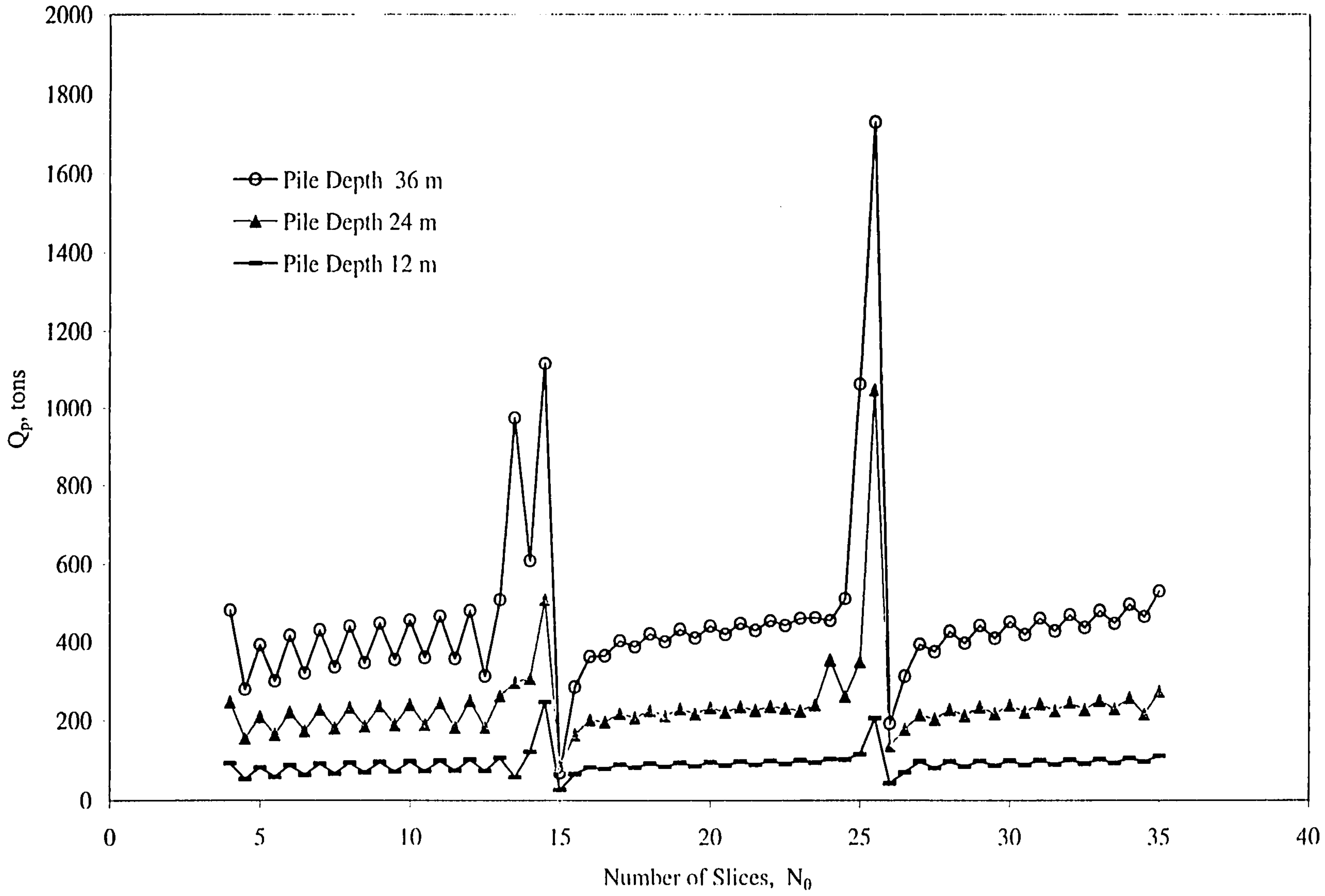

Figure 4.16 Percentage of error in N_q (% error)

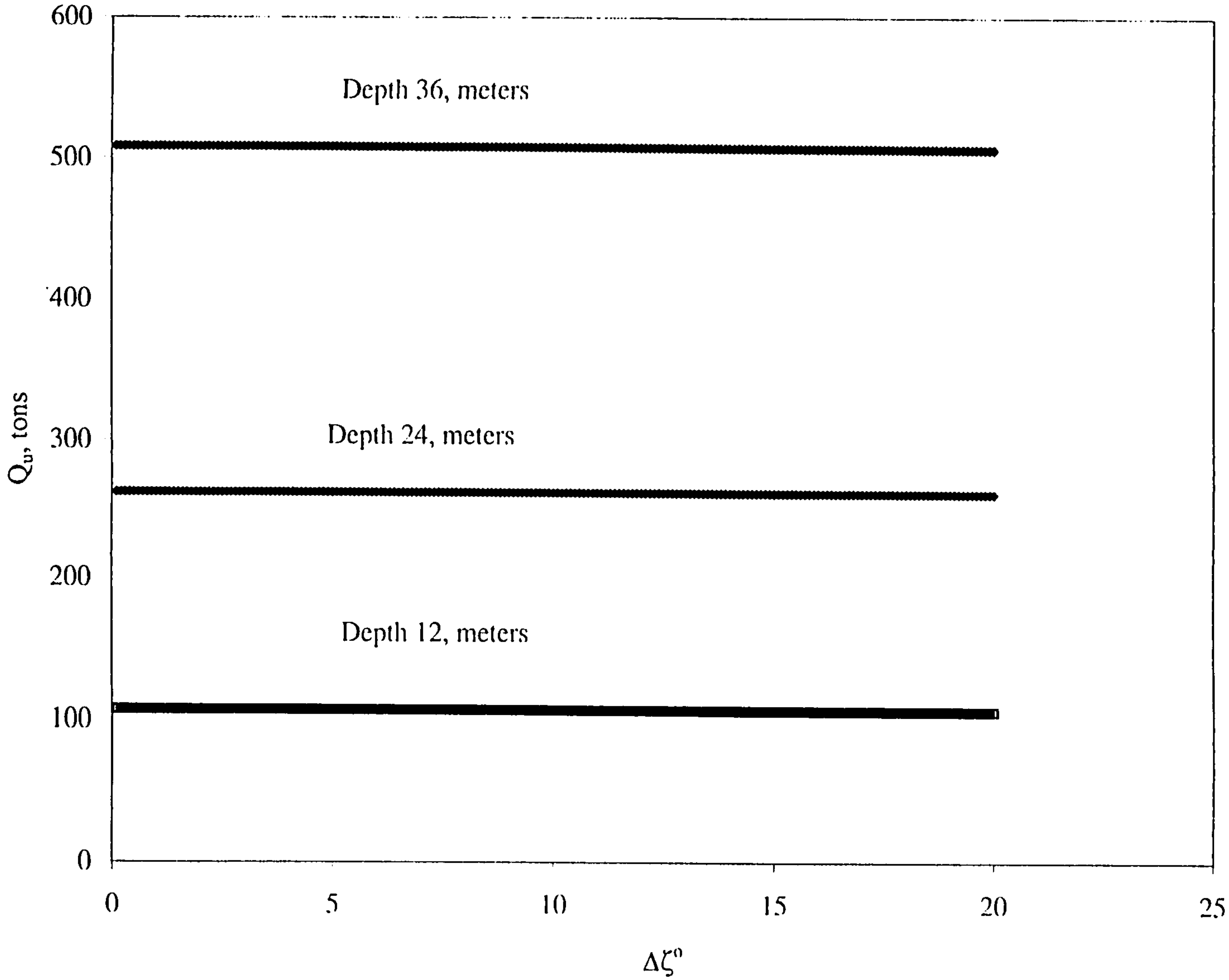

Figure 4.17 Changing of $\Delta\zeta$ Verses Q_u

The proposed theoretical model to predict the ultimate bearing capacity of a single pile in sand involves the following parameters: H_l, R, L_l, L_3& **r**, where these parameters are dependent on the input parameters: D, B, ϕ, δ and K_s.

Where:

H_l = Vertical height of mobilized skin resistance beneath the ground surface

R = Radius of influence at the ground surface

L_l = Vertical height of mobilized tip resistance area above the tip level

r = Radius of influence at the tip level

D = Embedded depth of the pile

B = Pile's diameter

ϕ = Angle of shearing resistance of sand

δ = Angle of friction between sand and pile's shaft

K_s = Coefficient of earth pressure on the pile shaft

The effect of the input parameters D, B, ϕ & δ on the model parameters H_l, R, L_l, L_3& **r** are introduced in the present section. Also the effect of various factors on the coefficient of earth pressure acting on the shaft, K_s, is introduced here. Since a new function to predicted K_s value was included in the proposed model.

The computation of N^*_q was carried out utilizing the implemented computer program G-Pile, using the following equation:

$$N^*_q = Q_p / (\gamma' * D * A_p) \quad ...(4.37)$$

4.6.1 Effect of Angle of Shearing Resistance ϕ on the Model Parameters

The following data were used to analyze the effect of angle of shearing resistance ϕ on the various model parameters: $\phi = 27^{o}$ to 42^{o}, D = 12.0 m up to 36.0 m, B = 0.30 m up to 0.50 m. $\delta/\phi = 0.7$.

4.6.1.1 Effect of Angle of Shearing Resistance ϕ on the Point Resistance Q_p

The effect of angle of shearing resistance ϕ on the dimensionless bearing capacity factor N^*_q is presented in Figure 4.18. Where a series of pile tests with depth equal to 12, 24, and 36 meters, $\phi/\delta = 0.7$ and pile diameter B = 0.3 m were examined. All other parameters were frozen and only ϕ were changed from $\phi = 27^{o}$ to 42^{o}. It has been shown that the magnitude of N^*_q is increased with the increase of ϕ in a nonlinear relationship. The increase of N^*_q due to the increase of ϕ is found to be semi linear in the range of $\phi = 27^{o}$ to 35^{o}, and nonlinear with a higher rate of increase in the range of $\phi > 35^{o}$. It is also one of the distinct feature of the new proposed model, the rate of change of N^*_q versus ϕ is varied between more than one mode. This trend is different than the previous theories, which assume one rate of change of ϕ versus N^*_q.

4.6.1.2 Effect of Angle of Shearing Resistance ϕ on the Radius of Influence at Tip "r"

Figure 4.19 shows the test results of the study of the effect of the angle of shearing resistance ϕ on the radius of influence at tip, "**r**". It has been shown that increasing ϕ resulted in an increase of "**r**" in a linear relationship. Because of the different slenderness ratio used for the pile tests, it could be also concluded that there is an increase in the radius of influence at tip, "**r**" with the increase of the pile depth. This parameter has a direct impact on the point

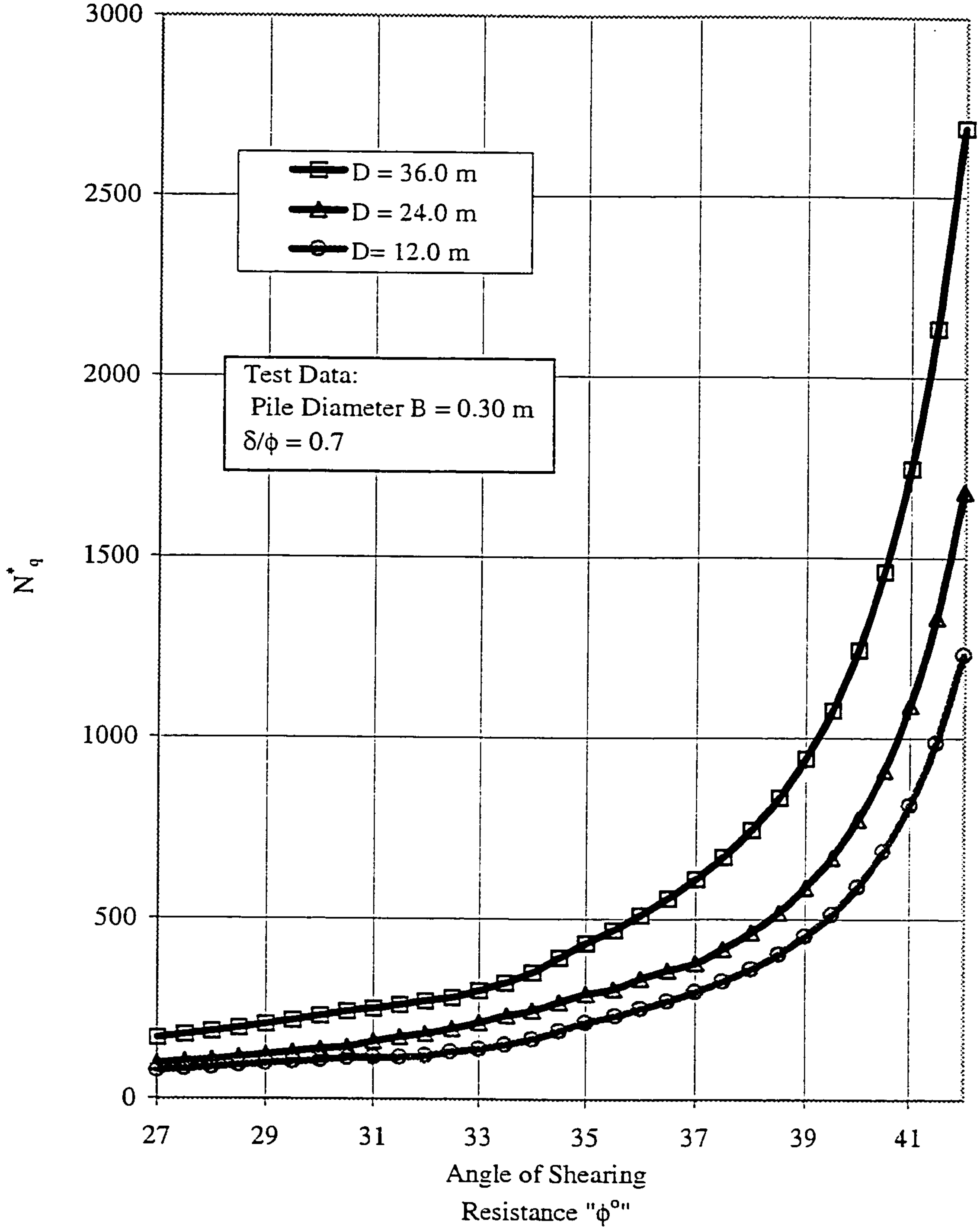

Figure 4.18 Angle of Shearing Resistance "φ" Versus Bearing Capacity Factor N^*_q

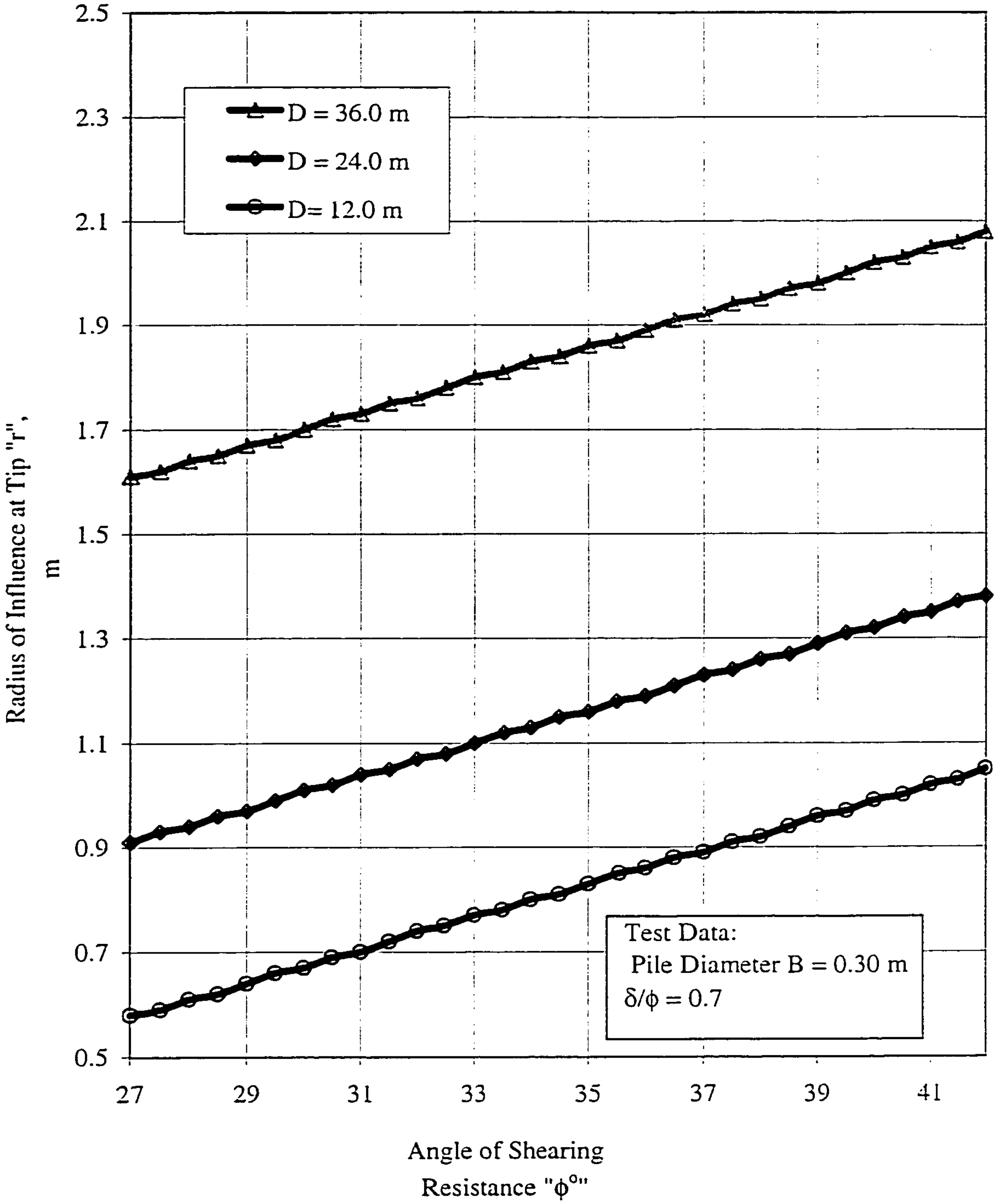

Figure 4.19 Angle of Shearing Resistance "ϕ" Versus Radius of Influence at Tip "r" for a Pile Diameter 0.30 m and Different Depths

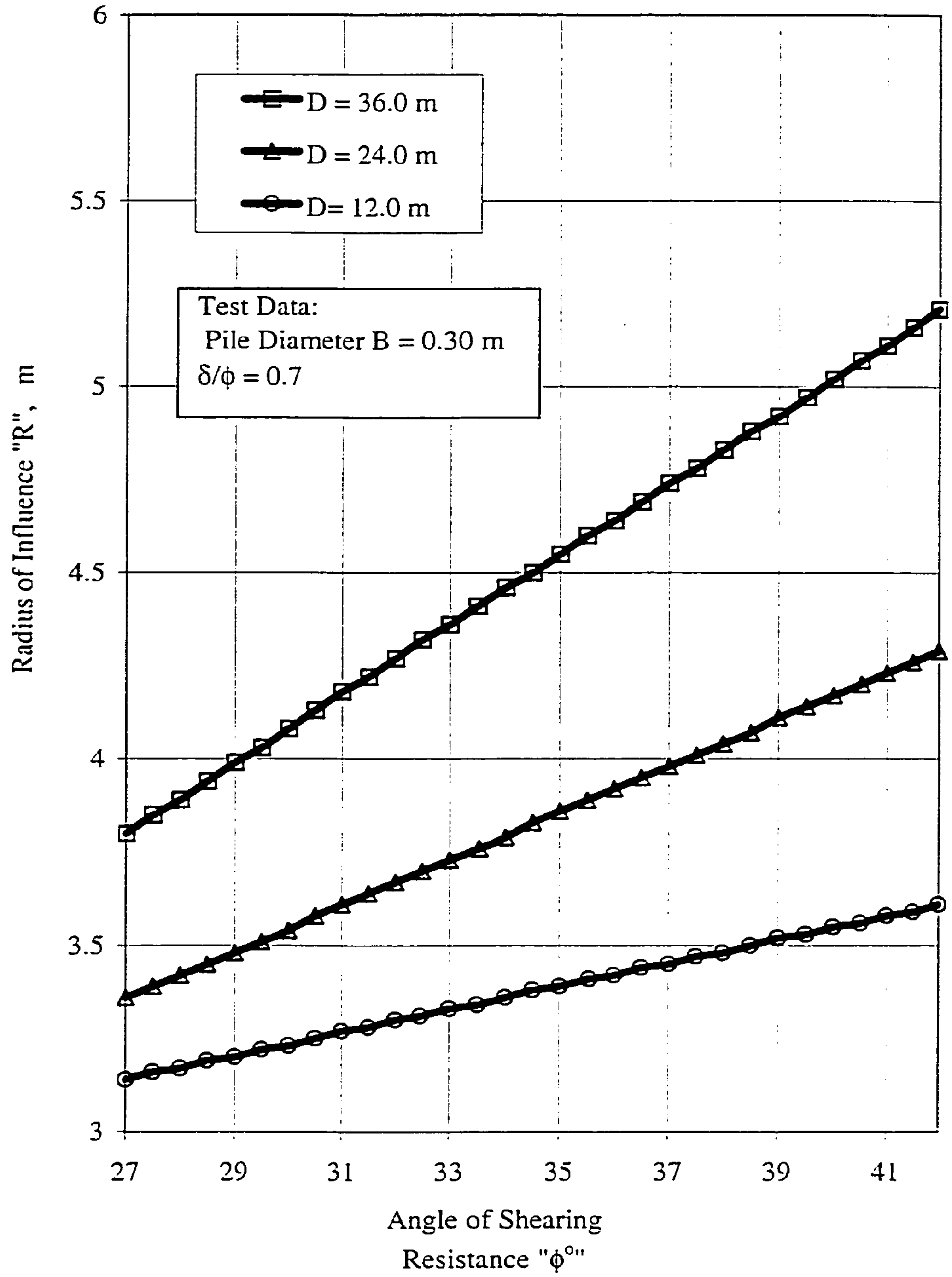

Figure 4.20 Angle of Shearing Resistance "φ" Versus Radius of Influence at Ground Level "R"

bearing capacity and it logically accepted to be increased versus the increase of ϕ.

4.6.1.3 Effect of Angle of Shearing Resistance ϕ on the Radius of Influence R

The effect of angle of internal friction of sand on the radius of influence at ground level "R" is presented in Figure 4.20 the radius of influence is increased with the increase of ϕ in a linear relationship. On the other hand it was found that R increased with the pile depth increase. The impact of ϕ on skin resistance is demonstrated with the increase of R due to the increase of ϕ. Where R is a major parameter in determining the skin resistance Q_s.

4.6.1.4 Effect of Angle of Shearing Resistance ϕ on the Vertical Distance H_l

The vertical distance H_l is the vertical dimension of the mobilized skin resistance zone on the pile shaft and it is located beneath the ground level. Figure 4.21 shows the effect of ϕ on the vertical distance H_l. The trend of H_l versus ϕ indicates a decrease of H_l with the increase of ϕ with a rate of 0.0005% per degree. This trend can be explained by the new features of the proposed model, which made it possible to take into account the effect of many factors at the same time. Some of these factors are affecting one parameter as an increase and some others affecting the same parameter as a decrease. It can be concluded here that H_l is decreased with pile depth.

4.6.1.5 Effect of Angle of Shearing Resistance ϕ on the Vertical Distance "L_l"

Vertical distance L_l is the vertical extension of mobilized tip resistance above the tip level. Figure 4.22 shows the effect of ϕ on L_l. It was found that ϕ does not affect L_l, and it took constant value with each pile depth. It can also concluded here that L_l increase with the increase of pile depth.

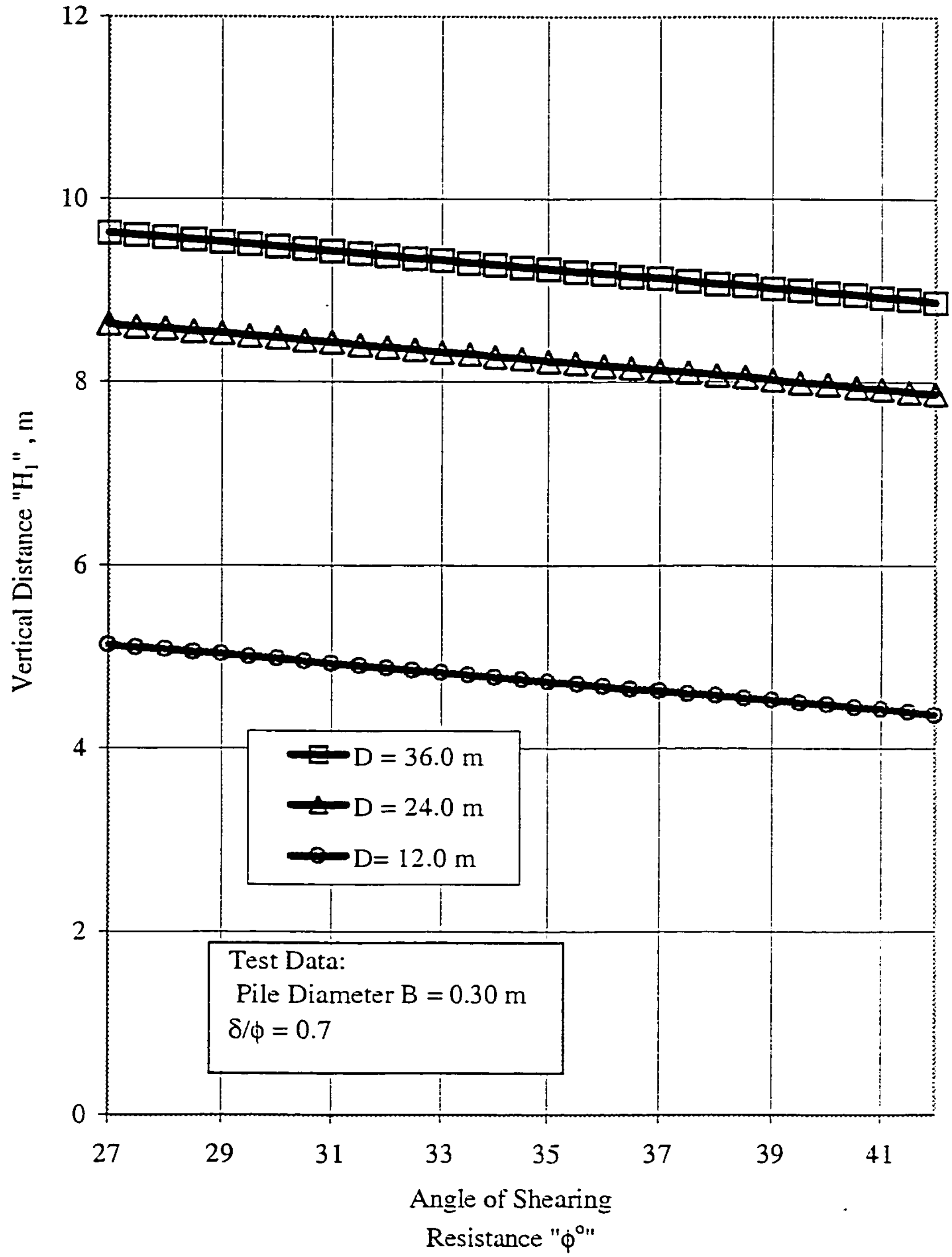

Figure 4.21 Angle of Shearing Resistance "ϕ" Versus Vertical Distance "H_1"

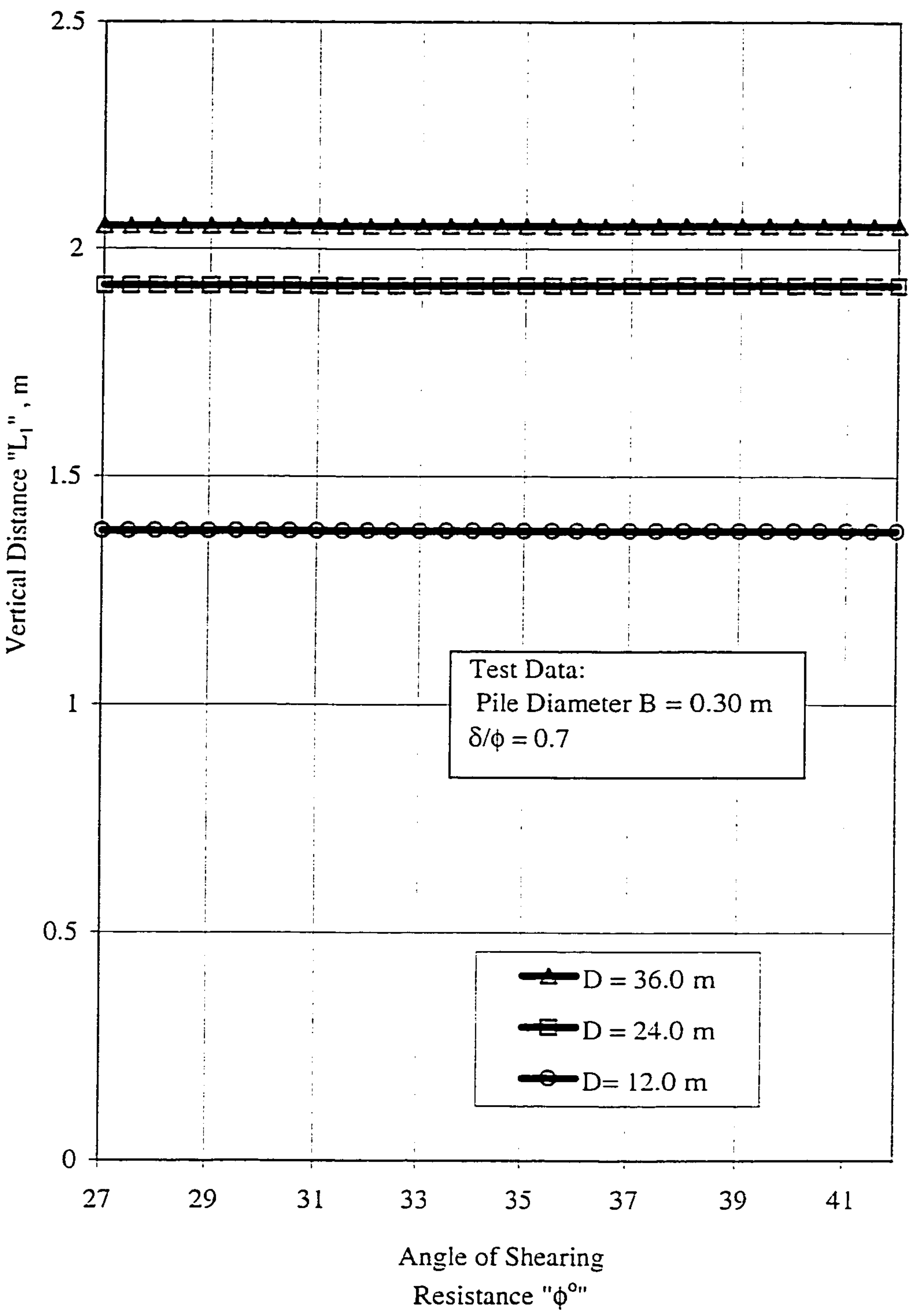

Figure 4.22 Angle of Shearing Resistance "ϕ" Versus Vertical Distance "L_1"

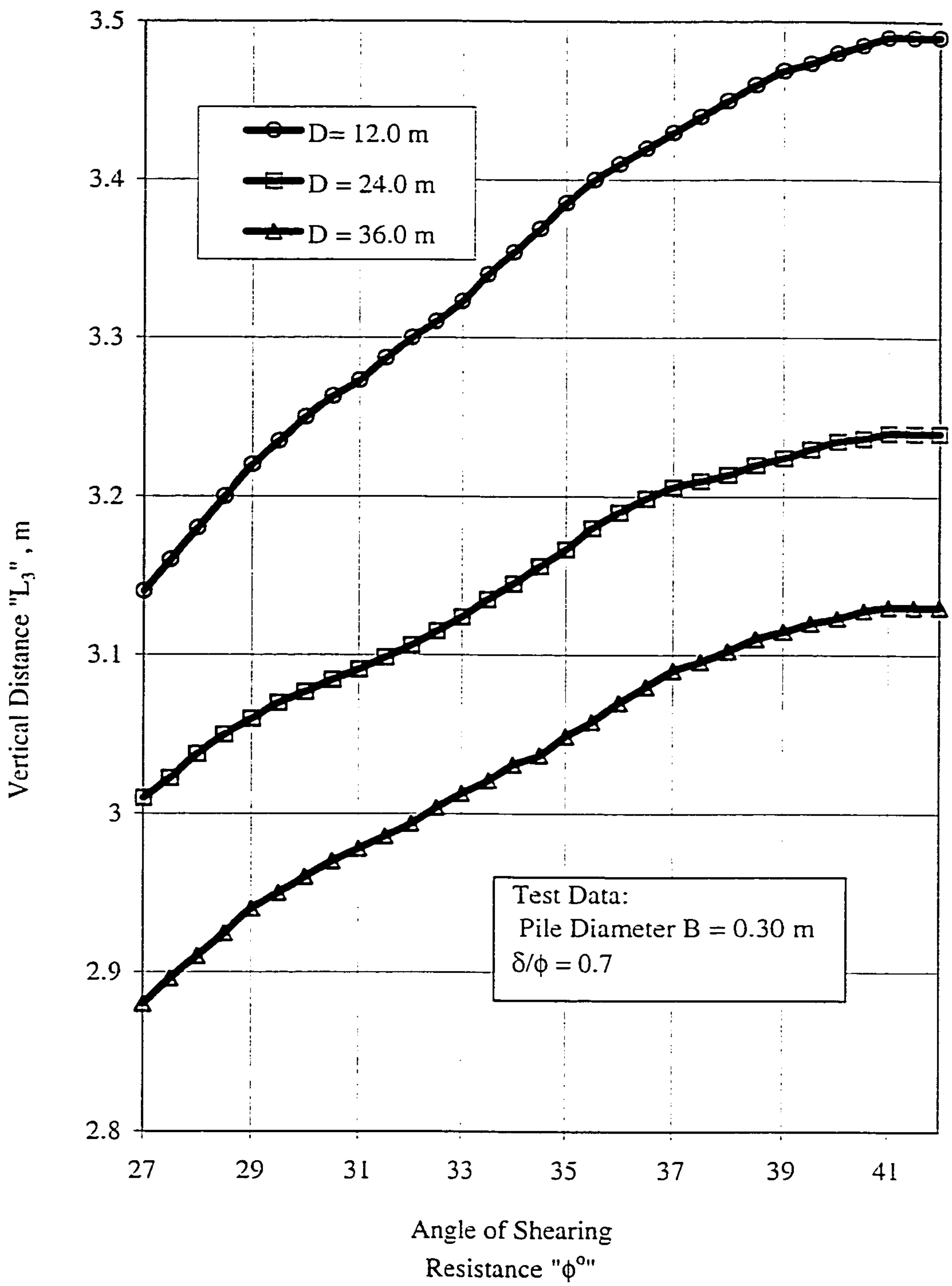

Figure 4.23 Angle of Shearing Resistance "φ" Versus Vertical Distance L_3

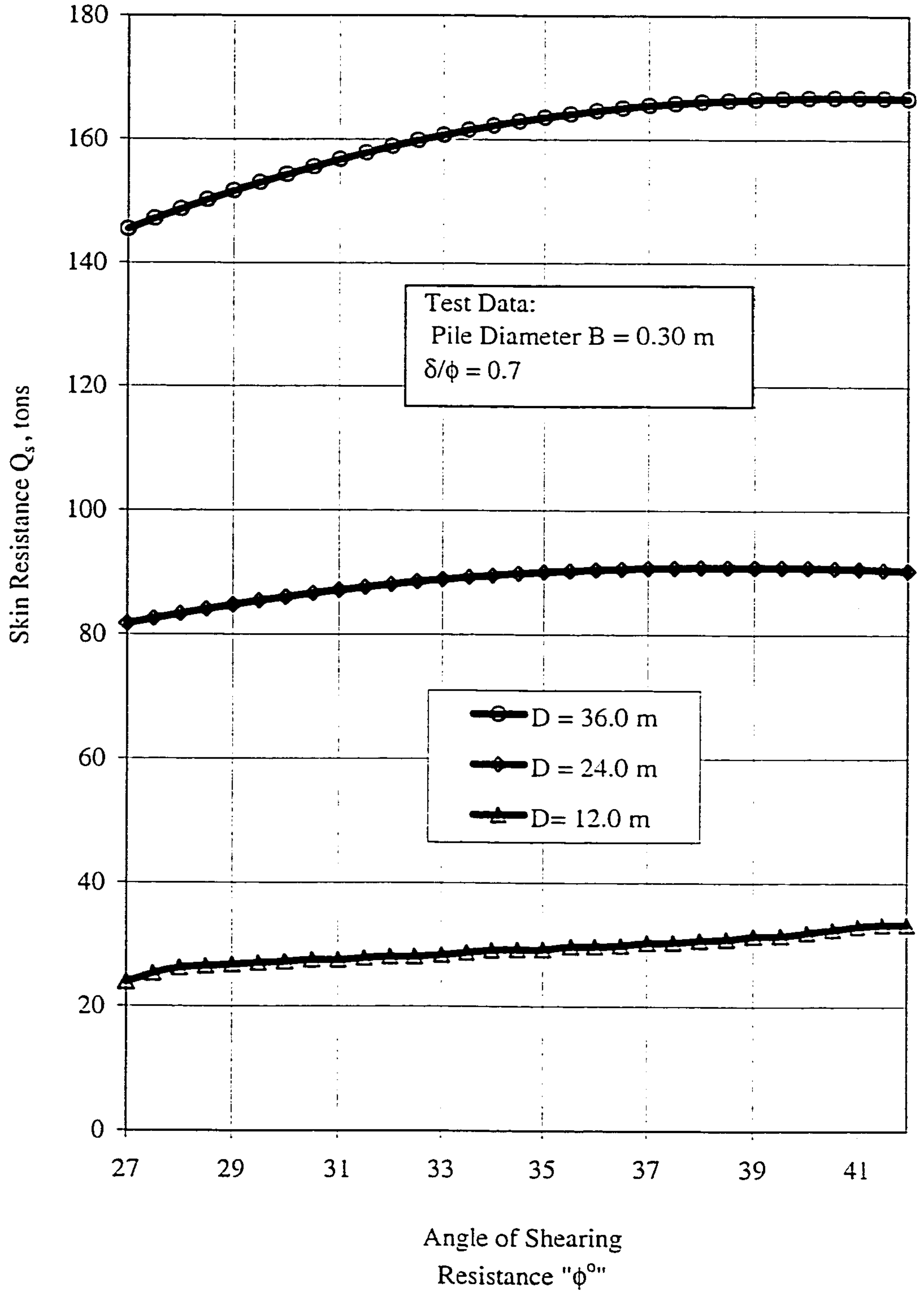

Figure 4.24 Angle of Shearing Resistance "ϕ" Versus Skin Resistance Q_s

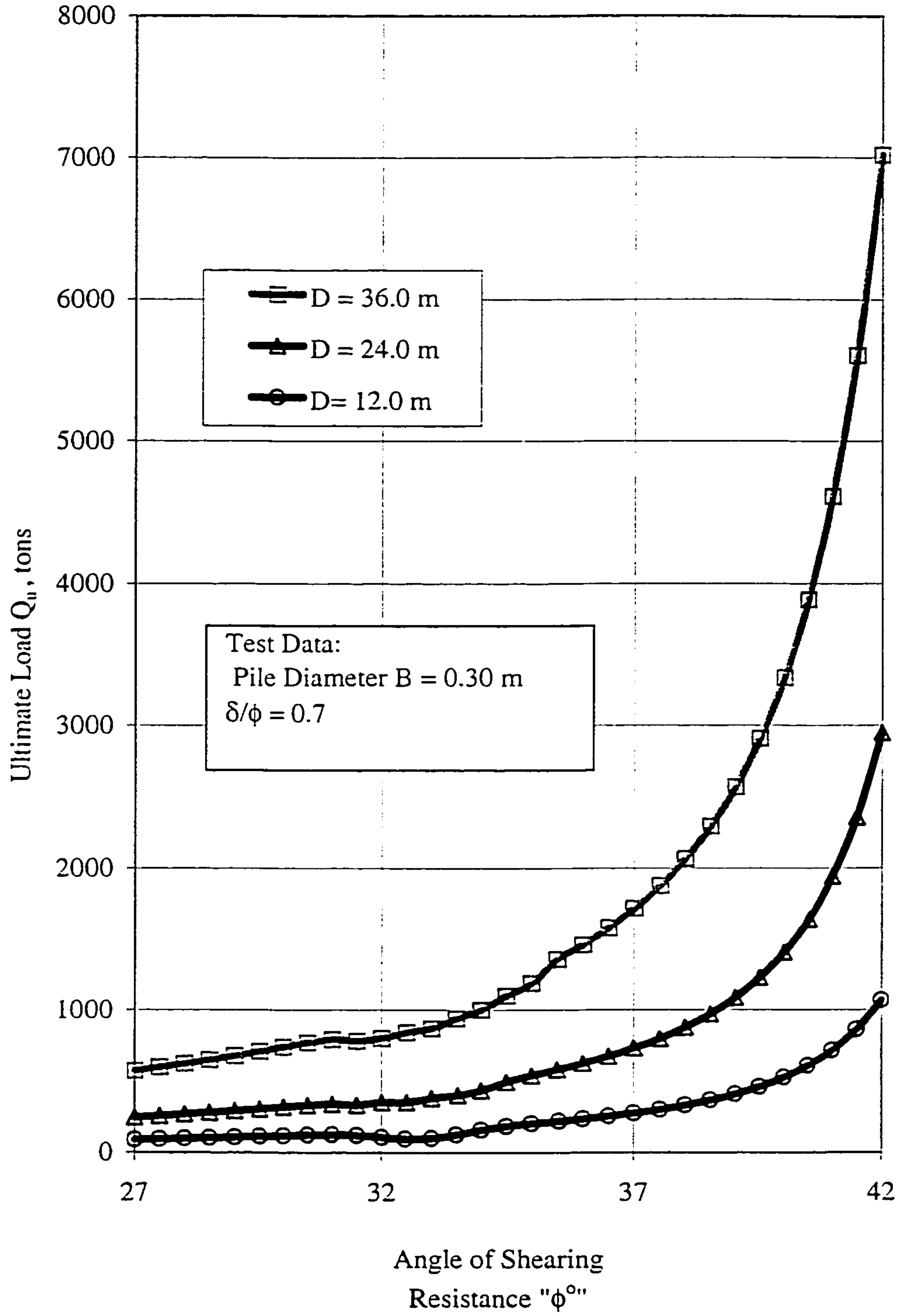

Figure 4.25 Angle of Shearing Resistance "ϕ" Versus Ultimate Load "Q_u"

4.6.1.6 Effect of Angle of Shearing Resistance ϕ on the Vertical Distance "L_3"

The variation of L_3 versus ϕ is shown in Figure 4.23. It demonstrates the increase of L_3 with the increase of ϕ in nonlinear variation. As it known that L_3 is the vertical extension of the failure pattern beneath the pile tip, it is logical to increase with the increase of ϕ, and resulted in increase of point resistance Q_p with the increase of ϕ.

4.6.1.7 Effect of Angle of Shearing Resistance ϕ on the Skin Resistance Q_s

The ultimate skin resistance Q_s is found to increase with the angle of shearing resistance ϕ as shown in Figure 4.24. This increase is relatively high for the piles with the higher relative depth, while the rate of increase is lower with the smaller relative pile depth.

4.6.1.8 Effect of Angle of Shearing Resistance ϕ on the Ultimate Load Q_u

Figure 4.25 demonstrates the increase of ultimate bearing capacity Q_u due to the increase of ϕ. Where the variation in Q_u is semi linear between $\phi = 27^o$ to 35^o and nonlinear between $\phi = 35^o$ and 42^o.

4.6.1.9 Effect of Angle of Shearing Resistance ϕ on the Coefficient of Earth Pressure K_s

As indicated in Figure 4.26 that K_s decreases with the increase of ϕ, furthermore it reaches higher values with smaller pile depths. This behavior is reflected on the proposed theoretical model which utilize variable coefficient of earth pressure K_s, which depends on the input parameters.

4.6.2 Effect of Shaft Roughness on the Model Parameters

To examine the effect of shaft roughness on the different model parameters, a series of pile load tests have been carried out with the following data: pile depths: 12.0, 18.0 & 24.0 meters,

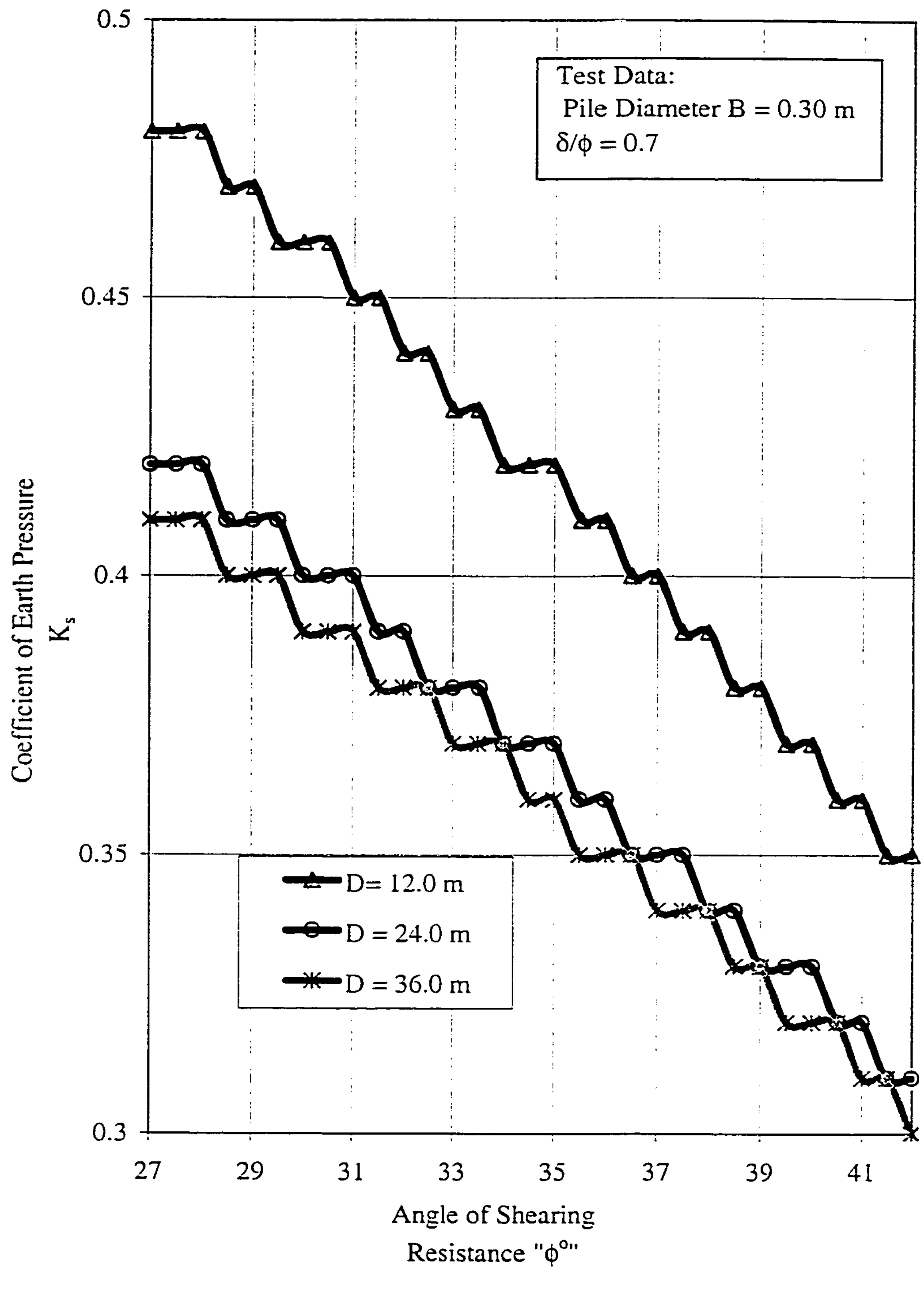

Figure 4.26 Angle of Shearing Resistance "ϕ" Versus Coefficient of Earth Pressure "K_s"

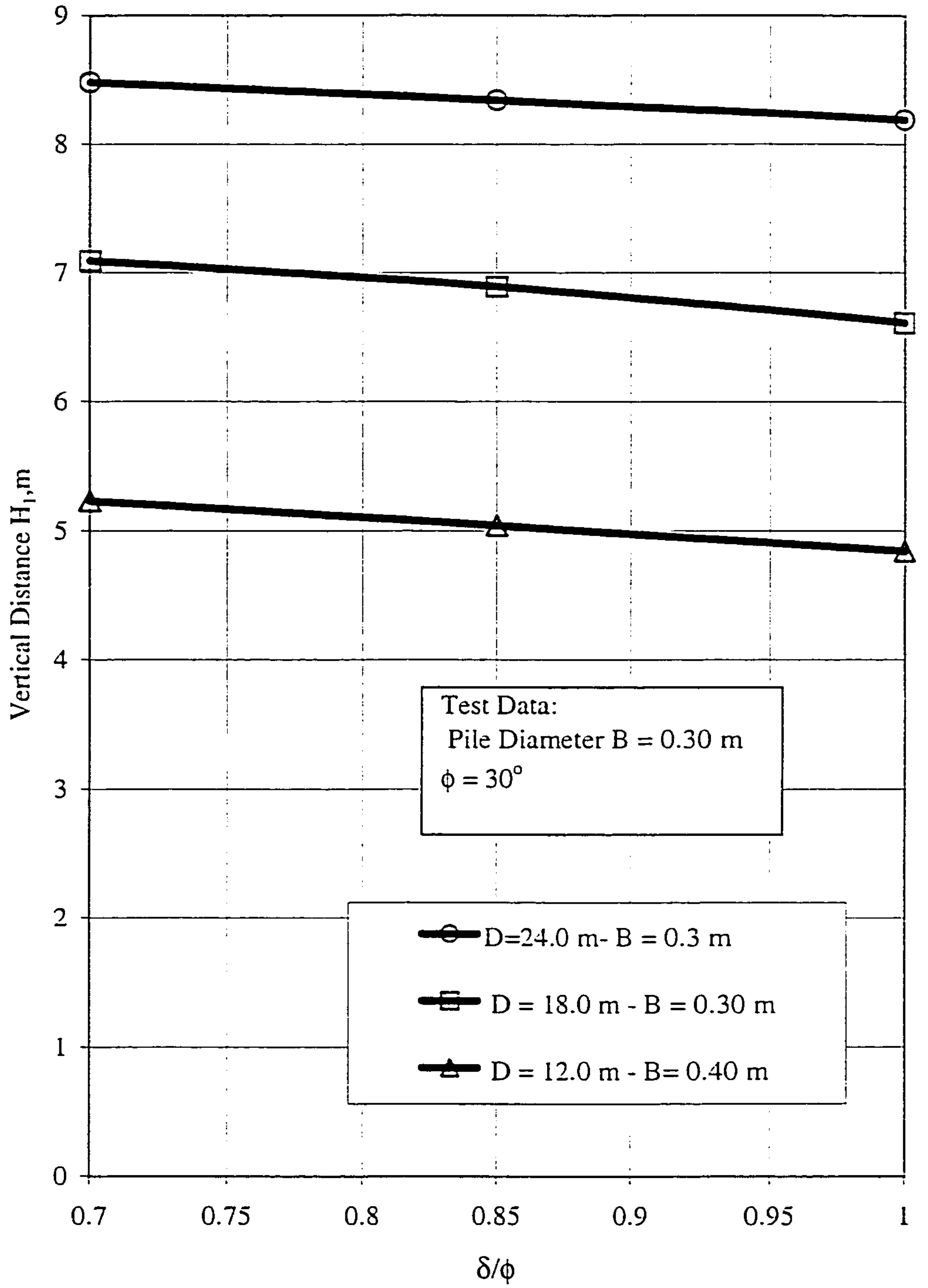

Figure 4.27 Effect of Shaft Roughness "δ/φ" on Vertical Distance H_1.

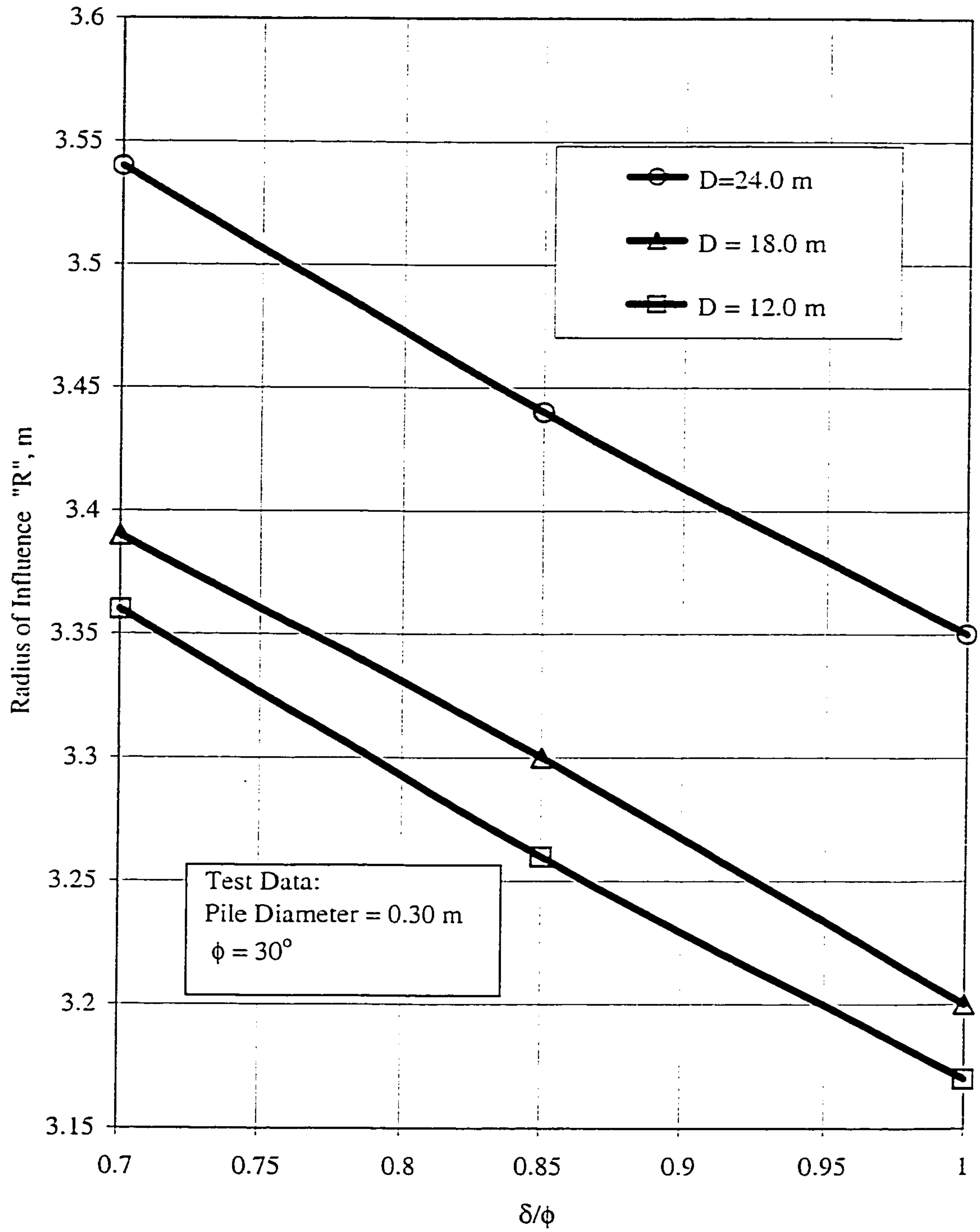

Figure 4.28 Effect of Shaft Roughness "δ/φ" on Radius of Influence "R"

pile diameter 0.30, 0.40 & 0.5 meters, $\phi = 30^o$.

4.6.2.1 Effect of Shaft Roughness on the Vertical Distance H_1

Figure 4.27 shows the variation of H_l versus the shaft roughness δ/ϕ. It is noticed that H_l decreases with the increase of the ratio δ/ϕ.

4.6.2.2 Effect of Shaft Roughness on Radius of Influence "R"

Figure 4.28 introduces the decrease of "R" due to the increase of shaft roughness δ/ϕ. This decrease is found to vary linearly.

4.6.2.3 Effect of Shaft Roughness on Coefficient of Earth Pressure K_s

In order to study the effect of shaft roughness on the coefficient of earth pressure K_s, acting on the pile shaft, a series of tests performed and resulting comparisons are shown in Figure 4.29. From Figure 4.29, it can be seen that a magnificent increase in K_s is produced with the increase of shaft roughness δ/ϕ.

From the analyses of the three parameters H_l, R & K_s which are enrolled in calculation of shaft resistance Q_s, it can concluded that the major impact on Q_s is resulted from the coefficient of earth pressure K_s.

4.6.2.4 Effect of Shaft Roughness on Ultimate Bearing Capacities: Q_u, Q_p & Q_s

The effect of shaft roughness on the two components of the ultimate bearing capacity Q_s and Q_p is demonstrated in Figure 4.30. As expected the ratio δ/ϕ is causing the ultimate skin resistance Q_s, to be increased, at a higher rate than Q_p.

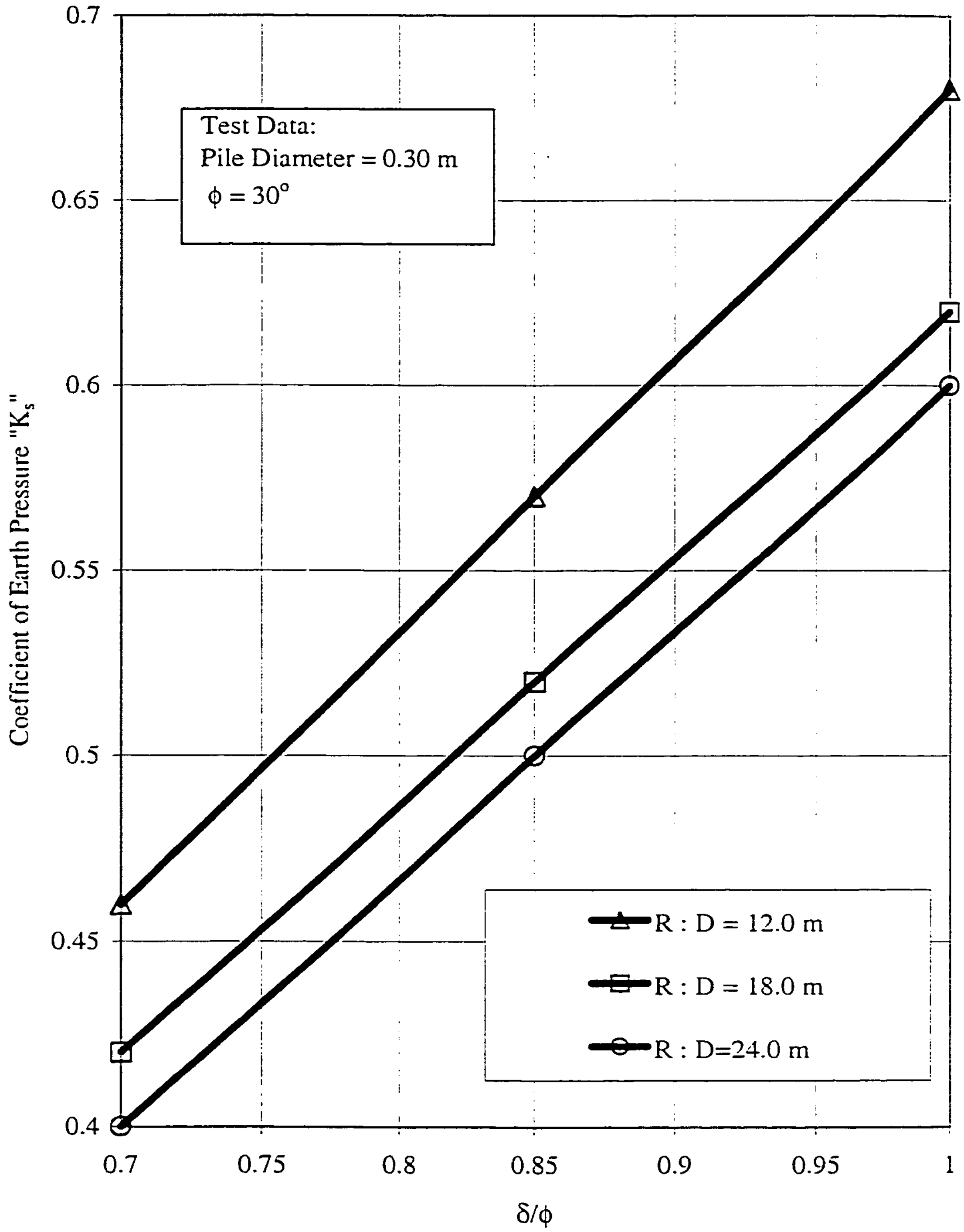

Figure 4.29 Effect of Shaft Roughness "δ/φ" on Coefficient of Earth Pressure "K_s"

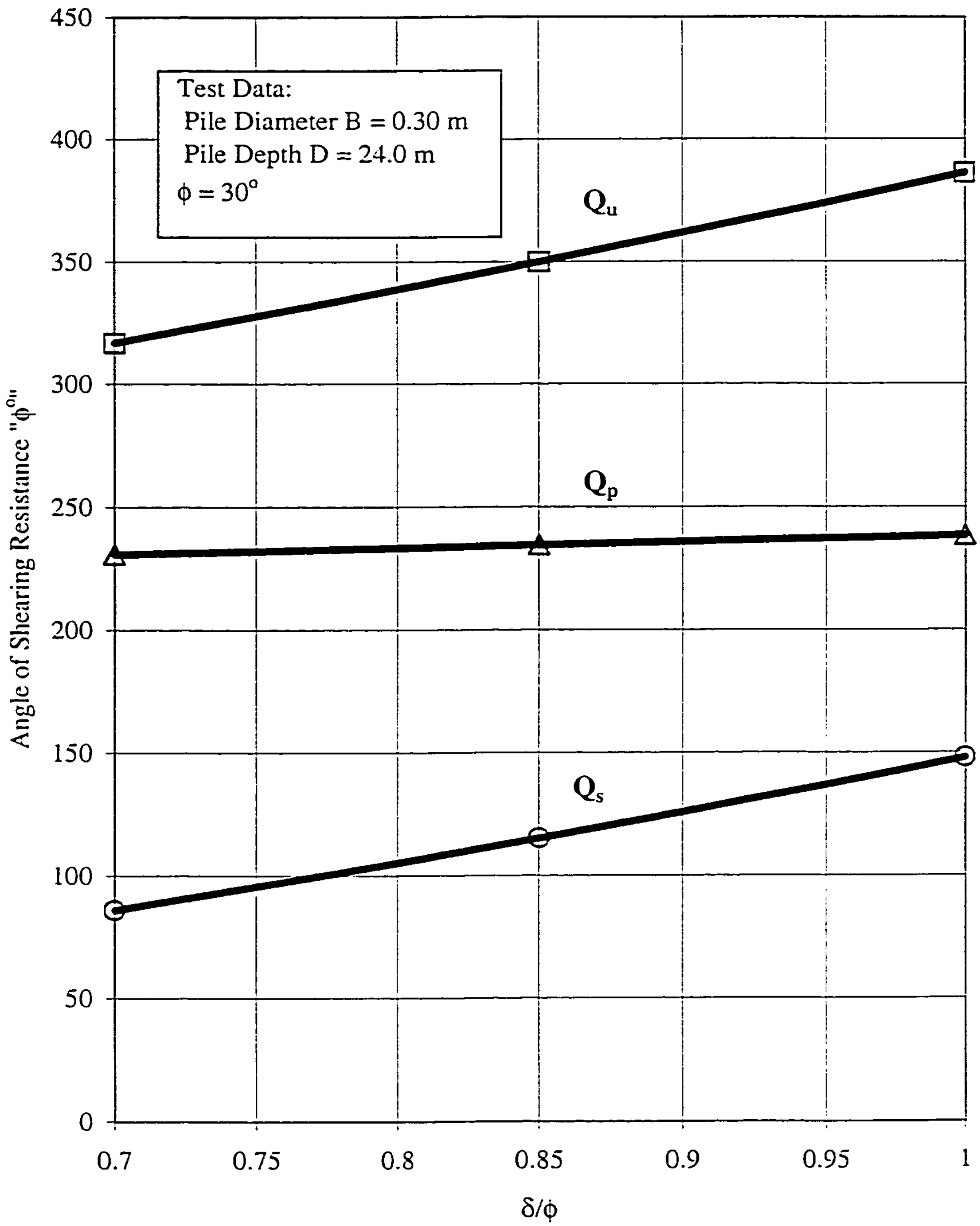

Figure 4.30 Effect of Shaft Roughness "δ/ϕ" on Ultimate Bearing Capacities: Q_u, Q_p, Q_s

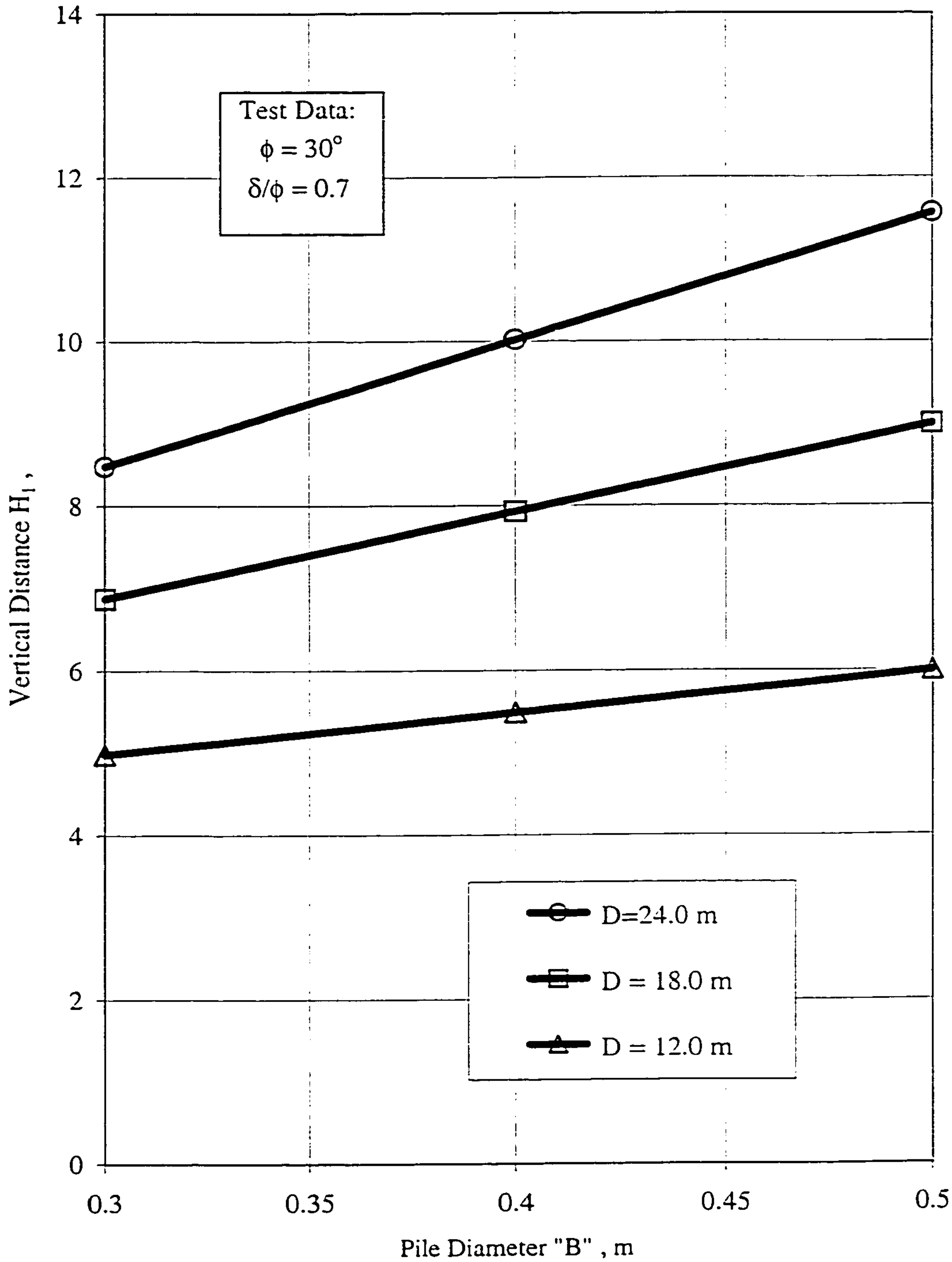

Figure 4.31 Pile Diameter "B" Versus Vertical Distance H_l

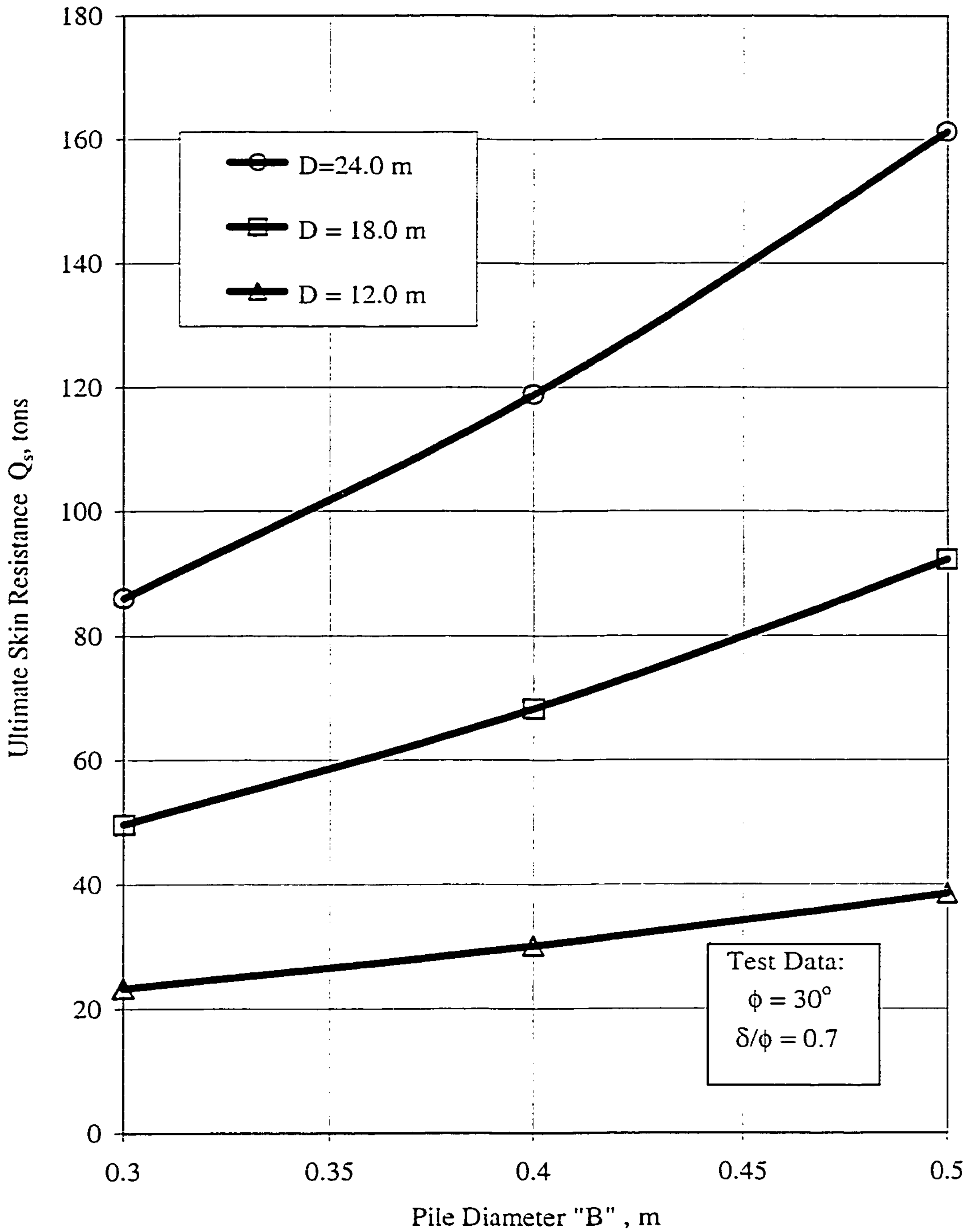

Figure 4.32 Pile Diameter "B" Versus Ultimate Skin Resistance Q_s

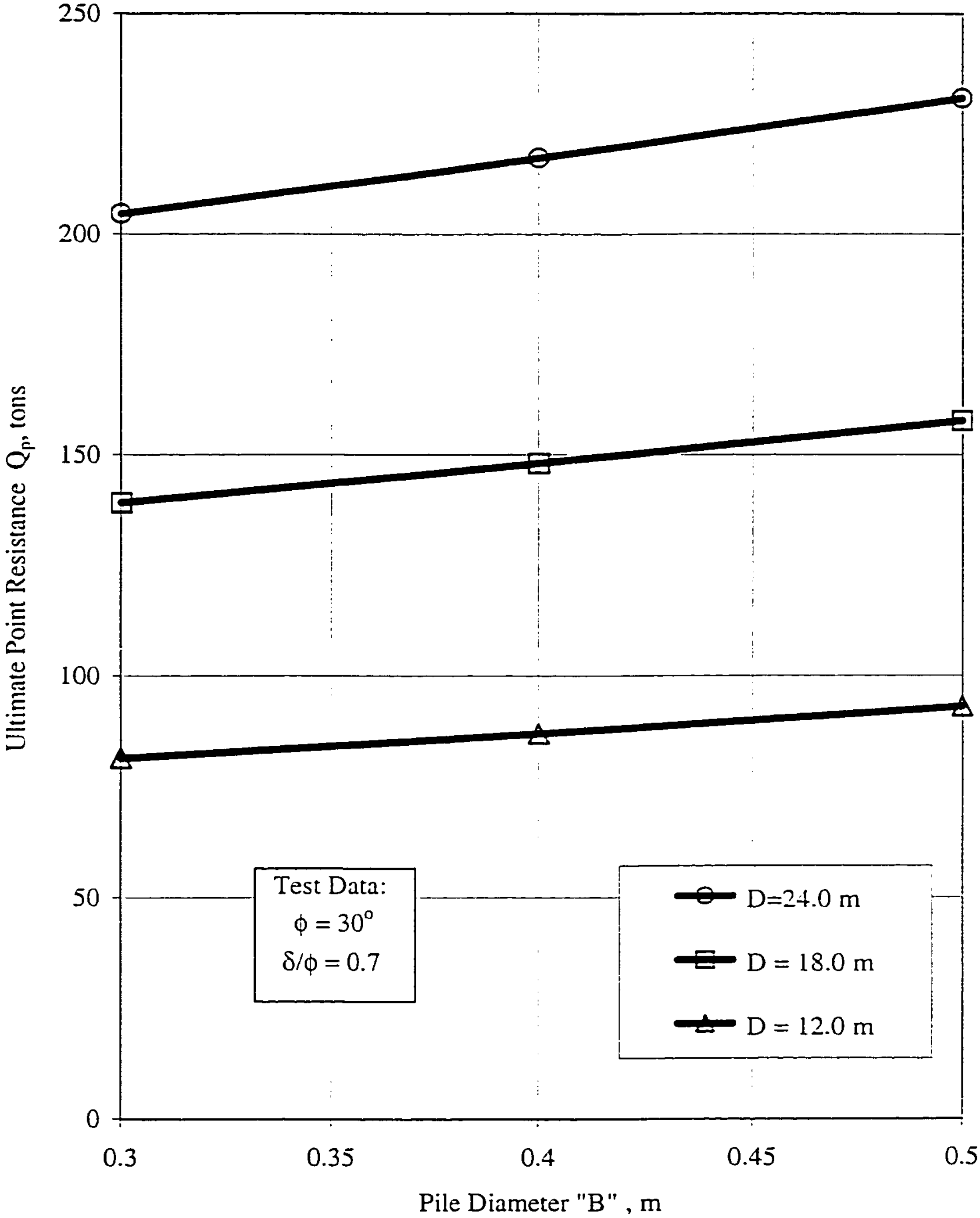

Figure 4.33 Pile Diameter "B" Versus Ultimate Point Resistance Q_p

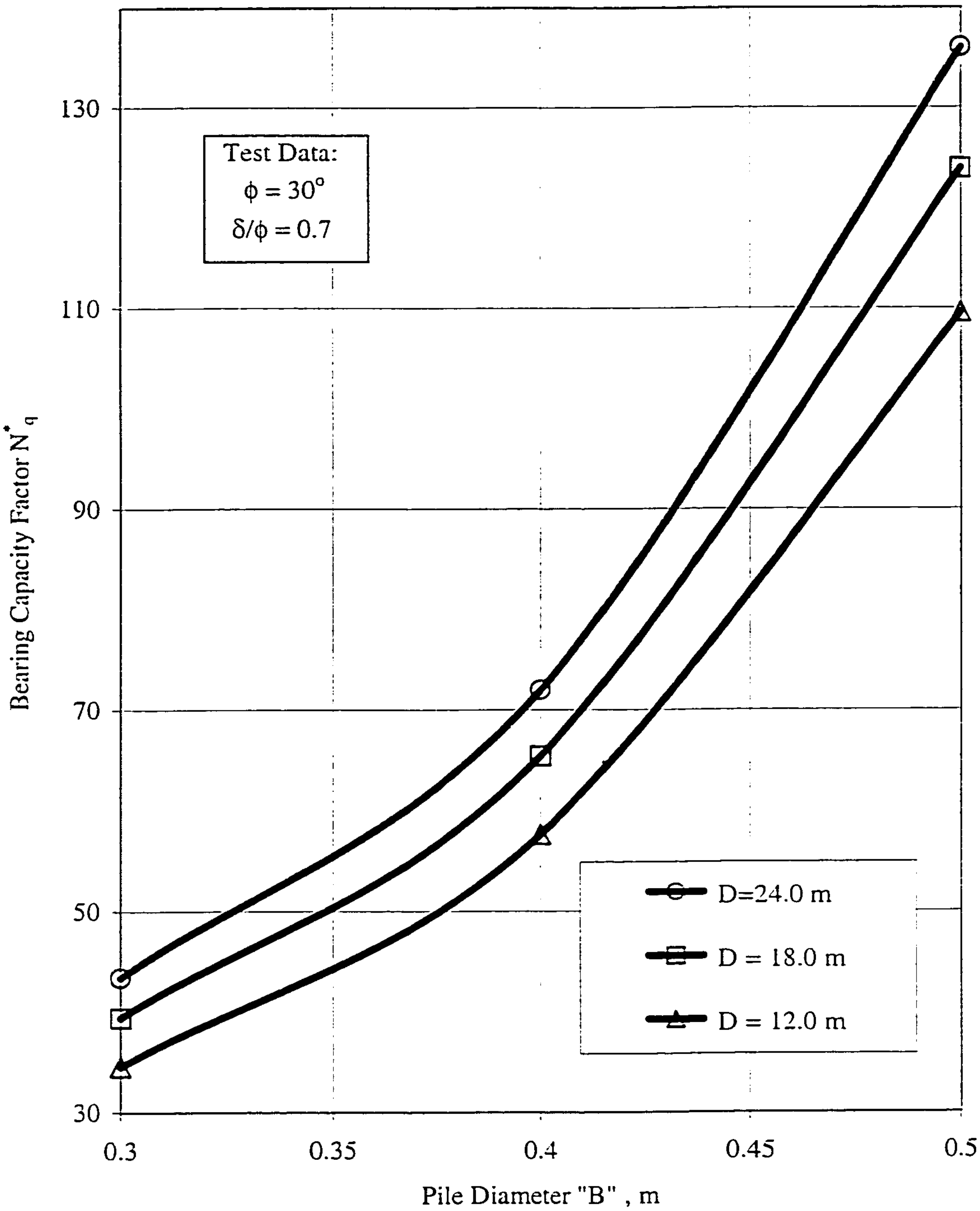

Figure 4.34 Pile Diameter "B" Versus Bearing Capacity factor N^*_q

4.6.3 Effect of Pile Width "B" on the Parameters of the Proposed Theoretical Model

The pile width "B" is introduced as an influencing factor for the prediction of the ultimate bearing capacity of a single pile in sand. In order to show the effect of this geometric factor on the different parameters used in the proposed model, a study for a series of pile tests has been performed and displayed in the Figures: 4. 31, 4. 32, 4.33 & 4.34. The input data for carried out tests are as follows: pile diameters B: 0.3, 0.4 & 0.5 meters, pile depth D: 12.0, 18.0 & 24.0 meters, $\phi = 30^o$ and $\delta/\phi = 0.7$.

4.6.3.1 Effect of Pile Diameter "B" on Vertical Distance H_1

Figure 4.31 shows the effect of Pile Diameter "B" on vertical distance H_1. It can be noted from Figure 4.31, that an increase of "B" results in an increase of the vertical distance H_1. Also it can be seen from this Figure that the rate of change is slightly higher with the depth, which implies that there is a combined effect for pile width and depth together on this factor.

4.6.3.2 Effect of Pile Diameter "B" on Ultimate Skin Resistance Q_s

Figure 4.32 shows the effect of Pile Diameter "B" on ultimate skin resistance Q_s. As can be seen from this Figure 4.32, the increase of the pile width "B", has tremendously increased the ultimate skin resistance. It can also be concluded that the pile depth "D" has a combined effect with pile width, where a relatively higher variation of increase was noticed with respect to "D".

4.6.3.3 Effect of Pile Diameter "B" on Ultimate Point Resistance Q_p

In studying the effect of pile width "B" on the ultimate point resistance Q_p, a series of pile load tests were performed and the comparison is shown in Figure 4.33. The increase of pile

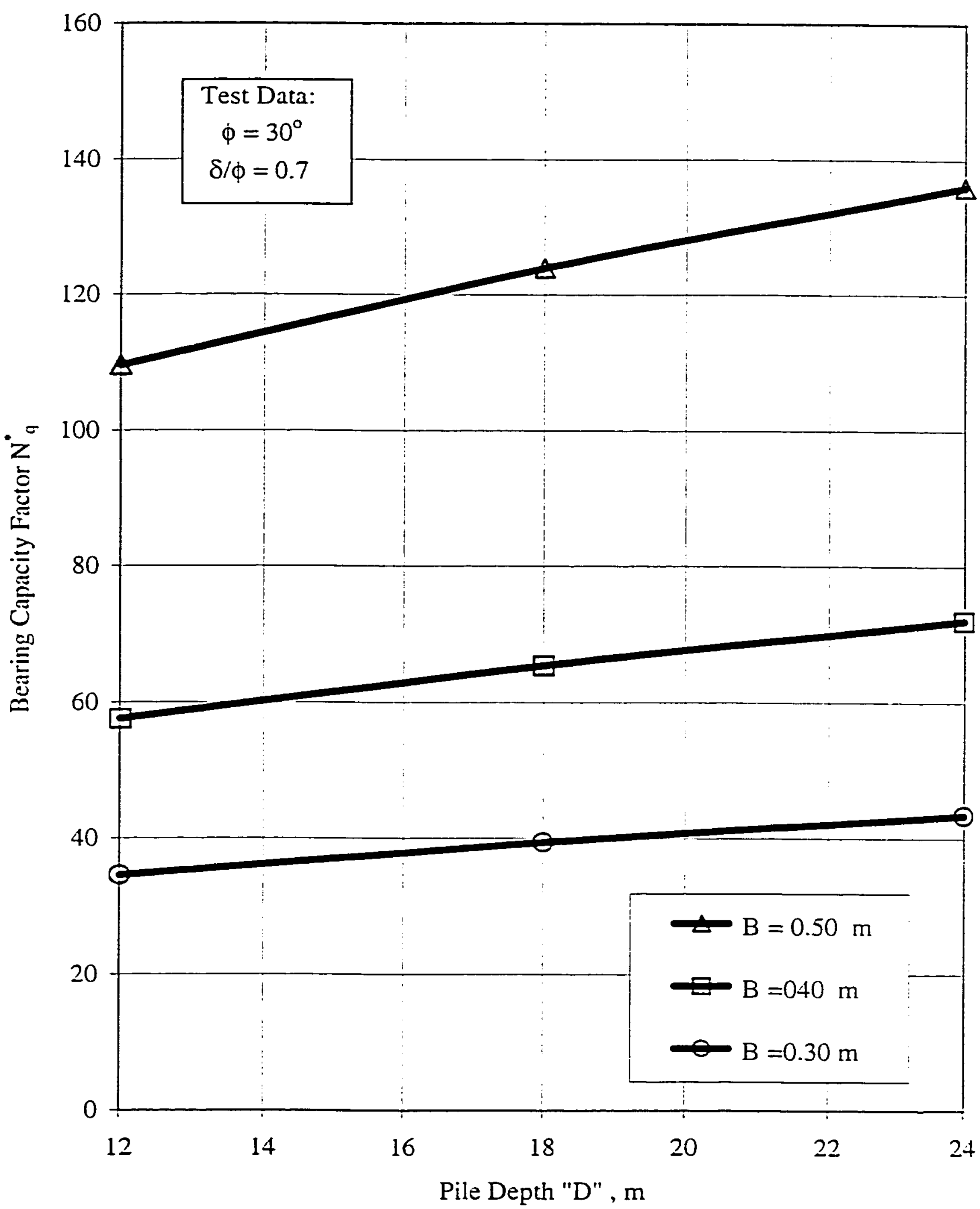

Figure 4.35 Pile Depth "D" Versus Bearing Capacity factor N^*_q

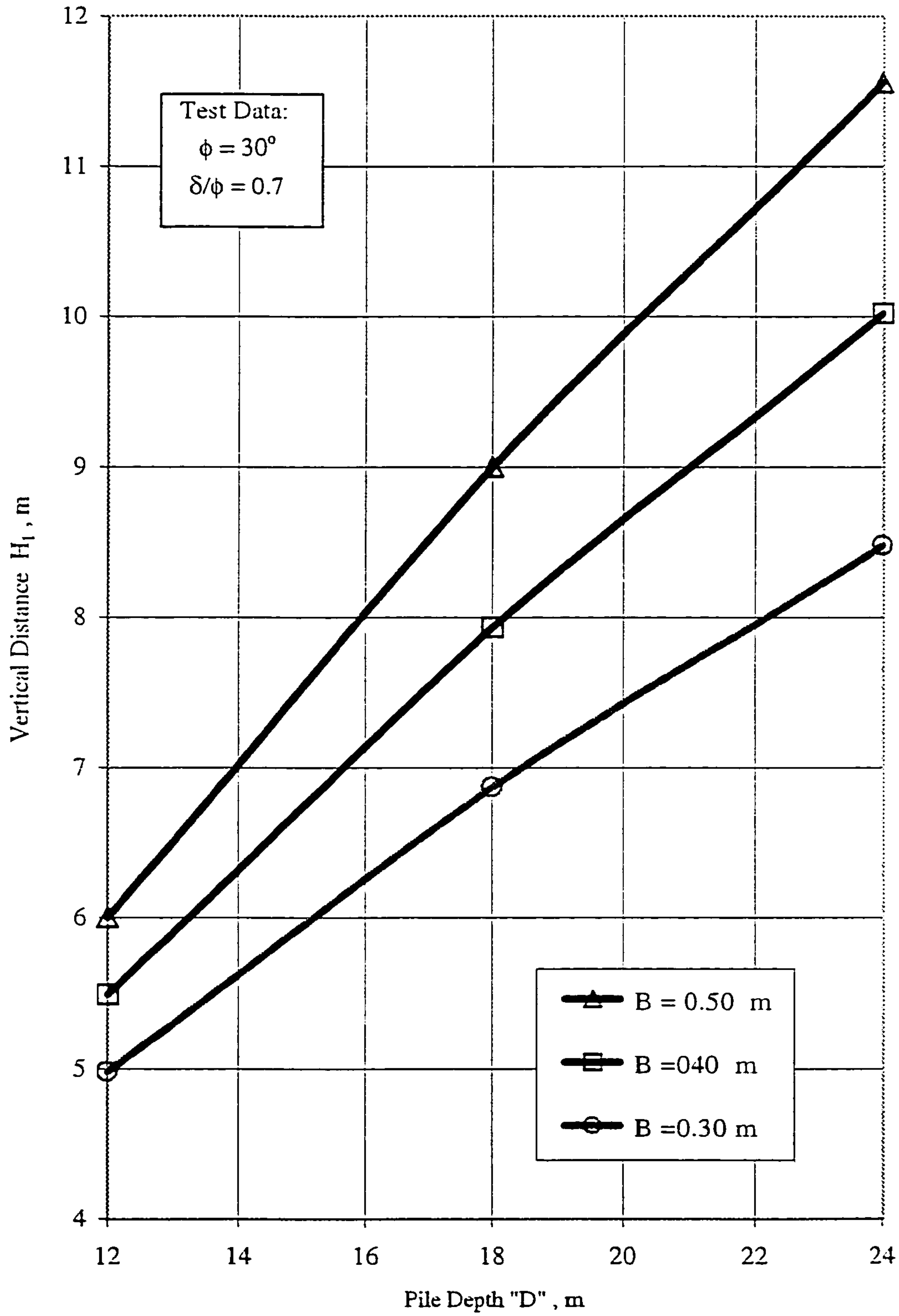

Figure 4.36 Pile Depth "D" Versus Vertical Distance H_1

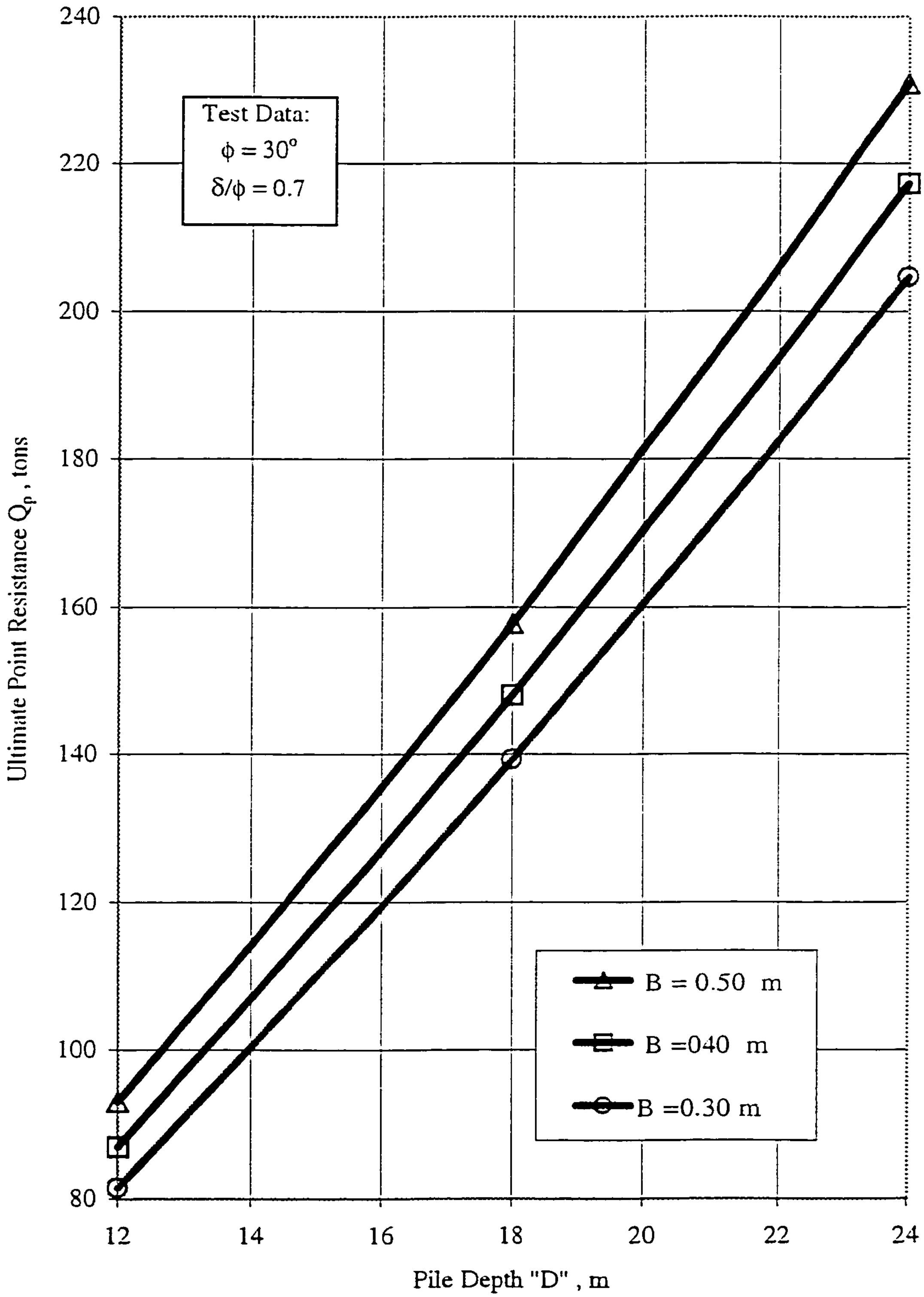

Figure 4.37 Pile Depth "D" Versus Ultimate Point Resistance Q_p

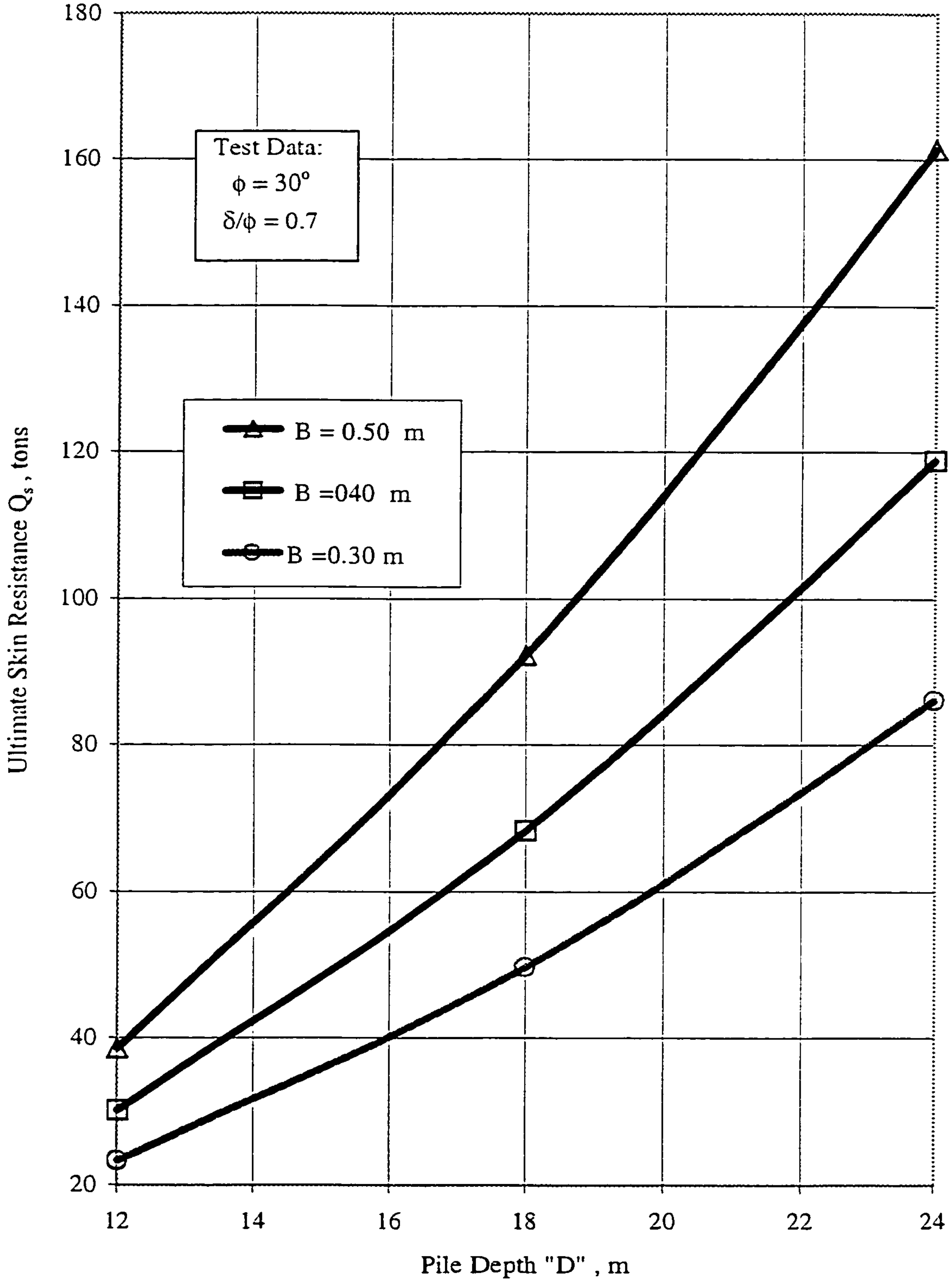

Figure 4.38 Pile Depth "D" Versus Ultimate Skin Resistance Q_s

diameter "B" resulted in an increase of the ultimate point resistance Q_p. It was found that the rate of variation also increased with respect to pile depth "D".

4.6.3.4 Effect of Pile Diameter "B" on Bearing Capacity factor N^*_q

Figure 4.34 shows the effect of pile width "B" on bearing capacity factor N^*_q, where it is found that the increase of "B" has resulted in an increase of N^*_q in a nonlinear relationship. The above analyses demonstrated the importance of considering the geometry of the pile in prediction the ultimate bearing capacity.

4.6.4 Effect of Pile Depth "D" on the Parameters of the Proposed Theoretical Model

In order to investigate the effect of pile depth "D" on the predicted ultimate bearing capacity, a series of load tests have been performed for pile diameter = 0.30 m, depths 12, 18 and 24 meters, ϕ = 30^o and δ/ϕ=0.7. The results of this study are shown in Figures 4.35, 4.36, 4.37, 4.38.

4.6.4.1 Effect of Pile Depth "D" on Bearing Capacity Factor N^*_q

Figure 4.35 shows the effect of pile depth "D" on bearing capacity factor N^*_q. It has been shown that N^*_q increases with depth in a linear function.

4.6.4.2 Effect of Pile Depth "D" on Vertical Distance H_1

Three series of pile tests with diameters 0.3, 0.4 and 0.5 were performed with ϕ =30^o, δ/ϕ = 0.7 and different depths as shown in Figure 4.36. The comparison between the three series shows that vertical distance H_1 is increased with the increase of the pile depth and width.

4.6.4.3 Effect of Pile Depth "D" on Ultimate Point and Skin Resistances Q_p & Q_s

The effect of pile depth on ultimate point resistance Q_p is shown in Figure 4.37. It is found that Q_p is increased with pile depth in a semi linear relationship.

Figure 4.38 shows the effect of pile depth "D" on ultimate point resistance Q_s, where it is found that Q_s is increased with pile depth in a semi nonlinear relationship.

4.7 General Remarks

The forgoing sensitivity analysis demonstrated the functionality of the parameters of the proposed theoretical model. Furthermore the new proposed model adopts the effect of many parameters which have been ignored by the previous theories developed for the same problem.

The new features in the proposed theoretical model can be summarized as follows:

1- The present model considers the effect of pile geometry, D and B on the predicted bearing capacity.

2- The coefficient of earth pressure acting on the shaft is a distinct feature of the present model, where a function of variable coefficient was established and used in the prediction of bearing capacity of a single pile.

3- The effect of relative roughness of the shaft is used to examine its effect on both components Q_s and Q_p. This feature could make the present model able to handle all types of pile materials easily.

4- The influence of pile depth on the bearing capacity of a single pile is considered and introduced. The dimensionless ratio D/B known in the literature to represent the pile geometry is loosing its appeal, simply because the same value of D/B could be common between a pile of dimensions, let's say 0.25 * 24.0 m and a long pile of dimensions 0.75*72 m, both would have the ratio of 96. There is a big difference in the geometry of both piles. At the same time the comparison between their behavior is extremely wide as it was proven through the previous sections. For this reason the solution introduced in the present research work will be presented by using the original dimensions of the pile itself without using ratios.

4.8 Model Verification

To assess the merit of the proposed theoretical model, a total of 27 well documented field load tests were used for verification purposes, which include:

I) Arkansas River Project (Mansur and Hunter, 1970): Seven load tests.

II) Low-sill structure, Old River, Louisiana, USA (Mansur and Kaufman, 1958): Seven load tests.

III) Two load test series consisting of six tests each carried out by Tavenas (1971) on a precast concrete Herkules pile and a steel H pile, respectively.

IV) Two load tests performed on a steel pipe pile by Vesic (1967b).

All Input data used in the analysis of 27 tests may be found in Table 4.1.

4.8.1 Arkansas Test Piles

The pile testing program for the Arkansas river navigation project is located on the east bank of the Arkansas river, about 20 miles downstream from Pine Bluff in Arkansas state, U.S.A. Removal of a layer to the depth of 20 ft. was carried out for preparations of the test area down to the top of the 100 ft. thick sand stratum. The standard penetration resistance was found to be increased with depth, varying from 20 to 40 blows per foot with an average of

Table 4.1 Data Used in Analysis of 27 Field Tests

Pile Test No.	Pile's Type	D (m)	B (m)	σ'_o (Tsf)	D_1 (m)	D_2 (m)	ϕ^o_1	ϕ^o_2	ϕ^o_{ave}	δ^o	K_o	Q_u Tons	Reference for Measured Q_u
Arkansas													
1	Steel Pipe	16.18	0.366	1.580	16.18	0.0	35	35	35.0	25.0	0.426	172.0	1) Hunter and Davisson (1969 [Table 2 p. 19] 2) Coyle and Castello (1981) [Table 3 p. 972-973]
2		16.093	0.457	1.540	16.09	0.0	34	34	34.0	25.0	0.441	242.0	
3		16.153	0.518	1.575	16.15	0.0	35	35	35.0	25.0	0.426	272.0	
10		16.153	0.433	1.543	16.15	0.0	34	34	34.0	25.0	0.441	242.0	
4	Concrete	12.25	0.457	1.184	12.25	0.0	35	35	35.0	30.0	0.426	200.0	
7	H	15.88	0.408	1.532	15.88	0.0	34	34	34.0	28.5	0.441	243.0	
Low-Sill													
1	H	24.69	0.405	2.198	14.94	9.75	28	36	31.2	21.8	0.482	292.0	Mansur and Kaufman (1958) [Table 3 p. 730]
2	Pipe	19.82	0.533	1.800	14.63	5.19	28	36	30.1	21.1	0.498	296.0	
3	H	21.64	0.405	1.900	15.85	5.79	28	36	30.1	21.6	0.498	151.0	
4	Steel Pipe	20.12	0.433	1.830	14.63	5.49	28	36	30.8	21.6	0.488	361.0	
5		13.72	0.433	1.260	13.72	0.0	28	36	28.0	19.6	0.531	117.0	
6		19.81	0.482	1.790	15.24	4.57	28	36	29.8	20.9	0503	329.0	
7		19.81	0.457	1.781	14.34	5.49	28	36	30.2	21.1	0.497	317.0	
Tavenas													
J-1	Precast Concrete	5.79	0.323	0.538	4.88	0.91	30	34	30.6	23.7	0.491	40.0	Tavenas (1971) [Table 2 p. 19]
J-2		8.84	0.323	0.843	4.88	3.96	30	34	31.8	24.5	0.473	55.0	
J-3		11.89	0.323	1.148	4.88	7.01	30	34	32.4	24.9	0.464	77.0	
J-4		14.94	0.323	1.453	4.88	10.06	30	34	32.7	25.1	0.460	95.0	
J-5		17.98	0.323	1.758	4.88	13.10	30	34	32.9	25.3	0.457	107.5	
J-6		21.03	0.323	2.063	4.88	16.15	30	34	33.1	25.4	0.454	120.5	
Tavenas													
H-1	Steel H Pile	5.49	0.347	0.507	4.88	0.61	30	34	30.4	23.8	0.494	20.0	Tavenas (1971) [Table 3 p. 21]
H-2		8.53	0.347	0.812	4.88	3.65	30	34	31.7	24.9	0.475	50.0	
H-3		11.58	0.347	1.117	4.88	6.70	30	34	32.3	25.4	0.466	80.0	
H-4		14.63	0.347	1.422	4.88	9.75	30	34	32.7	25.7	0.460	93.0	
H-5		17.68	0.347	1.727	4.88	12.8	30	34	32.9	25.9	0.457	105.0	
H-6		20.73	0.347	2.032	4.88	15.85	30	34	33.1	26.1	0.454	185.0	
Vesic													
H-14	Steel Pipe	11.98	0.457	1.461	3.66	8.32	31	38	35.9	25.0	0.414	347.0	Vesic (1967) [Table 19 p. 51]
H-15		15.03	0.457	1.788	3.66	11.37	31	38	36.3	25.0	0.408	421.0	

Table 4.2 Analysis Results for 27 Pile Load Tests

Pile Test No.	δ/ϕ	Present Model						Measured Q_u	Error e_R %
		N^*_q	Q_p	Equivalent K_s*tan δ	Q_s	Q_u	Q_s/Q_u		
Arkansas 1	0.71	65	116.37	0.3	47.5	163.9	0.29	172	4.73
2	0.74	80	217.60	0.35	67.1	284.7	0.24	242	-17.6
3	0.7	100	357.6	0.35	78.1	435.7	0.18	272	-60.1
10	0.74	77	188.73	0.28	51.2	239.9	0.21	242	0.85
4	0.86	85	177.73	0.3	33.6	211.4	0.16	200	-5.7
7	0.84	77.46	167.31	0.28	47.1	214.4	0.22	243	11.78
Low-Sill 1	0.7	56	170.78	0.28	104.1	274.9	0.38	292	5.8
2	0.7	50	216.23	0.27	86.8	303.02	0.29	296	-2.3
3	0.7	42	110.70	0.27	76.1	186.75	0.41	151	-23.7
4	0.7	65	188.61	0.35	94.38	282.99	0.33	361	21.6
5	0.7	40	79.96	0.3	38.0	117.96	0.32	117	-0.8
6	0.7	68	239.26	0.37	107.01	346.27	0.31	329	-5.25
7	0.7	58	182.51	0.32	87.30	269.81	0.32	317	14.89
Tavanas J-1	0.78	30	14.25	0.35	5.96	20.21	0.3	40	49.4
J-2	0.77	38	28.38	0.38	15.53	43.91	0.35	55	20.1
J-3	0.77	43	43.61	0.3	22. 40	66.01	0.34	77	14.2
J-4	0.77	47.5	60.52	0.33	38.87	99.38	0.39	95	-4.6
J-5	0.77	50	77.44	0.3	51.72	129.15	0.40	105	-23.0
J-6	0.77	55	100.57	0.3	71.41	171.97	0.42	120.5	-42.7
Tavanas H-1	0.8	20	10.40	0.33	5.41	15.81	0.34	20	20.9
H-2	0.79	42	34.93	0.38	15.50	50.43	0.31	50	-0.86
H-3	0.79	42	48.04	0.34	25.88	73.92	0.35	80	7.6
H-4	0.79	48	69.91	0.33	40.41	110.33	0.37	93	-18.6
H-5	0.79	50	88.49	0.29	52.15	140.64	0.37	105	-33.9
H-6	0.79	55.7	115.96	0.34	84.33	200.28	0.42	185	-8.2
Vesic H-14	0.7	84	216.32	0.47	63.46	279.78	0.23	347	19.3
H-15	0.7	100	315.7	0.42	87.21	402.91	0.22	421	4.2

about 20 blows per foot after site excavation. The ground water table was kept about 2 to 3 feet below the ground surface by a dewatering system installed around the test area. Only six test piles out of a total of 21 tests were considered relevant for use in the analysis which idealized the test site as a single layer deposit, having average physical properties summarized in Table 4.1. It can be seen in Table 4.2 that the calculated bearing capacity Q_u of the six selected test piles agreed well with their measured counterparts, incurring errors ranging only from about -17.6 percent to +11.78 percent, except for pile number 3 which encountered error exceeding +60%. This big error may be related to irregularity in the field measurements in the sight of the similar test condition: pile number 10, which has the same depth as pile number 3, the only difference being the pile width. For the present model, the consideration of pile width is working well so far, which is clear in the comparison of predicted Q_u for pile number 1 and pile number 2 in the same group, which are similar in all properties except the pile width.

4.8.2 Low-Sill Test Piles

The controlled spillway of Low-Sill structure is located on the west bank of the Mississippi River, 35 miles south of Natchez, Mississippi, U.S.A. The pile testing program included compression or compression/tension tests which were performed on two 14 in. steel H piles, and five steel pipe piles having diameters ranging from 16 to 20 inches. The soil profile for this site consists of 50 to 60 ft. of alternating strata of silts, sandy silts and silty sands overlying a clean sand stratum of varying thickness from 40 to 60 ft., which is in turn underlain by stiff clays. To account for the two-layered soil system an average angle of shearing resistance, ϕ is assumed as follows:

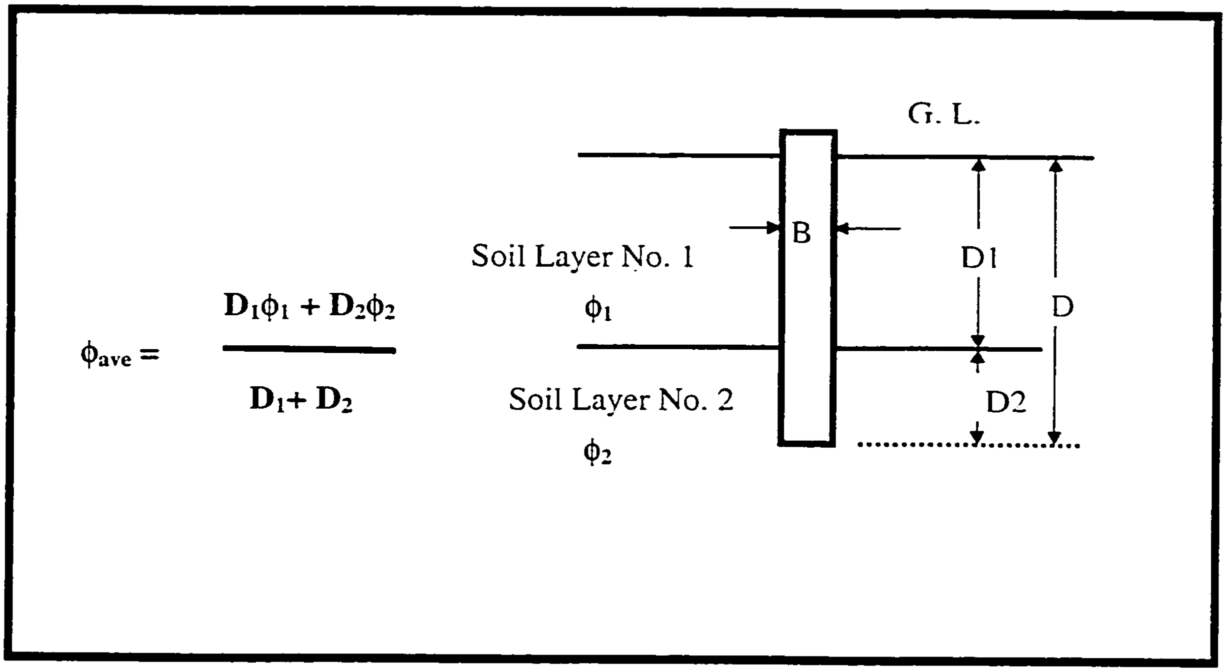

Figure 4.39 Procedure Followed to Determine Average Angle of Shearing Resistance for Two Layered Soil

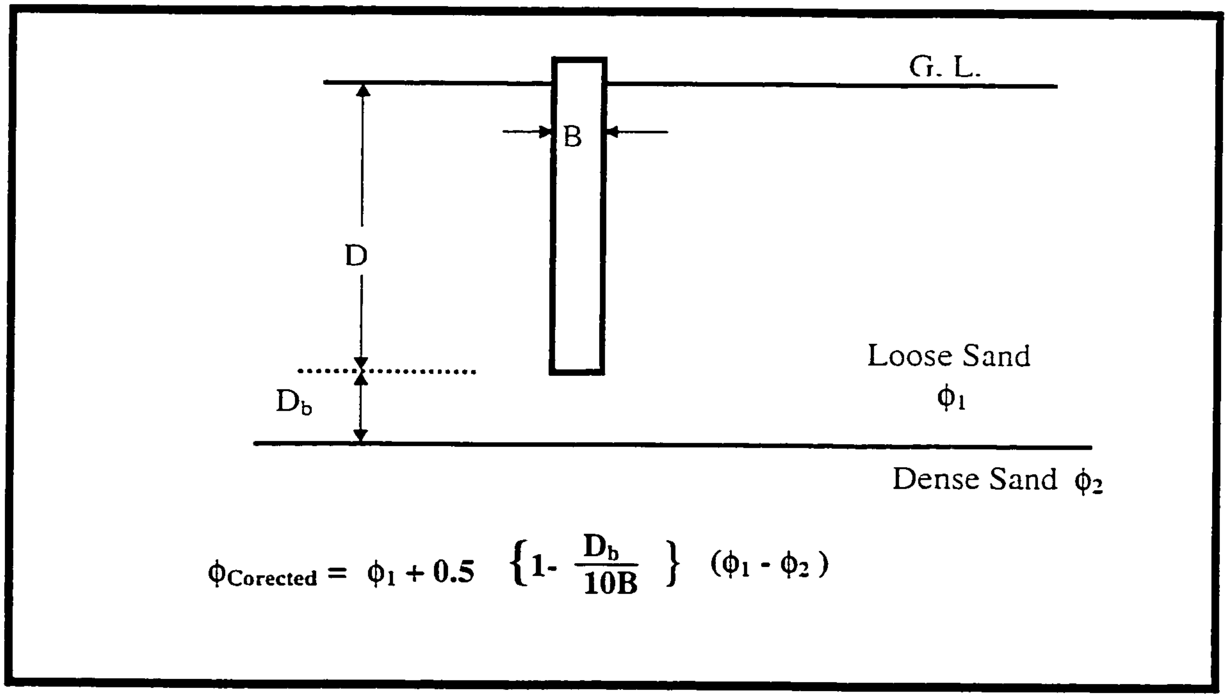

Figure 4.40 Procedure Followed to Determine Corrected Angle of Shearing Resistance for Layering Effect
(Vesic's Test No. H-11 and Low-Sill Test No. 5)

$$\phi_{ave} = \frac{\phi_1 D_1 + \phi_2 D_2}{D_1 + D_2} \qquad ...(4.38)$$

Where: ϕ_1, D_1 are denoting soil angle of shearing resistance and layer depth for layer 1.

ϕ_2, D_2 are denoting soil angle of shearing resistance and layer depth for layer 2.

This procedure is shown in Figure 4.39.The same procedure were followed for similar test sites and the summary is reported in Table 4.1.

A correction for the stiffening effect of the stronger sand layer located 4 ft. below the interface of the two layers is assumed as follows:

$$\phi_{Corrected} = \phi_1 + 0.5\left[1 - \frac{D_b}{10B}\right](\phi_1 - \phi_2) \qquad ...(4.39)$$

This procedure is shown in Figure 4.40. The corrected numerical values used in the analysis can be found in Table 4.1. Computed ultimate loads utilizing the suggested model, showed good agreement with their measured counterpart for the whole group, as indicated in Table 4.2, with errors ranging from -23.7 to +21.6 percent.

4.8.3 Tavenas' Field Tests:

A series of six load tests on a Herkules H800 precast concrete pile was performed by Tavenas (1971) as part of the embankment project of the St. Charles River in Quebec City, Quebec, Canada. The idealized geotechnical profile of the test site and physical properties of the dominant layers were shown in Figure 4.41a. The Herkules pile was driven and tested at depths of 19, 29, 39, 49, 59 and 69 ft., respectively. Axial loads were monitored by deformation gauges installed inside the pile shaft. Although all pile load tests were performed with the pile point located in the sand stratum, the first 16 ft. of the test pile was embedded in a loose crushed stone layer which had been dumped uncompacted under water. In the analysis, the same procedure introduced in Equation 4.30 was followed to account for the layering effects. The angle of shaft friction δ was determined as: $\delta=(2/3)(\phi_{ave}+5)$; this angle was suggested by Tavenas. Reasonable agreements between computed and measured pile bearing capacities were observed, indicating errors ranging from -23.0 to + 20.1 percent. Except for test number J-1 which was found to be underestimated by 49.4%, this test is a short pile, of D =5.79 m. In the same analysis for Tavenas H-Pile group, another short pile of 5.49 m was matched well: for these two piles J-1 and H-1 for the same site, the measured Q_u for test J-1 is 40 tons, while in the almost same test data H-1, the measured Q_u is half of test J-1. This should implies some irregularities in the field measurements. The same trend can be noticed for test number J-6,where it was overestimated by -42.7%. In a similar test in H-pile testing for Tavenas test number H-6 the results was in reasonable agreement -8.2%. For these reasons the two tests J-1 and J-6 will be excluded from the present error analysis.

4.8.4 Tavenas' Tests on H-Pile

Another load test series on a steel H-pile (type 12BP74), were carried out by Tavenas (1971) for the same project. This steel H-pile, which consisted of one 20 ft. section and five 10 ft. sections, was driven and tested at six depths of 18, 28, 38, 48, 58 and 68 ft., respectively. The same idealized geotechnical profile used to analyze the Herkules pile (see Fig. 4.41a) was assumed valid for the H-pile. The adapted numerical data values and the output results are shown in Table 4.1. From Table 4.2, it can be seen that there are fairly good agreements between computed and measured bearing capacities, with errors ranging from -18.6 percent to +20.6 percent. Errors exceeding -33 percent, however, were encountered in pile test No.

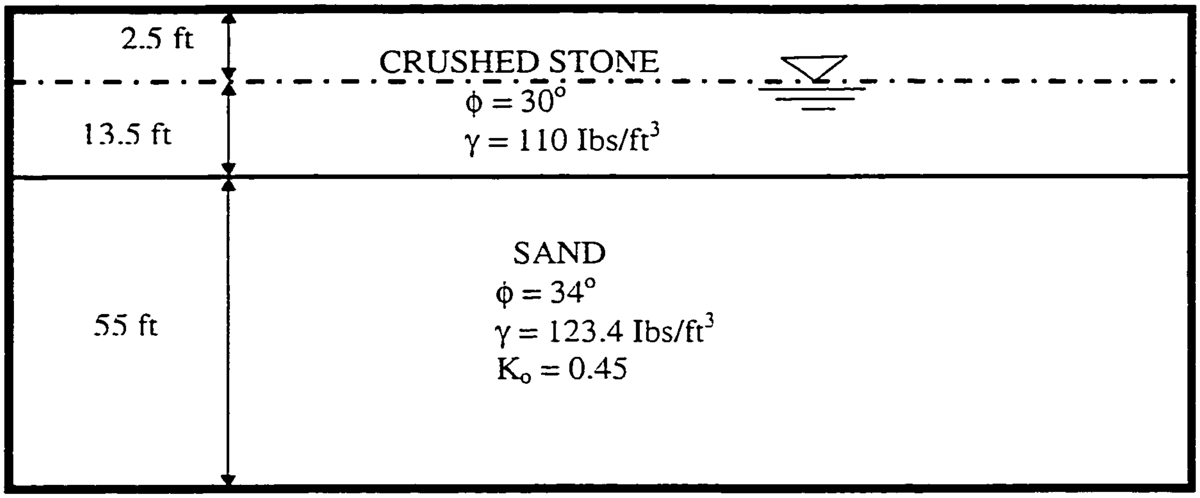

a - Tavanas' Test Site, (1971)

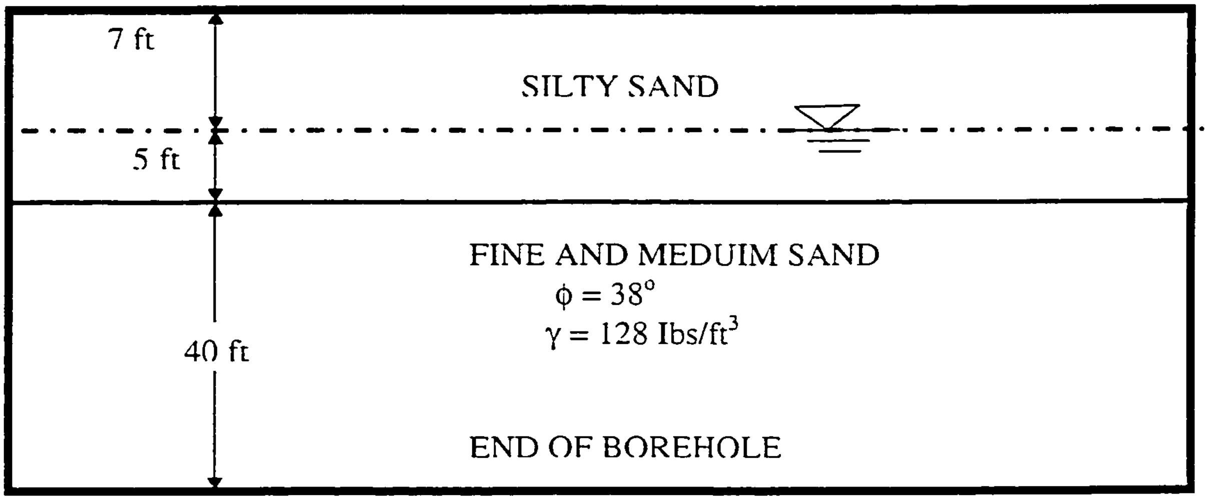

b - Vesic, (1967) Test Site

Figure 4.41 Idealized Geotechnical Profile of Tavanas' and Vesic Test Sites

H-5. In the analysis, the H-pile was explicitly assumed to be fully plugged and replaced by an equivalent circular pile having the same cross section area. If the flanges of the H pile were only partially plugged with soil then this assumption would lead to an overestimation of Q_u For these reasons, pile test No. H-5 will be excluded from a subsequent correlation study.

4.8.5 Vesic's Tests on Steel Pipe Pile

Two load tests were chosen from the testing program carried out by Vesic, (1967b); they are H-14 and H-15. These load tests were performed at the site of the future Ogeechee River bridge on Interstate Highway 16, in Effingham County, Georgia state, U.S.A. The site profile consisted of a silty sand layer down to about 12 ft., underlain by a fine to medium sand deposit. Figure 4.41b shows an idealized geotechnical profile and soil properties for the site. The test pile was closed end steel pipe pile with an 18 in. width, driven in five sections approximately 10 ft. long each and tested at nominal depths of 40 and 50 ft. Strain gauges were inserted on the internal walls of the pile sections to measure axial loads in the pile shaft at various depths. The same procedure previously followed to account for the two layered soil system, is adapted in this test series. The numerical values for analysis and obtained results are shown in Table 4.1 and 4.2 respectively.

The agreement between predicted and measured bearing capacities was found to be +19.2 percent for test No. H-14 and +4.2 percent for test No. H-15.

The error analysis results for the 27 tests are shown in Table 4.2. and Figure 4.42. The following remarks are due from Figure 4.42:

1- The over estimated capacities are 11 tests out of 23, - ve sign.

2- The under estimated capacities are 12 tests out of 23, + ve sign.

3- The tests agreed within 10% error are 52% of the total number of tests.

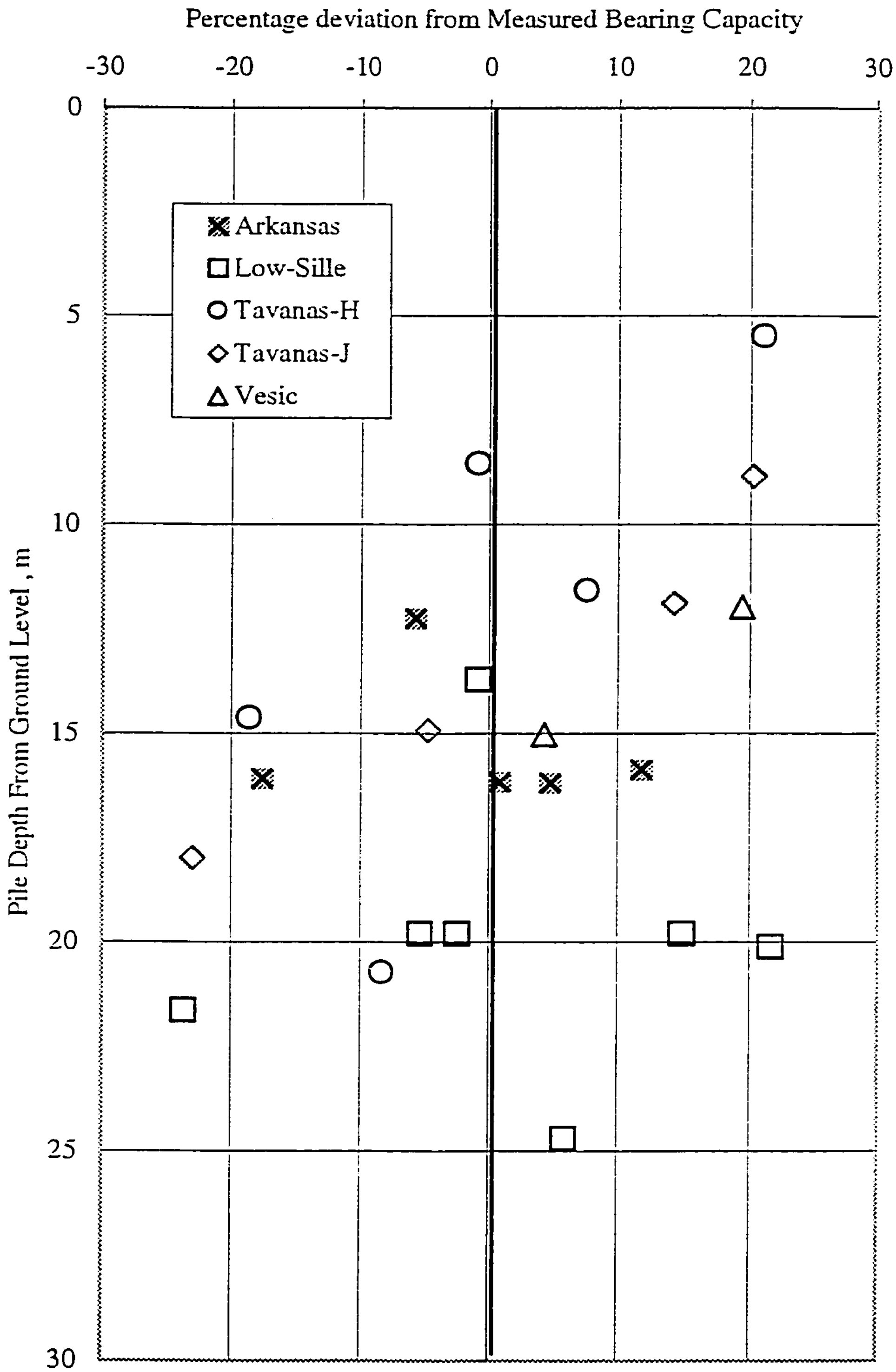

Figure 4.42 Comparison Between Measured and Predicted Bearing Capacity

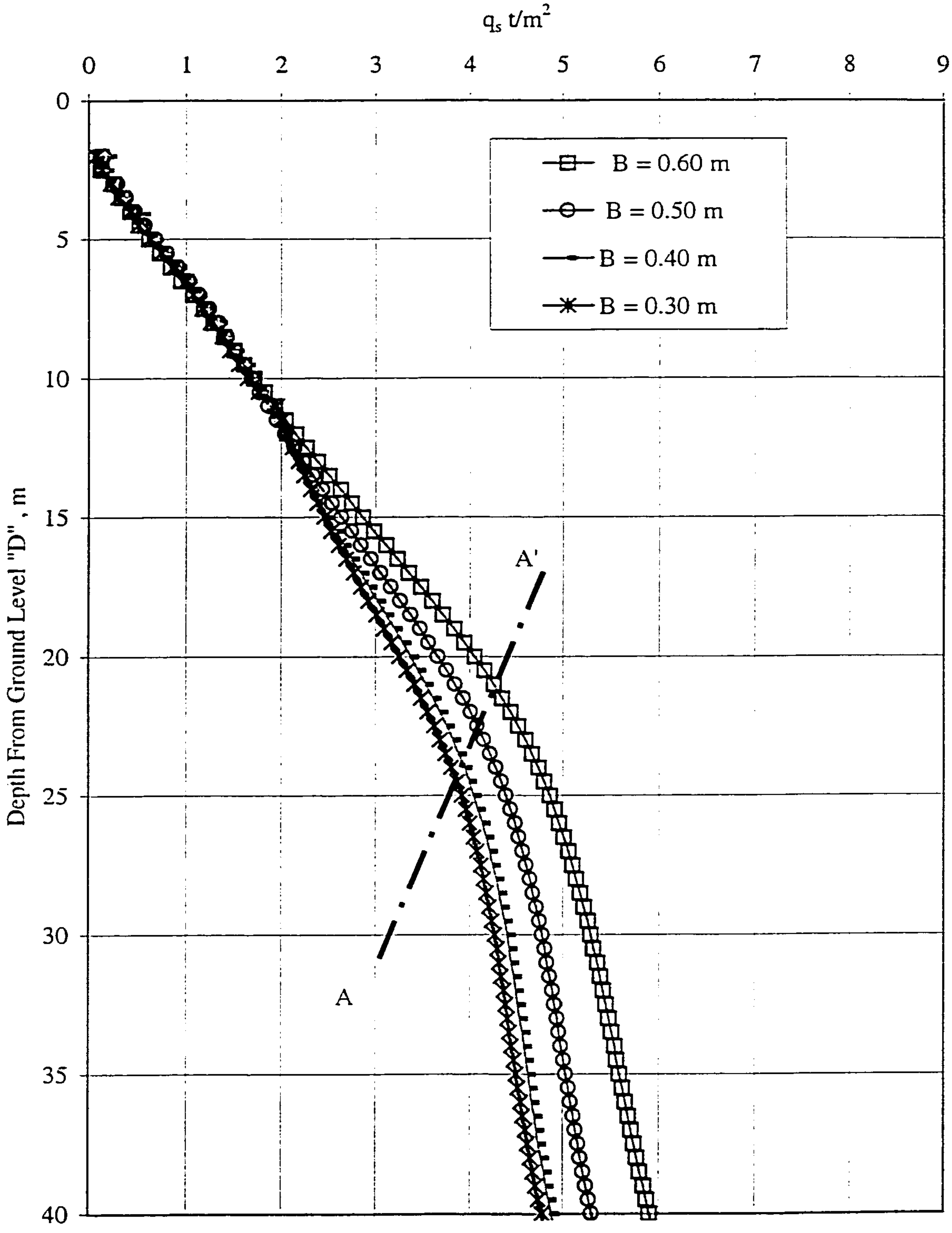

Figure 4.43 Unit Skin Friction q_s Versus Pile Depth "D" for Different Pile Diameters "B"(Case of ϕ =30°)

4- Tests agreed within 20% error are 83% of the total number.

5- The maximum error deviation did not exceed 23.6%.

6- The ratio Q_s/Q_u is ranging between 0.16 to 0.42.

4.9 Critical Depth

Figure 4.43 and 4.44 introduce plots of unit skin and unit point resistances versus pile depth for various pile diameters: 0. 30, 0.40, 0.50 & 0.60 m. Test data are $\phi = 30^o$, $\delta/\phi = 0.7$. It can be noted from Figure 4.43 that the unit of skin resistance is increasing with an increase of the depth up to approximate depth named $D_c = 28.5$ m in the case of pile width of 0.30 m, 28.0 m in case of B = 0.40, 27.0 m in case of B = 0.50 and 26.0 m in case of B = 0.60m. It is noticed that the critical depth in this case (skin resistance) is decreased with pile depth and width. It is important to note that below this depth, the unit of skin resistance tends to increase, at a lower rate.

This trend explains the phenomena of critical depth. It can be noted from this Figure that theo-cratical depth depends on pile diameter B, depth D and angle of shearing resistance ϕ.

To explore this trend in the case point resistance, a relationships between N_q and pile depth are plotted in Figure 4.44. Different trend was found in the case of point resistance (refer to Figure 4.44), where critical depths occurred between 14.0 m at B =0.30 up to 17.50 m at B=0.60m. Where the critical depth in increased with pile width and depth.

The rate of increase below that depth tends to behave as a slower increase in case of B = 0.30 m and B=0.40m, while it tends to have gradual but increasingly rapid increase in case of B = 0.50 and 0.60m. The line of critical depth is marked as B-B' in Figure 4.44.

This investigation could lead to the following conclusions:

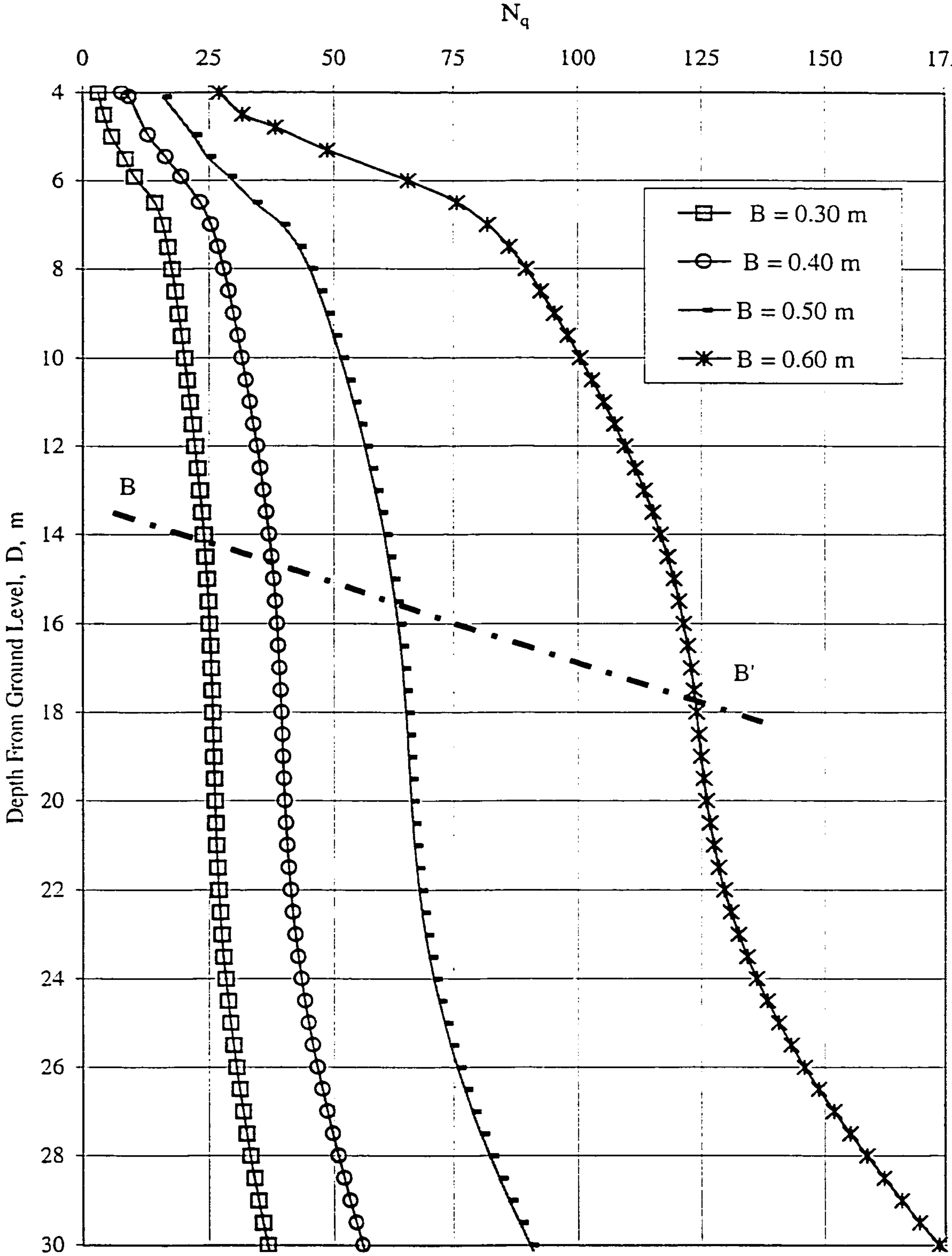

Figure 4.44 Bearing Capacity Factor N_q Versus "D" for Different Pile Diameters "B"
(Case of ϕ=30)

1- The critical depth is found, but below this depth a lower rate of increase of N_q & q_s occurs.

2- In some cases, like with a higher pile width, below the critical depth, the point resistance might be subjected to a rate of increase. This trend could benefit from more explanation in a future study.

3- It was found that a varied critical depth occurs depends on the pile width and depth and angle of shearing resistance ϕ. This trend also needs more explanations in further studies.

4.10 Design Charts

The preceded analysis made it possible to establish a new rational solution for the problem of bearing capacity of a single pile driven vertically in sand. It can be seen that the proposed theoretical model is capable to predict the two components of pile bearing capacity: Q_p and Q_s for a wide range of sand conditions. The proposed design procedure can handle pile depths from 4.0 m up to 30.0 m, pile widths from 0.30 m up to 0.60 m, angle of shearing resistance from 27^o up to 42^o, and shaft roughness ratio $\delta/\phi = 0.7$ to 1.0.

To predict the ultimate point bearing, a data produced by the program G-Pile were used in developing charts for the dimensionless factor N^*_q. Figures 4.45 to 4.49 are introducing the new design charts proposed for the bearing capacity factor N^*_q. It should be noted that this factor is introduced as a f unction of Pile depth D and width B in meters and the angle of shearing resistance of sand ϕ in degrees.

Prediction of Q_s can be determined easily if the factor (K_s*tan δ) is known. As was presented in the preceding sections of the present work, the varied failure pattern produced different mobilized skin friction surface areas. In this case it is recommended to simplify the use of these different mobilized skin friction areas to determine the skin friction component Q_s.

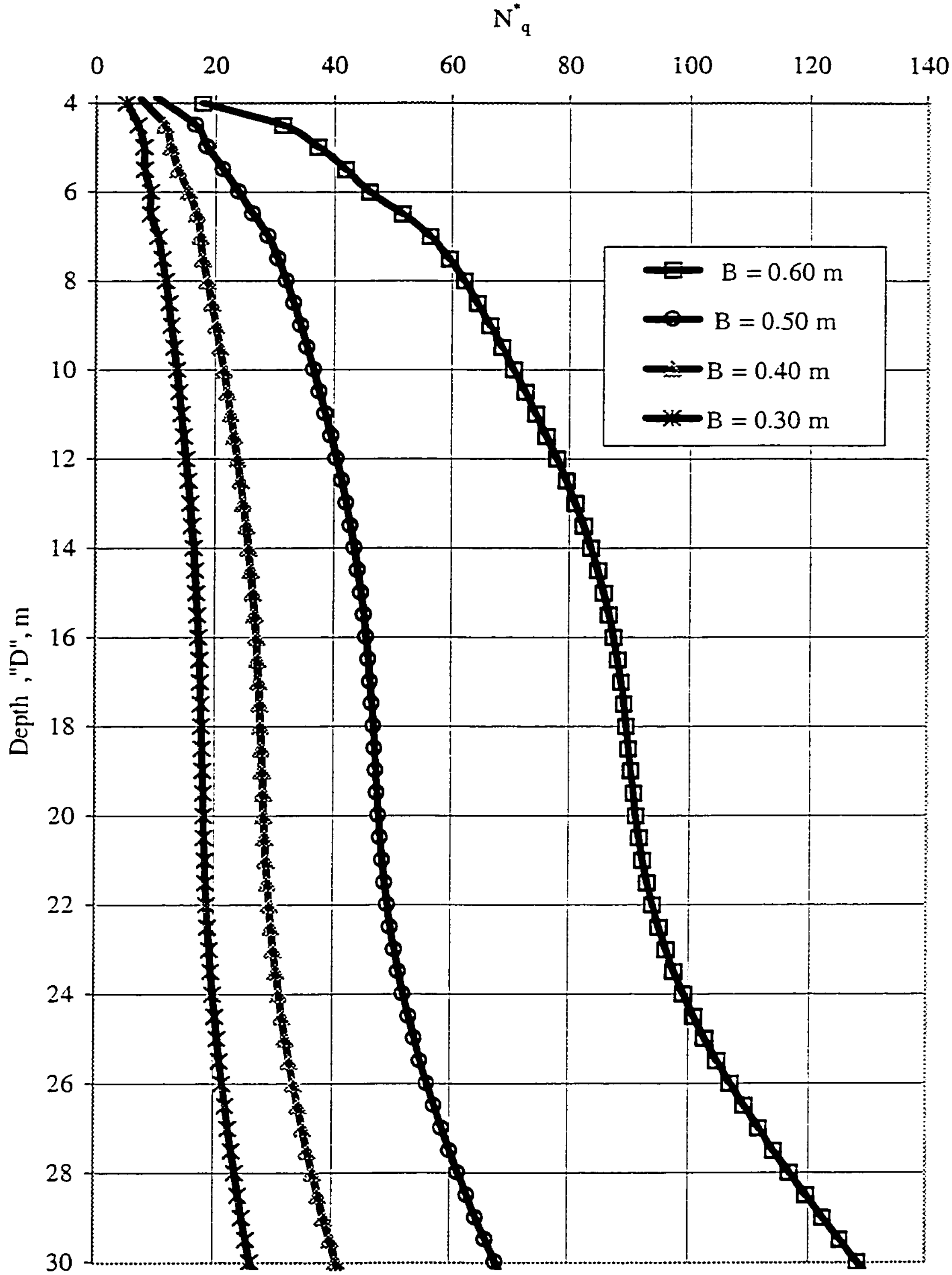

Figure 4.45 Bearing Capacity Factor N^*_q Versus Pile Depth "D" for Different Pile Diameters "B" (Case of ϕ =27°)

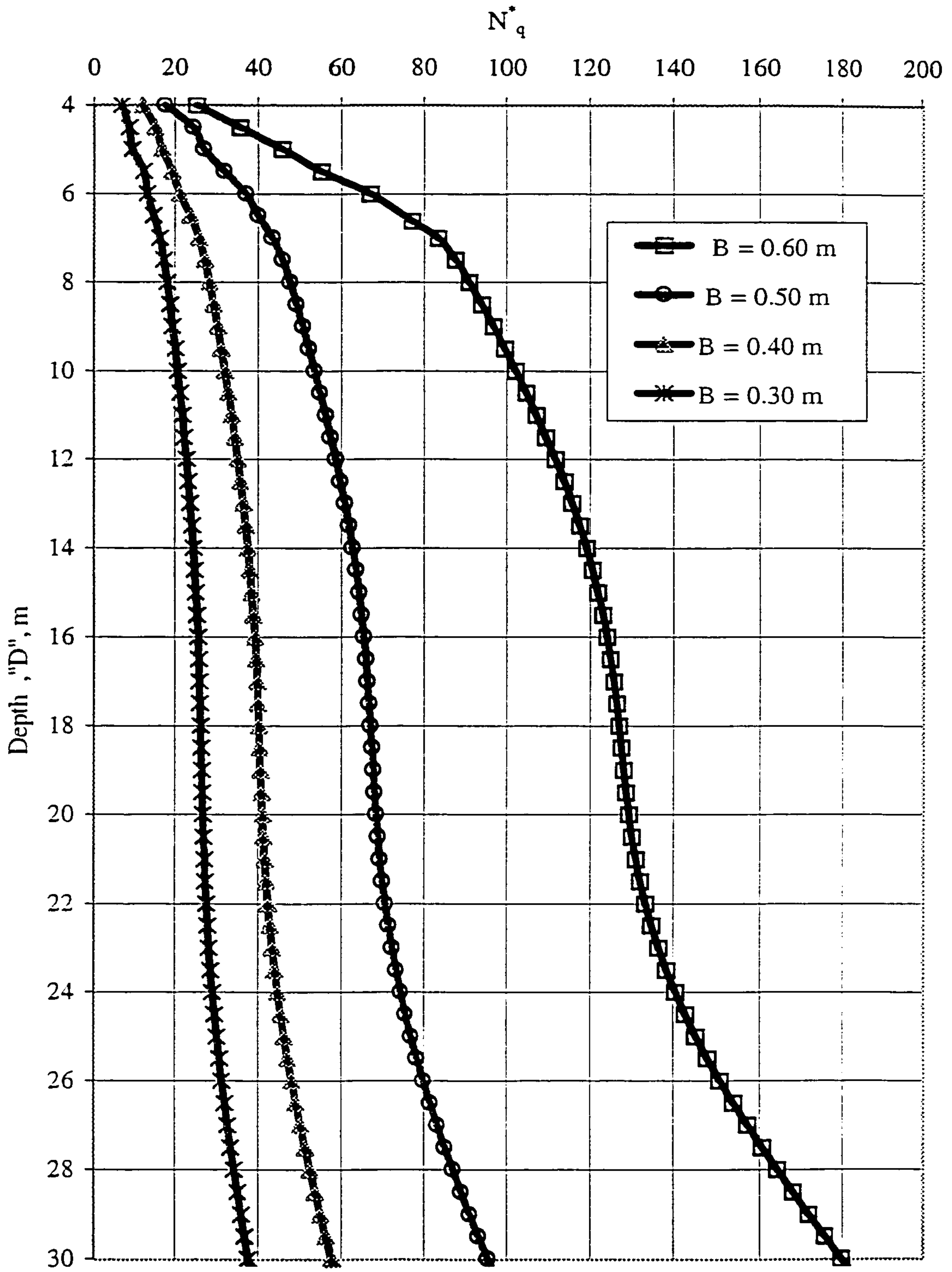

Figure 4.46 Bearing Capacity Factor N^*_q Versus Pile Depth "D" for Different Pile Diameters "B" (Case of ϕ =30°)

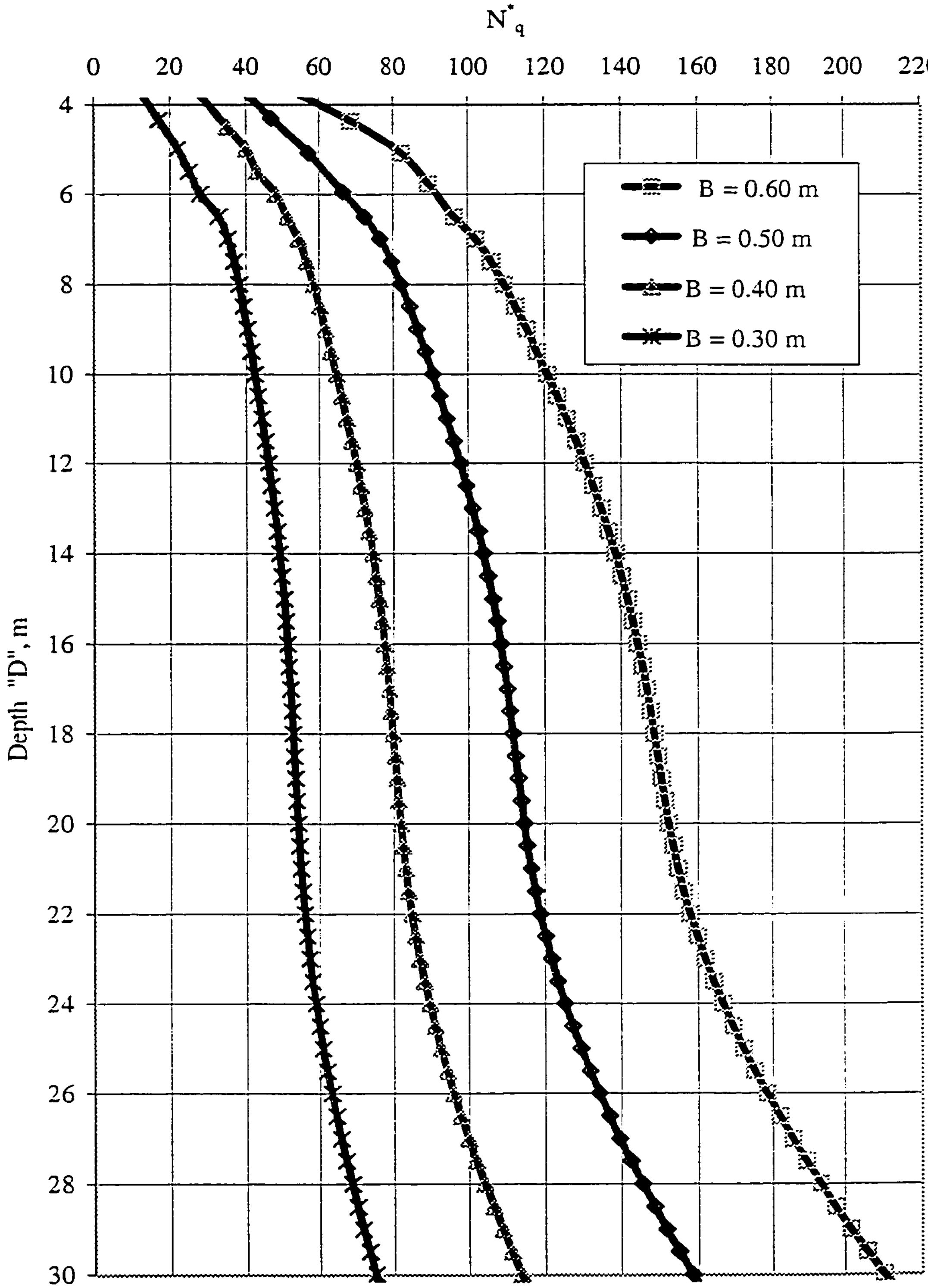

Figure 4.47 Bearing Capacity Factor N^*_q Versus Pile Depth "D" for Different Pile Diameters "B" (Case of ϕ =35°)

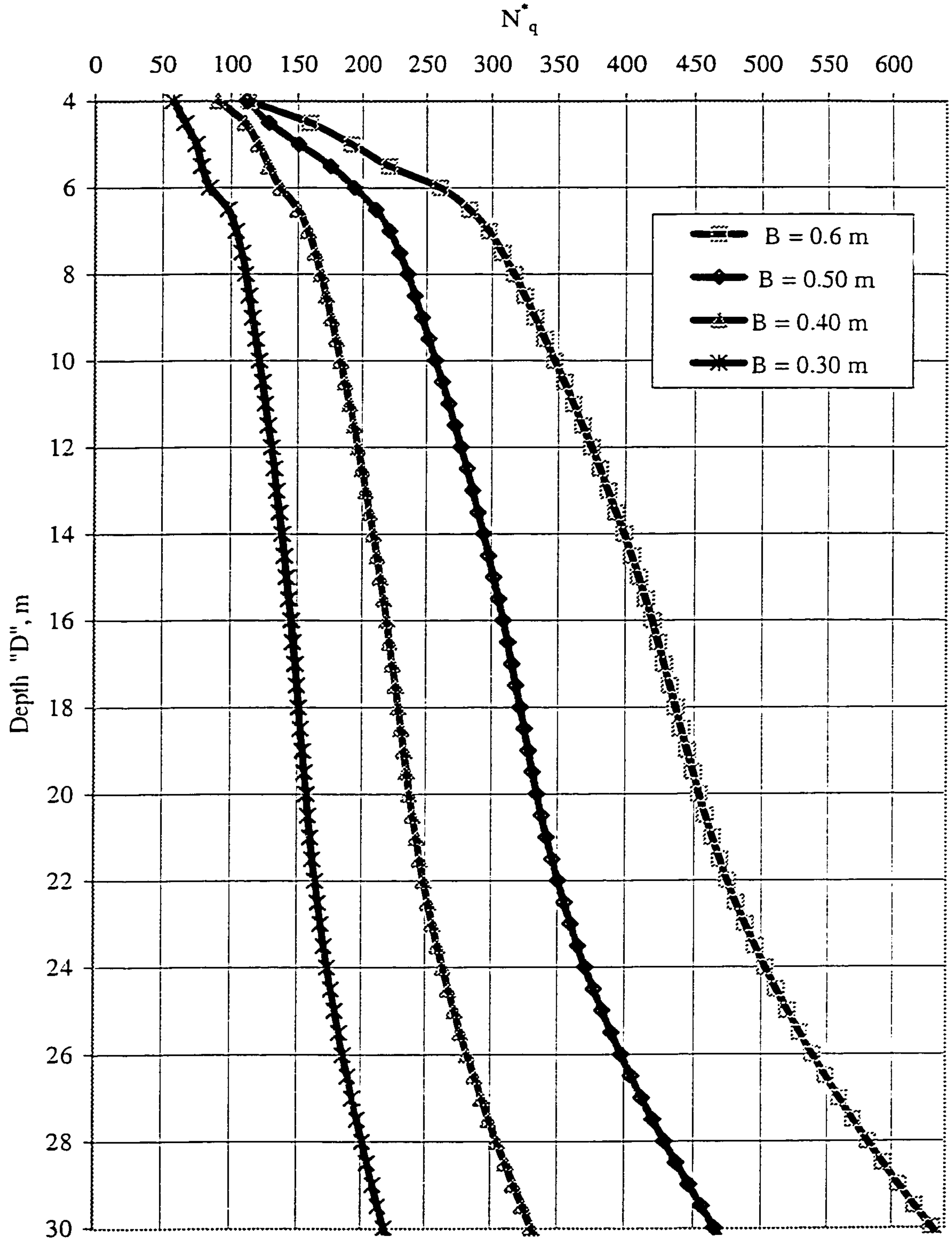

Figure 4.48 Bearing Capacity Factor N^*_q Versus Pile Depth "D" for Different Pile Diameters "B" (Case of ϕ =40°)

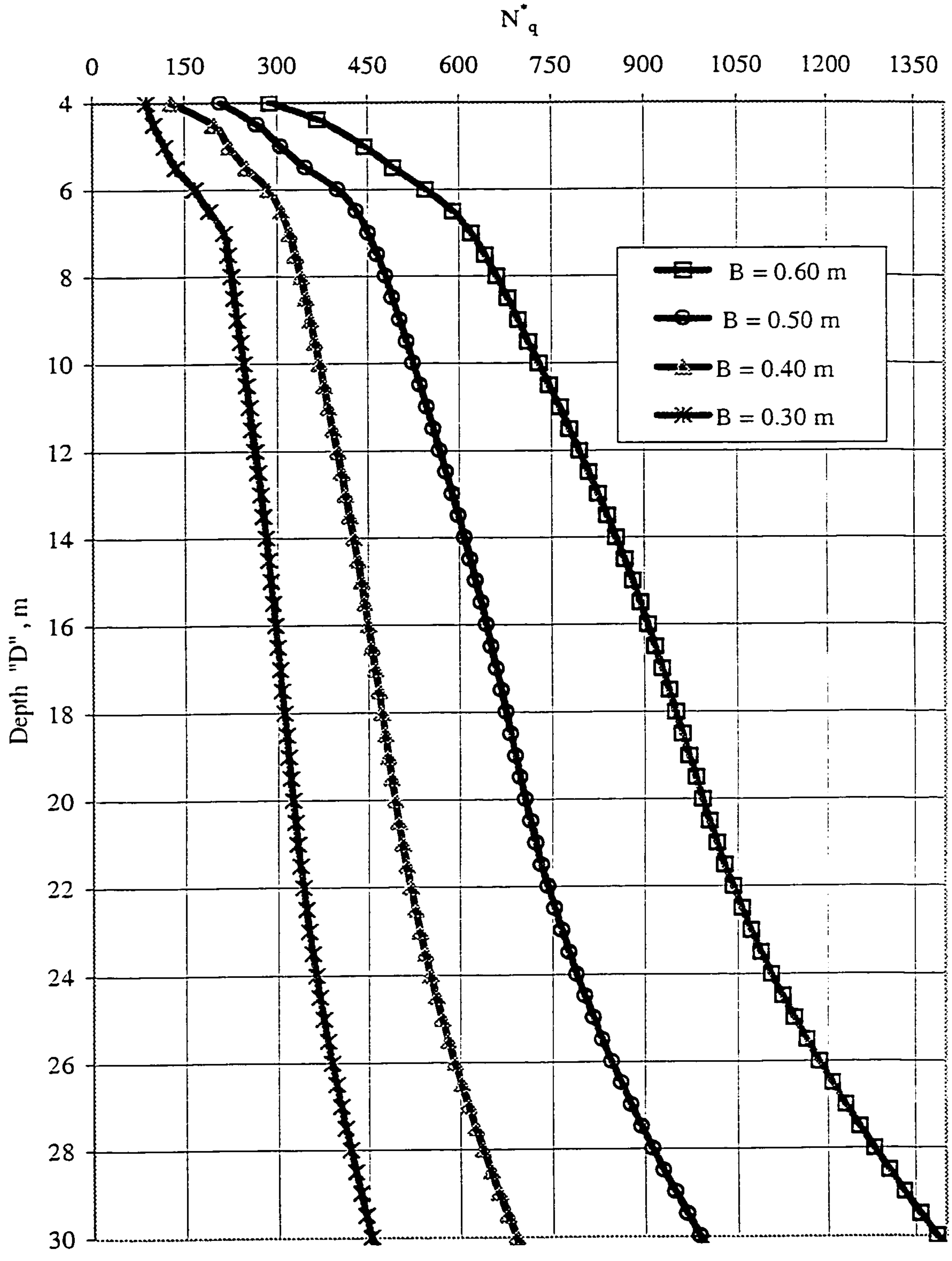

Figure 4. 49 Bearing Capacity Factor N^*_q Versus Pile Depth "D" for Different Pile Diameters "B" (Case of ϕ=42°)

The following steps were followed to produce a simplified formula that can be used in design charts for the factor (K_s*tan δ)

1- The program G-Pile was used to conduct pile load tests for pile depths ranging from 4.0 m up to 30.0 m, and pile diameters between 0.30 m up to 0.60 m.

2- The resulted component of skin resistance Q_S, in tons, was used to determine the equivalent factor (K_s*tan δ) as if the skin resistance were mobilized over the whole shaft area, using the following equation:

$$Q_S = \left(\frac{1}{2}K_S\gamma' D\tan\delta\right)A_S = f_S A_S \qquad \text{...(4.40)}$$

Where:

γ' = effective unit weight of sand (t/m^3)

$$f_s = 0.5\, K_S\, \gamma'\, D \tan\delta \quad (\text{t/m}^2) \qquad \text{...(4.41)}$$

So that the equivalent factor of ($K_s$tan δ) is given by:

$$K_S\tan\delta = \frac{2Q_S}{\gamma B D \pi} \qquad \text{...(4.42)}$$

Figures 4.50 to 4.54 introduce the equivalent factor of (K_s*tan δ) versus pile depth for different pile widths and shaft roughness ratios δ/ϕ. It should be noted that this factor is introduced as a function of Pile Depth D and width B (meters), angle of shearing resistance ϕ and shaft roughness δ/ϕ.

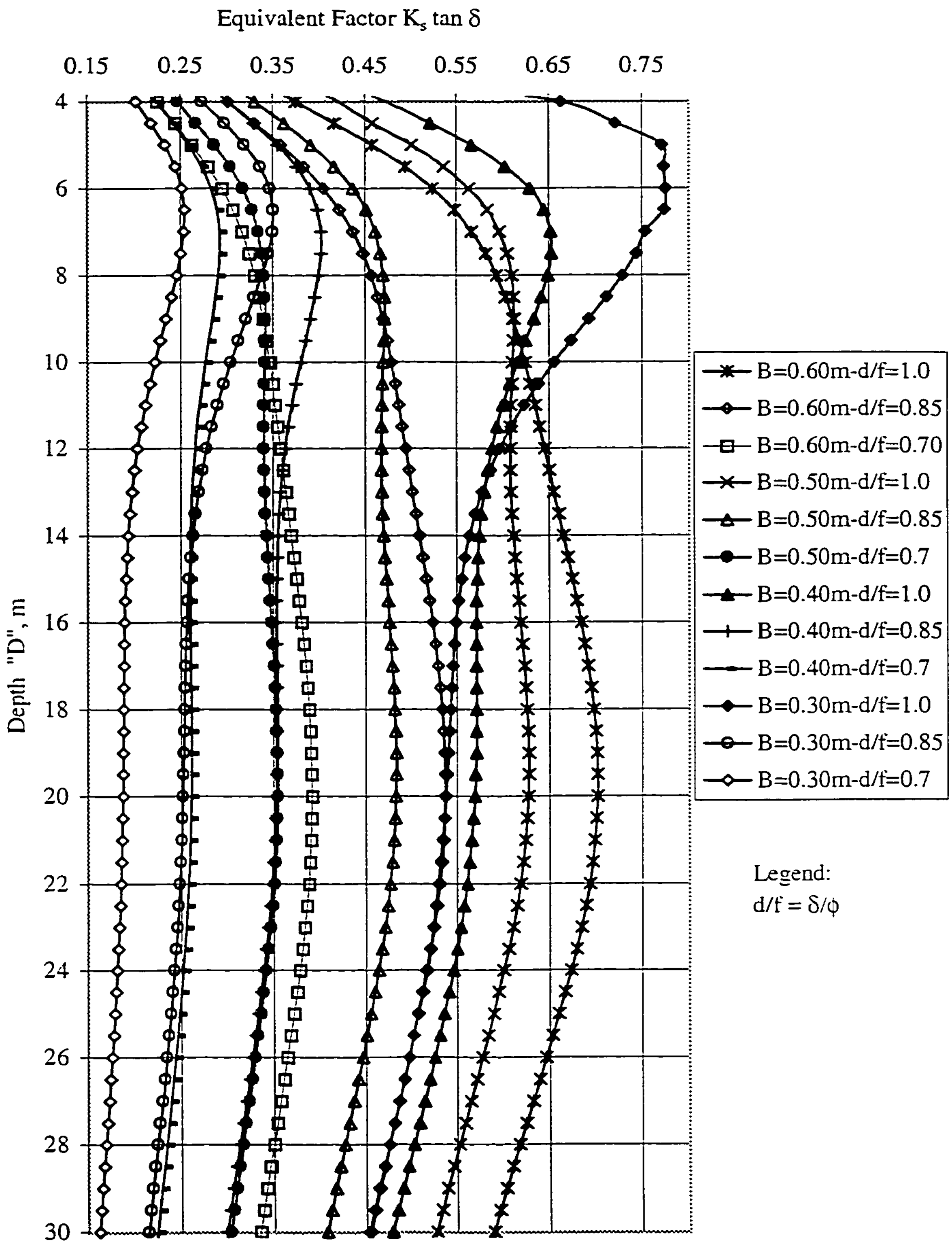

Figure 4.50 Equivalent Factor (K_s tan δ) Versus Depth "D" for Different Pile Diameters "B" (Case of ϕ=27°)

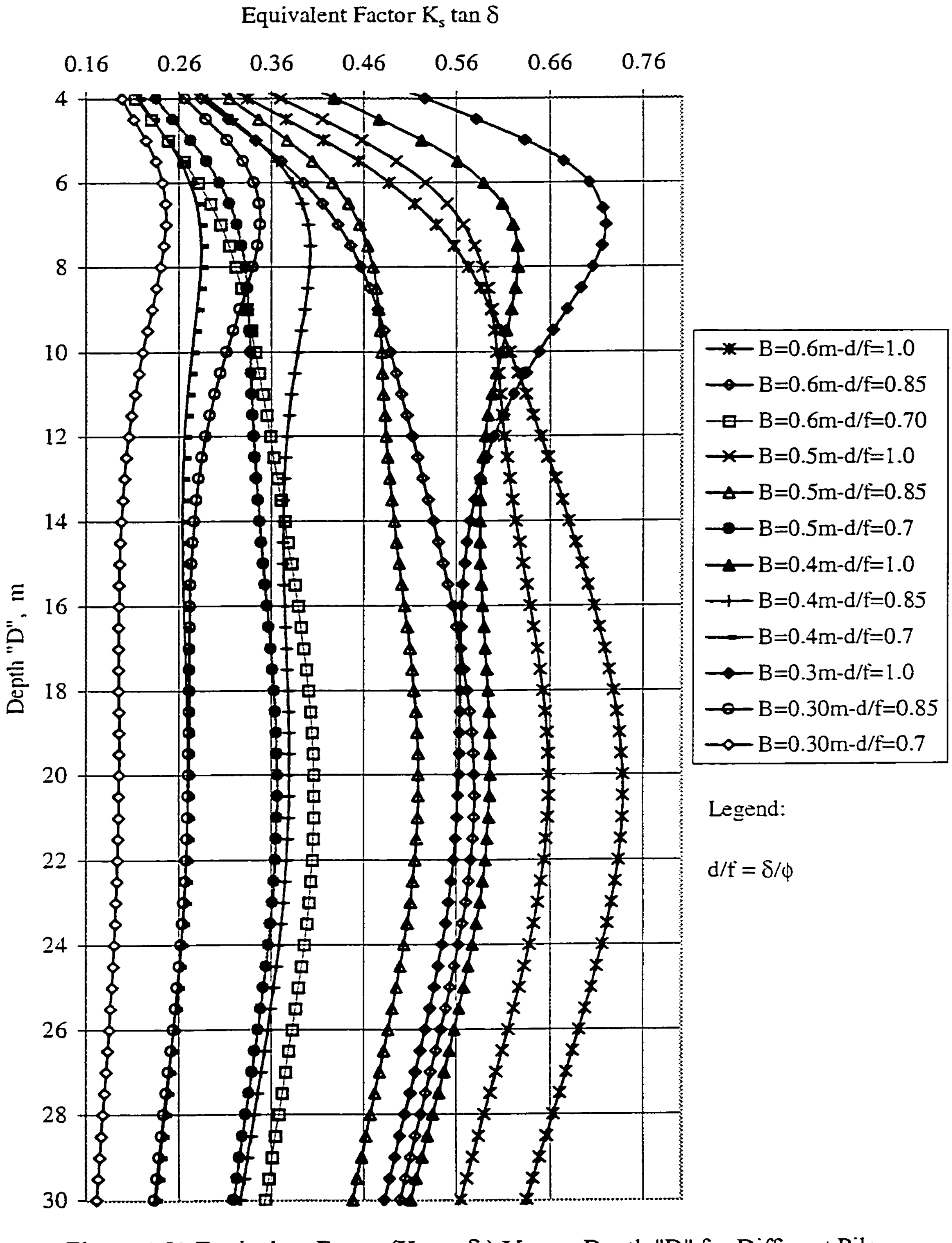

Figure 4.51 Equivalent Factor (K_s tan δ) Versus Depth "D" for Different Pile Diameters "B" (Case of ϕ=30°)

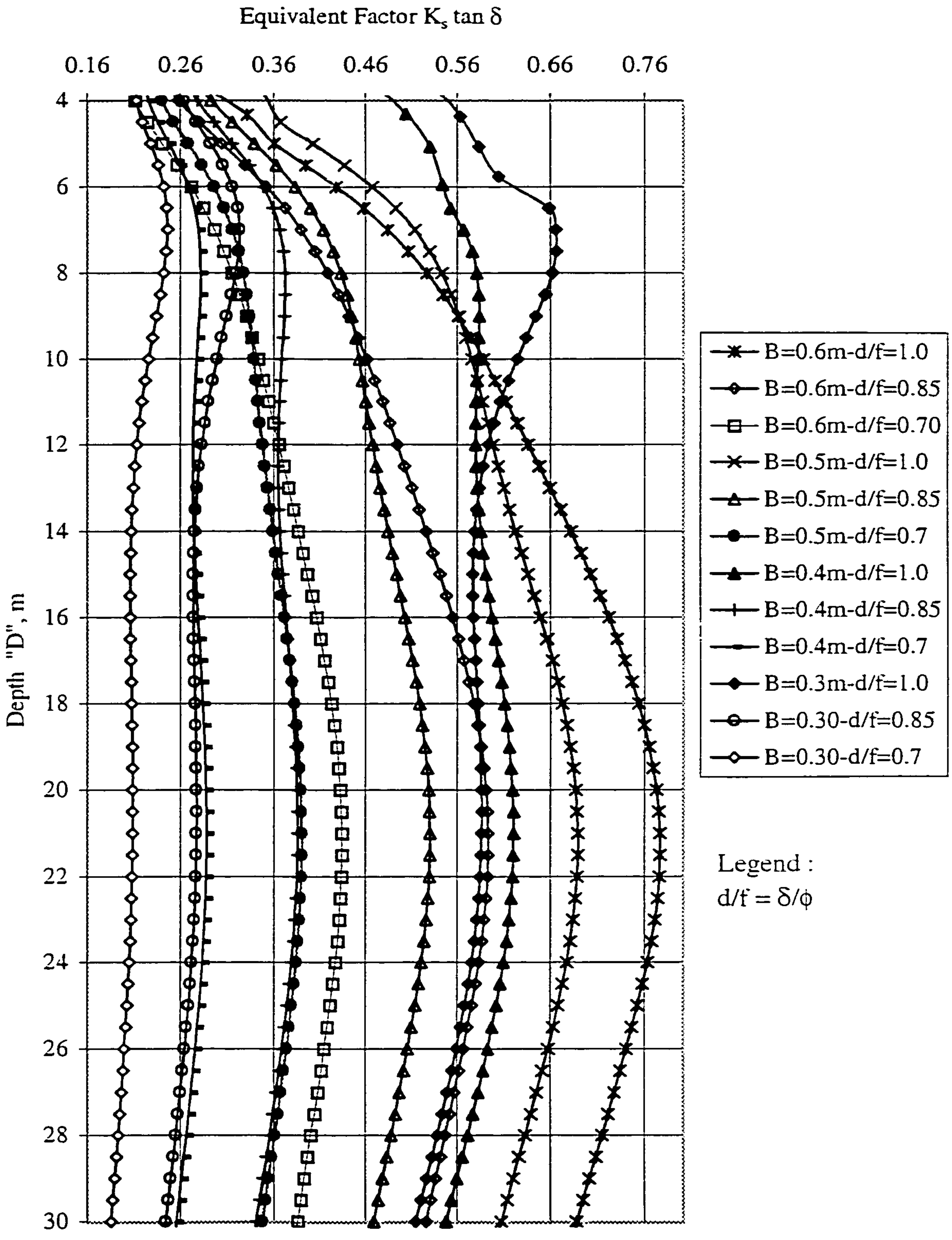

Figure 4.52 Equivalent factor (K_s tan δ) Versus Depth "D" for Different Pile Diameters "B" (Case of $\phi=35°$)

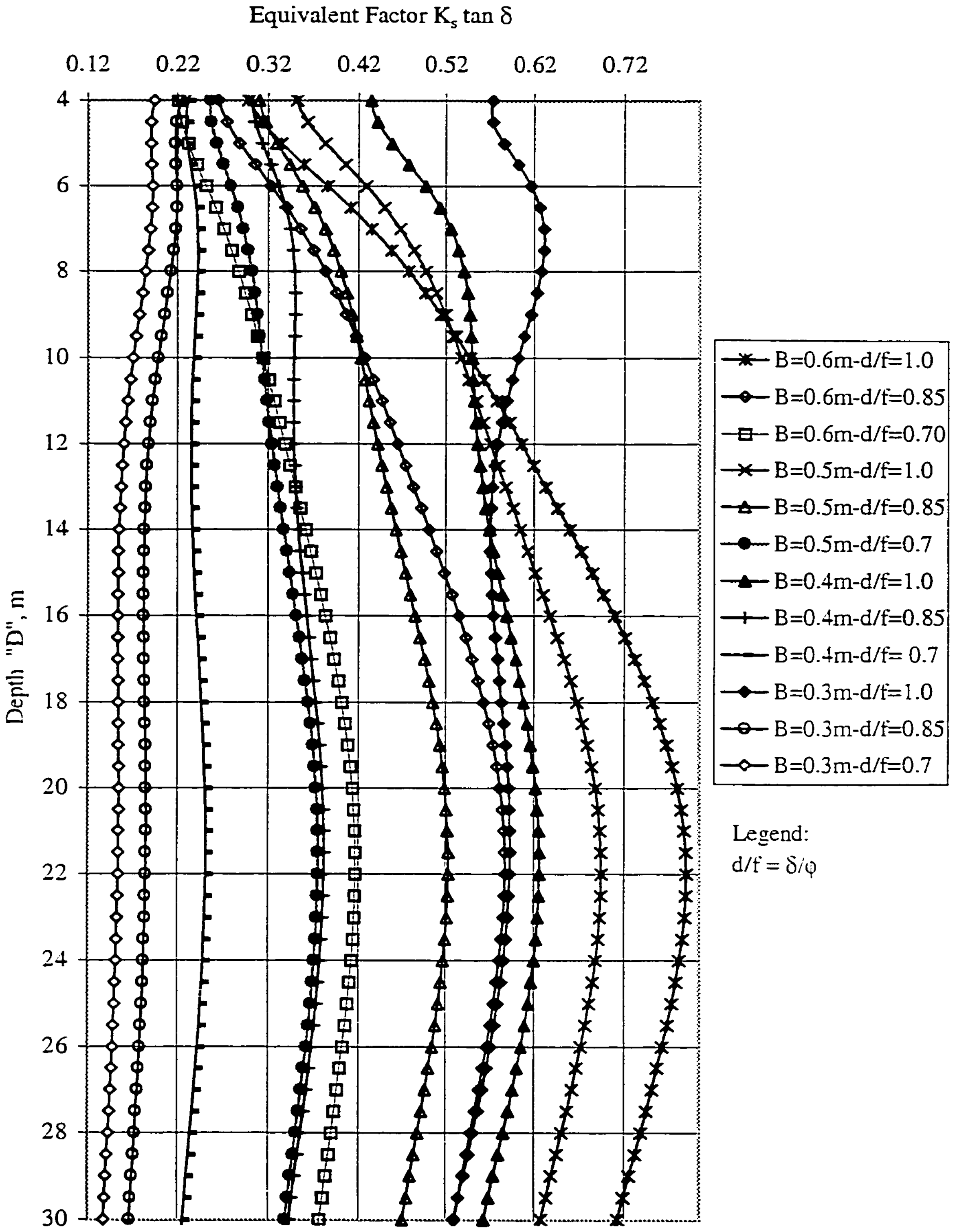

Figure 4.53 Equivalent Factor (K_s tan δ) Versus Depth "D" for Different Pile Diameters "B" (Case of ϕ=40°)

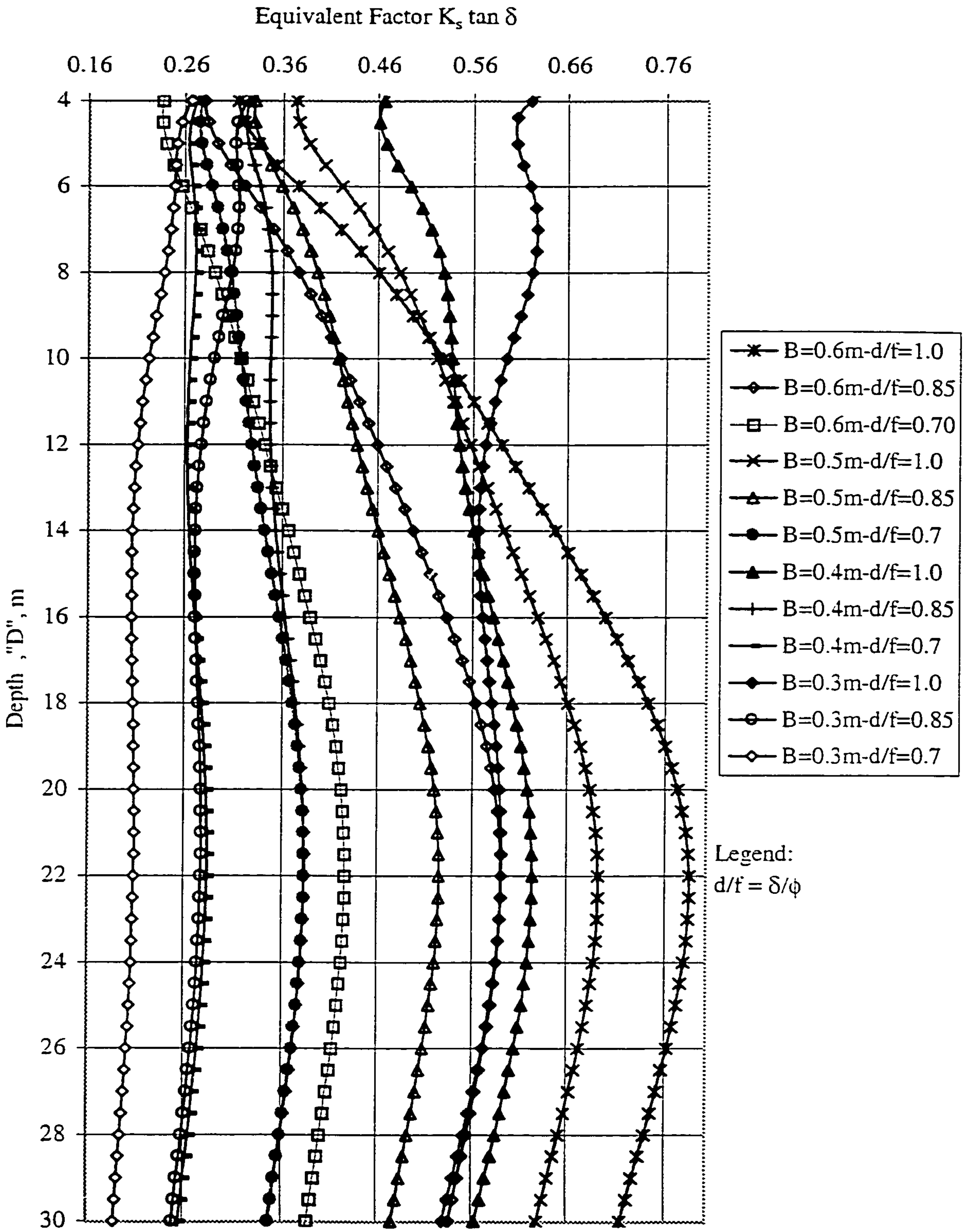

Figure 4.54 Equivalent Factor (K_s tan δ) Versus Depth "D" for Different Pile Diameters "B" (Case of ϕ=42°)

4.11 Recommended Design Procedure

On the basis of the proposed theoretical model, the recommended procedure to estimate the ultimate bearing capacity of a single pile in sand may be summarized as follows:

1- From the data of angle of shearing resistance ϕ, relative shaft roughness δ/ϕ, pile depth D and width B (meters), estimate the equivalent factor of skin resistance ($K_s \tan \delta$) Figures 4.50 to 4.54.

2- Multiply the equivalent factor of skin resistance ($K_s \tan \delta$) by $[(0.5*\gamma*D) * A_s]$, to determine the ultimate skin resistance Q_s (tons). Where γ in t/m^3.

3- Using the data: angle of shearing resistance ϕ, pile depth D and width B (meters), interpolate the bearing capacity factor N_q from Figures 4.45 to Figure 4.49.

4- Multiply N_q by ($\sigma' * D*A_p$) to determine the ultimate point resistance Q_p (tons). Where σ' in t/m^2.

5- The sum of Q_s and Q_p gives the ultimate bearing capacity Q_u (tons).

6- In the case of two layered soil, an average angle of shearing resistance ϕ_{ave} should be determined using Equation 4.30.

4.12 Limitations of the Proposed Method of Design

The suggested procedure for design is subject to the following limitations:

1- It is applicable to the driven piles in sand with range of $4.0 < D < 30.0$ meters. For short piles, a different failure mode may be applicable such as general shear failure mode.

2- In the case of overconsolidated sands, a different study is needed to develop values for the coefficient of earth pressure depending on the degree of consolidation of the sand.

CHAPTER 5

CONCLUSIONS AND RECOMMENDATIONS FOR FUTURE RESEARCH

5.1 General

Literature review has demonstrated a large discrepancies that exist among the different conventional theories for predicting the bearing capacity of a single pile in sand. Numerical and theoretical investigations were conducted in order to clarify the overlooked factors that have been omitted during the development of the previous theories.

5.2 Conclusions

Based on the results of the present investigation, the following conclusions can be drawn:

1- The results of the numerical model constitute the base to define the failure mechanism around a single pile in sand in the following zones of influences:

a- Zone I located immediately below the ground surface and extending downward to a distance equal to $0.25H_l$ and horizontally to a distance of R or radius of influence. This zone is subjected to a densification process due to pile loading and the ground subsidence. The soil is attacking the shaft, so that a case of passive earth pressure has been generated below the ground surface. It reflects the degree of mobilization of skin resistance which is highly mobilized below the ground surface and extended vertically downward to a limited vertical distance H_1.

b- Zone II which exists around the pile tip a few diameters above and a few diameters below with a total height of ($L_1 + L_2 + L_3$) and width: "r". It is also subjected to another densification process due to the opening process made by the advanced pile tip. In this zone it was observed that the pile tip is attacking the soil around, crushing and/or compacting the soil particles creating the active earth pressure condition. This process is deemed to influence the mobilization of tip resistance, which is resisted by the amount of overburden pressure. This reason is believed to be responsible for the limited zone of influence around the tip.

c- Zone III is located between the above two mentioned zones and is subjected to a loosening process and extends horizontally to a few diameters. In this zone the loosening process was found to be not enough to generate pressures against the shaft. This process is believed to limit the degree of mobilization of skin resistance to a vertical depth equal to distance H_l. This zone also could be called the neutral zone.

2- It was shown numerically that the failure mechanism around the shaft is developed in three separate areas: around the pile head (skin resistance) and around the tip (tip resistance). The third the area located between these two areas, which called neutral zone. It was observed that the acting stresses in the neutral zone are not enough to mobilize the skin resistance.

3- The volume shape of failure pattern due to mobilized skin resistance can be approximated into a converted cone, with its base at ground surface, assumed base width equal to R (radius of influence measured from pile axis) and vertical height equal to limited vertical distance H_l measured from the ground surface. These dimensions H_l and R were found to vary with ϕ, δ/ϕ, D & B.

4- Failure pattern due to mobilized tip resistance can be approximated to a compacted inverted cone just beneath the tip connected to a log spiral surface which is extended horizontally to a distance r, and reverted back into the shaft above the tip level by distance equal to L_1+L_2. The vertical depth of the converted cone is called, L_3. These dimensions were found to be vary with: ϕ, D & B.

5- Due to observations of the present study, it was assumed that a varied radius of influnce around the pile shaft is more realastic than a constant distance as it was considered in literature. The raduis of influce around the pile shaft was found to varies with depth.

6- The developed shear stresses on the shaft, τ_{xy} are dependent on shaft roughness δ/ϕ and vary with depth. Its distribution is not linear as suggested in previous theories; and it can be approximated to a bell shaped distribution.

7- The magnitude of σ_x acting on the shaft with depth . The maximum value of σ_x acting on the shaft is found immediately below the ground surface and decreases with depth.

8- The distribution of K_s is not a constant over the shaft and it varies with depth. This trend was reported by several authors, Kulhawy (1984), Meyerhof (1976), Werching. (1987) and Altaee, et al (1992 &1993). The variation of K_s may be ranged between ($K_s< K_o$) and ($K_s >K_p$) over the shaft.

9- A simplified method to predict the variable coefficient of earth pressure acting on the shaft,

K_s is developed and presented in the form of design charts.

10- The varied failure mechanism was utilized in developing theoretical model for predicting the bearing capacity of single pile in sand employing the Sarma method of slices and limit equlibrium technique. The punching shear failure was adapted as the principle mode of failure beneath the pile tip.

11- The parameters involved in the proposed theortical model were observed in a numerical parametric study and a separate predictive equation for each of them were implemented. Skin resistance parameters: H_l and R, are function of ϕ, δ/ϕ, D & B. Tip resistance parameters: L_1, L_2 L_3 and r, are function of ϕ, D & B. These implemented equations were employed in the theortical model calculations.

12- A computer program to facilitate the use of the new proposed theoretical model was developed and used extensively to develop design charts for the bearing capacity factors: N^*_q and equivalent factor ($K_s \tan\delta$).

13- The new proposed theoretical model has proven its capabilities of incorporating important features previously unaccounted for in most conventional bearing capacity theories of deep foundations:

a- A varied failure mechanism depends on factors other than the unique factor,ϕ; they are pile depth, D, and width, B, Shaft relative roughness ϕ/δ and angle of shearing resistance,ϕ.

b- Treatment of the pile bearing capacity problem under axisymmetric conditions; adopting punching shear failure as the principle failure mode.

c- New failure mechanism for skin resistance was developed, whereas the failure mechanism for tip only was considered in most of the previous theories.

14- The proposed theoretical model showed that a critical depth is observed. The unit skin resistance below the critical depth tends to increase at a lower rate than the rate of increase above that depth. Also the critical depth is varied with respect to angle of shearing resistance and pile geometry; diameter and depth. In the case of skin resistance, the critical depth in decreased with pile width and depth, and in the case of point resistance the critical depth in increased with pile width and depth. The proposed theoretical model seems to support the recent findings indicating that below the critical depth the resistances are not constant and tend to increase with depth.

15- The results of the present investigation the basis for a design procedure to estimate the ultimate bearing capacity of single pile in sand. Accordingly, design charts for both skin and tip resistances factors were presented. Ultimate bearing capacity estimated according to these design charts showed good agreement with field load test results, attested by the fact that more than 83% of these tests were predicted within minus or plus 20% of their measured counterpart in a correlation study involving 27 well documented field tests.

5.3 Recommendations for future research

Results of numerical analyses are always subjected to erroneous output, however, they have proven to be a good source of information about the behavior of single piles driven in sand. Further investigation is needed to enhance the presented model in this thesis:

1- Empirical improvements could be added to the numerical functions developed to predict the failure mechanism parameters: H_1, R, L_1, L_2, L_3 and r. These improvements could be developed through verification against field data including a large range of pile geometries and loading conditions to optimize the perdition function of these parameters.

2- Different types of pile geometries, like other cross section shapes, unsymmetrical loading, inclined piles and layered soil, should be the objectives of future studies.

3- It is recommended to extend the present study to clays and soils which possess both cohesion and friction.

4- Further studies should be done to investigate the effect of the over consolidation ratio of sand on the coefficient of earth pressure acting on the pile shaft, K_s.

5- The present study should be extended to non-displacement piles (case of K_o condition) or bored piles.

LIST OF REFERENCES

Altaee, A., Fellenius, B. H., and Evgin, E.,(1992-a), ***"Axial Load Transfer for Piles in Sand: I. Tests on an Instrumented Precast Pile"***, Cand. Geotech. Journal. 29: 11-20.

Altaee, A., Evgin E., and Fellenius, B. H.,(1992-b), ***"Axial Load Transfer for Piles in Sand: II. Numerical Analysis"***, Cand. Geotech. Journal, 29: 21-30.

Altaee, A., Evgin E., and Fellenius, B. H.,(1993), ***"Load Transfer for Piles in Sand and Critical depth"***, Cand. Geotech. Journal, 30: 455-463

Al-Wakati, Z.,(1975),***"On Problems of Soil Bearing Capacity at Depth."***, Ph. D. Thesis Duke University.

Armaleh, S.(1986),***"Analysis of Single and Group of Piles in Cohesionless Soils"***, Msc. Thesis, The University of Arizona.

Armaleh, S.,and Desai, C. S., (1987), "***Load-Deformation Response of Axially Loaded Piles.***", Journal of Geotechnical Engineering, Vol. 113,No.12, pp. 1483-1500.

Balaam, N.P., Poulus, H.G. & Booker, J. R.(1975),***"Finite Element Analysis of the Effect of Installation on Pile Load-Settlement Behaviour"***, Geotech. Engrg. 6, No. 1, 33-48.

Banerjee, P. K. (1978), ***"Analysis of Axially and Laterally Loaded Pile Groups"***, In Developments of in Soil Mechanics ed. C. Scott, Ch. 9, London: Applied Science Publishers.

Berezantzev,V.G. et al.(1961),***"Load Bearing Capacity and Deformation of Piled Foundations"***, Proc. 5th Int. Conf. Soil Mech. and Found. Engrg.,Vol. II,pp. 11-15.

Berezantzev,V.G. (1965),***"Design of Deep Foundation"***, Proc. 6th Int. Conf. Soil Mech. and Found. Engrg., Vol IV, pp 234-237.

Bond. AJ, Hight, D.W., and Jardine, RJ, (1997), ***"Design Of Piles In Sand In The Uk Sector Of The North Sea"***, Offshore and technology report. Health and safety executive. report # OTH 94 457, U.K.

Britto, A.M., (1988), ***"CRISP User's and Programmer's Guide"***, CUED.

Britto, A.M., and Gunn,M.J.,(1987),***"Critical State Soil Mechanics Via Finite Elements"***, John Wiley& Sons.

Britto, A.M.,(1995) ***"Private Communications"***

Broms,B.B. and Sliberman, J. O.,(1964),***"Skin Friction Resistance for Piles in Cohesionless Soils."***, Sols-Soils, No. 10, pp. 33-43.

Butterfield, R., and P. K. Banerjee (1971), ***"The Problem of Group-Pile Cap Interaction"***, Geotechnique, Vol. 21, No. 2, June, pp. 135-142.

Canadian Geotechnical Society,(1992), ***"Canadian Foundation Engineering Manual"***, Third Edition, Technical Committee on Foundations.

Chen,L., and Polous,H. G., (1993), ***"Analysis of Pile-Soil Interaction Under Lateral Loading Using Infinite and Finite Elements"***, Computers and Geotechnics 15, pp. 189-220.

Chow, Y. K. (1986), ***"Analysis of Vertically Loaded Pile Groups"***, Int. J. Numerical Anal. Meth Geomechs 10, 59-72.

Coyle, H. M.,and Reese,L. C., (1966), ***"Load Transfer for Axially Loaded Piles in Clay"***, J. Soil Mech. and Foundation Engrg. division, ASCE, vol. 92, March 1966, pp. 1-26.

Coyle, H.,and Suliman, I. H., (1967), ***"Skin Friction for Steel Piles in Sand"***, Int. Soil Mech. Found. div., ASCE, Vol. 93, SM6, pp. 261-278.

Coyle,H.,and Castello,R.R.,(1981)," ***New Design Correlations for Piles in Sand"***, Journal of Geotechnical Engineering, Vol. 107, No.Gt7, pp. 965-986.

D'Appolonia, E.D., and Romualdi,A.M.,(1963),***"Load Transfer In End-Bearing Steel H-Piles."***, Journal of Geotechnical Engineering. Vol. 89,No.SM2, Paper # 3450, pp. 1-25.

De Nicola, A. and Randolph, M., (1994)," ***Tensile and Compressive Shaft Capacity of Piles in Sand"***, Journal of Geotechnical Engineering, ASCE, 119,(12): 1952-1973.

Desai,C.S., (1974-a), ***"Numerical Design-Analysis for Piles in Sand."***, Journal of Geotechnical Engineering, Vol. 100, No. GT6, pp. 613-635.

Desai,C.S., et al., (1974-b), ***"Finite Element Analysis of The Colombia Lock Pile Foundation System"***, US Army Engineer Waterways Experiment station, Technical report No. S-74-6.

Duncan, J. M.,(1972)," ***Finite Element Analyses of Stresses and Movements in Dams, Excavations and Slopes: State -of-the-art."***, US Army Engineer Waterways Experiment Station, Proc. of Symposium held at Vicksburg, Mississippi "Applications of the Finite Element Method in Geotechnical Engineering" pp. 267-326.

Fellenius, B. H., (1995)," ***The Critical depth: How it came into being and why it does not exist"***, Proc. Instn Civ. Engrg, Geotech. Engrg, 113 Apr., PP. 107-111.

Finno R.J., et al(1989),***"Summary of Pile Capacity predictions and Comparison with Observed Behavior."***, Foundation Engineering Congress, pp. 356-385.

Fruco and Associates (1964)," ***Pile driving and Loading Tests, Lock and Dam No. 4,***

arkansas River and Tributaries Arkansas and Oklahoma.", U.S. Army Engineer District, Little Rock, Corps of Engineers.

Gunn,M.J., (1996) ***"Private communications".***

Hanna,T.H.,and Tan,R.S.H.,(1973),"***The Behavior of Long Piles Under Compressive Loads in Sand."***, Canadian Geotechnical Journal,Vol.10, No.3,pp.311-340.

Holloway, D. M. Clough,G.W.,and Vesic, A. S.,(1975)," ***The mechanics of pile-soil interaction in cohesionless soils"***, Final report of a research project school of Engrg.,Duke University, 280 pp.

Hu, G.(1965), ***"Bearing Capacity of Foundations with Overburden Shear"***, Sols-Soil, No. 13, pp. 11-18.

Jardine, R. J., Potts, D. M., Fourie, A. B. & Burland, J. B., (1986), ***"Studies of the Influence of Non-Linear Stress-Strain Characteristics in Soil-Structure Interaction"***, Geotechnique 36, No. 3,377-396.

Jardine, R. J.,and Lehane,B. M.,(1993), ***"Research Into the Behaviour of Offshore Piles: Field Experiments in Sand and Clay"***, OTH Rep. No. OTH 93 401, HSE Books, London, U.K.

Janbu, N., and Sennest, K. (1974), ***" Effective Stress Interpretation of In-Situ Penetration Tests"***, Proc. European Symposium on Penetration Testing, Stockholm, Vol. 2.2, pp. 181-193.

Janbu, N., (1976), "***Static bearing capacity of friction piles."***, Proc. 6 Th. European Conf. Soil Mech. and Found. Engr., Vol.1.2,pp.479-488.

Kerisel, J. (1961), ***"Foundations Profondes en Milieux Sableux: Variation de la Force Portant Limit en Fonction de la Densite, de la Profondeur, du Diametre et de la Vitesse d'Enfoncement"***, Proc. 5th Int. Conf. Soil Mech. and Found. Engr., Vol. 2 pp. 73-83.

Kerisel, J. (1964),***" Deep Foundations: Basic Experimental Facts"***, Proc. North American Conf. on Deep Foundations, Mexico City, Vol. I, pp. 5-44.

Kerisel, J. (1965),***" Point Resistance in Cohesionless Media at various Densities"***, Proc. 6th Int. Conf. Soil Mech. and Found. Engr., Vol. 3 pp. 265-269.

Kishida, H., (1967),***"The Ultimate Bearing Capacity of Pipe Piles in Sand"***, Proc. of the Third Asian Regional Conf. on Soil Mech. and Found. Engrg., pp. 196-255.

Kraft Jr., L. M., et al.,(1981),"***Theoretical t-z Curves",*** Journal of Geotechnical Engineering,Vol. 107, No.GT11, pp. 1521-1541.

Koumoto, T. & Meyerhof, G.G.,(1985)," ***Ultimate Bearing Capacity of Axially Loaded Piles Based on Three-Dimensional Analysis***", Computer and Geotechnics 1, 181-194.

Kulhaway, F.H., (1984),"***Limiting Tip and side resistance: Fact or Fallacy?***", Proc. of the ASCE, Symp. on Analysis and Design of Pile Foundations, Meyer J.R. Editor, Oct 1984, pp. 80-98.

Kulhaway, F.H., (1995), "***Critical depth: How it Came into Being and Why it Does not Exist***", Discussion, Proc. Instn Civ. Engrg, Geotech. Engrg, 119 Oct., PP. 244-245.

Law, K.T.,(1982), "***Numerical Analysis of Pile Loading and Pulling Tests***", Proc. of 4th Inter. Confer. on Num. meth. in Geomechanics, edmonton., pp. 825-833.

Lehane, B., (1992), "***Experimental Investigations of Pile Behaviour Using Instrumented Field Piles***", Ph.D. Thesis, University of London, U.K.

Lehane, B. M., Jardine, R. J., Bond, A. J., and Frank, R.,(1993), "***Mechanisms of Shaft Friction in Sand from Instrumented Pile Tests.***", Journal of Geotechnical Engineering, Vol. 119,No. 1, pp. 19-35.

Mansur, C.I., and Kaufman, R.I., (1958), "***Pile Tests Low-Sill Structure, Old River Louisiana***", A.S.C.E, TRANSACTIONS, Vol. 123, p. 715.

Mansur, C.I., and Hunter,A.H., (1970), "***Pile Tests--Arkansas River Project***", Journal of Geotechnical Engineering,Vol. 96, No. 5, pp.1545-1582.

Meibner,H., and Shen,Y.L.,(1994), "***Numerical model of a pile foundation with respect to the stress history.***", Proc. of third European conf. on Numerical methods in Geotechnical Engineering, Manchester /UK/ 7-9 September 1994, Balkema, Rotterdam. pp279-284.

Meyerhof,G.G.,(1951), "***The Ultimate Bearing Capacity of Foundations***", Geotechnique, Vol. 2, pp. 301-322.

Meyerhof,G.G.,(1959), "***Compaction of Sands and Bearing Capacity of Piles***", Journal of Geotechnical Engineering,Vol.85,No.SM6, pp.1-29.

Meyerhof,G.G., (1986),"***Theory and Practice of Pile Foundations***", Procedure of Int. Conference on Deep foundations, Beijing, Vol. 2, pp. 77-86.

Meyerhof, G. G.,(1976), "***Bearing Capacity and Settlement of Pile Foundations***", Journal of Geotechnical Engineering, Vol. 102,No. GT3, pp. 197-228.

Meyerhof,G.G.,(1983), "***Scale Effect of Ultimate Pile Capacity.***", Journal of Geotechnical Engineering,Vol.109,No.6, pp.797-806.

Mohan, D., et. al, (1963), "***Load Bearing Capacity of Piles.***", Geotechnique, Vol. 13, pp.76-

86.
Nguyen, T. Q., (1991), "*A Three Dimensional Model For Vertical Piles In Sand*", Ph.D. Thesis Civil Engineering Department, Concordia University, Montreal, Canada.

Nguyen,T. Q., and Hanna, A. M., (1991), "*A Three Dimensional Model For Single Piles In Sand*", Proceedings of the 4th international conference on piling and deep foundations Stresa, Italy 7-12 April 1991, pp. 421-429.

Norlund, R.L.,(1963),"*Bearing Capacity of Piles In Cohesionless Soils*", Journal of Geotechnical Engineering, Vol. 89,No. SM3, pp. 1-35.

Ottaviani,M. (1975), "*Three-Dimensional Finite Element Analysis of Vertically Loaded Pile Groups*", Geotechnique, 25, No. 2, 159-174.

Potyondy, J.G., (1961),"*Skin Friction Between Soils and Various Constru-ction Materials.*", Geotechnique, Vol. XI, No. 4, pp. 339-353.

Poulos, H.G., and Davis, E.H.,(1980), "*Pile Foundation Analysis and Design*", John Wiley and Sons Inc.,New York.

Poulos, H.G., (1989), "*Pile Behaviour - Theory and Application*", Geotechnique, 39, No. 3, pp. 365-415.

Prandtl, L.(1920), "*Uber die Harte Plastisher Korper*", Nachirichen Kon. Gesell. des Wissenschafften, Bottingen, Math. Phys. Klasse, pp. 74-85.

Randolph, M. F., (1977), "*A Theoretical Study of Performance of Piles*", Ph. D. Thesis, Cambridge University, U. K.

Randolph, M. F., (1985), "*Capacity of Piles Driven Into Dense Sand*", Technical report, No. CUED/D- Soils/TR -171, Engineering Dept., Cambridge University, U.K.

Randolph, M., Dolwin,J., and Beck,R.,(1994), "*Design of Driven Piles in Sand*", Geotechnique,44, No. 3, pp. 427-448.

Reese, L. C.,(1972), "*Use of Finite Elements in Foundation Engineering: State -of-the-art*", US Army Engineer Waterways Experiment Station, Proc. of Symposium held at Vicksburg, Mississippi "Applications of the Finite Element Method in Geotechnical Engineering" pp. 507-532.

Reissner, H. (1924), "*Zum Erdolruckproblem*", Proc. 1st Int. Conf. Appl. Mech., Delft, Holland, pp. 295-311.

Robinsky,E.I., and Morrison,C.F.,(1964),"*Effect of Shape and Volume on the Capacity of Model piles in Sand*", Canadian Geotechnical Journal, Vol. I, pp.189-204.

Robinsky,E.I., Sagar, W.L., and Morrison,C.F.,(1964),*"Sand displacement and compaction around model friction piles"*, Canadian Geotechnical Journal, Vol. I, pp.81-93.

Schultaze, E.,(1964),*"Experimental methods and Evaluation of some Loading Testa on Piles"*, Proceedings Symposium on Bearing Capacity of Piles, Roorkee, pp. 60-88.

Simonini, P.,(1994), *"A Finite element analysis of the tip bearing capacity of bored piles in sand."*, Proc. of 8th. Int. Conf. on Computer Methods and Advances in Geomechanics,Balkema,A.A.,Roterdam,Vol. 3,pp.2311-2316.

Szechy,C.,(1960), *"A New Pile Bearing Formula for Friction Piles in Cohesionless Sands."*, Symposium on Pile Foundations,Stckholm,pp.73-76.

Tavenas,F. A.,(1971), *"Load Tests Results on Friction Piles in Sand"*, Canadian Geotechnical Journal,Vol. 8 No. 7,pp.7-22.

Terzaghi, K., (1943), *"Theoretical Soil Mechanics"*, Wiley, New York, N.Y.

Trochanis,A.M., Bielk,J., and Christiano,P.,(1988), *"A Three-Dimensional Nonlinear Study of Piles Leading to Development of a Simplified Model"*, A Technical Report of Research, Civil Engineering, Carnegie Institute of Technology, Carnegie University U.S.A.

Trochanis,A.M., Bielk,J., and Christiano,P.,(1991), *"Three-Dimensional Nonlinear Study of Piles"*, Journal of Geotechnical Engineering, Vol. 117, No.3, pp.429-447.

Tucker, L.M., and Briaud, J., (1988), *"Analysis of the Pile Load Test Program at the Lock and Dam 26 Replacement Project"*, Texas A&M University, Civil Engrg. Department, a technical report prepared for U.S. Army Engineers, report # GL-88-11.

Skempton, A.W., et. al.,(1953), *"Theorie de la Force Portante des Pieux"*, Annales de l'Institut Technique du Batiment et des Travaux Publics, No. 63-64, pp. 285-289.

Stewart, D.P., Jewell,R. J. & Randolph, M.F., (1993),*" Numerical Modeling of Piled Bridge Abutments on Soft Ground"*, Computers and Geotechnics 15, pp. 21-46.

Valliappan, S., Lee, I.K. & Boonlualohr, P.(1974),*" Settlement of Piles in Layered Soils "*, Proc. 7th Biennial Conf., Aust. Road Res. Board, Adelaide 7, Pt 7, 144-153.

Vesic, A.S.,(1963), *"Bearing Capacity of Deep Foundations in Sand"*, Highway Research Record, No. 39, pp. 112-153.

Vesic, A.S.,(1964),*"Investigations of Bearing Capacity of Piles in Sand"*, Soil Mech. Lab. Report No. 3, Duke University, Durham, North Carolina, 16 pp.

Vesic, A.S.,(1967a),*"Ultimate Loads and Settlements of Deep Foundations in Sand"*, Proc. of A Symposium Bearing Capacity and Settlement of Foundations, Duke University, Durham, North Carolina, pp. 53-68.

Vesic, A.S.,(1967b)," ***A Study of Bearing Capacity of Deep Foundations***", Final Report, Project B-189, Georgia Institute of technology, Atlanta, Georgia, U.S.A.

Vesic, A.S.,(1977), "***Design of Pile Foundation*** ", National Cooperative Highway Research Program Synthesis of Practice No. 42, Transportation Research Board, Washington, D.C.

Wersching, S.N., (1987), "***The Development Of Shaft Friction And End Bearing For Piles In Homogenous And Layered Soils***", Ph.D. thesis, civil Engrg. Dept., Polytechnic of Wales, U.K.

Zaman,M. M., Najjar, Y.M., and Muqtadir,A., (1993)," ***Effects of Cap Thickness and Pile Inclination on the Response of a Pile Group Foundation by Three-Dimensional Nonlinear Finite Element Analysis***", Computers and Geotechnics 15, pp. 65-86.

Zeitlen, J. G., and S. Paikowsky (1982), "***Discussion: New Design Correlations for Piles in Sands***", JGED, ASCE, Vol. 108, GT 11, Nov., pp. 1515-1518.

Zienkiewicz, O.C., (1977), " ***The Finite Element Method***", 3rd ed., McGraw-Hill, New York, 787 pp.

Zytynsski (1976), See Britto & Gunn (1987).

APPENDIX I

APPLICATION OF SARMA'S METHOD OF SLICES

APPENIDX I

APPLICATION OF SARMA'S METHOD OF SLICES

Sarma, 1979, introduced his method to determine the stability analysis of embankment and slopes. In this method the soil enclosed within an assumed plane slip surface is divided into a number of slices which do not necessarly to have vertical or parallel sides.

In the following section the general method of slices by Sarma is introduced, as well as the application of this method in the present investigation.

A.1.1 The general method of Slices

The general geometry for the acting forces of a typical slice is shown in Figure A 1.1.

The equilibrium of the horizontal and vertical acting forces is given in the following equations:

$$E_i \cos \omega_i + X_i \sin \omega_i - E_{i+1} \cos \omega_{i+1} + X_{i+1} \sin \omega_{i+1} + FH_i$$

$$+ T_i \cos \alpha_i - N_i \sin \alpha_i = 0 \qquad \text{...(A 1.1)}$$

$$X_i \cos \omega_i - E_i \sin \omega_i - E_{i+1} \sin \omega_{i+1} - X_{i+1} \cos \omega_{i+1} - F_{vi} - W_i$$

$$+ T_i \sin \alpha_i + N_i \cos \alpha_i = 0 \qquad \text{...(A 1.2)}$$

X_i, X_{i+1} and T_i can be replaced as follows:

$X_i \quad = E_i \tan \phi_{si}$

$X_{i+1} = E_{i+1} \tan \phi_{si+1}$

$T_i \quad = N_i \tan \phi_{Bi}$

After simplification and termination of the unknown N_i, a form for E_{i+1} as a function of E_i can be established, where E_i should be known as an external acting force.

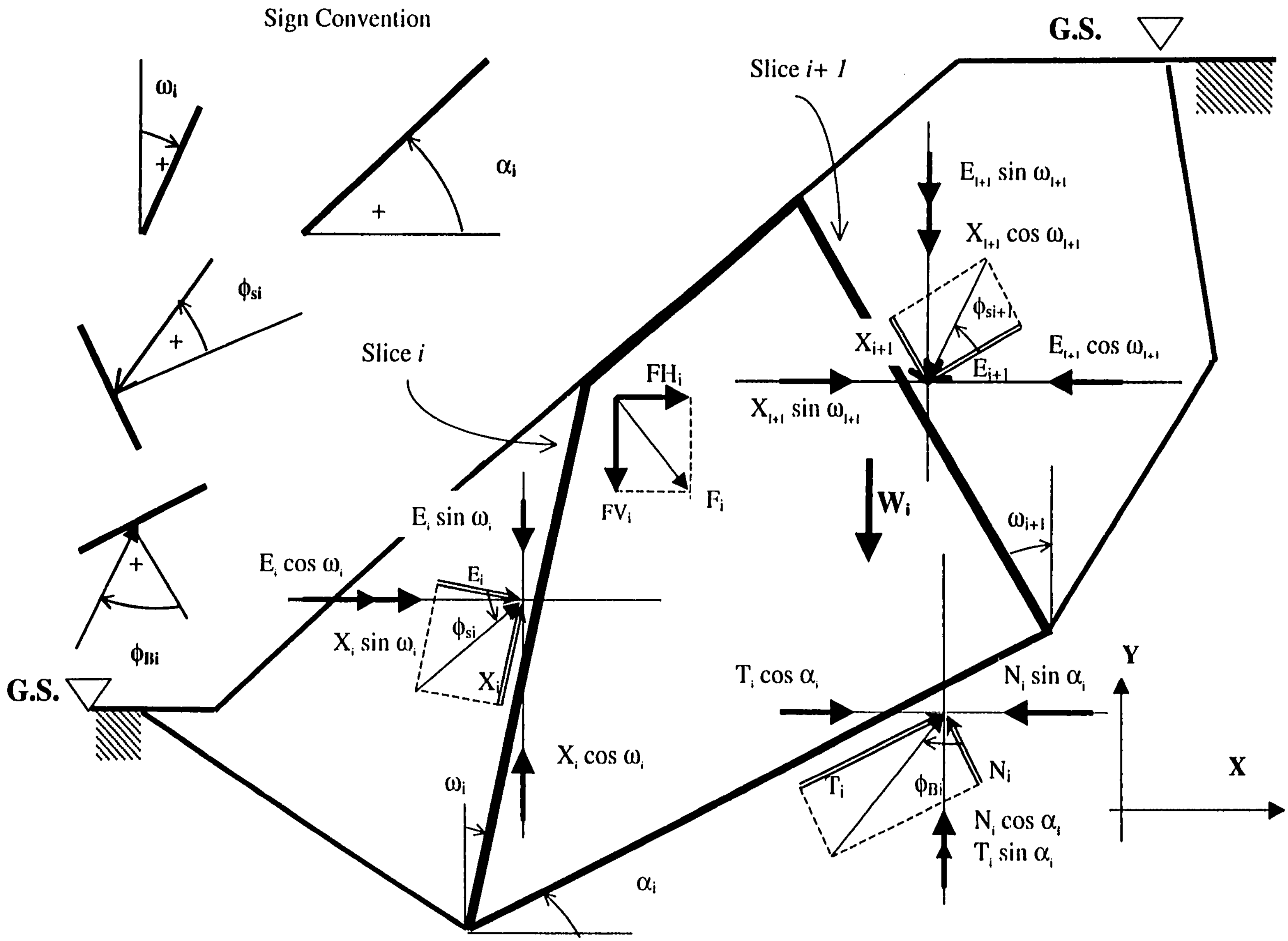

Figure A 1.1 General Geometry and Analysis for Slice Method.

$$E_{i+1} = \frac{\cos(\phi_{Bi} - \alpha_i + \phi_{Si} - \omega_i)\cos\phi_{si+1}}{\cos(\phi_{Bi} - \alpha_i + \phi_{Si+1} - \omega_{i+1})\cos\phi_{Si}}E_i$$

$$+\frac{(W_i + FV_i)(\cos\phi_{Si+1})\sin(\phi_{Bi} - \alpha_i)}{\cos(\phi_{Bi} - \alpha_i + \phi_{Si+1} - \omega_{i+1})}$$

$$+\frac{FH_i(\cos\phi_{Si+1})\cos(\phi_{Bi} - \alpha_i)}{\cos(\phi_{Bi} - \alpha_i + \phi_{Si+1} - \omega_{i+1})} \qquad \text{...(A 1.3)}$$

where:

E_i, E_{i+1} = normal forces acting on the sides of slice i

α_i = basal slope of slice i

ω_i, ω_{i+1} = inclinations of sides of slice i

ϕ_{Bi} = mobilized angle of shearing resistance at mid point of the base of slice i

ϕ_{Si}, ϕ_{Si+1} = average mobilized angles of shearing resistance along sides of slice i

W_i = weight of slice i

F_i = resultant of external forces acting on slice i (other than E_i, E_{i+1}, W_i, N_i and T_i)

FH_i and FV_i = horizontal and vertical components of F_i.

A.1.2 Application of Method of Slices Into Failure Mode

Figure A 1.2 shows the acting forces on zone I. Zone I is a triangle and only three sides are found. This zone can be treated as one slice and the following equations can be determined from the horizontal and vertical equilibrium:

$$\Delta E_1 = E_{RA} + R_{GA} * \sin(90\text{-}\phi\text{-}\beta) - R_{1A} \qquad \text{...(A 1.4)}$$

$$\Delta Q_{s1} = R_{GA1} * \cos(90\text{-}\phi\text{-}\beta) - W_{1A} \qquad \text{...(A 1.5)}$$

Where:

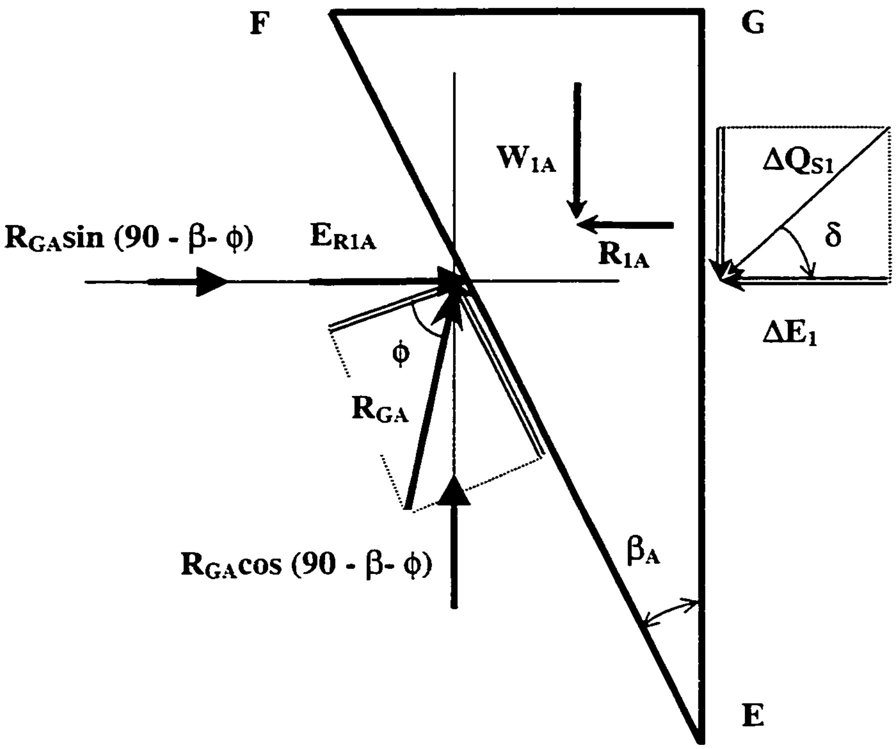

Figure A 1.2 Analysis of Acting Forces on Zone I As One Slice

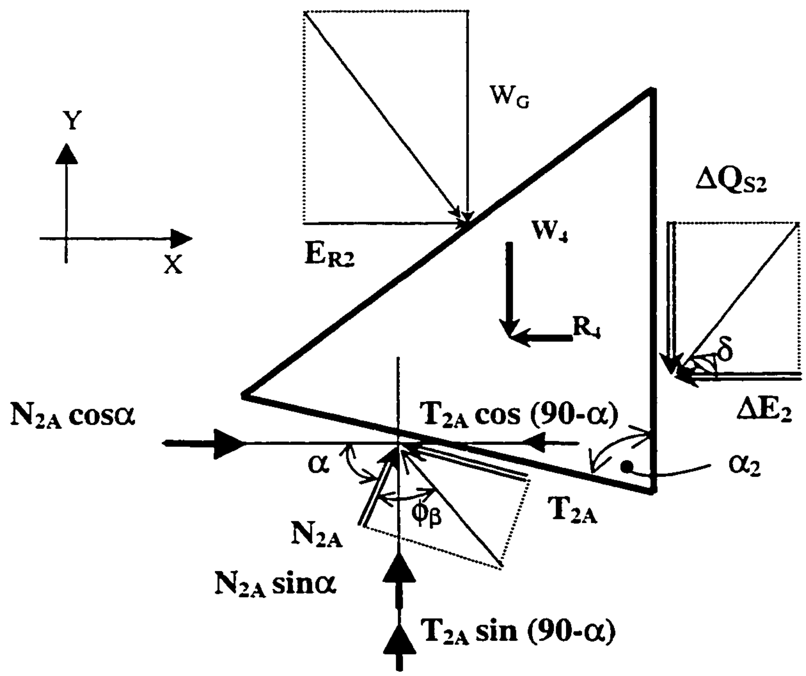

Figure A 1.3 Analysis of Acting Forces on Zone IV As One Slice

E_{RA} is given by equation 4.5.

R_{GA} = Ground reaction on surface FE and is equal to:

$$R_{GA} = 1/2\, \gamma\, H_1^2\, K_o \qquad \text{...(A 1.6)}$$

and :

$$K_o = 1 - \sin\phi \qquad \text{...(A 1.7)}$$

Acting forces on zone 4 is given in Figure A 1.3.

Equilibrium analysis of these forces led to the following equations:

$$N_{2A} \cos\alpha + E_{R2} - \Delta E_2 - R_4 - T_{2A} \cos(90-\alpha) = 0 \qquad \text{...(A 1.8)}$$

$$T_{2A} \sin(90-\alpha) + N_{2A} \sin\alpha - W_G - \Delta Q_{S2} - W_4 = 0 \qquad \text{...(A 1.9)}$$

Substitute:

$$T_{2A} = N_{2A} \tan\phi_\beta$$

$$\Delta Q_{S2} = \Delta E_2 \tan\delta$$

Where:

ϕ_β = Average mobilized angle of shearing resistance on base BC.

We get:

$$N_{2A} \cos\alpha - N_{2A} \tan\phi_\beta * \cos(90-\alpha) + E_{R2} - \Delta E_2 - R_4 = 0 \qquad \text{...(A 1.10)}$$

$$N_{2A} \sin\alpha + N_{2A} \tan\phi_\beta * \sin(90-\alpha) - W_G - \Delta E_2 \tan\delta - W_4 = 0 \qquad \text{...(A 1.11)}$$

$$N_{2A} [\cos\alpha - \tan\phi_\beta * \cos(90-\alpha)] + E_{R2} - \Delta E_2 - R4 = 0$$

$$N_{2A} [\sin\alpha + \tan\phi_\beta * \sin(90-\alpha)] - \Delta E_2 \tan\delta - W_4 - W_G = 0$$

By eliminating N_{2A} between the above two equations, it produces the following equation:

$$\left(\frac{\sin\alpha + \tan\phi_\beta \cdot \sin(90-\alpha)}{\cos\alpha - \tan\phi_\beta \cdot \cos(90-\alpha)}\right)(R_4 + \Delta E_2 - E_{R2}) - \Delta E_2 \tan\delta - W_G - W_4 = 0$$

Finally:

$$\Delta E_2 = \frac{W_{4G} + W_4 - A(R_4 - E_{R2})}{A - \tan\delta} \qquad \text{...(A 1.12)}$$

Where: $$A = \left(\frac{\sin\alpha + \tan\phi_\beta \cdot \sin(90-\alpha)}{\cos\alpha - \tan\phi_\beta \cdot \cos(90-\alpha)}\right)$$

Then:

$$\Delta Q_{S2} = \Delta E_2 \tan\delta \qquad \text{...(A 1.13)}$$

and:

$$N_{2A} = \frac{\Delta E_2 + (R_4 - E_{R2})}{\cos\alpha - \tan\phi_\beta \cos(90-\alpha)} \qquad \text{...(A 1.14)}$$

$$T_{2A} = N_{2A} \tan\phi_\beta \qquad \text{...(A 1.15)}$$

APPENDIX II
Computer Program "G-Pile"

Program List G-Pile

%******************


```
function [QS,Qp,Qu,L1,L3,rtip,H1,R,Nq,Ks] = DCR(D,phi,B,Delta,gama)

% Input parameters here:-
**********************************************************************
D =
B =
gama =
Phi =
Delta =
**********************************************************************
DEta = 1;
NCeta =13 ;
L2 =0.0001*D;
df=(dlta)/(fhi);

%  PARAMETERS CALCULATIONS HERE
**********************************************************************

% Ks
**********************************************************************
 XK=1.0/D;
 Ks25=1.194+XK*(-10.98+XK*(258.04+XK*(-1966.46+XK*(6405.12+XK*(-514.79)))));
 Ki = (1-sin(Phi*Y));
 KsI = Ks25 +( 0.0161*(fhi) - 0.4025);
 KsB=0.31+0.5015*(atan((D-23.57)/(-5.178))+1.571)/(3.142);
 Y3=(( B-0.25)/0.5)*KsB;

YK=0.37*(2.0*0.0045*(log(exp((df+0.34/2.0)/0.0045)+exp(0.84/0.0045))-
log(exp((0.84+0.34/2.0)/0.0045)+exp(df/0.0045)))+0.34)/(2.0*0.34);
Y2=0.36-YK;
  Ksi1=(KsI+Y3);
  Ksi=Ksi1*(1-Y2);

 Ks=Ksi*Ki;

% [R]
**********************************************************************
 XR1=log(D)*log(D);
 XR2=1.0/sqrt(D);
 XR3=exp(-D);
```

```
R25=-0.23+0.0096*XR1+0.93*XR2-0.88*XR3;
  xR=fhi-25;
RF=(-7.93E-21)+xR*0.0027;
 RD1=R25+RF;
Xx1=D;
Xx2=D*D;
Xx3=log(D)/(D*D);
Xx4=1.0/(D*D);
RB=0.055-0.00069*Xx1+(2.52E-06)*Xx2+10.53*Xx3 -8.701*Xx4;
 RB1=RD1 +RB ;
RI= RB1*D; %in meters
RD = 0.3*(0.6*(df-0.5)) ;
R = RI*(1- RD) ;

% [r]
*************************************************************************
r25=0.4281+4.89*(2.0*5.98*(log(exp((D+67.811/2.0)/5.98)+exp(54.91/5.98))-
log(exp((54.91+67.81/2.0)/5.98)+exp(D/5.98)))+67.81)/(2.0*67.811);
rB=0.004+0.293/(1.0+exp(-(D-13.672)/-2.621))
rI = r25 + ((0.75-B)/0.5)*rB

r1f=0.0315*(fhi-25);
rtip=(r25+r1f +rI);

% [H1]
*************************************************************************
H1D=(0.16+D*(0.571+D*(-0.024+D*0.000678)))/(1.0+D*(-
0.048+D*(0.0011+D*7.514E-06)));
  X2h=D*sqrt(D);
 X3h=log(D)/(D^2);
 X4h=exp(-D);
 Hf=-2.01+0.48*D-0.033*X2h+20.29*X3h -21.97*X4h;
HB=-3.66+(log(D))*(5.75+(log(D))*(1.89+(log(D))*(-7.56+(log(D))*(4.64+(log(D))*(-
1.065+(log(D))*0.086)))));
BR= ((0.75-B)/0.5)*HB;
H1rd = 0.0727*fhi - 1.2331;
H1 = H1D -  BR  -(dlta/fhi)*H1rd;


% [L3]
*************************************************************************
 X1L3=D;
 X2L3=D/log(D);
 X3L3=1.0/log(D);
 X4L3=log(D)/(D^2);
 L345=2.21-0.192*X1L3+1.09*X2L3-5.152*X3L3+22.23*X4L3;
```

```
L3red = -0.0223*(fhi) + 1.0025;
L3dif=((45-fhi)/20)*L3red;
L3=(L345-L3dif);
z1L3=exp(-0.5*((D+1.66)/2.11)*((D+1.66)/2.11));
z2L3=exp(-0.5*((fhi-32.771)/-0.772)*((fhi-32.771)/-0.772));
zL3=0.94-96.772*z1L3-0.435*z2L3+1424.37*z1L3*z2L3;
L3=L3*zL3;
L3Y=-0.292+(0.422/(1.0+exp(-(D-10.79+15.42/2.0)/2.57)))*(1.0-1.0/(1.0+exp(-(D-
10.79-15.42/2.0)/3.16)));
L3=L3*(1+L3Y);
%[L1]
*************************************************************************
L125=(0.031+D*(0.098+D*(-0.00373+D*0.00015)))/(1.0+D*(-
0.039+D*(0.00041+D*2.93E-05)));
L1f=(0.77+log(D)*(-0.32+log(D)*(-0.25+log(D)*(0.223+log(D)*(-
0.066+log(D)*0.0072)))))/(1.0+log(D)*(-0.51+log(D)*(-0.25+log(D)*(0.25+log(D)*(-
0.07+log(D)*0.0072)))));
L1dff=((fhi-25)/20)*L1f;
L1=L125;
L1z=-59.422-3.26*D-8.66*(sqrt(D)*log(D))+36.19*(D/log(D))-104.732*(1.0/(D^2));
L1=L1*L1z;

.........................................................................

RU= R-(B/2);
Lx=0.25 *H1;
Cx=Ks*gama*(0.25*H1);
Phi = Phi* Y ;
PG1    = ((R-(B/2))/3)+ (B/2);
PG4    = ((rtip-(B/2))/3)+ (B/2);

Ko = 1 - sin(Phi);
Ki = Ko;
Kp=(1+sin(Phi))/(1-sin(Phi));
format short
Beta = atan(RU /H1);
PhiB = Phi / 2;
W1A = (1/2) *( RU) * (H1) *PG1 * gama * DEta  ;
RGA= 0.25*gama*(H1^2)*Ko*R*DEta;
Geta= (90*Y)-Phi-Beta;
RI =0.25*gama *( H1^2)*(RU)* Ko  ;
R1A = 2 * RI * sin (DEta/2);
E1=0.0625*gama*R*H1^2*3*Ks*DEta;
DE1= E1+RGA*sin(Geta)   -0.5*R1A
QS1=DE1*tan (Delta)*(2*pi/DEta);
*************************************************************************
ru=rtip-(0.5*B);
```

```
AlphaI= atan((ru)/L2);
AlphaII=90*Y-AlphaI;
W4G= 0.25*gama*(2*D-L1-2*L2)*DEta*rtip ; % /2 = 0.5 r    weight of soil above
W4=0.5*gama*(ru)*(L1+L2)*PG4*DEta ;  % self weight of zone 4
R4=(0.5*gama*Ko*(2*D-L1)*(ru)*(L1+L2))*sin(DEta/2);
BI=( cos(AlphaI)-tan (PhiB)*cos(AlphaII))/(sin(AlphaI)+tan (PhiB)*sin(AlphaII));
DE2=(R4-BI*W4G-BI*W4)/( BI*tan(Delta)-1);
DE2=abs(DE2);
QS2=(DE2*tan(Delta)*(2*pi/DEta));
QS=QS1+QS2;
Calculation of Qp
**********************************************************************
N2A=(W4+W4G+DE2*tan(Delta))/(tan(PhiB)*sin(AlphaII)+sin (AlphaI));
T2A = N2A * tan(PhiB) ;
Epsi =atan(2*L3/B) ;
Ceta = (1.5*pi)-Epsi-AlphaI ;
DCeta = Ceta / NCeta;
s1 = (1 / Ceta) ;
s2 = (2*L2/B);
s3 = (cos(Epsi)) / (cos(AlphaI))   ;
B1 = s1 * (log(s2 * s3));
f1 = B / (2 * cos(Epsi))

 for i = 1 : NCeta + 1
        Er(i) = f1 * (2.718281829)^(B1 * (Ceta - (i-1) * DCeta));
 end

 for i = 1 : NCeta
        Ai(i) = .5 * Er(i) * Er(i + 1) * sin(DCeta);
 end

 for jj = 1 : NCeta
        L(jj) = (2 / 3) * f1 * (2.718281829)^ (B1 * (Ceta - ((jj-1) + .5) * DCeta));
 end


for k = 1: NCeta
         P(k) = (B / 2) + L(k) *( sin(pi-(AlphaI + ((k-1) - .5) * DCeta)));
         W(k) = Ai(k) * P(k) * (DEta) * gama;
 end

 for s = 1: NCeta +1

          OMIG(s) = pi-(AlphaI + (s-1) * DCeta) ;
 end
 for m = 1 : NCeta +1
```

```
 z1(m)= (Er(m) * cos((AlphaI + (m) * DCeta)-pi)+D) ;
 z2(m)=(Er(m) * cos((AlphaI + (m+1) * DCeta)-pi)+D);
 h(m) = z2(m)-z1(m);
 P(m) =  Er(m) *( sin(pi-(AlphaI + (m+1) * DCeta)));
 Alpha(m) = atan(h(m) / P(m));
 AlphaA(m)=Alpha(m)*(180/pi);
 end


 PhibM = -PhiB;
 for n = 1 : NCeta +1
  PhiS(n) = (PhibM) + (Phi - PhibM) * ((n-1) * DCeta / Ceta);
 end
for i = 1 : NCeta +1
 Phib(i) = (1 - ((.5 * (Ceta + (Ceta - ((i-1)* 2 + 1) * DCeta))) / Ceta)) * Phi;
end

for i = 1 : NCeta + 1
 z(i)= Er(i) * cos((AlphaI + (i-1) * DCeta)-pi)+D;
z(i) = Er(i) * cos(OMIG(i)) + D;
end
for j = 1: NCeta
  RII(j) = (1 / 3) * Ai(j) * (D + z(j) + z(j + 1)) * Ko * gama
  R2(j)  = 2 * RII(j) * sin(DEta / 2);
end
 N2(1) = N2A;

for i = 1 : NCeta
 U1 = (cos(Phib(i) - Alpha(i) + PhiS(i) - OMIG(i)) * cos(PhiS(i+ 1))) / (cos(Phib(i) -
Alpha(i) + PhiS(i+ 1) - OMIG(i+ 1)) * cos(PhiS(i)));
 U2 = (cos(PhiS(i + 1)) * sin(Phib(i) - Alpha(i))) / cos(Phib(i) - Alpha(i) + PhiS(i + 1) -
OMIG(i + 1));
 U3 = (cos(PhiS(i + 1)) * cos(Phib(i) - Alpha(i))) / cos(Phib(i) - Alpha(i) + PhiS(i + 1) -
OMIG(i + 1));
 N2(i+1) = U1 * N2(i) + U2 * W(i) - U3 * R2(i);
end
format bank
TN = -(N2(NCeta+1)) * tan(Phi);
Wc = (1 / 3) * ((pi * (B ^ 2)) / 4) * (DEta / Y) * (sin(Epsi)) * (gama);
Qp = (2 * (pi) / (DEta)) * ((N2(NCeta+1)) * cos(Epsi) + (TN) * sin(Epsi)) - Wc;
Qu=QS+Qp;
```

APPENDIX III

CONVERSION FACTORS

Appendix III

CONVERSION FACTORS

The following are the conversion factors for most used units in this thesis to comply with the S.I. units:

1 inch =	0.0833333 ft
1 inch =	2.54 cm
1 inch =	0.0254 m
1 ft^2 $\doteq$	0.092904 m^2
1 t/m^3 =	1000 kg/m^3
1 t/m^3 =	0.036127 pci
1 t/m^3 =	62.42796 pcf
1 t/m^3 =	9.8039 kN/m^3
1 kN/m^3 =	0.102 t/m^3
1 kN/m^3 =	0.003685 pci
1 kN/m^3 =	6.367666 pcf
1 kN/m^3 =	0.102 t/m^3
1 t/m^2 =	204.82 psf
1 t/m^2 =	1.4223 psi
1 t/m^2 =	9.8066 kpa
1 ton (force) =	2 kip
1 ton (force) =	8896.443 N
1 ton (force) =	8.8964433 kN